

# Geologic Studies in Alaska by the U.S. Geological Survey, 1994

Thomas E. Moore *and* Julie A. Dumoulin, *Editors*

---

U.S. GEOLOGICAL SURVEY BULLETIN 2152



UNITED STATES GOVERNMENT PRINTING OFFICE, WASHINGTON: 1996



**U.S. DEPARTMENT OF THE INTERIOR**

**BRUCE BABBITT, Secretary**

**U.S. GEOLOGICAL SURVEY**

**Gordon P. Eaton, Director**

For sale by  
U.S. Geological Survey, Map Distribution  
Box 25286, MS 306, Federal Center  
Denver, CO 80225

Any use of trade, product, or firm names in this publication is for descriptive purposes only and does not imply endorsement by the U.S. Government.

**COVER PHOTO:** View to the northeast of carbonate rocks (light colored rocks, foreground to left skyline) of the Lisburne Group (Mississippian and Pennsylvanian) and of the Baird Group (Devonian) overlain on a moderately east-dipping fault contact by ultramafic rocks (dark rocks to right of light colored rocks) of the Avan Hills mafic-ultramafic complex (Jurassic), western Brooks Range. The emplacement mechanism of the Siniktanneyak mafic-ultramafic complex, which is also located in the western Brooks Range and is similar to the Avan Hills mafic-ultramafic complex, is the subject of a paper by Morin and Moore in this volume.

# CONTENTS

Introduction	
Thomas E. Moore and Julie A. Dumoulin .....	1

## ENVIRONMENT AND CLIMATE

Acid mine drainage associated with volcanogenic massive sulfide deposits, Prince William Sound, Alaska	
Richard J. Goldfarb, Steven W. Nelson, Cliff D. Taylor, William M. d'Angelo, and Allen L. Meier .....	3
Environmental geochemistry of mercury deposits in southwestern Alaska: mercury contents in fish, stream-sediment, and stream-water samples	
John E. Gray, Allen L. Meier, Richard M. O'Leary, Carol Outwater, and Peter M. Theodorakos .....	17
Natural environmental effects associated with the Drenchwater zinc-lead- silver massive sulfide deposit with comparisons to the Red Dog and Lik deposits, west-central Brooks Range, Alaska	
Karen D. Kelley and Cliff D. Taylor .....	31
Environmental geochemistry of the McKinley Lake gold mining district, Chugach National Forest, Alaska	
T. P. Trainor, S. Fleisher, T.R. Wildeman, R.J. Goldfarb, and C.S. Huber .....	47

## HAZARDS AND RELATED STUDIES

Alaska earthquakes—1994	
Kent A. Pogleman, Charlotte A. Rowe, and William R. Hammond .....	59

## RESOURCES

Organic matter and thermal maturation of lower Paleozoic rocks from the Nixon Fork subterranean of the Farewell terrane, west-central and southwestern Alaska	
Stephen R. Jacobson, Robert B. Blodgett, and Loren E. Babcock .....	81
Rare-earth enrichment at Bokan Mountain, southeast Alaska	
John A. Philpotts, Cliff D. Taylor, and Phillip A. Baedeker .....	89

## GEOLOGIC FRAMEWORK

Gravity models of the Siniktanneyak mafic-ultramafic complex, western Brooks Range, Alaska: evidence for thrust emplacement of Brooks Range ophiolites	
Robert L. Morin, and Thomas E. Moore .....	101
Elemental and isotopic evidence for 2.1-Ga arc magmatism in the Kilbuck terrane, southwestern Alaska	
Elizabeth Moll-Stalcup, Joseph L. Wooden, Jack Bradshaw, and John N. Aleinikoff .....	111

GEOLOGIC FRAMEWORK—*Continued*

U-Pb zircon and titanite ages for augen gneiss from the Divide Mountain area, eastern Yukon-Tanana upland, Alaska, and evidence for the composite nature of the Fiftymile batholith Cynthia Dusel-Bacon and John N. Aleinikoff .....	131
Late Cretaceous age of the Middle Fork caldera, Eagle quadrangle, east-central Alaska Charles R. Bacon and Marvin A. Lanphere .....	143
Correlation of rock sequences across the Denali fault in south-central Alaska Béla Csejty, Jr., Chester T. Wrucke, Arthur B. Ford, Michael W. Mullen, J. Thomas Dutro, Jr., Anita G. Harris, and Phil F. Brease .....	149
Sandstone composition and provenance of the Orca Group, Chugach National Forest study area, south-central Alaska Patti J. Phillips .....	157
The pliosaurid <i>Megalneusaurus</i> : a newly recognized occurrence in the Upper Jurassic Naknek Formation of the Alaska Peninsula Robert E. Weems and Robert B. Blodgett .....	169
Geochemistry of the andesitic Admiralty Island Volcanics, an Oligocene rift-related basalt to rhyolite volcanic suite of southeastern Alaska Arthur B. Ford, Curtis A. Palmer, and David A. Brew .....	177

## BIBLIOGRAPHIES

U.S. Geological Survey reports on Alaska released in 1994 Ellen R. Reiser .....	205
Reports about Alaska in non-USGS publications released in 1994 that include USGS authors Ellen R. Reiser .....	213

## CONTRIBUTORS TO THIS BULLETIN

**Anchorage**

U.S. Geological Survey  
4200 University Drive  
Anchorage, Alaska 99508-4667

*Bradshaw, Jack (deceased)*  
*Nelson, Steven W.*  
*Phillips, Patti J.*

**Denver**

U.S. Geological Survey MS-  
Box 25046 Denver Federal Center  
Lakewood, Colorado 80225-0046

*Aleinikoff, John N., MS 963*  
*d'Angelo, William M., MS 973*  
*Goldfarb, Richard J., MS 973*  
*Gray, John E., MS 973*  
*Kelley, Karen D., MS 973*  
*O'Leary, Richard M., MS 973*  
*Meier, Allen L., MS 973*  
*Taylor, Cliff D., MS 973*  
*Theodorakos, Peter M., MS 973*

**Menlo Park**

U.S. Geological Survey MS-  
345 Middlefield Road  
Menlo Park, California 94025-3591

*Bacon, Charles R., MS 910*  
*Brew, David A., MS 904*  
*Csejtey, Béla, Jr., MS 904*  
*Dusel-Bacon, Cynthia, MS 904*  
*Fogleman, Kent A., MS 977*  
*Ford, Arthur B., MS 904*  
*Lanphere, Marvin A., MS 937*  
*Moore, Thomas E., MS 904*  
*Morin, Robert L., MS 989*  
*Mullen, Michael W., MS 904*  
*Reiser, Ellen R., MS 955*  
*Wooden, Joseph L., 937*  
*Wrucke, Chester T., MS 901*

**Reston**

U.S. Geological Survey  
National Center, MS-  
12201 Sunrise Valley Drive  
Reston, Virginia 22092

*Baedecker, Phillip A., MS 923*  
*Blodgett, Robert B., MS 970*  
*Harris, Anita G., MS 970*  
*Moll-Stalcup, Elizabeth, MS 959*  
*Palmer, Curtis A., MS 990*  
*Philpotts, John A., MS 923*  
*Weems, Robert E., MS 928*

**Others**

*Babcock, Loren E.*  
*Jacobson, Stephen R.*  
Department of Geological Sciences  
Orton Hall  
The Ohio State University  
155 S. Oval Mall  
Columbus, Ohio 43210

*Brease, Phil F.*  
Denali National Park and Preserve  
P.O. Box 9  
Denali Park, Alaska 99755

*Dutro, J. Thomas, Jr.*  
U.S. Geological Survey  
Rm E308, Museum of Natural History, MRC-137  
10th and Constitution NW  
Washington, D.C. 20560

*Fleisher, S.*  
*Trainor, T.P.*  
*Wildeman, T.R.*  
Department of Chemistry and Geochemistry  
Colorado School of Mines  
Golden, Colorado 80401

## CONTENTS

VII

*Hammond, William R.*  
*Rowe, Charlotte A.*  
Geophysical Institute  
University of Alaska  
P.O. Box 757320  
Fairbanks, Alaska 99775-0800

*Huber, C.*  
U.S. Forest Service  
Chugach National Forest  
3301 C. St., Suite 300  
Anchorage, Alaska 99503-3998

*Outwater, Carol*  
P.O. Box 222  
Dillingham, Alaska 99576



# Geologic Studies in Alaska by the U.S. Geological Survey, 1994

By Thomas E. Moore *and* Julie A. Dumoulin

## INTRODUCTION

This collection of 15 papers is the twentieth<sup>1</sup> in the annual series of U.S. Geological Survey (USGS) reports on the geology of Alaska. The series presents new or preliminary findings that are of interest to scientists in academia and industry, to land and resource managers, and to the public at large. The papers present brief topical studies on aspects of broader USGS programs that investigate the resources, hazards, and environment of Alaska. More comprehensive findings of these programs are reported elsewhere. The Geologic Studies in Alaska series brings together reports that cover a broad spectrum of earth science topics and highlights the diversity of USGS efforts in Alaska to meet the earth science needs of the Nation.

The papers in this volume are organized under three general headings that reflect the major theme areas of USGS research in Alaska: Environment and Climate, Hazards and Related Studies, and Resources. A fourth heading, Geologic Framework, consists of papers that discuss the results of basic research in the earth sciences of Alaska. The Geologic Framework papers provide scientific background information for present and future studies of the environment, paleoclimate, hazards, and energy and mineral resources of Alaska. Four articles in this volume focus on the environmental geochemistry of both undisturbed and developed mineral deposits found in northern, southwestern, or south-central Alaska (fig. 1). These papers discuss the contamination of surficial waters adjacent to mercury, gold, or sulfide deposits in the Arctic environment. Another paper reviews the magnitudes, locations of epicenters, and tectonic causes of earthquakes in Alaska during 1994 and describes the Alaska Earthquake Information Center, an earthquake monitoring organization in Fairbanks operated cooperatively by the USGS and the Geophysical Institute of the University of Alaska. Under the Resources heading, articles describe preliminary thermal maturation data from a prospective petroleum basin in southwestern Alaska and the distribution of enriched deposits of rare earth elements in southeastern Alaska. Geologic framework studies address aspects of tectonics, geochronology, isotopic geology, paleontology, sandstone petrography, and volcanology throughout Alaska. One of these papers describes a Jurassic pliosaurid marine reptile fossil found on the Alaska Peninsula, only the second such fossil reported from the Arctic region.

Two bibliographies at the end of the volume list reports about Alaska in USGS publications released in 1994 and reports about Alaska by USGS authors in non-USGS publications in 1994.

---

<sup>1</sup> From 1975 through 1988, the annual series was published as USGS Circulars; since 1988, it has been published in the more formal USGS Bulletin format. The series of reports was initially published under the title "The United States Geological Survey in Alaska: Accomplishments during 1975," but in 1986 its title was changed to "Geologic Studies in Alaska by the U.S. Geological Survey in 1985". This 1994 volume is the seventh volume in the bulletin format and the tenth volume since the change in title.



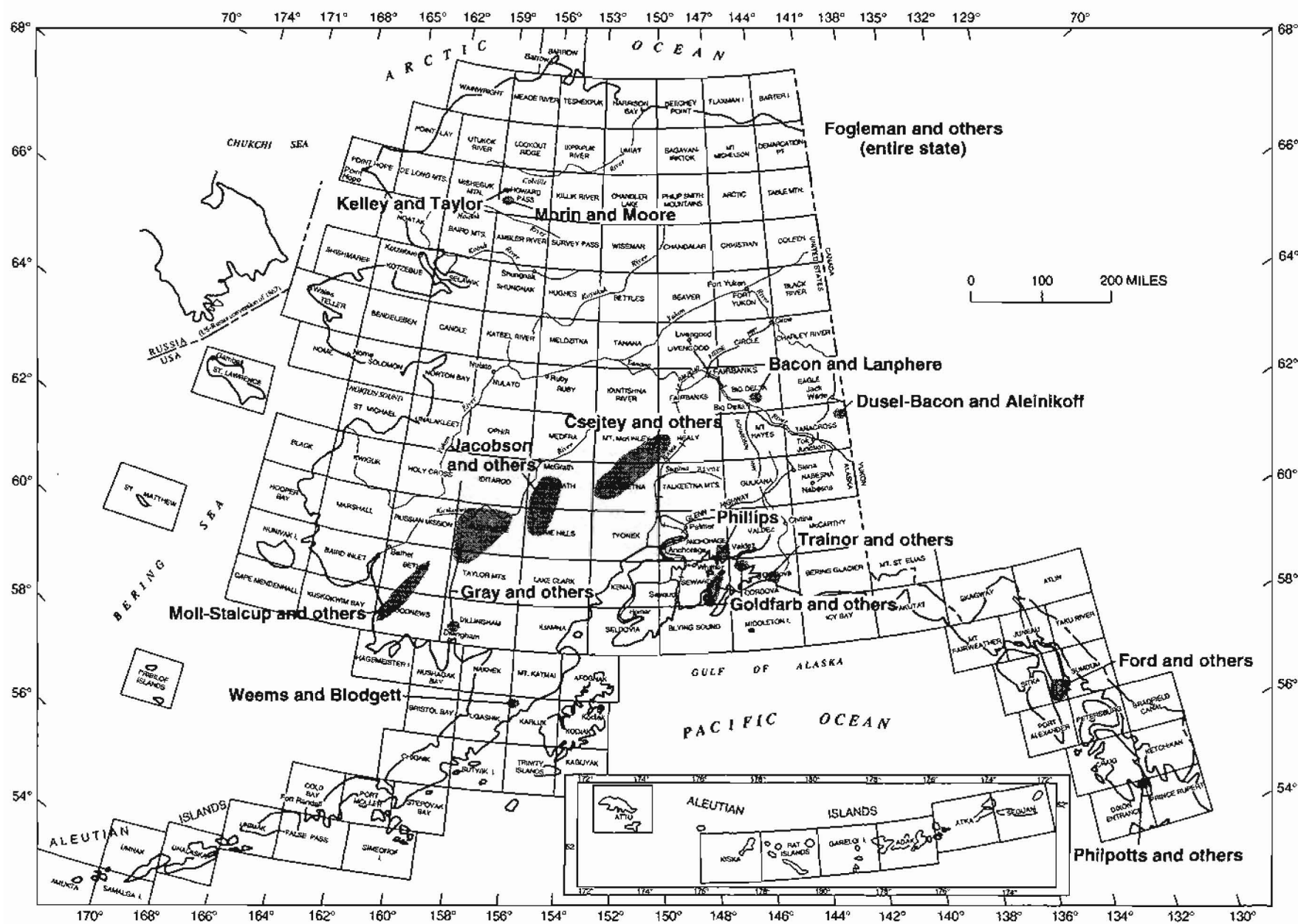


Figure 1. Index map of Alaska showing 1:250,000-scale quadrangles and locations of study areas discussed in this bulletin.

# Acid Mine Drainage Associated with Volcanogenic Massive Sulfide Deposits, Prince William Sound, Alaska

By Richard J. Goldfarb, Steven W. Nelson, Cliff D. Taylor, William M. d'Angelo, and Allen L. Meier

## ABSTRACT

Iron-copper-zinc-rich massive sulfide deposits are widespread in the metasedimentary and metavolcanic rocks of Prince William Sound. Acid drainage characterizes mine discharge that has interacted with many of the abandoned workings at the deposits. The most acidic waters are found flowing from the base of sulfide-rich tailings piles, with pH values as low as 2.6–2.7 at the Duchess and Blackbird mines on Latouche Island and 4.3 at the Rua Cove mine on Knight Island. At these acidic conditions, oxygenated mine waters contain dissolved loads of as much as 21,000 ppb Fe, 3,600 ppb Cu, 3,300 ppb Zn, 220 ppb Pb, 30 ppb Co, 150 ppb Ni, 27 ppb Cd, and 311 ppm  $\text{SO}_4^{2-}$ . Water at the surface of the 300-m-diameter flooded glory hole at the Beatson mine, the largest developed sulfide orebody in Prince William Sound, has a neutral pH and only slightly elevated metal values.

Acid mine drainage from the massive sulfide deposits could pose a local environmental hazard to wildlife. But given the relatively low discharge volumes through most workings and the high runoff in major stream channels, metal concentrations are immediately diluted to near background levels in the major streams. Discharge from the Beatson glory hole, estimated at 10 ft<sup>3</sup>/s, contained 650 ppb Fe, 380 ppb Zn, and 60 ppb Cu. These concentrations are about an order of magnitude greater than background concentrations measured above the mine workings and might be even greater during times of extensive leaching of tailings by snowmelt or heavy rains. It is uncertain whether these increased metal contents have any detrimental impact on the nearshore environment of Prince William Sound.

## INTRODUCTION

Volcanogenic massive sulfide (VMS) deposits are common in rocks of the Prince William Sound area. These Fe-Cu-Zn-rich deposits were prospected and developed in the early 1900's. Production ceased in the 1930's, and there has been no significant development work during the last 60 years. Today, abandoned workings remain on lands of

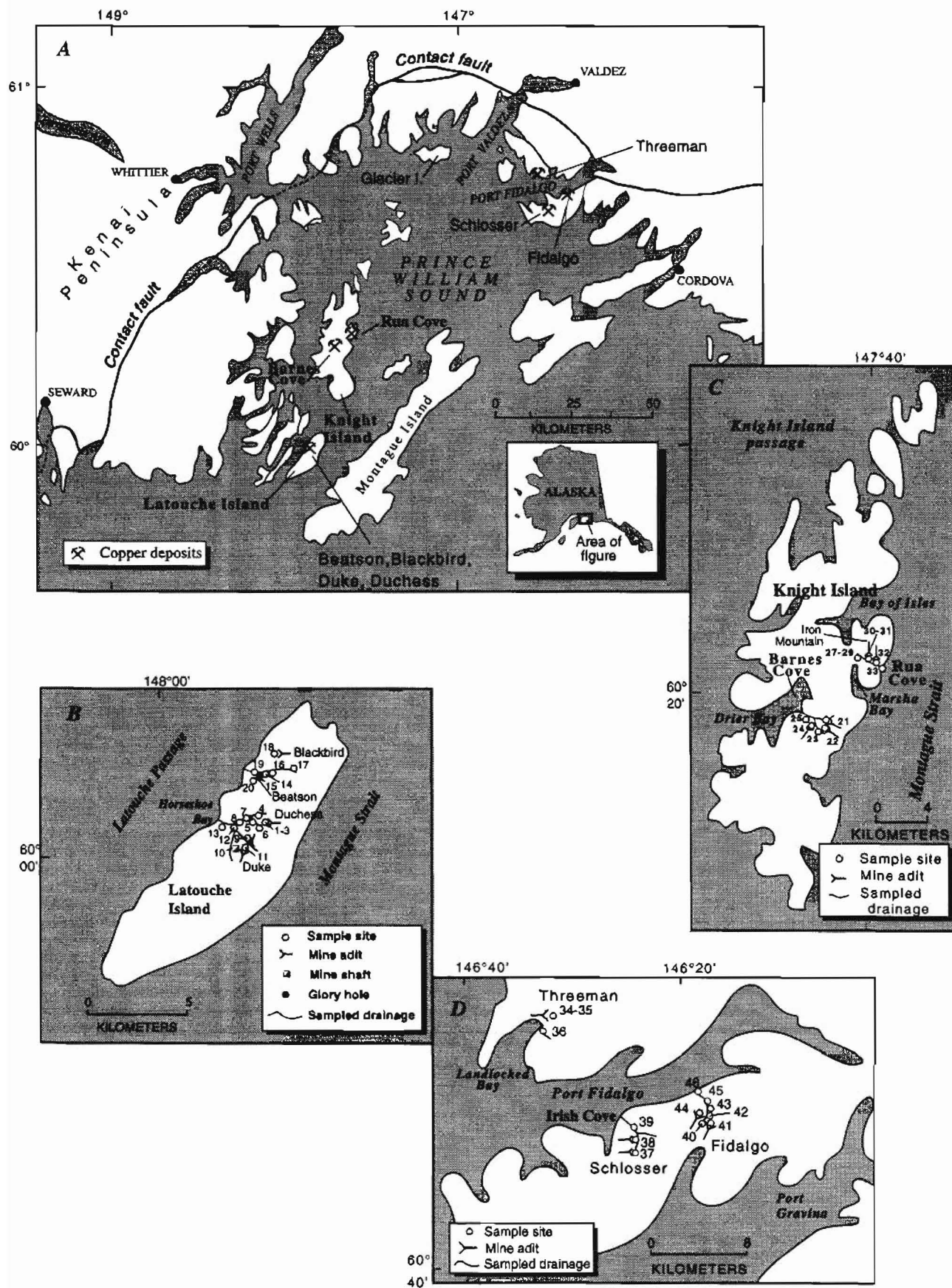
the Chugach National Forest and on private inholdings within the national forest.

The mine-waste piles, underground workings, and unmined ore zones have the potential to produce acidic and metal-rich discharge into local drainages. Such discharge, if present, could impact vegetation, aquatic life, and wildlife in Chugach National Forest and possibly impact the quality of fresh water used for human consumption on private inholdings and other developed areas. Many of the potentially impacted streams reach the shoreline of Prince William Sound after flowing short distances. Prior to our study, no detailed hydrogeochemical data existed that could be used to determine the presence and extent of acid mine drainage. During the summer of 1994, we therefore carried out an investigation to characterize stream-water chemistry in the vicinity of some of the ore deposits. Resulting data will provide land managers and regulators with valuable information needed for balanced land-use planning and for identification and prioritization of abandoned mine sites near public lands that may require cleanup.

## GEOLOGY AND DEVELOPMENT OF THE MINERAL DEPOSITS

The Prince William Sound region is underlain by Paleocene and Eocene graywacke, slate, and marine volcanic rocks of the Orca Group (Nelson and others, 1985) that compose part of an accretionary complex located seaward of the Contact fault. Volcanogenic massive sulfide deposits (fig. 1A) are hosted by both sedimentary rocks (turbidites) and volcanic units (ophiolite complexes) of the accretionary prism. The former are classified as Besshi-type deposits, whereas the latter are classified as Cyprus-type deposits. Crowe and others (1992) recently completed a detailed geologic investigation of the two deposit types in the area. The ore systems in both are dominated by a chalcopyrite-pyrite-pyrrhotite-sphalerite mineral assemblage. Ores in the Besshi-type deposits also commonly contain minor amounts of arsenopyrite and tetrahedrite. Typically, ore is present as conformable lenses of massive to semimassive sulfide that is interbedded with the volcanic or sedimentary rock hosts.

GEOLOGIC STUDIES IN ALASKA BY THE U.S. GEOLOGICAL SURVEY, 1994



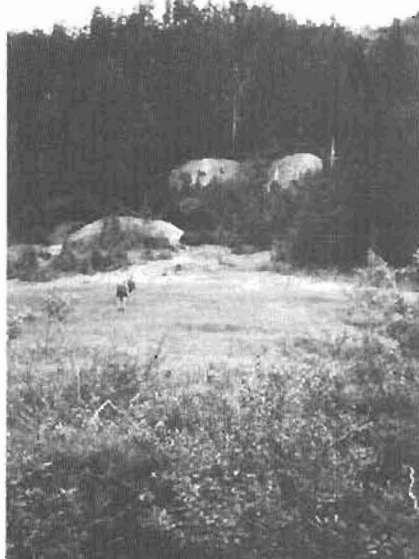
widespread disturbed zone in the study area and are dominated by a tailings pile upstream from a 300-m-diameter, flooded glory hole (fig. 2*B*). Discharge at the base of the glory hole travels through about 300 m of bedrock before flowing through piles of rusty fuel drums and other mine debris that have been consolidated into one large pile (fig. 2*C*).

Mine drainage from the Cyprus-type ores and background levels of metals in streams underlain by submarine basaltic rocks were determined from water samples collected on Knight Island (fig. 1*C*). Above Barnes Cove, we obtained water samples from a couple of small adits that contained iron- and copper-bearing sulfide minerals within

mafic dikes cutting basalt. One 2-m-wide stream, largely fed by snowmelt from the ridgetop, was sampled above the workings (site 23). Near the Rua Cove pyrite-pyrrhotite-chalcopyrite deposit, we collected samples upstream of workings, from discharge draining adits and tailings, and far downstream from all workings. Decaying 55-gallon drums leaking into the pond at site 29 may pose an organic contamination problem that was not addressed during the present study.

Both Besshi- and Cyprus-type ore deposits are exposed along Port Fidalgo (fig. 1*D*). We examined waters associated with volcanic-rock-hosted ore at the Threeman mine in Landlocked Bay, with sedimentary-rock-hosted massive

A



C



B



D



**Figure 2.** A, Iron-stained tailings piles adjacent to the Duchess mine, Latouche Island. B, Water-filled glory hole at the Beatson mine, Latouche Island. C, Drainage below the Beatson mine glory hole on Latouche Island and above its discharge into Prince William Sound. D, Mine discharge from one of the adits at the Schlosser mine along Port Fidalgo.



Sulfide layers generally range from centimeter-wide stringers to 3-m-wide lenses, although massive ore in a lens at the Beatson deposit reaches a maximum width of 90 m (Bateman, 1924). Typically, VMS orebodies are traceable for no more than a few hundred meters along strike.

Most of the VMS deposits were developed in the early 1900's on generally steep hillsides (Moffit and Fellows, 1950). The deposit workings range in size from small prospect pits with no production to small mines with underground tunnels on the order of hundreds of meters. The largest is the Beatson mine, which has a total length of more than 4 km of underground workings on five levels. Well-consolidated tailings piles, commonly 10-20 m in height, remain today adjacent to the adits and mine sites (fig. 2A). The tailings generally weather bright red owing to the oxidation of iron sulfide. Some tailings are devoid of vegetation except for bright-green to black moss that has grown around their bases, whereas other tailings support a dense growth of alder or spruce. The moss colonies are characteristic of new growth on copper-rich soils and are described in detail by Shacklette (1961). A few tailings piles on Latouche Island have recently been bulldozed into road surfaces and recreational cabin sites. Discharge both from open adits and from the bases of many of the tailings piles is generally bright red, although yellow and clear discharges are also sometimes present.

The Beatson mine was Alaska's second largest copper mine and contained the largest orebody mined in the Prince William Sound area. Unlike the other smaller VMS deposits in the study area, workings at the Beatson mine include a large glory hole that is now filled with water. Bateman (1924) indicated that the ore mined at the Beatson mine contained 12 percent by volume pyrite-pyrrhotite-chalcopyrite, and averaged 12.4 percent Fe and 2.2 percent Cu. Such grades likely are present in the remaining ore that can be observed along some of the walls of the flooded glory hole.

The volume of tailings exposed to the atmosphere is likely an important factor in controlling the amount of acid mine drainage. Tailings volumes near each deposit are directly related to the amount of production. Total copper production from the Beatson mine was  $5.43 \times 10^6$  tons, approximately two orders of magnitude greater than the combined production of the other VMS deposits in the study area. Consequently, the tailings pile at the Beatson mine is orders of magnitude larger than those near other workings. The Schlosser mine, the third largest copper mine from the Prince William Sound area, produced  $1.9 \times 10^4$  tons and created a correspondingly smaller amount of tailings. The

smallest producing mine that we studied, Knight Island Copper near Barnes Cove, produced 1 ton of ore, and the tailings are on the order of only  $10 \text{ m}^3$ .

## FIELD AND LABORATORY METHODS

Water samples were collected within, upstream, and downstream of mine workings on Latouche Island (fig. 1B), Knight Island (fig. 1C), and along Port Fidalgo (fig. 1D). All samples were collected over an exceptionally dry 8-day period in early August, 1994. No precipitation occurred during our field work, and the previous winter's snowpack was almost entirely melted. At each sample site, we measured water temperature, pH, and conductivity with standard meters and probes. We used Hach colorimetric kits in the field to determine alkalinity and dissolved oxygen. Resulting field measurements are summarized in tables 1-3. Samples for metal and anion analysis were collected in 60-mL polyethylene bottles following filtration through 0.45- $\mu$  filters. The sample collected for dissolved metals was acidified at the sites with concentrated nitric acid to a pH of less than 2.0.

Major, minor, and trace element contents of the acidified samples were determined by inductively coupled plasma-mass spectrometry (ICP-MS) (Meier and others, 1994). Concentrations for more than 60 elements were determined directly for each sample without preconcentration or dilution. Lower determination limits for most cations are at the parts per trillion level. Data for the more significant dissolved species—those likely to show greatest variation due to the impact of mining activity—are included in table 4. Concentration measurements for other elements were consistently below lower determination limits and thus are not included in the table. These include V (<0.1 ppb), As (<2 ppb), Mo (<0.1 ppb), Ag (<0.1 ppb), Sn (<0.3 ppb), Sb (<0.1 ppb), Te (<0.7 ppb), W (<0.1 ppb), Bi (<0.4 ppb), and U (<0.1 ppb). In the few cases where some of these elements are present at concentrations above the determination limits, we discuss the anomalies in the text.

Anions were determined on the filtered, unacidified waters using ion chromatography (Fishman and Pyen, 1979). Detection was by suppressed conductivity using peak height for quantification. Resulting data are listed in table 5.

## DESCRIPTION OF STUDY SITES

We collected samples near Besshi-type orebodies at the Duke, Duchess, Beatson, and Blackbird mines on Latouche Island (fig. 1B). Massive lenses of mostly pyrite, pyrrhotite, chalcopyrite, and (or) sphalerite in slate and graywacke characterize these deposits. The 300-m-long orebody at the Beatson mine consisted of massive pyrite, chalcopyrite, pyrrhotite, cubanite, and galena hosted in sedimentary rocks. The Beatson workings represent the most

**Figure 1.** A, Location map of the major volcanogenic massive sulfide deposits in rocks of the Orca Group, Prince William Sound area. B, Water sample sites on Latouche Island. C, Water sample sites on Knight Island. D, Water sample sites in the Port Fidalgo area.

by the pH of the waters themselves. At site 6, slightly acidic waters flowing through metasedimentary units are dilute calcium-bicarbonate-type waters. Major cation concentrations include 5,800 ppb Ca, 1,200 ppb Na, 380 ppb Mg, and 88 ppb K. Major anion concentrations include 2.2 ppm  $\text{Cl}^-$ , 4 ppm  $\text{SO}_4^{2-}$ , and 15 ppm  $\text{HCO}_3^-$ , the latter based on alkalinity at near-neutral pH. Metal levels in these background waters include 20 ppb Fe, 15 ppb Al, 3.5 ppb Mn, 1.4 ppb Zn, 0.3 ppb Cu, 0.2 ppb Co, <6 ppb Ni, <2 ppb As, <0.5 ppb Cr and Pb, and <0.1 ppb Mo, Ag, and Sb. The sample collected from Chisna Creek (site 36) is also a dilute calcium-bicarbonate-type water with similar concentrations of major cations and anions, despite the differing underlying volcanic lithology. A background copper level of 0.6 ppb was slightly greater than that for site 6, but lower levels of zinc (0.8 ppb) and iron (<20 ppb) were also measured. These differences are probably within analytical variation and are interpreted as insignificant.

A sample of poorly oxygenated ground water was collected in the vicinity of the Rua Cove workings (site 28). The sample was taken from a deeply emplaced, near-vertical pipe and was characterized by the most basic pH (8.77) and lowest dissolved-oxygen value (1.5 mg/L) from the study area. The relatively low Eh-high pH waters have noticeable enrichment in sulfate (22 ppm), vanadium (2.5 ppb), arsenic (3 ppb), molybdenum (1.3 ppb), and antimony (0.1 ppb). The high sulfate level indicates significant dissolution of pyrite that is likely disseminated within the volcanic rocks. We hypothesize that the extreme pH measurement is a product of adsorption of  $\text{H}^+$  by acid-consuming minerals within unexposed ultramafic rocks. Under such basic conditions, base metals will be totally sorbed (Smith and others, 1994) and the oxyanions will be more soluble.

Deep ground-water recharge, however, likely plays an insignificant role in contributing to total stream discharge in the study area. Mine workings are on steep slopes near the coastline, and most flowing water is believed to reflect primarily snowmelt infiltrating soils, with perhaps minor contributions from shallow ground water. The dissolved-oxygen data from streams and mine workings (tables 1–3) generally indicate oxygenated flow systems. Minor influx of deeper waters might be indicated by a low dissolved-oxygen measurement of 5 mg/L and anomalous antimony (0.1 ppb) and vanadium (0.1 ppb) at the Blackbird mine (site 18), and by anomalous concentrations of molybdenum (0.4–1 ppb) and vanadium (0.1–2.5 ppb) in surface waters below the Rua Cove (sites 30, 31, and 33) and Fidalgo (sites 41, 43, and 44) mine workings.

Samples of stream water above some of the mine workings provide indications of natural background concentrations in mineralized areas. These data allow for the estimation of metal content in surface waters that drain VMS occurrences that have not been disturbed by human activity. The presence of upstream, unmined mineral occurrences is readily identified through elevated iron, cop-

per, zinc, and sulfate concentrations relative to background estimates. We interpret slight enrichments in waters upstream from the Beatson mine (site 17) of 30 ppb Fe, 1.1 ppb Cu, 2.4 ppb Zn, and 5.0 ppm  $\text{SO}_4^{2-}$  as reflecting some interaction of waters with metalliferous soil and (or) rock. Similarly, concentrations of 40 ppb Fe, 3 ppb Zn, and 2 ppb Cu upstream from an adit at Barnes Cove (site 23) and 40 ppb Fe, 4.8 ppb Zn, and 1.3 ppb Cu above all workings in the Rua Cove area (site 27) are likely related to upstream sulfidized bedrock. Water flowing across sulfide-bearing bedrock above the upper adit at the Fidalgo workings contained natural background levels of 52 ppb Cu.

### ACID MINE DRAINAGE

Mine drainage is most acidic at the Duchess (site 3, pH = 2.61) and Blackbird (site 18B, pH = 2.74) mines, where the waters drain directly out of the bright-green bryophyte mats that surround the bases of the tailings. Near the Duchess mine, we examined water in a 1-m-wide shallow creek that captures the mine runoff. Water in this creek has a pH of 3.29 at a location 200 m downstream from the workings (site 4) and immediately above the confluence with a much larger, uncontaminated (pH = 6.91 at site 5) stream. The mine effluent has little detectable impact on the larger stream, as evidenced by the near-neutral pH that we recorded 200 m downstream from the junction (site 7).

Less acidic mine waters are associated with other VMS workings. Measured pH values that we interpret as partly the product of mining activity include 6.40 below a dump at the Duke mine (site 9), 6.28 in an adit at Barnes Cove (site 22), 4.31 below tailings at the lower Rua Cove adit (site 32), 5.70 within an adit at the Threeman mine (site 34), 6.10 in water flowing from an adit at the Schlosser mine (site 38), and 6.64 in an adit at the Fidalgo workings (site 41). We interpret these values as products of acid mine drainage, rather than acidic snowmelt, because of correspondingly high conductivities and (or) copper concentrations. In all cases, the pH values of waters in major drainages downstream from their confluence with the mine discharges are neutral to slightly alkaline. The amount of acid discharge from the mine workings is too limited to have a significant impact on the acidity of major streams within the humid, coastal environment.

Heavy metal solubilities are maximized where acidic conditions predominate, which in this study is generally at the bases of large tailings piles. Hence, maximum measured concentrations for most metals occur in the relatively acidic waters near the Duchess and Blackbird mines. At the Duchess mine, concentrations of as much as 12,000 ppb Fe, 760 ppb Cu, and 570 ppb Zn were recorded in waters downstream from the tailings piles (sites 2 and 3). Similarly, metal levels as high as 21,000 ppb Fe, 3,600 ppb Cu, and 3,300 ppb Zn characterized surface waters downstream from tailings at the Blackbird mine (site 18A). The

latter site also had measured values of 220 ppb Pb, 30 ppb Co, 9.6 ppb Cd, and 311 ppm  $\text{SO}_4^{2-}$ . The lead value exceeds the 15 ppb maximum contaminant level set by the Environmental Protection Agency (EPA) (National Primary Drinking Water Regulations, 40 CFR 141), and the sulfate, iron, copper, and cadmium values exceed State of Alaska maximum contaminant levels of 250 ppm, 300 ppb, 1,000 ppb, and 5 ppb (State of Alaska Drinking Water Regulations, 18 AAC 80.070), respectively. Thus, at least locally, metal levels are elevated to concentrations that could potentially be hazardous to wildlife.

Data from the Rua Cove and Duchess workings indicate that metal levels are typically one to two orders of magnitude higher below the tailings piles than they are within adits. We assume that this reflects the increased permeability and oxygenation once unconsolidated material is piled adjacent to the adits.

In the Port Fidalgo area, water in adits contained significantly greater concentrations of copper and zinc than in adits on Latouche and Knight Islands. We measured the following highly anomalous metal concentrations: 1,100 ppb Cu at the Threeman mine (site 34), 1,400 ppb Cu and 3,100 ppb Zn at the Schlosser mine (site 38), and 930 ppb Cu at the Fidalgo mine (site 41). None of these adits contained waters with more than 310 ppb Fe, and all waters associated with the Fidalgo mine workings contained less than 20 ppb Fe. Despite abundant iron sulfides in the adit wallrocks, the lack of strongly acidic pH values in waters at these workings is a limiting factor on iron mobility. Because of the relatively dry conditions during water sampling, there was no water flowing below the numerous dumps at the Schlosser and Fidalgo mines. But, given the high metal concentrations measured in waters in the adits, we hypothesize that acid mine drainage downstream from the dumps will be common during wetter periods.

Increased acidity related to acid mine drainage also mobilizes many minor and major elements. Concentrations of >3,000 ppb Al, 6,900 ppb Mg, and 250 ppb Mn were measured in acidic waters below the Duchess mine tailings. Waters below the Blackbird mine tailings carried >3,000 ppb Al, 36,000 ppb Mg, and 750 ppb Mn. Water flowing from a dump at the Duke mine workings contained 370 ppb Mn, and tailings at the Beatson mine had 390 ppb Mn.

### HYDROGEOCHEMISTRY OF THE BEATSON GLORY HOLE

The water-filled glory hole at the Beatson mine is about 500 m from the shoreline of Prince William Sound. It represents, therefore, a potential significant contaminant source to the marine environment. The water has a blue-green color, which suggests that it contains a significant amount of ferrous sulfate in solution. Discharge from the pit (fig. 2C) is largely through an old adit at its base and at a rate

that we measured to be about 10 ft<sup>3</sup>/s (site 19). If waters were relatively acidic, they would have the potential to transport significant amounts (that is, at the parts per million level) of iron, copper, and zinc into marine waters of Latouche Passage. Water in the pit had an acidic pH of 4.8 when measured by Shacklette (1961) in the summer of 1957. However, our measurements 37 years later indicate that water at the surface of the glory hole has a pH of 7.25 (site 15) and, where it discharges at the base, has pH values of 6.50–6.59 (sites 19, 20).

We suggest that some of the shift to a more neutral pH reflects a consolidation during the last few decades of the large tailings pile located above the glory hole. Recharge to the pit is mostly from a single, deeply incised channel that transects the consolidated tailings; there is little recharge through its banks, which are composed of consolidated tailings. Where this stream enters the glory hole, it has a pH of 7.10 and a conductivity of 50  $\mu\text{S}/\text{cm}$  (site 14), essentially identical to measurements along the stream above the tailings (site 17). Other possible causes of the shift to more alkaline waters in the pit could be the (1) gradual decrease of sulfide oxidation in the flooded pit and (2) flushing of the originally more acidic waters that initially filled the pit (Andy Nichol森, PTI Environmental Services, oral commun., 1994). These latter changes would have occurred during the period 30–60 years subsequent to cessation of mining.

The lack of acidic water limits the volume of potentially toxic metals that are transported downstream from the Beatson mine. Water sampled at the surface of the glory hole contains 30 ppb Fe, 21 ppb Cu, 39 ppb Zn, and 6.5 ppm  $\text{SO}_4^{2-}$ . These values are essentially identical to those determined for waters flowing through the tailings and into the pit. Levels for these parameters are approximately an order of magnitude greater for the discharge from the pit because of the slightly greater acidity at the base of the pit (sites 19, 20). This increased acidity probably results from interactions between the waters leaving the pit and tailings at the base of the pit and unmined ore along the adits that exit the pit.

## DISCUSSION

Volcanogenic massive sulfide deposits, widespread in the Prince William Sound area and elsewhere within the accreted terranes of the northern Pacific continental margin, are the ore deposit type most likely to produce metal-rich discharges. The high-sulfide contents of these ore systems and their association with non-carbonate host rocks lead to significant mobilization of trace metals. The weathering of VMS deposits can produce the most acidic, metal-rich mine drainage of any mineral deposit type (Smith and others, 1994). The severity of the acid mine drainage will be dependent on a number of factors, including sulfide

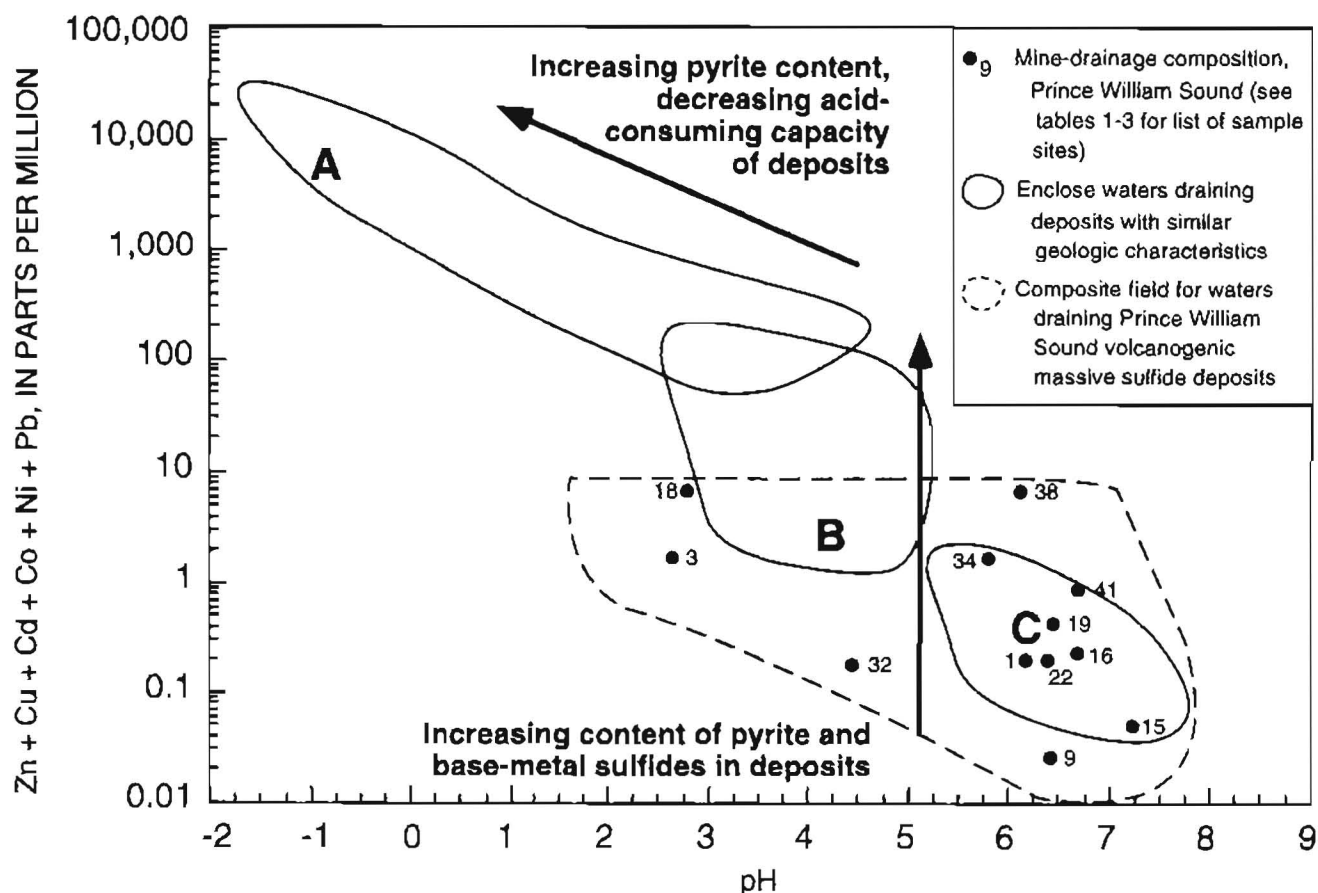
concentration, access of oxygen to the sulfides, local hydrology, and acid-neutralizing capacity of the host rocks.

Results from our investigation indicate that acid mine drainage will most likely present localized problems where surface waters percolate through tailings piles. Acidic waters ( $\text{pH} < 4.5$ ) leaching mine wastes near the Duchess and Blackbird mines have total base-metal contents ( $\text{Zn} + \text{Cu} + \text{Cd} + \text{Co} + \text{Ni} + \text{Pb}$ ) of between about 1 to 7 ppm (fig. 3) and Fe concentrations of as much as 21 ppm. Under these low-pH conditions, all of the heavy metals are relatively mobile and adsorption on iron-rich suspended material is not significant (Smith and others, 1992). Dissolved concentrations of these metals will be much lower in the more neutral waters in the study area because of adsorption. For example, hydrous iron oxides will sorb most copper in solution at pH values of  $\geq 4.5$  and most zinc at pH values of  $\geq 5.7$  (Smith and others, 1994).

Both the sedimentary and volcanic host rocks have buffering capacities intermediate between the low buffering capacity of granite and the high buffering capacities of

carbonate rocks. Generally, slightly calcareous mafic volcanic rocks, such as at Rua Cove, will have a higher buffering capacity than metasedimentary rock units (Glass and others, 1982). The sandstones of the Orca Group are dominated by plagioclase, quartz, K-feldspar, and lithic fragments, with calcite being only locally present in the matrix of some samples (Dumoulin, 1987). These differences might explain the more acidic and subsequently much more metal-rich waters draining the Duchess and Blackbird mine tailings relative to the waters draining the Rua Cove mine tailings.

We were surprised by the relatively less contaminated waters in the stream cutting through the enormous Beatson mine-tailings pile. The surface discharge, prior to emptying into the glory hole, has a neutral pH. As stated earlier, we believe this reflects a very low percentage of the flow percolating through the tailings themselves. The streambed itself was observed to be extremely clay-rich and impermeable where it meanders for about 100 m through the tailings, perhaps hindering significant interaction between water



**Figure 3.** Ficklin diagram plotting pH versus dissolved base metal content of mine-drainage waters. Fields A, B, and C, from Plumlee and others (1994), define fields for the West Shasta district VMS deposits, sulfide-rich vein deposits in rocks with low-buffering capacity, and sulfide-rich vein deposits in carbonate host rocks, respectively. Data from this study, with site numbers as listed in tables 1-3, indicate that volcanogenic massive sulfide mine waters in the humid Prince William Sound area are significantly less acidic and less metal rich than those in the more arid West Shasta district.



and sulfidized rocks. Along this length, concentrations of iron increase from 30 to 40 ppb, zinc from 2.4 to 40 ppb, and copper from 1.1 to 28 ppb, with all concentrations still one to three orders of magnitude lower than those in the waters draining the Duchess and Blackbird mine tailings. A small seep out of the Beatson mine tailings (site 16) contained 4,500 ppb Fe, but because copper and zinc concentrations were not similarly enriched and pH was near neutral, we believe water-rock interaction was relatively localized.

To obtain a better estimate of the leachability characteristics of the Beatson mine-tailings pile, we performed a synthetic precipitation leaching procedure (EPA method 1312) on a composite grab sample of the tailings. We used an extractant with pH of 5.0, approximately that of local snowmelt and rain water (Brabets, 1987), and a water:rock ratio of 20:1. The extract had a pH of 4.22 and concentrations of 36,000 ppb Fe, 1,400 ppb Cu, 37 ppb Zn, 420 ppb Pb, 2.6 ppb Co, 1 ppb Ni, and <3 ppb Cd as determined by ICP-MS. These data suggest that significantly more contaminated waters will be produced if a high degree of percolation through the Beatson mine tailings occurs. Whether or not such leaching activity leads to intermittent periods of acid mine drainage can only be determined by examining the Beatson workings during times of late spring snowmelt or heavy rainfall.

Values for pH of waters within most adits are between about 6 and 7 and appear to reflect precipitation in some cases (for example, sites 22, 24, 30, and 44) and water-rock interaction in others (sites 1, 34, 37, 38, and 41) based on interpretation of conductivity measurements. Total base-metal concentrations in excess of 1 ppm within adits from all three mine areas along Port Fidalgo (fig. 3) might reflect more permeable strata in this area relative to Knight and Latouche Islands. These data suggest that despite near-neutral pH values, copper and zinc remain relatively mobile in some waters that have interacted with unmined ore zones. The relatively low iron contents of these same waters (<20 to 310 ppb) indicate significant oxy-hydroxide precipitation without significant copper and zinc adsorption.

Hydrogeochemical data for mine drainage from the study area are similar to those from other VMS orebodies along the western Cordillera. Kilburn and others (1994) examined acid mine drainage near the Holden mine in mafic volcanic rocks of the eastern Cascades. They measured waters within adits with pH values of about 5 and metal concentrations of 370–580 ppb Fe, 570–580 ppb Cu, and almost 5,000 ppb Zn. Discharge from adjacent tailings contained 23,000–50,000 ppb Fe, 21–53 ppb Cu, and 130–3,800 ppb Zn at pH values of 2.8–2.9. The reason for the relatively low copper content of this latter drainage is uncertain.

Climate clearly plays a major role in defining the severity of acid mine drainage. In contrast to discharge from

VMS deposits in the relatively humid marine ecoregions of Prince William Sound and the Cascades, discharge below VMS deposits in more arid environments (for example, field A of fig. 3) may be even more toxic. Filipek and others (1987) and Alpers and Nordstrom (1991) examined drainage associated with Fe-Cu-Zn-rich VMS deposits in the West Shasta district of northern California within a less humid, chaparral forest and shrub province ecosystem. Extensive evaporation of waters and elevated air temperatures in the workings led to the formation of dripping mine waters with negative pH values. These acidic waters contained as much as 11 percent Fe, 2.3 percent Zn, and 0.5 percent Cu (Alpers and Nordstrom, 1991). Drainage discharging from the adits and tailings was characterized by pH values of as low as 2.35 and by metal values as high as 1,600 ppm Fe, 190 ppm Cu, and 156 ppm Zn (Filipek and others, 1987). These metal concentrations are approximately two orders of magnitude greater than the extreme values measured in our study and indicate that a more limited acid mine drainage problem exists in the cooler, wetter climate of Prince William Sound.

## CONCLUSIONS

Acid mine waters are prevalent in discharges below mine workings in the Prince William Sound area. Metal values in waters are only slightly elevated where VMS deposits are undeveloped. However, the waters become enriched in metals once the sulfide minerals are exposed and more easily oxidized, especially in relatively permeable tailings piles. The pH values of waters may locally decrease below 3.0, and total base-metal concentrations at the parts per million level may be present. In the Pacific coastal mountains, however, such acid drainage appears to be rapidly diluted to near-background levels within a few hundreds of meters of most workings.

This report describes only a first attempt to assess the acid discharge of mine waters in the Prince William Sound area. The impacts of seasonal variation have not been addressed and could be significant. Alpers and others (1994) identified seasonal variations in copper and zinc contents of waters draining VMS deposits in northern California. Our study was carried out during August, subsequent to the major snowmelt and during a relatively dry weather period in the summer of 1994. We expect that metal dispersion during the annual spring flushing by snowmelt could be significant. Also, other periods of high precipitation might release increased amounts of metals from exposed tailings. Our leaching test on the tailings pile at the Beatson mine indicates that it has the potential to yield significant dissolved metals during water-rock interaction.

The acid discharge below the VMS deposits represents a possible local hazard to wildlife and aquatic organisms. Without more data, however, it is uncertain as to whether

any of these abandoned mine lands pose a threat to Prince William Sound itself. Loring and Asmund (1989) noted that sulfide-rich mine tailings released into a fjord in Greenland led to base-metal enrichments in seaweed and mussels. Significant discharge volumes enter Prince William Sound within a few hundred meters of their exit from the bottom of the Beatson mine glory hole (fig. 2C). Our data indicate at least a two-orders-of-magnitude increase in zinc levels for these waters relative to those above the workings. It is uncertain if these levels increase with leaching of the upstream tailings during periods of increased runoff. If they do, analysis of near-shore waters and shellfish communities for anomalous metal concentrations may be warranted.

**Acknowledgments.**—This work was partly funded by the Office of Mineral Resources Center for Environmental Geochemistry and Geophysics. We thank the Chenega Corporation, Chugach Alaska Native Corporation, and Tahtlik Corporation for access to mine workings on their lands. Field sampling was aided by Barrett Cieutat, John McHugh, and Robert (Rollo) Eppinger. McHugh also performed the leaching test on the tailings sample from the Beatson mine, and Cieutat aided in berry picking. Captain Gary McWilliams of the research vessel *Hyak* made sure to navigate us to where we needed to go, and Kerry's efforts with the tasty meals and berry pies were greatly appreciated.

## REFERENCES CITED

- Alpers, C.N., and Nordstrom, D.K., 1991, Geochemical evolution of extremely acid mine waters at Iron Mountain, California—are there any lower limits to pH?, in Second International Conference on the Abatement of Acidic Drainage, Proceedings: MEND (Mine Environment Neutral Drainage), Ottawa, Canada, v. 2, p. 321–342.
- Alpers, C.N., Nordstrom, D.K., and Thompson, J.M., 1994, Seasonal variations of Zn/Cu ratios in acid mine waters from Iron Mountain, California, in Alpers, C.N., and Blowes, D.W., eds., *Environmental geochemistry of sulfide oxidation*, ACS Symposium Series 550: Washington, D.C., American Chemical Society, p. 324–344.
- Bateman, A.M., 1924, Geology of the Beatson copper mine, Alaska: *Economic Geology*, v. 19, p. 338–368.
- Brabets, T.P., 1987, Quantity and quality of urban runoff from the Chester Creek basin, Anchorage, Alaska: U.S. Geological Survey Water-Resources Investigations Report 86–4312, 58 p.
- Crowe, D.E., Nelson, S.W., Brown, P.E., Shanks, W.C., III, and Valley, J.W., 1992, Geology and geochemistry of volcanogenic massive sulfide deposits and related igneous rocks, Prince William Sound, south-central Alaska: *Economic Geology*, v. 87, p. 1722–1746.
- Dumoulin, J.A., 1987, Sandstone composition of the Valdez and Orca Groups, Prince William Sound, Alaska: U.S. Geological Survey Bulletin 1774, 37 p.
- Filipek, L.H., Nordstrom, D.K., and Ficklin, W.H., 1987, Interaction of acid mine drainage with waters and sediments of West Squaw Creek in the West Shasta mining district, California: *Environmental Science and Technology*, v. 21, no. 4, p. 388–396.
- Fishman, M.J., and Pyen, Grace, 1979, Determination of selected anions in water by ion chromatography: U.S. Geological Survey Water-Resources Investigations 79–101, 30 p.
- Glass, N.R., Arnold, D.E., Galloway, J.N., Henry, G.R., Lee, J.J., McFee, N.W., Norton, S.A., Powers, C.F., Rambo, D.L., and Schofield, C.L., 1982, Effects of acid precipitation: *Environmental Science and Technology*, v. 16, p. 162A–169A.
- Kilburn, J.T., Whitney, G.C., d'Angelo, W.M., Fey, D.L., Hopkins, R.T., Meier, A.L., Motooka, J.M., Roushey, B.H., and Sutley, S.J., 1994, Geochemical data and sample locality maps for stream sediment, heavy-mineral concentrate, mill tailing, water, and precipitate samples collected in and around the Holden mine, Chelan County, Washington: U.S. Geological Survey Open-File Report 94–680A, 33 p.
- Loring, D.H., and Asmund, G., 1989, Heavy metal contamination of a Greenland fjord system by mine wastes: *Environmental Geology and Water Sciences*, v. 14, no. 1, p. 61–71.
- Meier, A.L., Grimes, D.J., and Ficklin, W.H., 1994, Inductively coupled plasma mass spectrometry—a powerful analytical tool for mineral resource and environmental studies [abs.], in Carter, L.M.H., Toth, M.J., and Day, W.C., eds., *USGS research on mineral resources—1994, Part A—Program and Abstracts*, V.E. McKelvey Forum on Mineral and Energy Resources, 9th, Tucson, Ariz., February 22–25, 1993: U.S. Geological Survey Circular 1103-A, p. 67–68.
- Moffit, F.H., and Fellows, R.E., 1950, Copper deposits of the Prince William Sound district, Alaska: U.S. Geological Survey Bulletin 963-B, p. 47–80.
- Nelson, S.W., Dumoulin, J.A., and Miller, M.F., 1985, Geologic map of the Chugach National Forest, Alaska: U.S. Geological Survey Miscellaneous Field Studies Map MF-1645-B, 16 p., 1 sheet, scale 1:250,000.
- Plumlee, G.S., Smith, K.S., and Ficklin, W.H., 1994, Geoenvironmental models of mineral deposits, and geology-based mineral-environmental assessments of public lands: U.S. Geological Survey Open-File Report 94–203, 7 p.
- Shacklette, H.T., 1961, Substrate relationships of some bryophyte communities on Latouche Island, Alaska: *The Bryologist*, v. 64, no. 1, p. 1–16.
- Smith, K.S., Ficklin, W.H., Plumlee, G.S., and Meier, A.L., 1992, Metal and arsenic partitioning between water and suspended sediment at mine-drainage sites in diverse geologic settings, in Kharaka, Y.K., and Maest, A.S., eds., *Water-rock interaction: Seventh International Symposium on Water-Rock Interaction*, Park City, Utah, July 13–18, 1992, Proceedings: Rotterdam, A.A. Balkema, v. 1, p. 443–447.
- Smith, K.S., Plumlee, G.S., and Ficklin, W.H., 1994, Predicting water contamination from metal mines and mining wastes: U.S. Geological Survey Open-File Report 94–264, 112 p.

Reviewers: Lori Filipek and Karen Kelley

# Environmental Geochemistry of Mercury Deposits in Southwestern Alaska: Mercury Contents in Fish, Stream-Sediment, and Stream-Water Samples

By John E. Gray, Allen L. Meier, Richard M. O'Leary, Carol Outwater, and Peter M. Theodorakos

## ABSTRACT

Mercury is a heavy metal that can be toxic to humans when concentrations are high, especially in food sources. Mercury-rich lodes and abandoned mines scattered throughout southwestern Alaska represent a potential environmental hazard in the region. Concentrations of mercury were measured in fish, stream-sediment, and stream-water samples collected downstream from the mines and lodes to evaluate environmental mercury accumulation. Mercury concentrations in fish are useful for addressing the levels of mercury in the food chain that can eventually affect humans.

Freshwater fish collected downstream from the mercury lodes generally contain the highest mercury concentrations. Dolly Varden collected downstream from the Cinnabar Creek mine contain as much as 0.62 ppm Hg wet weight in muscle samples (edible fillets), but mercury concentrations are also elevated in Arctic grayling collected downstream from the Mountain Top mine (as much as 0.26 ppm in muscle samples) and at a site on the Kolmakof River (as much as 0.42 ppm Hg in muscle samples). The site studied on the Kolmakof River is downstream from mercury anomalies that suggest a possible undiscovered mercury lode. Arctic grayling and Dolly Varden, collected from background sites in southwestern Alaska, contain as much as 0.20 ppm Hg wet weight in muscle samples. Chum salmon collected from large rivers in southwestern Alaska contain the lowest mercury concentrations in muscle samples collected in the study, ranging up to 0.08 ppm Hg wet weight. The salmon results are important because these fish are a major food source to residents, and the low mercury concentrations suggest that mercury from the mines and deposits has not adversely affected the salmon. All mercury concentrations in fish collected in this study are below the 1 ppm wet weight concentration for edible fish established by the Food and Drug Administration (FDA) as the action level when mercury advisories are listed and sale of fish is restricted. In addition, all concentrations of mer-

cury in stream-water samples collected in the study are below the 2-ppb drinking-water maximum-contaminant level recommended by the State of Alaska.

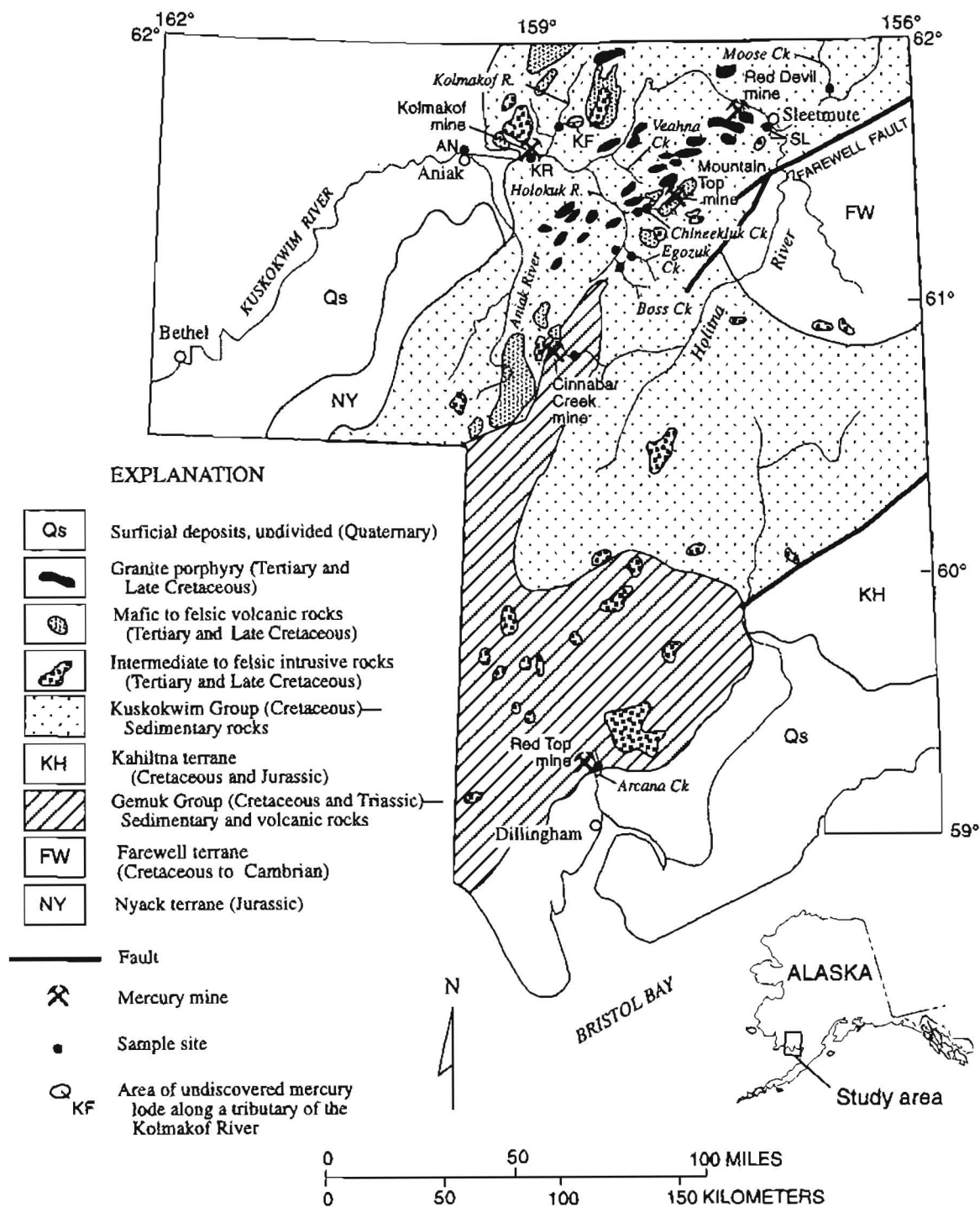
## INTRODUCTION

Mercury is a heavy metal of environmental concern because elevated concentrations can be toxic to living organisms. Mercury has no known metabolic purpose, and contaminations are regarded as undesirable and potentially hazardous (National Academy of Sciences, 1978). Present and past mercury uses include manufacture of electrical instruments, pharmaceuticals, plastics, agricultural fungicides, paper production, munitions, and in the extraction of gold (amalgamation) in mining. Most mercury toxicity problems are related to organic mercury compounds (Eisler, 1987), of which methylmercury is the most toxic to humans (Friberg and Vostal, 1972). Conversion of inorganic forms of mercury (for example, cinnabar) to methylmercury is mostly by the action of aerobic and anaerobic bacteria in organic-rich muds in streams and lakes (Wood, 1974; Gough and others, 1979). Methylmercury is volatile, water soluble, and concentrates in tissues (bioaccumulation) of fish and other aquatic organisms (Fenchel and Blackburn, 1979). Once mercury is converted to water-soluble forms, like methylmercury, it becomes readily available to biota (bioavailable), such as fish. Mercury can increase in concentration with increasing trophic position in the food chain (biomagnification). Concentration of mercury in fish provides an easy pathway for mercury to enter the food chain. The toxic nature of mercury has stimulated abundant environmental research (for example, Lindqvist, 1991).

Mercury lodes are scattered over a wide region covering several thousand square kilometers in southwestern Alaska (fig. 1). Several of the lodes were mined between the early 1900's and the 1980's, but they are not currently operating because of low prices and low demand for mercury. Approximately 41,000 flasks of mercury (1

flask=76 lb or 34.5 kg) have been produced from the region (Bundtzen and others, 1986). The presence of mercury lodes and abandoned mines in southwestern Alaska is

a potential hazard to residents and wildlife populations because drainage from the lodes and mines enters streams and rivers that are part of local ecosystems.



**Figure 1.** Location map of study area. Samples sites along the Kuskokwim River are AN (near Aniak), KR (near Kolmakof), and SL (near Sleetmute). Geology generalized from Cady and others (1955), Hoare and Coonrad (1959), Miller and others (1989), and Miller and Bundtzen (1994).



Environmental studies are an important part of the U.S. Geological Survey's (USGS) mineral resource assessment program. This study is part of continuing environmental investigations of mercury-rich mineral deposits in southwestern Alaska. Environmental studies of the southwestern Alaska mercury mines and deposits were recently initiated by the USGS (Gray and others, 1994); other studies conducted by the U.S. Fish and Wildlife Service provide baseline data for mercury in fish (Crayton, 1990; Snyder-Conn and others, 1992). Gray and others (1994) reported that fish (Arctic grayling), stream-sediment, and stream-water samples collected downstream from the Cinnabar Creek mine contained mercury concentrations elevated above those collected from a control site. However, Gray and others (1994) noted that the fish collected from Cinnabar Creek were unusually small, and any larger, predatory fish in Cinnabar Creek could potentially contain higher mercury concentrations. This is because mercury concentrations generally increase in larger predatory fish as a result of biomagnification (Eisler, 1987). Thus, fish higher in the food chain also need to be evaluated. Cinnabar Creek was the only southwest Alaska mercury deposit evaluated by Gray and others (1994), but widespread mercury lodes and mines in the region suggest that environmental aspects of other lodes must be evaluated in relation to well-constrained regional backgrounds (sites where no mercury lodes are known upstream). In addition, mercury concentrations in salmon and pike need to be evaluated because these fish are a common food source and the presence of mercury lodes throughout southwestern Alaska suggests that mercury might be elevated in these fish. Thus, the objectives of this study are to measure mercury concentrations in samples of fish, stream-sediment, and stream-water collected (1) downstream from several mines and lodes and (2) from several sites where no mercury lodes are known in order to thoroughly evaluate regional geochemical backgrounds. Mercury concentrations were also measured in salmon and pike to determine if these food sources contain elevated mercury. These data were then used to evaluate mercury hazards of the mercury mines and lodes in southwestern Alaska. Other heavy metals such as As, Cd, Pb, Cu, Sb, and Zn were also measured in the samples because these metals can also be of environmental concern. Sites were studied downstream from the Cinnabar Creek, Mountain Top, and Red Top mines, as well as a locality on the Kolmakof River downstream from a probable undiscovered mercury occurrence (fig. 1). These localities were chosen for study because streams draining the mines and lodes were large enough to support fish habitat. Samples were collected from background sites on Boss Creek, Egozok Creek, Holokuk River, Moose Creek, and Veahna Creek (fig. 1). Salmon were collected from two sites along the Kuskokwim River (one at Aniak and one adjacent to the Kolmakof mine) and from the background site on the

Holokuk River. Northern pike were collected from a site on the Kuskokwim River near Sleetmute.

## GEOLOGY

Rocks in the study area primarily consist of sedimentary and volcanic rocks of the Triassic and Cretaceous Gemuk Group and the Cretaceous Kuskokwim Group. The Gemuk Group consists of massive siltstone interbedded with lesser amounts of chert, volcanic rocks, graywacke, and limestone (Cady and others, 1955). The Gemuk Group is interpreted to comprise part of a volcanic-arc complex (Box, 1985). Rocks of the Kuskokwim Group consist of thick sequences of intercalated sandstone and shale, with minor conglomerate and volcanic rocks (Cady and others, 1955; Miller and Bundtzen, 1994). The Kuskokwim Group consists primarily of deep-water turbidites and lesser shallow-shoreline-facies rocks (Miller and Bundtzen, 1994). Rocks of the Gemuk and Kuskokwim Groups are locally cut or overlain by Late Cretaceous and Tertiary intrusions and volcanic rocks. Mercury lodes in southwestern Alaska show a close spatial association to the Late Cretaceous and early Tertiary intrusions (Cady and others, 1955). The mercury lodes generally consist of small, discontinuous veins that rarely exceed a few meters in width and a few tens of meters in strike length. Mercury ores are geochemically simple, commonly containing over one percent each of Hg, Sb, and As, but are generally poor in base and precious metals. Most of the mercury lodes were located by tracing occurrences of placer cinnabar upstream to sources (Webber and others, 1947; Sainsbury and MacKevett, 1965). The lodes developed into mines were typically worked by a few individuals that operated small, on-site retorts.

At the Cinnabar Creek mine, sedimentary rocks of the Gemuk Group are cut locally by Late Cretaceous and Tertiary mafic dikes (Sainsbury and MacKevett, 1965). Mercury ores there are high grade and consist of massive replacements, disseminations, and vug fillings of cinnabar in quartz-carbonate veins that cut siltstone, graywacke, and an altered dike. At Cinnabar Creek, native mercury and lesser stibnite and pyrite are also found (Sainsbury and MacKevett, 1965). Native mercury is common in sheared and brecciated sedimentary rocks. The mine is located near the headwaters of Cinnabar Creek and consists of a small open-pit about 50 m long, 15 m wide, and 10 m deep. Ore averaging about 3 to 4 percent mercury was retorted on site, and several hundred flasks of mercury were recovered (Sainsbury and MacKevett, 1965). Veins containing cinnabar and native mercury in the open pit, and small ore piles at the mine site are sources of mercury that have eroded into Cinnabar Creek. Particulate (detrital) cinnabar grains and occasional beads of native mercury have been observed in stream-sediment samples collected from Cinnabar Creek (Gray and others, 1991).

The Red Top deposit is also underlain by sedimentary rocks of the Gemuk Group; a diabase dike of Late Cretaceous or early Tertiary age cuts the sedimentary rocks near the mine (Sainsbury and MacKevett, 1965). Cinnabar is found in quartz-carbonate veins and vein breccias that cut the sedimentary rocks. Mineralized veins and breccias are generally a few centimeters wide with maximum lengths of about 50 m. Ore was removed from underground workings and trenches totaling a few hundred meters in length. Ore containing greater than 2 percent mercury was reported from the mine (Webber and others, 1947), but only minor cinnabar is present in small ore piles near adit portals. Cinnabar retorted on site produced about 60 flasks of mercury (Sainsbury and MacKevett, 1965).

Rocks at the Mountain Top mine consist of sandstone and shale of the Kuskokwim Group that are cut locally by small Late Cretaceous and Tertiary mafic dikes (Sorg and Estlund, 1972). Vuggy, quartz-carbonate veins containing cinnabar are found in faulted and brecciated dikes that cut sedimentary rocks of the Kuskokwim Group. There are about 15 trenches that total roughly 500 m in length at Mountain Top; small ore piles with visible cinnabar are present near the trenches. Ore containing 1 to 2 percent mercury was reported from Mountain Top (Sorg and Estlund, 1972). About 165 flasks of mercury were recovered from this locality (Miller and others, 1989). Ore was presumably processed in a small retort found at the mine.

Rocks along the Kolmakof River site studied also consist of sandstone and shale of the Kuskokwim Group that are cut locally by small Late Cretaceous and Tertiary dikes (Cady and others, 1955). This site was selected for study because stream-sediment samples collected from an upstream tributary contain as much as 5.6 ppm Hg, and associated heavy-mineral-concentrate samples contain as much as 50 percent cinnabar (Gray and others, 1993). These results indicate the possible presence of undiscovered cinnabar lodes upstream, although none have been identified yet in this drainage basin.

Basins selected for background study on Boss Creek, Egozuk Creek, Holokuk River, Moose Creek, and Veahna Creek are underlain by sandstone and shale of the Kuskokwim Group that are cut locally by small Late Cretaceous and Tertiary intrusions (Cady and others, 1955; Miller and others, 1989). No cinnabar-bearing lodes or significant geochemical anomalies are known in these drainage basins.

## METHODS

### SAMPLE COLLECTION

Samples collected for study were primarily fish, but stream-sediment and stream-water samples were also col-

lected from most sites. All samples were collected from the active stream channel. Most fish were collected with spinning rods equipped with artificial lures, but those collected downstream from the Red Top mine were captured in gill net traps. Several fish (usually 5-10) were generally collected from a single site on a given stream or river; however, fish were collected from two sites on Chineekluk Creek downstream from the Mountain Top mine. The most commonly observed fish at the sites studied was Arctic grayling (*Thymallus arcticus*), and thus grayling represent the majority of the fish sampled. However, Dolly Varden (*Salvelinus malma*) were collected from some streams when grayling were rare or not present. Both Arctic grayling and Dolly Varden are freshwater fish that are common foods of residents and sportsmen in southwestern Alaska, and therefore they were appropriate to evaluate mercury contents in fish that are commonly consumed. Chum salmon (*Oncorhynchus keta*), coho salmon (*Oncorhynchus kisutch*), and northern pike (*Esox lucius*) are also common foods; these are migratory fish that were collected from large rivers in the study area to evaluate regional mercury hazards. Sculpin (*Scorpaena guttata*) were collected downstream from the Red Top mine to evaluate mercury concentrations in a bottom-feeding fish. Collected fish were dissected and muscle (edible fillets) and liver samples were saved for analysis. Muscle samples were analyzed for mercury because they are a common food source in the region. Livers generally concentrate heavy metals, and thus concentrations of mercury in livers help identify trends in the data. Sculpin collected were too small for dissection and were analyzed whole.

Stream-sediment samples were collected from stream-channel detritus for measurement of trace-metal concentrations. Collected stream-water samples included (1) an unfiltered sample collected in a glass bottle, acidified with nitric acid and potassium dichromate, for total mercury concentration; (2) a sample filtered through a 0.45- $\mu$ m membrane into a glass bottle, acidified with nitric acid and potassium dichromate, for dissolved mercury concentration; (3) an unfiltered sample collected in a polypropylene bottle, acidified with nitric acid, for other total trace-metal concentrations; and (4) a sample filtered through a 0.45- $\mu$ m membrane into a polypropylene bottle, acidified with nitric acid, for other dissolved trace-metal concentrations.

Stream-water pH, conductivity, alkalinity, and turbidity were also measured at the sites studied, but there was little variation in these measurements. The pH of the stream waters are neutral to slightly alkaline and varied between 7.1 and 8.4. These results are consistent with the mineralogy of the mercury deposits since cinnabar has an extremely low solubility in water (Hem, 1970) and does not readily form acid drainage because of its chemical and physical resistance during weathering. Thus, acid mine drainage downstream from abandoned mercury mines is probably not of environmental concern.

**Table 1.** Data for Arctic grayling (gyl) and Dolly Varden (doly) collected from background sites on Boss Creek (BS), Egozok Creek (EZ), Holokuk River (HK), Moose Creek (MC), and Veahna Creek (VH)

[Analysis of Hg by cold-vapor atomic absorption spectrophotometry (CVAAS); Sb, As, Ag, Bi, Cd, Cu, Mo, Pb, and Zn by inductively coupled plasma-mass spectrometry (ICP-MS); fish weights are whole body measured on site; concentrations are in parts per million wet weight; n.d., not determined]

Sample	Tissue	Fish weight (g)	Hg ppm	Sb ppm	As ppm	Ag ppm	Bi ppm	Cd ppm	Cu ppm	Mo ppm	Pb ppm	Zn ppm
BS1gylM	muscle	260	0.14	<0.4	<0.4	<0.4	<0.7	<0.5	0.6	<0.4	<0.4	10
BS2gylM	muscle	255	.12	<.4	<.4	<.4	<.7	<.5	.6	<.4	<.4	9
BS3gylM	muscle	300	.14	<.4	<.4	<.4	<.7	<.5	.6	<.4	<.4	8
BS4gylM	muscle	325	.20	<.4	<.4	<.4	<.7	<.5	.6	<.4	<.4	8
BS5gylM	muscle	405	.17	<.4	<.4	<.4	<.7	<.5	.7	<.4	<.4	8
BS1gylL	liver	260	.19	<.4	<.4	<.4	<.7	<.5	2	<.4	<.4	21
BS2gylL	liver	255	.18	<.4	<.4	<.4	<.7	<.5	2	<.4	<.4	16
BS3gylL	liver	300	.20	<.4	<.4	<.4	<.7	<.5	2	<.4	<.4	20
BS4gylL	liver	325	.27	<.4	<.4	<.4	<.7	<.5	2	<.4	<.4	19
BS5gylL	liver	405	.18	<.4	<.4	<.4	<.7	<.5	2	<.4	<.4	12
EZ1gylM	muscle	500	.12	.01	.1	<.1	<.1	<.01	.4	<.01	.02	7
EZ2gylM	muscle	245	.08	<.01	<.1	<.1	<.1	<.01	.3	<.01	<.01	5
EZ3gylM	muscle	240	.09	<.01	.1	<.1	<.1	<.01	.5	<.01	<.01	5
EZ4gylM	muscle	190	.10	<.01	<.1	<.1	<.1	<.01	.3	<.01	<.01	6
EZ5gylM	muscle	520	.14	<.01	<.1	<.1	<.1	.01	.5	<.01	<.01	5
EZ6gylM	muscle	530	.13	<.01	.1	<.1	<.1	.01	.7	<.01	<.01	6
EZ1gylL	liver	500	.24	<.4	<.4	<.4	<.7	<.5	2	<.4	<.5	22
EZ2gylL	liver	245	.15	<.4	<.4	<.4	<.7	<.5	2	<.4	<.5	21
EZ3gylL	liver	240	.11	<.4	<.4	<.4	<.7	<.5	2	<.4	<.5	20
EZ4gylL	liver	190	.13	<.4	<.4	<.4	<.7	<.5	2	<.4	<.5	21
EZ5gylL	liver	520	.19	<.4	<.4	<.4	<.7	<.5	2	<.4	<.5	22
EZ6gylL	liver	530	.15	<.4	<.4	<.4	<.7	<.5	2	<.4	<.5	20
HK1gylM	muscle	310	.10	.02	<.1	<.1	<.1	.01	.4	<.01	.01	8
HK2gylM	muscle	350	.08	<.01	.1	<.1	<.1	<.01	.3	<.01	<.01	7
HK3gylM	muscle	300	.14	<.01	<.1	<.1	<.1	<.01	.3	<.01	<.01	5
HK4gylM	muscle	320	.12	<.01	<.1	<.1	<.1	<.01	.5	<.01	<.01	6
HK5gylM	muscle	420	.09	<.01	<.1	<.1	<.1	.01	.3	<.01	<.01	6
HK6gylM	muscle	305	.09	<.01	.1	<.1	<.1	<.01	.3	<.01	<.01	6
HK7gylM	muscle	230	.08	<.01	.1	<.1	<.1	<.01	.3	<.01	<.01	5
HK1gylL	liver	310	.10	<.4	<.4	<.4	<.7	<.5	2	<.4	<.5	21
HK2gylL	liver	350	.13	<.4	<.4	<.4	<.7	<.5	5	<.4	<.5	21
HK3gylL	liver	300	.13	<.4	<.4	<.4	<.7	<.5	2	<.4	<.5	18
HK4gylL	liver	320	.22	<.4	<.4	<.4	<.7	<.5	5	<.4	<.5	27
HK5gylL	liver	420	.14	<.4	<.4	<.4	<.7	<.5	2	<.4	<.5	22
HK6gylL	liver	305	.13	<.4	<.4	<.4	<.7	<.5	4	<.4	<.5	22
HK7gylL	liver	230	.08	<.4	<.4	<.4	<.7	<.5	2	<.4	<.5	13
MC1gylM	muscle	375	.16	<.01	<.1	<.1	<.1	<.01	.2	<.01	.02	6
MC1gylL	liver	375	.20	<.4	<.4	<.4	<.7	<.5	2	<.4	<.5	22
VH1gylM	muscle	110	.07	<.01	.1	<.1	<.1	<.01	.4	<.01	<.01	11
VH1dolyM	muscle	680	.14	<.01	1.2	<.1	<.1	<.01	1	<.01	<.01	5
VH2dolyM	muscle	55	<.02	.01	.1	<.1	<.1	<.01	.6	<.01	<.01	4
VH1gylL	liver	110	.11	<.4	.1	<.4	<.7	<.5	.8	<.4	<.5	10
VH1dolyL	liver	680	.01	<.4	.4	<.4	<.7	<.5	20	<.4	<.5	42

**ANALYTICAL METHODS**

Mercury was measured in the fish samples using the cold-vapor atomic absorption spectrophotometry (CVAAS)

method of O'Leary (in press). Fish tissues were also analyzed for a multielement suite by an inductively coupled plasma-mass spectrometry (ICP-MS) technique modified from Meier and others (1994). All concentrations in fish are reported on a wet-weight basis (tables 1-4).

**Table 2.** Data for Dolly Varden (doly) and Arctic grayling (gyl) collected from Cinnabar Creek (CC), Chineekluk Creek (CHE-east site and CHW-west site), and the Kolmakof River (KF)

[Analysis of Hg by cold-vapor atomic absorption spectrophotometry (CVAAS); Sb, As, Ag, Bi, Cd, Cu, Mo, Pb, and Zn by inductively coupled plasma-mass spectrometry (ICP-MS); fish weights are whole body measured on site; concentrations are in parts per million wet weight; n.d., not determined]

Sample	Tissue	Fish weight (g)	Hg ppm	Sb ppm	As ppm	Ag ppm	Bi ppm	Cd ppm	Cu ppm	Mo ppm	Pb ppm	Zn ppm
CC1dolyM	muscle	230	0.62	0.01	0.1	<0.1	<0.1	<0.01	0.5	0.01	0.02	5
CC2dolyM	muscle	550	.23	.01	.1	<.1	<.1	<.01	.4	.01	.01	6
CC3dolyM	muscle	710	.08	<.01	.2	<.1	<.1	<.01	.3	<.01	.01	5
CC4dolyM	muscle	480	.43	.01	.1	<.1	<.1	<.01	.5	<.01	.02	6
CC1gylM	muscle	480	.15	<.01	.1	<.1	<.1	.01	.9	<.01	.01	7
CC1dolyL	liver	230	1.3	<.4	<.4	<.4	<.7	<.5	2	<.4	<.5	32
CC2dolyL	liver	550	.29	<.4	<.4	<.4	<.7	<.5	2	<.4	<.5	38
CC3dolyL	liver	710	.10	<.4	<.4	<.4	<.7	<.5	5	<.4	<.5	39
CC4dolyL	liver	480	.68	<.4	<.4	<.4	<.7	<.5	5	<.4	<.5	49
CC1gylL	liver	480	.26	<.4	<.4	<.4	<.7	<.5	2	<.4	<.5	26
CHE1gylM	muscle	355	.12	.01	.3	<.1	<.1	.01	.4	<.01	<.01	9
CHE2gylM	muscle	430	.26	.01	.2	<.1	<.1	.01	.4	<.01	<.01	5
CHW3gylM	muscle	230	.08	.01	.1	<.1	<.1	.01	.3	<.01	.01	5
CHW4gylM	muscle	305	.08	.01	.2	<.1	<.1	.01	.7	<.01	<.01	5
CHW5gylM	muscle	105	.07	.01	.2	<.1	<.1	.01	.6	<.01	<.01	6
CHE1gylL	liver	355	.16	<.4	<.4	<.4	<.7	<.5	3	<.4	<.5	23
CHE2gylL	liver	430	.35	<.4	<.4	<.4	<.7	<.5	2	<.4	<.5	21
CHW3gylL	liver	230	.15	<.4	<.4	<.4	<.7	<.5	4	<.4	<.5	25
CHW4gylL	liver	305	.13	<.4	<.4	<.4	<.7	<.5	4	<.4	<.5	24
CHW5gylL	liver	105	.13	<.4	<.4	<.4	<.7	<.5	2	<.4	<.5	20
KF1gylM	muscle	290	.09	.01	<.1	<.1	<.1	.01	.3	.01	.02	5
KF2gylM	muscle	315	.14	.01	<.1	<.1	<.1	.01	.4	.01	.01	5
KF3gylM	muscle	135	.08	.01	<.1	<.1	<.1	.01	.4	<.01	.03	6
KF4gylM	muscle	220	.10	.01	.1	<.1	<.1	.01	.3	.02	<.01	6
KF5gylM	muscle	140	.09	.01	.1	<.1	<.1	.01	.3	<.01	.04	5
KF6gylM	muscle	500	.42	.01	<.1	<.1	<.1	.01	.3	<.01	<.01	4
KF1gylL	liver	290	.24	<.4	<.4	<.4	<.7	<.5	3	<.4	<.5	23
KF2gylL	liver	315	.22	<.4	<.4	<.4	<.7	<.5	2	<.4	<.5	24
KF3gylL	liver	135	.14	<.4	<.4	<.4	<.7	<.5	1	<.4	<.5	20
KF4gylL	liver	220	.18	<.4	<.4	<.4	<.7	<.5	2	<.4	<.5	22
KF5gylL	liver	140	.16	<.4	<.4	<.4	<.7	<.5	2	<.4	<.5	20
KF6gylL	liver	500	.92	<.4	<.4	<.4	<.7	<.5	1	<.4	<.5	15

In the laboratory, stream-sediment samples were dried at temperatures below 50°C, sieved to minus-80 mesh, and pulverized. The sediments were analyzed for mercury by CVAAS following the technique of Kennedy and Crock (1987). Concentrations of Sb, As, Ag, Au, Bi, Cd, Cu, Mo, Pb, and Zn were determined in the stream-sediment samples by an inductively coupled plasma-atomic emission spectrometry (ICP-AES) technique (Motooka, 1988). The stream-water samples were also analyzed for Hg by CVAAS using a modified version of the technique of Kennedy and Crock (1987), and for Sb, As, Ag, Au, Bi, Cd, Cu, Mo, Pb, and Zn by ICP-MS (Meier and others, 1994). The analytical results for stream-sediment and stream-water samples are shown in table 5.

## RESULTS

### BACKGROUND SITES

Fish, stream-water, and stream-sediment samples were collected from several sites (fig. 1) to determine regional geochemical controls for this study. Arctic grayling collected from these sites contain mercury concentrations ranging from 0.07 to 0.20 ppm in muscle and 0.08 to 0.27 ppm in liver (table 1) and generally have low mercury concentrations relative to the other grayling collected in the study. Stream-water samples collected from background sites contain mercury concentrations below the 0.10 ppb lower limit of determination (table 5). These results are consistent with



**Table 3.** Data for sculpin and coho salmon collected downstream from the Red Top mine

[Analysis of Hg by cold-vapor atomic absorption spectrophotometry (CVAAS); fish weights are whole body measured on site; Hg concentrations are in parts per million wet weight]

Sample	Tissue	Fish weight (g)	Hg (ppm)
RTsculpA	whole body	6.9	0.06
RTsculpB	whole body	8.6	.06
RTsculpC	whole body	6.2	.02
RTsculpD	whole body	6.2	.05
RTsculpF	whole body	2.7	.02
RTsculpG	whole body	7.3	.02
RTsculpH	whole body	8.2	.03
RTsculpI	whole body	8.1	.03
RTsculpJ	whole body	5.2	.02
RTsculpK	whole body	5.9	.01
RTsculpL	whole body	6.9	.02
RTsculpM	whole body	5.4	.02
RTsculpN	whole body	5.3	.05
RTsculpO	whole body	2.8	.09
RTsculpP	whole body	6.7	.05
RTsculpQ	whole body	3.6	.04
RTsculpR	whole body	3.2	.06
RTsculpS	whole body	3.3	.12
RTsculpT	whole body	4.1	.02
RTsculpU	whole body	3.4	.10
<hr/>			
RTcohoE	muscle	21	.08
RTcohoIA	muscle	11	.14
RTcohoIB	muscle	12	.08
RTcohoIC	muscle	9.3	.08
RTcohoID	muscle	8.0	.03
RTcohoIE	muscle	11	.06
RTcohoIF	muscle	8.4	.06
RTcohoIG	muscle	5.3	.06
RTcohoIH	muscle	6.9	.03
RTcohoII	muscle	6.4	.04

the low concentrations of mercury observed in natural surface waters, commonly less than 0.1 ppb (Wershaw, 1970). Other trace metals in the stream-water samples from background sites are also low and generally below limits of determination (table 5). Stream-sediment samples collected from background sites generally contain less than 0.5 ppm Hg. Mercury concentrations in fish, stream-water, and stream-sediment samples collected from these sites are similar, but slightly more variable, than those reported from other studies in the region (Crayton, 1990; Snyder-Conn and others, 1992; Gray and others, 1994).

#### CINNABAR CREEK MINE

Fish collected from Cinnabar Creek, about 10 km downstream from the mine, contain the highest mercury concen-

trations in this study (table 2, fig. 2). Four Dolly Varden samples collected from Cinnabar Creek contain 0.08 to 0.62 ppm Hg in muscle and 0.10 to 1.3 ppm Hg in liver (table 2). One Arctic grayling collected from Cinnabar Creek in this study contains 0.15 ppm Hg in muscle and 0.26 ppm Hg in liver. The muscle sample of Dolly Varden containing 0.62 ppm Hg exceeds mercury concentrations in muscle samples of grayling (0.47 ppm) previously collected from Cinnabar Creek (Gray and others, 1994), but the fish collected for this study were larger (ranging from 230 to 710 g in weight) than the grayling collected by Gray and others (1994), which ranged from 9 to 45 g. In addition, Dolly Varden are higher in trophic position than grayling, and the higher mercury concentrations in the Dolly Varden are possibly a result of biomagnification. Dolly Varden are also migratory fish and probably feed along portions of the stream closer to the mine, where mercury concentrations are much higher. Other trace-metal concentrations in fish collected from Cinnabar Creek are considered low, and most are below analytical limits of determination (table 2).

The stream-sediment sample collected from Cinnabar Creek contains 1.0 ppm Hg, which is higher in mercury than the background sites (table 5). Previous studies have reported mercury concentrations in excess of 36 ppm in stream-sediment samples collected within about 7 km from the Cinnabar Creek mine (Gray and others, 1991). These results indicate that stream sediments in Cinnabar Creek contain abundant mercury.

The stream-water samples collected from Cinnabar Creek contain low concentrations of mercury and other trace metals. Mercury concentrations in the stream-water samples are 0.19 ppb (unfiltered) and <0.10 ppb (filtered). Antimony concentrations in the filtered stream-water sample were 0.4 ppb and 0.8 ppb in the unfiltered sample. All other trace metals in the stream-water samples are below analytical limits of determination. The presence of trace amounts of mercury and antimony in these stream waters is consistent with the presence of cinnabar, native mercury, and stibnite in the upstream Cinnabar Creek deposit.

#### MOUNTAIN TOP MINE

The Mountain Top mine is located at the headwaters of a tributary of Chineeekluk Creek, about 15 km upstream from the two collection sites (fig. 1). Five Arctic grayling collected from Chineeekluk Creek contain mercury concentrations varying from 0.07 to 0.26 ppm in muscle and 0.13 to 0.35 ppm in liver (table 2). The grayling muscle containing 0.26 ppm Hg is slightly higher in mercury than grayling from background sites (fig. 2). The elevated mercury in the grayling suggests that, as in Cinnabar Creek, mercury from the Mountain Top deposit has been converted to a form of mercury (probably methylmercury) that is bioavailable to fish in Chineeekluk Creek. Other trace-metal

**Table 4.** Data for chum salmon, coho salmon, and northern pike collected from the Kuskokwim River (AN-at Aniak, KR-at the Kolmakof mine, and SL-near Sleetmute) and the Holokuk River (HK)

[Analysis of Hg by cold-vapor atomic absorption spectrophotometry (CVAAS); Sb, As, Ag, Bi, Cd, Cu, Mo, Pb, and Zn by inductively coupled plasma-mass spectrometry (ICP-MS); fish weights are whole body wet weights measured on site; concentrations are in parts per million wet weight]

Sample	Tissue	Fish weight (kg)	Hg ppm	Sb ppm	As ppm	Ag ppm	Bi ppm	Cd ppm	Cu ppm	Mo ppm	Pb ppm	Zn ppm
AN1chumM	muscle	3.2	0.03	<0.4	0.4	<0.4	<1	<0.6	0.8	<0.5	<0.6	5
AN2chumM	muscle	3.2	.05	<.4	<.4	<.4	<1	<.6	.7	<.5	<.6	5
AN3chumM	muscle	3.1	.05	<.4	<.4	<.4	<1	<.6	<.7	<.5	<.6	4
AN4chumM	muscle	3.0	.04	<.4	.4	<.4	<1	<.6	.7	<.5	<.6	4
AN5chumM	muscle	1.8	.04	<.4	.6	<.4	<1	<.6	1	<.5	<.6	6
AN1chumL	liver	3.2	.04	<.4	<.4	.7	<1	1	30	<.5	<.6	24
AN2chumL	liver	3.2	.04	<.4	<.4	1	<1	1	47	<.5	<.6	24
AN3chumL	liver	3.1	.03	<.4	<.4	1	<1	1	71	<.5	<.6	93
AN4chumL	liver	3.0	.04	<.4	<.4	1	<1	1	91	<.5	<.6	29
AN5chumL	liver	1.8	.03	<.4	<.4	2	<1	3	64	<.5	<.6	28
HK1chumM	muscle	2.7	.06	<.4	.6	<.4	<1	<.6	2	<.5	<.6	8
HK2chumM	muscle	2.3	.08	<.4	<.4	<.4	<1	<.6	.9	<.5	<.6	9
HK1chumL	liver	2.7	.06	<.5	.7	3	<1	2	140	<.5	<.6	41
HK2chumL	liver	2.3	.05	<.5	<.4	3	<1	2	120	<.5	<.6	31
KRcoho1M	muscle	.92	.03	.01	.4	<.4	<1	<.6	.6	<.5	<.6	6
KRcoho1L	liver	.92	.04	<.4	<.4	<.4	<1	<.6	30	<.5	<.6	30
SL1pikeM	muscle	.75	.28	<.4	.2	<.4	<.1	<.1	.2	<.1	<.1	17
SL2pikeM	muscle	.98	.25	<.4	.3	<.4	<.1	<.1	.1	<.1	<.1	6
SL3pikeM	muscle	.96	.19	<.4	.3	<.4	<.1	<.1	.1	<.1	<.1	4
SL4pikeM	muscle	1.5	.31	<.4	.3	<.4	<.1	<.1	.2	<.1	<.1	5

concentrations in these fish are similar to those from background sites and are not of environmental concern.

Stream-sediment and stream-water samples were not collected from Chineekluk Creek for this study because such samples were previously collected about 5 km downstream from the Mountain Top mine (Gray and others, 1991). In the Gray and others (1991) study, mercury concentrations were 12 ppm in a stream-sediment sample and 0.10 ppb in a stream-water sample. Although these samples were collected about 10 km upstream from the site sampled in this study, the results indicate significant concentrations of mercury in the stream-sediment sample but low-level mercury concentrations in the stream-water sample.

### KOLMAKOF RIVER

Fish, stream-sediment, and stream-water samples were collected from the Kolmakof River about 5 km downstream from a tributary where stream-sediment samples contain as much as 5.6 ppm Hg (Gray and others, 1993). No mercury lodes have been discovered in this drainage basin, perhaps because of the low, poorly exposed terrain. This site was selected for study because it represents an area where natu-

rally occurring mercury concentrations (baselines) can be reported prior to any mining. A stream-sediment sample collected from this site contains 5.7 ppm Hg, but the stream-water sample contained less than 0.10 ppb Hg (table 5). Six Arctic grayling collected from the Kolmakof River contain mercury concentrations from 0.08 to 0.42 ppm in muscle and 0.14 to 0.92 ppm in liver (table 2). The grayling containing 0.42 ppm Hg in muscle is elevated above mercury concentrations in fish muscle samples collected from background sites (fig. 2). Other trace-metal concentrations in fish, stream-sediment, and stream-water samples collected from the Kolmakof River are similar to those from background sites.

### RED TOP MINE

Study of the Red Top mine was conducted in cooperation with Carol Outwater and Ward Jones, residents of Dillingham. Only fish were collected for this part of the study because equipment was not available for stream-sediment and stream-water sampling. Fish collected downstream from the Red Top mine contain low concentrations of mercury, ranging from 0.01 to 0.12 ppm in whole-body samples

**Table 5.** Geochemical data for stream-sediment and stream-water samples collected from Cinnabar Creek (CC), Kolmakof River (KF), Kuskokwim River (KR-at the Kolmakof mine and AN-near Aniak), Boss Creek (BS), Egozuk Creek (EZ), Holokuk River (HK), Moose Creek (MC), and Veahna Creek (VH)

[Analysis of Hg by cold-vapor atomic absorption spectrophotometry; Sb, As, Ag, Au, Bi, Cd, Cu, Mo, Pb, and Zn determined by inductively coupled plasma-atomic emission spectrometry (ICP-AES) in stream-sediment samples and by inductively coupled plasma-mass spectrometry (ICP-MS) in stream-water samples; concentrations for sediments are in parts per million (ppm) and for waters are in parts per billion (ppb); n.d., not determined; sample suffix RA, raw water, sample suffix FA, filtered water]

Sediments	Hg (ppm)	Sb (ppm)	As (ppm)	Ag (ppm)	Au (ppm)	Bi (ppm)	Cd (ppm)	Cu (ppm)	Mo (ppm)	Pb (ppm)	Zn (ppm)
CC4200S	1.0	1.9	16	<0.07	<0.1	<1.0	0.1	37	0.99	7.3	100
KF4304S	5.7	<1.0	6.1	<.07	<.1	<1.0	.1	14	.44	6.0	81
KR4306S	28	<1.0	6.6	<.07	<.1	<1.0	.2	27	.65	8.9	78
BS4301S*	.02	1.3	9.3	<.07	<.1	<1.0	.1	28	.65	10	110
EZ4302S*	.03	1.3	9.0	<.07	<.1	<1.0	.1	30	.71	9.5	110
HK4300S*	<.02	<1.0	8.3	<.07	<.1	<1.0	.1	32	1.0	8.6	110
MC4100S*	.33	10	5.4	<.07	<.1	<1.0	.08	17	.26	4.4	91
VH4303S*	.45	<1.0	11	<.07	<.1	<1.0	.1	17	.65	7.4	89
AN4308S*	.08	1.0	17	.21	.4	<1.0	.2	14	.94	8.7	67

waters	Hg (ppb)	Sb (ppb)	As (ppb)	Ag (ppb)	Au (ppb)	Bi (ppb)	Cd (ppb)	Cu (ppb)	Mo (ppb)	Pb (ppb)	Zn (ppb)	pH
CC4200RA	0.19	0.8	<2	<0.1	<0.1	<0.6	<1	<1	<0.4	<0.6	<2	7.1
CC4200FA	<.10	.4	<2	<.1	<.1	<.6	<1	<1	<.4	<.6	<2	
KF4304RA	<.10	.2	<2	<.1	<.1	<.6	<1	1	<.4	.9	9	7.5
KF4304FA	n.d.	<.2	<2	<.1	<.1	<.6	<1	.9	.2	<.6	<2	
KR4306RA	<.10	.3	<2	<.1	<.1	<.6	<1	2	.6	1	7	7.7
KR4306FA	n.d.	.2	<2	<.1	<.1	<.6	<1	.8	.7	<.6	<2	
BS4301RA*	<.10	<.2	<2	<.1	<.1	<.6	<1	<1	<.4	<.6	<2	7.1
BS4301FA*	<.10	<.2	<2	<.1	<.1	<.6	<1	<1	<.4	<.6	<2	
EZ4302RA*	<.10	<.2	<2	<.1	<.1	<.6	<1	<1	<.4	<.6	<2	8.4
EZ4302FA*	<.10	<.2	<2	<.1	<.1	<.6	<1	<1	<.4	<.6	<2	
HK4300RA*	<.10	<.2	<2	<.1	<.1	<.6	<1	<1	<.4	<.6	<2	7.4
HK4300FA*	<.10	<.2	<2	<.1	<.1	<.6	<1	<1	<.4	<.6	<2	
MC4100RA*	<.10	<.2	<2	<.1	<.1	<.6	<1	<1	<.4	<.6	<2	8.1
MC4100FA*	<.10	<.2	<2	<.1	<.1	<.6	<1	<1	<.4	<.6	<2	
VH4303RA*	<.10	<.2	<2	<.1	<.1	<.6	<1	1	<.4	<.6	<2	7.6
VH4303FA*	<.10	<.2	<2	<.1	<.1	<.6	<1	<1	<.4	<.6	<2	
AN4308RA*	<.10	<.2	<2	<.1	<.1	<.6	<1	<1	<.4	<.6	<2	7.1
AN4308FA*	<.10	<.2	<2	<.1	<.1	<.6	<1	2	<.4	<.6	<2	

\*Indicates background sites.

of sculpin, and from 0.03 to 0.14 ppm in muscle samples of coho salmon (table 3). These mercury concentrations are similar to those in fish collected from background sites throughout the region.

### ADDITIONAL SITES

Sites along the Kuskokwim and Holokuk Rivers were studied to evaluate possible mercury bioaccumulation in fish that constitute major food sources. Salmon collected from the Kuskokwim and Holokuk Rivers have the lowest

concentrations of mercury in fish muscle samples collected in this study (table 4). Chum salmon collected from the Kuskokwim and Holokuk Rivers contain mercury concentrations ranging from 0.03 to 0.08 in muscle, and 0.03 to 0.06 in liver. Similarly, mercury in the stream-water and stream-sediment samples collected from these two sites is also low (table 5). One coho salmon collected from the Kuskokwim River adjacent to the Kolmakof mercury mine also contains low mercury concentrations, 0.03 ppm in muscle and 0.04 ppm in liver (table 4), even though the stream-sediment sample contains 28 ppm Hg. The high mercury concentration in this stream-sediment sample is a

result of erosion of cinnabar from the deposit into the stream channel at this site.

Northern pike (also a local food source) collected from the Kuskokwim River, about 4 km upstream from Sleetmute and about 12 km upstream from the Red Devil mine, contain mercury concentrations ranging from 0.19 to 0.31 ppm in muscle samples (table 4). Although these mercury concentrations are higher than those in background Arctic grayling and salmon collected in the region, they are much lower than mercury found in fish collected near the abandoned mercury mines. Pike are large, predatory fish (that is, higher in trophic position than grayling), and the mercury results for pike suggest some mercury biomagnification. Other trace-metal concentrations in the pike are not of environmental concern.

## INTERPRETATIONS

Some stream-sediment, stream-water, and fish samples collected below mercury mines contain mercury concentrations elevated above background values. A stream-water sample collected below the Cinnabar

Creek mine contains 0.19 ppb Hg, whereas background stream waters in the region typically contain less than 0.10 ppb Hg. Mercury concentrations in all stream-water samples is below both the 2-ppb drinking-water maximum-contaminant level recommended by the State of Alaska (Alaska Department of Environmental Conservation, 1994) and the 2.4 ppb maximum instream concentration recommended by the U.S. Environmental Protection Agency (EPA) (Environmental Protection Agency, 1992). However, mercury concentrations in some stream-water samples exceed the 0.012 ppb level that the EPA indicates may result in chronic effects to aquatic life. To evaluate possible aquatic life effects in the study area, edible portions of fish were analyzed to determine if mercury concentrations exceed the 1.0 ppm (wet weight) action level established by the Food and Drug Administration (FDA) (Federal Register, 1979).

Mercury concentrations in samples of freshwater fish collected downstream from the Cinnabar Creek and Mountain Top mercury mines, as well as those from the site on the Kolmakof River, exceed background values. Fish containing the highest mercury concentrations were 0.62 ppm in muscle and 1.3 ppm in liver samples from

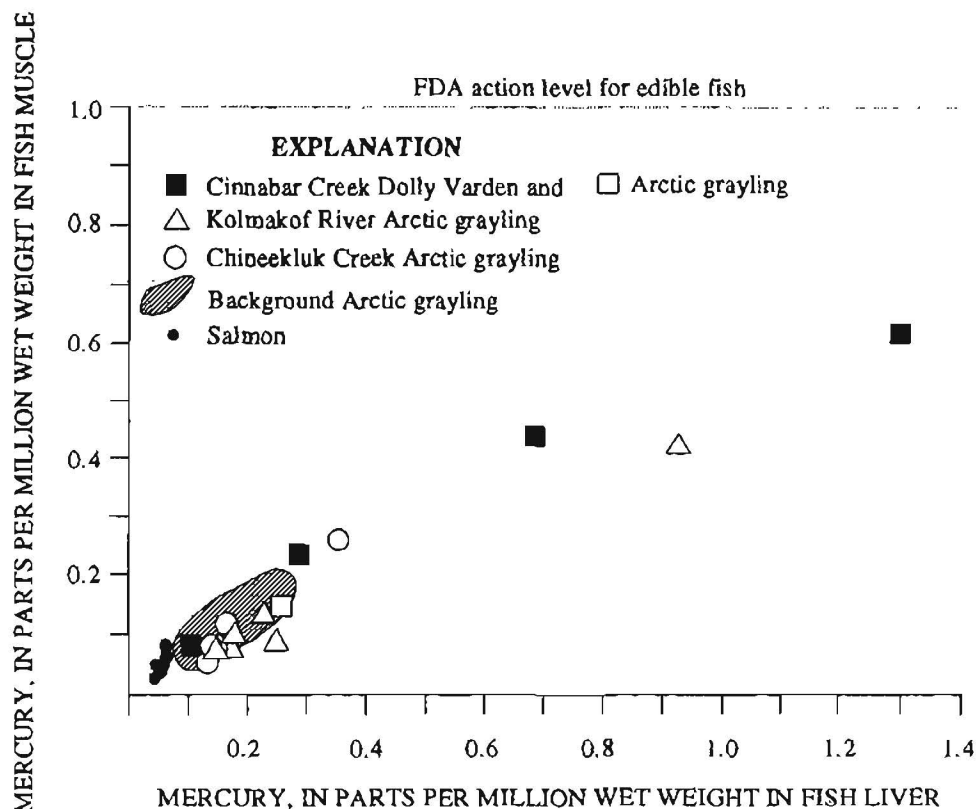


Figure 2. Plot of mercury in fish muscle versus mercury in fish liver from samples collected in this study.

Dolly Varden collected from Cinnabar Creek. Mercury concentrations as much as 0.47 ppm in muscle samples were also found in Arctic grayling collected from Cinnabar Creek (Gray and others, 1994). Mercury concentrations in the Dolly Varden and Arctic grayling collected from Cinnabar Creek are several times greater than those in fish collected from background sites in this study (fig. 2). Although the fish collected downstream from abandoned mercury mines and lodes contain elevated mercury concentrations in comparison to regional backgrounds, all mercury concentrations in samples of fish muscle are below the 1-ppm action level for edible fish established by the FDA. This is the concentration at which mercury advisories are listed and sale of fish is restricted by the FDA. A Dolly Varden liver sample collected from Cinnabar Creek contains 1.3 ppm Hg, but fish liver is not usually eaten by humans, and this concentration does not violate the FDA action level.

The elevated mercury concentrations in fish are interpreted to be a result of upstream mercury mines in the case of Cinnabar Creek and Mountain Top, and of undiscovered mercury lodes upstream from the site studied on the Kolmakof River. Mercury concentrations in these fish indicate that mercury introduced from the mines is bioavailable to the fish. In the stream environment, inorganic mercury (mostly cinnabar) is probably converted to organic mercury (methylmercury) and then passed onto fish through stream water, as well as through food sources such as invertebrate animals and other smaller fish that live in these streams. Such transfer of mercury to fish through food sources has been noted in freshwater ecosystems (Huckabee and others, 1979; Boudou and others, 1991). Mercury concentrations in water are low, even downstream from sources, because of the high volatility of mercury and its tendency to be sorbed by clays, microcrystalline oxides, sediment, and organic matter (Jenne, 1970). Although mercury concentrations in stream waters are generally less than 0.10 ppb, mercury is readily accumulated by fish when it is in a form that is biologically available in water.

Sculpin and coho salmon were collected downstream from the Red Top mine near Dillingham. Mercury concentrations in these fish were low, ranging from 0.01 to 0.12 ppm in samples of whole-body sculpin and 0.03 to 0.14 ppm in coho salmon muscle samples. These mercury concentrations are similar to those in freshwater fish reported in other studies (Crayton, 1990; Snyder-Conn and others, 1992; Gray and others, 1994). Results for the sculpin and coho salmon collected downstream from the Red Top mine suggest that (1) mercury has not had time to bioaccumulate because these fish are small and young; (2) there is little mercury in the stream environment, even though the stream drains a mercury mine; or (3) mercury in the stream draining the mine is not in a form that is biologically available to fish.

Salmon are an important subsistence and sport fish in southwestern Alaska, but salmon collected from the

Kuskokwim and Holokuk Rivers contain the lowest mercury concentrations of all the fish-muscle samples collected in this study. These results were not unexpected because salmon have a long ocean cycle and only return to freshwater streams and lakes for a short time to spawn. Northern pike (also a local food source) collected from the Kuskokwim River near Sleetmute contains mercury concentrations slightly elevated above background values but significantly lower than fish collected downstream from mercury mines. The salmon and pike were collected from large rivers and streams, and these data suggest that the influx of mercury from the naturally occurring mines and lodes is not large enough to adversely affect these fish. However, additional studies of salmon and pike need to be conducted because the sample population and distribution were not large enough to reach firm conclusions concerning mercury concentrations in these fish.

## SUMMARY

All concentrations of mercury in stream-water samples collected in this study are below the 2-ppb drinking-water maximum-contaminant level. Field measurements of pH indicate that stream waters draining mercury mines are neutral to slightly alkaline and are similar to background values. The dominant ore mineral in the mercury deposits is cinnabar, which is highly insoluble in water, resistant to physical and chemical weathering, and does not easily form acid drainage during weathering. Such near-neutral pH values are important because significant acid-drainage problems can result downstream from some sulfide-bearing mineral deposits and mines. However, acid formation in streams below the mercury mines in southwestern Alaska is probably insignificant environmentally.

Samples of muscle from Dolly Varden and Arctic grayling collected downstream from southwestern Alaska mercury mines and lodes contain mercury concentrations elevated above background values. The highest mercury concentration in fish is 0.62 ppm in a muscle sample and 1.3 ppm (wet weight) in a liver sample from a Dolly Varden collected below the Cinnabar Creek mine. However, all mercury concentrations in fish are below the 1 ppm wet-weight action level for edible fish established by the FDA as the concentration at which sale of fish is restricted.

Concentrations of mercury were also measured in salmon from large rivers to evaluate mercury levels in fish that constitute major food sources in the region. Chum salmon collected from the Kuskokwim and Holokuk Rivers contain the lowest mercury concentrations in muscle samples in the study, ranging from 0.03 to 0.08 ppm wet weight. Northern pike is another common food in the region, and samples collected from the Kuskokwim River near Sleetmute contain 0.19 to 0.31 ppm Hg wet weight in



muscle. All of these mercury concentrations are also well below the FDA action level.

Subsistence and sport fishing are common in southwestern Alaska, but the area is sparsely populated. The sites with the highest mercury concentrations in fish are distant from towns and unlikely to be frequent fishing sites. Mercury concentrations in fish collected in this study are below levels considered to be toxic to humans, but effects on organisms higher in the food chain remain to be addressed.

**Acknowledgments.**—The authors thank Mollie Malcolm, Jerry Motooka, and Joel Sadler (USGS) for chemical analyses. Jim Acker (Alaska Helicopters), Mike Balen (U.S. Bureau of Mines), Marti Miller (USGS), and Dr. Isadore Yablon (sport fisherman) assisted with sample collection. Discussions with Elizabeth Bailey (USGS), Tom Bundtzen (State of Alaska Geological and Geophysical Surveys), Elaine Snyder-Conn (U.S. Fish and Wildlife Service), and June McAtee and Rob Retherford (Calista Corporation) were helpful in the development of this study. Calista Corporation also provided access to their lands and encouraged these studies. Special thanks goes to Ward Jones for initiating studies with Carol Outwater around the Red Top mercury mine near Dillingham; without his assistance, this part of the study would not have been possible.

## REFERENCES CITED

- Alaska Department of Environmental Conservation, 1994, Drinking water regulations: State of Alaska, Department of Environmental Conservation report 18-ACC-80, 195 p.
- Boudou, A., Delnomdedieu, M., Georgescauld, D., Ribeyre, F., and Saouter, E., 1991, Fundamental roles of biological barriers in mercury accumulation and transfer in freshwater ecosystems (analysis at organism, organ, cell, and molecular levels): *Water, Air, and Soil Pollution*, v. 56, p. 807–822.
- Box, S.E., 1985, Mesozoic tectonic evolution of the northern Bristol Bay region, southwestern Alaska: Santa Cruz, Calif., University of California; Ph.D. dissertation, 199 p.
- Bundtzen, T.K., Kline, J.T., Clautice, K.H., and Adams, D.D., 1986, Minerals potential, Department of Natural Resources Kuskokwim planning block, Alaska: Alaska Division of Geological and Geophysical Surveys, Public Data File 86-53e, 44 p.
- Cady, W.M., Wallace, R.E., Hoare, J.M., and Webber, E.J., 1955, The central Kuskokwim region, Alaska: U.S. Geological Survey Professional Paper 268, 132 p.
- Crayton, W.M., 1990, Report of findings, placer mining impacts—Tuluksak River: U.S. Fish and Wildlife Service, Anchorage, Alaska, unpublished report, 20 p.
- Eisler, Ronald, 1987, Mercury hazards to fish, wildlife, and invertebrates: a synoptic review: Fish and Wildlife Service Biological Report 85(1.10), 90 p.
- Environmental Protection Agency, 1992, Water quality standards; establishment of numeric criteria for priority toxic pollutants; states' compliance; final rule: Federal Register, 40 CFR Part 131, v. 57, no. 246, p. 60847–60916.
- Federal Register, 1979, Action level for mercury in fish, shellfish, crustaceans, and other aquatic animals: comment from the Department of Health, Education, and Welfare, Food and Drug Administration, v. 44, no. 14, p. 3990–3993.
- Fenchel, T., and Blackburn, T.H., 1979, Bacteria and mineral cycling: London, England, Academic Press, 225 p.
- Friberg, Lars, and Vostal, Jaroslav, 1972, Mercury in the environment: CRC Press, Cleveland, Ohio, 215 p.
- Gough, L.P., Shacklette, H.T., and Case, A.A., 1979, Element concentrations toxic to plants, animals, and man: U.S. Geological Survey Bulletin 1466, 80 p.
- Gray, J.E., Goldfarb, R.J., Detra, D.E., and Slaughter, K.E., 1991, Geochemistry and exploration criteria for epithermal tin-bar and stibnite vein deposits in the Kuskokwim River region, southwestern Alaska: *Journal of Geochemical Exploration*, v. 41, p. 363–386.
- Gray, J.E., Theodorakos, P.M., Bradley, L.A., and Bullock, J.H., Jr., 1993, Favorable areas for metallic mineral resources in and near the Horn Mountains, Sleetmute quadrangle, southwestern Alaska, in Dusel-Bacon, Cynthia, and Till, Alison, eds., *Geologic studies in Alaska by the U.S. Geological Survey, 1992*: U.S. Geological Survey Bulletin 2068, p. 79–90.
- Gray, John, Theodorakos, Peter, Budahn, James, and O'Leary, Richard, 1994, Mercury in the environment and its implications, Kuskokwim River region, southwestern Alaska, in Till, Alison B., and Moore, Thomas, E., eds., *Geologic studies in Alaska by the U.S. Geological Survey, 1993*: U.S. Geological Survey Bulletin 2107, p. 3–13.
- Hem, J.D., 1970, Chemical behavior of mercury in aqueous media, in *Mercury in the Environment*: U.S. Geological Survey Professional Paper 713, p. 19–24.
- Hoare, J.M., and Coonrad, W.L., 1959, Geology of the Russian Mission quadrangle, Alaska: U.S. Geological Survey Miscellaneous Geologic Investigations Map I-292, scale 1:250,000.
- Huckabee, J.W., Elwood, J.W., and Hildebrand, S.G., 1979, Accumulation of mercury in freshwater biota, in Nriagu, J.O., ed., *The Biogeochemistry of mercury in the environment*: New York, Elsevier/North-Holland Biomedical Press, p. 277–302.
- Jenne, E.A., 1970, Atmospheric and fluvial transport of mercury, in *Mercury in the environment*: U.S. Geological Survey Professional Paper 713, p. 40–45.
- Kennedy, K.R., and Crock, J.G., 1987, Determination of mercury in geological materials by continuous flow, cold-vapor, atomic-absorption spectrophotometry: *Analytical Letters*, v. 20, p. 899–908.
- Lindqvist, O., ed., 1991, Mercury as an environmental pollutant—Proceedings from the International Conference, Gävle, Sweden, June 11–13, 1990: *Water, Air, and Soil Pollution*, v. 56, 847 p.
- Meier, A. L., Grimes, D.J., and Ficklin, W.H., 1994, Inductively coupled plasma mass spectrometry—a powerful analytical tool for mineral resource and environmental studies [abs.], in Carter, L.M.H., Toth, M.I., and Day, W.C., eds., *USGS research on mineral resources—1994, Part A—Program and Abstracts*, V.E. McKelvey Forum on Mineral and Energy Resources, 9th, Tucson, Ariz., February 22–25, 1993: U.S. Geological Survey Circular 1103-A, p. 67–68.

- Miller, M.L., Belkin, H.E., Blodgett, R.B., Bundtzen, T.K., Cady, J.W., Goldfarb, R.J., Gray, J.E., McGimsey, R.G., and Simpson, S.L., 1989, Pre-field study and mineral resource assessment of the Steetmute quadrangle, southwestern Alaska: U.S. Geological Survey Open-File Report 89-363, 115 p., 3 plates, scale 1:250,000.
- Miller, M.L., and Bundtzen, T.K., 1994, Generalized geologic map of the Iditarod quadrangle, Alaska, showing potassium-argon, major-oxide, trace-element, fossil, paleocurrent, and archaeological sample localities: U.S. Geological Survey Miscellaneous Field Studies Map MF-2219-A, 1 sheet, scale 1:250,000.
- Motooka, J.M., 1988, An exploration geochemical technique for the determination of preconcentrated organometallic halides by ICP-AES: *Applied Spectroscopy*, v. 42, no. 7, p. 1293-1296.
- National Academy of Sciences, 1978, *An assessment of mercury in the environment*: National Academy of Sciences, Washington, D.C., 185 p.
- O'Leary, R.M., in press, *The determination of mercury and selenium in eight Argonne Premium coal samples by cold vapor and hydride atomic absorption spectrometry*, in Palmer, C.A., ed., *The chemical analysis of Argonne Premium coal samples*: U.S. Geological Survey Bulletin, p. J1-J11.
- Sainsbury, C.L., and MacKevett, E.M., Jr., 1965, Quicksilver deposits of southwestern Alaska: U.S. Geological Survey Bulletin 1187, 89 p.
- Snyder-Conn, E., Patton, T., Bertram, M., Scannell, P., and Anthony, C., 1992, Contaminant baseline data for water, sediments, and fish of the Nowitna National Wildlife Refuge, 1985-1988: U.S. Fish and Wildlife Service, Fairbanks, Alaska, Ecological Services Technical Report NAES-TR-92-02.
- Sorg, D.H., and Estlund, M.B., 1972, Geologic map of the Mountain Top mercury deposit, southwestern Alaska: U.S. Geological Survey Miscellaneous Field Studies Map MF-449.
- Webber, B.S., Bjorklund, S.C., Rutledge, F.A., Thomas, B.I., and Wright, W.S., 1947, Mercury deposits of southwestern Alaska: U.S. Bureau of Mines Report of Investigations 4065, 57 p.
- Wershaw, R.L., 1970, Sources and behavior of mercury in surface waters, in *Mercury in the environment*: U.S. Geological Survey Professional Paper 713, p. 29-31.
- Wood, J.M., 1974, Biological cycles for toxic elements in the environment: *Science*, v. 183, no. 4129, p. 1049-1052.

Reviewers: Ronald Severson and Richard Goldfarb





# Natural Environmental Effects Associated with the Drenchwater Zinc-Lead-Silver Massive Sulfide Deposit with Comparisons to the Red Dog and Lik Deposits, West-Central Brooks Range, Alaska

By Karen Duttweiler Kelley and Cliff D. Taylor

## ABSTRACT

The Drenchwater deposit is a shale-hosted stratiform zinc-lead-silver massive sulfide deposit in the west-central Brooks Range. Analytical results of water samples from the undisturbed deposit indicate natural metal contamination occurs in stream water owing to leaching and weathering of the deposit. Water samples collected from Discovery and lower Drenchwater Creeks, which drain the mineralized zone on the west side, contain minimum pH values of 4.2 and dissolved concentrations of Al, Fe, Mn, Cd, Co, Cu, Ni, Pb, and Zn that are 4 to 116 times greater than the concentrations in water upstream from the deposit in upper Drenchwater Creek. Most notable are concentrations in Discovery Creek as high as 1 ppm Al, 3 ppm Fe, 6 ppb Cd, and 1,400 ppb Zn. Water conductivity also increases from an average of 67.2  $\mu\text{S}/\text{cm}$  above the deposit to 107.2  $\mu\text{S}/\text{cm}$  in water collected below the deposit. The effects of these low-pH, metal-rich waters are evident for at least 1.7 km below the mineralized area. Although dissolved Cd, Co, Fe, Ni, and Zn are still enriched by factors of 2–57 times at these distances, Cu and Pb are close to background levels in samples collected 0.4 to 1.7 km downstream.

Stream-water samples from False Wager Creek, which partially drains the deposit on the east side, are relatively more acidic and metal rich than either lower Drenchwater or Discovery Creek. The high acidity of the creek water is reflected by pH values of 3.2 or lower over the entire 4.5-km distance sampled. False Wager Creek water contains elevated concentrations of As and Sb, as well as Fe, Cd, Co, Cu, Ni, Pb, and Zn. The most acidic water contains the highest concentrations of metals; one water sample with a pH of 2.8 contains 53 ppm Al, 270 ppm Fe, 9 ppb Pb, and 2,000 ppb Zn. In addition, the sulfate concentrations in False Wager Creek water are extremely high, from 480 to 1,180 ppm. Although the source of the metals in the lower part of False Wager Creek is probably from weathering of the deposit, the headwaters of

False Wager Creek, 2 km above areas of known base-metal mineralization, also contain low-pH, metal-rich waters. These metal-rich waters are attributed either to zones of abundant pyrite, without associated base-metal sulfides, or to mineralized areas that have not yet been identified.

The data from the Drenchwater deposit provide an interesting comparison with natural waters draining the Red Dog and Lik stratiform massive sulfide deposits in the westernmost part of the Brooks Range. The low pH and high-total-metal contents of waters from Drenchwater are similar to those from the Red Dog deposit prior to mining, although the total metal concentrations in water from the Red Dog deposit are many times greater than at Drenchwater, probably owing in large part to the relatively greater extent of surface exposure and to the higher grade of the Red Dog deposit. In contrast, water samples collected below the mineralized zone at Lik have pH values of 6.2 to 8.1 and, with the exception of zinc, the metal contents are low compared with water draining the Drenchwater deposit. These differences can be attributed to the presence of carbonate rocks at Lik, which serve to buffer acidic, metal-rich waters.

## INTRODUCTION

The Drenchwater deposit is located in the west-central Brooks Range within the National Petroleum Reserve in Alaska (NPRA) (fig. 1). It is a zinc-lead-silver massive sulfide deposit hosted primarily by carbonaceous black shale and siliceous mudstone, similar to the sedimentary exhalative Lik and Red Dog deposits in the western Brooks Range. Unlike the Lik and Red Dog deposits, the Drenchwater deposit has not been drilled or mined.

A study was undertaken to determine the natural background concentrations and extent of natural metal contamination in water samples from the Drenchwater deposit area. This area is ideally suited for such a study because it offers a means to determine the natural environmental

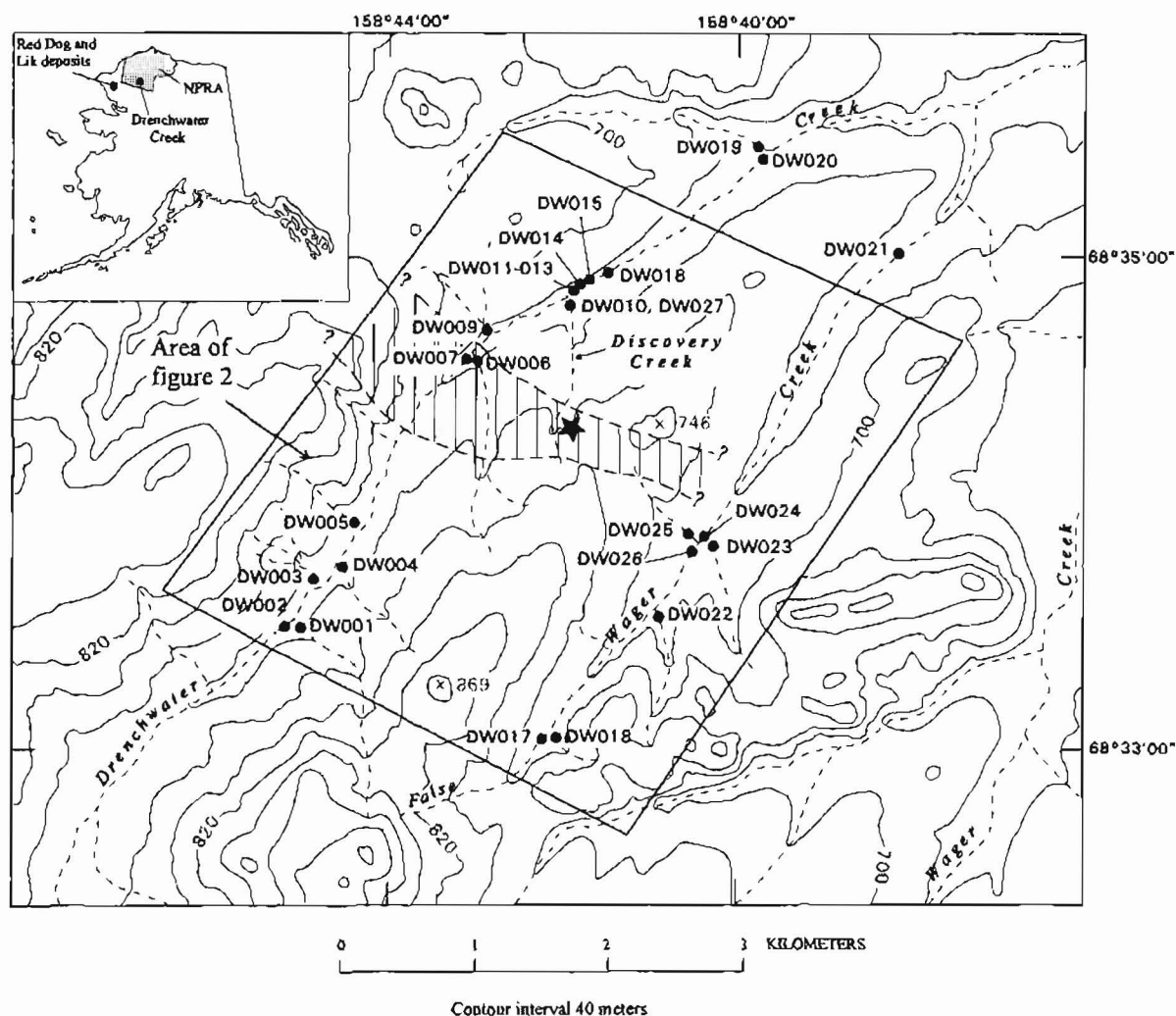
effects associated with mineral deposits prior to human disturbance. Knowledge of the natural background concentrations of metals in mineralized areas is helpful for devising realistic plans for remediation and monitoring programs. For example, it may not be scientifically reasonable or technically possible to remediate water to standards that are lower than local natural background concentrations. In addition, characterizing the environmental behavior of a specific deposit may help predict the environmental effects likely to result from future proposed mining of a deposit with similar geologic characteristics.

Geoenvironmental models have been developed by Plumlee and others (1993, 1994) and Smith and others (1994) to characterize the environmental behavior of specific types of deposits in Colorado. These models are based on descriptive and empirical studies of the natural

and human-induced environmental effects associated with mineral deposits. Data from the present study may be used to develop a similar model for sedimentary exhalative deposits in the arctic environment.

## PREVIOUS WORK

During fieldwork by the U.S. Geological Survey (USGS) in 1950-53, 1976, and 1977, iron staining was observed in dark-gray chert and shale along Drenchwater Creek (Tailleur and others, 1977) that was similar to staining observed at Red Dog Creek in the western Brooks Range (Tailleur, 1970). In the late 1970's, detailed investigations were undertaken by the USGS at Drenchwater Creek as part of a regional assessment of the southern part of the NPRA. Stream-sediment geochemical studies



**Figure 1.** Map showing Drenchwater Creek area and locations of water samples. Solid black circles indicate water sample sites; star denotes location of semimassive sulfides. Hatched zone shows area of alteration and disseminated base-metal mineralization. Insert shows location of Drenchwater Creek within the National Petroleum Reserve in Alaska (NPRA) and locations of Red Dog and Lik deposits.

were conducted by Theobald and others (1978), and soil geochemistry and ground magnetic geophysical studies were completed by Metz and others (1979). Additional geologic and geochemical studies of the area include Churkin and others (1978), Jansons and Baggs (1980), Jansons and Parke (1981), Jansons (1982), and Nokleberg and Winkler (1982).

In the summers of 1990–1994, the USGS conducted geologic mapping and geochemical sampling in the Howard Pass quadrangle as part of the Alaska Mineral Resource Assessment Program (AMRAP). During this work, detailed stream-sediment, nonmagnetic heavy-mineral-concentrate, and rock samples were collected from the Drenchwater Creek and surrounding areas in the western part of the Howard Pass quadrangle (Kelley and others, 1992). Other studies include soil geochemical sampling by the U.S. Bureau of Mines in conjunction with Kennecott Exploration (Meyer and Kurtak, 1992); gravity surveys by the USGS (Meyer and Kurtak, 1992); and detailed mapping of lithologies and alteration by Werdon (in press), which is part of an ongoing Ph.D. thesis. There has been no drilling because of the location of the study area within the NPRA.

## GEOLOGY

The Drenchwater Creek area lies within an east-west-trending fold and thrust belt of Paleozoic and Mesozoic rocks that extends along the entire western and central Brooks Range. Upper Paleozoic sedimentary rocks within this belt host several stratiform massive sulfide and barite mineral deposits. Largest among these are the Red Dog and Lik zinc-lead-silver-barite deposits in the westernmost part of the Brooks Range (Moore and others, 1986; Forrest and Sawkins, 1987). The Drenchwater deposit is located in the west-central Brooks Range, about 175–180 km east of the Red Dog and Lik deposits (fig. 1).

The Drenchwater deposit is hosted dominantly by black carbonaceous shale and chert of the Mississippian and Pennsylvanian Kuna Formation of the Lisburne Group (Patton and Tailleir, 1964; Mull and others, 1982; Dumoulin and others, 1993). The Kuna Formation also hosts the Red Dog and Lik deposits in the westernmost part of the Brooks Range (Ellersieck and others, 1990; Mayfield and others, 1990). Regionally, the Kuna Formation intertongues with light-colored platform carbonate rocks that are also assigned to the Lisburne Group (Mull and others, 1982; Ellersieck and others, 1990; Mayfield and others, 1990). In the western and central Brooks Range, rocks of the Lisburne Group depositionally overlie clastic sedimentary rocks of the Upper Devonian and Lower Mississippian Endicott Group (Mull and others, 1982) and underlie fine-grained sedimentary rocks of the

Pennsylvanian to Jurassic Etivluk Group (Mull and others, 1982).

The Drenchwater Creek area is shown on figure 2. Three structural plates have been defined (Nokleberg and Winkler, 1982; Werdon, in press): the Two Cubs, Drenchwater, and Spike Camp thrust plates. The Drenchwater thrust plate is distinguished from the other thrust plates by the presence of stratiform sulfide mineralization, altered volcanic rocks, and a high proportion of sooty black carbonaceous shale and siliceous mudstone (Werdon, in press). Mississippian to Permian parts of the stratigraphic section are structurally repeated at least four times within the Drenchwater thrust plate. High-angle north-trending faults offset stratigraphic units at nearly perpendicular angles to the thrust plates.

In the Drenchwater Creek region, the Kuna Formation is at most 70 m thick (Dumoulin and others, 1993; Werdon, in press). Preservation of laminae and the high organic component suggest that anoxic or dysaerobic bottom-water conditions prevailed during its deposition (Dumoulin and others, 1993). Limestone and dolomite occur locally as laminae and thin beds in siliceous mudstone but overall comprise only a minor part of the stratigraphic section (Nokleberg and Winkler, 1982; Werdon, in press).

In the Drenchwater thrust plate, the Kuna Formation contains significant amounts of volcanic rocks (Nokleberg and Winkler, 1982; Werdon, in press). The volcanic rocks consist primarily of submarine felsic tuffaceous rocks. Mafic rocks occur at two localities in the eastern part of the Drenchwater thrust plate (fig. 2). At least four felsic to intermediate intrusive domes and flows occur within, or near, the felsic tuffaceous volcanic pile (Werdon, in press). The volcanic pile may be as thick as 300 m (along Discovery Creek) but is generally less than 100 m (Werdon, in press). Biotite from the least altered massive igneous unit in the central part of the Drenchwater thrust plate yielded a K-Ar age of  $319 \pm 10$  Ma (Tailleur and others, 1966).

## ALTERATION AND MINERALIZATION

Alteration assemblages, determined for sedimentary and volcanic rocks in the Drenchwater thrust plate (Werdon, in press), consist predominantly of quartz, kaolinite, dickite, and carbonates. Lesser amounts of pyrite, fluorite, illite, white mica, epidote, and leucoxene are also present. In the tuffaceous volcanic rocks and intrusive domes, kaolinite and dickite are the most abundant clay alteration minerals, although illite and white mica partially replace feldspar phenocrysts in some of the intrusive rocks. The highest concentration of illite and white mica (up to 25 volume percent) is in the volcanic breccia

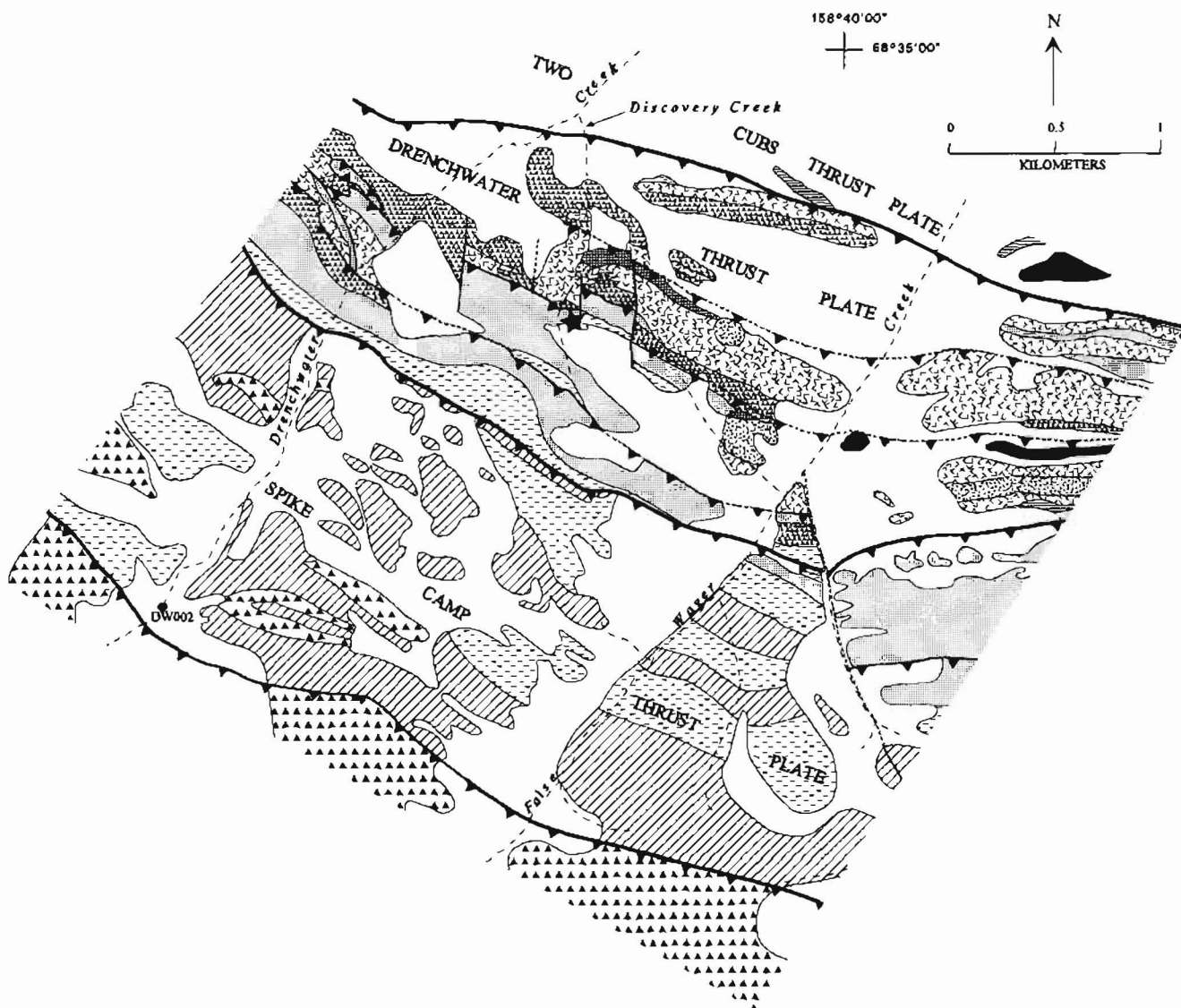
adjacent to the intrusive dome along Discovery Creek (fig. 2).

Carbonate alteration is present throughout the volcanic pile but its relation, if any, to mineralization or hydrothermal silicification is not clear. Fluorite is present within highly foliated, carbonate-altered felsic volcanic tuffs along Discovery Creek (Werdon, in press).

Mineralization is spatially associated with hydrothermal silicification and bleaching of black carbonaceous shale and siliceous mudstone. Silicification and mineralization appear to be concentrated primarily in a single, thrust-repeated siliceous horizon near the top of the Kuna Formation, although black shale and mudstone exposed

along Drenchwater Creek (Werdon, in press) appears to be weakly mineralized. Additionally, volcanic breccia units are silicified and mineralized.

Sphalerite is the predominant sulfide mineral, but variable amounts of galena, pyrite, and marcasite, minor amounts of fluorite, and trace amounts of barite are also present. Minute sulfosalt grains are present within galena and account for anomalous concentrations of antimony, arsenic, and silver. Copper-bearing minerals are notably absent (Werdon, in press). Sulfide minerals exhibit a wide variety of textures. Within the study area, four primary types of mineralization have been defined based on textures and spatial distribution (Werdon, in press):



**Figure 2.** Geologic map of the Drenchwater Creek area. Geology of the Drenchwater and Two Cubs thrust plates from Werdon (in press); geology of the Spike Camp thrust plate from Nokleberg and Winkler (1982). Background water sample along Drenchwater Creek (DW002) is shown for reference.



semimassive, disseminated, layered or diagenetic, and volcanic breccia cement.

Semimassive sulfides crop out along Discovery Creek in hydrothermally recrystallized silica rocks with mottled, diffusely layered, and brecciated textures. The semimassive sulfides are relatively coarser grained, higher in grade, and contain more galena than the disseminated type of mineralization. A bulk sample from this outcrop grades 10.5 percent Zn, 0.9 percent Pb, and 30.2 g/t (gram per metric ton) Ag (Kurtak and others, 1995).

The low-grade disseminated type of mineralization consists of fine-grained sulfide minerals (primarily sphalerite) that are sparsely distributed within bleached and silicified, laminated gray shale and mudstone. This is the most common form of mineralization; it extends laterally for over 3.3 km (Kurtak and others, 1995) and is present within several of the repeated thrust sheets within the Drenchwater thrust plate (Werdon, in press). A bulk sample yielded concentrations of 15.2 percent Zn, 3.2 percent Pb, and 60 g/t Ag (Kurtak and others, 1995).

The layered or diagenetic type of mineralization consists of thin, alternating laminations of sulfides and black carbonaceous shale (Werdon, in press) that are exposed along the banks of Drenchwater Creek. The sulfides are interpreted to have formed by diagenetic growth in metal-enriched unconsolidated muds.

The outcrops of volcanic breccia (fig. 2), located along the east bank of Discovery Creek and further to the south and east, are mineralized and represent the fourth style of mineralization. Within these breccias, clasts are cemented or replaced by quartz, sphalerite, pyrite, galena, and fluorite (Werdon, in press). Silica has variably replaced primary volcanic textures, minerals, clasts, and interclast material.

Overall, the Drenchwater deposit exhibits features of both volcanogenic massive sulfide and sedimentary exhalative deposits (Werdon, in press). Although the spatial association of mineralization with volcanic rocks and alteration patterns centered around intrusions is consistent with volcanogenic massive sulfide models, a sedimentary exhalative model for the formation of the deposit is favored. The lack of copper and stringer-type mineralization, the small percentage of high-temperature alteration minerals (such as illite and white mica), the laterally extensive silicification, and the Ag-Ba-F-Fe-Pb-Zn metal assemblage suggest a dominantly low-temperature basinal fluid source that is characteristic of sedimentary exhalative deposits (Werdon, in press).

## METHODS

### SAMPLE COLLECTION AND FIELD METHODS

Water samples were collected on July 14 and 15, 1994, from Drenchwater and False Wager Creeks and smaller tributaries (fig. 1). During this time, the weather was sunny with an average air temperature of about 40°F. Snowmelt was observed to be above average for this time of year.




At each site, the water temperature was recorded, and the pH and specific conductivity were measured using standard digital meters after adjusting for temperature. Water samples were collected in polyethylene bottles that had been rinsed with 10 percent nitric acid. Three separate samples, each designated for different types of analyses, were obtained: (1) an unfiltered acidified sample for determination of total metal content, (2) a filtered (0.45- $\mu$ m membrane filter) acidified sample for determination of dissolved trace element content, and (3) a filtered unacidified sample for anion analyses. Samples for anion analyses were kept cool until analysis.

### ANALYTICAL METHODS





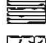
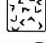



Major and minor element concentrations were determined for filtered acidified and unfiltered acidified water samples by inductively coupled plasma-atomic emission spectroscopy (ICP-AES) and inductively coupled plasma-


### EXPLANATION

#### Rocks and cover materials of Permian and younger age

-  Tundra cover
-  Cretaceous to Permian sedimentary rocks—Sandstone, siltstone, mudstone, and chert with lesser amounts of shale
-  Permian sedimentary rocks—Pyritic siltstone, mudstone, chert, and shale

#### Rocks of Mississippian and Pennsylvanian age

-  Black medium-bedded chert of the Kuna Formation
-  Silicified mudstone and shale of the Kuna Formation
-  Black shale and mudstone of the Kuna Formation
-  Limestone and dolomite
-  Felsic tuff
-  Volcanic breccia
-  Intrusive domes and flows
-  Mafic igneous rocks—Mafic intrusive rocks and mafic tuff
-  Semimassive sulfides

-  Thrust fault—Dashed where approximately located or concealed. Sawtooth on upper plate. Faults shown in black separate major thrust plates. Faults shown in gray are intraplate faults

-  Fault—Dashed where approximately located or concealed

mass spectrometry (ICP-MS) in the laboratories of the USGS, Branch of Geochemistry. The relative standard deviation for the ICP-AES method is 10 percent (Briggs, 1990). The ICP-MS method is semiquantitative but allows for determination of more than 60 elements directly from the water sample without the need for preconcentration or dilution and with detection limits in the sub-part-per-billion range (Meier and others, 1994). The standard deviation may be as high as 25 percent for some elements (A.L. Meier, U.S. Geological Survey, oral commun., 1994).

Anions were determined on the filtered unacidified stream-water sample using ion chromatography (Fishman and Pyen, 1979). The relative standard deviation for this method is about 10 percent.

## RESULTS

Streambed material in most tributaries in the Drenchwater Creek area consists of coarse gravel to small cobbles. Although streamflow measurements were not recorded during this study, streamflow data are available for streams in the western Brooks Range (Dames & Moore, 1983) that are approximately equivalent in slope, drainage-basin area, and stream length to those in the Drenchwater Creek area. Based on data for late spring and summer (Dames & Moore, 1983, p. IV-27), flow rates of Drenchwater and False Wager Creeks are estimated to be between 25 and 125 ft<sup>3</sup>/s; smaller tributaries to these creeks have estimated flow rates of 5 to 35 ft<sup>3</sup>/s for this time of year.

The analytical results for water samples are listed in tables 1–3. Only trace element data from filtered acidified samples are shown and discussed in this paper. These data represent the concentrations of metals dissolved in the water. For graphical purposes throughout this paper, when elements were below the determination limit of the analytical method, those values were replaced by a value equal to 70 percent of the determination limit (Miesch, 1976). This procedure allows illustration of samples with low concentrations without altering data interpretation.

### SIGNATURE ELEMENTS

Previous geochemical studies indicated that stream-sediment samples collected from drainages surrounding the Drenchwater deposit contain anomalous concentrations of Ag, As, Ba, Cd, Cu, Mn, Ni, Pb, Sb, and Zn (Theobald and others, 1978; Kelley and others, 1992). To determine which elements in water samples are indicative of mineralization, a comparison was made between compositions of water collected from Discovery Creek, which drains mineralized areas (the average of samples DW010 and DW027; fig. 1), with water collected from the head-

waters of Drenchwater Creek, about 3 km above the confluence with Discovery Creek (background sample DW002). The background sample reflects primarily the chemistry of black shale, pyritic siltstone, mudstone, and chert; it is upstream from any known mineralized areas. The ratio of selected metal concentrations in Discovery Creek water to those in upper Drenchwater Creek is referred to as the enrichment factor. The results indicate that Discovery Creek is enriched in Al, Fe, Mn, Cd, Co, Cu, Ni, Pb, and Zn (fig. 3). Of these elements, Fe, Mn, Co, Pb, and Zn show the greatest enrichment (19–116 times), whereas Al, Cd, Cu, and Ni are less enriched (4 to 14 times). Enrichment factors of the anions  $\text{SO}_4^{2-}$ ,  $\text{Cl}^-$ , and  $\text{F}^-$  are 4.1, 1.6, and 5.1, respectively (only sample DW010 was used in calculations of the anions because a filtered unacidified sample was not taken at site DW027). Conductivity, which shows strong positive correlation with  $\text{SO}_4^{2-}$  concentration, is 2.3 times greater in water from Discovery Creek relative to upper Drenchwater Creek water. The pH values are lower in Discovery Creek (Table 1), indicating an increase in acidity relative to upper Drenchwater Creek. Other elements identified by Kelley and others (1992) as anomalous in stream-sediment samples draining the Drenchwater deposit (Ag, As, and Sb) were either not determined or were below the lower limit of determination in water samples from Discovery and Drenchwater Creeks.

### DRENCHWATER CREEK

To determine the extent of natural metal contamination from the Drenchwater deposit, water samples were collected from Drenchwater and False Wager Creeks, both upstream and downstream from areas of known mineralization. The data from Drenchwater Creek indicate that water samples collected downstream of the confluence with Discovery Creek tend to have lower pH, higher conductivity, and are enriched in Al, Fe, Mn, Cd, Co, Cu, Pb, and Zn relative to upper Drenchwater Creek (table 2, fig. 4). Many metals such as Cd, Co, Fe, and Zn are still enriched by a factor of 2–57 times in samples as far as 1.7 km downstream of the confluence. However, other metals, including Cu and Pb, are close to background levels in samples collected 0.4 to 1.7 km downstream (fig. 4). Similarly, the pH values are near-neutral to neutral within 0.4 km of the confluence.

### FALSE WAGER CREEK

Except for samples from three tributaries draining into False Wager Creek near the center of the study area (DW022, DW023, and DW025; fig. 1), water samples collected from False Wager Creek are highly acidic, with

**Table 1.** Temperature, conductivity, and pH values of water samples from the Drenchwater Creek area

Sample No.	Latitude	Longitude	Temperature (°C)	pH	Conductivity (µS/cm)
DW001	68 33 30	158 44 49	2	6.7	128
DW002	68 33 32	158 45 03	6	7.2	56
DW003	68 33 43	158 44 45	2	6.8	51
DW004	68 33 45	158 44 26	2	6.7	63
DW005	68 33 57	158 44 16	2	6.7	38
DW006	68 34 35	158 42 56	5	5.7	104
DW007	68 34 35	158 43 03	9	7.0	78
DW009	68 34 43	158 42 51	5	5.6	129
DW010	68 34 48	158 41 56	3	4.3	129
DW011	68 34 51	158 41 54	3	4.3	128
DW012	68 34 51	158 41 54	10	6.5	91
DW013	68 34 51	158 41 54	6	5.3	100
DW014	68 34 52	158 41 50	5	4.9	108
DW015	68 34 53	158 41 48	7	5.6	97
DW016	68 34 57	158 41 24	10	6.5	91
DW017	68 33 03	158 42 17	4	2.8	2,150
DW018	68 33 03	158 42 07	3	3.1	1,410
DW019	68 35 25	158 39 45	6	7.2	74
DW020	68 35 22	158 39 44	9	6.7	92
DW021	68 34 58	158 38 22	10	3.2	979
DW022	68 33 33	158 40 54	6	7.0	127
DW023	68 33 51	158 40 17	12	6.5	144
DW024	68 33 51	158 40 26	8	3.1	1,269
DW025	68 33 51	158 40 33	13	6.6	96
DW026	68 33 48	158 40 34	8	3.1	1,242
DW027	68 34 48	158 41 56	3	4.2	128

pH values of less than 3.2 over the entire 4.5-km distance sampled; they also contain elevated concentrations of all signature elements identified in the Drenchwater Creek drainage basin. Concentrations of Al, Fe, Mn, Cd, Co, Cu, Ni, Pb, and Zn in samples from False Wager Creek are high (table 2). The chemistry of the False Wager Creek water samples is best illustrated on a plot of pH versus total metal content (fig. 5), which clearly shows the higher acidity and metal contents of False Wager Creek relative to either lower Drenchwater Creek or Discovery Creek.

The  $\text{SO}_4^{2-}$  concentrations in False Wager Creek, which range from 480 to 1,180 ppm (table 3), are 10 to 24 times greater than the concentrations in Discovery Creek. Elements such as antimony and arsenic that were below detection limits in most water samples from Discovery and Drenchwater Creeks have high concentrations in False Wager Creek; concentrations of antimony range from 0.1 to 0.3 ppb, and arsenic concentrations are 4 to 26 ppb (table 2).

Interestingly, even water samples collected from the headwaters of False Wager Creek (DW017 and DW018; fig. 1) exhibit natural contamination. These samples are 2 km upstream from known mineralized areas (fig. 1). The pH values are extremely low (2.8–3.1) and the sum of dissolved metal contents (Cd+Co+Cu+Ni+Pb+Zn) are high (2,200 to 2,600 ppb). At locality DW017, a hard, bright-orange ferricrete layer covers the bottom of the stream, and cements the stream pebbles and cobbles. Analyses by x-ray diffraction revealed that most of this material is crystalline jarosite [ $\text{KFe}_3(\text{SO}_4)_2(\text{OH})_6$ ], with variable amounts of quartz, kaolinite, and amorphous iron oxides (S.J. Sutley, U.S. Geological Survey, written commun., 1994). Similar orange-yellow claylike material was collected from the stream bank on the north side of DW018. Jarosite, quartz, and minor amounts of amorphous iron oxides were the primary minerals identified in this sample. Both of these iron oxide samples contain low concentrations of base metals (K.D. Kelley, unpublished data).

**Table 2.** Geochemical data for filtered acidified water samples from the Drenchwater Creek area

[FA, filtered (0.45-µm membrane filter) acidified, Al, Fe, Mg, and Na in parts per million (ppm); all other values in parts per billion (ppb), \*, analyses by inductively coupled plasma-atomic emission spectrography (ICP-AES); all other analyses by inductively coupled plasma-mass spectrometry (ICP-MS)]

Sample No.	Al*	Fe*	Mg*	Mn*	Na*	As	Ba	Cd	Co	Cu	Ni	Pb	Sb	Zn
DW001FA	0.1	0.4	3	320	0.5	<0.9	27	< 2	3	3	36	< 0.3	< 0.1	88
DW002FA	< .1	< .06	1	14	.4	< .9	39	< 2	.2	< .9	4	< .3	< .1	12
DW003FA	< .1	< .06	2	3	.4	< .9	31	< 2	< .1	1	< 4	< .3	< .1	12
DW004FA	< .1	.09	2	10	.6	< .9	38	< 2	< .1	< .9	5	< .3	< .1	12
DW005FA	< .1	.07	1	3	.5	< .9	44	< 2	< .1	1	< 4	< .3	< .1	5
DW006FA	.2	.2	3	120	.4	< .9	48	< 2	.7	2	10	4	< .1	67
DW007FA	< .1	.3	2	65	.4	< .9	39	< 2	.9	2	10	< .3	< .1	73
DW009FA	.6	.1	3	220	.5	< .9	38	< 2	2	14	15	4	< .1	150
DW010FA	1	3	1	480	.1	< .9	32	6	6	7	22	5	< .1	1,400
DW011FA	1	3	1	490	.1	< .9	32	5	6	8	25	5	< .1	1,400
DW012FA	.1	2	2	170	.4	< .9	40	< 2	3	2	16	.4	< .1	380
DW013FA	.7	2	2	390	.3	< .9	35	4	6	6	27	3	< .1	1,100
DW014FA	.7	2	1	400	.2	< .9	35	4	5	5	22	3	< .1	1,000
DW015FA	.5	2	2	380	.3	< .9	36	4	6	7	27	2	< .1	1,000
DW016FA	< .1	1	2	240	.4	< .9	38	2	3	2	23	< .3	< .1	580
DW017FA	53	270	5	2,200	1	26	21	6	48	260	290	9	.3	2,000
DW018FA	95	150	3	1,100	3	4	23	5	47	67	180	10	< .1	1,900
DW019FA	< .1	.09	2	7	.2	< .9	34	< 2	< .1	.9	< 4	< .3	< .1	16
DW020FA	< .1	2	2	220	.4	< .9	36	3	4	2	27	< .3	< .1	690
DW021FA	31	87	8	3,400	2	5	32	8	44	120	250	3	< .1	2,600
DW022FA	< .1	< .06	5	5	2	< .9	51	< 2	< .1	< .9	< 4	< .3	< .1	3
DW023FA	< .1	.9	6	760	1	< .9	44	< 2	13	2	100	< .3	< .1	290
DW024FA	44	130	7	2,900	2	8	29	6	48	140	230	4	.1	2,000
DW025FA	< .1	.09	1	84	.2	< .9	65	< 2	.2	< .9	< 4	< .3	< .1	4
DW026FA	43	130	7	2,700	2	7	30	6	43	130	210	4	.1	1,900
DW027FA	1	3	1	430	0.1	< .9	31	5	6	8	24	4	< .1	1,400



**Table 3.** Geochemical data for filtered unacidified water samples from the Drenchwater Creek area[FU, filtered (0.45- $\mu$ m membrane filter) unacidified; all values in parts per million (ppm); filtered unacidified sample was not taken at site DW027]

Sample No.	F <sup>-</sup>	Cl <sup>-</sup>	SO <sub>4</sub> <sup>2-</sup>	NO <sub>3</sub> <sup>-</sup>
DW001FU	0.08	0.12	49	< 0.2
DW002FU	< .05	< .10	12	< .2
DW003FU	< .05	.13	16	< .2
DW004FU	.06	.11	22	< .2
DW005FU	< .05	< .10	12	< .2
DW006FU	.07	.10	43	< .2
DW007FU	.09	.11	24	< .2
DW009FU	.14	< .10	54	.4
DW010FU	.18	.11	49	< .2
DW011FU	.18	.11	47	< .2
DW012FU	.14	< .10	31	< .2
DW013FU	.15	< .10	41	< .2
DW014FU	.16	.14	40	< .2
DW015FU	.16	< .10	37	< .2
DW016FU	.14	< .10	32	< .2
DW017FU	.52	< .4	1,180	< .2
DW018FU	.55	1.0	964	< .2
DW019FU	< .05	.12	18	< .2
DW020FU	.14	< .10	32	< .2
DW021FU	.28	.13	480	< .2
DW022FU	< .05	< .10	46	< .2
DW023FU	.10	< .10	57	< .2
DW024FU	.52	.27	629	< .2
DW025FU	.16	< .10	19	< .2
DW026FU	.49	.29	610	< .2

## DISCUSSION

The data from Discovery and Drenchwater Creeks clearly show that weathering of the undisturbed (undeveloped or unmined) Drenchwater deposit has resulted in natural metal contamination of streams draining the deposit. Typically, these waters have an average pH of about 5 and a sum of dissolved metal content of 1,000 ppb (fig. 5). Waters from False Wager Creek are relatively more acidic and metal rich than either Discovery Creek or lower Drenchwater Creek. The source of some of the metals observed in the lower stretches of False Wager Creek (DW021) may also be from weathering of mineralized rocks. Disseminated sulfide minerals occur in a southeast-trending zone west of False Wager Creek near the center of the study area, and massive sulfide float was reported in frost boils (Kurtak and others, 1995) between a small tributary (sample DW023) and the main drainage of False Wager Creek (sample DW026; fig. 1). The acidic, metal-rich waters at the headwaters of False Wager Creek

are not as easily explained. Many of the shale and chert samples observed in float along upper False Wager Creek contain variable amounts of disseminated pyrite. In addition, black chert with iron stains derived from weathering of sulfide minerals is prominent in a few zones at the headwaters of False Wager Creek, upstream from samples DW017 and DW018 (Nokleberg and Winkler, 1982). Sulfide minerals other than pyrite were not observed, and most of the iron-stained cherts contain low concentrations of Ag (2-7 ppm), Pb (15-150 ppm), and Zn (<200 ppm) (Nokleberg and Winkler, 1982), indicating that sulfide minerals such as galena and sphalerite are not common in these zones. In addition, stream-sediment and heavy-mineral-concentrate samples collected from the headwaters of False Wager Creek and Wager Creek to the east do not contain anomalous concentrations of base metals. Although the presence of metal-rich, low-pH waters from upper False Wager Creek suggests possible undiscovered base-metal mineralization, it is also possible that abundant accumulations of pyrite, without accompa-

nying base-metal sulfide minerals, have produced the acidic,  $\text{SO}_4^{2-}$  and metal-rich waters that have contaminated upper False Wager Creek.

False Wager Creek water remains acidic over a distance of 4.5 km, even though water with near-neutral pH (6.5–7.0; samples DW022, DW023, DW025) flows into the creek near the central part of the basin. This indicates that (1) the source of the acidic water at the headwaters of False Wager Creek is not present in the central part of the basin, and (2) the low-pH water (3.2) collected from False Wager Creek near the confluence with Drenchwater Creek is due largely to the acidic water originating near the headwaters, 4.5 km upstream. Carbonate rocks, which typically buffer the acidity towards neutral pH and reduce the metal content of water (Plumlee and others, 1993), are notably absent in the False Wager Creek basin (fig. 2); this may have allowed the low-pH waters to remain acidic for distances downstream of 4.5 km or more.

If abundant pyrite is the source of acidic, metal-rich water in False Wager Creek, then it is unclear why the waters that drain the immediate area of the Drenchwater deposit are not more acidic. The deposit contains abundant pyrite, and, like the upper False Wager Creek area, there are surrounding zones of chert that are iron-stained

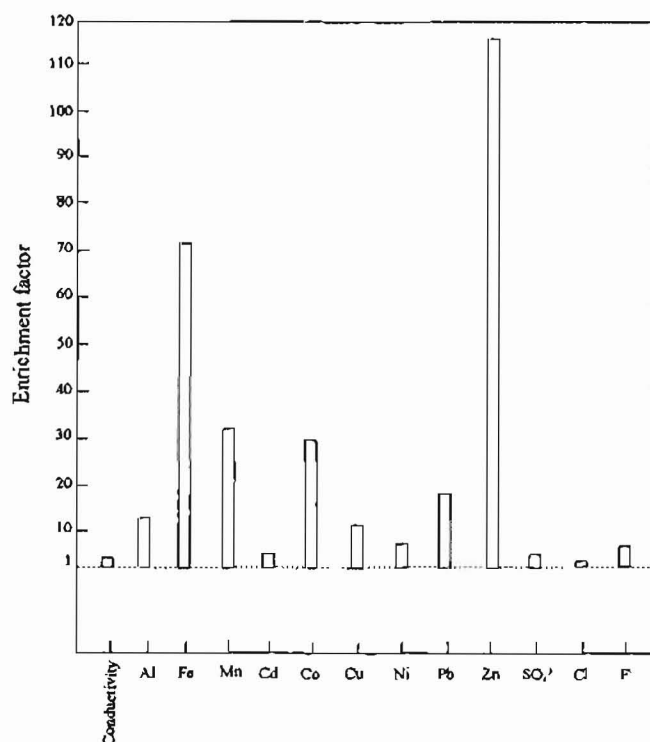
from weathering of pyrite (Nokleberg and Winkler, 1982). Furthermore, there are no carbonate rocks exposed along Discovery Creek (fig. 2), although there are abundant carbonate alteration minerals associated with the deposit (Weldon, in press). Reactions with these carbonate minerals may help reduce the acidity of Discovery Creek water and may explain the relative difference in acidity between Discovery Creek (pH of 4.3) and False Wager Creek (pH of 2.8 to 3.2).

### COMPARISON TO THE RED DOG AND LIK DEPOSITS

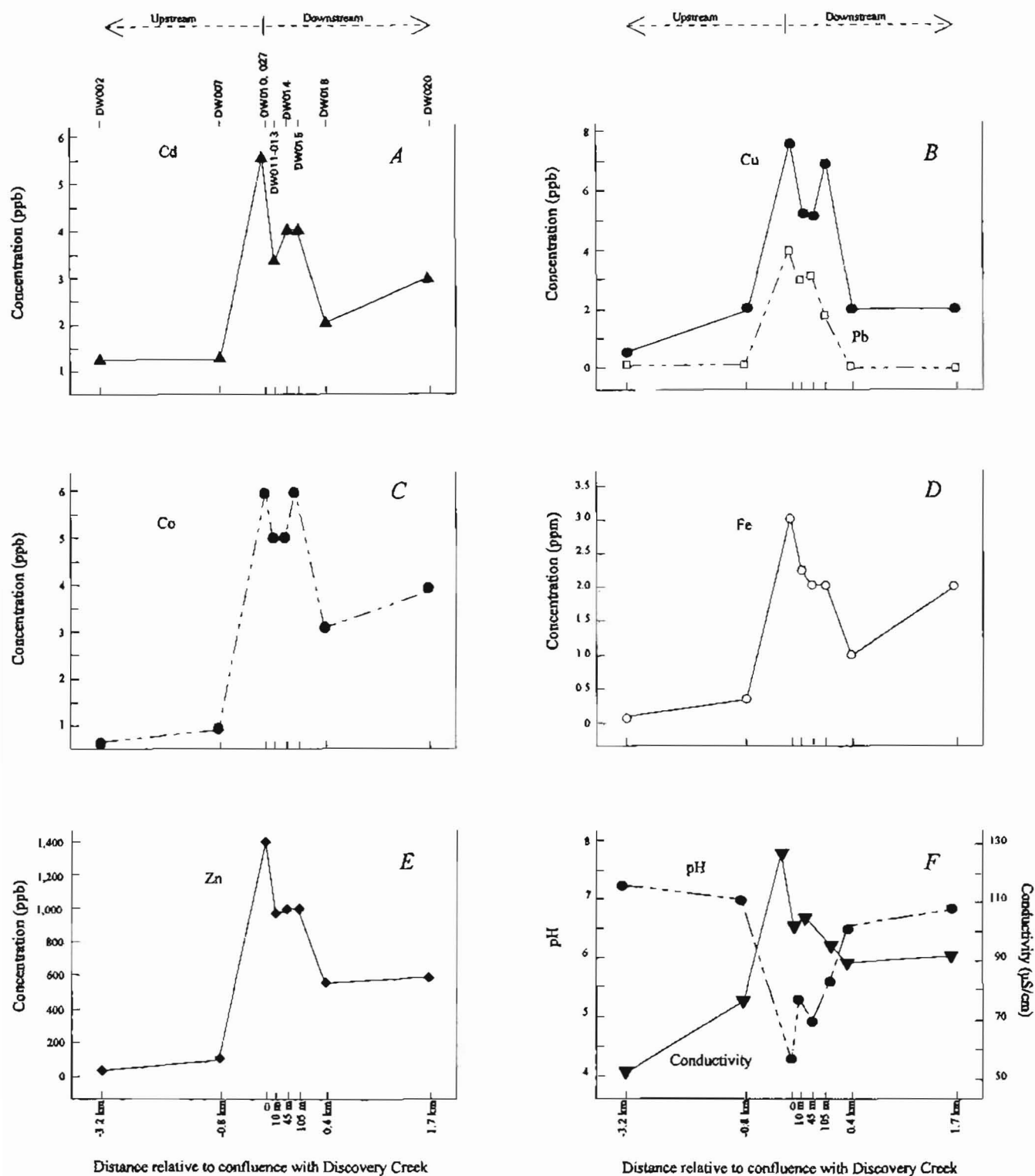
To evaluate the significance of the results from the Drenchwater Creek area, we compared our results with water chemistry from the Red Dog and Lik deposits in the western Brooks Range. All three deposits occur in similar geologic settings, contain similar types and styles of mineralization, and are hosted by rocks of similar age and composition. The only major differences likely to affect water chemistry are the relative size and extent of exposure of the deposits at the surface, the presence of carbonate rocks in the section, and the proportion of pyrite in the ore.

The Red Dog deposit contains announced geologic reserves of 85 million tonnes of 17 percent zinc, 5 percent lead, and 82 g/t silver (Moore and others, 1986; Koehler and Tikkanen, 1991). Recent exploration drilling has delineated an additional zone of zinc-lead mineralization 450 m north of the current open pit mine (Kilburn, 1995). Preliminary estimates show that the new extension could contain at least 73 million tonnes of 14 percent zinc and 3 percent lead (Anchorage Daily News, September 15, 1995). The deposit is hosted by black siliceous shale and chert. Other than thin beds of limestone that are interlayered with sequences of shale, siltstone, and mudstone, carbonate rocks are absent in the immediate deposit area (Moore and others, 1986). Most mineralization at Red Dog is massive, chaotic, or fragmentally textured. Major sulfides in decreasing order of abundance are sphalerite, pyrite, marcasite, and galena (Moore and others, 1986). Pyrite-rich zones are uncommon and small (<10 m × <100 m; Schmidt and Zierenberg, 1988). The Red Dog deposit was discovered because it was exposed at the surface, and streams in the area are red owing to precipitation of iron oxide derived from the leaching and weathering of sulfides. Mining began in 1990 and has continued to the present.

A two-year baseline study was conducted prior to mining at Red Dog that included seasonal water-quality data from Red Dog Creek and surrounding tributaries and rivers (Dames & Moore, 1983; Runnels and others, 1992). The data reveal natural contamination of stream and



**Figure 3.** Enrichment factors for water samples. Enrichment factor defined as ratio of Discovery Creek samples (mineralized drainage) to Drenchwater Creek sample upstream from confluence with Discovery Creek (background drainage).

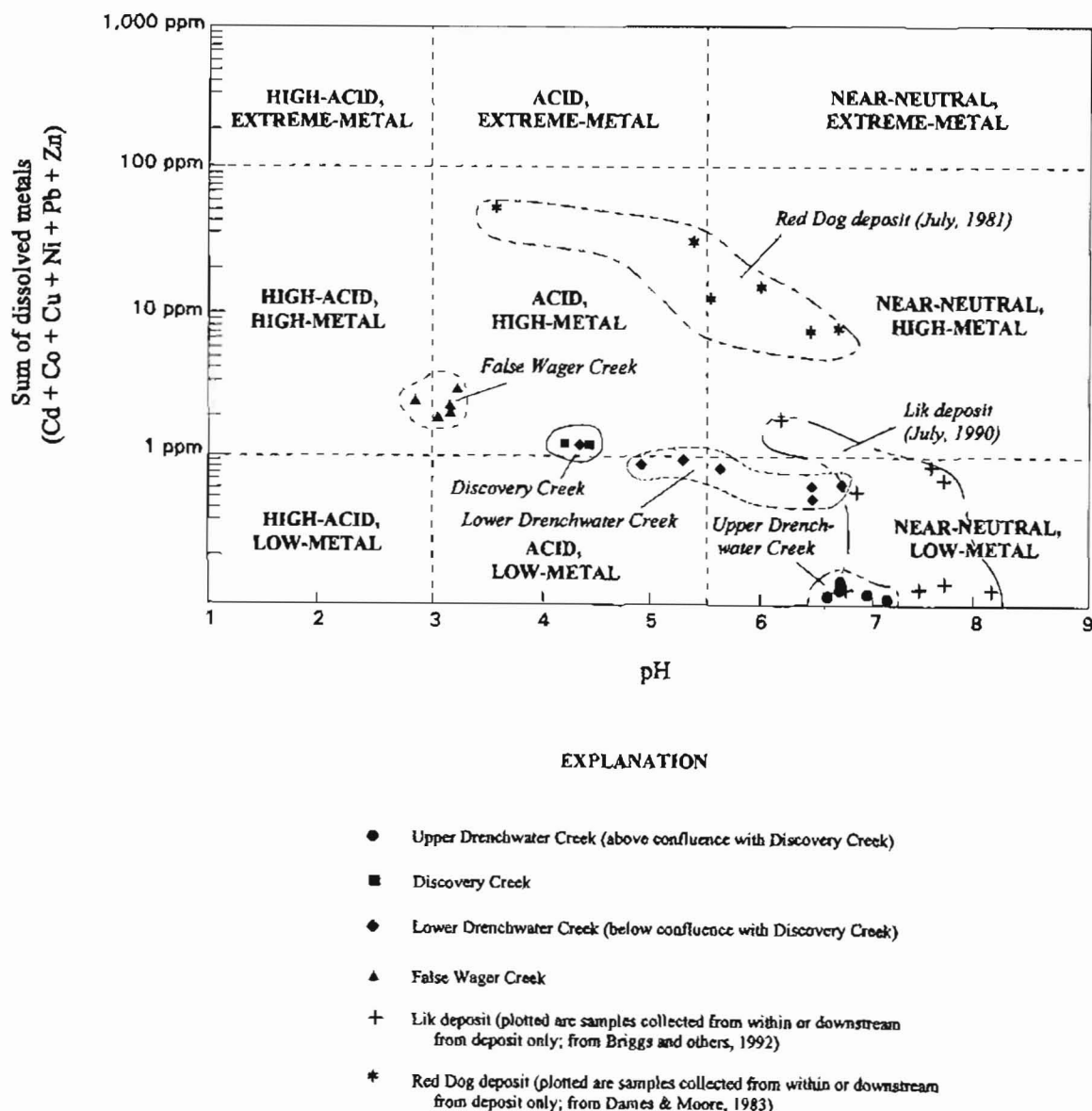


**Figure 4.** Concentrations of (A) Cd, (B) Cu and Pb, (C) Co, (D) Fe, (E) Zn, and (F) pH and conductivity in Drenchwater Creek water samples. Iron concentrations are in parts per million (ppm); all other concentrations in parts per billion (ppb). Concentrations of elements in two samples from Discovery Creek (DW010 and DW027) were averaged, as were three samples collected 10 m downstream from confluence with Discovery Creek (DW011-013).

groundwaters by leaching of metals from the nondisturbed orebody. Waters collected from streams draining the deposit during late spring and summer of 1981 (that is, the same time of year as this study) had reported pH values as low as 3.5 and lead, zinc, and cadmium concentrations of 2,100 ppb, 40,400 ppb, and 396 ppb, respectively (Dames & Moore, 1983). Concentrations of lead, zinc, and cadmium reportedly were even greater in waters collected during other times of the year, with maximum con-

centrations reaching 2,250 ppb Pb, 272,000 ppb Zn, and 800 ppb Cd (Runnells and others, 1992). The higher metal concentrations in water from Red Dog Creek relative to Drenchwater and Discovery Creeks is probably due to the relatively greater extent of surface exposure of the Red Dog deposit and (or) the higher grade of mineralization.

The Lik deposit, which has not been mined but has been extensively drilled, contains reserves of at least 21.77



**Figure 5.** Diagram adapted from Plumlee and others (1993) showing the relation between pH and metal content of water samples from the Drenchwater Creek area. Water samples from the Lik and Red Dog (premining) deposits also shown for comparison. All three deposits are hosted dominantly by black shale and chert; however, carbonate rocks exposed near the Lik deposit buffer the acidity and metal-carrying capacity of the waters. The high metal contents in waters from the Red Dog deposit relative to either Drenchwater or Lik may be explained by the greater extent of surface exposure of the Red Dog deposit and (or) the higher grade of mineralization.

million tonnes grading 9 percent Zn, 3.1 percent Pb, and 48 g/t Ag (Bundtzen and others, 1994). Black shale and chert are the primary host rocks for the deposit. A thick section of Mississippian carbonate platform rocks crops out immediately upstream from the surface expression of the orebody (Sable and Dutro, 1961; Mayfield and others, 1990). Where exposed at the surface or within 45 m of the surface, the mineralized body at Lik is about 15-20 m wide. It strikes northeast and dips steeply to the northwest. Within the deposit are zones of complex and brecciated textures, in addition to laminar and nodular sulfides (Forrest, 1983). Intervals of black shale and chert are commonly interlayered with mineralized zones. Sulfide minerals present are sphalerite, galena, pyrite, and marcasite.

Water samples were collected by the USGS (K.D. Kelley, E.A. Bailey, and B.A. Cieutat) in July 1991 from streams draining the Lik deposit. The compositions of these water samples (Briggs and others, 1992) differ from those collected near the Drenchwater deposit, particularly in the pH of the water and in the concentrations of most metals (table 4; fig. 5). The Lik stream-water samples are near-neutral to neutral, with a minimum pH of 6.2 in water downstream from the deposit (table 4). Most water samples contain relatively low total metal contents (fig. 5). Only one sample collected from a small tributary draining the deposit contained concentrations of Cd (5 ppb), Ni (51 ppb), and Zn (2,000 ppb) that are comparable to levels detected in lower Drenchwater and Discovery Creeks. The only metal that showed a consistently high concentration in water samples below the deposit was zinc, which ranged from 380 to 2,000 ppb. These data show that even in water with neutral pH, natural concentrations of metals, particularly zinc, can exceed nonmineralized background values. Other studies of nonacidic waters adjacent to ore deposits yield similar results (Runnells and others, 1992; Plumlee and others, 1993).

Differences in water chemistry between the Drenchwater and Lik deposits may be attributed to the presence of carbonate rocks in the headwaters of most creeks that drain the Lik deposit; carbonate minerals such as calcite consume acid and can reduce the acidity and concentrations of some metals.

## CONCLUSIONS

The data show that the undisturbed Drenchwater deposit is the source of natural contamination in Discovery Creek and lower Drenchwater Creek. The pH values of water from these creeks are low (as low as 4.2), and metals that are enriched in these waters relative to upper Drenchwater Creek include Al, Fe, Mn, Cd, Co, Cu, Ni, Pb, and Zn.

The headwaters of False Wager Creek exhibit greatly elevated metal concentrations relative to Discovery Creek. These waters are highly acidic (pH values as low as 2.8) and contain high values of base metals and sulfate. The source of these acidic waters is either (1) base-metal mineral occurrences similar to the Drenchwater deposit that have not yet been recognized or are not exposed, or (2) pyritic rocks without associated base-metal sulfides. If the source is abundant pyrite, it serves as an example of the extreme acid-generating nature of pyritic rocks in the absence of carbonate rocks or other buffers.

A comparison of the stream-water data from the Drenchwater deposit with data from the Red Dog and Lik deposits shows some interesting similarities and contrasts. Many of the metals that are enriched in waters draining the Drenchwater deposit are also enriched in Red Dog Creek water, but concentrations of metals are many times higher in the latter. This is likely a result of a higher grade of mineralization and a greater extent of exposure of sulfide minerals at the surface at Red Dog relative to Drenchwater Creek. In the case of Lik, concentrations of all metals except zinc are decreased relative to the Red Dog and Drenchwater deposits owing to the presence of carbonate rocks, which buffer the acidity and metal-carrying capacity of stream water.

The knowledge of natural background concentrations and extent of natural metal contamination in water from the Drenchwater deposit area may be useful for devising realistic plans for remediation and monitoring programs. For example, it may not be technically possible to remediate water to standards that are lower than local natural background concentrations. In addition, the comparison of the data from natural waters draining the Drenchwater, Lik, and Red Dog deposits contributes to the development of a model that characterizes the environmental behavior of sedimentary exhalative deposits. Data from deposits in other physiographic settings are required in order to complete such a geoenvironmental model.

*Acknowledgments.*—We thank the Bureau of Land Management (BLM) for access to the Drenchwater Creek area and for permission to camp at the Ivotuk airstrip. Mike Kunz, an archaeologist with the BLM who had a camp within 6 miles of ours, helped with logistics of camp and helicopter work. We gratefully acknowledge the efforts of Dave Taylor, who served as a volunteer from the USGS Volunteer for Science Program; Dave was our cook and camp manager, as well as field assistant. Jeanine Schmidt (Branch of Alaskan Geology, USGS) helped with some of the water sampling. The chemists who provided analyses include Al Meier and Molly Malcolm (ICP-MS), Paul Briggs (ICP-AES), Bill d'Angelo (ion chromatography), and Steve Sutley (XRD). Steve Wilson helped the senior author run some preliminary  $\text{SO}_4^{2-}$  analyses on water samples. Discussions with Bill

**Table 4.** Maximum concentrations and minimum pH for filtered stream-water samples from the Drenchwater deposit area compared with data from the Red Dog and Lik deposits, western Brooks Range

[ND, no data available; \*, data from one site only; data for Lik deposit from Briggs and others (1992); data for Red Dog deposit from Dames &amp; Moore (1983)]

Deposit	Number of samples	pH	Cd ppb	Co ppb	Cu ppb	Ni ppb	Pb ppb	Zn ppb
<b>Upgradient of the deposit</b>								
Lik	6	7.5	< 1	< 3	< 10	< 5	< 10	12
Red Dog	2	6.5	3	ND	ND	ND	9.2	190
Upper Drenchwater Creek	5	6.7	< 2	3	3.1	< 4	< .3	88
Upper False Wager Creek	3	2.8	6	48	260	290	10	2,000
<b>Within or downstream from the deposit</b>								
Lik	7	6.2	5	< 3	< 10	51	< 10	2,000
Red Dog	6	3.5	396	< 7*	11*	< 5*	2,100	40,400
Lower Drenchwater Creek	7	4.2	6	6	8	27	5	1,400
Lower False Wager Creek	2	3.2	8	44	120	250	4	2,600

d'Angelo and Steve Wilson about water chemistry helped in our interpretation. Prior to field work, discussions with Kathy Smith and Geoff Plumlee greatly helped in determining needed field sampling equipment and methods for sampling.

## REFERENCES CITED

- Briggs, P.H., 1990, Elemental analysis of geological material by inductively coupled plasma-atomic emission spectrometry, in Arbogast, B.F., ed., *Quality assurance manual for the Branch of Geochemistry*, U.S. Geological Survey: U.S. Geological Survey Open-File Report 90-668, p. 83-91.
- Briggs, P.H., Motooka, J.M., Bailey, E.A., Cieutat, B.A., Burner, S.A., Kelley, K.D., and Ficklin, W.H., 1992, Analytical results of soil, stream sediment, panned concentrate, and water samples from the Lik deposit, northwestern Brooks Range, Alaska: U.S. Geological Survey Open-File Report 92-15A (paper version) and 92-15B (diskette version).
- Bundtzen, T.K., Swainbank, R.C., Clough, A.H., Henning, M.W., and Hansen, E.W., 1994, Alaska's mineral industry 1993: Alaska Division of Geological and Geophysical Surveys Special Report 48, 84 p.
- Churkin, Michael, Jr., Mayfield, C.F., Theobald, P.K., Barton, H.N., Nokleberg, W.J., Winkler, G.R., and Huie, C., 1978, *Geological and geochemical appraisal of metallic mineral resources, southern National Petroleum Reserve in Alaska*: U.S. Geological Survey Open-File Report 78-70A, 82 p.
- Dames & Moore, 1983, *Environmental baseline studies, Red Dog project: Water Quality Report*, chapt. 3, prepared by L.A. Peterson and Associates, Inc., for the Red Dog Mine Project, Cominco, Alaska, Inc., Anchorage, Alaska.
- Dumoulin, J.A., Harris, A.G., and Schmidt, J.M., 1993, Deep-water lithofacies and conodont faunas of the Lisburne Group, west-central Brooks Range, Alaska, in Dusel-Bacon, Cynthia, and Till, A.B., eds., *Geological Studies in Alaska by the U.S. Geological Survey, 1992: U.S. Geological Survey Bulletin 2068*, p. 12-30.
- Ellersieck, Inyo, Curtis, S.M., Mayfield, C.F., and Tailleur, I.L., 1990, Reconnaissance geologic map of the Delong Mountains A-2 and B-2 quadrangles and part of the C-2 quadrangle, Alaska: U.S. Geological Survey Miscellaneous Investigations Series Map I-1931, 2 sheets, 1:63,360.
- Fishman, M.J., and Pyen, Grace., 1979, Determination of selected anions in water by ion chromatography: U.S. Geological Survey Water-Resources Investigations 79-101, 30 p.
- Forrest, Kimball, 1983, *Geologic and isotopic studies of the Lik deposit and the surrounding mineral district, DeLong Mountains, western Brooks Range, Alaska*: Minneapolis, University of Minnesota, Ph.D. dissertation, 161 p.
- Forrest, Kimball, and Sawkins, F.J., 1987, Geologic setting and mineralization of the Lik deposit: implications for the tectonic history of the western Brooks Range, in Tailleur, I.L., and Weimer, Paul, eds., *Alaskan North Slope geology: Society of Economic Paleontologists and Mineralogists Field Trip Guidebook 50*, p. 295-305.
- Jansons, Uldis, 1982, Zinc-lead occurrences in and near the National Petroleum Reserve in Alaska: U.S. Bureau of Mines Mineral Lands Assessment Report MLA 121-82, 55 p.
- Jansons, Uldis, and Baggs, D.W., 1980, Mineral investigations of the Misheguk Mountain and Howard Pass quadrangles, Alaska: U.S. Bureau of Mines Open-File Report 38-80, 76 p.
- Jansons, Uldis, and Parke, M.A., 1981, 1978 mineral investigations in the Misheguk Mountain and Howard Pass quadrangles, Alaska: U.S. Bureau of Mines Open-File Report 26-81, 195 p.
- Kelley, K.D., Borden, J.C., Bailey, E.A., Fey, D.L., Motooka, J.M., and Roushey, B., 1992, Geochemically anomalous areas in the west-central part of the Howard Pass Quadrangle, National Petroleum Reserve, Brooks Range,



- Alaska—evidence for sediment-hosted Zn-Pb-Ag-Ba mineralization, in Bradley, D.C. and Dusel-Bacon, Cynthia, eds., *Geologic studies in Alaska by the U.S. Geological Survey*, 1991: U.S. Geological Survey Bulletin 2041, p. 60–69.
- Kilburn, John, 1995, Cominco strikes new zone at Red Dog: *The Northern Miner*, v. 81, no. 23, p. 1.
- Koehler, G.F., and Tikkanen, G.D., 1991, Red Dog, Alaska: discovery and definition of a major zinc-lead-silver deposit, in Hutchinson, R.W., and Grauch, R.I., eds., *Historical perspectives of genetic concepts and case histories of famous discoveries: Economic Geology Monograph 8*, p. 268–274.
- Kurtak, J.M., Hicks, R.W., Weldon, M.B., Meyer, M.P., and Mull, C.G., 1995, Mineral investigations in the Colville Mining District and Southern National Petroleum Reserve in Alaska: U.S. Bureau of Mines Open-File Report 8-95, 217 p.
- Mayfield, C.F., Curtis, S.M., Ellersieck, Inyo, and TAILLEUR, I.L., 1990, *Reconnaissance geologic map of the DeLong Mountains A-3 and B-3 quadrangles and parts of the A-4 and B-4 quadrangles, Alaska*: U.S. Geological Survey Miscellaneous Investigations Series Map I-1929, 2 sheets, scale 1:63,360.
- Meier, A.L., Grimes, D.J., and Ficklin, W.H., 1994, Inductively coupled plasma mass spectrometry—a powerful analytical tool for mineral resource and environmental studies [abs.], in Carter, L.M.H., Toth, M.I., and Day, W.C., eds., *USGS research on mineral resources—1994, Part A—Program and Abstracts, Ninth V.E. McKelvey Forum on Mineral and Energy Resources*, 9th, Tucson, Ariz., February 22–25, 1993: U.S. Geological Survey Circular 1103-A, p. 67–68.
- Metz, P.A., Robinson, M.S., and Lueck, Larry, 1979, Baseline geochemical studies for resource evaluation of lands—geophysical and geochemical investigations of the Red Dog and Drenchwater Creek mineral occurrences: Juneau, Alaska, U.S. Bureau of Mines, Alaska Field Operations Center report under Grant G0177176, 21 p.
- Meyer, M.P., and Kurtak, J.M., 1992, Results of the 1991 U.S. Bureau of Mines Colville Mining District Study: U.S. Bureau of Mines Open-File Report 75-92, 101 p.
- Miesch, A.T., 1976, Geochemical survey of Missouri—methods of sampling, laboratory analysis, and statistical reduction of data: U.S. Geological Survey Professional Paper 954-A, 39 p.
- Moore, D.W., Young, L.E., Modene, J.S., and Plahuta, J.T., 1986, Geologic setting and genesis of the Red Dog zinc-lead-silver deposit, western Brooks Range, Alaska: *Economic Geology*, v. 81, no. 7, p. 1696–1727.
- Mull, C.G., TAILLEUR, I.L., Mayfield, C.F., Ellersieck, Inyo, and Curtis, S., 1982, New upper Paleozoic and lower Mesozoic stratigraphic units, central and western Brooks Range, Alaska: *American Association of Petroleum Geologists Bulletin*, v. 66, no. 3, p. 348–362.
- Nokleberg, W.J., and Winkler, G.R., 1982, Stratiform zinc-lead deposits in the Drenchwater Creek area, Howard Pass quadrangle, northwestern Brooks Range, Alaska: U.S. Geological Survey Professional Paper 1209, 22 p.
- Patton, W.W., Jr., and TAILLEUR, I.L., 1964, Geology of the upper Killik-Iktiklik region, Alaska: U.S. Geological Survey Professional Paper 303-G, p. 409–499.
- Plumlee, G.S., Smith, K.S., and Ficklin, W.H., 1994, Geoenvironmental models of mineral deposits, and geology-based mineral-environmental assessments of public lands: U.S. Geological Survey Open-File Report 94-203, 7 p.
- Plumlee, G.S., Smith, S.M., Toth, M.I., and Marsh, S.P., 1993, Integrated mineral-resource and mineral-environmental assessments of public lands: applications for land management and resource planning: U.S. Geological Survey Open-File Report 93-571, 15 p.
- Runnells, D.D., Shepherd, T.A., and Angino, E.E., 1992, Metals in water—determining natural background concentrations in mineralized areas: *Environmental Science and Technology*, v. 26, p. 2316–2323.
- Sable, E.G., and Dutro, J.T., 1961, New Devonian and Mississippian formations in the DeLong Mountains, northern Alaska: *American Association of Petrology Bulletin*, v. 45, no. 5, p. 585–596.
- Schmidt, J.M., and Zierenberg, R.A., 1988, Lateral variations of ore, and reconstruction of the Red Dog Zn-Pb-Ag deposit, Noatak District, Alaska [abs.]: *Geological Society of America Abstracts with Program*, v. 20, no. 7, p. A–37.
- Smith, K.S., Plumlee, G.S., and Ficklin, W.H., 1994, Predicting water contamination from metal mines and mining wastes—notes from a workshop presented at the International Land Reclamation and Mine Drainage Conference, and the Third International Conference on the Abatement of Acidic Drainage, Pittsburgh, Pennsylvania, April 24, 1994: U.S. Geological Survey Open-File Report 94-264, 112 p.
- TAILLEUR, I.L., 1970, Lead-, zinc-, and barite-bearing samples from the western Brooks Range, Alaska, with a section on petrography and mineralogy, by G.D. Eberlein and Ray Wehr: U.S. Geological Survey Open-File Report 70-319, 16 p.
- TAILLEUR, I.L., Ellersieck, I.F., and Mayfield, C.F., 1977, Mineral resources of the western Brooks Range, in Blean, K.M., ed., *The United States Geological Survey in Alaska: Accomplishments during 1976*: U.S. Geological Survey Circular 751-B, p. B24–B25.
- TAILLEUR, I.L., Kent, B.H., Jr., and Reiser, H.N., 1966, Outcrop geologic maps of the Nuka-Etiviluk region, northern Alaska: U.S. Geological Survey Open-File Report 66-128, scale 1:63,360.
- Theobald, P.K., Barton, H.N., Billings, T.M., Frisken, J.G., Turner, R.L., and VanTrump, George, Jr., 1978, Geochemical distribution of elements in stream sediment and heavy-mineral concentrate samples in the southern half of the National Petroleum Reserve, Alaska: U.S. Geological Survey Open-File Report 78-517, scale 1:500,000.
- Weldon, M.B., in press, Drenchwater Alaska: sedimentary exhalative deposit, volcanogenic massive sulfide deposit, or both?, in Raines, G.L., ed., *Geology and ore deposits of the American Cordillera—Geological Society of Nevada Symposium Proceedings*.

Reviewers: Geoff Plumlee and Steve Smith



# Environmental Geochemistry of the McKinley Lake Gold Mining District, Chugach National Forest, Alaska

By T.P. Trainor, S. Fleisher, T.R. Wildeman, R.J. Goldfarb, and C.S. Huber

## ABSTRACT

The McKinley Lake mining district, located in the Chugach National Forest, was examined to identify any natural or mine-induced contamination to the local drainages leading to McKinley Lake. Small, gold-bearing quartz veins that contain a few percent pyrite and arsenopyrite are scattered throughout the district. Waters were sampled from inside mine workings, along drainages below the workings, and in drainages upstream of any mining disturbances. Soils near mines and rock samples from tailings dumps were collected to determine their metal-leaching characteristics and acid generation/acid neutralization potential.

Background levels of iron and arsenic in natural stream waters collected distal to mineralized veins were  $\leq 20$  ppb and 3–13 ppb, respectively, at pH values of 7.5–7.7. In the vicinity of mineralized outcrops, but upstream from known workings, arsenic levels reached natural background levels of 32 ppb. Toxicity characteristic leaching procedure and acid generation/neutralization tests of soils and rocks, respectively, showed that metals had low leaching potential and that the mineral occurrences had very limited acid-generating potential. This was confirmed by the analyses of waters collected directly from mine workings, where the lowest pH was 6.4. Maximum concentrations of 650 ppb Fe at one site and 94 ppb As at a second site were measured for stagnant waters near one of the workings. Such locally elevated metal levels, however, are not present in the major drainages upstream from McKinley Lake and downstream from mine workings. These streams have background metal concentrations, which indicates that acid mine drainage and heavy-metal contamination are not significant problems in the mining district.

## INTRODUCTION

This study was undertaken at the request of the United States Forest Service to determine the extent of "natural" and mine-induced contamination to the environment from

the McKinley Lake mining district in the Chugach National Forest, south-central Alaska. Streams in the district eventually discharge into McKinley Lake, an important salmon spawning ground and a recreational fishing resource in the summer. The study was carried out with support of the Cordova Ranger District of the Chugach National Forest and is a collaborative effort between the Department of Chemistry and Geochemistry of the Colorado School of Mines, the U.S. Forest Service, and the U.S. Geological Survey (USGS).

The McKinley Lake mining district is located approximately 20 km east-southeast of Cordova and 0.5 km north of McKinley Lake (fig. 1). The district contains small gold-bearing vein occurrences scattered over an area of 2 to 3 km<sup>2</sup> along steep, densely forested slopes. It is accessed by hiking 4 km along the McKinley Lake trail starting from "mile 20" on the Copper River Highway.

The McKinley Lake area was prospected and mined for gold prior to World War II. Although gold-bearing quartz veins are widespread, their small size and discontinuous nature resulted in very limited production. Total production from the district was only 16 oz gold and 9 oz silver recovered from the McKinley Lake mine (Jansons and others, 1984); gold grades averaged 0.25 oz/ton (Haney and Jansons, 1987).

As discussed by Haney and Jansons (1987), early reports on this area describe numerous tunnels and cuts. However, there is much inconsistency among the reports on the locations and names of all the workings. Most likely, total workings in the district consisted of about 18 adits, numerous open cuts, 2 shafts, and 1 ball mill (Jansons and others, 1984). During this study, we located 4 adits, 2 inclined shafts, and 2 open cuts within the district.

Gold-bearing, mesothermal quartz veins typically contain a few percent sulfide minerals. In an oxidizing environment, sulfide species are unstable and weather to produce acids and to mobilize metals into streams (for example, see Smith and others, 1994). Many mobilized metallic species are potentially toxic to humans and aquatic life. Even where these mineral deposits are undeveloped, natural weathering processes result in soils and

streams becoming enriched in metals (Runnells and others, 1992). The mobility and concentrations of the inorganic species in the secondary environment depend on the volume of sulfidized rock, the accessibility of minerals in the rock to air and water, the susceptibility of the minerals to weathering, and the subsequent pH and redox potential of the waters that control element solubilities (Smith and others, 1994). The pH is controlled to a large extent by the buffering capacity imparted to the waters

from the weathering of carbonate and silicate minerals in the country rock. The mobility of many heavy metals, though, may be hindered because under some chemical conditions they will adsorb to solid matter.

Oxidation of sulfide minerals in abandoned mine workings and in adjacent tailing piles, such as those of the McKinley Lake district, has the potential to contaminate the environment with heavy metals and to produce a detrimental impact on wildlife. Drainage of acid water

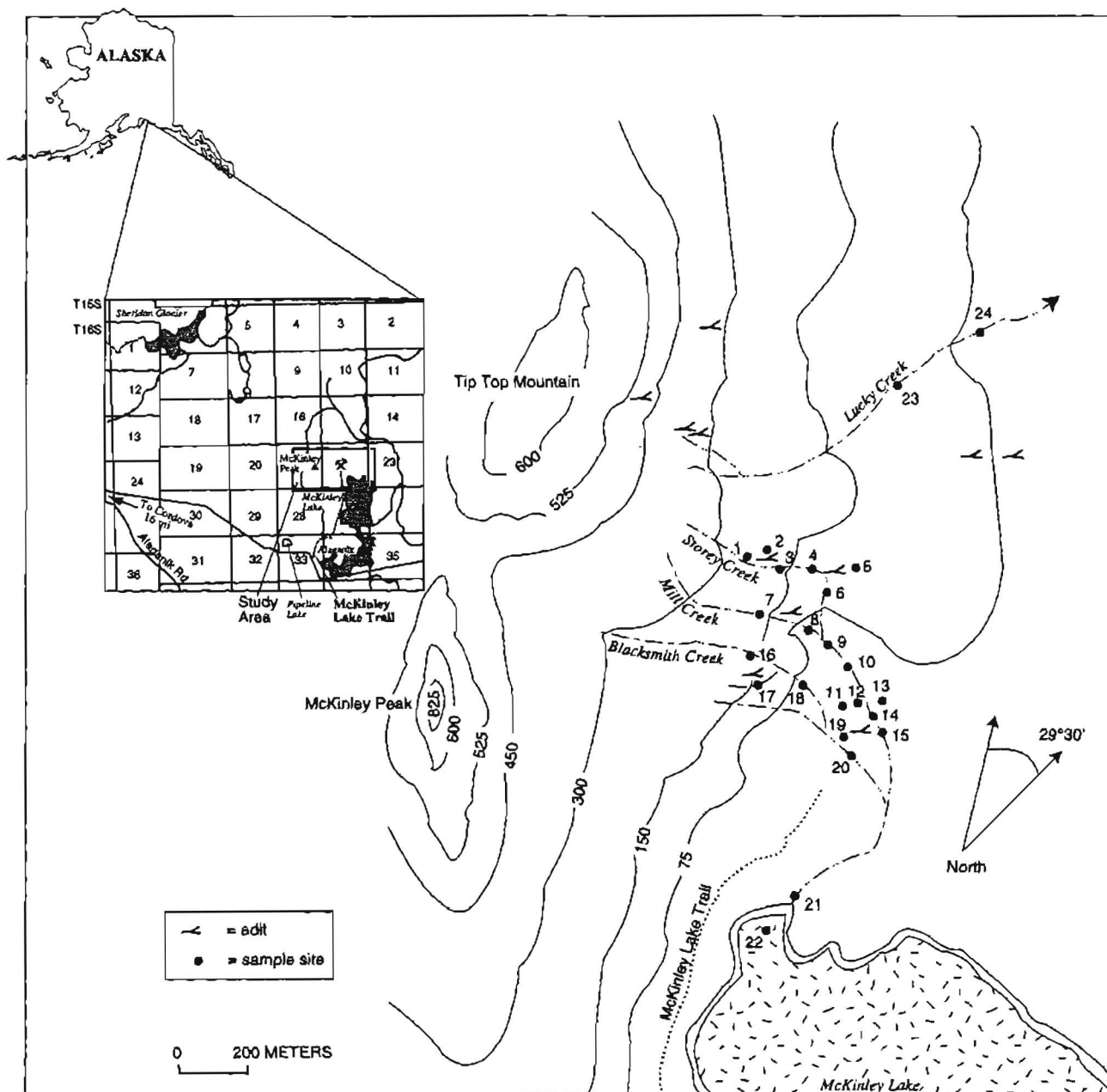


Figure 1. Location of mine workings and stream-water sample sites from the McKinley Lake mining district, south-central Alaska. Contours shown in meters.

from mines introduces increased levels of inorganic species, including sulfate and heavy metals, into surface and ground waters.

To assess the impact of natural and man-induced weathering of sulfide minerals in gold-bearing veins on the local hydrogeochemistry in the McKinley Lake mining district, we collected water samples from sites both downstream and upstream of the mine workings. Analyses were performed to determine concentrations of metals and major anions. Soils from the workings were also sampled and analyzed to determine levels of lead, arsenic, and mercury. Leaching tests were performed on the soils to determine their potential for yielding significant amounts of arsenic, cadmium, lead, mercury, and silver. Additionally, rock samples were taken from the rock dumps to determine their potential for acid production and neutralization. These combined data will indicate the extent and impact of acid mine drainage from a small gold district on the local ecosystem.

## GEOLOGY AND MINERAL OCCURRENCES

The McKinley Lake mining district is underlain by Paleocene and Eocene graywacke, slate, and argillite of the Orca Group. These metasedimentary rocks represent turbidites that were deposited in deep-sea fans and accreted to the southern Alaskan continental margin by 50 Ma (Plafker and others, 1994). During accretion and associated deformation in the Eocene, granitic plutons were emplaced into the flysch. One of these, the 52-Ma McKinley Lake pluton, is located about 1.5 km northwest of the gold-bearing veins now exposed in the district (Winkler and Plafker, 1993). Coeval with this tectonism and plutonism, the flysch was regionally metamorphosed to lower greenschist facies.

Gold-bearing quartz veins in the district are present as both simple fissure veins that are rarely more than 10 cm thick (Haney and Jansons, 1987) and stockwork systems up to 13 m wide (Jansons and others, 1984). The veins are both concordant and discordant to bedding in the host rocks; discordant veins are restricted to the relatively competent graywacke units (Haney, 1982). Pyrite, arsenopyrite, stibnite, pyrrhotite, and galena are reported in various veins (Jansons and others, 1984; Haney and Jansons, 1987). Generally, total sulfide contents are less than 1–2 percent of the vein material, but we have observed some veins that contain massive clots of arsenopyrite. Analysis of one relatively sulfide-rich vein sample indicated 3 percent Fe, 1.5 percent As, 1 ppm Ag, 160 ppm Au, 0.18 ppm Hg, 70 ppm Pb, 30 ppm Sb, and 5 ppm W (Richard Goldfarb, unpub. data). Sulfidization of metasedimentary rocks adjacent to veins is also typical.

Both disseminated pyrite and arsenopyrite are common within a few meters of the veins. The timing of vein emplacement is uncertain but probably was coeval with the Eocene metamorphism and plutonism.

Four groups of workings are clustered within the mining district (Richelson, 1934; Haney and Jansons, 1987). The only past production is minor and came from the claims of what was known as the McKinley Mining group, which were developed by adits located along Storey, Mill, and Blacksmith Creeks. Work during our study was concentrated in the area surrounding this group of claims because they drain into McKinley Lake, which is located a few kilometers downstream (fig. 1). The other major group of claims is the Lucky Strike group, located near the head of Lucky Creek. During this study, two samples were collected along Lucky Creek. Less extensive prospects in the Riley and Bear Creek claim groups (the former located about 600 m east of the Lucky Strike claim group and the latter near the top of Tip Top Mountain) were not included in the present study since these creeks do not drain into McKinley Lake.

## FIELD AND ANALYTICAL INVESTIGATIONS

Sample sites (fig. 1) were chosen to best determine background and mine-induced levels of metals in waters and soils of the district. Water samples were taken from 17 sites at intervals along the major drainages; from 6 adits, cuts, and shafts; and directly from McKinley Lake. The sampled creeks were typically 0.3 to 1.6 m wide and less than 30 cm deep, with flows generally less than 2 ft<sup>3</sup>/s. Soil and rock samples were also taken from tailings piles and stream banks at many water sample sites. The information recorded at each site included water temperature, pH, conductivity, alkalinity, and discharge (table 1). Conductivity and pH were determined using standard meters, and alkalinity was measured by titration with sulfuric acid to pH 4.8. Discharge was approximated using cross-sectional surveys and float measurements of velocity. At a few of the sample sites, dissolved oxygen was determined using a standard meter. Measurements of 10 to 12 mg/L indicated that water in the streams was relatively saturated with respect to oxygen. Dissolved oxygen values of 6 to 8 mg/L from a cut, shaft, and adit in the workings of the McKinley Mining group indicate some oxygen depletion in these mine waters.

At each site, two water samples were collected in 250 mL polyethylene bottles for chemical analysis. One of these was filtered through a 0.45- $\mu$ m filter and then acidified with reagent-grade concentrated nitric acid to a pH less than 2.0 for cation analysis. Each acidified sample was subsequently analyzed for 56 elements by inductively

Table 1. Field measurements and site descriptions for hydrogeochemical sampling, McKinley Lake district

Site No.	Temp. (°C)	Conductivity (µS/cm)	Dissolved oxygen (mg/L)	pH	Alkalinity at pH=4.8 (as ppm CaCO <sub>3</sub> )	Discharge <sup>1</sup> ft <sup>3</sup> /s	Site Description
1	7	27	-	7.5	11	s	Head of Storey Creek
2	6	56	-	7.2	22.8	0	Inside upper adit, Storey Creek
3	7	35	-	7.6	17.6	s	Along Storey Creek
4	8	27	-	7.4	14.2	s	Along Storey Creek
5	8	19	-	7.4	14.8	0.52	Inside lower adit, Storey Creek
6	8	17	-	7.5	21.9	s	Along Storey Creek
7	7	23	-	7.7	25.3	s	Head of Mill Creek
8	7.5	23	-	7.7	23	0.8	Upper Mill Creek
9	7	23	-	7.6	23.4	7.5	Along Mill Creek
10	9	40	11.5	7.7	22.2	1.5	Along Mill Creek
11	8.5	61	6	6.6	34.8	0	Inclined shaft just north of the mill
12	9	43	6	6.6	29.8	0	Pool of water in open cut
13	11.5	17	8.6	5.8	3.6	0	Mouth of inclined shaft along Mill Creek
14	10	38	10.8	7.5	24.4	0.93	Along Mill Creek
15	9	40	12.2	7.9	21.9	2.3	Mill Creek below old mill
16	6	74	11	7.3	29.6	s	Above adit, North Fork of Blacksmith Creek
17	7	55	11.8	7.7	28.6	s	Above adit, head of Blacksmith Creek
18	7	50	10.4	7.4	29.6	s	Below adit, Blacksmith Creek
19	8	46	7.8	6.4	18.2	0	Inside lower adit, McKinley Lake workings
20	9	47	11.2	7.8	27.9	0.4	South of mill, Blacksmith Creek
21	9.5	17	-	7.4	14.2	1.9	Along Mill Creek
22	14	17	-	7.4	10	lake	McKinley Lake
23	-	-	-	-	-	-	110 m elevation on Lucky Creek
24	-	-	-	-	-	-	65 m elevation on Lucky Creek

<sup>1</sup>stagnant, 0=flowing but <0.1 ft<sup>3</sup>/s.

coupled plasma-mass spectrometry (ICP-MS) at the USGS laboratories in Denver, Colorado (Meier and others, 1994). The second, unfiltered and unacidified sample was analyzed in Denver for chloride, nitrate, phosphate, sulfate, bromide, and fluoride by ion chromatography (Fishman and Pyen, 1979).

Two unfiltered water samples, one acidified and one unacidified, were collected in 1 L polyethylene bottles at a few additional sample sites for analysis by Commercial Testing & Engineering Company of Anchorage, which had been contracted by the U.S. Forest Service. Metals were analyzed by an inductively coupled plasma-atomic emission spectroscopy (ICP-AES) 23-element scan, and chloride, nitrate, nitrite, phosphate, and sulfate were analyzed by ion chromatography. The acidified samples were also analyzed for arsenic, lead, silver, and antimony by graphite-furnace atomic absorption spectrometry in Anchorage because of the lower determination limits of this technique for those elements.

Soil samples were taken from seven sites, both along streams and from adits, and were analyzed by Commercial Testing & Engineering Company. Prior to analysis,

each sample was digested with nitric acid and hydrogen peroxide. Lead and arsenic were then analyzed by graphite-furnace atomic absorption spectrometry, and mercury was analyzed by cold-vapor atomic absorption spectrometry. Some samples also had a toxicity characteristic leaching procedure (TCLP) test performed. This test simulates the leaching of elements from a solid sample by wash with acetic acid. It is the standard test required by the U.S. Environmental Protection Agency (EPA) to determine the mobility of contaminants from wastes.

Rock samples were collected from dumps near the lower adit of the McKinley Lake workings (between lower Blacksmith and Mill Creeks), the adit along Blacksmith Creek, and the lower adit along Storey Creek. Tests were performed by McLelland Labs of Sparks, Nevada to determine the acid-generation and acid-neutralization potential (AGP/ANP) of these samples. These tests determine the total reduced-sulfide content of each sample and the net ability of a sample to generate acid by oxidation of sulfides. This information is compared with the total carbonate carbon in each sample. The carbonate minerals consume acid in the weathering process and provide a



buffering effect on the system. The comparison provides a measure of the net potential of a sample to generate or consume acid.

## HYDROGEOCHEMICAL RESULTS

Concentrations of the more abundant cations are reported in table 2. Sample sites 1, 7, 16, and 17 are located above any known workings (fig. 1), and water samples from these locations contain background metal concentrations; that is, the chemistry of these waters has not been impacted by human-induced mining disturbances. Calcium was the dominant cation in solution, typically varying in concentration between 3,000 and 11,000 ppb. In almost all samples (table 2), values for iron were below 100 ppb and for all other metals below 10 ppb. The most anomalous measurements were 650 ppb Fe, 94 ppb As, 38 ppb Zn, 7 ppb Cu, 1 ppb Cd, and 1 ppb Ag.

The data for measured major anions are listed in table 3. Little variability between samples characterized the analyses for nitrate, nitrite, phosphate, fluoride, and bromide, and these species are omitted from the table. Maximum sulfate and chloride levels are 6,000 ppb and 1,900 ppb, respectively. Calculated alkalinities were determined from measurements of  $\text{Ca}^{2+}$  and pH using the assumption that dissolved carbonate species contribute most of the alkalinity (for examples, see Hem, 1992).

The difference between calculated alkalinity and the measured alkalinity is a means of defining the quality of the water analyses. At about half of the sample sites, the calculated values are within 5 ppm (as  $\text{CaCO}_3$ ) of measured values (table 3). Therefore, the majority of the alkalinity in these waters is clearly carbonate alkalinity, with the dissolution of carbonate minerals from the flysch strongly regulating the water chemistry. Differences of >5 ppm for the other sites reflect, in part, extremely low contents of dissolved species, which cause a high likelihood of inaccuracies in measurements of both alkalinity and calcium. For example, calcium concentrations of waters at sites 12 and 18 (table 2) are relatively low at 1,200 ppb, and these are the two sites with a >20 ppm difference between calculated and measured alkalinities. Because measured alkalinity values are always greater than values calculated from  $\text{Ca}^{2+}$  for sites with significant differences, we suggest that noncarbonate species also contribute to alkalinity in the study area. Such species might include organic, hydroxide, and silicate ligands derived from the soils and rocks.

In table 3, we have also identified samples for which a cation/anion balance is not obtained. A sample is considered within the acceptable range of cation/anion balance if  $|\Sigma \text{anions} - \Sigma \text{cations}| \leq$  the quality calculation, where the quality calculation is defined as  $0.1065 +$

$0.0155 \Sigma \text{anions}$  (Tchobanoglous and Schroeder, 1985). Site 12 is the only location where a balance is not observed. We suggest that, based on abundant organic material in the relatively stagnant water at this sample site, organic anions were overlooked during analysis.

## ANALYSIS OF RESULTS

### HYDROGEOCHEMISTRY

Results of chemical analyses indicate that the water chemistry is little affected by the mining activity. The only significant impact is a localized increase in arsenic, iron, and acidity due to the dissolution of sulfide minerals. Background levels of arsenic dissolved in waters range between about 3 and 13 ppb, based on measurements from stream sites located above mine workings on Storey (site 1), and Blacksmith (site 17) Creeks. Anomalous levels of dissolved arsenic, measured for filtered samples collected in and near workings on Mill and Blacksmith Creek (sites 11, 16, 19, 20), range between 28 and 94 ppb (table 2). Two of these samples exceed the level of 50 ppb established by the EPA as the safe drinking-water standard. Background levels for iron and pH in streams in the study area are  $\leq 20$  ppb and 7.5–7.7, respectively. Near some of the workings, however, we have identified mine drainage waters containing as much as 650 ppb Fe and having pH values as low as 6.4.

Examination of data for unfiltered water samples analyzed by atomic absorption spectroscopy indicates that some arsenic was likely sorbed onto suspended material. For example, the concentration of arsenic determined by this method for water from site 17 is twice that of filtered water analyzed by ICP-MS from the same site. We suggest that the relatively high background concentration of 20 ppb for an unfiltered water sample collected on Mill Creek above known mineral occurrences (site 7) reflects both dissolved and sorbed arsenic and not just the concentration of arsenic in solution.

Water samples were taken from within a number of the workings. The most anomalous waters were identified from within the lower adit of the McKinley Lake workings located between Mill and Blacksmith Creeks and approximately 45 m west of the ball mill (site 19). At the time of sampling, water in the adit was stagnant, but it does appear to flow occasionally and drain down a trail that leads into Blacksmith Creek. Some old pipes are present in the sampled pool and the sediments have a reddish tinge indicating the presence of iron oxy-hydroxide. The acidic pH of 6.4 and anomalous concentrations of arsenic (94 ppb), silver (0.3 ppb), iron (90 ppb), and sulfate (4,000 ppb) indicate the dissolution of arsenic- and iron-bearing sulfide minerals. At the measured pH

Table 2. Cation data for water samples from the McKinley Lake mining district.

[Filtered samples were analyzed by inductively coupled plasma-mass spectrometry (ICP-MS) for Na, Mg, Al, Ca, Fe, Cu, Zn, As, Cd, and Sb; unfiltered samples were analyzed by inductively coupled plasma-atomic emission spectroscopy (ICP-AES) for the same elements (excluding Sb) as well as for Si, Ag, As, and Pb; all K analyses were performed by atomic absorption spectroscopy on filtered samples; all data are in parts per billion]

Site No.	Na	Mg	Al	K	Ca	Fe	Cu	Zn	As <sup>2</sup>	Ag	Cd	Sb	Pb	Si <sup>3</sup>	As <sup>4</sup>
1	690	210	72	120	3000	20	1.2	3.3	3	<0.1	<0.7	0.1	<0.5	1500	<5
2	300	100	55	70	2000	<20	.6	3.5	9.3	<.1	<.7	<.1	<.5	-	-
3	660	200	27	120	3200	<20	.9	1.6	7	.9	<.7	.2	<.5	1500	9
4 <sup>1</sup>	1500	320	<50	-	5800	<50	<25	<25	<50	<25	<25	-	<5	1700	6
5	850	350	14	150	5500	<20	.7	3.3	9.2	<.1	<.7	.2	<.5	1700	10
6	830	320	14	150	5700	<20	.5	2.2	11	<.1	<.7	.4	<.5	-	-
7 <sup>1</sup>	1500	290	<50	-	8200	<50	<25	<25	<50	<.1	<25	<5	<5	2100	20
8	700	230	1100	340	3600	80	7	38	8.5	<.1	1	.2	2.6	-	-
9 <sup>1</sup>	1700	340	<50	-	7200	<50	<25	<25	<50	<25	<25	-	<5	1800	6
10	930	360	8	150	7100	<20	.3	2.1	12	<.1	<.7	.3	<.5	2100	11
11	1100	600	8	180	13000	30	.4	3.6	51	.2	<.7	.4	<.5	2100	54
12 <sup>1</sup>	1900	570	<50	-	1200	650	<25	<25	<50	<25	<25	-	<5	2100	47
13	400	110	36	70	700	20	.9	5.4	4	.2	<.7	<.1	<.5	1100	11
14	970	360	12	140	7100	<20	.8	2.7	12	.4	<.7	.4	<.5	-	-
15	950	380	11	170	7200	20	1.2	5.7	11	<.1	.9	.3	<.5	2000	11
16	1100	460	5	180	11000	<20	<.3	1.1	32	<.1	<.7	.4	<.5	-	-
17	600	200	24	100	4700	<20	.3	2.6	13	<.1	<.7	.2	<.5	2200	26
18 <sup>1</sup>	1900	420	<50	-	1200	<50	<25	<25	<50	1	<25	<5	<5	2200	36
19	1000	460	11	140	6600	90	1	8	94	.3	1	.3	<.5	1800	91
20	840	320	67	150	7100	94	.4	3	28	<.1	<.7	.3	<.5	-	-
21	940	350	44	130	4600	50	.4	.9	4	.2	<.7	.2	<.5	1600	<5
22 <sup>1</sup>	1200	280	60	-	4200	94	<25	<25	<50	<25	<25	-	<5	910	<5
23 <sup>1</sup>	1600	300	<50	-	6000	<50	<25	<25	<50	<25	<25	-	<5	1500	6
24 <sup>1</sup>	1500	290	<50	-	5100	<50	<25	<25	<50	<25	<25	-	<5	1500	<5

<sup>1</sup> Samples from these sites were unfiltered

<sup>2</sup> Arsenic measured by ICP-MS on filtered samples and ICP-AES for unfiltered samples

<sup>3</sup> Silica measured on unfiltered samples only

<sup>4</sup> Arsenic measured by atomic absorption spectroscopy on unfiltered samples

and given that the waters are moving out to an oxidizing environment, the majority of iron in solution will precipitate out as solid iron hydroxide ( $\text{Fe}(\text{OH})_3$ ) (Rose and others, 1979; Pontius, 1990).

A few hundred meters northwest of the lower McKinley Lake adit, and along the west side of Mill Creek, a flooded shaft (site 11) and a pool in an open cut (site 12) both had water with a pH of 6.6. The water in the shaft was filled with organic debris and also was characterized by anomalous arsenic (51 ppb), silver (0.2 ppb), and calcium (13,000 ppb) concentrations. Water in an unfiltered sample from the adjacent cut contained 47 ppb As and 650 ppb Fe. The high level of iron is probably the result of contributions from old pipe and ore-cart tracks that run over the cut. The cause of the increased calcium concentration in waters from the shaft is uncertain, but it might reflect increased calcium solubility in more acidic conditions and (or) dissolution of calcite in the vein systems and wall-rock alteration halos.

Water was sampled from a second open cut, near the mouth of another shaft, on the opposite side of Mill Creek (site 13). A measured pH of 5.8 was the most acidic value found during this study. An arsenic concentration of 4 ppb, an iron concentration of 20 ppb, and low levels for most other metals suggest that the sampled water was mostly rain water that had little interaction with the gold-bearing vein material. Waters from inside both adits along Storey Creek also showed little influence from mining activity (sites 2 and 5). Although the upper adit did have a relatively high conductivity (56  $\mu\text{S}/\text{cm}$ ), arsenic and iron were both at background levels.

Data from water samples collected along the stream channels indicate rapid dilution of mine discharge. Values for pH were always 7.3 or greater in waters outside of mine workings. The two water samples collected on Lucky Creek (sites 23 and 24), below a series of upstream adits, contained <5 to 6 ppb As and are not impacted by the sulfide-bearing veins or the mining activity.

Table 3. Anion data for water samples from the McKinley Lake mining district

[Calculated alkalinities were determined subsequent to conversion of ion data to milliequiv./L; resulting calculated values assume all alkalinity as  $\text{HCO}_3^-$  because all concentrations of  $\text{CO}_3^{2-}$  were  $<0.1$  ppm; values in bold indicate significant variation between measured and calculated alkalinity (column 6) or significant cation/anion imbalance (column 9); all values for ion concentrations were converted to milliequiv./L for anion/cation calculations; measurements were not made on samples from sites 23 and 24]

Site No.	$\text{Cl}^-$ (ppb)	$\text{SO}_4^{2-}$ (ppb)	Measured alkalinity (as ppm $\text{CaCO}_3$ )	Calculated alkalinity (as ppm $\text{CaCO}_3$ )	Calculated minus actual alkalinity (ppm)	Sum cations (meq./L)	Sum anions (meq./L)	Sum anions minus sum cations (meq./L)	Quality calculation <sup>1</sup>
1	1000	1700	11	7.5	-3.5	0.201	0.214	0.01	0.11
2			22.8	5.0	-17.8	.123	.100	-.02	.11
3			17.6	8.0	-9.6	.209	.160	-.05	.11
4			14.2	14.5	.3	.381	.290	-.09	.11
5	1000	3400	14.8	13.8	-1.0	.345	.374	.03	.11
6	1000	1800	21.9	14.3	-7.6	.352	.351	.00	.11
7	1000	2900	25.3	20.5	-4.8	.498	.499	.00	.11
8			23	9.0	-14.0	.240	.180	-.06	.11
9			23.4	18.0	-5.4	.461	.360	-.10	.11
10	1200	3400	22.2	17.8	-4.4	.429	.460	.03	.11
11	1600	3900	34.8	32.4	-2.4	.752	.775	.02	.12
12			29.8	3.0	-26.8	.189	.060	-.13	.11
13	1100	1100	3.6	1.7	-1.9	.064	.089	.03	.11
14			24.4	17.8	-6.6	.431	.355	-.08	.11
15	1200	3400	21.9	18.1	-3.8	.438	.466	.03	.11
16	300	1900	29.6	27.5	-2.1	.641	.598	-.04	.12
17	300	1300	28.6	11.8	-16.8	.280	.271	-.01	.11
18	1300	6000	29.6	3.0	-26.6	.177	.222	.04	.11
19	1900	4000	18.2	16.5	-1.7	.415	.466	.05	.11
20			27.9	17.8	-10.1	.422	.356	-.07	.11
21	1000	1900	14.2	11.5	-2.7	.304	.298	-.01	.11
22	1100	3000	10	10.5	.5	.285	.303	.02	.11

<sup>1</sup> Quality calculation is defined as  $0.1065 + 0.0155(\text{sum of the anions})$

Samples collected along Storey Creek, downstream from adits, show background levels of iron and arsenic (sites 3, 4, and 6). A concentration of 0.9 ppb Ag in a water sample collected downstream from the upper adit on Storey Creek (site 3) may be related to the mining activity. This value suggests that the leached vein material may be enriched in electrum but carries relatively low volumes of sulfide minerals.

Water data from one sample along Mill Creek (site 8), above its junction with Storey Creek, shows anomalous levels for many metals, including aluminum, iron, copper, zinc, cadmium, tin, and lead; aluminum concentrations are two orders of magnitude greater than background (table 2), and tin levels increase from a background of  $<0.3$  ppb to 13 ppb. Scattered debris from the mining activity, including aluminum and tin cans, and iron pipes are found near the creek. The anomalies are derived from runoff through this garbage. Analysis of a sample collected a few hundred meters farther downstream (site 9), just below the influx from Storey Creek, indicates alumi-

num levels are rapidly diluted back down to background levels. Further downstream along Mill Creek, influx from the lower mine workings has little impact on water quality (sites 14 and 15). Iron, arsenic, and pH measurements show little variation from background levels, with a slight increase in silver (site 14) being the only noticeable change in hydrogeochemistry.

Interpretation of the data from samples collected on Blacksmith Creek above all known workings indicates that anomalous arsenic levels are a likely natural consequence of water-rock interaction in areas of unmined mesothermal gold veins (sites 16 and 17). The concentration of 32 ppb As in waters upstream from the upper adit on the creek (site 16) is essentially identical to that of 36 ppb As collected just below the adit (site 18). Iron levels and pH for waters on Blacksmith Creek, however, appear little affected by either the mineral occurrences or mining disturbances. A calcium concentration of 11 ppm, and consequently the highest measured conductivity in the study of  $74 \mu\text{S}/\text{cm}$ , may relate to widespread calcite re-

sulting from the hydrothermal activity. Concentrations of 28 ppb As and 94 ppb Fe near the bottom of Blacksmith Creek (site 20) reflect contributions from both upstream adits and runoff from the hillside to the north that hosts the old mill workings.

The two samples collected farthest down the drainage net were collected near the mouth of Mill Creek (site 21) and from McKinley Lake itself (site 22). Both are characterized by background levels of <5 ppb As and pH measurements of 7.4. However, the creek has an iron concentration of 50 ppb, whereas the lake has an iron concentration of 94 ppb. Both values are notably greater than measured upstream background concentrations. The elevated concentration from the creek is likely due to upstream mining contamination, whereas we hypothesize that the even higher level in lake waters is largely due to more reducing conditions in the relatively stagnant water body.

### SOIL AND ROCK GEOCHEMISTRY

Soil samples from throughout the study area are strongly anomalous in arsenic (table 4) relative to typical rocks that contain a few tens of parts per million arsenic (Rose and others, 1979). A soil collected about 10 m west of the lower McKinley adit (site 19) contained 3,500 ppm As, clearly reflecting an abundance of detrital arsenopyrite. Soils collected near other workings contained between 99–370 ppm As. A soil collected near the mouth of Mill Creek also contained 99 ppm As (site 21). This suggests transport of detrital sulfide grains downstream and deposition in overbank accumulations. Concentrations of as much as 29 ppm Pb and 0.75 ppm Hg in soils adjacent to some of the workings also reflect weathering of mine waste.

TCLP tests on five of the seven soil samples (table 4) indicate metals are relatively insoluble. If the results from a TCLP test indicate a metal value in excess of 100 times the safe drinking-water standard of the EPA, then the sample is considered to pose a threat to water quality (EPA method 1311, SW/846, 40CFR261). None of the tested soils showed such elevated values for any of the measured metals. Even the soil with 3,500 ppm As was characterized by a relatively low leaching potential of the arsenic; its arsenic concentration (120 ppb) was only about two and a half times greater than the safe drinking-water standard.

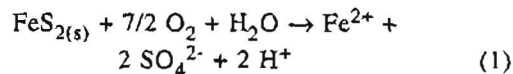
Acid-generation/neutralization tests were conducted on quartz-veined and weakly sulfidized metasedimentary rocks collected from dumps near the lower McKinley (site 19), lower Storey Creek (site 5), and upper Blacksmith Creek (site 18) adits (table 5). Pastes made from all rocks had neutral to alkaline pH values, suggestive of little acid-production potential. The sample from the McKinley adit

dump did show a slightly greater potential to generate acid than to neutralize acid when the calculations are based on total sulfur content of the rock. However, the abundances of sulfide and carbonate are extremely low. Also, when the calculation was based on sulfide content (likely the major acid-producing species), the McKinley sample shows a slightly greater potential to neutralize acid than to generate acid. This result indicates that acid mine drainage should not be a concern at these gold occurrences. The rock samples taken from the Blacksmith Creek and Storey Creek workings also show a net acid-neutralization over acid-production potential.

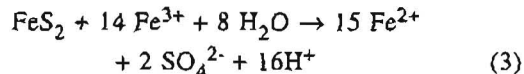
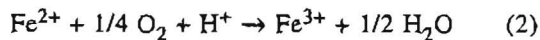
### DISCUSSION

In general, the only sites that show notable arsenic contamination are the lower McKinley adit (site 19) and the nearby flooded shaft and open cut (sites 11 and 12). The concentrations of arsenic at these sites are strongly anomalous relative to normal background levels, although the pH values and levels for other heavy metals are not significantly impacted. Two of these sites have levels of arsenic above the EPA's drinking-water quality standard of 50 ppb. However, the downstream concentrations of arsenic in the major drainage are not impacted by the limited discharge from these workings and are well below the drinking-water standard. Anomalous levels of other metals in the waters at a single site along Mill Creek (site 8) are attributed to contributions from metallic debris adjacent to the creek, and they too are quickly diluted downstream.

The dissolution of pyrite and arsenopyrite is the major contributor to observed variability in pH and arsenic concentrations within the study area. The following equation represents the acid-producing dissolution of pyrite:



Acid continues to be released during oxidation of the released  $\text{Fe}^{2+}$  to  $\text{Fe}^{3+}$ , as follows:



Hydrous oxide minerals are precipitated during the acid-producing reactions, represented by the following:



Table 4. Concentrations of As, Hg, and Pb in soils from the McKinley Lake mining district and results of toxicity characteristic leaching procedure (TCLP) tests of these soil samples for five metals, carried out according to EPA method 1311

[Pb and As were determined by graphite-furnace atomic absorption spectroscopy; Hg was determined by cold-vapor atomic absorption spectroscopy, all data are in parts per million]

Site No.	As	Hg	Pb	Ag	As	Cd	Hg	Pb
Soils				Soil Extracts				
3	140	0.11	16	<0.1	0.005	<0.5	<0.0001	<1
5	99	<.10	12	<.1	.005	<.5	<.001	<1
13	140	<.10	11	---	---	---	---	---
15	250	.45	23	<.1	.025	<.5	<.0001	<1
18	370	<.10	13	<.1	.160	<.5	.002	<1
19	3500	.75	29	<.1	.120	<.5	<.001	<1
21	99	<.10	10	---	---	---	---	---

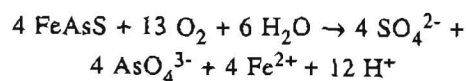
Table 5. Results of modified acid-base accounting static acid-generation/neutralization tests on rock samples from the lower McKinley, Blacksmith Creek, and Storey Creek adits

[Data for total sulfur and sulfide are reported in percent; acid-generation potential (AGP), acid-neutralization potential (ANP), and net-neutralization potential (NNP) are reported as CaCO<sub>3</sub> equivalents per 1,000 tons of rock]

Adit	Paste pH	Total S (%)	Sulfide S (%)	AGP total	AGP sulfide	ANP	NNP total	NNP sulfide
Lower McKinley	7.25	0.500	0.290	15.6	9.1	12	-3.6	+2.9
Blacksmith	7.75	.068	.024	2.1	.8	30	+27.9	+29.2
Storey	8.92	.096	.024	3.0	.8	50	+47.0	+49.2

The formation and precipitation of iron hydroxide (in equation 4), which is highly insoluble in the range of pH values of the sites that we sampled, drives the former reactions (equations 2 and 3) and produces much of the measured sulfate and acidity (Wildeman, 1991).

The TCLP tests indicate that much of the arsenic and other metals in the soils, in part derived from weathered, sulfide-rich rock, remain relatively immobile. However, dissolution of arsenopyrite still contributes some amount of arsenic and additional acidity into the drainage network in the McKinley Lake area. Arsenic concentrations of 32 ppb upstream from mine workings along Blacksmith Creek (site 16) indicate that such a process is naturally occurring within the McKinley Lake watershed. The net reaction for the oxidation of arsenopyrite is represented by the following equation:



Arsenic can subsequently be transported in dissolved form as either an arsenite (As<sup>3+</sup>) or arsenate (As<sup>5+</sup>) species, largely depending on local redox potential (Cherry and others, 1979). Under reducing conditions, dissolved arsenic will migrate as H<sub>3</sub>AsO<sub>3</sub>. In the more oxidizing environment characteristic of Mill Creek and its tributaries, H<sub>2</sub>AsO<sub>4</sub><sup>-</sup> will dominate under acid conditions and HAsO<sub>4</sub><sup>2-</sup> will dominate in alkaline waters (fig. 2). However, arsenic mobility is likely greatly restricted because the arsenate readily adsorbs to amorphous Fe hydroxides (Smith and others, 1992), which are also likely products of pyrite and arsenopyrite dissolution. We therefore suggest that in mining districts such as McKinley Lake, arsenic mobility will consistently be relatively low and extreme hydrogeochemical (>100 ppb As) arsenic anomalies are unlikely. But because humic acids derived from decaying organic material compete with arsenate for sites on solids (Xu and others, 1991), episodic elevated arsenic levels in the waters of McKinley Lake cannot be ruled out. Such anomalous arsenic levels would be favored if,



during certain periods, there is an abundance of decomposing vegetation in the McKinley Lake drainage network.

## CONCLUSIONS

Detailed study of stream waters in the McKinley Lake mining district shows that there is little detrimental effect on water quality from the old mine workings. Although rocks and soils derived from mine waste are enriched in iron and arsenic, much of the metal is relatively immobile in solution. Stagnant pools of water in mine workings, however, may contain 50–100 ppb As. Such local concentrations could be hazardous to wildlife if they were used as a long-term drinking source.

Arsenic contamination and acid mine drainage are the obvious environmental concerns that we attempted to address in this study. However, other less obvious concerns that we did not examine still could have significant impact on local wildlife and aquatic life. Anomalous amounts of mercury in rock and in soils at sites 15 and 19 suggest that evaluation of waters for mercury content

is probably warranted. More significantly, if mercury was used at the mill for amalgamation purposes during gold recovery, then mercury could indeed be an environmental concern in the McKinley Lake mining district. The field work for this study was carried out during mid-summer, and we are uncertain as to whether initial spring runoff could have carried greater metal concentrations, which may have accumulated in the weathering environment over the winter months. Finally, McKinley Lake represents a major sink for suspended material transported from the mine workings. A reconnaissance-level sampling program of lake-bottom sediments, with analyses particularly for arsenic and mercury, would indicate any possible problems that might impact salmon runs or other aquatic life.

The McKinley Lake mining district contains relatively small deposits with only minor development. But results similar to those reported here would be expected for mine drainage waters from larger and more developed gold-bearing quartz vein deposits. The low-sulfide mineral content of the ore, as well as the associated carbonate alteration that provides a buffer for mine effluent, do not favor significant acid production. Therefore, relative to mine drainage waters associated with many other mineral deposit types, those draining gold-bearing quartz veins are less contaminated. In fact, metal concentrations in waters draining Alaska's largest gold mine, Alaska-Juneau, are consistently below the state's drinking water maximum allowable level (Gray and Sanzalone, 1996).

**Acknowledgments.**—We greatly appreciate the logistical support and encouragement of the Cordova Ranger District of the Chugach National Forest, and especially Bruce Campbell, Dixon Sherman, and John Crouse. We also thank Bill d'Angelo, Al Meier, Molly Malcolm, and John McHugh for their help with some of the analytical efforts.

## REFERENCES CITED

- Cherry, J.A., Shaikh, A.U., Tallman, D.E., and Nicholson, R.V., 1979, Arsenic species as an indicator of redox conditions in groundwater: *Journal of Hydrology*, v. 43, p. 373–392.
- Fishman, M.J., and Pyen, Grace, 1979, Determination of selected anions in water by ion chromatography: U.S. Geological Survey Water-Resources Investigations 79-101, 30 p.
- Gray, J.E., and Sanzalone, R.F., eds., 1996, Environmental studies of mineral deposits in Alaska: U.S. Geological Survey Bulletin 2156, in press.
- Haney, J.M., 1982, Geology of the McKinley Lake gold prospect area, Chugach National Forest, south-central Alaska: Socorro, N. Mex., New Mexico Institute of Mining and Technology, M.S. thesis, 52 p.
- Haney, J.M., and Jansons, Uldis, 1987, Geology of the McKinley Lake gold area, Chugach National Forest, southcentral Alaska: U.S. Bureau of Mines Open-File Report 32-87, 40 p.

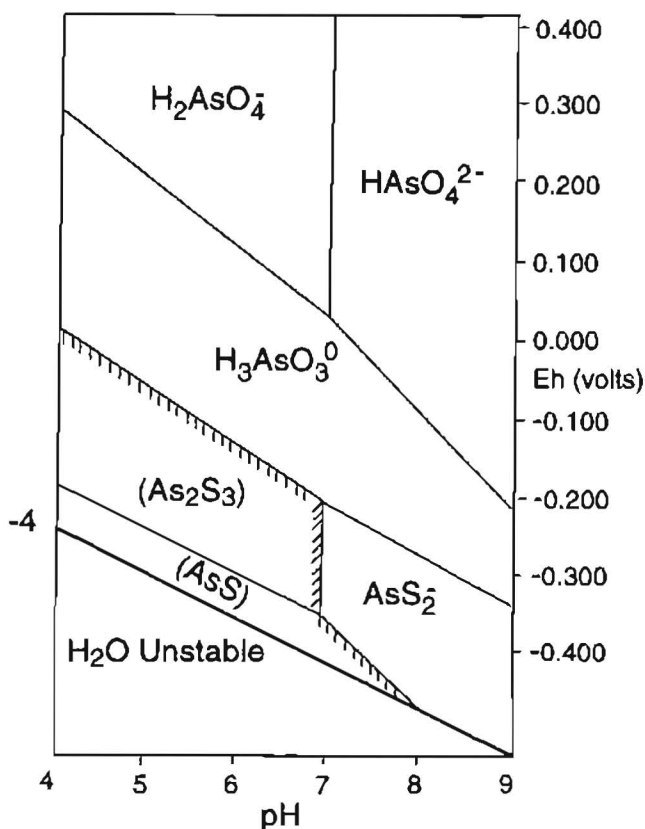


Figure 2. Eh-pH diagram for the As-S-H-O system at 25°C,  $10^{-7.176}$  mol/L As, and  $10^{-3}$  mol/L S (from Cherry and others, 1979). The hatched area reflects the stability field for solid sulfide mineral phases.



- Hem, J.D., 1992, Study and interpretation of the chemical characteristics of natural water: U.S. Geological Survey Water-Supply Paper 2254, 263 p.
- Jansons, Uldis, Hoekzema, R.B., Kurtak, J.M., and Fechner, S.A., 1984, Mineral occurrences of the Chugach National Forest, southcentral Alaska: U.S. Bureau of Mines MLA Report 5-84, 43 p., 2 pls.
- Meier, A.L., Grimes, D.J., and Ficklin, W.H., 1994, Inductively coupled plasma mass spectrometry—a powerful analytical tool for mineral resource and environmental studies [abs.], in Carter, L.M.H., Toth, M.I., and Day, W.C., eds., U.S. Geological Survey Research on mineral resources—1994, Part A—Program and Abstracts, Ninth V.E. McKelvey Forum on Mineral and Energy Resources, 9th, Tucson, Ariz., February 22–25, 1993: U.S. Geological Survey Circular 1103-A, p. 67–68.
- Plafker, George, Moore, J.C., and Winkler, G.R., 1994, Geology of the southern Alaska margin, in Plafker, George, and Berg, H.C., eds., The geology of Alaska: Boulder, Colo., Geological Society of America, The Geology of North America, v. G-1, p. 389–449, pl. 12.
- Pontius, F.W., 1990, Water quality and treatment (4th ed.): New York, McGraw-Hill, 1194 p.
- Richelson, W.A., 1934, Report on the Pioneer, Lucky Strike and Rileys prospects at McKinley Lake, Lower Copper River region, Alaska: Bear Creek Mining Co., unpublished company report, 9 pp.
- Rose, A.W., Hawkes, H.E., and Webb, J.S., 1979, Geochemistry in mineral exploration (2d ed.): London, Academic Press, 657 p.
- Runnells, D.D., Shepherd, T.A., and Angino, E.E., 1992, Metals in water—determining natural background concentrations in mineralized areas: Environmental Science and Technology, v. 26, p. 2316–2323.
- Smith, K.S., Ficklin, W.H., Plumlee, G.S., and Meier, A.L., 1992, Metal and arsenic partitioning between water and suspended sediment at mine-drainage sites in diverse geologic settings, in Kharaka, Y.K., and Maest, A.S., eds., Water-rock interaction: Seventh International Symposium on Water-Rock Interaction, Park City, Utah, July 13–18, 1992, Proceedings: Rotterdam, A.A. Balkema, v. 1, p. 443–447.
- Smith, K.S., Plumlee, G.S., and Ficklin, W.H., 1994, Predicting water contamination from metal mines and mining wastes: U.S. Geological Survey Open-File Report 94-264, 112 p.
- Tchobanoglous, George, and Schroeder, E.D., 1985, Water quality: Reading, Mass., Addison-Wesley Publishing Company, 768 p.
- Wildeman, T.R., 1991, Drainage from coal mines—chemistry and environmental problems, in Peters, D.C., ed., Geology in coal resource utilization: Fairfax, Va., Tech Books, p. 499–511.
- Winkler, G.R., and Plafker, George, 1993, Geologic map of the Cordova and Middleton Island quadrangles, southern Alaska: U.S. Geological Survey Miscellaneous Investigations Series Map I-1984, scale 1:250,000.
- Xu, H., Allard, B., and Grimvall, A., 1991, Effects of acidification and natural organic matter on the mobility of arsenic in the environment: Water, Air, and Soil Pollution, v. 57–58, p. 267–278.

Reviewers: Jim Crock and John McHugh



# Alaska Earthquakes—1994

By Kent A. Fogleman, Charlotte A. Rowe, and William R. Hammond

## ABSTRACT

Alaska is one of the world's most seismically active regions associated with subduction and volcanism. Earthquakes occur over practically the entire state. The greatest concentration of earthquakes is along the Pacific margin, where the Pacific plate is being subducted beneath southern Alaska and the Aleutian Islands. Historical and current seismicity along the Aleutian volcanic arc is dominated by activity west of the Alaska Peninsula. In 1994, 79 of the 103 magnitude 4.5 and larger shocks located in Alaska and western Canada occurred in the Aleutian Islands. The largest shock located during 1994 was a shallow, body-wave magnitude ( $m_b$ ) 6.0 event in the Fox Islands, but the most widely felt earthquake was an  $m_b$  5.4 event located 77 kilometers (km) southwest of Anchorage at a depth of 49 km. Two notable earthquakes are (1) the largest, well-constrained deep shock yet located in the Aleutian Wadati-Benioff zone east of longitude 156°W., an  $m_b$  4.6 event at 219-km depth, and (2) the largest crustal shock ever located beneath the edifice of Mount Spurr volcano, a magnitude ( $M_L$ ) 2.8 event at a depth of 1 km below the top of the volcano. The Alaska Earthquake Information Center (AEIC) located more than 4,400 earthquakes in 1994 using data recorded by the joint U.S. Geological Survey/University of Alaska seismograph network.

## INTRODUCTION

Alaska spans 4,800 km of the seismically active boundary between the oceanic Pacific and continental North American plates (fig. 1) and has one of the world's highest levels of earthquake activity associated with subduction and volcanism. The historical record indicates that approximately 11 percent of the world's earthquakes occur in Alaska, even though the land area of Alaska is only about three-tenths of 1 percent of the surface area of the world (Davies, 1984). Magnitude 7 and larger shocks are about three times more frequent in southern Alaska than in California (Page, 1994). Three of the ten largest

earthquakes in the world in this century originated in Alaska on the boundary between the Pacific and North American plates (Kanamori, 1977; Johnson and others, 1994). In 1964, the eastern end of the Aleutian subduction zone spawned the moment magnitude ( $M_W$ ) 9.2 Prince William Sound earthquake (fig. 2), the second largest earthquake of this century. The other two earthquakes occurred in the western and central parts of the Aleutian Islands—the 1965  $M_W$  8.7 Rat Islands earthquake (rank no. 5) and the 1957  $M_W$  8.6 Andreanof-Fox Islands earthquake (rank no. 7).

The seismicity of Alaska stems primarily from the interaction of the Pacific and North American plates. The northwestward motion of the Pacific plate relative to the North American plate (fig. 2) is accommodated by right-lateral, strike-slip faulting in western Canada and southeast Alaska on the Queen Charlotte–Fairweather fault system; by underthrusting and subduction of the Pacific plate along the Aleutian main thrust zone (megathrust), which extends from the eastern Gulf of Alaska to the central Aleutians; and by right-lateral, strike-slip faulting in the western Aleutians (Estabrook and Jacob, 1991). The Aleutian megathrust intersects the seafloor at the Aleutian trench, which forms part of the near-surface expression of the Pacific–North American plate boundary. In the northeastern Gulf of Alaska (fig. 1), between the Fairweather fault and the eastern end of the Aleutian trench, the plate boundary is transitional and complex. The relative motion is distributed among at least three fault systems (Lahr and Plafker, 1980). At the northern end of the Fairweather fault, the primary component of plate motion is transferred to the Chugach–St. Elias fault, then to a series of thrust faults between the Pamplona and Kayak Island zones, and finally to the Aleutian megathrust. Much of this complexity arises from the collision between the North American plate and the Yakutat terrane, a composite oceanic–continental terrane sutured to the top of the Pacific plate (Plafker, 1987). The Yakutat terrane is subducting beneath the North American plate to the west of longitude 144°W. and accreting to the North American plate to the east (Page, 1994). The horizontal compressional stress resulting from this collision is transmitted inland across the eastern half of the State and also

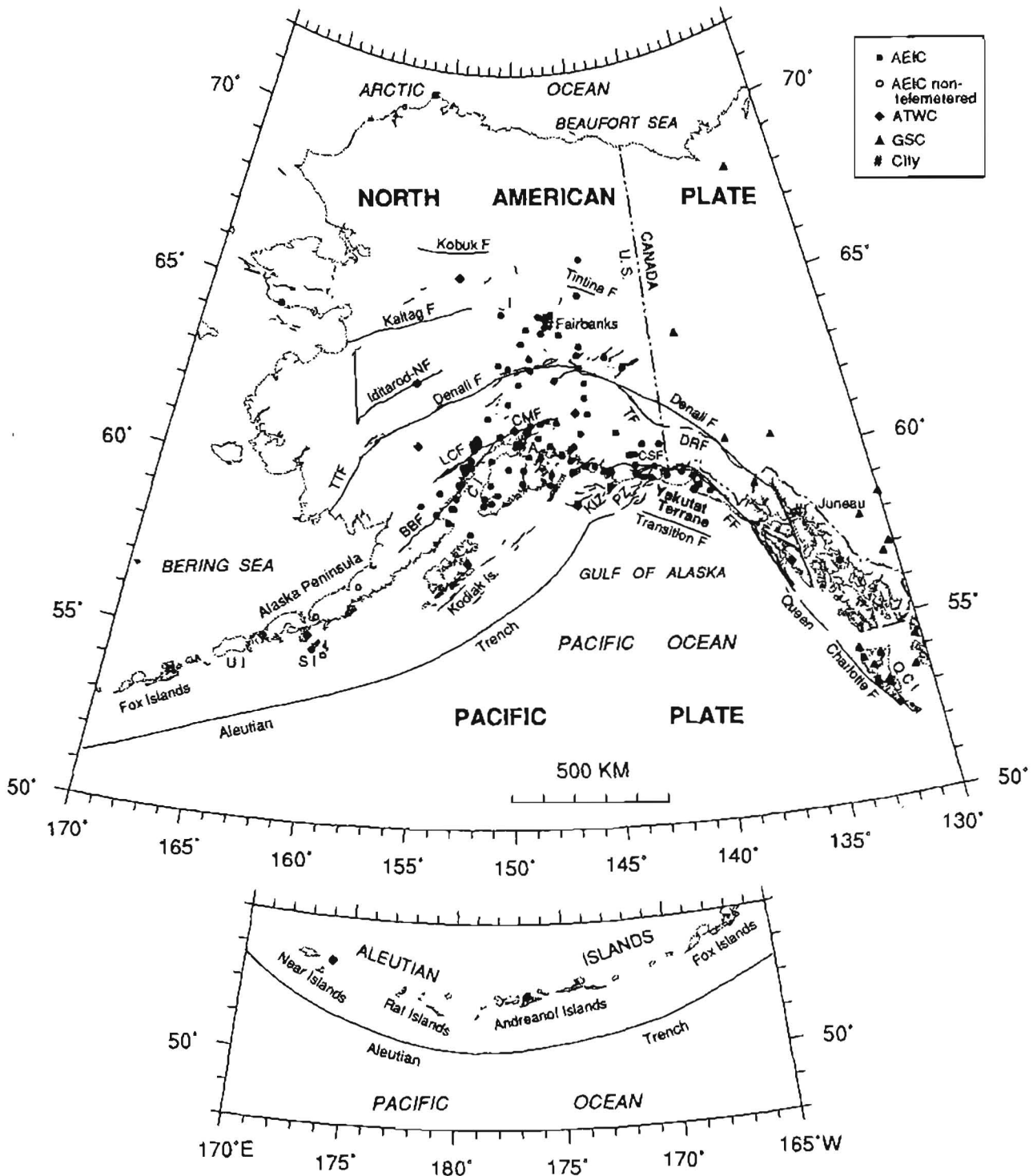
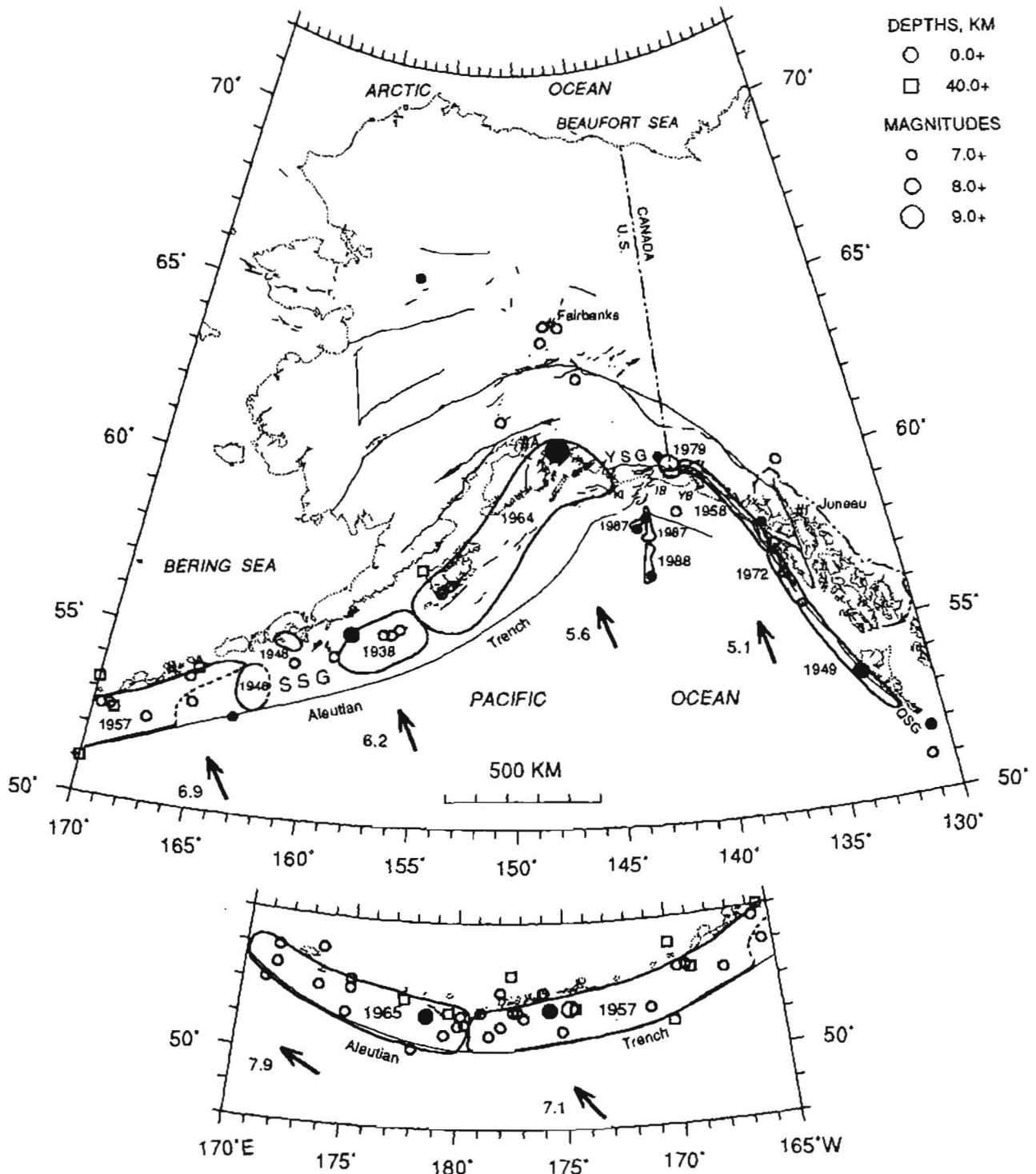


Figure 1. Map of seismograph stations in Alaska and western Canada operated during 1994. Symbol type corresponds to operating institution as indicated: AEIC, Alaska Earthquake Information Center; ATWC, Alaska Tsunami Warning Center; GSC, Geological Society of Canada. Solid lines show Neogene and younger faults (from Plafker and others, 1994). Fault abbreviations: BBF, Bruin Bay fault; CMF, Castle Mountain fault; CSF, Chugach-St. Elias fault; DRF, Duke River fault; FF, Fairweather fault; LCF, Lake Clark fault; Iditarod-NF, Iditarod-Nixon Fork fault; KIZ, Kayak Island zone; PZ, Pamplona zone; TF, Totschunda fault; TTF, Togiak-Tikchik fault; Also: A, Anchorage; CI, Cook Inlet; QCI, Queen Charlotte Islands; SI, Shumagin Islands; UI, Unimak Island.



**Figure 2.** Epicenters of 73 magnitude 7.0 or greater earthquakes from 1900 to 1994 (modified from Plafker and others, 1994) and aftershock zones (heavy line, dashed where inferred) of the largest earthquakes to have ruptured each segment (year of event listed) of the plate boundary (modified from Davies and others, 1981; Rogers, 1986). Solid symbols are earthquakes referred to in the text. Arrows show motion of Pacific plate relative to North American plate, with velocities in centimeters per year (DeMets and others, 1990). Symbol type corresponds to depth, and size is proportional to magnitude. Faults as in figure 1. Abbreviations: A, Anchorage; IB, Icy Bay; KI, Kayak Island; YB, Yakutat Bay; QSG, Queen Charlotte Islands seismic gap; SSG, Shumagin seismic gap; YSG, Yakutataga seismic gap.

seaward into the Pacific plate (Lahr and others, 1988; Page and others, 1991; Estabrook and Jacob, 1991).

The seismicity related to various tectonic elements can be divided into five distinct source zones: (1) plate-boundary earthquakes along the interface between the Pacific plate and the North American plate, (2) trench and unsubsucted oceanic intraplate earthquakes within the Pacific plate beneath or seaward of the Aleutian trench and the Transition fault, (3) Wadati-Benioff zone (WBZ) earthquakes within the subducted part of the Pacific plate landward of the Aleutian trench, (4) North American plate earthquakes, exclusive of those along the Aleutian and Wrangell volcanic axes, and (5) volcanic-axis earthquakes within the North American plate along the axis of active volcanoes.

Annual reviews of the seismic activity in Alaska are necessary in order to build a sound seismological basis for evaluating the State's long-term and intermediate-term earthquake potential. The purpose of this paper is to review the 1994 seismicity located in Alaska and western Canada by the Alaska Earthquake Information Center (AEIC) and the U.S. Geological Survey's National Earthquake Information Center (NEIC). We also provide an overview of the tectonics of Alaska and western Canada, a description of the functions of the AEIC, and summaries of much of the previous work on Alaskan and western Canadian seismicity for the benefit of readers who are not familiar with these topics.

## ALASKA EARTHQUAKE INFORMATION CENTER

The AEIC monitors earthquakes in Alaska, provides rapid information on felt earthquakes, and disseminates information about earthquakes and seismic hazards to government officials, the media, the public, and the earth-science community worldwide. Established in 1988, the AEIC is operated cooperatively by the U.S. Geological Survey (USGS) and the Geophysical Institute of the University of Alaska (UAGI). The main center of operations is located at the Geophysical Institute in Fairbanks.

Most of the earthquakes located by the AEIC originate in a "core" area in central and southern Alaska, between latitudes 57°N. and 67°N. and longitudes 135°W. and 156°W. (approximately 1,300,000 km<sup>2</sup> or 500,000 mi<sup>2</sup>). The AEIC reports also routinely include earthquakes provided by the NEIC for the larger region, between latitudes 48°N. and 75°N. and longitudes 130°W. to 170°E. Since 1990, the AEIC has located approximately 24,000 earthquakes in Alaska and western Canada.

Three types of reports are issued regularly by the AEIC: 1. Information Release—a one-page release is issued via fax and electronic mail within two hours of the

occurrence of any shock with magnitude  $\geq 4.0$  or for events smaller than magnitude 4 when they are felt. This release contains the preliminary hypocenter parameters, distances to nearby cities, and felt information (104 releases were issued in 1994, of which 44 contained felt information). 2. Weekly Seismicity Report—a several-page document is mailed within seven days of the end of each week. This report includes highlights of recent activity, epicenter maps, a preliminary listing of events, and felt reports and magnitudes augmented by the NEIC Quick Epicenter Determinations (QED). The first formal report in this series (no. 33-93) is for the week of August 13–19, 1993 (33rd week); however, weekly seismicity reports have been informally released since November 1989. 3. Earthquakes in Alaska—this multipage monthly report is issued about seven months following the close of a particular month. It includes epicenter maps and hypocenter cross sections, as well as locations, felt reports, and magnitudes based on additional information from the NEIC monthly Preliminary Determination of Epicenters (PDE) reports and from other seismic observatories (Fogleman and others, 1994).

The AEIC normally analyzes data from the joint USGS/UAGI seismograph network, which currently incorporates 117 stations, and from 15 stations operated by the Alaska Tsunami Warning Center (ATWC) in Palmer, Alaska. Most of the stations are located in central and southern Alaska (fig. 1). The majority of the 155 channels of data recorded at the AEIC are from short-period, vertical-component analog stations. Data are also received from 8 short-period, three-component analog stations, 5 short-period, vertical-component digital stations, and 4 broadband, three-component digital stations. Eight digital, three-component broadband stations were also operated by the UAGI along the Alaska Peninsula and in the Shumagin Islands during 1994 but were not recorded locally in Fairbanks. Waveforms and phase readings from these stations were occasionally combined with the data processed in Fairbanks. Phase readings obtained from data recorded by seismographs (instruments used to record the passing of seismic waves) located in western Canada and operated by the Geological Survey of Canada (GSC) are routinely combined with the AEIC data.

Shallow (depth < 30 km) shocks in southern coastal Alaska cannot be routinely determined by the AEIC regional network with sufficient precision to attribute individual shocks to the subducting plate, the interplate megathrust, or the overriding plate. The NEIC routinely fixes focal depths to 33 km for earthquakes whose character on seismograms (records of earthquakes produced on seismographs) indicates a shallow focus but whose depth is not satisfactorily determined by the data. Focal mechanisms and depth phases such as *pP* give information about the fault planes and stresses sufficient to determine the responsible source zone. The NEIC routinely interprets data from broadband displacement seismograms



to obtain focal depths (for events with  $m_b \geq 5.8$ ). The  $pP$  depth phase is a seismic wave that is reflected from the surface of the earth at a point near the epicenter and follows the initial  $P$ -wave by an interval proportional to the depth of the source.

Focal mechanisms are usually based on the first arrival times of  $P$ -waves and their corresponding directions of motion (first motions), which are traced back to a hypothetical focal sphere (a small imaginary sphere enclosing the earthquake focus). The first motion of each  $P$ -wave is alternately a compression or a dilatation. Their distribution (radiation pattern) on the sphere is used to divide the area surrounding the focus into four quadrants (such that adjacent quadrants have opposite polarities) separated by two orthogonal planes. Since the  $P$ -wave motion is null along these planes, they are called nodal planes. One of these planes corresponds to the fault plane; the other plane is perpendicular to the direction of fault movement and is called the auxiliary plane. Additional information such as geological trends, linear aspects of aftershock distributions, etc., is necessary to select which plane is the proper fault plane. The style of faulting, the direction of the fault slip, and the orientation of the  $P$ - (pressure) and  $T$ - (tension) axes can be inferred from these fault planes. The  $P$ - and  $T$ -axes are the bisectors of the dilatational and compressional quadrants of the focal mechanism, respectively, and provide the compressional and extensional strain directions for the two possible faults (Zoback and Zoback, 1991).

An alternative method to derive the source mechanism of an earthquake is based on the analysis of radiation patterns of long-period body waves (waves that travel from the earthquake source through the body of the earth), surface waves (waves that travel only in the outermost layers of the earth), and free oscillations (vibrations of the earth as a whole at different frequencies called normal modes) of the earth. By calculating the excitation of the normal modes from a particular earthquake source, an iterative inversion procedure can be used to derive the earthquake mechanism and total moment (Gilbert, 1971). The Harvard University centroid moment tensor (CMT) solutions reported in this paper use the long-period body- and mantle-wave moment-tensor inversion method of Dziewonski and others (1981). Moment-tensor solutions are generally limited to earthquakes with magnitudes exceeding 5.5 (Dziewonski and others, 1981).

Various magnitude formulas or scales are used to calculate the size of earthquakes. Each scale is defined for use with a particular type of seismograph and recording range and has its own inherent limitations; however, when used properly, each can be viewed as an extension of the previous one. The local magnitude ( $M_L$ ) scale, which is an approximation of the original Richter scale (Richter, 1958), is used for earthquakes recorded at seismic stations less than 600 km from the earthquake's epicenter.

$M_L$  magnitudes are usually reported for events with magnitudes smaller than 4-6. Beyond 600 km, body-wave ( $m_b$ ) and surface-wave ( $M_S$ ) magnitudes are used. These magnitudes are not typically calculated below magnitude  $m_b$  3.5 and  $M_S$  4.0. The  $m_b$  and  $M_S$  scales are equal at magnitude 6.75; above this value,  $M_S > m_b$ , and below it,  $M_S < m_b$  (Richter, 1958). Consequently, the  $m_b$  scale is used below magnitude 6.75 and  $M_S$  above. Kanamori (1977) showed that the  $M_S$  scale tends to saturate (underestimate the magnitude) for earthquakes beyond about magnitude 8 and thus introduced the moment magnitude ( $M_W$ ) scale for such great earthquakes. Unlike the other magnitude scales which are based upon the ground-motion amplitudes of seismic waves as measured on seismographs, the  $M_W$  scale is based upon the seismic moment. The seismic moment is directly proportional to the product of the average displacement (slip) and rupture area (mainshock-aftershock zone) on the fault and the rigidity of the rock that was faulted.  $M_W$  magnitudes are often reported for shocks smaller than magnitude 8 when they have been calculated.

The term "intensity," as applied to earthquakes, represents a subjective number based on the observed effects and damages on people, human-made structures, and the Earth's surface at a particular location. Intensities assigned by the AEIC and NEIC are based on the Modified Mercalli (MM) intensity scale of 1931 (Wood and Neumann, 1931), which ranges in steps from I to XII. The subjective effects on people described in the MM intensity scale of 1931 are not reliable considerations for assigning values above the intensity IV level (Stover and Coffman, 1993). Intensities of V and above are assigned primarily on the effects on human structures and their contents; this has been the practice of the USGS for the last decade. The abridged version of the scale is given in table 1. MM intensities of IV and larger observed for 1994 earthquakes are reported in this paper. Lower intensities are reported in addition when needed to depict the extent of the felt area.

## NOTABLE LARGE EARTHQUAKES DURING 1994

The overall pattern of seismicity for Alaska during 1994 is best examined using 103 events greater than or equal to magnitude 4.5, the approximate magnitude level at which the earthquake catalog is complete for the entire state (fig. 3). These shocks include 31 with magnitudes  $m_b$  5.0 to 6.0 (table 2). The seismicity is dominated by activity along the Aleutian arc west of long 160°W., where 79 of the shocks with  $M_L$  or  $m_b$  magnitudes  $\geq 4.5$  and 27 shocks with  $m_b$  5.0 to 6.0 occurred. The largest 1994 shock in Alaska, a shallow  $m_b$  6.0 earthquake, occurred

**Table 1.** Modified Mercalli intensity scale of 1931 (modified from Stover and Coffman, 1993, p. 6–7)

---

I.	Not felt -- except rarely, under especially favorable circumstances.
II.	Felt indoors by few, especially on upper floors. Hanging objects sometime swing.
III.	Felt indoors by several; motion usually rapid vibration. Duration estimated in some cases. Hanging objects may swing slightly. Vibration is like passing of light, or lightly, loaded trucks.
IV.	Felt by many to all. Hanging pictures swing in numerous instances. Trees and bushes shake slightly. Vibration is like passing of heavy truck. Standing motor cars rock noticeably. Buildings shake moderately to strongly. Walls creak loudly. Observers describe the shaking as "strong."
V.	Hanging pictures fall. Trees and bushes shake moderately to strongly. People have difficulty standing or walking. Felt moderately by people in moving vehicles. Some dishes and glassware break. Occasional cracked windows. Many small or unstable objects overturn.
VI.	Many small objects fall from shelves and (or) many glassware items or dishes break. Damage slight in poorly built buildings. Plaster falls or cracks in small amounts. Furniture overturns in many instances. Moderately heavy furnishings move.
VII.	Damage negligible in buildings of good design and construction, slight to moderate in well-built ordinary buildings, and considerable in poorly built or badly designed buildings, adobe houses, old walls, spires, etc. Many chimneys crack, as do some walls. Plaster falls in considerable to large amounts, as does some stucco. Numerous windows and some furniture break. Cornices from towers and high buildings fall. Heavy furniture overturns, with damage from breaking. Concrete irrigation ditches have considerable damage.
VIII.	Trees shake strongly -- branches and trunks break off, especially in palm trees. Sand and mud ejects in small amounts. Flow and temperature of spring and well waters change temporarily or permanently; dry wells renew flow. Slight damage in brick structures built to withstand earthquakes and considerable in ordinary substantial buildings. Partial collapse in racked, tumbled-down wooden houses in some cases. Panel walls in frame structures are thrown out, breaking off decayed piling. Solid stone walls crack and break severely. Wet ground observed to some extent. Chimneys, columns, monuments, factory stacks, and towers twist or fall. Very heavy furniture conspicuously moves or overturns.
IX.	Damage considerable in masonry structures built to withstand earthquakes. Some wood-frame houses built to withstand earthquakes thrown out of plumb. Damage great in substantial masonry buildings with some collapse. Frame buildings wholly shift off foundations. Reservoirs have serious damage. Underground pipes sometimes break. Ground cracks are conspicuous.
X.	Damage serious to dams, dikes, and embankments and severe to well-built wooden structures and bridges, with some destroyed. Dangerous cracks occur in excellent brick walls. Most masonry and frame structures and their foundations are destroyed. Railroad rails bend slightly. Buried pipelines tear apart or crush endwise. Open cracks and broad wavy folds appear in cement pavements and asphalt roads. Ground cracks, especially where loose and wet, up to widths of several inches; fissures up to a yard in width run parallel to canal and stream banks. Sand and mud shift horizontally on beaches and flat land. Water level changes in wells. Water is thrown on banks of canals, lakes, rivers, etc.
XI.	Damage severe to wood-frame structures and great to dams, dikes, and embankments. Few, if any, masonry structures left standing. Large well-built bridges destroyed by the wrecking of supporting piers or pillars. Wooden bridges are affected less. Railroad rails bend greatly and thrust endwise. Buried pipelines completely put out of service. Ground disturbances are frequent and widespread, varying with type of material. Water ejects in large amounts charged with sand and mud. Significant sea waves (tsunami) occur.
XII.	Nearly all structures damaged greatly or destroyed. Ground disturbances great and varied, with numerous shearing cracks. Fault slips in firm rock, with notable horizontal and vertical offsets. Surface and underground water channels disturbed and modified greatly. Lakes dam and rivers deflect. Waves seen on ground surfaces. Objects thrown into the air.

---

on July 29 in the Fox Islands. Three aftershocks with  $m_b$  5.0, 4.3, and 5.4 occurred in the first six hours after the mainshock. The depths of the mainshock and of the  $m_b$  5.4 aftershock were constrained by NEIC to 11 km (using broadband displacement seismograms) and to 22 km (using  $pP$  phases), respectively. The Harvard CMT solutions (reported by the NEIC) for the mainshock and for the  $m_b$  5.4 aftershock exhibit reverse faulting on a shallow plane dipping to the north-northwest and striking to the west-southwest. The CMT solutions of the mainshock and largest aftershock suggest that these shocks were thrust events on the plate-boundary interface.

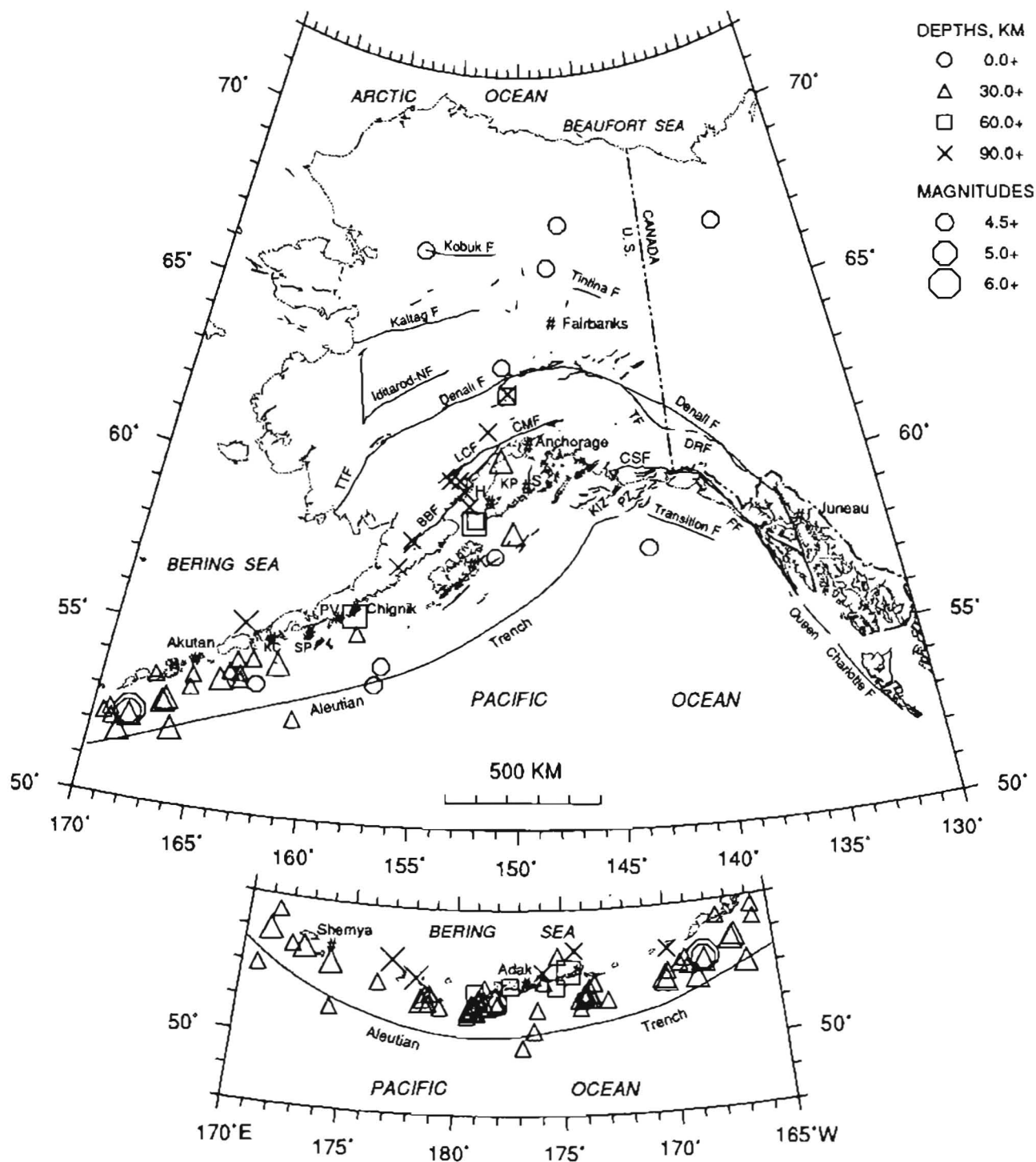
The second largest shock of 1994 ( $m_b$  5.8) struck on April 5 in the Andreanof Islands. The NEIC reported a depth of 20 km from broadband displacement seismo-

grams. The April shock was preceded by two possible foreshocks—an  $m_b$  5.3 shock on March 13 in the same location as the mainshock and an  $m_b$  5.0 event on March 18 approximately 20 km southwest of the mainshock—and was followed by an  $m_b$  4.6 shock on July 18. The Harvard CMT solution from the NEIC for the April earthquake suggests shallow-angle, reverse faulting on a west-southwest-striking, north-northwest-dipping plane, which is compatible with the occurrence of the event on the Aleutian megathrust.

Two other magnitude 5.5 or larger shocks occurred in the Aleutians in 1994: an  $m_b$  5.5 event on May 4 in the Fox Islands slightly landward of the Aleutian trench and an  $m_b$  5.6 event on October 10 in the Andreanof Islands. The Harvard CMT solution for the May 4 shock exhibits

almost pure normal faulting on either of two moderately-dipping planes that strike northeast-southwest approximately parallel to the local strike of the Aleutian trench.

Normal slip is typical in the central and eastern Aleutians for shocks located near the trench; the inferred rupture planes for these shocks trend strictly trench-parallel (Taber



**Figure 3.** Epicenters of 103 earthquakes with magnitudes of 4.5 and larger in Alaska and western Canada for 1994: 47 in upper plot, 69 in lower plot (13 events common to both). Aleutian arc events west of long 160°W. are National Earthquake Information Center epicenters. Symbol type corresponds to depth, and size is proportional to magnitude. Faults and fault abbreviations as in figure 1. Abbreviations: H, Homer; K, Kodiak; KC, King Cove; KP, Kenai Peninsula; PV, Perryville; S, Seward; SP, Sand Point.

Table 2. Source parameters of magnitude 5.0 or greater earthquakes in Alaska for 1994

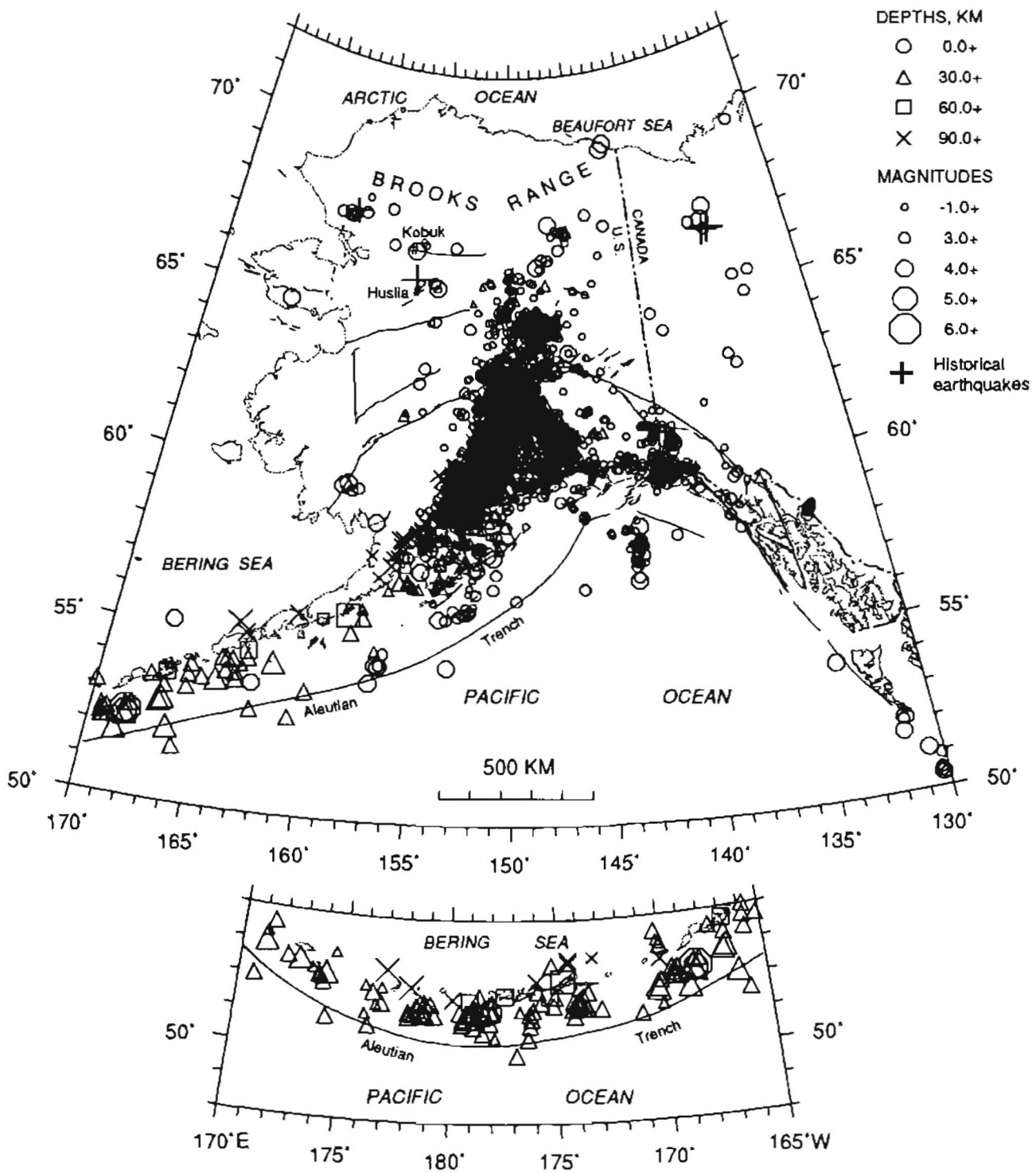
[Events are listed in chronological order. The following data are given for each event:

1. Date And Time in Coordinated Universal Time (UTC): month (Mo), day (Dy), hour (Hr), minute (Mn), and second (Sec). To convert to Alaska Standard Time (AST) or Alaska Daylight Time (ADT), subtract 9 or 8 hours, respectively.
2. Latitude and Longitude of epicenter in degrees (Deg) and minutes (Min).
3. Dep. depth of focus in kilometers (Km). One kilometer equals 0.62 mile. Symbols after the depth indicate the following:  
 N = Depth was fixed at 33 km for earthquakes whose character on seismograms indicates a shallow focus but whose depth is not satisfactorily determined by the data;  
 D = Depth was restrained by the computer program based on two or more compatible pP phases and (or) unidentified secondary arrivals used as pP;  
 G = Depth was fixed by a geophysicist at other than 33 km.
4. Mag, the AEIC local magnitude  $M_L$  is the preferred magnitude, unless it is unavailable or the NEIC reports a body-wave magnitude  $m_b \geq 4.5$  (the magnitude level at which the earthquake catalog is complete for all of Alaska). All magnitudes reported in this table are NEIC  $m_b$  magnitudes.
5. Region, region of occurrence.
6. MM Intensity Report, felt report from the NEIC PDE reports. Intensities assigned by the NEIC are based on the Modified Mercalli (MM) intensity scale of 1931 (table 1).

Date Mo Dy	Time Hr Mn Sec	Latitude Deg Min	Longitude Deg Min	Dep Km	Mag $m_b$	Region and MM Intensity Report
2 5	23 49 13.77	51 48.48N	170 08.70W	33N	5.1	Fox Islands.
2 6	05 55 08.27	51 54.84N	170 12.72W	33N	5.1	Fox Islands.
3 13	03 11 28.68	51 24.00N	178 08.94W	33N	5.3	Andreanof Islands.
3 18	00 11 54.79	51 14.70N	178 40.20W	33N	5.0	Andreanof Islands.
4 5	09 35 44.88	51 17.76N	178 09.12W	20G	5.8	Andreanof Islands.
4 16	08 37 32.98	52 27.72N	176 57.72E	139	5.1	Rat Islands.
4 20	16 8 41.40	52 54.36N	166 48.00W	33N	5.0	Fox Islands.
4 21	16 55 27.56	52 35.10N	172 47.88E	33N	5.0	Near Islands.
4 25	00 19 07.78	60 48.82N	151 01.54W	49	5.4	Kenai Peninsula. Felt V Anchorage, Cooper Landing, Fort Richardson and Kenai; IV at Big Lake, Butte, Eagle River, Hope, Ninilchik, Palmer, Seward, Seward, Sheep Creek, Sterling, Tyonek, and Wasilla; III at Homer and Soldotna; II at Fairbanks.
5 4	11 47 20.39	51 49.26N	168 41.10W	33N	5.5	Fox Islands.
6 25	12 15 13.62	58 58.53N	152 28.11W	66	5.2	Kodiak Island region.
7 14	18 38 09.83	55 24.18N	163 48.84W	167D	5.2	Unimak Island. Felt IV at King Cove; III at Akutan and Sand Point.
7 29	00 17 45.41	52 23.88N	168 19.98W	11G	6.0	Fox Islands.
7 29	01 13 01.21	52 17.04N	168 18.96W	33N	5.0	Fox Islands.
7 29	05 42 27.63	52 20.58N	168 20.52W	22D	5.4	Fox Islands.
8 5	08 14 10.30	52 13.80N	174 14.70E	33N	5.1	Near Islands. Felt IV on Shemya.
8 5	18 28 10.21	51 08.04N	179 17.64W	33N	5.2	Andreanof Islands.
8 6	01 02 52.04	51 05.10N	179 10.32W	33N	5.1	Andreanof Islands.
9 1	01 17 47.25	52 46.20N	166 59.22W	33N	5.2	Fox Islands.
9 1	16 15 17.37	52 06.18N	166 21.24W	33N	5.3	South of Aleutian Islands.
9 3	02 53 03.08	51 17.52N	178 56.04W	33N	5.1	Andreanof Islands.
9 5	02 59 41.47	55 59.22N	158 26.16W	62D	5.3	Alaska Peninsula. Felt V at Chignik, IV at Chignik Lagoon and Perryville; III at Sand Point.
9 11	14 52 52.43	51 56.34N	178 09.30E	99D	5.1	Rat Islands.
9 15	19 48 23.40	54 21.42N	161 51.56W	50D	5.2	Alaska Peninsula. Felt V at King Cove; IV at Cold Bay and Sand Point.
9 19	19 35 26.00	52 10.38N	174 44.46W	64D	5.1	Andreanof Islands. Felt IV on Adak.
9 28	05 37 35.00	51 18.17N	178 23.28E	33N	5.1	Rat Islands.
10 10	21 06 53.70	51 28.32N	173 53.16W	33N	5.6	Andreanof Islands.
10 12	10 33 21.37	51 39.06N	173 54.24W	33N	5.1	Andreanof Islands.
12 8	03 29 11.90	52 59.40N	171 05.76E	33N	5.0	Near Islands.
12 15	04 42 12.26	58 41.30N	150 16.81W	39	5.0	Gulf of Alaska. Felt IV at Birchwood, Homer and Seward; III at Anchorage, Cooper Landing, Kasilof, Kodiak and Ninilchik.
12 26	03 08 17.78	53 41.28N	164 28.80W	33N	5.3	Unimak Island Region.

and others, 1991; Estabrook and Jacob, 1991). The  $m_b$  5.6 October event had five aftershocks ( $m_b$  4.3, 4.9, 4.5, 4.7, and 5.1) within 48 hours; all six of these shocks had depths fixed at 33 km. The CMT solution exhibits low-angle, reverse slip on a west-northwest-striking, north-northeast-dipping plane, which suggests that the shock occurred on the Aleutian megathrust.

The largest shock in 1994 beneath continental Alaska ( $m_b$  5.4) occurred on April 25. Its location, approximately 77 km southwest of Anchorage at a depth of 49 km, places it within the subducting Pacific plate. The moderately well-constrained focal mechanism has a tension axis ( $T$ -axis) aligned west-northwest in the dip direction of the subducted plate similar to that found for events in the



**Figure 4.** Epicenters of 4,626 earthquakes in Alaska and western Canada for 1994: 4,523 in upper plot, 129 in lower plot (26 events common to both). Events along the Alaska Peninsula and Aleutian arc west of long 160°W, are provided by the National Earthquake Information Center. The magnitude level for which the earthquake catalog is complete varies across the state owing to uneven station spacing. Earthquake data are more complete and hypocenters are more accurate in regions where station density is greatest (fig. 1). Symbol type corresponds to depth, and size is proportional to magnitude. Epicenters of 4 historical earthquakes in northwest Canada and western Alaska referred to in the text are indicated by plus symbol, "+." Faults as in figure 1.



Aleutian WBZ beneath southern Alaska (Lahr and others, 1993, 1994). The earthquake triggered an unusually vigorous aftershock sequence for a WBZ shock in the Cook Inlet region; 22 events of magnitude  $M_L$  1.5 to 2.3 occurred within 24 hours. Typically few, if any, aftershocks are detected for such events. In an article published in the Anchorage Daily News, the AEIC requested information from people who felt the earthquake. In response, 397 earthquake questionnaires were returned. They were supplemented with 19 questionnaires that had been sent by the NEIC to post offices, fire stations, and police stations in and near the felt region. While only 8 percent of the questionnaires have been assigned an intensity value to date, preliminary results show that the event was felt over an area of approximately 120,000 km<sup>2</sup> (46,000 mi<sup>2</sup>) in southern and central Alaska. It caused MM intensity V effects in Kenai, Cooper Landing, Anchorage, and Fort Richardson (32 km southwest, 75 km southeast, 77 km northeast, and 88 km northeast, respectively, of the epicenter), intensity IV effects as far as Seward to the south (118 km away) and Palmer to the northeast (135 km away), and intensity II effects as far as 500 km away in Fairbanks.

Two other magnitude 5 or greater shocks occurred in southern Alaska during 1994. On June 25, an  $m_b$  5.2 event occurred beneath southern Cook Inlet at a depth of 66 km. It was followed by two shocks on July 2 and 9 with  $M_L$  2.4 and 3.2, respectively. The poorly controlled focal mechanism suggests strike-slip faulting with a small dip-slip component. The subhorizontal  $T$ -axis is aligned north-west-southeast in the dip direction of the subducted plate, and the  $P$ -axis is aligned with the strike of the subducted plate. These orientations of the  $T$ - and  $P$ -axes are similar to those found by numerous authors for Aleutian WBZ shocks beneath Cook Inlet (Lahr, 1975; Engle, 1982; Pulpan and Frohlich, 1985; Lahr and others, 1993, 1994).

The second notable event is an  $m_b$  5.0 earthquake that occurred on December 15, in the Gulf of Alaska south of the Kenai Peninsula at a poorly constrained depth of 39 km. The earthquake was felt with MM intensity IV effects at Homer and Seward (128 km northwest and 165 km northeast, respectively, of the epicenter) and intensity III effects as far away as Kodiak and Anchorage (160 km southwest and 283 km north, respectively, of the epicenter). The December 15 shock is the largest event to occur within a 100-km radius from its epicenter since an  $m_b$  5.5 event in 1973. The 1973 shock occurred at a depth of 12 km and was about 50 km southeast of the 1994 shock. The poorly controlled focal mechanism of the December 15 event suggests normal, oblique faulting with an east-west-oriented subhorizontal  $T$ -axis and a  $P$ -axis with an intermediate dip to the north-northwest. The orientations of the  $T$ - and  $P$ -axes are consistent with the axes orientations found by Lahr and others (1994) for earthquakes at approximately 50-km depth in the Aleutian WBZ (southern Alaska segment).

## OTHER FEATURES OF THE 1994 SEISMICITY

For 1994, the AEIC analyzed more than 7,000 recorded events (many of which were noise, calibration signals, glacierquakes, quarry or mine blasts, teleseisms, etc.) and located 4,427 earthquakes. The NEIC reported an additional 185 regional shocks located primarily along the Aleutian Islands, and the Pacific Geoscience Center (PGC) of the Geological Survey of Canada provided locations for 14 events in southeastern Alaska. The magnitude level for event location varies across the state due to uneven station spacing and hypocenter depth. Within the area where the regional network is densest (roughly a triangle bounded by: latitude (lat) 59.5°N., longitude (long) 139.0°W.; lat 59.0°N., long 155°W.; and lat 66.0°N., long 148.0°W.), the 1994 catalog is reasonably complete for shallow (depth < 30 km) earthquakes of about magnitude  $M_L$  2.0 and larger. The magnitude threshold at which the catalog is complete increases with increasing depth for the events in the WBZs. For earthquakes deeper than 100 km in the southern Alaska segment of the Aleutian WBZ, the catalog is complete above about magnitude  $M_L$  2.7. Focal depths for shallow shocks generally are not well constrained owing to the relatively large distances between stations and the misfit of the regional velocity models to the actual velocities within the crust.

## PLATE-BOUNDARY EARTHQUAKES

Historically, most of the seismic energy in Alaska and western Canada is released in earthquakes of magnitude 7 and greater that occur on the primary plate interface as right-lateral, strike-slip events in western Canada, southeast Alaska, and the western Aleutians, and as thrust-type earthquakes from the Gulf of Alaska toward the central Aleutians (Taber and others, 1991; Page and others, 1991; Rogers and Horner, 1991). The dip of the plate boundary along the Aleutian trench varies from a minimum of 4-5° in the Gulf of Alaska to a maximum of 25-30° in the central Aleutians (Taber and others, 1991). Beneath a certain depth, estimated to be about 40 km in the Aleutian arc (Davies and House, 1979) and about 20 km in the northern Prince William Sound region (Page and others, 1989, 1992), the interface is believed to slip aseismically.

Nearly the entire 5,300-km-long plate boundary in Alaska and western Canada north of lat 50°N. has experienced a series of shocks in this century ranging in size from  $M_S$  7.0 to  $M_W$  9.2 (fig. 2; Page and others, 1991; Taber and others, 1991; Rogers and Horner, 1991). The rupture zones of these large events, defined by the extent of their aftershock zones, tend to abut rather than over-



lap, except for several small regions that have been identified as "seismic gaps." Seismic gaps are areas of seismically active plate margins that have not recently ruptured, but where future large earthquakes are expected (for example, Mogi, 1968; Sykes, 1971; Kelleher and Savino, 1975; McCann and others, 1980). Three seismic gaps have been identified in Alaska and western Canada: the Shumagin, the Queen Charlotte Islands, and the Yakutat seismic gaps (fig. 2).

The Shumagin seismic gap in the Shumagin Islands region south of the Alaska Peninsula extends about 225 km from the east end of the aftershock zone of the 1946  $M_S$  7.4 earthquake (near long 161.5°W.) and the western end of the 1938  $M_W$  8.2 earthquake (near long 158.4°W.; Taber and others, 1991). The largest shock to occur in the Shumagin seismic gap in 1994 was an  $m_b$  5.2 shock at a depth of 50 km on September 15 (fig. 4). The Harvard CMT solution suggests strike-slip faulting on near-vertical planes striking northwest-southeast and northeast-southwest. The location, depth, and CMT solution of this event places it within the subducting Pacific plate and not on the Aleutian megathrust.

The Queen Charlotte Islands seismic gap in western Canada extends from the south end of the aftershock zone of the 1949  $M_W$  8.1 Queen Charlotte Islands earthquake (near lat 52.4°N.; fig. 2) to the epicenter of the mainshock of the 1970  $M_S$  7.1 Cape St. James earthquake (near lat 51.8°N.; Rogers, 1986). An earthquake of magnitude 7.5 or greater would be required to completely fill this 75-km-long seismic gap and can be expected to have a combined strike-slip and thrusting mechanism with a minor thrust component similar to the 1970 Cape St. James earthquake immediately to the south (Rogers, 1986). The largest shocks to occur within this seismic gap since 1954 are in the magnitude 4 class (Rogers, 1986). The most notable seismicity in 1994 near the Queen Charlotte-Fairweather fault system (fig. 4) occurred within and around the Queen Charlotte Islands seismic gap (10 shocks with magnitudes from  $M_L$  3.2 to  $m_b$  4.2). Three events with  $m_b$  magnitudes of 3.5, 4.0, and 4.1 occurred within the southern half of the seismic gap (near lat 52°N., long 131.5°W.). The largest shock in the tight cluster of earthquakes near lat 50.3°N. and long 130.3°W. was an  $m_b$  4.2 event on July 15. This event was preceded by two events on July 10 and 11 ( $M_L$  3.2 and  $m_b$  3.5, respectively) and was followed by an  $m_b$  3.8 shock on November 2. An isolated  $m_b$  4.2 event occurred on July 7 off the northwest end of Graham Island (lat 53.9°N., long 133.9°W.). All of the earthquakes along the Queen Charlotte fault in 1994 had focal depths fixed at either 10 or 18 km.

The Yakutat seismic gap, which extends for about 175 km along the coast of southern Alaska from the western limit of the 1979  $M_W$  7.3 St. Elias earthquake aftershock zone (Stephens and others, 1980; Estabrook and

others, 1992) near Icy Bay to the eastern extent of the 1964 rupture near Kayak Island (fig. 2), experienced two  $M_W$  8.1 shocks in 1899 that ruptured the transitional segment between Kayak Island and the western extent of the 1958  $M_W$  7.7 Fairweather Fault earthquake near Yakutat Bay (McCann and others, 1980; Page and others, 1991). This seismic gap is considered a likely site for an  $M_S$  7.8 or greater thrust earthquake within the next few decades (McCann and others, 1980; Lahr and others, 1980; Jacob, 1984).

Seismicity of the Yakutat seismic gap region has been monitored nearly continuously since 1974 (Fogleman and others, 1993). During this period (1974–1994), the spatial distribution of seismicity, in a belt extending 90 km inland from the coast, has remained relatively stable. It is characterized by broad concentrations of shallow seismicity (fig. 5) beneath Icy Bay, Waxell Ridge, and the Copper River Delta separated by areas of relative quiescence. The most active area has been the aftershock zone of the St. Elias earthquake, both prior to and since 1979, which involved low-angle, north-northwest-directed thrusting (Estabrook and others, 1992) at depths between 10–15 km (Stephens and others, 1980) in a zone that is, at least locally, no more than 2–3 km thick (Page and others, 1984). Stephens and others (1992) found that hypocenters of better-recorded shocks in the diffuse patch of seismicity near Waxell Ridge, at the center of the Yakutat seismic gap, are concentrated near a depth of 12 km, comparable to the depth of the Aleutian megathrust as defined by the seismicity beneath the St. Elias area. The largest earthquakes located within the gap since 1971 are in the magnitude 4 class. Two shallow magnitude 3 shocks were located within the gap in 1994: an  $M_L$  3.4 shock that occurred on January 3, with an epicenter about 25 km east of the Waxell Ridge concentration of seismicity (lat 60.4°N., long 142.3°W.), and an  $M_L$  3.2 event that occurred on July 3 southwest of Waxell Ridge (lat 60.4°N., long 143.6°W.). The shallow foci computed for these two events (5 and 0 km, respectively) are poorly constrained; consequently, it is uncertain whether these events originated in the overriding plate or on the megathrust.

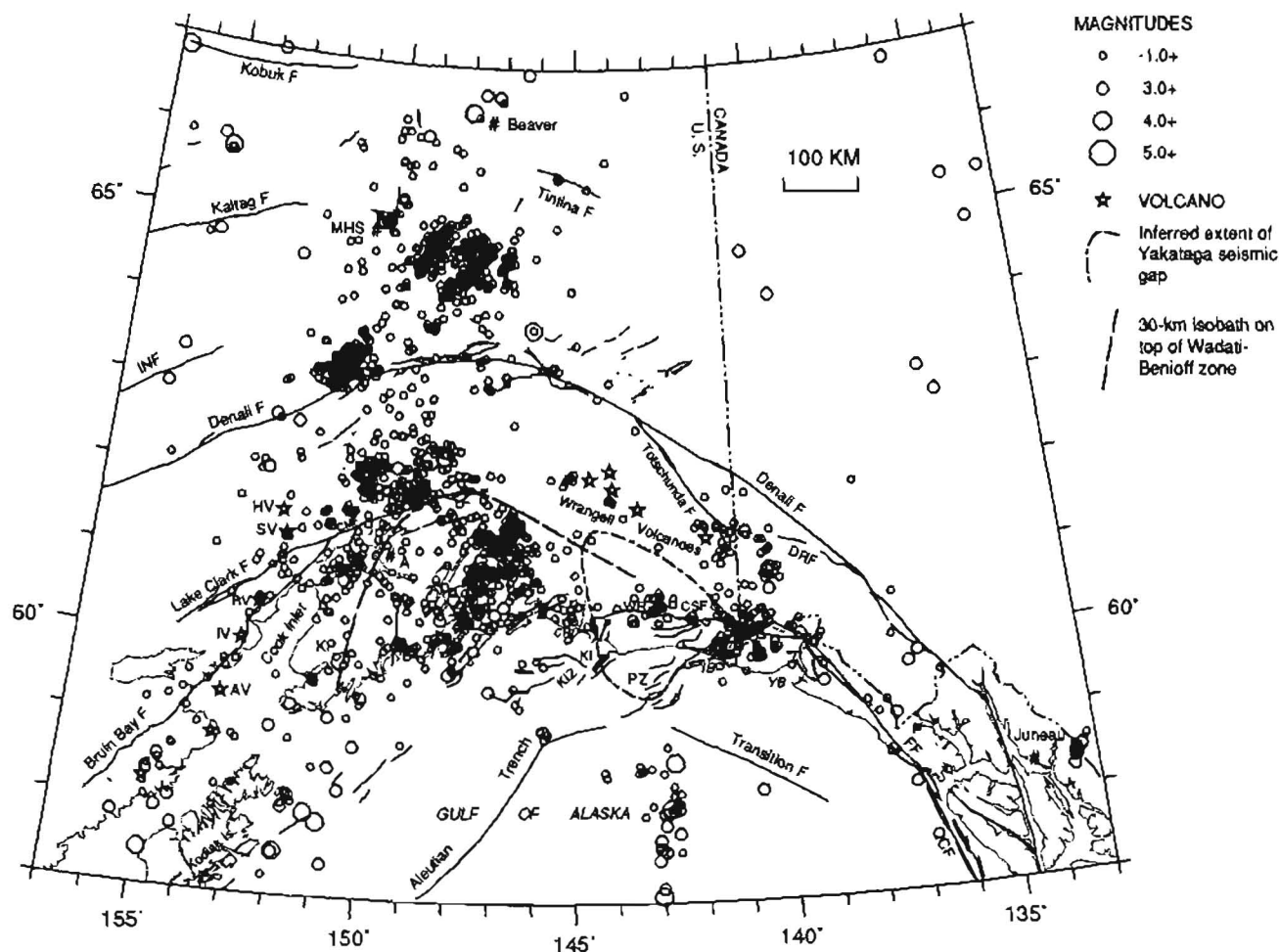
## TRENCH AND UNSUBDUCTED OCEANIC INTRAPLATE EARTHQUAKES

The apparent rate of historical (Taber and others, 1991; Page and others, 1991) and current seismicity for earthquakes within the Pacific plate beneath or seaward of the Aleutian trench and the Transition fault is low compared with other parts of the subduction zone (figs. 3, 4). The most active area encompasses the aftershock zones (fig. 2) of the 1987 ( $M_W$  7.2 and  $M_W$  7.8) and 1988 ( $M_W$  7.7) Gulf of Alaska earthquakes (Lahr and others, 1988; Hwang and Kanamori, 1992). These major

intraplate, strike-slip oceanic events occurred in the northern Gulf of Alaska along conjugate trends in a region where seismicity had not been previously located. The two largest events ruptured a composite, 250-km-long, north-striking fault in the Pacific plate south of the Yakataga seismic gap and are among the largest oceanic intraplate earthquakes ever recorded (Page and others, 1991). Large oceanic intraplate shocks are rare and usually involve normal or thrust faulting away from the trench within the unsubducted portion of the plate (Lahr and others, 1988). Lahr and others (1988) suggested that these events reflect shear stress in the Pacific plate seaward of the boundary between the locked Yakataga seismic gap and the Aleutian megathrust segment that slipped in the great 1964 earthquake. The latitudes and magnitudes of the largest shocks located in 1994 in the aftershock zones

of the 1987–1988 shocks are 58.7°, 58.1°, 57.1°N., and  $M_L$  4.0, 4.5, 4.0, respectively (figs. 4, 5). The focal depths of trench and unsubducted oceanic intraplate earthquakes located by AEIC are routinely fixed at 10 km below sea level owing to poor hypocentral control.

In contrast to the Gulf of Alaska shocks, which extend as far as several hundred kilometers south of the Aleutian trench, most of the events detected along the rest of the Aleutian arc during 1994 (fig. 4) extend only 50 to 60 km oceanward of the trench. This pattern is consistent with the results of an ocean-bottom seismometer (OBS) study in the central Aleutians (Frohlich and others, 1982), where events were shallower than 20 km and extended up to 10 km landward and 60 km oceanward of the trench axis. Focal mechanisms of historical and 1994 events oceanward of the trench in the Aleutian Is-



**Figure 5.** Epicenters of 1,959 earthquakes with depths shallower than 30 km in southern and central Alaska and western Canada for 1994. Earthquake data are more complete in regions where station density is greatest (fig. 1). Quaternary volcanoes (stars): AV, Augustine volcano; HV, Hayes volcano; IV, Iliamna volcano; RV, Redoubt volcano; SV, Spurr volcano. Also: CMF, Castle Mountain fault; CSF, Chugach–St. Elias fault; DRF, Duke River fault; FF, Fairweather fault; INF, Iditarod–Nixon Fork fault; KIZ, Kayak Island zone; PZ, Pamplona zone; QCF, Queen Charlotte fault; A, Anchorage; CRD, Copper River Delta; IB, Icy Bay; KI, Kayak Island; KP, Kenai Peninsula; MHS, Manley Hot Springs; WR, Waxell Ridge; YB, Yakutat Bay.

lands are consistent with normal faulting, and the tension axis is approximately perpendicular to the trench (Taber and others, 1991). The trench-parallel normal faulting may reflect either spatial-temporal variations of bending stresses related to the earthquake cycle of great earthquakes at each plate boundary or may be a stationary feature related to permanent differences along the arc in the degree of coupling at the plate interface (Taber and others, 1991; Estabrook and Jacob, 1991).

The largest shock beneath or seaward of the Aleutian trench during 1994, an  $m_b$  5.3 shock on September 1 (fig. 4), occurred beneath the trench (lat 52.1°N., long 166.3°W.) and was preceded by an  $m_b$  4.4 event on July 7 (approximately 70 km southeast of the September shock). A notable, diffuse cluster of earthquakes occurred in 1994 centered near lat 54.5°N. and long 156.8°W. The largest shock in this cluster, an  $m_b$  4.9 earthquake on October 24, occurred slightly landward of the trench. This event was followed within 8 minutes by an  $M_L$  3.9 aftershock (approximately 20 km north-northeast of the mainshock) and was preceded by an  $M_L$  3.2 foreshock on October 22 (about 5 km west of the mainshock). The October earthquakes were preceded by two nearby earthquakes: an  $M_L$  4.1 shock on January 13 and an  $m_b$  4.7 shock on September 5 (approximately 5 km east and 60 km southwest, respectively, of the  $m_b$  4.9 October 24 event).

## WADATI-BENIOFF ZONE EARTHQUAKES

Wadati-Benioff seismic zones are associated with both the northwest- to north-dipping Aleutian volcanic arc and the north-northeast-dipping Wrangell volcanic arc (fig. 6). Although the Aleutian volcanic arc terminates at Hayes volcano (lat 61.6°N., long 152.4°W.; fig. 6), the associated WBZ continues about 350 km farther north to lat 64.25°N. (fig. 6). Along the Aleutian WBZ west of long 156°W. (fig. 4), relatively few events can clearly be identified as WBZ activity owing to poor depth resolution (the majority of the events are held to 33-km depth by the NEIC.) The largest shocks in 1994 west of long 156°W. with depths greater than 33 km were six magnitude 5 events (fig. 3; table 2): (1) an  $m_b$  5.1 shock on April 16 at 139-km depth in the Rat Islands (lat 52.5°N., long 177.0°E.); (2) an  $m_b$  5.2 event on July 14 at 167-km depth north of Unimak Island (lat 55.4°N., long 163.8°W.), which was felt at King Cove (110 km southeast of the epicenter) with MM intensity IV effects; (3) an  $m_b$  5.3 earthquake on September 5 at 62-km depth beneath the Alaska Peninsula (56.0°N., 158.5°W.), which caused MM intensity V effects at Chignik and intensity IV effects at Chignik Lagoon and Perryville (34 km north, 41 km north,

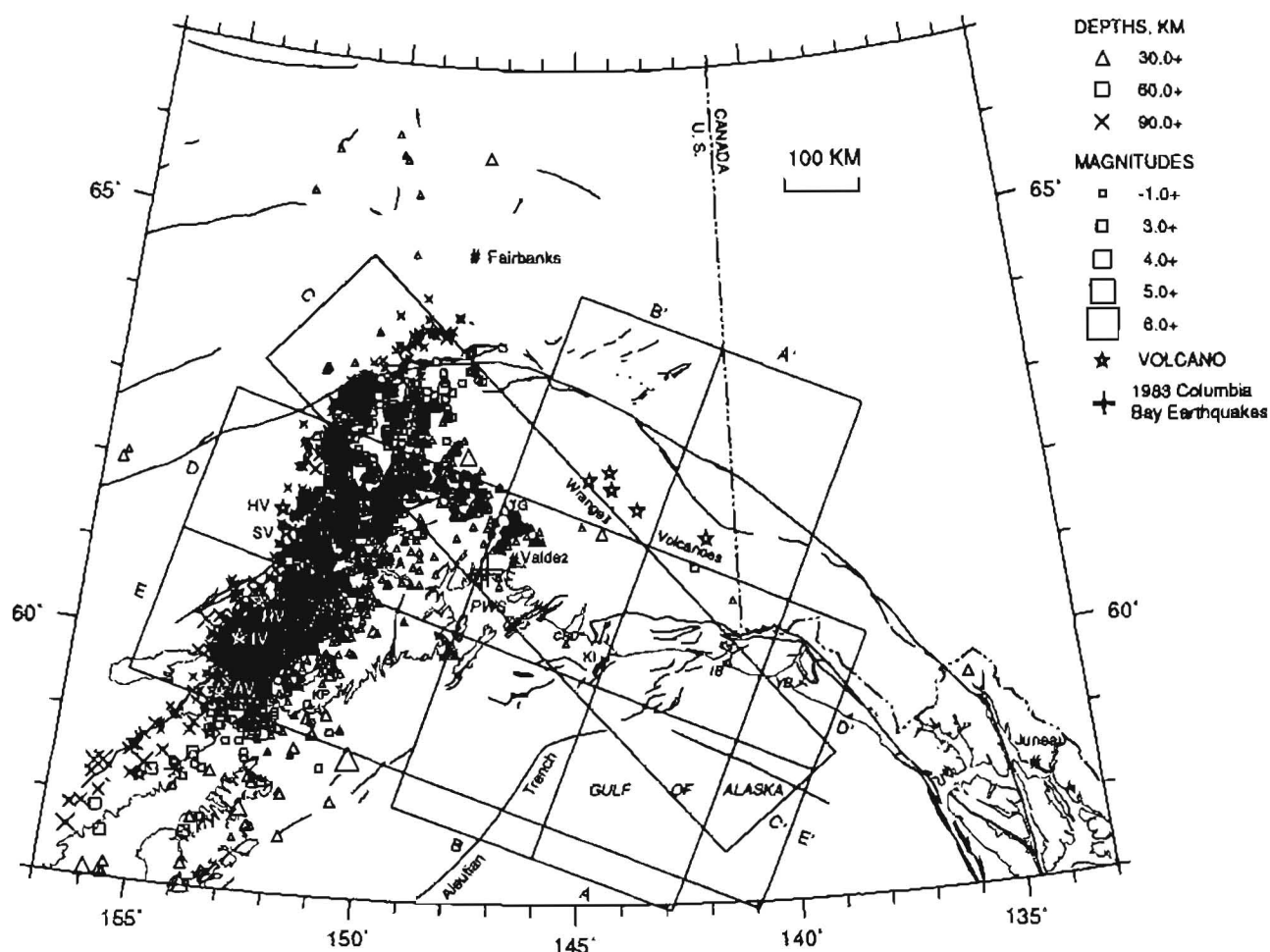
and 45 km west, respectively, of the epicenter); (4) an  $m_b$  5.1 earthquake on September 11 at 99-km depth in the Rat Islands (lat 51.9°N., long 178.2°E.); (5) an  $m_b$  5.2 shock on September 15 at 50-km depth south of the Alaska Peninsula (lat 54.3°N., long 161.9°W.), which was felt with MM intensity V effects at King Cove and MM intensity IV effects at Cold Bay and Sand Point (83 km north-northwest, 108 km northwest, and 140 km northeast, respectively, of the epicenter); and (6) an  $m_b$  5.1 event on September 19 at 64-km depth beneath the Andreanof Islands (lat 52.2°N., long 174.7°W.), which caused MM intensity IV effects at Adak (139 km west-southwest of the epicenter). The largest WBZ shocks east of long 156°W. in 1994, the  $m_b$  5.4 shock on April 25, the  $m_b$  5.2 event on June 25, and the  $m_b$  5.0 December 15 earthquake, were previously discussed in the section on notable large earthquakes.

West and north of the Cook Inlet region, the distribution of earthquakes in 1994 below 30-km depth is dominated by activity within the Aleutian WBZ (fig. 6). This zone dips 8–10° west-northwestward beneath the Kenai Peninsula and Anchorage and steepens to a 50° dip west of Cook Inlet (fig. 7, sections C–C', D–D', E–E'). The apparent steepening of the dip to nearly 90° at the deep end of the sections is an artifact of locating events using a flat-layered velocity model (McLaren and Frohlich, 1985). The Aleutian WBZ west of Cook Inlet dips at an angle between 30° (Davies and House, 1979) in the Shumagin Islands and 60° (Engdahl and Gubbins, 1987) in the Adak region. Beneath both the southern Kenai Peninsula and Anchorage, the upper surface of the Aleutian WBZ is at a depth of 29 to 35 km, whereas beneath the volcanic arc west of Cook Inlet, it is at a depth of about 100 km. The average dip of the shallow (depth < 30 km) part of the zone is about 7° beneath Prince William Sound (Page and others, 1991). On a regional scale using only events with well-constrained focal depths, the thickness of the Aleutian WBZ ranges from 10 to 15 km beneath Prince William Sound (Page and others, 1994) and from 15 to 35 km beneath the western Kenai Peninsula, Cook Inlet, and the volcanoes west of Cook Inlet (fig. 7, sections C–C', D–D', E–E'). The maximum focal depth for 1994 earthquakes in southern Alaska varies along the length of the WBZ from 219 km near Iliamna volcano (fig. 7, section E–E') to 150 km beneath Hayes volcano (fig. 7, section D–D') and 151 km beneath the Alaska Range (fig. 7, section C–C'). The deepest shocks in the Aleutian WBZ west of long 160°W. for 1994 were at depths of 210 and 200 km beneath the Bering Sea (lat 52.75°N., long 174.4°W.) on June 24 ( $m_b$  4.1) and December 27 ( $m_b$  4.7), respectively. The maximum focal depth of earthquakes in the Aleutian Islands from previous years varies from 250 to 300 km (Taber and others, 1991).

The geometry of the Aleutian WBZ changes along strike, as documented by studies of teleseismically and regionally recorded earthquakes (Van Wormer and others, 1974; Lahr, 1975; Davies, 1975; Agnew, 1980; Pulpan and Frohlich, 1985). At approximately lat 59°N. in lower Cook Inlet, the strike of the WBZ abruptly changes direction from about 40° east of north to 25° east of north, coincident with a similar northward bend in the strike of the associated chain of volcanoes (fig. 6). About 400 km farther north along strike (near lat 62.5°N.), the strike changes trend from about 25° east of north to 60° east of north. The Aleutian WBZ seismicity east of the Cook Inlet region ends abruptly along a northwest-trending line that approximately parallels the direction of plate convergence.

The rate and character of the 1994 seismicity in the shallow and deep (depth < 45 km) parts of the Aleutian

WBZ are significantly different, with a higher level of activity in the deep part of the zone beneath the western Kenai Peninsula, Cook Inlet, and the volcanic arc. The distribution of seismicity exhibits a significant component of spatial and temporal clustering. Clustering is more common in the shallow WBZ, where significant aftershock sequences occur as exemplified by those following the two  $m_b$  6.2 1983 Columbia Bay earthquakes (fig. 6, near lat 61.0°N., long 147.2°W.). These earthquakes involved normal faulting on a steeply northwestward-dipping plane between depths of 22 to 35 km (Page and other, 1985, 1989). In contrast, few, if any, aftershocks are typically detected following shocks in the deep part of the WBZ. The north-northeast-trending swath of seismicity centered at lat 61.5°N., long 146.5°W. beneath the Tazlina Glacier (figs. 5, 6), is a persistent but diffuse concentration of events not associated with an aftershock



**Figure 6.** Epicenters of 2,433 earthquakes with depths equal to and below 30 km in southern and central Alaska for 1994. Symbol type corresponds to depth, and size is proportional to magnitude. Boxes indicate selection areas for hypocenters shown in figure 7. Faults as in figure 5. Abbreviations: AV, Augustine volcano; HV, Hayes volcano; IV, Iliamna volcano; RV, Redoubt volcano; SV, Spurr volcano; CRD, Copper River Delta; IB, Icy Bay; KI, Kayak Island; KP, Kenai Peninsula; PWS, Prince William Sound; TG, Tazlina Glacier; YB, Yakutat Bay.

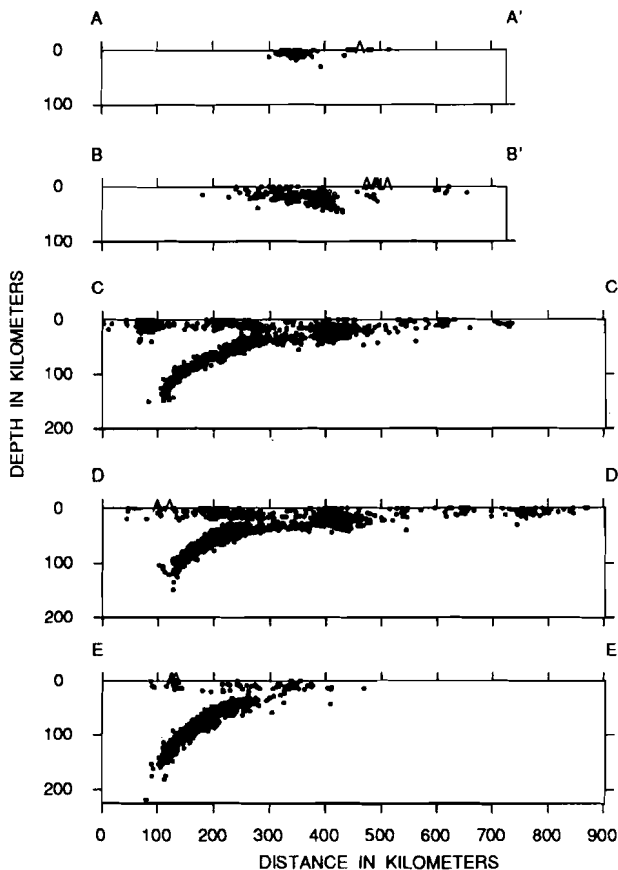
sequence. Relocated events in the Tazlina Glacier cluster have depths between 25 and 45 km (Page and others, 1989). Spatial clustering in the WBZ west of Prince William Sound is conspicuous (fig. 6) with concentrations of events deeper than 30 km about 60 km north-northwest of Anchorage (lat 61.7°N., long 149.6°W.) and events deeper than 110 km beneath Iliamna volcano (lat 60°N., long 153°W.) and Mt. McKinley (lat 63°N., long 150.3°W.). Some regions are relatively quiet, such as in the vicinity of the two points lat 60.8°N., long 152.5°W. and lat 62.5°N., long 150.2°W.

An unusually deep (219 km), moderate size ( $m_b$  4.6) earthquake occurred in 1994 on December 10 in the Aleutian WBZ east of long 156°W., about 250 km southwest of Anchorage. Only three other shocks with well-constrained depths greater than 200 km have been located in the WBZ in southern Alaska since 1971, when the USGS seismic network began operation (Fogleman and others, 1993). A moderately well-constrained focal

mechanism for the recent event indicates that its  $T$ -axis is oriented about 15° counterclockwise of the dip direction of the WBZ beneath Cook Inlet and that its  $P$ -axis trends north-south. These axis orientations are consistent with what Lahr and others (1994) found for WBZ shocks in southern Alaska below about 75-km depth.

Relatively few events occurred in 1994 in the weakly active Wrangell WBZ (fig. 6; fig. 7, sections A–A', B–B'), which dips to the north-northeast beneath the Wrangell volcanoes (Stephens and others, 1984; Page and others, 1989; Fogleman and others, 1993). The difference in the rates of seismicity between the Wrangell and Aleutian WBZ zones may be due to thermal or age differences in the descending plate (Stephens and others, 1984), or to the relatively small component of plate convergence (about 3.7 cm/yr) in the downdip direction of the Wrangell WBZ (Estabrook and others, 1992). Page and others (1989) found that the seismicity in the Aleutian and Wrangell zones appears to be continuous, at least in the depth range 20–45 km, and may define adjacent limbs of a buckle in the subducted Pacific plate. The largest shock located in the Wrangell WBZ during 1994 is an  $M_L$  3.1 event on August 24 at 42-km depth (lat 61.5°N., long 144.3°W.). The moderately well-constrained focal mechanism exhibits predominantly strike-slip faulting with an east-west-trending, subhorizontal  $T$ -axis and a north-south-trending  $P$ -axis oriented downdip. Although few well-constrained solutions are available for the Wrangell seismic zone, the axis orientations of the August shock are compatible to those found by Page and others (1989) for the largest ( $m_b$  4.6) Wrangell shock (52-km depth) yet recorded by the regional network. The stress field within the Wrangell WBZ is unknown because of the low level of seismicity (Page and others, 1989).

The stress orientation within the Aleutian WBZ east of long 156°W., inferred from focal-mechanism solutions of earthquakes since 1970, generally is characterized by in-plane, downdip tension (Page and others, 1991; Lahr and others, 1994). This stress orientation is consistent with the idea that the Pacific plate acts as a stress guide that propagates the body forces upward from the deeper parts of the subducted slab (Lahr and others, 1994). The stress orientation of the Aleutian WBZ west of long 156°W., inferred from historical focal mechanisms, varies in both time and space along the arc (Taber and others, 1991) and cannot be simply characterized.



**Figure 7.** Vertical cross sections of better-constrained hypocenters (horizontal errors  $\leq 5$  km, vertical errors  $\leq 10$  km) in southern and central Alaska for 1994. Section locations indicated in figure 6. Quaternary volcanoes plotted as triangles above zero depth. No vertical exaggeration.

## NORTH AMERICAN PLATE EARTHQUAKES

Crustal earthquakes within the North American plate occur over most of the state (figs. 3–5). Seismicity is highest in southern and central Alaska and decreases northward away from the plate boundary. Historically, the only region of Alaska that appears to be aseismic is the North



Slope (Page and others, 1991), the part of Alaska north of the Brooks Range. The fault-plane solutions from the historical data in southern, central, and northern Alaska typically indicate strike-slip and reverse-slip motion with northwest- to north-oriented compressional axes, whereas solutions from west-central Alaska generally indicate normal-slip motion with northerly oriented tensional axes (Page and others, 1991; Estabrook and Jacob, 1991). Both the distribution of historical seismicity and the available focal mechanisms are consistent with the theory that the seismicity within the North American plate, excluding west-central Alaska, results from stresses arising from the collision of the Pacific and North American plates along the northern Gulf of Alaska (Lahr and Plafker, 1980; Davies, 1983; Estabrook and others, 1988; Page and others, 1991; Estabrook and Jacob, 1991). Page and others (1995) offer a seismotectonic model for east-central Alaska that attributes the seismicity east of about long 150°W. to the clockwise rotation of elongate, northeast-oriented blocks caused by right-lateral shear between the bounding right-lateral strike-slip Denali and Tintina fault systems in response to convergence between the Pacific and North American plates. The rotation is manifest by left-lateral faults striking northeast to north-northeast at a high angle to the bounding right-lateral fault systems.

The distribution of 1994 crustal seismicity is diffuse and the majority of the events cannot be clearly associated with mapped fault traces (figs. 3–5). The diffuse character of the seismicity outside of the densest part of the regional network may be partially attributed to the degraded detection capability of the network. Shallow (depth < 30 km) shocks located seaward of the 30-km isobath on the Aleutian-Wrangell WBZ in southern Alaska in 1994 (fig. 5) are discussed in the sections on plate-boundary and WBZ shocks. Shallow shocks located landward of the 30-km isobath and landward of the Queen Charlotte–Fairweather fault system in 1994 are in the North American plate. Several conspicuous concentrations are seen in southern and central Alaska in the 1994 data (fig. 5): (1) a diffuse group of shocks along and south of the Duke River fault on the U.S.–Canada border, (2) a diffuse north-northeast-trending band of seismicity near long 150°W. beneath the upper Cook Inlet, (3) a east-west-trending zone of shocks north of the Castle Mountain fault, (4) a northeast-trending cluster of epicenters about 80 km long north of the Denali fault near long 151°W., and (5) a broadly distributed pattern of activity in the Fairbanks area with a general northeast-southwest grain and several distinct zones.

To some degree, the apparent scatter of the seismicity in eastern Alaska and western Canada near the Duke River fault reflects errors in the locations of the epicenters. Recent shocks located from both regional (Horner, 1983) and local (Power, 1988) recordings reveal that the

seismicity is mostly concentrated in the vicinity of the Duke River fault. An unusual crustal shock of magnitude  $M_L$  4.3 occurred on February 2 south of the Duke River fault (lat 61°N., long 140.2°W.) in an area devoid of mapped Neogene and younger faults. This event had a poorly constrained depth (nominally at 0 km) and was followed within 6 hours by three aftershocks with magnitudes  $M_L$  2.4, 3.1, and 2.0.

The north-northeast-trending zone of diffuse seismicity beneath northern Cook Inlet and the east-west-trending zone north of the Castle Mountain fault (fig. 5) clearly lie above the Aleutian WBZ (fig. 7, sections C–C', D–D'). The northern Cook Inlet activity follows a broad fold and thrust belt. Two new stations, one three-component and one single-component vertical, were installed near Anchorage in the summer of 1994 to help investigate the nature of the persistent seismicity and to evaluate the hazard that buried faults within this zone may pose to Anchorage and the surrounding area.

The rate of activity for magnitude 2 and smaller shocks in the northeast-trending cluster of epicenters north of the Denali fault near long 151°W. (fig. 5) appears to have increased threefold since November 1993 relative to the previous four years. The rate of magnitude 3 and larger shocks has remained constant since at least 1990. The cause of the apparent increase in microseismicity is under investigation. Two magnitude 4 shocks occurred in November in this cluster within a few kilometers of one another (lat 63.5°N., long 151.1°W.). The  $m_b$  4.6 mainshock on November 7 occurred at a depth of 12 km. It was preceded 50 minutes earlier by an  $M_L$  2.4 foreshock and followed within 4 hours by three aftershocks with magnitudes  $M_L$  2.4, 2.0, and 2.7. The  $M_L$  4.3 shock of November 17 occurred at a depth of 11 km. This event was preceded 18 hours earlier by an  $M_L$  2.9 foreshock and followed within 20 hours by five aftershocks with  $M_L$  1.8, 2.6, 2.8, 2.0, and 2.2. The patterns of *P*-wave first motions for the mainshocks are almost identical. Although the focal mechanisms are poorly controlled and allow either reverse or strike-slip solutions, they have horizontal, northwest-trending *P*-axes that are consistent with the *P*-axis orientations of historical solutions (Page and others, 1991). The northeast-striking nodal planes for the reverse solution are nearly parallel to the trend of the seismic cluster, which indicates that the events are probably due to reverse-slip motion on a northeast-trending fault.

An  $M_L$  4.0 earthquake occurred in 1994 on October 17 in central Alaska, approximately 50 km north of the Denali fault (lat 64°N., long 146.1°W.). The event was followed 21 minutes later by an  $M_L$  2.8 aftershock. The patterns of first motions for the mainshock and the aftershock are almost identical. The mainshock's well-controlled focal mechanism has a subhorizontal, north-



northeast- to south-southwest-oriented  $P$ -axis and allows reverse slip on either a steep southwest-dipping plane or a shallow northwest-dipping plane. The northeast-striking nodal plane for the thrust solution is near a series of northeast-oriented mapped faults, which indicates that the mainshock and aftershock are probably due to reverse-slip motion (with a significant component of left-lateral motion) on a northeast-trending fault.

Activity in the Fairbanks area in 1994 displays a northeast-southwest grain with several noteworthy clusters and trends (fig. 5). The easternmost cluster is the Salcha seismic zone (Biswas and Tytgat, 1988), approximately 40 km southeast of Fairbanks, which is characterized by a conspicuous, narrow band of activity approximately 50 km long. Although the current and historical seismicity suggest the presence of a northeast-trending fault, no fault with Quaternary displacement has yet been recognized (Cluff and others, 1974). Farther west is the Fairbanks seismic zone (Gedney and others, 1980), a diffuse zone of epicenters about 40 km wide and 150 km long. On November 2, an  $M_L$  3.3 shock occurred 12 km northeast of Fairbanks at a depth of 14 km. This quake produced MM intensity III to intensity V effects throughout the Fairbanks area. The quake awakened many residents, rattled houses, knocked items off shelves, and shifted one fuel tank on its mounting. The well-constrained focal mechanism solution for this event indicates left-lateral strike-slip motion on a northeast-striking vertical plane. This solution is consistent with the northeast-southwest trend of seismicity in the Fairbanks area and with the mechanisms for historical activity in the Salcha seismic zone (Wickens and Hodgson, 1967; Hammond and others, 1993) and in the Fairbanks seismic zone (Matumoto and others, 1968). West of the Fairbanks seismic zone is the Minto Flats seismic zone (Biswas and Tytgat, 1988), a diffuse northeast-trending zone of earthquakes about 100 km long. A magnitude  $M_L$  4.0 earthquake occurred in this zone (lat 65.1°N., long 150.4°W.) on December 17 at a depth of 11 km. It was felt with MM intensity III to intensity IV effects at Manley Hot Springs, 14 km southwest of the epicenter. The event was followed 10 hours later by an  $M_L$  3.0 aftershock. An  $m_b$  4.6 event that occurred on March 30 about 180 km north of Fairbanks (lat 66.5°N., long 148.0°W.) has a poorly constrained depth (fixed to 20 km) and was felt with MM intensity IV effects at Beaver, 29 km to the southeast.

Notable crustal shocks in northeast Alaska in 1994 (fig. 4) include an  $m_b$  4.9 earthquake on January 5 in northern Alaska near lat 67.6°N., long 147°W. The mainshock was preceded by an  $M_L$  3.7 foreshock on January 3 and was followed by five aftershocks with magnitudes ranging from  $M_L$  3.8 to 2.5. The northernmost earthquakes located in Alaska in 1994 are an  $M_L$  4.2 shock on July 5 and an  $M_L$  4.3 shock on July 17, both in the

northeast Brooks Range (lat 69.7°N., long 143°W.). Correlations between specific shocks and geologic structures for events in northeast Alaska are not possible with the low occurrence rate and poor precision of the historical (Page and others, 1991) and current data.

Earthquakes in western and southwestern continental Alaska include an  $M_L$  4.4 event on February 10, which occurred in southwestern Alaska beneath the Kuskokwim Mountains (lat 59.6°N., long 159.1°W.). It was preceded by two shocks ( $M_L$  4.0 and 3.5) on February 9 and followed by an  $M_L$  3.3 event on February 11. These four earthquakes may be associated with the northeast-southwest-trending Togiak-Tikchik strand of the Denali fault system. On April 10, an  $M_L$  4.6 shock and two aftershocks ( $M_L$  2.5 and 2.6) occurred in western Alaska near the western end of the east-west trace of the Kobuk fault (lat 66.6°N., long 156.5°W.). The fault locally displaces late Quaternary deposits in a dextral sense (Brogan and others, 1975). The mainshock produced MM intensity IV effects at Kobuk, located 10 km to the north-northwest. On September 3, an  $M_L$  4.1 shock occurred 64 km east of Huslia (lat 66°N., long 155.6°W.) near the epicenter of the 1958  $M_S$  7.3 Huslia earthquake, the largest event in the historical record in western Alaska (Page and others, 1991). The 1958 shock involved normal slip on either a shallow, north-northwest-dipping plane or a steep, south-southwest-dipping plane (Page and others, 1991, fig. 13, p. 64). An unusual swarm of eight events occurred in northwestern Alaska in December 1994 centered near lat 67.5°N., long 162°W. The events ranged in magnitude from 3.0 to 3.8 and had depths fixed at 10 km. The location of this activity is near the epicenter of the 1981  $m_b$  5.3 earthquake, the largest event in the historical record of continental Alaska north of lat 66.5°N. (Page and others, 1991, table 1, p. 50 and table 2, p. 56; Stover and Coffman, 1993, seismicity map, p. 8). The 1981 shock involved normal slip on either a shallow, south-southwest-dipping plane or a steep, north-northeast-dipping plane (Page and others, 1991, fig. 13, p. 64.)

Among other seismogenic features of note in southern Alaska in 1994 is the moderate level of shallow seismicity south, east, and northeast of Kodiak Island (figs. 4, 5). Four magnitude 4 shocks occurred there where a belt of northeast-trending submarine faults of Quaternary age is mapped. The foci of these shocks are poorly constrained, and it is uncertain whether these events occurred in the North American plate or on the Aleutian megathrust. Elsewhere, an  $M_L$  4.1 shock was recorded on February 1 and located at 10-km depth beneath the southern Kenai Peninsula (lat 59.8°N., long 150.7°W.; fig. 5). It has a well-constrained focal mechanism that indicates almost pure normal-slip motion on either of two moderately dipping, north-northwest-striking planes. This solution is consistent with previous studies of recent seismicity in this

area that indicate that the shallow crust above the megathrust is in tension (Stephens and others, 1982).

Relatively few events were located in southeastern Alaska in 1994 (figs. 4, 5). A curious series of events are clustered near the Wright Glacier (lat 58.4°N., long 133.5°W.), about 50 km east of Juneau (Rowe and others, 1994). The historical record indicates that clustered events occur at this location in a repeated cycle: events begin in the late spring (May) of each year and increase in rate through the fall (October), but they are largely absent during other months. The Wright Glacier seismicity cannot be located by the current AEIC regional network. Hypocenters of 14 events from October 1 to 9, 1994, with magnitudes between 1.7 and 3.2 and depths fixed to 5 or 10 km have been provided by Robert Horner of the GSC, Pacific Geoscience Center, Sidney, British Columbia. The cyclic behavior of the cluster is not consistent with regional tectonic stresses being the sole source of the activity. The cluster's proximity to large tidewater and alpine glaciers suggests an ice-related source for the events; however, waveforms of these earthquakes are notably different from other glacier events observed on the southern Alaska coast. Causes for the temporal pattern of events are being investigated and may involve elevated pore pressures at depth related to surface-water input from seasonal glacier melt and rainfall.

The largest earthquakes in northwestern Canada in 1994, an  $m_b$  4.4 shock on May 29 and an  $m_b$  4.7 event on October 10 (near lat 67°N., long 135.5°W.), occurred beneath the Richardson Mountains, Yukon Territory near the two largest historical shocks known to have occurred in the northern Yukon Territory (north of about lat 66°N. and west of about long 134°W.). The May 29 and June 5, 1940 Richardson Mountain earthquakes ( $M_S$  6.2 and 6.5, respectively) were located about 20 km apart (lat 66.8°N., long 135.3°W. and lat 66.9°N., long 135.8°W., respectively) and had focal depths ranging from 15 to 11 km for the May rupture sequence and 10 to 7 km for the June sequence (modeling of teleseismic and regional body waves indicated a complex rupture sequence for each event, consisting of two to three subevents; Cassidy and Bent, 1993). The 1940 shocks were interpreted by Cassidy and Bent (1993) to involve right-lateral motion along a west-dipping, north-south-trending fault plane based on the focal mechanisms, the relative locations of the subevents, and the north-south-trending Richardson fault array (a complex shear zone that extends from the Arctic Ocean in the north to the Mackenzie Mountains in the south near lat 66°N.).

### VOLCANIC-AXIS EARTHQUAKES

Small, shallow earthquakes along the volcanic axes of both the Aleutian (Cook Inlet segment) and Wrangell

arcs are detected by the AEIC seismograph network. The 1994 shocks along the Cook Inlet segment of the Aleutian volcanic axis form a diffuse band punctuated by clusters beneath Spurr, Redoubt, and Augustine volcanoes (fig. 5; fig. 7, sections  $D-D'$ ,  $E-E'$ ). The largest shallow earthquake ( $M_L$  2.8) yet located beneath the edifice of Mount Spurr volcano (3,375 m above sea level) occurred on October 28, 1994, at a computed depth of 1 km below the top of the volcano. This event is one of only 15 crustal shocks larger than magnitude 2 since 1971 that have been located by the regional network within a 10-km radius of the summit of Mount Spurr, whose Crater Peak vent last erupted in 1992 (Power and others, in press).

### CONCLUSION

The overall pattern of 1994 seismicity in Alaska and western Canada is generally similar to that observed since at least 1988 when the AEIC was established and the USGS and UAGI seismograph networks were merged. Most of the earthquakes located in 1994 occurred in southern and central Alaska, the Alaska Peninsula, and the Aleutian Islands. The higher rate of earthquake activity in central and southern Alaska (about 85 percent of the total number of earthquakes located in 1994) relative to the Alaska Peninsula and the Aleutian Islands reflects the greater concentration of seismograph stations in those regions.

The 1994 seismicity is best examined using events greater than or equal to magnitude 4.5 (the approximate magnitude level at which the earthquake catalog is complete for Alaska and western Canada). This seismicity is dominated by activity along the Aleutian arc west of long 160°W. where 77 percent of the 103 events with  $m_b \geq 4.5$ , 87 percent of the 31 events with  $m_b \geq 5.0$ , and all four of the events with  $m_b \geq 5.5$  occurred. The three largest Aleutian shocks ( $m_b$  6.0, 5.8, and 5.6) probably occurred on the Pacific-North American plate boundary based on their focal mechanisms (low-angle, reverse faulting on north-northwest-dipping plane) and shallow depths. In central and southern Alaska the largest events ( $m_b$  5.4, 5.2, and 5.0) were Aleutian WBZ shocks (depths of 49, 66, and 39 km, respectively). The stress orientation of these events inferred from their focal mechanism solutions is characterized by inplate, downdip tension. This stress orientation is consistent with the pattern seen for Aleutian WBZ shocks in southern Alaska since 1971, when the USGS southern Alaska seismograph network began operation.

Two notable 1994 earthquakes are the largest, well-constrained shock yet located deeper than 200 km in the Aleutian WBZ east of long 156°W. (an  $m_b$  4.6 event at 219 km depth on December 10), and the largest crustal shock ever located beneath the edifice of Mount Spurr

volcano (an  $M_L$  2.8 event at 1-km depth below the top of the volcano on October 28).

## REFERENCES CITED

- Agnew, J.D., 1980, Seismicity of the central Alaska Range, Alaska, 1904–1978: Fairbanks, University of Alaska, M.S. thesis, 88 p.
- Biswas, N.N. and Tytgat, Guy, 1988, Intraplate seismicity in Alaska: *Seismological Research Letters*, v. 59, p. 227–233.
- Brogan, G.E., Cluff, L.S., Korranga, M.K., and Stemmmons, D.B., 1975, Active faults of Alaska: *Tectonophysics*, v. 29, p. 73–85.
- Cassidy, John F., and Bent, Allison L., 1993, Source parameters of the 29 May and 6 June, 1940 Richardson Mountains, Yukon Territory, earthquakes: *Bulletin of the Seismological Society of America*, v. 83, no. 3, p. 636–659.
- Cluff, L.S., Stemmmons, D.B., Brogan, G.E., and Korranga, M.K., 1974, Basis for pipeline design for active-fault crossings for the Trans-Alaska Pipeline System: Houston, Tex., Alyeska Pipeline Service Company, 115 p.
- Davies, J.N., 1975, Seismological investigations of plate tectonics in south-central Alaska: Fairbanks, University of Alaska, Ph.D. dissertation, 193 p.
- , 1983, Seismicity of the interior of Alaska: a direct result of Pacific–North American Plate convergence? [abs.]: *Eos (American Geophysical Union Transactions)*, v. 64, p. 90.
- , 1984, Alaska's earthquakes: *The Northern Engineer*, Geophysical Institute, University of Alaska Fairbanks, v. 16, no. 4, p. 8–13.
- Davies, J.N., and House, Leigh, 1979, Aleutian subduction zone seismicity, volcano-trench separation, and their relation to great thrust-type earthquakes: *Journal of Geophysical Research*, v. 84, p. 4583–4591.
- Davies, John, Sykes, Lynn, House, Leigh, and Jacob, Klaus, 1981, Shumagin seismic gap, Alaska Peninsula; history of great earthquakes, tectonic setting, and evidence for high seismic potential: *Journal of Geophysical Research*, v. 86, no. B5, p. 3821–3855.
- DeMets, C., Gordon, R.G., Argus, D.F., and Stein, S., 1990, Current plate motions: *Geophysics Journal International*, v. 101, p. 425–478.
- Dziewonski, A.M., Chou, T.-A., and Woodhouse, J.H., 1981, Determination of earthquake source parameters from waveform data for studies of global and regional seismicity: *Journal of Geophysical Research*, v. 86, no. B4, p. 2825–2852.
- Engdahl, E.R., and Gubbins, D., 1987, Simultaneous travel-time inversion for earthquake location and subduction zone structure in the central Aleutian Islands: *Journal of Geophysical Research*, v. 92, p. 13,855–13,862.
- Engle, K.Y., 1982, Earthquake focal mechanism studies of Cook Inlet area: Alaska: Fairbanks, University of Alaska, M.S. thesis, 81 p.
- Estabrook, C.H., and Jacob, K.H., 1991, Stress indicators in Alaska. in Stemmmons, D.B., Engdahl, E.R., Zoback, M.D., and Blackwell, D.D., eds., *Neotectonics of North America*: Boulder, Colo., Geological Society of America, Decade of North American Geology Map Volume 1, p. 387–399.
- Estabrook, C.H., Nabelek, J.L., and Lerner-Lam, A.L., 1992, Tectonic model of the Pacific–North American plate boundary in the Gulf of Alaska from broadband analysis of the 1979 St. Elias, Alaska, earthquake and its aftershocks: *Journal of Geophysical Research*, v. 97, no. B5, p. 6587–6612.
- Estabrook, C.H., Stone, D.B., and Davies, J.N., 1988, Seismotectonics of northern Alaska: *Journal of Geophysical Research*, v. 93, p. 12,026–12,040.
- Fogleman, K.A., Lahr, J.C., Stephens, C.D., and Page, R.A., 1993, Earthquake locations determined by the southern Alaska seismograph network for October 1971 through May 1989: U.S. Geological Survey Open-File Report 93–309, 54 p.
- Fogleman, K.A., Rowe, C.A., Stephens, C.D., and Hammond, W.R., 1994, Earthquakes in Alaska: Alaska State Seismologist's Reports (Periodical series. 12 issues/year: reports #91-01 to 91-09 and 93-01 were published in 1994).
- Frohlich, Cliff, Billington, Selena, Engdahl, E.R., and Malahoff, A., 1982, Detection and location of earthquakes in the central Aleutian subduction zone using land and ocean-bottom seismograph stations: *Journal of Geophysical Research*, v. 87, p. 6853–6864.
- Gedney, Larry, Estes, Steve, and Biswas, Nirenda, 1980, Earthquake migration in the Fairbanks, Alaska, seismic zone: *Bulletin of the Seismological Society of America*, v. 70, p. 223–241.
- Gilbert, Freeman, 1971, Excitation of the normal modes of the earth by earthquake sources: *Geophysical Journal of the Royal Astronomical Society*, v. 22, p. 223–226.
- Hammond, W.R., Lahr, J.C., Rowe, C.A., and Benoit, J.P., 1993, The Salcha seismic zone near Fairbanks, Alaska [abs.]: *Eos (American Geophysical Union Transactions)*, v. 74, no. 43, p. 417–418.
- Horner, R.B., 1983, Seismicity in the St. Elias region of northwestern Canada and southeastern Alaska: *Bulletin of the Seismological Society of America*, v. 73, no. 4, p. 1117–1137.
- Hwang, L.J., and Kanamori, Hiroo, 1992, Rupture processes of the 1987–1988 Gulf of Alaska earthquake sequence: *Journal of Geophysical Research*, v. 97, no. B13, p. 19,881–19,908.
- Jacob, K.H., 1984, Estimates of long-term probabilities for future great earthquakes in the Aleutians: *Geophysical Research Letters*, v. 11, p. 295–298.
- Johnson, Jean M., Tanioka, Yuichiro, Ruff, Larry J., Satake, Kengi, Kanamori, Hiroo, and Sykes, Lynn R., 1994, The 1957 Great Aleutian earthquake: *Pageoph*, v. 142, no. 1, p. 3–28.
- Kanamori, Hiroo, 1977, The energy release in great earthquakes: *Journal of Geophysical Research*, v. 82, no. 20, p. 2981–2987.
- Kelleher, John, and Savino, John, 1975, Distribution of seismicity before large strike slip and thrust-type earthquakes: *Journal of Geophysical Research*, v. 80, no. 2, p. 260–271.
- Lahr, J.C., 1975, Detailed seismic investigation of Pacific–North American plate interaction in southern Alaska: Columbia University, New York, N.Y., Ph.D. dissertation, 141 p.

- Lahr, J.C., Fogleman, K.A., Stephens, C.D., and Page, R.A., 1993, Stresses within the Pacific plate of southern Alaska [abs.]: *Eos (American Geophysical Union Transactions)*, v. 74, no. 43, p. 95.
- Lahr, J.C., Page, R.A., and Stephens, C.D., 1988, Unusual earthquakes in the Gulf of Alaska and fragmentation of the Pacific plate: *Geophysical Research Letters*, v. 15, no. 13, p. 1483-1486.
- Lahr, J.C., and Plafker, George, 1980, Holocene Pacific-North American plate interaction in southern Alaska; implications for the Yakataga seismic gap: *Geology*, v. 8, p. 483-486.
- Lahr, J.C., Stephens, C.D., Hasegawa, H.S., and Boatwright, John, 1980, Alaskan seismic gap only partially filled by 28 February 1979 earthquake: *Science*, v. 207, p. 1351-1353.
- Lahr, J.C., Stephens, C.D., Page, R.A., and Fogleman, K.A., 1994, Characteristics of the Aleutian Wadati-Benioff zone seismicity beneath southern Alaska: SUBCON, Interdisciplinary Conference on the Subduction Process, Catalina Island, California, 1994, p. 301-303.
- Matumoto, T., Gumper, F., and Sbar, M., 1968, A study of microaftershocks following Fairbanks earthquake of June 21, 1967 [abs.]: *Eos (American Geophysical Union Transactions)*, v. 49, p. 294.
- McCann, W.R., Perez, O.J., and Sykes, L.R., 1980, Yakataga seismic gap, southern Alaska: seismic history and earthquake potential: *Science*, v. 207, p. 1309-1314.
- McLaren, J.P., and Frohlich, Cliff, 1985, Model calculations of regional network locations for earthquakes in subduction zones: *Bulletin of the Seismological Society of America*, v. 75, no. 2, p. 397-413.
- Mogi, Kiyoo, 1968, Some features of recent seismic activity in and near Japan, (1): *Bulletin of the Earthquake Research Institute, University of Tokyo*, v. 46, p. 1225-1236.
- Page, R.A., 1994, Comparison of knowledge of earthquake potential in the San Francisco Bay and Anchorage regions, in *Earthquake Alaska—are we prepared?: U.S. Geological Survey Open-File Report*, 94-218, p. 31-42.
- Page, Robert A., Biswas, Nirendra N., Lahr, John C., and Pulpan, Hans, 1991, Seismicity of continental Alaska, in Slemmons, D.B., Engdahl, E.R., Zoback, M.D., and Blackwell, D.D., eds., *Neotectonics of North America*: Boulder, Colo., Geological Society of America, *Decade of North America Geology Map Volume 1*, p. 47-68.
- Page, R.A., Brocher, T.M., Stephens, C.D., Lahr, J.C., Fogleman, K.A., and Fisher, M.A., 1994, Piggyback subduction at the eastern end of the Aleutian trench and the giant asperity that ruptured in the Great 1964 earthquake: SUBCON, Interdisciplinary Conference on the Subduction Process, Catalina Island, Calif., 1994, p. 152-154.
- Page, R.A., Hassler, M.H., Stephens, C.D., and Criley, E.E., 1984, Fault zone geometry of the 1979 St. Elias, Alaska, earthquake, in Bartsch-Winkler, Susan, and Reed, K.M., eds., *The United States Geological Survey in Alaska: Accomplishments during 1982*: U.S. Geological Survey Circular 939, p. 65-67.
- Page, R.A., Lahr, J.C., Stephens, C.D., Fogleman, K.A., Brocher, T.M., and Fisher, M.A., 1992, Seismicity and stress orientation in the Alaska subduction zone after the great 1964 earthquake and speculation on the origin of a giant asperity [abs.]: *Wadati Conference on Great Subduction Earthquakes*, Fairbanks, Alaska, 1992, p. 31-32.
- Page, R.A., Plafker, George, and Pulpan, Hans, 1995, Block rotation in east-central Alaska: a framework for evaluation earthquake potential?: *Geology*, v. 23, no. 7, p. 629-632.
- Page, R.A., Stephens, C.D., Fogleman, K.A., and Maley, R.P., 1985, The Columbia Bay, Alaska, earthquakes of 1983, in Bartsch-Winkler, Susan, and Reed, K.M., eds., *The United States Geological Survey in Alaska: Accomplishments during 1983*: U.S. Geological Survey Circular 945, p. 80-83.
- Page, R.A., Stephens, C.D., and Lahr, J.C., 1989, Seismicity of the Wrangell and Aleutian Wadati-Benioff zones and the North American plate along the Trans-Alaska Crustal Transect, Chugach Mountains and Copper River basin, southern Alaska: *Journal of Geophysical Research*, v. 94, p. 16,059-16,082.
- Plafker, George, 1987, Regional geology and petroleum potential of the northern Gulf of Alaska continental margin, in Scholl, D.W., Grantz, Arthur, and Vedder, J.G., eds., *Geology and resource potential of the continental margin of western North America and adjacent ocean basins*: American Association of Petroleum Geologists Circum-Pacific Earth Science Series, v. 6, p. 229-268.
- Plafker, George, Gilpin, L.M., and Lahr, J.C., 1994, Neotectonic map of Alaska, in Plafker, George, and Berg, H.C., eds., *The geology of Alaska*: Boulder, Colo., Geological Society of America, *The Geology of North America*, v. G-1, pl. 12, scale 1:2,500,000.
- Power, J.A., Jolly, A.D., Page, R.A., and McNutt, S.R., 1995, Seismicity and forecasting of the 1992 eruptions of Crater Peak vent, Mt. Spurr, Alaska: an overview, in Keith, T.E.C., ed., *The 1992 eruptions of Crater Peak vent, Mount Spurr volcano, Alaska*: U.S. Geological Survey Bulletin 2139, p. 149-160.
- Power, M.A., 1988, Mass movement, seismicity, and neotectonics in the northern St. Elias Mountains, Yukon: Edmonton, University of Alberta, M.S. thesis, 125 p.
- Pulpan, Hans, and Frohlich, Cliff, 1985, Geometry of the subducted plate near Kodiak Island and the lower Cook Inlet, Alaska, determined from relocated earthquake hypocenters: *Bulletin of the Seismological Society of America*, v. 75, p. 791-810.
- Richter, C.F., 1958, *Elementary seismology*: San Francisco, Calif., W.H. Freeman and Co., 768 p.
- Rogers, Garry C., 1986, Seismic gaps along the Queen Charlotte fault: *Earthquake Prediction Research*, v. 4, p. 1-11.
- Rogers, Garry C., and Horner, Robert B., 1991, An overview of western Canadian seismicity, in Slemmons, D.B., Engdahl, E.R., Zoback, M.D., and Blackwell, D.D., eds., *Neotectonics of North America*: Boulder, Colo., Geological Society of America, *Decade of North American Geology Map Volume 1*, p. 69-76.
- Rowe, C.A., Wolf, L.W., and Horner, R.B., 1994, Periodic seismicity near Wright Glacier, SE Alaska-British Columbia border [abs.]: *Eos (American Geophysical Union Transactions)*, v. 75, no. 44, p. 478.
- Stephens, C.D., Fogleman, K.A., Lahr, J.C., and Page, R.A., 1984, Wrangell Benioff zone, southern Alaska: *Geology*, v. 12, p. 373-376.
- Stephens, C.D., Lahr, J.C., Fogleman, K.A., and Horner, R.B.,



- 1980, The St. Elias, Alaska, earthquake of 28 February 1979: regional recording of aftershocks and short-term pre-earthquake seismicity: *Bulletin of the Seismological Society of America*, v. 70, no. 5, p. 1607–1633.
- Stephens, C.D., Lahr, J.C., Page, R.A., and Fogleman, K.A., 1992, Recent seismicity in and near the Yakataga seismic gap, southern Alaska [abs.]: *Wadati Conference on Great Subduction Earthquakes*, Fairbanks, Alaska, 1992, p. 30.
- Stephens, C.D., Lahr, J.C., and Rogers, J.A., 1982, Review of earthquake activity and current status of seismic monitoring in the region of the Bradley Lake Hydroelectric Project, southern Kenai Peninsula, Alaska: November 27, 1980–November 30, 1981: U.S. Geological Survey Open-File Report 82-417, 26 p.
- Stover, C.W., and Coffman, J.L., 1993, Seismicity of the United States, 1568–1989 (revised): U.S. Geological Survey Professional Paper 1527, 418 p.
- Sykes, L.R., 1971, Aftershock zones of great earthquakes, seismicity gaps and earthquake prediction for Alaska and the Aleutians: *Journal of Geophysical Research*, v. 76, p. 8021–8041.
- Taber, J.J., Billington, Selena, and Engdahl, E.R., 1991, Seismicity of the Aleutian Arc, in Slemmons, D.B., Engdahl, E.R., Zoback, M.D., and Blackwell, D.D., eds., *Neotectonics of North America*: Boulder, Colo., Geological Society of America, Decade of North American Geology Map Volume 1, p. 29–46.
- Van Wormer, J.D., Davies, John, and Gedney, Larry, 1974, Seismicity and plate tectonics in south central Alaska: *Bulletin of the Seismological Society of America*, v. 64, p. 1467–1475.
- Wickens, A.J., and Hodgson, J.H., 1967, Computer re-evaluation of earthquake mechanisms solutions 1922–1962: Ottawa, Canada, Publications of the Dominion Observatory, v. 33, no. 1, 560 p.
- Wood, H.O., and Neumann, Frank, 1931, Modified Mercalli Intensity Scale of 1931: *Seismological Society of America Bulletin*, v. 21, no. 4, p. 277–283.
- Zoback, Mark D., and Zoback, Mary Lou, 1991, Tectonic stress field of North America and relative plate motions, in Slemmons, D.B., Engdahl, E.R., Zoback, M.D., and Blackwell, D.D., eds., *Neotectonics of North America*: Boulder, Colo., Geological Society of America, Decade of North American Geology Map Volume 1, p. 339–366.

Reviewers: Lynn D. Dietz and Robert A. Page





# Organic Matter and Thermal Maturation of Lower Paleozoic Rocks from the Nixon Fork Subterrane of the Farewell Terrane, West-Central and Southwestern Alaska

By Stephen R. Jacobson, Robert B. Blodgett, and Loren E. Babcock

## ABSTRACT

Middle Cambrian and Upper Cambrian(?) sedimentary rocks from two areas of the Nixon Fork subterrane of the Farewell terrane, west-central and southwestern Alaska, have low concentrations of total organic carbon. Transmitted-light microscopic analyses show that kerogen, including acritarchs, contained in some of the samples was heated beyond the oil- and gas-generating windows.

## INTRODUCTION

This paper provides quantitative data on source rock characteristics for sedimentary units in a subterrane that was investigated for its petroleum potential by several major oil companies and other organizations in the 1980's (see Smith and others, 1984; Palmer and others, 1985). We describe total organic carbon (TOC) contents and thermal maturation of organic matter from samples of lower Paleozoic limestones collected from the Nixon Fork subterrane of the Farewell terrane in west-central and southwestern Alaska. Studied samples were collected from gray and black limestones that were deposited in inferred deep-shelf environments (see Babcock and others, 1993, 1995; St. John, 1994; St. John and Babcock, 1994). Gray to black limestones often contain sufficiently high quantities of organic carbon to qualify as petroleum source rocks (for example, Cook and Enos, 1977; Cook and Taylor, 1977; Tissot and Welte, 1984; Christiansen and others, 1985). Carbonate petroleum source rocks are well documented in both marine and lacustrine lithofacies (for example, Jones, 1984; Palacas, 1988). Carbonate source rock lithofacies can vary from marls to lime mudstones (Palacas, 1988). Samples from the Nixon Fork subterrane were analyzed as part of ongoing work to better understand the basin history and tectonic provenance of the Proterozoic and lower Paleozoic section in the subterrane (Blodgett, 1983; Blodgett and Gilbert, 1983, 1992a,b; Bundtzen and Gilbert, 1983; Gilbert and Bundtzen, 1983;

Blodgett and Clough, 1985; Miller and others, 1989; Babcock and Blodgett, 1992; Babcock and others, 1993, 1994; St. John, 1994; St. John and Babcock, 1994). In this part of our study, we sought to evaluate some unnamed lower Paleozoic strata that are part of the Nixon Fork subterrane for their petroleum source rock potential.

The Nixon Fork subterrane was originally defined (Patton, 1978) as being characterized primarily by a distinctive succession of lower and middle Paleozoic platform carbonate rocks. To the east, this shallow-water succession of strata grades into stratigraphically equivalent, deeper water basinal lithofacies (Blodgett, 1983; Blodgett and Gilbert, 1983, 1992a,b; Bundtzen and Gilbert, 1983; Gilbert and Bundtzen, 1983; Blodgett and Clough, 1985) that have been mapped as part of the Dillinger, East Fork, and Minchumina terranes. Further work (Decker and others, 1994) suggests that the units that were previously assigned to the Nixon Fork, Dillinger, East Fork, and Minchumina tectonostratigraphic terranes (Jones and others, 1987) are genetically related. Decker and others (1994) proposed the name Farewell terrane to embrace these entities and reduced each of them in rank to subterrane of the Farewell. Babcock and others (1994) showed that not all of the strata present in the Nixon Fork subterrane are Paleozoic or younger in age; a succession of Late(?) Proterozoic, mixed carbonate and siliciclastic rocks, more than 600 m thick, is also present. The age was based on (1) a similarity to other inferred Late Proterozoic strata in Alaska, (2) a stratigraphic position below Middle Cambrian strata, and (3) a lack of macrofossils and trace fossils.

## STUDY AREAS

Samples reported here are from unnamed Middle Cambrian and Upper Cambrian(?) rocks that crop out in two areas of the Nixon Fork subterrane of the Farewell terrane, west-central and southwestern Alaska (fig. 1). Some samples used for the analyses (table 1) were collected from richly fossiliferous limestones in an east-west-

trending anticlinorium in the Holitna basin (fig. 1). All three of these sample sites are from the NW 1/4, sec. 27, T. 11 N., R. 42 W., Sleetmute A-2 quadrangle (1:63,360 series). Other samples (table 1) were collected from ridges west of Lone Mountain (fig. 1; see Babcock and others, 1994) in sec. 11 and sec. 14, T. 28 N., R. 30 W., McGrath C-4 quadrangle (1:63,360 series).

## STRATIGRAPHY

Samples used for the analyses reported here (table 1) were collected from unnamed stratigraphic units of Middle Cambrian age in the Holitna basin and from unnamed stratigraphic units of Middle Cambrian and Late Cambrian(?) age in the Lone Mountain area (fig. 1). Middle Cambrian and Upper Cambrian(?) rocks from the Holitna basin and the Lone Mountain area are part of a Late(?) Proterozoic and lower Paleozoic succession of shelf carbonate and siliciclastic strata that exceeds 950 m in thickness (Babcock and others, 1993, 1994, 1995; St. John, 1994). The stratigraphic successions present in the Holitna basin and in the Lone Mountain area appear to be the same, but stratigraphic relationships are less complicated in the ridges west of Lone Mountain (Babcock and others, 1994) than they are in the Holitna basin.

Three limestone samples (84RB126, 84RB133, and SA102) from the Holitna basin (fig. 1) are biostratigraphically dated using trilobites, most of which are of Siberian aspect (Palmer and others, 1985; Babcock and Blodgett, 1992; St. John, 1994; St. John and Babcock, 1994; Babcock and others, 1995). Sample 84RB126 is early Middle Cambrian in age in North American terms (Palmer and others, 1985); abundant trilobites present in this wackestone suggest a correlation with the *Anabaraspis* Zone of the Amgan Stage of Russia (as used by Egorova and others, 1982). Samples 84RB133 and SA102 were collected from beds that are stratigraphically higher than sample 84RB126. These two samples are late Middle Cambrian age in North American terms (Palmer and others, 1985); abundant trilobites present in these wackestones suggest a correlation with the *Anoplenus henrici* Zone to the *Anomocarioides limbataeformis* Zone of the Mayan Stage of Russia (as used by Egorova and others, 1982; see St. John, 1994).

All remaining samples reported herein (table 1) are from limestone beds present in ridges west of Lone Mountain (figs. 1, 2). Samples 7/29/93/8 and 7/25/93/2 were collected from low knobs formed by light- to medium-gray limestone beds and thin intercalated beds of gray-green siltstone. In the Lone Mountain area, two such knobs, formed by limestone beds about 1–2 m thick, are present in a roughly 30-m-thick succession that is dominated by gray-green siltstones.

Samples 7/29/93/8 and 7/25/93/2 were collected from the upper limestone ridge (fig. 2). Both are highly stylolitized wackestones, and sample 7/29/93/8 contains sparse trilobites that suggest a late Middle Cambrian age. Samples 7/29/93/3, 7/29/93/11, and 7/29/93/12 were collected from an unnamed succession of rocks that is at least 300 m thick and that seems to conformably overlie the unnamed Middle Cambrian unit (fig. 2). The samples reported herein were collected from near the base of the unit. The unit is dominated by black, platy lime mudstones; carbonate breccias up to 10 m in thickness are present in a 30-m-thick interval that begins about 20 m up from the base of the unit. Samples 7/29/93/11 and 7/29/93/3 are from black, platy lime mudstones that underlie the breccia interval, and sample 7/29/93/12 is from a lime mudstone clast (light-gray color) in one of the breccia beds. Identifiable fossils have not been found in this unnamed unit, but the unit is tentatively assigned to the Late Cambrian near the base and to the Early Ordovician higher in the section (Babcock and others, 1994), based on its stratigraphic position above rocks of Middle Cambrian age and on the inferred age of the carbonate breccia beds. In various localities worldwide, such as the Cordilleran region of North America (Taylor and Cook, 1976; Cook and Taylor, 1977; Leslie and others, 1991), the Appalachian area of North America (Kindle and Whittington, 1958; Hubert and others, 1977), Greenland (Ineson and others, 1994), and China (Gao and Duan, 1985; Rees and others, 1992), thick carbonate breccia beds resembling the ones near Lone Mountain are present in deep-shelf to shelf-edge environments near the Cambrian-Ordovician boundary. Because the black, platy lime mudstone interval above the breccia-containing interval near Lone Mountain exceeds 250 m in thickness, it is likely that the unit was deposited in part during the Ordovician Period.

## ANALYSES

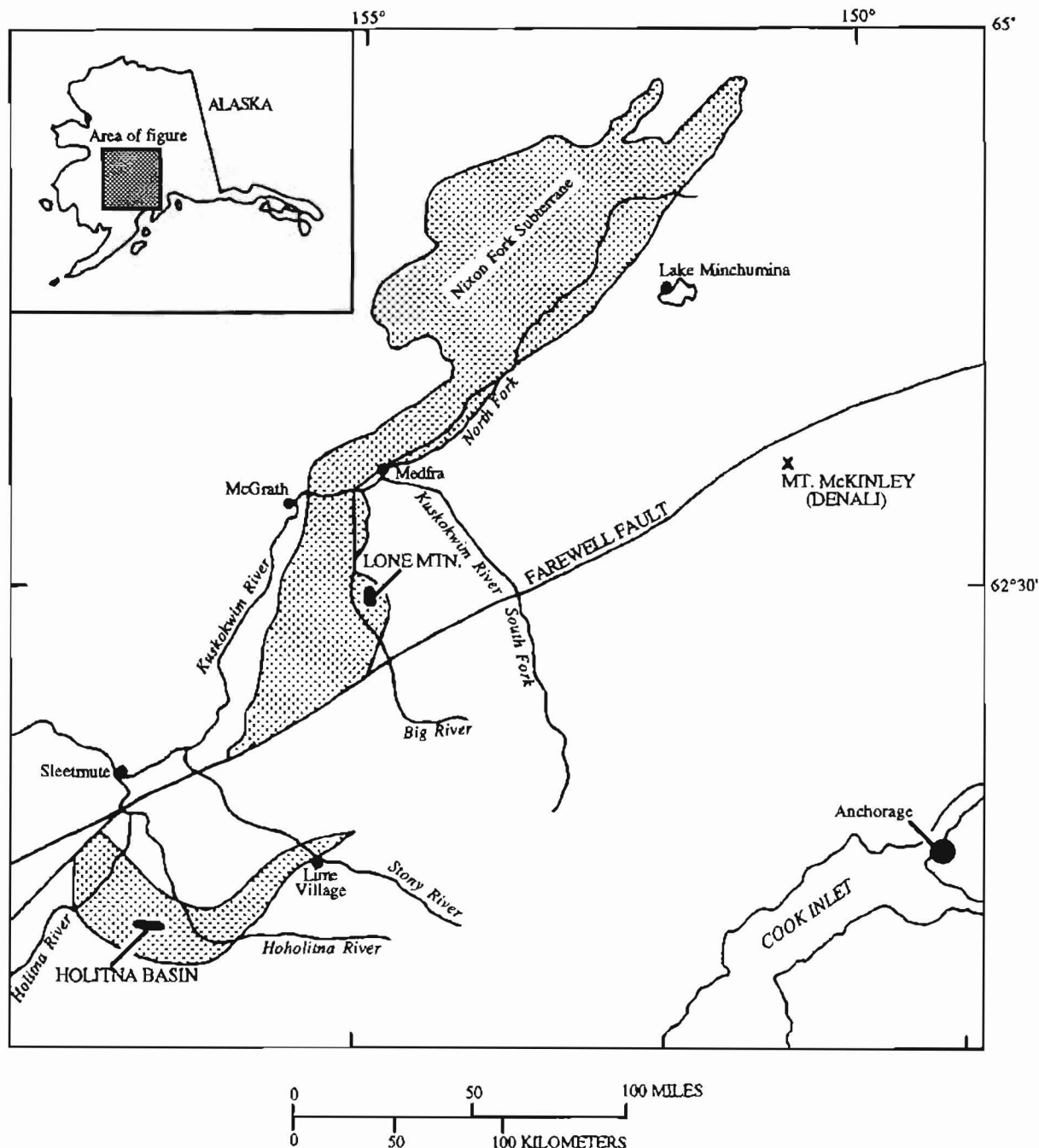
To evaluate the unnamed lower Paleozoic stratigraphic units for their petroleum source rock potential, we selected eight samples for TOC analyses. Our intention was to discover which samples had sufficient organic matter (greater than 0.40 weight percent) to warrant further examination with Rock-Eval pyrolysis. The results from TOC analysis led us to select two samples for transmitted-light microscopy to help clarify our interpretation of the thermal maturation of this part of the stratigraphic succession in the Nixon Fork subterranean.

The results of TOC analyses are shown in table 1. The data show that all eight samples yielded minimal detectable amounts of organic carbon. Results range from 0.01 to 0.06 weight percent organic carbon. These values

are far below the minimum values needed to obtain reliable results from Rock-Eval pyrolysis. Low concentrations could be caused by low original organic content, sedimentary dilution, oxidation, or thermal maturation. Therefore, to determine why the total organic carbon values were low, we prepared strew (disseminated kerogen)

mount slides from demineralized rock samples to evaluate the organic matter using transmitted-light microscopy.

Samples 84RB126 and 84RB133 from the Holitna basin were selected for analysis of organic matter by transmitted-light microscopy. The samples weighed about 10 g each and were prepared using standard palynological



**Figure 1.** Index map of part of west-central Alaska showing location of the Nixon Fork subterranean of the Farewell terrane (stippled areas); modified from Blodgett and Gilbert (1992a) and Babcock and others (1994). Shaded regions are the Holitna basin, an area of Proterozoic and lower Paleozoic sedimentary rock exposures in an east-west-trending anticlinorium in the Sleetmute A-2 quadrangle; and Lone Mountain, an area of Proterozoic and lower Paleozoic sedimentary rock exposures in the vicinity of Lone Mountain, McGrath B-4 and C-4 quadrangles.

**Table 1.** Total organic carbon (TOC) data for limestone samples from unnamed lower Paleozoic stratigraphic units in the Nixon Fork subterrane of the Farewell terrane, west-central and southwestern Alaska

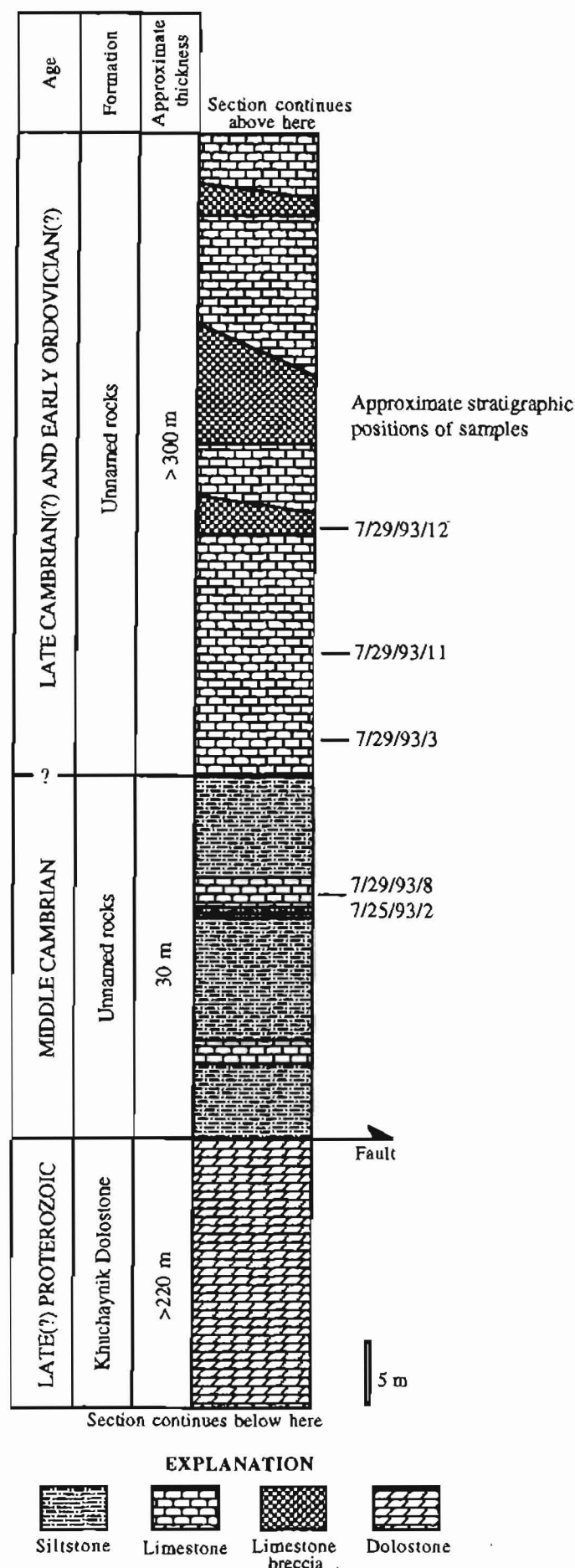
Sample number	Location	TOC (wt %)
84RB126	Holitna basin	0.04
84RB133	Holitna basin	.01
SA102	Holitna basin	.01
7/29/93/2	Lone Mountain	.02
7/25/93/2	Lone Mountain	.01
7/29/93/3	Lone Mountain	.01
7/29/93/11	Lone Mountain	.02
7/29/93/12	Lone Mountain	.06

techniques, omitting the oxidation step. Demineralization was accomplished by first treating pea-sized rock particles with hydrochloric acid to dissolve carbonate minerals. Then the samples were washed. Following washing, hydrofluoric acid was used to dissolve silicate minerals. The samples were not oxidized with nitric acid during preparation. The remaining organic residue was mounted on microscope slides and examined with a transmitted-light microscope.

Sample 84RB126 contains sparse organic matter, which is consistent with its TOC value of 0.04 weight percent. The kerogen is composed of structureless, opaque, dark-brown to black particles and rare translucent grayish-brown acritarchs. The opaque material ranges in size from about 2 to 150  $\mu\text{m}$  in long dimension. These particles have either angular or rounded boundaries. The rounded structureless particles may represent acritarchs up to 150  $\mu\text{m}$  in diameter. Straplike particles with long dimensions up to 150  $\mu\text{m}$  are also present. Their width is generally one-fifth to one-third the long dimension. The color of both the opaque structureless kerogen and the translucent acritarchs suggests that they have reached a stage of advanced thermal maturation.

Sample 84RB133 has even less organic matter (TOC = 0.01 weight percent) than sample 84RB126. The organic particles are somewhat smaller, with a few reaching 75  $\mu\text{m}$  in their longest dimension. Acritarchs, especially sphaeromorphs, are present; they have diameters of 10 to 50  $\mu\text{m}$ . One acanthomorphic acritarch was

**Figure 2.** Generalized columnar stratigraphic section of some Late(?) Proterozoic and lower Paleozoic rocks in the area of Lone Mountain, McGrath C-4 quadrangle. Approximate stratigraphic positions of samples are indicated at right.



found. Also present are slightly larger (30 to 60  $\mu\text{m}$ ), opaque, carbonized subspherical particles (acritarchs?) and angular structureless kerogen particles. The opaque material ranges from dark brown to black, and the translucent acritarchs are grayish brown.

## INTERPRETATION

The shapes and sizes of the acritarchs recovered are consistent with a marine paleoenvironment. However, age-diagnostic forms were not found. Associated trilobites (Palmer and others, 1985; Babcock and Blodgett, 1992; St. John 1994; St. John and Babcock, 1994) also indicate marine paleoenvironments.

The thermal maturation of palynomorphs has been codified by many workers (for example, Gutjahr, 1966; Correia, 1967; Staplin, 1969). The scheme used here is that of Jones and Edison (1978). The method is based on the progressive darkening of pollen and spores with their increasing exposure to heat. This carbonization process occurs with many kinds of palynomorphs, such as pollen, spores, dinoflagellate cysts, and acritarchs, although their thermal alteration index (TAI) values may vary slightly owing to different chemical compositions and wall thicknesses, primarily at initial stages of thermal maturation. However, at the advanced thermal maturation found in these Alaskan samples, the chemical composition of these diverse palynological components becomes more similar. This similarity is shown especially in the application of elemental analysis or Rock-Eval pyrolysis for thermally mature systems (for example, Jones, 1984; Tissot and Welte, 1984; Espitalié and others, 1985; Peters, 1986; Clayton, 1988; Jacobson, 1991). Therefore, the advanced thermal maturation of the acritarchs described here can be viewed with some confidence.

The low concentrations of organic matter in all eight studied samples suggest that their host rocks cannot be considered candidates for petroleum source rocks in the Holitna basin or the Lone Mountain area. The dark-brown to grayish-brown color of the acritarchs and the brittleness and dark-brown to black color of the opaque, structureless organic matter collectively suggest a thermal maturation beyond oil and gas generation. These interpretations are tentative because the preparations have such sparse kerogen concentrations that definitive description of the entire organic matter assemblage is not possible. Additional insight will require larger samples.

## CONCLUSIONS

Samples from the studied units in the Nixon Fork subterranean of the Farewell terrane have low concentrations of preserved organic matter due to the combined

factors of (1) low original concentrations of deposited organic constituents as determined from the miniscule volumes of refractory organic residue in the rocks, and (2) advanced thermal maturity, as demonstrated by the color of rare acritarchs and the absence of measurable pyrolysis values (see, for example, Tissot and Welte, 1984; Peters, 1986). We interpret these rocks to have already generated small, and probably noncommercial, amounts of oil or gas. Samples were heated beyond the oil- and gas-generating windows.

**Acknowledgments.**—We are grateful to Bill Beebe, Area Forester, Alaska Department of Natural Resources, Division of Forestry, McGrath, Alaska, for arranging helicopter support that permitted us to conduct field studies. Raymond Sullivan, San Francisco State University, collected one of the samples from the Holitna basin. James St. John, The Ohio State University, assisted with field work in the Lone Mountain area. Karen Tyler, The Ohio State University, assisted with the drafting of figure 1. Field work was partly supported by a grant from the National Geographic Society, and laboratory work was partly supported by a grant from the National Science Foundation, both to Babcock. Geochemical analyses were performed by Humble Geochemical Services (Humble, Texas). Slides of organic matter were prepared by National Petrographic Services (Houston, Texas).

## REFERENCES CITED

- Babcock, L.E., and Blodgett, R.B., 1992, Biogeographic and paleogeographic significance of Middle Cambrian trilobites of Siberian aspect from southwestern Alaska [abs.]: Geological Society of America Abstracts with Programs, v. 24, no. 5, p. 4.
- Babcock, L.E., Blodgett, R.B., and St. John, James, 1993, Proterozoic and Cambrian stratigraphy and paleontology of the Nixon Fork terrane, southwestern Alaska, in Ortega-Gutiérrez, Fernando, Coney, P.J., Centeno-García, Elena, and Gómez-Caballero, Arturo, eds., Proceedings of the First Circum-Pacific and Circum-Atlantic Terrane Conference: Universidad Nacional Autónoma de México, Guanajuato, México, p. 5–7.
- , 1994, New Late(?) Proterozoic-age formations in the vicinity of Lone Mountain, McGrath Quadrangle, west-central Alaska, in Till, A.B., and Moore, T.E., eds., *Geologic Studies in Alaska by the U.S. Geological Survey, 1993*: U.S. Geological Survey Bulletin 2107, p. 143–155.
- Babcock, L.E., St. John, James, Jacobson, S.R., Askin, R.A., and Blodgett, R.B., 1995, Neoproterozoic to Early Paleozoic geologic history of the Nixon Fork subterranean of the Farewell terrane, Alaska [abs.]: Geological Society of America Abstracts with Programs, v. 27, no. 5, p. 2–3.
- Blodgett, R.B., 1983, Paleobiogeographic affinities of Devonian fossils from the Nixon Fork terrane, southwestern Alaska, in Stevens, C.H., ed., *Pre-Jurassic rocks in western North American suspect terranes*: Los Angeles, Calif.,



- Society of Economic Paleontologists and Mineralogists, Pacific Section, p. 125-130.
- Blodgett, R.B., and Clough, J.G., 1985, The Nixon Fork terrane—part of an in-situ peninsular extension of the Paleozoic North American continent [abs.]: Geological Society of America Abstracts with Programs, v. 17, no. 6, p. 342.
- Blodgett, R.B., and Gilbert, W.G., 1983, The Cheenectuk Limestone, a new Early(?) to Middle Devonian formation in the McGrath A-4 and A-5 quadrangles, west-central Alaska: Alaska Division of Geological and Geophysical Surveys Professional Report 85, 6 p., scale 1:63,360.
- 1992a, Upper Devonian shallow-marine siliciclastic strata and associated fauna and flora, Lime Hills D-4 quadrangle, southwest Alaska, in Bradley, D.C., and Dusel-Bacon, Cynthia, eds., *Geologic studies in Alaska by the U.S. Geological Survey, 1991: U.S. Geological Survey Bulletin 2041*, p. 106-113.
- 1992b, Paleogeographic relations of lower and middle Paleozoic strata of southwest and west-central Alaska [abs.]: Geological Society of America Abstracts with Programs, v. 24, no. 5, p. 8.
- Bundtzen, T.K., and Gilbert, W.G., 1983, Outline of geology and mineral resources of the upper Kuskokwim region, Alaska: *Journal of the Alaska Geological Society*, v. 3, p. 101-117.
- Christiansen, F.G., Nøhr-Hansen, H., Rolle, F., and Wrang, P., 1985, Preliminary analysis of the hydrocarbon source rock potential of central and western North Greenland: *Grønlands Geologiske Undersøgelse, Rapports*, v. 126, p. 117-128.
- Clayton, J.L., 1988, Role of amount and type of organic matter in recognition of petroleum source rocks, in Magoon, L.B., ed., *Petroleum systems of the United States: U.S. Geological Survey Bulletin 1870*, p. 16-18.
- Cook, H.E., and Enos, Paul, eds., 1977, Deep-water carbonate environments: Society of Economic Paleontologists and Mineralogists, Special Publication No. 25, 336 p.
- Cook, H.E., and Taylor, M.E., 1977, Comparison of continental slope and shelf environments in the Upper Cambrian and lowest Ordovician of Nevada, in Cook, H.E., and Enos, Paul, eds., *Deep-water carbonate environments: Society of Economic Paleontologists and Mineralogists, Special Publication No. 25*, p. 51-81.
- Correia, M., 1967, Relations possibles entre l'état de conservation des éléments figurés de la matière organique (microfossiles palynoplantologiques) et l'existence de gisements d'hydrocarbures: *Revue de l'Institut Français du Pétrole*, v. 22, p. 1285-1306.
- Decker, John, Bergman, S.C., Blodgett, R.B., Box, S.E., Bundtzen, T.K., Clough, J.G., Coonrad, W.L., Gilbert, W.G., Miller, M.L., Murphy, J.M., Robinson, M.S., and Wallace, W.K., 1994, Geology of southwestern Alaska, in Plafker, George, and Berg, H.C., eds., *The geology of Alaska: Boulder, Colo., Geological Society of America, The Geology of North America*, v. G-1, p. 285-310, pl. 3.
- Egorova, L.I., Shabanov, Y.Y., Pegel, T.V., Savitsky, V.E., Suchov, S.S., and Chernysheva, N.E., 1982, Mayskiy yarusa stratotipicheskoy mestnosti (sredniy kembriy yugo-vostoka Sibirskoy platformy) [The Mayan Stage of the stratotype locality (Middle Cambrian of the south-eastern Siberian Platform)]: *Trudy Mezhdomestvennyy Stratigraficheskiy Komitet SSSR*, v. 8, 146 p. [In Russian].
- Espitalié, J., Deroo, G., and Marquis, F., 1985, Rock Eval pyrolysis and its applications [preprint]: *Revue de l'Institut Français du Pétrole*, Rueil, France.
- Gao Zhenzhong, and Duan Taizhong, 1985, Gravity-displaced deposits of Cambrian deep-water carbonates in west Hunan and east Guizhou: *Acta Sedimentologica Sinica*, v. 3, p. 7-22 [In Chinese with English summary].
- Gilbert, W.G., and Bundtzen, T.K., 1983, Paleozoic stratigraphy of the Farewell area, southwest Alaska Range, Alaska [abs.]: Alaska Geological Society Symposium, New Developments in the Paleozoic Geology of Alaska and the Yukon, Anchorage, Alaska, 1983, Program and Abstracts, p. 10-11.
- Gutjahr, C.C.M., 1966, Carbonization of pollen grains and spores and their application: *Leidse Geologische Mededelingen*, v. 38, p. 1-30.
- Hubert, J.F., Suchecki, R.K., and Callahan, R.K.M., 1977, The Cow Head Breccia: sedimentology of the Cambro-Ordovician continental margin, Newfoundland, in Cook, H.E., and Enos, Paul, eds., *Deep-water carbonate environments: Society of Economic Paleontologists and Mineralogists, Special Publication No. 25*, p. 125-154.
- Ineson, J.R., Surlyk, Finn, Higgins, A.K., and Peel, J.S., 1994, Slope apron and deep shelf sediments of the Brønland Fjord and Tavsens Iskappe Groups (Lower Cambrian-Lower Ordovician), North Greenland: stratigraphy, facies, and depositional setting: *Grønlands Geologiske Undersøgelse, Bulletin*, v. 169, p. 7-24.
- Jacobson, S.R., 1991, Petroleum source rocks and organic facies, in Merrill, R.K., ed., *Source and migration processes and evaluation techniques: Treatise of petroleum geology, handbook of petroleum geology: Tulsa, Okla., American Association of Petroleum Geologists*, p. 3-11.
- Jones, D.L., Silberling, N.J., Coney, P.J., and Plafker, George, 1987, Lithotectonic terrane map of Alaska (west of the 141st Meridian): U.S. Geological Survey Miscellaneous Field Studies Map MF-1874-A, 1 sheet, scale 1:250,000.
- Jones, R.W., 1984, Comparison of carbonate and shale source rocks, in Palacas, J.G., ed., *Petroleum geochemistry and source rock potential of carbonate rocks: American Association of Petroleum Geologists, Studies in Geology No. 18*, p. 163-180.
- Jones, R.W., and Edison, T.A., 1978, Microscopic observation of kerogen related to geochemical parameters with emphasis on thermal maturation, in Oltz, D.F., ed., *Symposium in geochemistry: low temperature metamorphism of kerogen and clay minerals: Los Angeles, Calif., Society of Economic Paleontologists and Mineralogists, Pacific Section*, p. 1-12.
- Kindle, C.H., and Whittington, H.B., 1958, Stratigraphy of the Cow Head region, western Newfoundland: *Geological Society of America Bulletin*, v. 69, p. 315-342.
- Leslie, S.A., Isaacson, P.E., Repetski, J.E., and Weideman, W.L., 1991, Upper plate rocks of the Roberts Moun-



- Society of Economic Paleontologists and Mineralogists, Pacific Section, p. 125-130.
- Blodgett, R.B., and Clough, J.G., 1985, The Nixon Fork terrane—part of an in-situ peninsular extension of the Paleozoic North American continent [abs.]: Geological Society of America Abstracts with Programs, v. 17, no. 6, p. 342.
- Blodgett, R.B., and Gilbert, W.G., 1983, The Cheenectuk Limestone, a new Early(?) to Middle Devonian formation in the McGrath A-4 and A-5 quadrangles, west-central Alaska: Alaska Division of Geological and Geophysical Surveys Professional Report 85, 6 p., scale 1:63,360.
- 1992a, Upper Devonian shallow-marine siliciclastic strata and associated fauna and flora, Lime Hills D-4 quadrangle, southwest Alaska, in Bradley, D.C., and Dusel-Bacon, Cynthia, eds., *Geologic studies in Alaska by the U.S. Geological Survey, 1991: U.S. Geological Survey Bulletin 2041*, p. 106-113.
- 1992b, Paleogeographic relations of lower and middle Paleozoic strata of southwest and west-central Alaska [abs.]: Geological Society of America Abstracts with Programs, v. 24, no. 5, p. 8.
- Bundtzen, T.K., and Gilbert, W.G., 1983, Outline of geology and mineral resources of the upper Kuskokwim region, Alaska: *Journal of the Alaska Geological Society*, v. 3, p. 101-117.
- Christiansen, F.G., Nøhr-Hansen, H., Rolle, F., and Wrang, P., 1985, Preliminary analysis of the hydrocarbon source rock potential of central and western North Greenland: *Grønlands Geologiske Undersøgelse, Rapports*, v. 126, p. 117-128.
- Clayton, J.L., 1988, Role of amount and type of organic matter in recognition of petroleum source rocks, in Magoon, L.B., ed., *Petroleum systems of the United States: U.S. Geological Survey Bulletin 1870*, p. 16-18.
- Cook, H.E., and Enos, Paul, eds., 1977, Deep-water carbonate environments: Society of Economic Paleontologists and Mineralogists, Special Publication No. 25, 336 p.
- Cook, H.E., and Taylor, M.E., 1977, Comparison of continental slope and shelf environments in the Upper Cambrian and lowest Ordovician of Nevada, in Cook, H.E., and Enos, Paul, eds., *Deep-water carbonate environments: Society of Economic Paleontologists and Mineralogists, Special Publication No. 25*, p. 51-81.
- Correia, M., 1967, Relations possibles entre l'état de conservation des éléments figurés de la matière organique (microfossiles palynoplantologiques) et l'existence de gisements d'hydrocarbures: *Revue de l'Institut Français du Pétrole*, v. 22, p. 1285-1306.
- Decker, John, Bergman, S.C., Blodgett, R.B., Box, S.E., Bundtzen, T.K., Clough, J.G., Coonrad, W.L., Gilbert, W.G., Miller, M.L., Murphy, J.M., Robinson, M.S., and Wallace, W.K., 1994, Geology of southwestern Alaska, in Plafker, George, and Berg, H.C., eds., *The geology of Alaska: Boulder, Colo., Geological Society of America, The Geology of North America*, v. G-1, p. 285-310, pl. 3.
- Egorova, L.I., Shabanov, Y.Y., Pegel, T.V., Savitsky, V.E., Suchov, S.S., and Chernysheva, N.E., 1982, Mayskiy yarusa stratotipicheskoy mestnosti (sredniy kembriy yugo-vostoka Sibirskoy platformy) [The Mayan Stage of the stratotype locality (Middle Cambrian of the south-eastern Siberian Platform)]: *Trudy Mezhdomestvennyy Stratigraficheskiy Komitet SSSR*, v. 8, 146 p. [In Russian].
- Espitalié, J., Deroo, G., and Marquis, F., 1985, Rock Eval pyrolysis and its applications [preprint]: *Revue de l'Institut Français du Pétrole*, Rueil, France.
- Gao Zhenzhong, and Duan Taizhong, 1985, Gravity-displaced deposits of Cambrian deep-water carbonates in west Hunan and east Guizhou: *Acta Sedimentologica Sinica*, v. 3, p. 7-22 [In Chinese with English summary].
- Gilbert, W.G., and Bundtzen, T.K., 1983, Paleozoic stratigraphy of the Farewell area, southwest Alaska Range, Alaska [abs.]: Alaska Geological Society Symposium, New Developments in the Paleozoic Geology of Alaska and the Yukon, Anchorage, Alaska, 1983, Program and Abstracts, p. 10-11.
- Gutjahr, C.C.M., 1966, Carbonization of pollen grains and spores and their application: *Leidse Geologische Mededelingen*, v. 38, p. 1-30.
- Hubert, J.F., Suchecki, R.K., and Callahan, R.K.M., 1977, The Cow Head Breccia: sedimentology of the Cambro-Ordovician continental margin, Newfoundland, in Cook, H.E., and Enos, Paul, eds., *Deep-water carbonate environments: Society of Economic Paleontologists and Mineralogists, Special Publication No. 25*, p. 125-154.
- Ineson, J.R., Surlyk, Finn, Higgins, A.K., and Peel, J.S., 1994, Slope apron and deep shelf sediments of the Brønland Fjord and Tavsens Iskappe Groups (Lower Cambrian-Lower Ordovician), North Greenland: stratigraphy, facies, and depositional setting: *Grønlands Geologiske Undersøgelse, Bulletin*, v. 169, p. 7-24.
- Jacobson, S.R., 1991, Petroleum source rocks and organic facies, in Merrill, R.K., ed., *Source and migration processes and evaluation techniques: Treatise of petroleum geology, handbook of petroleum geology: Tulsa, Okla., American Association of Petroleum Geologists*, p. 3-11.
- Jones, D.L., Silberling, N.J., Coney, P.J., and Plafker, George, 1987, Lithotectonic terrane map of Alaska (west of the 141st Meridian): U.S. Geological Survey Miscellaneous Field Studies Map MF-1874-A, 1 sheet, scale 1:250,000.
- Jones, R.W., 1984, Comparison of carbonate and shale source rocks, in Palacas, J.G., ed., *Petroleum geochemistry and source rock potential of carbonate rocks: American Association of Petroleum Geologists, Studies in Geology No. 18*, p. 163-180.
- Jones, R.W., and Edison, T.A., 1978, Microscopic observation of kerogen related to geochemical parameters with emphasis on thermal maturation, in Oltz, D.F., ed., *Symposium in geochemistry: low temperature metamorphism of kerogen and clay minerals: Los Angeles, Calif., Society of Economic Paleontologists and Mineralogists, Pacific Section*, p. 1-12.
- Kindle, C.H., and Whittington, H.B., 1958, Stratigraphy of the Cow Head region, western Newfoundland: *Geological Society of America Bulletin*, v. 69, p. 315-342.
- Leslie, S.A., Isaacson, P.E., Repetski, J.E., and Weideman, W.L., 1991, Upper plate rocks of the Roberts Moun-

- tains thrust, northern Independence Range, northeast Nevada: the Late Cambrian(?) to Middle Ordovician Snow Canyon Formation of the Valmy Group, in Cooper, J.D., and Stevens, C.H., eds., *Paleozoic paleogeography of the western United States-II*: Los Angeles, Calif., Society of Economic Paleontologists and Mineralogists, Pacific Section, p. 475-486.
- Miller, M.L., Belkin, H.E., Blodgett, R.B., Bundtzen, T.K., Cady, J.W., Goldfarb, R.J., Gray, J.E., McGimsey, R.G., and Simpson, S.L., 1989, Pre-field study and mineral resource assessment of the Sleetmute quadrangle, southwestern Alaska: U.S. Geological Survey Open-File Report 89-363, 115 p.
- Palacas, J.G., 1988, Characteristics of carbonate source rocks of petroleum, in Magoon, L.B., ed., *Petroleum systems of the United States*: U.S. Geological Survey Bulletin 1870, p. 20-25.
- Palmer, A.R., Egbert, R.M., Sullivan, Raymond, and Knoth, J.S., 1985, Cambrian trilobites with Siberian affinities, southwestern Alaska [abs.]: *American Association of Petroleum Geologists Bulletin*, v. 69, p. 295.
- Patton, W.W., Jr., 1978, Juxtaposed continental and oceanic-island arc terranes in the Medfra quadrangle, west-central Alaska, in Johnson, K.M., ed., *The United States Geological Survey in Alaska: Accomplishments during 1977*: U.S. Geological Survey Circular 772-B, p. B38-B39.
- Peters, K.E., 1986, Guidelines for evaluating petroleum source rocks using programmed pyrolysis: *American Association of Petroleum Geologists, Bulletin*, v. 70, p. 318-329.
- Rees, M.N., Robison, R.A., Babcock, L.E., Chang, W.T., and Peng, S.C., 1992, Middle Cambrian eustasy: evidence from slope deposits in Hunan Province, China [abs.]: *Geological Society of America Abstracts with Programs*, v. 24, no. 7, p. A108.
- Smith, T.N., Blodgett, R.B., and Clough, J.G., 1984, Preliminary analysis of the petroleum potential and stratigraphy of the Holitna basin, southwest Alaska [abs.]: *Geological Society of America Abstracts with Programs*, v. 16, no. 5, p. 334.
- St. John, James, 1994, Systematics and biogeography of some upper Middle Cambrian trilobites from the Holitna basin, southwestern Alaska: Columbus, The Ohio State University, M.S. thesis, 90 p.
- St. John, James, and Babcock, L.E., 1994, Biogeographic and paleogeographic implications of Middle Cambrian trilobites of extra-Laurentian aspect from a native terrane in southwestern Alaska [abs.]: *Geological Society of America Abstracts with Programs*, v. 26, no. 5, p. 63.
- Staplin, F.L., 1969, Sedimentary organic matter, organic metamorphism, and oil and gas occurrence: *Canadian Petroleum Geology Bulletin*, v. 17, p. 47-66.
- Taylor, M.E., and Cook, H.E., 1976, Continental shelf and slope facies in the Upper Cambrian and lowest Ordovician of Nevada: *Brigham Young University Geology Studies*, v. 23, no. 2, p. 181-214.
- Tissot, B.P., and Welte, D.H., 1984, *Petroleum formation and occurrence* (2nd ed.): New York, Springer-Verlag, 699 p.
- Reviewers: Rosemary A. Askin and David A. Rohr

# Rare-Earth Enrichment at Bokan Mountain, Southeast Alaska

By John A. Philpotts, Cliff D. Taylor, and Philip A. Baedeker

## ABSTRACT

A suite of 11 granite and vein-dike samples of low radioactivity from Bokan Mountain (Alaska's only producer of uranium) and a granodiorite and two metabasalt samples of local country rock have been analyzed for rare-earth elements, yttrium, zirconium, hafnium, niobium, thorium, and uranium. The samples constitute a crude 3-km geochemical transect southeast from the peripheral peralkaline granites of the Bokan Mountain stock along mineralized pegmatite and aplite vein dikes. Unusually high concentrations, in excess of 2 percent each, were obtained for total rare earths, yttrium, and zirconium as oxides. Hafnium and niobium concentrations were also high, reaching 0.06 and 0.3 percent, respectively, as oxides.  $\text{ThO}_2$  reached 0.05 percent, and  $\text{U}_3\text{O}_8$  values were as high as 0.02 percent. These maximum enrichments are about 50 times typical crustal values for thorium and uranium; 100 times crustal values for total rare earths, zirconium, hafnium, and niobium; and 1,000 times crustal values for yttrium. The enrichment in yttrium is paralleled by unusually high concentrations of heavy rare earths relative to light rare earths. The limited differences in slope of the chondrite-normalized rare-earth patterns suggest that the rare-earth abundances in the stock and vein-dike samples are dominated by only two or three constituent phases. All of the stock and vein-dike samples have pronounced negative europium anomalies of similar size ( $\text{Eu}/\text{Eu}^* = 0.27 \pm 0.04$ ). The sign and size of the europium anomalies are consistent with extensive feldspathic igneous fractionation. The relative invariance of the europium anomalies indicates either that all of these samples formed at the same petrogenetic stage or that effectively only trivalent europium was involved in any relative fractionation among these particular samples, which might indicate oxidizing conditions. The similarity in the overall rare-earth patterns and in the europium anomalies of all the stock and vein-dike samples indicates that the enriched elements were derived from igneous sources rather than by hydrothermal-cell leaching of local country rocks. The country rocks have quite different patterns and lack appreciable europium anomalies. The relatively low tho-

rium and uranium contents and ore-grade levels of other elements in the vein-dike samples support the possible occurrence of ore deposits of rare earths, yttrium, zirconium, hafnium, and niobium without significant radioactivity.

## INTRODUCTION

Bokan Mountain (lat  $54^{\circ}55'$  N., long  $132^{\circ}9'$  W.) is located between the South Arm of Moira Sound and the West Arm of Kendrick Bay on southern Prince of Wales Island in the Dixon Entrance D1 quadrangle, 60 km southwest of the town of Ketchikan (figs. 1, 2). The locality became notable in 1955 when airborne and subsequent ground surveys identified areas of radioactivity due to concentrations of uranium and thorium minerals. A dozen major prospects and numerous other occurrences having uranium and thorium enrichment were found in the vicinity. Of these, only the Ross Adams deposit has proven to be economically viable to date. The Ross Adams mine was active intermittently between 1957 and 1971 and produced 94,000 short tons of high-grade uranium ore averaging 1 percent  $\text{U}_3\text{O}_8$ , the only uranium production to date from Alaska (Roppel, 1991).

The discovery and mining of uranium ore stimulated geological interest in the area. Details of the local geology and of the thorium- and uranium-rich mineral occurrences have been reported by MacKevett (1963), Collot (1981), Thompson and others (1982), Warner and Mardock (1987), Thompson (1988), Barker and Mardock (1988), and Warner and Barker (1989). Bokan Mountain is a crudely circular stock composed of peralkaline granite, about  $10 \text{ km}^2$  in area. It is surrounded by an albitized contact metamorphic aureole about 3 km across. The metamorphic aureole extends out into the local country rocks that consist of Phanerozoic island-arc sedimentary, volcanic, and plutonic rocks. Armstrong (1985), on the basis of Rb-Sr isochron analysis, interpreted the Bokan Mountain stock as a  $151 \pm 5$ -Ma (Late Jurassic) intrusion into  $432 \pm 19$ -Ma (Early Silurian) country rock. The geologic map of Gehrels (1992) divides the Bokan Mountain stock

into a core of riebeckite granite porphyry (with subordinate aplitic fely-aegirine granite) surrounded by an outer annulus that is predominantly aegirine granite porphyry (fig. 2). The Bokan Mountain stock intrudes country rock that consists predominantly of Late Ordovician and (or) Early Silurian quartz monzonite and granite and Late Ordovician quartz diorite and diorite (fig. 2). Collot (1981) interpreted the stock as the apex of a large composite intrusion made up largely of outer aegirine granite around a core of arfvedsonite granite. Thompson and others (1982) and Thompson (1988) suggest no less than 12 mappable intrusive phases are present in the complex. In their interpretation, a key feature for the formation of mineralizing fluids is the subsidence or collapse of the central part of the complex that led to the emplacement of ring dikes, devolatilization of the magma, and a change from aegirine granite to riebeckite granite crystallization. Mineralogically, the granites of the Bokan Mountain stock are composed largely of various proportions of quartz, potassic feldspar, albite, aegirine, and soda-iron amphibole; accessory minerals include zircon, ilmenite, magnetite, allanite, xenotime, monazite, fluorite, and uranotorite (MacKevett, 1963; Thompson and others, 1982; Warner and Mardock, 1987; Thompson, 1988; Warner and Barker, 1989).

The thorium-uranium deposits occur as pegmatites, vein dikes, and pipelike bodies that are all closely associated with the stock both spatially and genetically and are believed to have formed during devolatilization of the magma; the mineralization is thought to be of magmato-hydrothermal origin (Thompson and others, 1982; Thompson, 1988). Uranotorite, uranoan thorianite, and uraninite, the dominant radioactive minerals, often fill open spaces within the pegmatites and vein dikes. Alteration is characterized by albitization and silicification of the igneous host rock and destruction of potassium feldspars. Iron and manganese oxides locally mark the position of shear zones and faults along which the fluid travelled. Later movement on these faults has offset some of the mineralization (MacKevett, 1963). Temperature estimates obtained for water-rich and carbon dioxide-rich inclusions in late-stage quartz and independently from sulfur isotopes in coexisting sulfide phases are in the hydrothermal range from 150 to 450°C; the isotopic composition of oxygen in calcite indicates magmatic rather than meteoric water (Thompson, 1988).

Although most of the early work focused on the uranium occurrences, MacKevett (1963) recognized abnormal rare-earth element (REE) enrichments in some of the rocks as one of the more interesting petrologic and geochemical features of mineralized samples from Bokan Mountain. MacKevett (1963) reported La, Ce, and Nd concentrations up to 1 percent, Nb values up to 0.1 percent, and Zr values of more than 10 percent, in aplite dikes. The resources of REE, Y, Zr, and Nb in Bokan Mountain granites and vein dikes has been the specific emphasis in a number of recent reports from the U.S. Bureau of Mines (Warner and Mardock, 1987; Warner and Barker, 1989). In the most detailed study to date of enrichments of elements in addition to thorium and uranium, Warner and Barker (1989) reported indicated and inferred resources (in millions of pounds) of 43 and 198, respectively, for total REE as oxides; 28 and 105 for  $Y_2O_3$ ; 170 and 467 for  $ZrO_2$ ; 20 and 76 for  $Nb_2O_5$ ; 8.5 and 19 for  $TbO_2$ ; and 3.3 and 8.5 for  $U_3O_8$ . Warner and Barker (1989) reported the following maximum concentrations: total REE, 4.0 percent; Y, 3.0 percent; Zr, 9.7 percent; Nb, 2.8 percent; Th, 12.8 percent; and U, 2.4 percent.

The processes leading to ore-level enrichment of REE in deposits other than placers are not fully understood. The world's largest REE deposit at Bayan Obo, China, for example, is currently both of uncertain age and origin (Philpotts and others, 1991). Many enrichments of REE, however, are associated with the carbonatite or silicate facies of alkalic igneous complexes. Further study and genetic modeling of the REE-alkalic igneous rock association is attractive at Bokan Mountain for a number of reasons: (1) unusually high enrichments of REE and other elements indicate an unusually high degree of fraction-

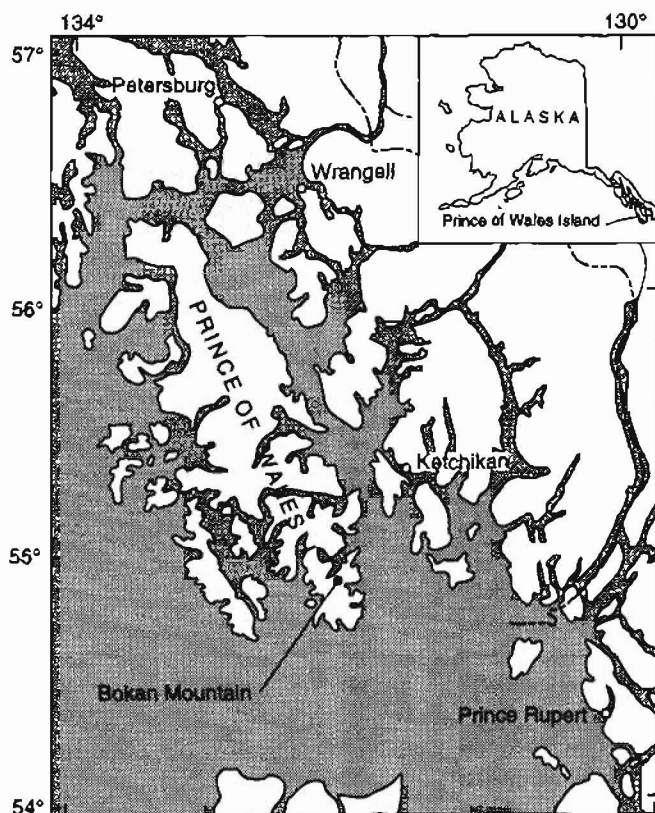


Figure 1. Location of Bokan Mountain on Prince of Wales Island, southeast Alaska.

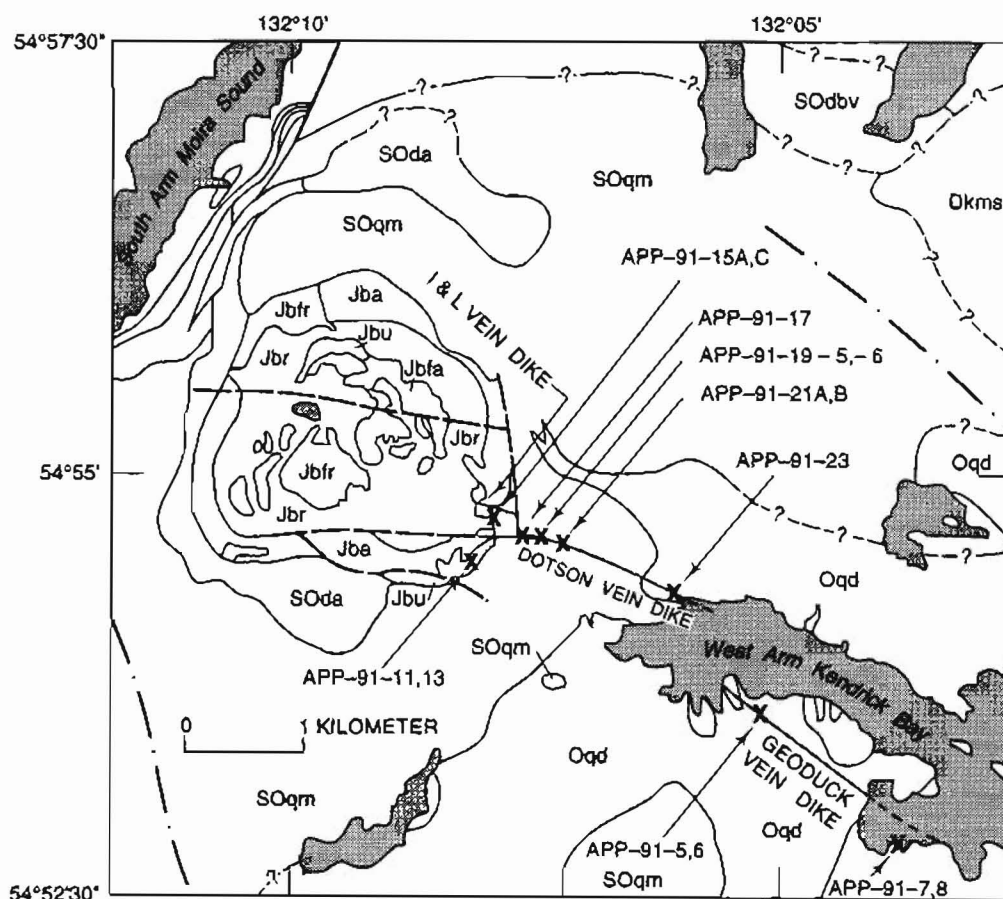


ation; (2) unlike typical REE ore deposits, HREE (that is, the heavy REE, Gd to Lu) are particularly enriched at Bokan Mountain, and this enrichment could have economic significance should demand rise for one or more of the HREE; (3) the Alexander terrane host rocks are relatively simple, being derived from juvenile (mantle-derived) magmas that are largely free from contamination by old continental crust (Samson and others, 1989); and (4) a petrologic scenario for the genesis of the Bokan Mountain stock has been proposed (Thompson, 1988) and appears reasonable. The purpose of the present note is to further test this scenario and to extend the modeling of the igneous rocks and the vein dikes via genetic interpretation of the abundances of the elements of potential economic interest, especially the REE. It is further anticipated that a comprehensive model for the evolution of Bokan

Mountain might be very useful for elucidating the petrogenesis of other similar but much less well studied alkaline igneous bodies elsewhere in southeast Alaska.

The term "vein dike" is used here for dikes and veins at Bokan Mountain that include pegmatitic, aplitic, and quartz-cored varieties. The vein dikes show bifurcating and anastomosing tendencies, particularly away from the stock, and they are perhaps more precisely thought of as systems rather than as individual bodies. We interpret the vein dikes as products of gradational magmatic and hydrothermal activity.

In the present paper we report chemical analyses for REE, Y, Zr, Hf, and Nb in a small suite of samples collected from the outer granitic annulus of Bokan Mountain and from the Dotson and the Geoduck vein-dike systems (fig. 2). The Dotson vein dike is a major mineralized



**Figure 2.** Sample sites (X) and the location (after Warner and Barker, 1989) of the Dotson, Geoduck, and I & L vein dikes on the southeast flank of Bokan Mountain. Geologic map modified from Gehrels (1992); all map units from Gehrels (1992). Bokan Mountain Granite map units (all Jurassic): Jbr, riebeckite granite porphyry; Jba, aegirine granite porphyry; Jbfr, fine-grained riebeckite granite porphyry; Jbfa, felty-aegirine granite; Jbu, granite, undivided. Country rock map units: Dkms, mudstone and siltstone unit of Early Devonian Karheen Formation; SOda and SOdbv, argillite and shale unit and basaltic to andesitic volcanic rock unit, respectively, of Ordovician and Early Silurian(?) Descon Formation; SOqm, Late Ordovician and (or) Early Silurian quartz monzonite and granite; Oqd, Late Ordovician quartz diorite and diorite. Faults are shown by long-dash lines where approximately located and by dash-dot lines where inferred from aerial photographs.

feature at Bokan Mountain. It is bounded by steeply dipping fractures (Staatz, 1978). The northwestern terminus appears to be at a right-lateral offset of the "I & L" vein-dike system, which continues to the periphery of the stock (fig. 2). The Dotson vein dike extends for about 3 km to the southeast with reasonably good width (usually  $\geq 1$  m) and exposure on the flanks of the mountain (Warner and Barker, 1989). The Geoduck vein dike occurs to the southeast of the Dotson vein dike, farther away from the stock. The Dotson and Geoduck vein dikes are therefore well suited for studying relationships between the vein dikes and the stock, as well as any changes in composition along the lengths of the vein dikes.

These vein-dike systems were the specific focus of the mineralogical and geochemical study of Staatz (1978). They were also included in the detailed but geographically broader descriptions of the vein-dike systems by Warner and Mardock (1987) and Warner and Barker (1989). In contrast with much of the earlier work, our focus is entirely on samples having low radioactivity. This difference in emphasis was planned so as to broaden the coverage and with the thought that, in light of the extensive airborne and ground surveying, any significant undiscovered mineral deposits in the area are not likely to be radioactive. Although the U-Th and REE groups can both be enriched in late stage granite differentiates, they are not highly coherent geochemically. In systems highly enriched in both U-Th and REE such as at Bokan Mountain, the two groups of elements are generally partitioned largely into different mineral phases. In the vein-dike systems around Bokan Mountain, REE, Nb, and Zr appear to be inversely correlated with U and Th (Warner and Mardock, 1987; Warner and Barker, 1989). Thus, there is the possibility of economic mineral deposits of Y, REE, Zr, Hf, or Nb showing little or no radioactivity at Bokan Mountain. Low radioactivity can be advantageous for resource exploitation. Radioactive elements, especially Th, are often a nuisance byproduct because precautionary measures are required for their handling and processing.

Sampling by Staatz (1978), Warner and Mardock (1987), Barker and Mardock (1988), and Warner and Barker (1989) included many composite and channel samples that are well suited for estimating potential grades and tonnages but not so well suited for paragenetic studies or for petrogenetic interpretation. Furthermore, many of the earlier chemical data were obtained by semiquantitative emission spectroscopy. This is a useful technique, but it does not have the quality provided by the analytical data we report here, which is particularly necessary for the petrogenetic interpretation of the REE data.

## SAMPLE LOCATIONS

Sample locations are shown in figure 2. The sample nomenclature we use is given in table 1. Granite samples

11 (that is, APP-91-11) and 13 were collected from the periphery of the stock, about 100 m south of the Ross Adams open pit. Granite samples 15A and 15C were selected from talus immediately southwest (fig. 2) of the I & L vein-dike system (Staatz, 1978) because they have more distinctly porphyritic textures than those of granite samples 11 and 13. The in situ locations of granites 15A and 15C are unknown, but their geochemistry clearly links them to the stock, and sample 15A closely fits the description given by Warner and Barker (1989) for border-zone pegmatite. Samples 17, 19-5, and 19-6 (all quartz-albite-potassic feldspar pegmatites) and samples 21A and 21B are from locations on the Dotson vein dike that are increasingly distal from the stock. The feldspar in 21A is albite with normative feldspar composition of  $\text{Or}_{30}\text{Ab}_{96}\text{An}_0$ , whereas in 21B it is largely potassic feldspar (normative  $\text{Or}_{80}\text{Ab}_{20}\text{An}_0$ ). Sample 21B was interpreted in the field to be from a vein dike interfingering with host sample 21A, although the exact relationship was obscure. The trace element signature of 21A, however, is also vein dike-like. It appears likely that 21A also represents a vein dike. Alternatively, based on the chemistry, it is possible that 21A could represent Ordovician and (or) Silurian country rock or Mesozoic granite admixed or metasomatized with about 5 percent enriched vein-dike material; there is, however, no available geologic or petrographic information to support such an interpretation. Sample 23, a quartz-albite aplite, was collected about 1 km southeast of sample 21 (that is, farther from the stock). The intervening distance, the bifurcating nature of the vein dikes, and the heavy undergrowth make it uncertain whether the sample is from the extension of the Dotson vein dike or from a nearby parallel vein dike. Sample 6, a quartz-albite aplite, was collected 1.2 km to the southeast of sample 23. Sample 6, however, is from another extensive vein dike, the Geoduck system (Warner and Barker, 1989). The Geoduck trends to the southeast along the southern edge of the West Arm of Kendrick Bay (fig. 2). Sample 5 was taken from the metabasalt country rock that hosts the Geoduck vein dike in this vicinity. Sample 7 was collected from a basalt dike and sample 8 from the local Ordovician and (or) Silurian granodiorite country rock cut by the dike. Samples 7 and 8 were collected about 4 km southeast of the outer-annulus granite of Bokan Mountain and are likely free from albitization or any other metasomatic effects associated with the stock.

## ANALYTICAL METHODS

Concentrations of REE, Zr, Hf, U, and Th were determined by instrumental neutron activation analysis (INAA). Sample aliquots of about 0.5 g each were irradiated for 6.5 hours on a TRIGA reactor (U.S. Geological Survey, Denver); following a 6-day cooling period, the samples were counted four times over a period of 8 weeks



**Table 1.** Oxide weight percents for sums of measured (m-) and total (t-) REE, Y, Zr, Hf, Nb, Th, and U in Bokan Mountain granites, vein dikes, and country rocks[Analysts: Philip Baedeker, Michael Doughien, David Fey, and Paul Briggs.  $\text{ZrO}_2$  is not reported for sample APP-91-5 because the correction for fission product interference exceeds 50 percent of the value]

Sample No.	Rock type	m- $\text{RE}_2\text{O}_3$ %	t- $\text{RE}_2\text{O}_3$ %	$\text{Y}_2\text{O}_3$ %	$\text{ZrO}_2$ %	$\text{HfO}_2$ %	$\text{Nb}_2\text{O}_5$ %	$\text{ThO}_2$ %	$\text{U}_3\text{O}_8$ %
<b>BORDER ZONE GRANITES</b>									
APP-91-11	Aegirine granite	0.093	0.102	0.0024	0.151	0.00376	0.0073	0.00222	0.00085
APP-91-13	Amphibole granite	.14	.16	.0089	.052	.00135	.019	.0156	.0014
APP-91-15A	Granite porphyry	.014	.018	.0051	.218	.00516	.0046	.00140	.000948
APP-91-15C	Aegirine granite	.015	.018	.0036	.124	.00295	.0086	.0032	.000724
<b>DOTSON VEIN DIKE</b>									
APP-91-17	Qtz-Ab-Kfs pegmatite	0.113	0.17	0.018	2.53	0.0508	0.0110	0.00978	0.00752
APP-91-19-5	Qtz-Ab-Kfs pegmatite	.101	.19	.23	3.30	.0634	.0099	.00339	.0113
APP-91-19-6	Qtz-Ab-Kfs pegmatite	.35	.49	.28	2.62	.0496	.086	.0132	.0115
APP-91-21A	Albite granite	.107	.14	.067	.060	.00131	.014	.00547	.00229
APP-91-21B	Kfs pegmatite	1.7	2.4	2.3	2.00	.0344	.090	.0559	.0175
APP-91-23	Qtz-Ab aplite	.47	.53	.048	.045	.00116	.24	.00464	.0112
<b>GEODUCK VEIN DIKE</b>									
APP-91-6	Qtz-Ab aplite	0.57	0.70	0.27	0.753	0.0124	0.30	0.0247	0.0166
<b>COUNTRY ROCKS</b>									
APP-91-5	Metabasalt	0.0055	0.0072	0.0029		0.000220	0.00027	0.000195	0.000075
APP-91-7	Metabasalt dike	.0035	.0052	.0029	0.015	.00029	.00027	.000024	<.00005
APP-91-8	Granodiorite	.0075	.0084	.0006	.012	.000290	.00026	.000439	.00015

for the determinations. Yttrium was determined by inductively coupled plasma-atomic emission spectrometry (ICP-AES). Nb was determined by ICP-AES following a chemical separation of the sample. All of the determinations are expected to be accurate to within 10 percent of the reported value (Baedecker, 1987).

## RESULTS AND DISCUSSION

The sums of the *measured* REE concentrations in each sample as weight-percent oxide ( $m\text{-RE}_2\text{O}_3$ ) are given in table 1, and the individual measured REE concentrations as parts per million by weight of the element in the sample are shown in table 2. Concentrations of REE not measured directly may be interpolated with a high degree of confidence because the REE are a very coherent group of elements (see figs. 3-5). Estimated *total* REE sums, which include interpolated values for REE not directly measured, are also reported in table 1 as weight-percent oxide ( $t\text{-RE}_2\text{O}_3$ ). The weight percents for the oxides of Y, Zr, Hf, and Nb are also given, along with those for Th and U, which again are noted to be relatively low.

Chondrite-normalized REE abundance patterns are given in figures 3-5. The normalized patterns for the four samples with relatively flat slope for the HREE are shown in figure 3. Normalized patterns for the six samples with normalized HREE abundances that increase up to the values for Yb or Lu are displayed in figure 4. The relative enrichment of the heaviest REE is less in sample 19-6 than in the other samples in figure 4, and this sample may be a type intermediate between the figure 3 samples and the other figure 4 samples. Patterns for the metabasalt (samples 5, 7) and granodiorite (sample 8) country rocks and for vein-dike sample 23 are shown in figure 5. Sample 23 has a pattern of decreasing (light to heavy) REE abundances that is quite different from those of the other vein-dike samples.

Each of the three country rock samples has its own unique pattern (fig. 5). Sample 7, which is from a basalt dike, has low La and Ce abundances indicative of a depleted source. The sample 7 REE pattern resembles that of MORB (mid-ocean-ridge basalt; for example, Philpotts and others, 1969). The lack of any significant Eu anomaly in this sample indicates that it represents primitive melt (that is, it has undergone little low-pressure feldspar fractionation since leaving the mantle). Sample 5, another metabasalt, also appears to be primitive (that is, no Eu anomaly). The enriched La and Ce abundances in sample 5 suggest either a much lower degree of partial melting than for sample 7 or a source that was not depleted by prior melting events. The REE pattern of sample 5 is similar to that of many diabases and continental flood basalts (Philpotts and Schnetzler, 1968a). Both basalt samples 7 and 5 have been altered, and this alteration

might have modified their REE patterns to some degree. However, the power and utility of the REE in petrogenetic interpretation derive, in part, from the relative immobility of these elements (for example, Philpotts and others, 1969). The fact that the three country rock REE patterns shown in figure 5 are each distinct certainly argues against any significant postemplacement regional homogenization of REE. If the REE pattern of country rock sample 8 has not been modified by regional metamorphism, then the lack of a Eu anomaly again suggests little differentiation involving feldspar and hence mantle rather than crustal derivation. The slope of the REE pattern, particularly for the HREE, might indicate an affinity with the tonalite-trondjemite suite. The country rock samples are discussed further below only in relation to the Bokan Mountain granites and vein dikes, which are the focus of this paper.

The degree of HREE enrichment apparent in figures 3 and 4 is unusual for rocks with such high total REE abundances, although greisens sometimes show such patterns. Most REE ores are, like sample 23 (fig. 5), strongly enriched in LREE (that is, the light REE, La to Sm). The LREE-enriched pattern of sample 23 may reflect its position as the most distal of our Dotson vein-dike samples. The REE data of Staatz (1978), when plotted as chondrite-normalized patterns, show HREE-enriched or bowl-shaped patterns for samples from the I & L vein dikes (which are proximal to the stock) but LREE enrichment like that in sample 23 for his three samples from the Dotson vein dike. The Dotson vein dike is located farther from the stock than are the I & L vein dikes (fig. 2). Similarly, Warner and Mardock (1987) reported general proximal HREE enrichment and distal LREE enrichment in the vein dikes. Warner and Mardock (1987) and Warner and Barker (1989) concluded that there is variation in composition along the vein dikes. They noted that U and Th concentrations and the U/Th ratio are high in vein dikes in and near the Bokan Mountain stock, whereas REE, Zr, and Nb are enriched in distal parts of the vein dikes. They also note that the textures of the vein dikes tend to change from pegmatitic near the stock to aplitic away from it.

The compositions of our samples appear to fit some of these previously noted trends. Three of our four most distal samples (21A, 23, and 6) are quartz-albite granite or aplite (table 1). Of these, aplite samples 6 and 23 have the second and third highest REE contents (table 1) of our samples, respectively, and sample 6 also has the highest Nb concentration (0.3 percent  $\text{Nb}_2\text{O}_5$ ). However, the potassium-feldspar-bearing pegmatite sample 21B has the highest REE (2.4 percent  $t\text{-RE}_2\text{O}_3$ ) and Y contents (2.3 percent  $\text{Y}_2\text{O}_3$ ); sample 21B also has 2.0 percent  $\text{ZrO}_2$ . Somewhat higher  $\text{ZrO}_2$  concentrations were obtained for the proximal Dotson pegmatite sample 17 (2.53 percent) and especially for the middle Dotson pegmatite samples

**Table 2.** Rare-earth element concentrations in parts per million by weight (ppm) and europium anomalies (Eu/Eu\*) in granites, vein dikes, and country rocks at Bokan Mountain

[Analyst: Philip Baedeker. Missing Ho values indicate unacceptable counting uncertainty]

Sample No.		Ce	Nd	Sm	Eu	Tb	Ho	Yb	Lu	Eu/Eu*
	ppm	ppm	ppm	ppm	ppm	ppm	ppm	ppm	ppm	
<b>BORDER-ZONE GRANITES</b>										
APP-91-11	195	388	170	20.9	1.09	0.891		17.3	2.81	0.31
APP-91-13	292	619	241	48.1	3.22	3.63		16.6	2.32	.29
APP-91-15A	19.7	44.1	22	6.54	.665	1.62	4.0	16	2.67	.28
APP-91-15C	25.7	55.9	20	4.5	.40	.937	2.6	14	2.28	.27
<b>DOTSON VEIN DIKE</b>										
APP-91-17	102	270	110	33.2	4.3	17.9	60	340	46	0.27
APP-91-19-5	40.6	78	63	28	4.86	24.6	90	490	67.0	.29
APP-91-19-6	541	1130	530	186	18.7	49.6	110	390	52.6	.26
APP-91-21A	227	393	150	46.9	4.85	13.8	20	52	5.62	.25
APP-91-21B	3220	5860	2400	771	79.0	295	500	1360	153	.23
APP-91-23	1140	1950	710	198	16.4	19.6		12	.986	.29
<b>GEODUCK VEIN DIKE</b>										
APP-91-6	1200	2420	780	237	22.6	51.3	70	189	22.2	0.26
<b>COUNTRY ROCKS</b>										
APP-91-5	9.03	19.6	11	3.1	1.04	0.63		2.50	0.356	0.96
APP-91-7	2.9	9.1	9.8	3.43	1.20	.72		2.6	.37	.97
APP-91-8	17.4	31.4	12	2.3	.627	.21		.65	.085	1.07

19-5 (3.3 percent) and 19-6 (2.62 percent).  $\text{HfO}_2$  concentration reaches 0.0634 percent in sample 19-5. Clearly there is some relative fractionation of these elements among the various samples, and this fractionation is perhaps most likely due to differences in mineralogy.

The rough parallelism of parts of the REE patterns for most of the stock and vein-dike samples suggests that they have a close genetic link. Differences in the absolute level of REE among these samples may be due in part to the dilution effect of phases with low-REE concentrations, such as quartz, feldspar, and possibly pyroxene. The similarity in the REE patterns suggests that the REE in these samples are likely dominated by the same few (two or three?) major REE-bearing components. These phases may have very similar REE patterns regardless of the rock in which they occur. The slopes of the LREE in all the stock and vein-dike samples, and especially the pattern for aplite sample 23 (fig. 5), indicate that one or more of the phases contributing REE is LREE enriched with increasing depletion toward heavier REE; preliminary petrographic studies suggest bastnaesite and mona-

zite as likely candidates. The patterns in figure 3 further suggest a component phase with enriched but relatively unfractionated normalized HREE. The patterns in figure 4 indicate a phase with REE showing increasing enrichment up to Yb or Lu. Yttrium- and zirconium-rich phases appear to be contributing these enrichments of HREE. Mineralogical investigations currently underway are expected to identify these phases more precisely. Once the phases have been identified, published partitioning information may be useful for constraining the REE patterns of parental fluids and setting boundary conditions on likely source material and the type and extent of the fractionation processes involved.

The Eu anomalies give another indication of the close genetic bond between all of the stock and vein-dike samples that is even better than that revealed by the general similarities of their normalized REE patterns. Clearly, the stock and vein-dike samples displayed in figures 3, 4, and 5 have pronounced negative Eu anomalies. This is in distinct contrast to the patterns of the country rock samples (fig. 5), which show little if any Eu anomalies. The Eu

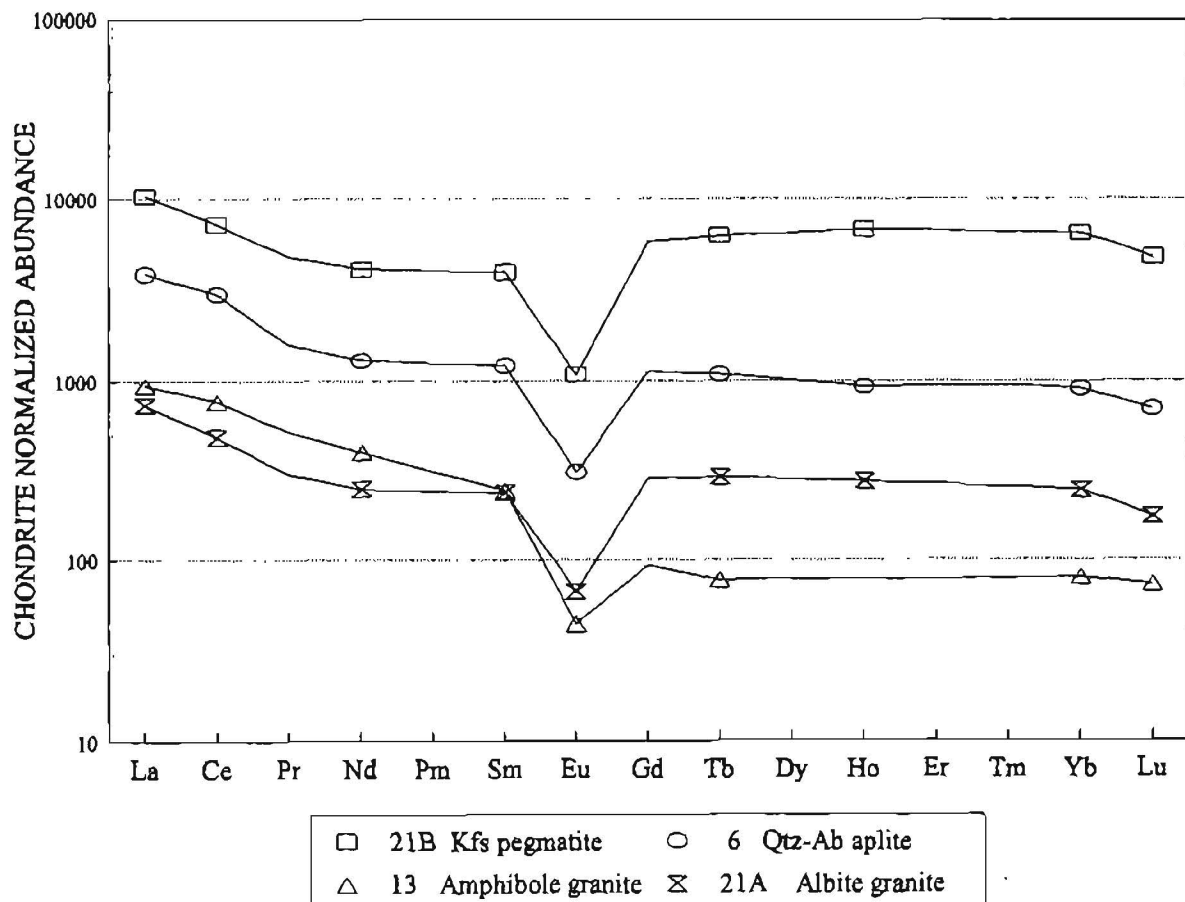


Figure 3. Chondrite-normalized REE abundance patterns for samples from the Dotson vein dike (samples 21A, 21B), the Geoduck vein dike (sample 6), and border-zone granite (sample 13) with relatively flat slopes for the heavy REE. The patterns are interpolated from measured values represented by the symbols.

anomalies in the stock and vein-dike samples are unusual in that they all show very similar depletion of Eu relative to the abundances of neighboring REE. Europium anomalies arise in igneous rocks because Eu can be partly divalent and may therefore be fractionated from the other (trivalent) REE, especially by minerals such as the feldspars that take up excess amounts of (divalent) Eu relative to its concentration in the environment of crystallization (Philpotts and Schnetzler, 1968b, 1969; Philpotts, 1970). In the ratio defining the Eu anomaly ( $\text{Eu}/\text{Eu}^*$ ), "Eu" represents measured Eu, whereas "Eu\*" is a hypothetical trivalent Eu abundance value obtained by interpolation of the REE pattern of the other (trivalent) REE. The geometric mean of chondrite-normalized Sm and Gd values [that is,  $(\text{Sm} \times \text{Gd})^{1/2}$ ] was used here for the  $\text{Eu}^*$  values in calculating the Eu anomalies. Gd was not measured in these samples, so we have instead adopted Gd values that in our judgment best fit the patterns defined by the measured abundances of the trivalent REE as shown in figs 3–5. The similarity between the stock and vein-dike Eu anomalies may be readily seen in the values given

in the right-hand column of table 2. The Eu anomalies for the stock and vein-dike samples all fall between  $0.27 \pm 0.04$ . There is no clear trend of  $\text{Eu}/\text{Eu}^*$  in the stock and vein-dike samples. Indeed, considering the  $\pm 15$  percent range in  $\text{Eu}/\text{Eu}^*$  in terms of likely sampling-errors, analytical-errors, and curve-fitting errors, the Eu anomalies might be identical in all of the stock and vein-dike samples.

The Eu anomaly results provide several petrogenetic insights. First, the similarity of the Eu anomalies of the Bokan Mountain granites and vein dikes indicates that the REE in each of these samples are very closely linked genetically. For each sample, whether granite, pegmatite or aplite, albite-rich or potassic, the REE have come from the same source without any intervening fractionation of Eu relative to other REE. Secondly, the source of the REE was igneous rather than the local country rocks because the latter lack appreciable Eu anomalies (fig. 5). Whole-rock Eu anomalies are expected to vary significantly with degree of fractionation in any igneous or hydrothermal system in which feldspar is being crystallized or put into solution or melt, as long as a significant frac-

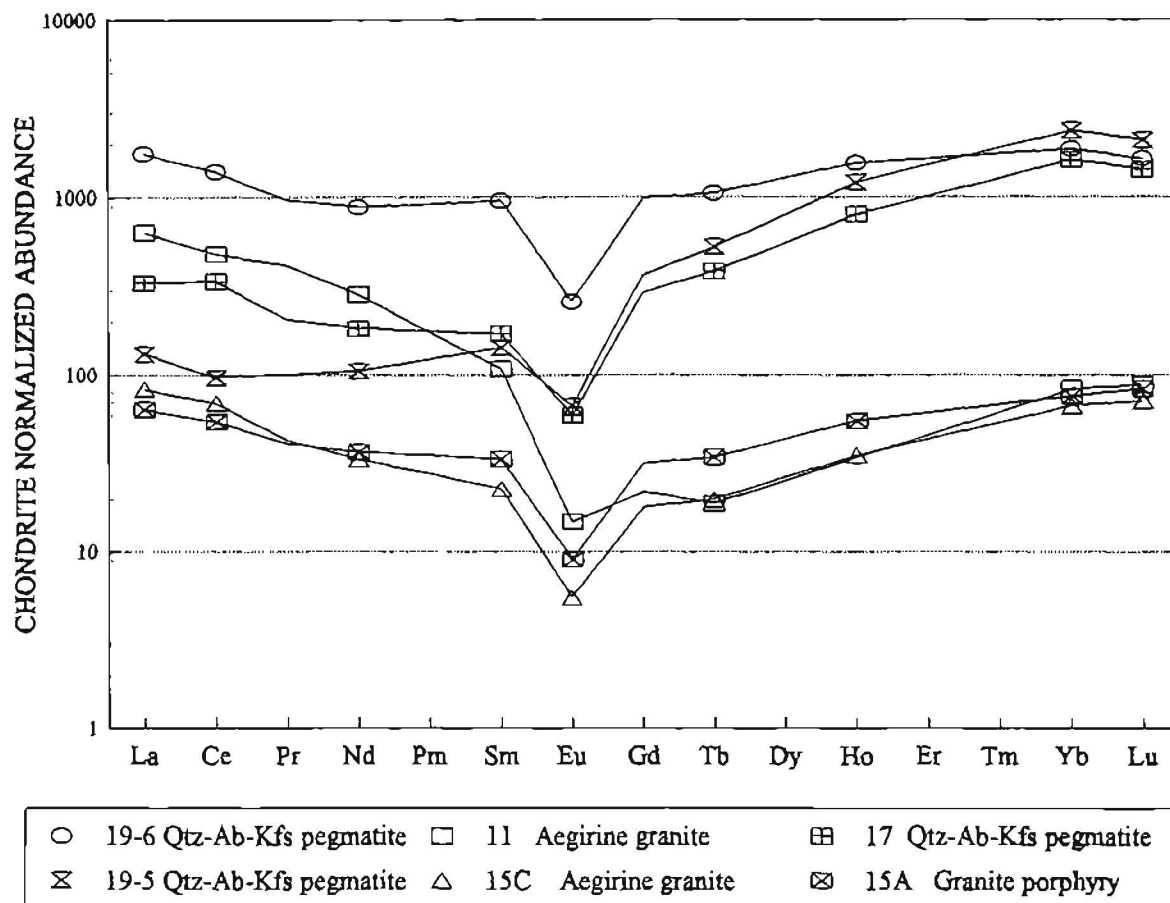


Figure 4. Chondrite-normalized REE abundance patterns for Bokan Mountain stock granite (samples 11, 15A, 15C) and Dotson vein dike (samples 17, 19-5, 19-6) samples with heavy REE abundances increasing up to Yb or Lu. Note the change in scale from figure 3.

tion of the Eu in the system is in a divalent state. Nd and Sr isotopic results on a granite from the Bokan Mountain stock (Samson and others, 1989) indicate that the granite was most likely derived from the mantle or possibly from primitive mantle derived-material such as MORB or island-arc basalt. It is very unlikely that any sizable volume of such source materials would have large negative Eu anomalies. Therefore, the anomalies presumably developed during the fractionation event that produced the Bokan Mountain granites. The size of the Eu anomaly indicates extensive fractionation, and this conclusion would be consistent with the unusual composition, including the enriched trace element suite, of all of granite and vein-dike samples associated with the stock.

The invariance of the stock and vein-dike Eu anomalies can be interpreted several ways. In the first hypothesis, it is assumed that whole-rock Eu anomalies were still capable of further evolution but that all of our stock and vein-dike samples (or more precisely the phases dominating their REE abundances) were generated at exactly the same paragenetic stage. This might not seem a very

plausible hypothesis. For one thing, the feldspathic nature of these rocks suggests that Eu/Bu\* might be subject to rapid change. However, MacKevett (1963) concluded that the thorium-uranium mineralization, the pegmatites, and the aplites were all coeval. Thompson (1988) concluded that the mineralization event was rapid and essentially contemporaneous with the hydrothermal alteration. It is not impossible, therefore, for all of our vein-dike and (outer-border) stock samples to be from the same evolutionary stage.

A second hypothesis is that all of the REE in these samples came from the same source, but that Eu anomalies stopped evolving prior to any differentiation/fractionation of the various rocks (and their constituent REE minerals). One possibility is that conditions became sufficiently oxidizing at some stage for the Eu to be effectively all in the trivalent state. Such an oxidative scenario receives support from the observation that the Bokan Mountain rocks are clearly enriched in ferric iron (for example, aegirine, iron oxides, etc.). However, verification of this hypothesis would require information on the

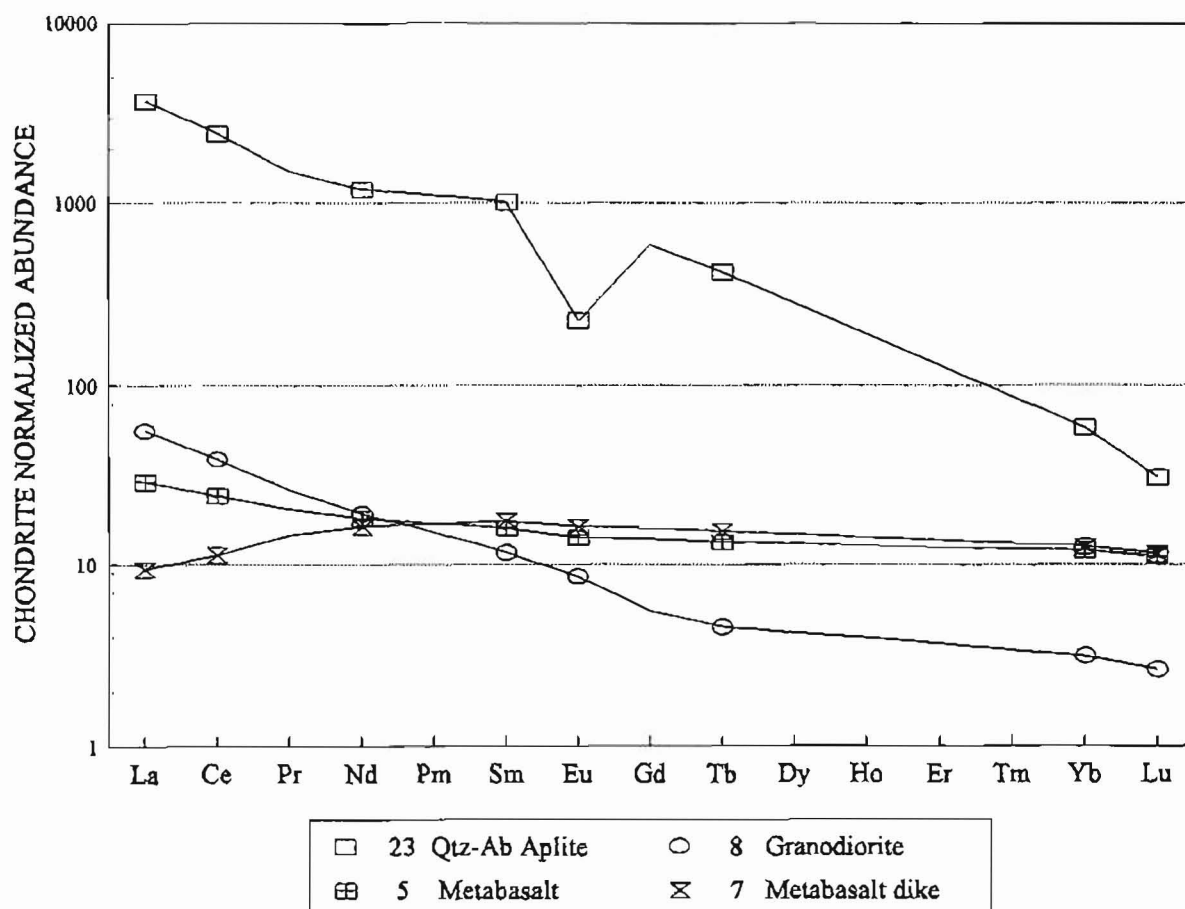


Figure 5. Chondrite-normalized REE abundance patterns for Bokan Mountain area country rocks (samples 5, 7, 8) and for the distal Dotson vein-dike sample (sample 23).



partitioning of the REE between equilibrated phases within the rocks, including phases with potential for anomalies such as feldspar. The concentration of Eu in feldspar relative to that in equilibrated phases is a function, in part, of the valence state of the Eu. This partitioning information is not currently available for these samples.

A third possibility is that the system was still reduced enough for the existence of divalent Eu, but that Eu anomalies stopped evolving because there was no longer any significant precipitation or solution of minerals containing excess (divalent) Eu. This explanation seems unlikely in such a feldspathic system.

Finally, a feldspar effect might be inconsequential if the amount of REE partitioned into feldspar diminished owing to changes in feldspar composition or structure, or to changes in temperature, pressure, or other environmental factors. In this fourth scenario, mineral phases containing excess (divalent) Eu may still have been crystallizing or dissolving, but partitioning of REE into such phases was too low to affect the rest of the system. These minerals would show Eu anomalies (unless they were swamped by REE contributions from inclusions or other contaminants), but their concentrations of Eu and the other REE would have negligible impact on the rest of the system, including the whole-rock REE pattern.

Based on the information currently available, we cannot choose any one of these scenarios over the others with confidence as an explanation of the invariant Eu anomaly. Indeed, more than one factor may have been involved. Further interpretation of the REE data should be possible as more information on the mineralogy is obtained. One aspect of the REE geochemistry, however, has already received mineralogic corroboration. Pegmatite sample 17 (fig. 4) has a distinctly higher Ce/La ratio than that of any of the other stock or vein-dike samples. This deviation is not as well constrained as it might have been if Pr abundances had been determined, but the high Ce/La ratio of sample 17 does suggest a positive Ce anomaly. Of all the REE, Ce is the only element that can show significant stability in the tetravalent state, and this can result in anomalous Ce abundances relative to those of neighboring (trivalent) REE. Typically, Ce anomalies are encountered in samples from oxygenated weathering or sedimentary environments (Goldberg, 1961). However, late-stage activity in igneous rocks can also show Ce anomalies (Goldschmidt, 1958). This appears to be the case for sample 17, inasmuch as we have identified cerianite (natural  $Ce^{4+}O_2$ ) by scanning electron microscope and electron microprobe analyses as a coating in vugs in this rock. Cerianite has not been found in any of the other samples. We interpret the cerianite as being deposited during the late stages of the REE mineralizing event.

## SUMMARY AND CONCLUSIONS

In summary, 14 samples were selected for analysis, on the basis of their low radioactivity, from a geochemical transect that extends from the border granites of the Jurassic Bokan Mountain stock southeast along the Dotson and Geoduck vein dikes that are associated with the stock and into surrounding country rock. Some of the samples show potential ore-level concentrations of REE, Y, Zr, Hf, and Nb.

The three country rock samples that were analyzed were meta-igneous rocks. Their chondrite-normalized REE abundance patterns were found to lack Eu anomalies. The lack of Eu anomalies is consistent with the primitive, mantle-derived nature of many of the rocks in the Alexander terrane.

Most of the samples from the stock and the vein dikes were found to be unusually enriched in HREE. The LREE-enriched nature of a distal aplite sample from the Dotson vein dike suggests that the HREE enrichment that is characteristic of these rocks may diminish away from the stock. This diminished HREE enrichment is presumed to be due to changes in mineral proportions. There is also a tendency for vein dikes proximal to the stock to be alkali feldspar pegmatites, whereas distal vein dikes are quartz albite granites and aplites. The REE patterns of the stock and vein-dike samples appear to be dominated by only a few REE-bearing minerals. These include bastnaesite and monazite, along with as yet unidentified Y-rich and Zr-rich minerals. The mineral cerianite was found in one sample and appears responsible for the higher whole-rock Ce/La ratio of this sample.

The stock and vein-dike samples all show similar large negative Eu anomalies. The Eu anomalies indicate that the Jurassic igneous rocks were the source of the REE in all of the stock and vein-dike samples. Inasmuch as the mantle source material that was likely parental to the Jurassic granites is unlikely to have had anomalous Eu, the Eu anomaly is presumed to have formed by feldspar fractionation during the differentiation event that produced the granite. The invariance of the Eu anomaly in the stock and vein-dike samples might indicate that these rocks all formed at the same paragenetic stage. This would be consistent with a previously proposed petrologic model for the genesis of these rocks. Other possibilities, however, are that the Eu anomaly stopped developing at some stage in the evolution of these rocks either because all the Eu became trivalent or because feldspar was no longer an important mineral in the fractionation of the REE. Additional mineralogic studies are required in order to check these other possible explanations.

*Acknowledgments.*—We thank Jim Barker of Interior Development, Fairbanks, Alaska, and R. "Red" Dotson, resident on the claim at the time of our visit. Their local

knowledge and assistance with the logistics were of inestimable help in the collection of samples and in the appreciation of the geological context. We also thank Gary McWilliams, Captain of the research vessel *HYAK*, for providing efficient and cost-effective transportation; and Holly Hughes for board. Finally we thank our colleagues Michael Doughten, David Fey, and Paul Briggs for providing high-quality chemical analyses.

## REFERENCES CITED

- Armstrong, R.L., 1985, Rb-Sr dating of the Bokan Mountain granite complex and its country rocks: *Canadian Journal of Earth Sciences*, v. 22, p. 1233-1236.
- Baedecker, P.A., ed., 1987, *Methods for geochemical analysis: U.S. Geological Survey Bulletin 1770*, 151 p.
- Barker, J.C., and Mardock, C.L., 1988, Lithophile metal, REE-Y-Nb deposits on southern Prince of Wales Island, Alaska, in Carson, D.J.T., and Vassiliou, A.H., eds., *Process mineralogy VIII: The Minerals, Metals, and Materials Society*, p. 139-157.
- Collot, B., 1981, *Le granite albitique hypercalin de Bokan Mountain (S.E. Alaska) et ses mineralizations U-Th. Sa place dans la cordilliere canadienne*: Montpellier, France, Montpellier II University, PhD dissertation, 238 p.
- Gehrels, G.E., 1992, *Geologic map of the southern Prince of Wales Island, southeastern Alaska*: U.S. Geological Survey Miscellaneous Investigations Map I-2169, scale 1:63,360.
- Goldberg, E.D., 1961, Chemistry in the oceans, in Sears, M., ed., *Oceanography*: Washington, D.C., American Association for the Advancement of Science, Publication No. 67, p. 583-597.
- Goldschmidt, V.M., 1958, *Geochemistry*: Oxford, England, Clarendon Press, 730 p.
- MacKevett, E.M., Jr., 1963, *Geology and ore deposits of the Bokan Mountain uranium-thorium area, southeastern Alaska*: U.S. Geological Survey Bulletin 1154, 125 p.
- Philpotts, J. A., 1970, Redox estimation from a calculation of  $\text{Eu}^{2+}$  and  $\text{Eu}^{3+}$  concentrations in natural phases: *Earth and Planetary Science Letters*, v. 9, no. 3, p. 257-268.
- Philpotts, J. A., and Schnetzler, C. C., 1968a, Genesis of continental diabbases and oceanic tholeiites considered in light of rare-earth and barium abundances and partition coefficients, in Ahrens, L. H., ed., *Origin and distribution of the elements*: Oxford, England, Pergamon Press, p. 939-947.
- 1968b, Europium anomalies and the genesis of basalts: *Chemical Geology*, v. 3, p. 5-13.
- 1969, Europium anomalies and the genesis of basalt: a reply: *Chemical Geology*, v. 4, p. 461-465.
- Philpotts, J. A., Schnetzler, C. C., and Hart, S. R., 1969, Submarine basalts: Some K, Rb, Sr, Ba, and rare-earth data bearing on their alteration, modification by plagioclase and possible source materials: *Earth and Planetary Science Letters*, v. 7, p. 293-296.
- Philpotts, J. A., Tatsumoto, M., Li, X., and Wang, K., 1991, Some Nd and Sr isotopic systematics for the rare earth deposit at Bayan Obo, China: *Chemical Geology*, v. 90, p. 177-188.
- Roppel, Patricia, 1991, *Fortunes from the Earth: an history of the base and industrial minerals of southeast Alaska*: Manhattan, Kans., Sunflower University Press, 139 p.
- Samson, S.D., McClelland, W.C., Patchett, P.J., Gebrels, G.E., and Anderson, R.G., 1989, Evidence from neodymium isotopes for mantle contributions to Phanerozoic crustal genesis in the Canadian Cordillera: *Nature*, v. 337, p. 705-709.
- Staat, M.H., 1978, I and L uranium and thorium vein system, Bokan Mountain, southeastern Alaska: *Economic Geology*, v. 73, p. 512-523.
- Thompson, T.B., 1988, *Geology and uranium-thorium mineral deposits of the Bokan Mountain Granite Complex, southeastern Alaska*: *Ore Geology Reviews*, v. 3, p. 193-210.
- Thompson, T.B., Pierson, J.R., and Lytle, T., 1982, Petrology and petrogenesis of the Bokan Granite Complex, southeastern Alaska: *Geological Society of America Bulletin*, v. 93, p. 898-908.
- Warner, J.D., and Barker, J.C., 1989, Columbian- and rare earth element-bearing deposits at Bokan Mountain, southeastern Alaska: U.S. Bureau of Mines Open File Report 33-89, 196 p.
- Warner, J.D., and Mardock, C.L., 1987, Rare earth element-, niobium-, thorium-, and uranium-bearing dikes at Bokan Mountain, southeast Alaska [abs.]: *Geological Society of America Abstracts with Programs*, v. 19, no. 6, p. 461.

Reviewers: Bruce R. Doe and Jeffrey N. Grossman

# Gravity Models of the Siniktanneyak Mafic-Ultramafic Complex, Western Brooks Range, Alaska: Evidence for Thrust Emplacement of Brooks Range Ophiolites

By Robert L. Morin and Thomas E. Moore

## ABSTRACT

Mafic-ultramafic complexes, including ophiolites, in the western Brooks Range are associated with unmetamorphosed late Paleozoic and early Mesozoic passive-margin strata that were imbricated in the Jurassic and Early Cretaceous. Many workers have hypothesized that the ophiolites were emplaced during the deformation as once-extensive thrust sheets whose erosional remnants now form klippen at high structural levels in the Brooks Range. However, gravity data indicating that at least one complex is as thick as 11 km have led some workers to dispute this hypothesis.

This paper provides detailed gravity data coverage for the Siniktanneyak mafic-ultramafic complex in the western Brooks Range in an attempt to determine the thickness of the ophiolite exposed there. Two gravity models have been constructed using constraints based on published and unpublished geologic mapping and with densities based on laboratory measurements of hand samples collected from outcrop. These models show that the Siniktanneyak Mountain ophiolite has a maximum crustal thickness of about 3.0 km. The great lateral extent of the body, as much as 35 km, in comparison to its thickness indicates that the ophiolite is a sheetlike body. The shape of the Siniktanneyak Mountain ophiolite is consistent with the hypothesis of thrust emplacement for at least some of the Brooks Range ophiolites.

## INTRODUCTION

The Brooks Range in northern Alaska is a Mesozoic and Cenozoic north-vergent fold and thrust belt that contains a series of mafic-ultramafic complexes that extend discontinuously for 200 km along the crest of the orogen (fig. 1). The mafic-ultramafic complexes are associated with deformed but unmetamorphosed late Paleozoic and early Mesozoic passive-margin strata that were imbricated in the Jurassic and Early Cretaceous. The mafic-ultramafic

complexes have an exposed thickness of up to 5 km and have been divided into structurally lower assemblages that consist of oceanic volcanic rocks and associated sedimentary rocks and structurally higher assemblages that consist of ophiolite (Mull, 1982). The Brooks Range ophiolites are mostly incomplete and consist largely of the lower, intrusive parts of the standard ophiolitic succession described by Coleman (1977). The structurally lower assemblage of volcanic rocks is distinguished from sparse extrusive rocks of the ophiolitic assemblage by age and geochemical differences (Moore and others, 1994).

Most workers have interpreted the mafic-ultramafic complexes as fragments of ocean crust that were emplaced by thrusting onto the more distal parts of the passive margin of North America in a south-dipping (using present coordinates) subduction zone (for example, Roeder and Mull, 1978; Box, 1985; Mayfield and others, 1988; Moore and others, 1994). These workers have interpreted the mafic-ultramafic complexes as klippen that are the synformal erosional remnants of extensive allochthons of oceanic volcanic and ophiolitic rocks that were emplaced from the south. The upper, ophiolitic, parts of the klippen of mafic-ultramafic complexes (collectively called the Misheguk Mountain allochthon) are thought to represent allochthonous suprasubduction-zone oceanic crust, whereas the lower volcanic parts (collectively called the Copter Peak allochthon) are interpreted to be fragments of upper oceanic crust that were accreted and assembled in a subduction zone beneath the ophiolitic assemblage. Both assemblages were later obducted together onto the passive margin of North America during underthrusting of North America beneath the oceanic arc.

Although general geologic map patterns and other data support this model (see Moore and others, 1994), geologic relations of many of the mafic-ultramafic complexes are not known in detail and some workers have presented data that argue against an allochthonous origin. Karl (1992) reported that geochemical data and steep contacts indicate that part of the informally named Maiyumerak Mountains mafic-ultramafic complex (fig. 1) is not far traveled and instead formed in a late Paleozoic rift

basin within the passive-margin succession. Preliminary analysis of the gravity anomaly associated with the informally named Asik Mountain mafic-ultramafic complex (fig. 1) indicated that the gabbro producing the anomaly is about 8 km thick (Barnes and TAILLEUR, 1970), and more recent 2 1/2 dimensional gravity modeling suggests that the Asik body may be on the order of 11 km in thickness (Morin, 1993). Thicknesses of this magnitude, if representative of all of the mafic-ultramafic complexes of the Brooks Range, are probably inconsistent with the thin-skinned, allochthonous origin proposed for the bodies. Considering observations such as these, Warren Hamilton (written communication to D. Barnes, 1987) suggested that the mafic-ultramafic complexes of the Brooks Range are instead the erosional remnants of arc volcanoes that intruded the underlying passive-margin strata prior to deformation and were later imbricated and thrust northward with the passive-margin strata in the Early Cretaceous. This model would explain the apparent deep crustal root of the Asik Mountain mafic-ultramafic complex and the presence of thrust faults bounding many of the complexes,

but it would not require the large amounts of shortening needed for obduction of oceanic rocks onto continental rocks.

The purpose of this paper is to model the gravity anomaly associated with the Siniktanneyak mafic-ultramafic complex, which is located at the eastern end of the area of exposure of the mafic-ultramafic complexes in the western Brooks Range (fig. 1). The Siniktanneyak complex includes both lower volcanic and upper ophiolitic parts and is apparently typical of the other Brooks Range mafic-ultramafic complexes in most respects. A moderately detailed geologic map (Nelson and Nelson, 1982) provides geologic control for this body. The large gravity anomaly associated with the Siniktanneyak mafic-ultramafic complex indicates that a large body of mafic rocks is present at depth there. Gravity modeling of the anomaly is undertaken to determine the thickness and shape of the mafic and ultramafic rocks of this complex. We postulate that the thickness and shape of the complex are indicative of their mechanism of emplacement: a thin, sheetlike configuration for the body would provide evidence of an

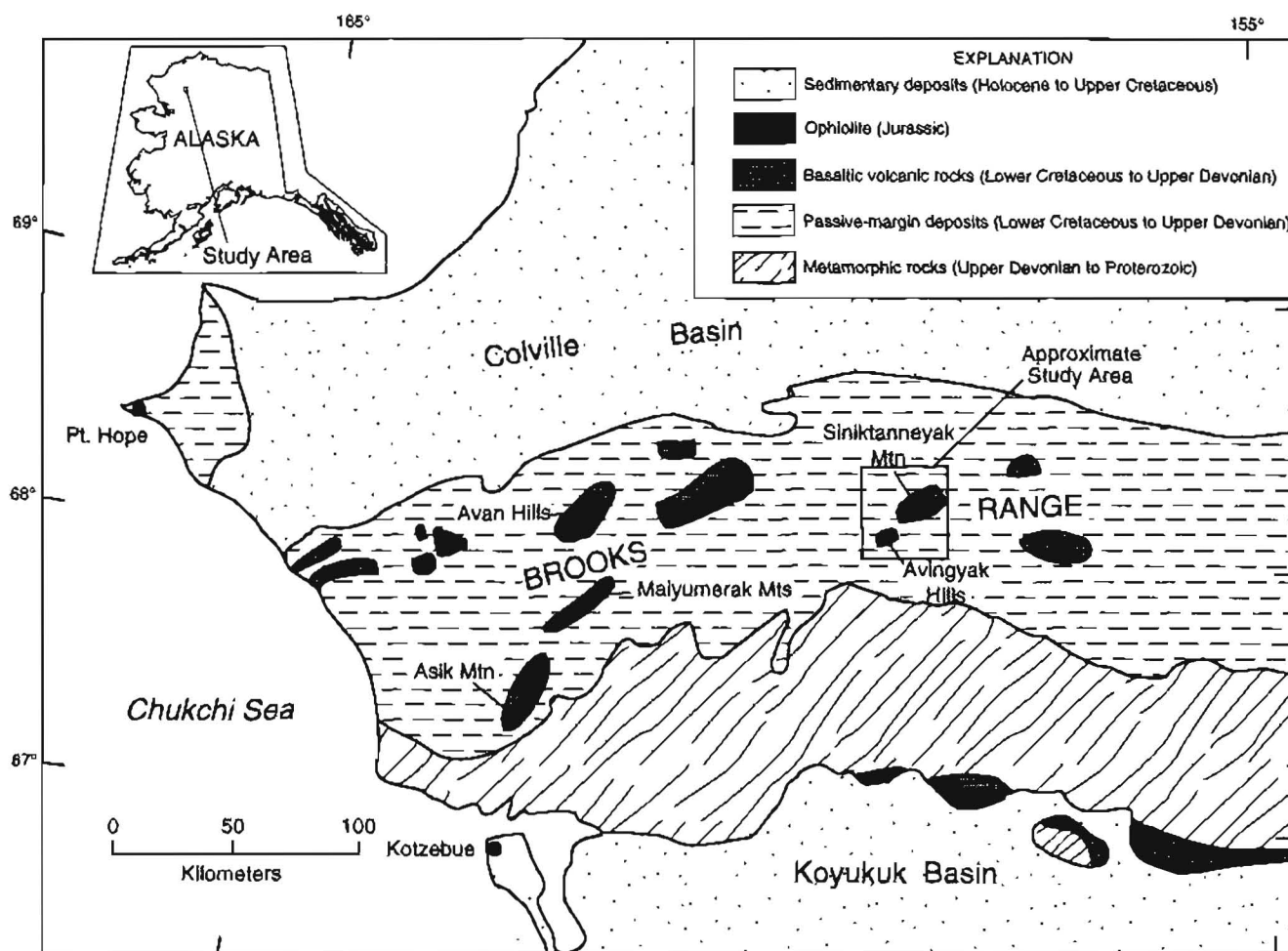


Figure 1. Map showing locations of mafic-ultramafic complexes in the western Brooks Range.



allochthonous origin, whereas a thick, deeply rooted configuration would be consistent with an intrusive origin.

## LOCAL GEOLOGY

The informally named Siniktanneyak mafic-ultramafic complex is located in the southwestern part of the Howard Pass 1:250,000 quadrangle in northern Alaska at about lat 68°20' N. and long 158°25' W. (fig. 1). Mafic and ultramafic rocks are well exposed over a 300-km<sup>2</sup> area in this region, which includes Siniktanneyak Mountain and a prominent but unnamed mountain located about 7 km to the northeast of Siniktanneyak Mountain (fig. 2). Although the Siniktanneyak mafic-ultramafic complex is bounded on the south by Quaternary sedimentary deposits, mafic and ultramafic rocks are reported in the Avingyak Hills, about 20 km to the southwest (fig. 2). The Avingyak Hills exposures may indicate that mafic and ultramafic rocks extend continuously in the subsurface from Siniktanneyak Mountain to the Avingyak Hills, making the complex as much as 35 km long in long dimension.

Geologic mapping by Nelson and Nelson (1982) of the Siniktanneyak Mountain area shows that intrusive rocks are exposed in the central part of the mafic-ultramafic complex and are surrounded by an outer zone of pillow basalt (fig. 2). The intrusive rocks comprise the lower part of an ophiolite, which they referred to as the Siniktanneyak Mountain ophiolite. Sheeted dikes, mafic volcanic rocks, and tuffaceous rocks that comprise the upper part of an ophiolite were reported from the western part of the Siniktanneyak mafic-ultramafic complex (Bickerstaff and others, 1993) but were not mapped by Nelson and Nelson (1982) and are not shown on figure 2. As mapped, the ophiolite consist of two principal units: (1) layered, medium- to coarse-grained olivine-pyroxene gabbro with cumulate textures (unit Jcg on fig. 2); and (2) medium-grained ultramafic rocks that consist of dunite with lesser amounts of wehrlite, harzburgite, pyroxenite, and chromitite (unit Jum on fig. 2). The ultramafic rocks are locally partly serpentinized but contain generally less than about 10 percent serpentine minerals. Horneblende-pyroxene gabbro with isotropic textures (unit Jhg on fig. 2) and sparse plagiogranite (included in unit Jp on fig. 2) are exposed in the northern part of the ophiolite. A U-Pb zircon age of  $170 \pm 3$  Ma has been obtained from plagiogranite in this area and indicates that the ophiolite crystallized in the Middle Jurassic (Moore and others, 1993). The pillow basalt unit (unit Dpb on fig. 2) consists of fault slices of basalt, diabase, mafic tuffs, and breccia with low-grade metamorphic assemblages. Thin units of limestone, locally with Devonian fossils, and radiolarian chert are structurally interleaved with the pillow basalts. The contacts of the pillow basalt

unit against the ophiolitic lithologies are moderate-dipping faults that place the ophiolitic rocks on top of the pillow basalt (Nelson and Nelson, 1982).

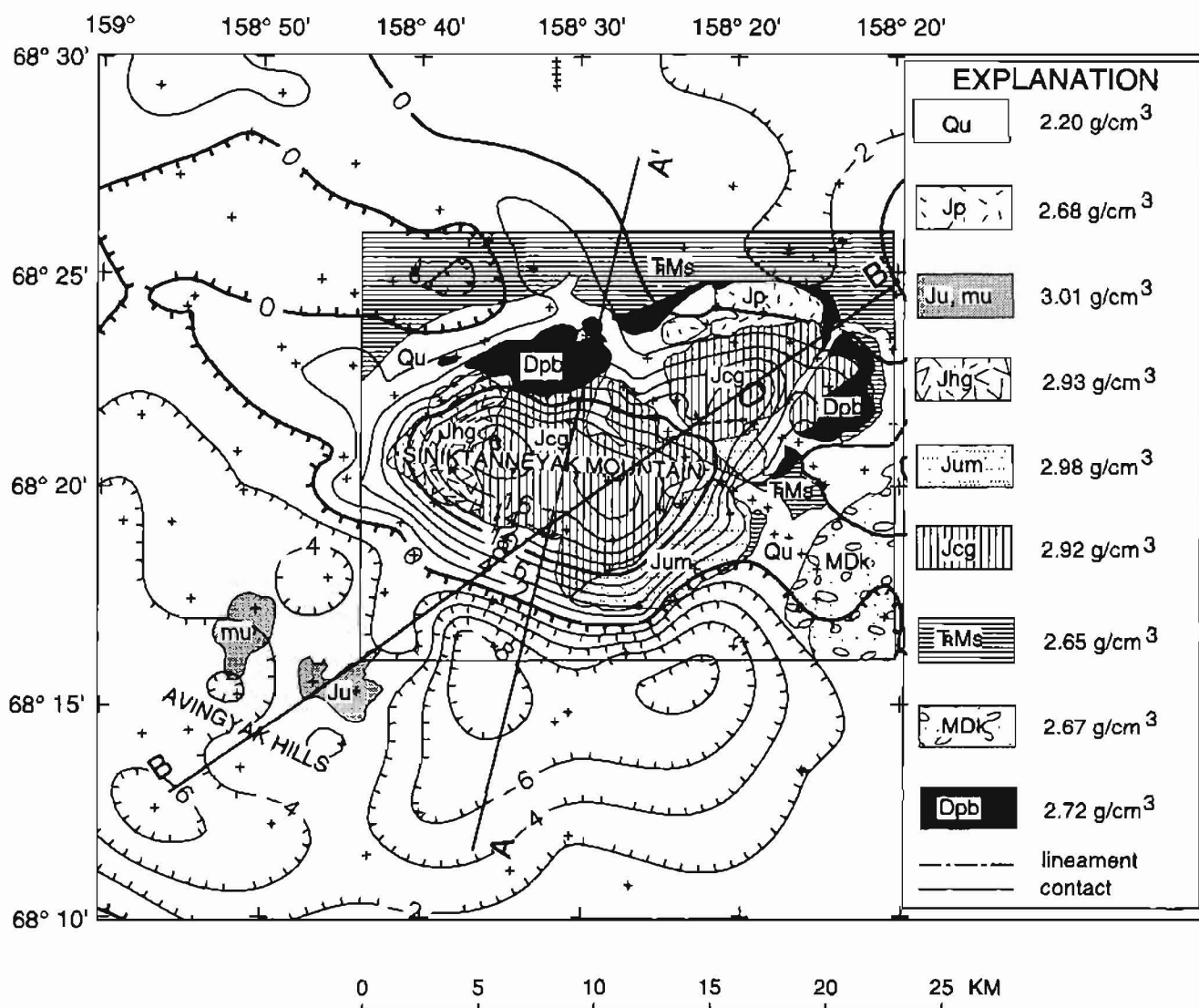
The country rocks of the Siniktanneyak mafic-ultramafic complex are Devonian to Triassic sedimentary rocks of continental origin. East of the complex, the sedimentary succession consists of Upper Devonian and Mississippian deltaic, quartz-rich clastic rocks of the Hunt Fork Shale, Noatak Sandstone, Kanayut Conglomerate, and Kayak Shale (Endicott Group); Mississippian and Pennsylvanian black marine shale and chert of the Kuna Formation (Lisburne Group); and Permian and Triassic marine siliceous shale, chert, and silicified limestone of the Etivluk Group. This sequence comprises the Endicott Mountains allochthon succession of Mull (1982). Nelson and Nelson (1982) simplified this stratigraphy by mapping a lower sandstone unit that consists predominantly of the Upper Devonian and Lower Mississippian? rocks of the Kanayut Conglomerate (unit MDk on fig. 2) and an upper unit that consists of the marine shale, siliceous shale, and chert that comprise the Kayak Shale, Kuna Formation, and Etivluk Group (unit TMs on fig. 2). Although both units of Nelson and Nelson (1982) have undergone contractional deformation, they have generally retained their relative stratigraphic positions and display the effects of the deformation mainly through internal thickening. The Kanayut Conglomerate in this area has an original stratigraphic thickness of less than 500 m but, because of contractional deformation, has a structural thickness of several kilometers. Likewise, the overlying shale- and chert-rich units have a probable cumulative stratigraphic thickness of about 200 m but a structural thickness of almost 500 m. The region bordering the mafic-ultramafic complex on the north and west was not mapped in detail by Nelson and Nelson (1982) but is portrayed on the smaller scale map of Mayfield and others (1988). The latter map shows that a thrust sheet (Ipnayik River allochthon), composed principally of sedimentary rocks like those of unit TMs but with a 100-m-thick unit of thin-bedded limestone and diabase assigned to the Lisburne Group, is exposed in this area. Because this thrust sheet is lithologically similar to and is inferred to rest on rocks of units TMs at depth (Mayfield and others, 1988), we have included it in unit TMs for the purpose of this study. Elsewhere, Quaternary deposits obscure the country rocks.

Along the eastern margin of the complex where the contacts are best exposed, the fine-grained upper part of the sedimentary succession is overlain by the volcanic rocks of the Siniktanneyak mafic-ultramafic complex on moderately dipping faults. The stratigraphy and bedding attitudes of sedimentary rocks bordering the eastern margin of the complex indicate that these rocks dip west beneath the mafic-ultramafic complex (Gil Mull, Alaska Division of Geological and Geophysical Surveys, oral

commun., 1994). Although the structural relations of the mafic-ultramafic complex with the adjacent sedimentary units are not known along other margins of the complex, the observed relations suggest that the Siniktanneyak mafic-ultramafic complex is a rootless body that is underlain at depth by sedimentary rocks like those bordering the complex. Nelson and Nelson (1982) estimated that the Siniktanneyak Mountain ophiolite is over 1 km thick and depicted a thickness of 1 km or less for the volcanic lower part of the complex.

## GEOPHYSICAL COVERAGE AND METHODS

Gravity coverage in the Siniktanneyak Mountain area consists of several data sets collected over a number of years. Data were collected at 12 stations in the Siniktanneyak Mountain region in 1961, 1965, and 1981 along fixed-winged aircraft and helicopter traverses. Measurements were made at an additional 18 stations in 1976 as



**Figure 2.** Isostatic gravity map of Siniktanneyak Mountain. Contour interval is 2 mGal. Lithologic units: Qu, Quaternary surficial deposits, undivided; Jp, Jurassic plutonic rocks; Ju, Jurassic ultramafic rocks of Avingyak Hills; mu, mafic and ultramafic rocks of Avingyak Hills, undifferentiated; Jhg, Jurassic hornblende-pyroxene gabbro; Jum, Jurassic ultramafic rocks; Jcg, Jurassic cumulus gabbro; TMs, Mississippian to Triassic sedimentary rocks, undivided; MDk, Devonian and Mississippian(?) rocks of Kanayut Conglomerate; Dpb, Devonian pillow basalt. Geology from Nelson and Nelson (1982), J. Schmidt (written commun., 1991), and I.L. Tailleux (written commun., 1992). +, gravity station.



part of the National Petroleum Reserve in Alaska (NPRA) seismic and gravity program. The Alaska Division of Geological and Geophysical Surveys (ADGGS) collected data at 82 stations in 1976 and 1979 as part of a study of Siniktanneyak Mountain (Steve Hackett, ADGGS, written commun., 1980). These data were processed by the senior author and were used as a guide for locating 73 additional stations in 1992.

The gravity data were reduced at a density of  $2.67 \text{ g/cm}^3$ , which is average crustal density, with corrections made for terrain and isostatic compensation. The data were then gridded by computer with a spacing of 0.1 km. An additional grid was made that represents the nonlinear regional gravity gradient in this area. This grid was subtracted from the original grid, leaving a grid that isolated the anomaly associated with Siniktanneyak Mountain. Gravity values were extracted from this grid along the profiles shown in figures 2 and 3. The regional gravity gradient was adjusted slightly along individual profiles during the modeling procedure. Topographic profiles were extracted from a 0.1-km grid of the topography. This grid was produced from a geographic grid of elevations averaged over 1/4-minute compartments. These profiles are used to show the topographic surface in the gravity models.

The geologic map of Nelson and Nelson (1982) with modified unit ages (Moore and others, 1993) was used for primary geologic control in the study area (figs. 2, 3). Mapping by I.L. Tailleux, (USGS, written commun., 1992) provided coverage of a small outcrop of ultramafic rocks in the Avingyak Hills. The regional geology beyond the extent of Nelson and Nelson (1982) was taken from a geologic map by Schmidt and others (J. Schmidt, USGS, written commun., 1991) and the regional map of Mayfield and others (1988).

Gravity modeling requires good gravity coverage, good control of the specific gravities of the geologic units that are modeled, and geologic surface control, all of which are now available in the Siniktanneyak Mountain area. The modeling program (Saltus and Blakely, 1993) calculates an anomaly based on the volume and shape of the geologic units and the density of those units. This anomaly is then compared to the observed anomaly, which is extracted from the gravity data. Modifications are then made to the volume of the geologic units by changing their dimensions until the calculated anomaly matches the observed anomaly (figs. 4, 5).

To obtain densities of the various units, samples were collected throughout the study area. A suite of 82 surface rock samples was collected by S. Hackett, S. Nelson, W. Nelson, and the senior author. Locations of samples other than the authors were provided by S. Hackett (S. Hackett, ADGGS, written commun., 1980). Rock sample sites were grouped according to geologic map units. Samples that fell close to unit contacts or samples that had densities that were very different from the average densities within

a given map unit were not used. Of the 85 samples collected, 64 were used to calculate the density values of the mapped units (table 1). Some of the model densities differ slightly from the calculated mean. They were modified to meet the constraints of the mapped geology and the observed gravity. The largest change was to unit Dpb, a pillow basalt, which was lowered from  $2.76 \text{ g/cm}^3$  to  $2.72 \text{ g/cm}^3$ . Because this unit contains many types of rock besides basalt and displayed a large range in densities (standard deviation  $0.135 \text{ g/cm}^3$ ), the model density is well within the range of the measured densities. Quaternary deposits were not collected for density measurements; an assumed density of  $2.20 \text{ g/cm}^3$  was used for this unit.

An isostatic gravity map with a 2-mGal contour interval plotted over the geology of Nelson and Nelson (1982) (fig. 2) shows the locations of the gravity profiles and gravity stations used to produce the map. The gabbros and ultramafic rocks of the Siniktanneyak Mountain ophiolite are associated with high-amplitude positive gravity anomalies (fig. 2). The largest anomaly, which is centered over cumulate gabbros and ultramafic rocks on Siniktanneyak Mountain, is an oval-shaped anomaly that trends approximately N.  $75^\circ$  W. This anomaly is about 17 km long and 14 km wide and has an amplitude of about 20 mGal. A smaller positive anomaly, located over cumulate gabbros that form the unnamed mountain to the northeast of Siniktanneyak Mountain, is almost triangular in shape with sides about 7 km long, but it is masked somewhat by the larger anomaly. The amplitude of this smaller anomaly is about 10 mGal. A small, circular +4-mGal anomaly, located just east of the 10-mGal anomaly, is probably associated with the volcanic rocks of the lower part of the mafic-ultramafic complex but was not investigated further for this study. Although mafic and ultramafic rocks are also present in the Avingyak Hills, only a broad, shallow anomaly with an amplitude of 2 mGal is present there. A large-dimensioned negative anomaly located to the south of Siniktanneyak Mountain can also be seen in figure 2. This anomaly, which is associated with alluvial deposits, is rectangular in shape, trends east-west, and is about 20 km long and 10 km wide with an amplitude of about 5 mGal.

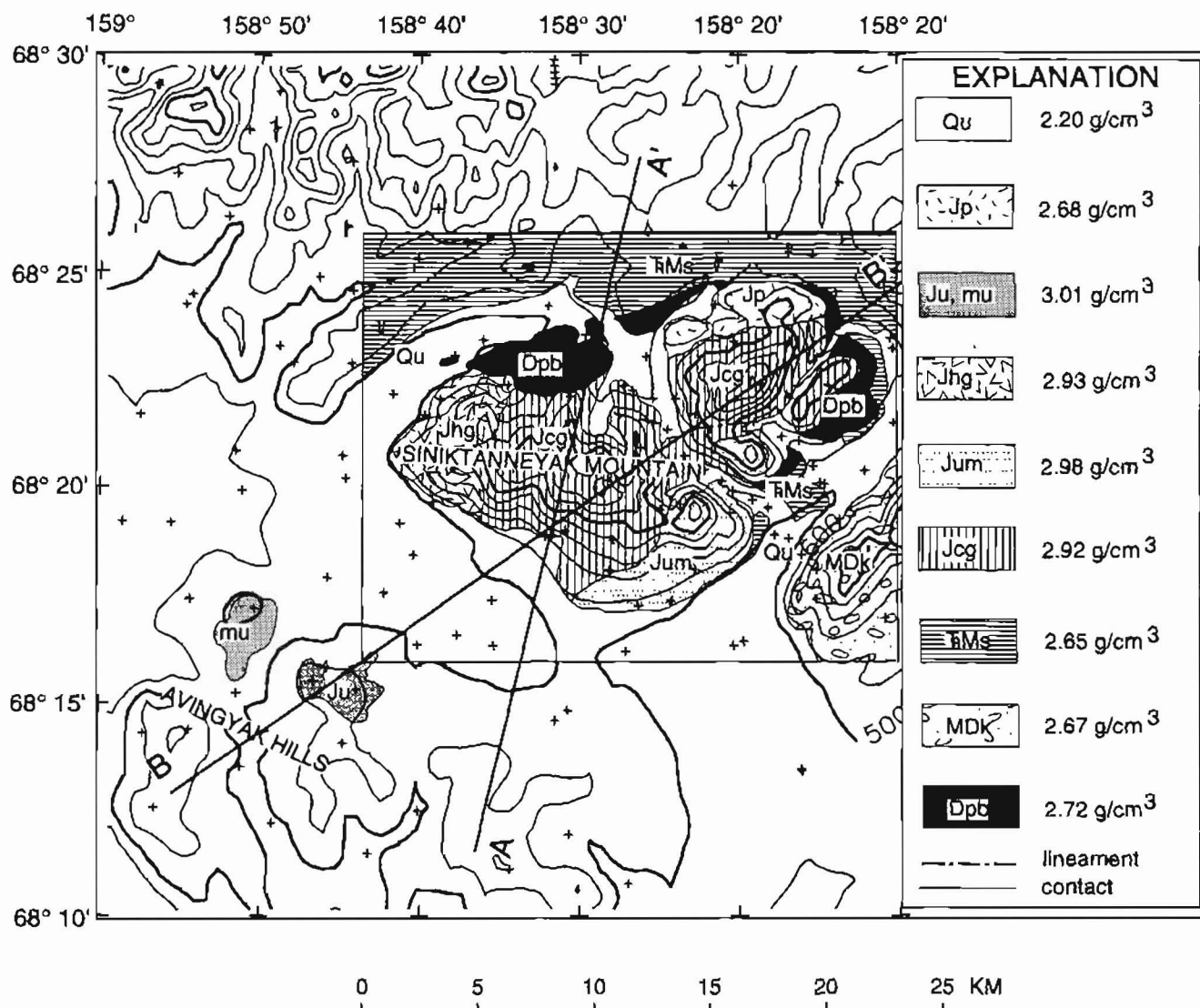
A topographic map with a 100-m contour interval was also plotted over the geology of Nelson and Nelson (1982) (fig. 3). This map shows that alluvium has filled in around most of Siniktanneyak Mountain and may be obscuring part of the mafic-ultramafic complex. A steep gravity gradient (fig. 2) extends several kilometers to the south and southwest of the mafic-ultramafic complex and indicates that part of the complex is buried there.

Because of the high density of the ophiolitic rocks of the Siniktanneyak mafic-ultramafic complex, modeling cannot determine the thickness of the volcanic unit (unit Dpb) that may underlie the ophiolitic upper part of the

complex. In addition, the densities of the volcanic rocks are so close to those of the clastic units east of the complex (unit MDk) that a very large range in the thickness of the volcanic rocks could be modeled. For these reasons, the shape and thickness of the volcanic lower part of the Siniktanneyak mafic-ultramafic complex were not modeled, and this unit was instead included with unit MDk, except where exposed at the surface.

Two gravity profiles were modeled (figs. 4, 5) to interpret the subsurface structure of the Siniktanneyak

mafic-ultramafic complex. Profile A-A' is perpendicular to the gravity contours of the largest gravity anomaly. This profile is designed to yield the most accurate interpretation of the depth of the causative body. Profile B-B' was located to investigate the relation between the largest anomaly associated with the Siniktanneyak mafic-ultramafic complex and the smaller anomaly located to the northeast of Siniktanneyak Mountain. Both models are 2 1/2 dimensional, with the distance in and out of the model estimated from the geologic map of Nelson and Nelson (1982).



**Figure 3.** Topographic map of Siniktanneyak Mountain. Contour interval is 100 m. Lithologic units: Qu, Quaternary surficial deposits, undivided; Jp, Jurassic plutonic rocks; Ju, Jurassic ultramafic rocks of Avingyak Hills; mu, mafic and ultramafic rocks of Avingyak Hills, undifferentiated; Jhg, Jurassic hornblende-pyroxene gabbro; Jum, Jurassic ultramafic rocks; Jcg, Jurassic cumulus gabbro; TMs, Mississippian to Triassic sedimentary rocks, undivided; MDk, Devonian and Mississippian(?) rocks of Kanayut Conglomerate; Dpb, Devonian pillow basalt. Geology from Nelson and Nelson (1982), I. Schmidt (written commun., 1991), and I.L. Tailleux (written commun., 1992). +, gravity station.

### PROFILE A-A'

The gravity model (fig. 4) along profile A-A' (figs. 2, 3) is a nearly north-south profile that begins to the south of Siniktanneyak Mountain on alluvial and sedimentary deposits and continues over the Siniktanneyak mafic-ultramafic complex to sedimentary deposits to the north. A regional linear gradient of 0.20 mGal/km, in addition to the nonlinear gradient previously removed, was removed from the observed profile. Modeling suggests that the gravity low on the southern end of profile A-A' (fig. 2) is caused by Quaternary sedimentary deposits that may be as thick as 0.5 km assuming a density of 2.20 g/cm<sup>3</sup>. The cumulus gabbro unit (unit Jcg) appears to be flat lying and may be as thick as 2.5 km. The cumulus gabbro continues under alluvium south of the surface exposures of the unit at about a 10° dip for about 4.0 km.

The cumulus gabbro may extend beneath alluvium for an additional 5 km, but this extension of cumulus gabbro could be no more than 0.5 km in thickness. To the north, the steep gradient between the cumulus gabbro unit and the pillow basalt unit (Dpb) (fig. 2) suggests that the contact between these two units is nearly vertical. This contact was interpreted to be a steep thrust fault by Nelson and Nelson (1982). A near-vertical fault was also shown by Nelson and Nelson (1982) between the pillow basalt unit (Dpb) and shale and chert-rich rocks of undivided sedimentary rocks unit (TMs). Modeling suggests that a steep contact is possible there if the unit (TMs) is very thin at the contact and thickens to the north to about 2 km. However, this configuration yields a good match to the observed gravity only if the density of unit MDk is raised to 2.70 g/cm<sup>3</sup>. Another possible solution, shown in figure 4, portrays unit Dpb as a northward-thinning wedge

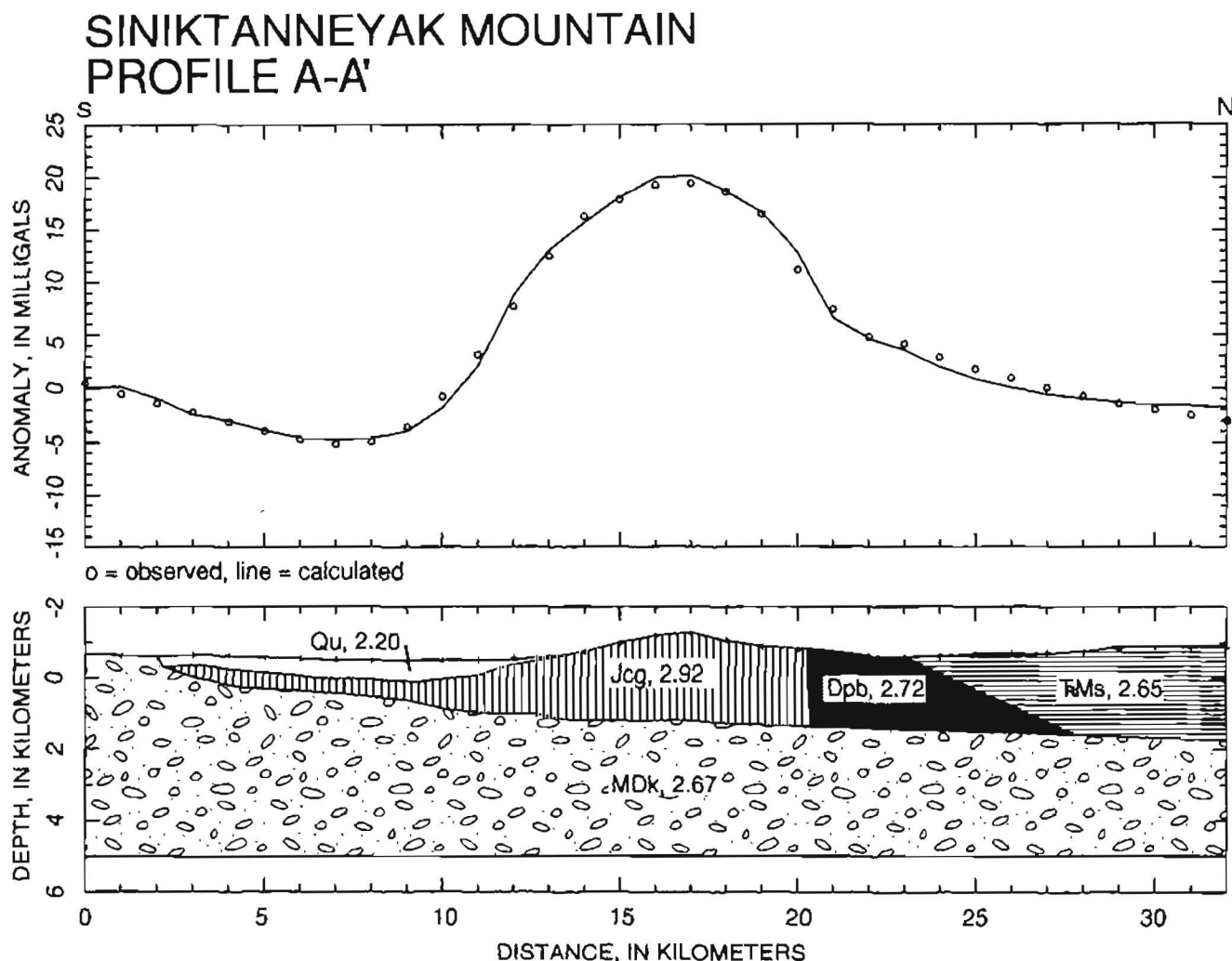


Figure 4. Gravity model of profile A-A'. Surface geology taken from Nelson and Nelson (1982). Gravity-model bodies: 2.20 g/cm<sup>3</sup>, Qu-Quaternary surficial deposits, undivided; 2.92 g/cm<sup>3</sup>, Jcg-Jurassic cumulus gabbro; 2.72 g/cm<sup>3</sup>, Dpb-Devonian pillow basalt; 2.65 g/cm<sup>3</sup>, TMs, Mississippian to Triassic sedimentary rocks, undivided; 2.67 g/cm<sup>3</sup>, MDk-Devonian and Mississippian(?) rocks of Kanayut Conglomerate.

that pinches out in the subsurface beneath a northward-thickening wedge composed of unit TMs. The best fit with the observed gravity is made if the contact between the two units dips to the northwest at about 25° as shown in figure 4. In either case, the modeled thickness of unit TMs is much greater than that expected for the unit. The increased thickness may be explained by the presence of a thrust sheet in this area (Ipsnavik River allochthon) that was included in unit TMs. Gravity coverage is sparse north of the exposures of unit Dpb, however, so additional gravity coverage and geologic mapping will be necessary to further constrain the gravity model in this area.

### PROFILE B-B'

Profile B-B' (fig. 2) cuts across the cumulus gabbro unit and the large anomaly associated with it. It also transects the smaller anomaly (also over cumulus gabbro)

that is located in the mountain northeast of Siniktanneyak Mountain. A regional linear gradient of 0.14 mGal/km, in addition to the nonlinear gradient previously removed, was removed from the observed profile. The model (fig. 5) shows the base of the cumulus gabbro as relatively flat lying and the gabbro as about 2.5 to 3.0 km thick where it is present beneath the largest anomaly. Beneath the unnamed mountain northeast of Siniktanneyak Mountain, cumulus gabbro is modeled as about 1.0 km thick. The change in thickness between the two areas is best modeled as a near-vertical fault that cuts the gabbro. As modeled, the fault has a vertical separation of about 1.5 km with the northeastern side up relative to the southwestern side. Inspection of the geologic map of Nelson and Nelson (1982) shows that the proposed vertical fault that cuts cumulus gabbro on profile B-B' may lie in the linear, northwest-trending valley that separates Siniktanneyak Mountain and the unnamed mountain to the northeast (fig. 3). Alternatively, the fault may correspond to a promi-

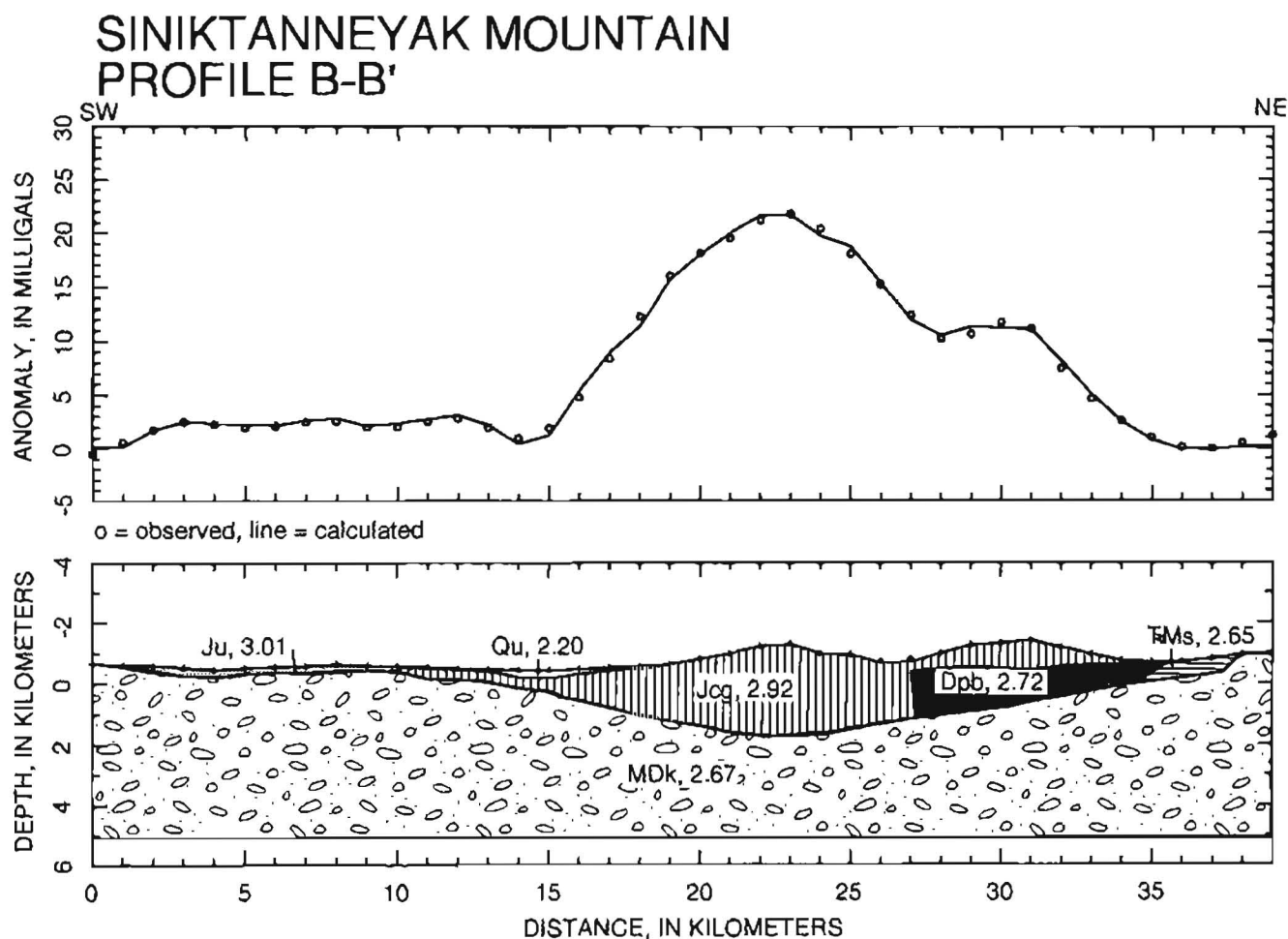


Figure 5. Gravity model of profile B-B'. Surface geology taken from Nelson and Nelson (1982) and I.L. Tailleux (written commun., 1992). Gravity model bodies: 3.01 g/cm<sup>3</sup>, Ju-Jurassic ultramafic rocks from Avinyak Hills; 2.92 g/cm<sup>3</sup>, Jcg-Jurassic cumulus gabbro; 2.72 g/cm<sup>3</sup>, Dpb-Devonian pillow basalt; 2.65 g/cm<sup>3</sup>, TMs-Mississippian to Triassic sedimentary rocks; 2.67 g/cm<sup>3</sup>, MDk-Devonian and Mississippian rocks (?) of Kanayut Conglomerate.

**Table 1.** Average rock densities of samples collected in the vicinity of Siniktanneyak Mountain

Unit	Number of samples	Mean density	Standard deviation	Value used in profile:	
				A	B
Jp	3	2.68	0.061		
Ju	4	3.01	0.114	--	3.01
Jhg	7	2.93	0.054	--	--
Jum	10	2.98	0.050	--	--
Jcg	21	2.91	0.075	2.92	2.92
UMs	6	2.63	0.056	2.65	2.65
MDk	2	2.67	0.007	2.67	2.67
Dpb	11	2.76	0.135	2.72	2.72

nent west-trending lineament that was identified from air photos (Nelson and Nelson, 1982). This lineament also intersects profile *B-B'* at the point where there is the major change in thickness of the cumulus gabbro. Because of the similar densities of units Dpb and MDk, it is not possible to resolve whether the basal contact of the volcanic, lower part of the Siniktanneyak mafic-ultramafic complex is cut by the near-vertical fault, which would constrain the relative age of the fault as either older or younger than the time of emplacement of the mafic-ultramafic complex.

The gravity anomaly associated with Siniktanneyak Mountain extends to the south and southwest of the exposures of cumulus gabbro, indicating that the mafic-ultramafic complex is partly buried beneath alluvial cover in this area (fig. 2). Modeling of the gravity anomaly indicates that the cumulus gabbro extends for at least 5.0 km to the southwest under the alluvium at a dip of about 10° and could continue farther if the gabbro is less than 0.5 km thick.

Exposures of ultramafic rocks located in the Avingyak Hills about 10 km southwest of Siniktanneyak Mountain (figs. 2, 3) are associated with a subdued gravity anomaly. Outcrop samples from this area have an average density of 3.01 g/cm<sup>3</sup> and have been identified as mafic and ultramafic rocks similar to those of the Siniktanneyak Mountain ophiolite (John Cady, USGS, written commun., 1994). The presence of these exposures raises the possibility that the gabbro and ultramafic rocks of the Siniktanneyak mafic-ultramafic complex continue southward uninterrupted beneath the alluvium from Siniktanneyak Mountain to the Avingyak Hills.

This hypothesis is modeled in figure 5. Since ultramafic rocks are exposed in the Avingyak Hills at the southwestern end of the profile (I. Tailleux, written commun., 1992), the Avingyak Hills are shown as being underlain by ultramafic rocks. The small amplitude of the

anomaly associated with the rocks of the Avingyak Hills suggests that the thickness of ultramafic rocks in this area is no more than 0.2–0.3 km. The shape of the anomaly indicates that the ultramafic rocks maintain approximately the same thickness across the Avingyak Hills. The ultramafic rocks are shown in figure 5 as abutting against the cumulate gabbro of Siniktanneyak Mountain at an arbitrary contact about 10 km north of the southern end of the profile. The position of the contact is uncertain because the Avingyak Hills have not been mapped in detail, but the differences in density between gabbro and ultramafic rocks are insufficient to significantly alter the model. The modeling shown in figure 5 indicates that if the Siniktanneyak Mountain ophiolite extends uninterrupted from Siniktanneyak Mountain to the Avingyak Hills, the southernmost 15 km of the body is a thin sheet that has a thickness of less than 0.5 km.

## CONCLUSIONS

Gravity models over the Siniktanneyak mafic-ultramafic complex (figs. 4, 5) show possible solutions of the subsurface geology that satisfy the observed gravity measurements taken on the surface. These models are constrained by the surface geology mapped by Nelson and Nelson (1982) and by densities of rock samples collected on the surface from this complex and the surrounding geologic units. Where profile *A-A'* crosses profile *B-B'*, the modeled thickness of the cumulus gabbro is about the same, indicating good agreement between the two models.

In general, the Siniktanneyak Mountain ophiolite appears to be a flat-bottomed or slightly keel-shaped body that has a maximum thickness of about 3.0 km. The main part of the ophiolite is approximately 20 km across where transected by profile *B-B'*, but it may continue southward into the Avingyak Hills for 15 km as a flat sheet less than 0.5 km thick. Although we are unable to constrain the thickness of the volcanic, lower part of the Siniktanneyak mafic-ultramafic complex, the 3-km-or-less thickness of the ophiolitic upper part of the complex in light of its possible 35-km extent strongly suggests that it is a sheetlike unit. A sheetlike configuration is consistent with models that call for thrust emplacement of the ophiolite in a Jurassic and Early Cretaceous thin-skinned décollement-type orogenic belt (for example, Roeder and Mull, 1978; Mull, 1982; Nelson and Nelson, 1982; Mayfield and others, 1988) but is not consistent with an intrusive origin for the body. The sheetlike configuration for the Siniktanneyak Mountain ophiolite suggests that this body differs greatly in thickness from the 11-km-thick Asik Mountain mafic-ultramafic complex in the western Brooks Range. It is unclear why these mafic-ultramafic complexes differ in shape so significantly. The difference in thickness may have been caused by different



origins for the bodies or by differences in their subsequent tectonic histories. At present, it is uncertain whether the thickness of the Siniktanneyak mafic-ultramafic complex is typical of other Brooks Range ophiolites.

The gravity models help constrain the internal structural characteristics of the Siniktanneyak mafic-ultramafic complex. The modeling agrees with Nelson and Nelson's (1982) interpretation of a near-vertical fault between cumulate gabbro and volcanic rocks north of Siniktanneyak Mountain and suggests the presence of a previously unrecognized near-vertical fault that displaces the cumulate gabbro in the subsurface northeast of Siniktanneyak Mountain. The detailed nature of the margins of the mafic-ultramafic complex is not well constrained by the gravity data, but the data do suggest that rocks of unit TMs have been both overthrust and underthrust along the northern and northeastern margins of the complex. The high-angle faults and conflicting relations may be the result of multiple periods of deformation between the Jurassic and Tertiary. Additional geologic map and gravity data are needed to more accurately delineate the structural configuration and kinematic history along the margins of the mafic-ultramafic complex.

## REFERENCES CITED

- Barnes, D.P. and TAILLEUR, I.L., 1970, Preliminary interpretation of geophysical data from the lower Noatak River basin, Alaska: U.S. Geological Survey Open-File Report, 15 p.
- BICKERSTAFF, DAMON, HARRIS, R.A., and MILLER, M.A., 1993, The crustal section of the Siniktanneyak Mountain ophiolite, Brooks Range, Alaska [abs.]: Geological Society of America Abstracts with Programs, v. 25, no. 5, p. 9.
- Box, S.E., 1985, Early Cretaceous orogenic belt in northwestern Alaska: internal organization, lateral extent, and tectonic interpretation, in Howell, D.G., ed., Tectonostratigraphic terranes of the circum-Pacific region: Houston, Tex., Circum-Pacific Council for Energy and Mineral Resources (American Association of Petroleum Geologists), Earth Science series, no. 1, p. 137-145.
- Coleman, R.G., 1977, Ophiolites: ancient oceanic lithosphere?: New York, Springer-Verlag, 229 p.
- Karl, Susan M., 1992, Arc and extensional basin geochemical and tectonic affinities for Maiyumerak basalts in the western Brooks Range in Bradley, Dwight C., and Ford, Arthur B., eds. Geologic studies in Alaska by the U.S. Geological Survey, 1990: U.S. Geological Survey Bulletin 1999, p. 141-155.
- Mayfield, Charles F., TAILLEUR, IRVIN L., and ELLERSIECK, INYO, 1988, Stratigraphy, structure, and palinspastic synthesis of the western Brooks Range, northwestern Alaska, in Gryc, George, ed., Geology and exploration of the National Petroleum Reserve in Alaska, 1974 to 1982: U.S. Geological Survey Professional Paper 1399, p. 143-186.
- Moore, Thomas E., Aleinikoff, John N., and Walter, Marianne, 1993, Middle Jurassic U-Pb crystallization age for Siniktanneyak Mountain ophiolite, Brooks Range, Alaska [abs.]: Geological Society of America Abstracts with Programs, v. 25, no. 5, p. 124.
- Moore, T.E., WALLACE, W.K., BIRD, K.J., KARL, S.M., MULL, C.G., and DILLON, J.T., 1994, Geology of northern Alaska, in Plafker, George, and Berg, H.C., eds., The geology of Alaska: Boulder, Colo., Geological Society of America, The Geology of North America, v. G-1, p. 49-140.
- Morin, Robert L., 1993, Mafic and ultramafic rocks of the northwestern Brooks Range of Alaska produce nearly symmetric gravity anomalies [abs.]: Geological Society of America Abstracts with Programs, v. 25, no. 5, p. 124.
- Mull, C.G., 1982, The tectonic evolution and structural style of the Brooks Range, Alaska: an illustrated summary, in Powers, R.B., ed., Geologic studies in the Cordilleran thrust belt: Denver, Colo., Rocky Mountain Association of Geologists, v. 1, p. 1-45.
- Nelson, Steven, W. and Nelson, Willis H., 1982, Geology of the Siniktanneyak Mountain ophiolite, Howard Pass quadrangle, Alaska: U.S. Geological Survey Miscellaneous Field Studies Map MF-1441, scale 1:63,360.
- Roeder, Dietrich, and Mull, C.G., 1978, Tectonics of Brooks Range ophiolites, Alaska: American Association of Petroleum Geologists Bulletin, v. 62, p. 1696-1702.
- Saltus, R.W., and Blakely, R.J., 1993, Hypermag, an interactive, 2- and 2 1/2-dimensional gravity and magnetic modeling program: version 3.5: U.S. Geological Survey Open-File Report 93-287, 39 p.

Reviewers: David A. Ponce and Robert C. Jachons

# Elemental and Isotopic Evidence for 2.1-Ga Arc Magmatism in the Kilbuck Terrane, Southwestern Alaska

By Elizabeth Moll-Stalcup, Joseph L. Wooden, Jack Bradshaw, and John Aleinikoff

## ABSTRACT

The Kilbuck terrane is an isolated crustal sliver of Precambrian crust that was accreted to southwestern Alaska by mid-Cretaceous or earlier time. The terrane is composed primarily of tonalite, trondhjemite, and granite gneiss and minor amphibolite, pelitic schist, and marble. Major and trace element data indicate that most of the plutonic rocks formed in an arc environment because the tonalite, trondhjemite, and granite gneisses are enriched in alkali elements and light rare-earth elements (LREE) relative to Nb and Ta. All but one of the amphibolites are chemically distinct from the tonalite suite and from each other, and they do not have compositions typical of arc-related rocks. U-Pb geochronology indicates that most of the plutonic rocks cooled at about 2.1 Ga and were reheated at 1.77 Ga. All of the tonalite gneisses and all but one of the granite gneisses give Nd model ages of about 2.1 Ga, indicating that the suite represents newly generated (or newly recycled) crust formed from mantle. One granite gneiss has a Nd model age of 2.7 Ga but a U-Pb zircon age similar to the other tonalite gneisses, indicating that it is probably part of the same magmatic event but has assimilated sufficient Archean bedrock to alter its Nd isotopic composition.

## INTRODUCTION

Much of southern Alaska and the western Cordillera formed by the accretion of a large number of tectonostratigraphic terranes to the North American continent in Cretaceous time. Most of these accreted terranes are parts of island arcs or oceanic crust that are Mesozoic or Cenozoic in age. Sandwiched between these terranes in southwestern Alaska is a block of Early Proterozoic tonalite gneiss, granite gneiss, and amphibolite and rare pelitic schists and marbles called the Kilbuck terrane (fig. 1). Recent U-Pb ages, Nd model ages, and major and trace element data on the Kilbuck terrane indicate that the terrane contains the oldest rocks in Alaska (Box and others, 1991) and that it represents the roots of a 2.1-Ga continental-margin arc.

Prior to recognition of the terrane concept, metamorphic rocks of the Kilbuck terrane were thought to represent the uplifted basement rocks that underlie this part of Alaska (Hoare and Coonrad, 1961). The Kilbuck terrane is now known to be an isolated crustal sliver, without crustal roots, that is surrounded on all sides by younger accreted oceanic terranes (Hoare and Coonrad, 1979; Box and others, 1991). Turner and others (1983) reported a Precambrian U-Pb zircon age from the Kilbuck terrane. Box and others (1991) published a short preliminary report based on a single zircon age from a small isolated block of the Kilbuck terrane northeast of the main body. In this paper we present additional U-Pb zircon ages, Sr and Nd isotopic data, and major and trace element geochemistry on the main part of the Kilbuck terrane to better constrain the age and composition of this enigmatic terrane and to assess its tectonic affinity.

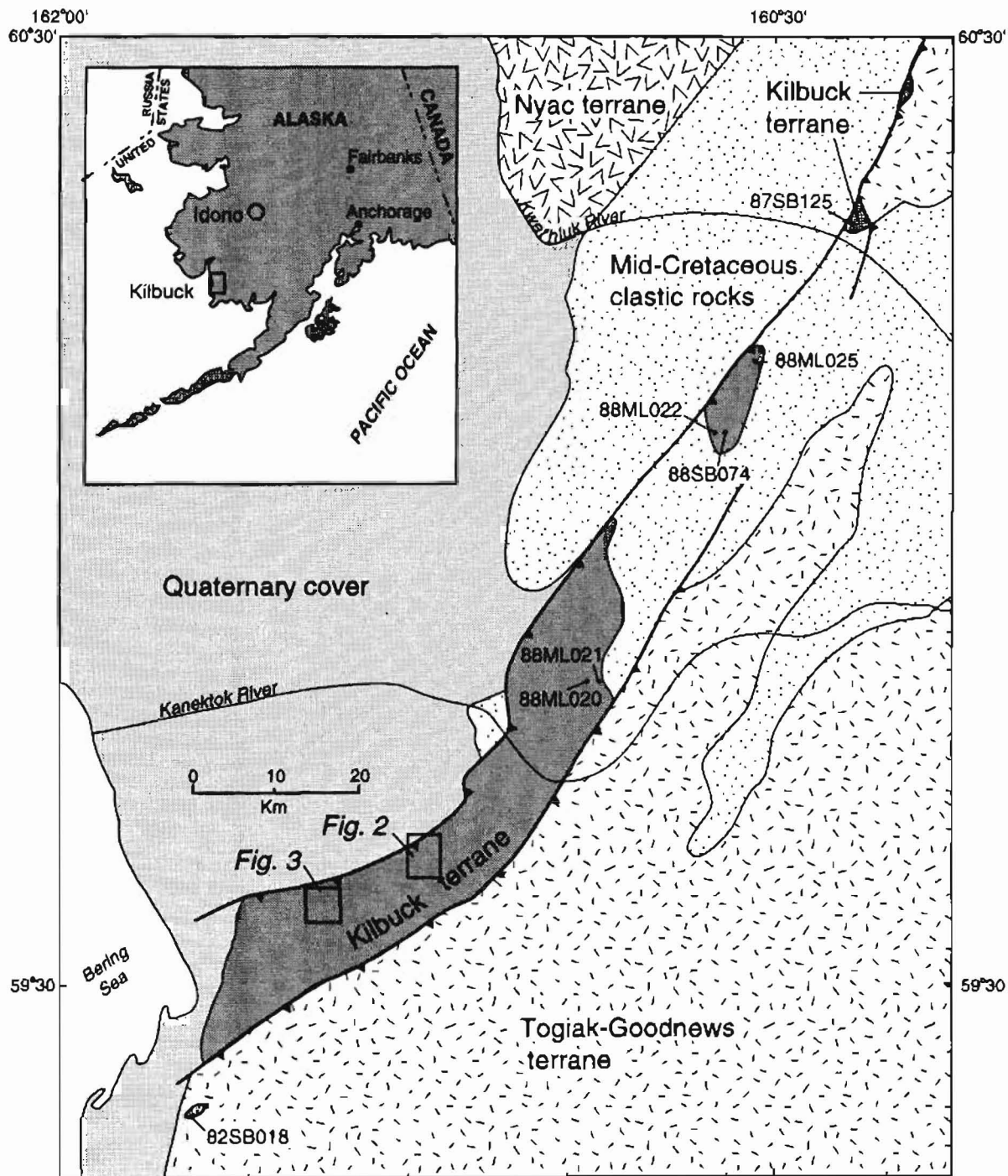
Amphibolite-facies gneisses that yield similar U-Pb and Nd model ages are located 250 km northwest of the Kilbuck terrane (the informally named Idono complex of Miller and others (1991; see fig. 1) but are not known elsewhere in Alaska or in the North American Cordillera (Box and others, 1991). The striking similarities in rock types, U-Pb ages, and Nd model ages between the Idono and Kilbuck terranes suggest that the two terranes represent a single crustal fragment that was accreted to North America and then was offset 250 km by later strike-slip faulting. Although Bowring and Podosek (1989) suggested that large parts of western North America are underlain by 2.0- to 2.4-Ga crust, most other rocks in the North American Cordillera that have zircon ages of about 2 Ga generally have older Nd model ages, and those with Nd model ages of 2 Ga have younger U-Pb zircon ages (R.R. Parrish, oral commun., 1991).

## SETTING AND DESCRIPTION OF ROCK TYPES

The Kilbuck terrane consists of a long narrow body (12 km × 80 km) and three smaller bodies along strike to the northeast (fig. 1). This terrane consists chiefly of biotite, hornblende, or muscovite orthogneiss, flanked lo-

cally on the northeast and southwest by a sequence of marble and impure quartzite. The tonalite and granite gneisses that comprise the bulk of the terrane do not contain mineral assemblages that are sensitive to changes in pressure and temperature. Preliminary mineral composi-

tion data from amphibolite orthogneisses in the Kilbuck terrane indicate that these rocks were metamorphosed to eclogite and upper amphibolite facies (12–13 kbar, 550–600° C), suggesting that the entire terrane experienced high pressures and temperatures.



**Figure 1.** Map showing the location of the Kilbuck terrane and its relation to two oceanic terranes, the Nyac terrane, a Mesozoic volcanic arc terrane, and the Togiak-Goodnews composite terrane. The Nyac, Togiak-Goodnews, and Kilbuck terranes are overlain by mid-Cretaceous clastic rocks. Inset map shows the location of the informally named Idono complex of Miller and others (1991).

The Kilbuck terrane is structurally overlain by Mesozoic oceanic-arc rocks of the Togiak-Goodnews composite terrane on the southeast. The geometry of these terranes is interpreted by Box and others (1991) to be the result of collision and underthrusting of the Kilbuck terrane beneath the Togiak-Goodnews terrane in Early Cretaceous time. All three terranes are overlain by mid-Cretaceous clastic rocks of the Kuskokwim Group.

The metaplutonic rocks of the Kilbuck terrane are best exposed in the Thumb Mountain area (fig. 2), where four distinct metaplutonic rock associations are recognized. The most abundant rock association is a suite of layered, weakly to well-foliated diorite, tonalite, and trondhjemite gneiss. Common mineral assemblages in this

suite are plagioclase, hornblende,  $\pm$ biotite,  $\pm$ quartz, and  $\pm$ potassium feldspar. The second rock association is clinopyroxene-biotite quartz diorite gneiss (pyroxene diorite gneiss) that is coarse grained, weakly foliated, and locally displays relict igneous textures, such as euhedral plagioclase and albite twinning. Contacts between the pyroxene diorite gneiss and the diorite, tonalite, and trondhjemite gneiss appear to be gradational; the transition from pyroxene diorite gneiss to diorite gneiss is marked by progressive development of a tectonic fabric and replacement of pyroxene by hornblende. The diorite, tonalite, trondhjemite gneiss and pyroxene diorite gneiss are also not distinguished from each other on the basis of chemical composition. Rather, the pyroxene diorite gneiss (sample 88JB177a) represents the most mafic end member of a chemically continuous suite of rocks from diorite through tonalite to trondhjemite, herein referred to as the tonalite gneiss suite. The third rock association is a distinctive medium-grained, pink- to pale pink- to cream-colored granite gneiss. The granite gneiss is exposed as pods, tens of meters across, and as cross-cutting pygmatic dikes and veins that locally invade rocks of the tonalite gneiss suite. The granite gneiss contains variable amounts of biotite and ranges from well-foliated biotite granite gneiss to biotite-poor leucocratic granite gneiss to pink pegmatitic granite gneiss; some biotite-poor rocks contain distinct biotite-rich schlieren. All types of granite gneiss are lumped into the granite gneiss suite, even though isotopic and element data given below indicate that they are not all the same age or composition. Also included in the granite gneiss suite are pink-colored, coarse-grained granite augen gneiss that occurs locally as rubble near the eastern margin of the terrane. The relation between this augen gneiss and the tonalite gneiss suite or more common types of granite gneiss is uncertain. The fourth rock association consists of various types of amphibolites that contain hornblende  $\pm$  garnet  $\pm$  clinopyroxene  $\pm$  plagioclase. The amphibolites occur as discordant dikes and concordant discontinuous layers, a few centimeters to a few meters thick, within rocks of the tonalite gneiss suite. Thin zones of pelitic schist and impure marbles are interlayered with garnet amphibolites in a few small areas on Thumb Mountain, but their relation to the more dominant gneissic rocks is uncertain.

## METHODS

Half of the samples were collected on foot traverses from geographically restricted areas near Thumb Mountain in 1988 (fig. 2) and Snow Gulch in 1989 (fig. 3). The remaining samples were collected by helicopter-supported field crews from isolated localities in the northern part of the terrane (fig. 1). Samples with the prefix 87SB, 88SB, or 88ML were cleaned, crushed, and powdered at the

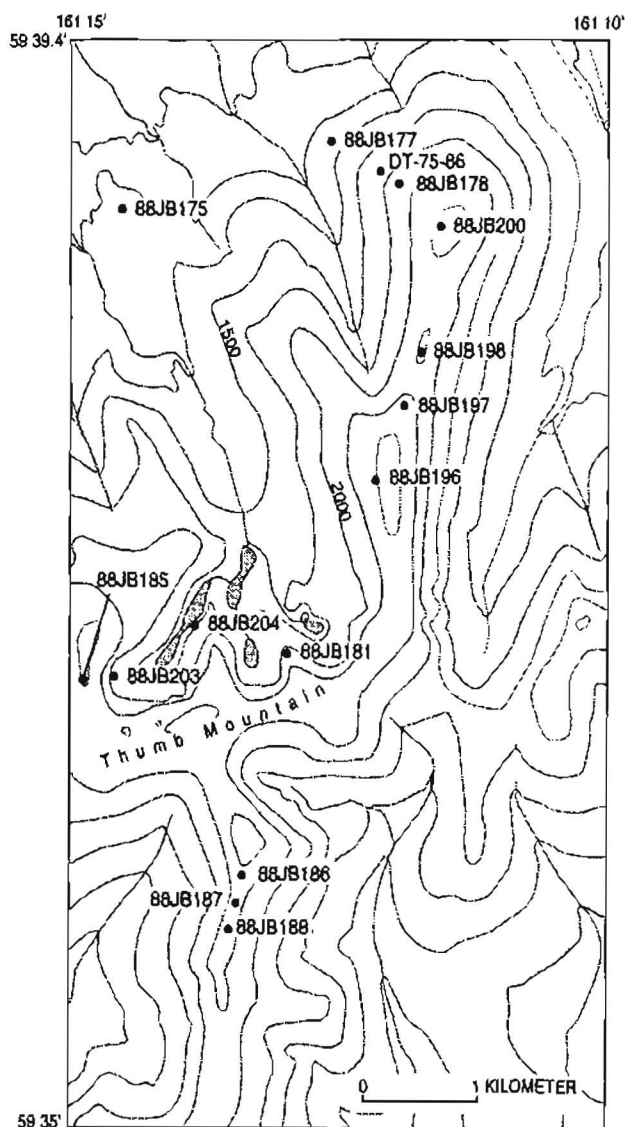


Figure 2. Map of the central part of Thumb Mountain, showing the location of samples collected in 1988. Contour interval is 250 ft. Small shaded areas are lakes.



USGS labs in Menlo Park, Calif.; those with the prefix 88JB or 89JB were prepared at the USGS labs in Anchorage, Alaska. An agate shatterbox was used to powder the rocks in Menlo Park and the samples with the prefix 89JB. A tungsten-carbide shatterbox was used to powder samples with the prefix 88JB and these samples have contaminated Ta values. Major and trace element data are given in tables 1 and 2. Methods for U-Pb zircon and common Pb isotope analyses are modified from Krogh (1973). Sr and Nd samples were analyzed as follows. Approximately 0.1 g of rock powder, spiked for Sm and Nd, was dissolved in HF in a sealed Savillex beaker and left on a hot plate overnight at 100° C. A small amount of 7 N HNO<sub>3</sub> was added, and the samples were heated until all the liquid had evaporated. They were then spiked for Rb and Sr and capped and returned to the hot plate for 1 week. Samples were again heated until dry with the addition of a small amount of 7 N HNO<sub>3</sub>. Samples were dissolved in 6 N HCl, capped on the hot plate overnight, and then heated until dry. Sr, Rb, and the rare-earth elements were separated using a cation exchange column using HCl as eluant. Rb samples were further purified on a second cation exchange column using HCl as eluant. Nd and Sm were separated on a third column using methylactic acid with a pH of 4.6. Total analytical blanks are less than 0.1 ng for Rb, Sr, Sm, and Nd.

Nd and Pb isotopic compositions were analyzed using a Finnigan-Mat 262 mass spectrometer with dynamic simultaneous collections of isotopes. Pb, Sm, Sr and Rb were analyzed by static simultaneous collection. Sr and Sm were analyzed using a single Ta filament, Nd was analyzed using double Re filaments, and Pb and Rb were

analyzed using single Re filaments. The average measured value of <sup>87</sup>Sr/<sup>86</sup>Sr for National Bureau of Standard's SRM987 is 0.710240. Nd isotopic compositions were monitored by an internal laboratory standard that gave an average value for <sup>143</sup>Nd/<sup>144</sup>Nd of 0.512136±0.000009 during the year the samples were analyzed. The average values for rock standards analyzed in this laboratory during the time these are as follows: <sup>87</sup>Sr/<sup>86</sup>Sr for BCR-1=0.704995, BHVO-1=0.703432, and AGV-1=0.703975; <sup>143</sup>Nd/<sup>144</sup>Nd for BCR-1=0.512635, BHVO-1=0.512969, and AGV-1=0.512786; and <sup>208</sup>Pb/<sup>204</sup>Pb for AGV-1=38.370, <sup>207</sup>Pb/<sup>204</sup>Pb for AGV-1=15.597, and <sup>206</sup>Pb/<sup>204</sup>Pb for AGV-1=18.896.

## MAJOR AND TRACE ELEMENT GEOCHEMISTRY

Rocks of the tonalite gneiss suite range from intermediate to felsic (55–75 percent SiO<sub>2</sub>) and are characterized by low K<sub>2</sub>O contents relative to Na<sub>2</sub>O contents and generally high Sr contents (fig. 4). Sr, FeO\* (total Fe as FeO), CaO, and MgO generally decrease with increasing SiO<sub>2</sub>, with the exception of one trondhjemite sample (87SB125b), which has an extremely high Sr content for its SiO<sub>2</sub> content (fig. 4). Trondhjemitic gneisses have between 68 and 75 percent SiO<sub>2</sub>, between 4.0 and 5.5 percent Na<sub>2</sub>O, and generally less than 2.5 percent K<sub>2</sub>O following the definition of trondhjemite given in Barker (1979), but slightly more FeO\*+MgO (3.0–4.1 percent) than Barker's limit of 3.4 percent. All the trondhjemites are slightly corundum normative; the tonalitic gneisses are diopside normative. The entire tonalite suite is LREE enriched (fig. 5). Most samples show little or no europium anomaly (Eu/Eu\*=0.7–1.0). REE patterns for two trondhjemitic gneisses plot below the other rocks in the suite and have small positive Eu anomalies (Eu/Eu\*=1.1–1.4), probably indicating plagioclase accumulation or metamorphic segregation. The entire tonalite suite is enriched in alkalis (Rb, Ba, and K) and depleted in Nb and Ta relative to La (fig. 5; table 1), similar to rocks from modern arcs (Hawkesworth and others, 1993). Th contents are low relative to the other alkali elements, but negative Th anomalies like these are not uncommon in modern arcs and may be related to the composition of the subducted sediments (Plank and Langmuir, 1993). Alternatively, Th may have been expelled during metamorphism.

The granite gneiss suite is chemically diverse, and not all of the granite gneisses can be related to the tonalite gneiss suite or to each other by igneous processes, such as crystal fractionation. For example, data for the granite gneiss suite do not fall along smooth lines when combined with data for the tonalite gneiss suite on Harker diagrams (fig. 4). Even though the SiO<sub>2</sub> contents of the

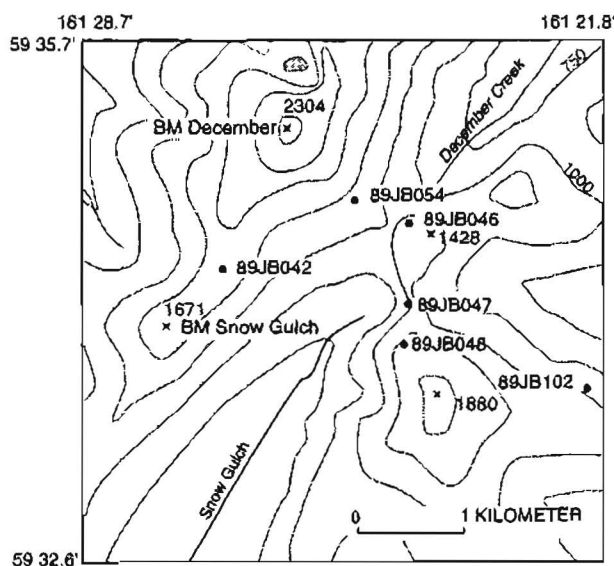


Figure 3. Map showing the location of samples collected from the Snow Gulch area in 1989. Contour interval is 250 ft. Small shaded area is a lake.



**Table 1.** Major and selected trace element data for rocks from the Kilbuck terrane

(Major elements in weight percent; trace elements in parts per million. All major oxides, except FeO, CO<sub>2</sub>, H<sub>2</sub>O<sup>+</sup>, and H<sub>2</sub>O<sup>-</sup>, by X-ray fluorescence following the methods of Taggart and others (1990). FeO determined by titration following the method of Papp and others (1990). CO<sub>2</sub> and H<sub>2</sub>O determined by the methods of Norton and Papp (1990). Trace elements determined by energy-dispersive X-ray fluorescence by the method described in Baedeker (1987). na, not accurately determined. Nb values in italics were isolated by ion exchange chromatography and analyzed by inductively coupled plasma (analyst: T.L. Fries, Menlo Park, Calif.). Sr and Rb values in italics were analyzed by isotope dilution mass spectrometry by the first author at the USGS in Menlo Park, Calif. Samples with the prefix SB or ML were analyzed for major elements by the USGS in Lakewood, Colo. (analysis: J.E. Taggart, A. Bartel, and D. Siems) and for trace elements by the USGS in Menlo Park (analyst: J. Kent); those with the prefix JB were analyzed in Anchorage, Alaska (analyst: Z.A. Brown). FeO, CO<sub>2</sub>, H<sub>2</sub>O<sup>+</sup> and H<sub>2</sub>O<sup>-</sup> were analyzed by wet chemistry in Menlo Park (analyst: S.T. Pribble).)

Rock type	Tonalite gneiss suite										
	Tonalite gneiss							Trondhjemitic gneiss			
Sample no.	88JB 177a	88JB 181d	88ML 020	88JB 178b	82SB 018a	88SB 074c	88JB 204a	87SB 125b	88ML 021	88JB 186b	88ML 025
SiO <sub>2</sub>	55.10	56.10	57.80	58.60	61.50	62.00	62.70	69.10	69.00	68.40	73.50
Al <sub>2</sub> O <sub>3</sub>	17.70	16.20	17.70	17.10	16.30	16.30	16.40	16.10	15.40	14.70	13.80
TiO <sub>2</sub>	.86	.91	.71	.84	.87	.85	.54	.30	.35	.40	.42
Fe <sub>2</sub> O <sub>3</sub>	2.38	2.95	2.61	2.11	2.20	2.79	1.56	1.46	1.24	1.20	2.38
FeO	5.09	5.45	4.01	4.30	2.79	3.34	3.13	.84	1.78	1.61	.44
MnO	.16	.14	.11	.09	.09	.08	.08	.04	.04	.04	.02
MgO	4.00	4.62	2.99	2.73	2.32	2.05	2.15	.85	1.19	1.27	.41
CaO	6.96	5.73	6.16	5.36	4.79	4.23	4.06	2.68	2.82	1.97	1.09
Na <sub>2</sub> O	4.52	4.50	4.65	4.70	4.12	4.36	4.69	5.41	4.43	4.94	4.03
K <sub>2</sub> O	1.50	1.33	1.30	1.82	3.08	1.99	2.66	1.66	2.35	2.53	2.17
P <sub>2</sub> O <sub>5</sub>	.41	.40	.32	.31	.41	.30	.24	.10	.14	.15	.07
H <sub>2</sub> O <sup>+</sup>	.89	1.43	1.16	1.12	.78	1.23	1.02	.49	.71	1.14	1.09
H <sub>2</sub> O <sup>-</sup>	.18	.14	.12	.17	.05	.06	.12	<.01	.11	.15	.04
CO <sub>2</sub>	.04	.02	<.01	.01	.11	.02	.13	.01	.02	.97	.27
SUM	99.79	99.92	99.64	99.26	99.41	99.60	99.48	99.04	99.58	99.47	99.73
SiO <sub>2</sub> <i>anhydrous</i>	55.52	56.71	58.50	59.53	62.26	62.84	63.62	69.65	69.74	70.23	74.75
Rb	56.4	32	29.4	75	70	76	59.8	22.0	39.7	51.9	40
Sr	1000.2	716	1073.3	838	680	680	695.9	1075.0	425.6	429.7	210
Ba	646	642	800	686	920	1100	1080	1100	1000	949	1100
Nb	11	11	6.9	10	13.5	10	8.9	8	7.4	9.7	8.4
Zr	143	240	148	284	240	315	170	345	120	215	345
Y	16	25	16	24	28	28	13	24	<10	16	24

two suites overlap, the granite gneiss suite has distinctly higher K<sub>2</sub>O contents (fig. 4A). The granite gneiss suite is characterized by high and variable SiO<sub>2</sub> (63–79 percent), K<sub>2</sub>O (3.5–7.6 percent), and Rb contents (fig. 4; table 1). REE patterns are also highly variable (fig. 6); granitic gneisses have LREE contents that are both higher and lower than those of the tonalite suite; HREE contents are similar to those of the tonalite suite (table 2). Most samples have slightly to moderately negative Eu anomalies (Eu/

Eu\*=0.4–1.0; fig. 6). The anomalous REE pattern of sample 88ML022a probably reflects igneous layering or metamorphic segregation. This sample is a pink leucocratic vein composed primarily of quartz, plagioclase, and potassium feldspar. The sample consists almost entirely of SiO<sub>2</sub>, Al<sub>2</sub>O<sub>3</sub>, Na<sub>2</sub>O, and K<sub>2</sub>O (table 1). It has very low REE contents and a large positive Eu anomaly (Eu/Eu\*=8.1), probably indicating the accumulation of feldspar, because feldspars have low concentration of all REEs

Table 1. Major and selected trace element data for rocks from the Kilbuck terrane—Continued

Rock type	Granite gneiss suite												
Sample no.	88JB 181e	88JB 197b	88JB 200a	88ML 022a	88ML 022b	88JB 203a	88JB 185a	88JB 198a	87SB 125a	89JB 046d	89JB 046f	89JB 054	89JB 102
SiO <sub>2</sub>	72.10	73.50	74.60	75.10	74.90	75.10	77.00	76.20	79.00	63.00	70.70	72.60	68.60
Al <sub>2</sub> O <sub>3</sub>	13.90	13.50	13.00	13.50	13.60	13.40	12.60	10.40	11.80	17.60	14.00	13.90	15.00
TiO <sub>2</sub>	.25	.16	.26	<.02	.11	.07	.06	.60	.08	.49	.37	.32	.42
Fe <sub>2</sub> O <sub>3</sub>	.70	.60	.52	.20	.67	.31	.14	1.95	.40	1.24	1.06	.94	1.37
FeO	.93	.60	.78	.09	.32	.36	.24	.95	.13	2.14	1.48	.41	1.48
MnO	.02	<.02	<.02	<.02	<.02	<.02	<.02	.05	.01	.04	<.02	.02	.03
MgO	.65	.32	.31	.11	.26	.24	.15	1.06	.20	1.58	.68	.36	1.12
CaO	1.40	.70	.59	.31	.86	.49	.45	1.76	.36	3.32	1.64	.76	1.90
Na <sub>2</sub> O	4.23	3.33	3.47	2.39	3.45	3.83	3.86	.33	3.50	4.56	2.83	3.39	3.92
K <sub>2</sub> O	4.42	5.58	5.12	7.59	4.57	5.05	4.70	3.65	4.24	3.54	5.54	5.45	4.46
P <sub>2</sub> O <sub>5</sub>	.08	<.05	<.05	<.05	<.05	<.05	<.05	<.05	.01	.20	.11	.06	.17
H <sub>2</sub> O <sup>+</sup>	.46	.55	na	.27	.50	.35	na	1.64	.24	.94	.58	.51	.79
H <sub>2</sub> O <sup>-</sup>	.10	.14	na	.02	.04	.09	na	.09		.14	.10	.10	.10
CO <sub>2</sub>	.12	.10	<.01	<.01	<.01	<.01	<.01	.49	.04	<.01	.14	<.01	<.01
SUM	99.36	99.08	98.65	99.58	99.28	99.29	99.20	99.17	100.01	98.79	99.23	98.82	99.36
SiO <sub>2</sub> <i>anhydrous</i>	72.99	74.73	75.55	75.63	75.83	75.94	77.60	78.52	78.97	64.47	71.84	73.92	69.67
Rb	54.2	88.4	136.0	162	144.07	164.9	115	68	78	80	88	142	130
Sr	263.3	328.4	114.7	265	187.18	86.6	59	161	52	890	500	205	405
Ba	640	1180	893	1100	1400	379	81	1260	480	1700	1800	1200	790
Nb	7.2	9.7	15	5.1	16	26	15	11	14	<10	<10	12	10
Zr	217	216	203	16	106	106	73	486	62	132	260	255	186
Y	17	12	18	<10	10	23	13	24	5	12	28	22	16

except Eu (fig. 6). Indeed, the REE pattern for this sample is similar in shape and concentrations to published REE data for feldspars (Schnetzler and Philpotts, 1970). The host rock (sample 88ML022b) for the vein has more normal REE abundances and a small negative Eu anomaly ( $\text{Eu}/\text{Eu}^* \approx 0.65$ ). Complementary REE patterns are probably the result of metamorphic segregation. Leucocratic layers in the gneiss are very REE poor because they are contain primarily REE-poor minerals, such as feldspar and quartz. Most of the REE that were in the original rock are concentrated in the darker gneiss layers, and these layers have more normal REE patterns.

Spidergram plots of data from most of the granite gneisses also show negative Nb and Ta anomalies (fig. 7) similar to those for samples from the tonalite gneiss suite and for rocks erupted in modern arcs. The granite gneisses, however, have much more evolved major and trace ele-

ment compositions (usually >70 percent SiO<sub>2</sub> and >4 percent K<sub>2</sub>O) than typical island-arc volcanic rocks and probably require some interaction with continental crust (that is, rocks more siliceous than the mantle or oceanic crust). Some of the granite gneisses have K<sub>2</sub>O and SiO<sub>2</sub> contents that are too high (7.6 weight percent and 79 weight percent, respectively) and Na<sub>2</sub>O contents that are too low (0.33 weight percent) to represent igneous compositions. Although these elements have been clearly modified since igneous formation, other elements, such as Ba, Sr, Th, Nb, Ta, and the REE, are remarkably similar to those in unaltered calc-alkalic granites.

The amphibolites are chemically diverse, although most appear to be metabasalts. One sample (88JB187d) has a LREE-enriched REE pattern (fig. 8) similar to nearby rocks of the tonalite gneiss suite and may be a more mafic part of that suite, but it lacks the high Sr concentra-

Table 1. Major and selected trace element data for rocks from the Kilbuck terrane—Continued

Rock type	Amphibolite					Metapelite	
Sample no.	88JB 187d	88JB 175g	88JB 196a	89JB 042	89JB 047	89JB 048a	88JB 188a
SiO <sub>2</sub>	47.80	48.60	54.50	47.90	48.40	48.70	60.40
Al <sub>2</sub> O <sub>3</sub>	16.60	13.40	12.90	12.70	13.70	12.80	19.70
TiO <sub>2</sub>	1.58	2.16	2.02	2.99	2.13	2.23	.72
Fe <sub>2</sub> O <sub>3</sub>	3.43	3.31	4.12	3.33	3.03	3.91	3.12
FeO	9.07	12.60	10.70	12.50	10.60	12.60	5.03
MnO	.27	.26	.32	.24	.21	.26	.03
MgO	7.04	5.83	3.42	5.87	6.66	5.87	2.06
CaO	7.58	10.60	6.80	10.30	9.84	9.90	.42
Na <sub>2</sub> O	4.20	2.32	2.75	2.22	2.11	2.33	.93
K <sub>2</sub> O	.48	.19	.80	.30	1.06	.53	4.57
P <sub>2</sub> O <sub>5</sub>	.33	.18	.30	.26	.20	.22	.05
H <sub>2</sub> O <sup>+</sup>	1.59	.52	1.12	1.40	1.90	.98	2.58
H <sub>2</sub> O <sup>-</sup>	.14	.10	.14	.07	.15	.07	.13
CO <sub>2</sub>	<.01	.01	.11	<.01	.11	<.01	<.01
Total	100.11	100.08	100.00	100.08	100.10	100.40	99.74
SiO <sub>2</sub> <i>anhydrous</i>	48.10	48.20	54.60	48.58	49.42	49.02	62.25
Rb	6.3	4.6	20.9	<10	22	22	163.0
Sr	222.3	104.4	151.1	166	205	154	102.6
Ba	52	37	241	54	250	64	433
Nb	7.5	16	17	16	12	12	16
Zr	104	123	202	182	124	142	176
Y	22	53	67	48	30	46	45

tions that characterize those rocks. The other five analyzed samples are apparently unrelated to the tonalite gneiss suite because they have much lower Na<sub>2</sub>O (fig. 4A) and Al<sub>2</sub>O<sub>3</sub> and much higher Nb, TiO<sub>2</sub>, and FeO\* contents (table 1) than the tonalite gneiss suite. These metabasalts are tholeiitic because of their high Fe contents. The tholeiitic samples all have flat REE patterns (fig. 8) and higher HREE contents than the tonalites (table 2). Sample 88JB187d has a small negative Nb anomaly (fig. 8); sample 88JB196a may have a very small one. Both samples have elevated Ta contents due to contamination from a tungsten-carbide shatterbox, which makes it hard to determine if a true Nb-Ta anomaly is present.

The single sample of pelitic schist also has a LREE-enriched REE pattern similar to the tonalite gneiss suite, but the pattern is more strongly concave down between Ce and Gd than are any of the patterns of the igneous rocks (fig. 9). The spidergram is difficult to interpret be-

cause Ta values were contaminated during grinding. But if Ta is ignored, the low Nb value suggests that the rock had a small Nb and Ta anomaly. There is no clear evidence for the age of the pelitic schists or their relations to the other rocks. They could be derived, at least in part, by erosion of the tonalite gneiss suite. Their metamorphic fabric suggests that the pelitic schists were part of the Kilbuck terrane by the time of metamorphism, probably by 1.77 Ga.

## U-Pb GEOCHRONOLOGY

One trondhjemite gneiss sample (87SB125b), two tonalite gneiss samples (88JB177a, 88JB204a), and two granite gneiss samples (88ML022b and DT-75-86) were dated using U-Pb zircon methods (table 3). Only the trondhjemite gneiss sample and one of the granite gneiss

**Table 2.** Additional trace element data for selected samples

[Trace elements in parts per million. Analyzed by long-count instrumental neutron activation analysis (INAA); methods described by Baedeker (1987). na, not accurately determined. Trace element values in italics analyzed by the first author by isotope dilution mass spectrometry at the USGS laboratory in Menlo Park, Calif. Samples with the prefix ML or SB were analyzed by R.J. Knight, J.R. Budahn, R.E. McGregor and R.B. Vaughn; samples with the prefix JB were analyzed by J.R. Budahn at the USGS laboratory in Lakewood, Colo.]

Rock type	Tonalite gneiss suite								
	Tonalitic gneiss					Trondhjemitic gneiss			
Sample no.	88JB 177a	88ML 020	82SB 018a	88SB 074c	88JB 204a	87SB 125b	88ML 021	88JB 186b	88ML 025
La	34.9	31.2	35.9	60.2	32.7	14.1	24.1	30	57.4
Ce	81.5	70.5	73.1	125	73.8	25.4	48.2	66.5	118
Nd	40.4	33.7	30.8	52.3	32.5	11.7	17.9	29.4	50.8
Sm	7.6	6.0	5.5	8.3	5.7	1.9	2.9	5.3	8.5
Eu	2.1	1.74	1.53	1.76	1.49	.67	.94	1.27	2.15
Gd	5.85	4.75	4	5.97	3.85	na	2.25	4.57	6.5
Tb	.796	.562	.544	.787	.513	.149	.276	.578	.844
Ho	.943	.679	na	.928	.614	na	na	.732	1
Tm	.352	.257	.26	.345	.245	na	.125	na	.375
Yb	2.05	1.53	1.52	2.10	1.49	.287	.797	1.5	2.06
Lu	.297	.219	.22	.309	.223	.037	.115	.208	.289
Ni	48.6	0	23.1	18.3	33.2	10	12.1	15.9	—
Zn	97.5	80.7	70.5	78.4	68.7	33.4	37.9	42.6	50.2
Cr	51.2	17.4	26	19.6	12.3	7.3	12.7	8.57	1.61
U	.497	.412	.39	.728	.263	<2	.439	.765	.353
Th	.862	1.20	.89	3.81	.399	.119	1.13	3.7	3.61
Ta	1.25	.508	.55	.490	1.26	.069	.328	1.46	.367
Hf	3.84	4.14	5.53	6.94	4.3	2.63	3.17	5.65	9.48
Co	52.4	19.6	15	13.0	54.9	4.85	6.75	52.9	2.02
Sc	18.5	15.3	15	12.4	12.8	3.2	4.99	7.85	7.78
Sb	.0811	na	0	na	.0914	<.1	na	.0733	0

samples yield independent ages ( $2070 \pm 15$  Ma and  $2052 \pm 27$  Ma, respectively; figs. 10A, D). The tonalite gneisses have insufficient spread in their Pb-U ratios to yield independent ages, but together they give an age of  $2060 \pm 3$  Ma (fig. 10B). The remaining granite gneiss gives an age of  $2040 \pm 90$  Ma (fig. 10C), but this age is more discordant than the other ages. The lower intercepts of all samples are not considered meaningful because all have very large uncertainties—in fact, all but one have larger uncertainties than their ages. We were not able to date the amphibolites and most of the granite gneisses by U-Pb methods because the other samples we collected failed to yield zircons.

A single sphene age of 1770 Ma was obtained on the same sample of granite orthogneiss (DT-75-86) that gave a U-Pb zircon age of 2052 Ga (fig. 10D; table 3). Since

sphene is reset at about 550°C (Hanson and others, 1971), this age probably indicates that amphibolite-grade metamorphism occurred at about 1770 Ma.

## Nd MODEL AGES

Twelve samples were analyzed for Nd isotopes, and model ages were calculated using the equations of Liew and McCulloch (1985) (table 4). Nd model ages calculate the time that a magma separated from a depleted mantle reservoir having a high Sm/Nd ratio. Once a magma has separated from the mantle, it will "grow"  $^{143}\text{Nd}$  from the decay of Sm at a different rate than its source, depending on its Sm/Nd ratio. The model age is calculated by extrapolating back to the point when the magma had the

Table 2. Additional trace element data for selected samples—Continued

Rock type	Granite gneiss suite										
Sample no.	88JB 197b	88JB 200a	88ML 022a	88ML 022b	88JB 185a	88JB 198a	87SB 125a	89JB 046d	89JB 046f	89JB 054	89JB 102
La ppm	141	46.7	1.64	27.1	1.24	143	8.6	33.9	80.5	39.4	40.0
Ce	223	104	1.81	51.1	6.32	305	16.1	56.8	149.0	72.0	77.0
Nd	71.9	35.9	1.03	16.1	1.4	115	6.6	23.0	58.3	33.0	30.0
Sm	8.5	5.6	.175	2.90	.39	15.6	1.5	3.6	10.2	5.9	5.8
Eu	1.2	.807	.487	.573	.092	3.12	.366	1.040	1.280	1.300	1.000
Gd	3.82	4.0	na	2.87	.488	9.58	na	nd	nd	nd	nd
Tb	.436	.49	.0260	.318	.0879	1.04	.172	.29	.91	.531	.58
Ho	.453	.537	na	na	.134	.934	na	nd	nd	nd	nd
Tm	na	na	na	na	na	na	na	nd	nd	nd	nd
Yb	.76	1.02	.214	.888	.377	1.87	.53	.67	2.33	1.20	1.70
Lu	.105	.155	.0353	.119	.0564	.286	.072	.092	.289	.166	.24
Ni	15.4	10.2	2.81	4.6	6.79	35.2	<10	22	<10	<8	24
Zn	7.66	25.2	4.15	24.6	1.72	38.8	8.5	57	37	31.2	41
Cr	2.52	5.53	.881	3.36	4.78	3.56	1.54	17	5.4	.69	9.3
U	3.35	1.15	.409	2.49	1.86	1.23	1.18	.21	.42	.59	1.3
Th	45.3	14.8	5.83	14.8	19	32	18.6	2.88	9.84	5.43	12.1
Ta	2.72	2.5	.402	1.47	2.31	1.69	1.045	.2	.65	.742	.61
Hf	5.62	6.86	.650	3.31	3.12	14.8	2.2	2.82	7.23	6.44	5.57
Co	103	90.8	.349	1.32	73.9	63.4	.61	9.37	4.35	1.48	5.6
Sc	1.96	3.19	.491	2.91	1.17	5.54	1.54	5.7	5.25	3.62	6.58
Sb	.11	.0846	.0228	.0250	.0705	.0593	.053	<.07	<.07	<.06	<.06

same isotopic composition as the source and is most successful when the source and the magma have markedly different Sm/Nd ratios. One must assume that the present Sm/Nd ratio of the analyzed rock has remained unmodified since formation, and that the magma formed directly from partial melting of the mantle. It also must be assumed that the isotopic composition of the source is the same as that of the modeled mantle-evolution curve (Arndt and Goldstein, 1987).

All of the tonalite gneisses and most of the granite gneisses have Nd isotopic compositions that indicate they were separated from a depleted mantle source at about 2.1 Ga (fig. 11). Granite gneiss sample 88ML022b gives a Late Archean model age (about 2.7 Ga) but has a U-Pb zircon age similar to that of the tonalite gneiss suite (fig. 10C). Two of the three amphibolites have Sm/Nd ratios that are not significantly different from mantle (that is, they have flat or almost flat REE patterns) and are not suitable for calculating Nd model ages (Arndt and Goldstein, 1987) because their Nd evolution curves are nearly parallel to the mantle-evolution line. These amphibolites are not shown on figure 11. The third amphibolite

(88JB187d) is LREE enriched and yields a more meaningful Nd model age that is similar to that of the tonalite gneiss suite (fig. 11).

## Rb-Sr SYSTEMATICS

Rb, Sr, and  $^{87}\text{Sr}/^{86}\text{Sr}$  analyses of igneous rocks or minerals are a potential source of information about the age and initial Sr isotopic composition of the rocks. However, they only yield meaningful results if all of the analyzed rocks or minerals started with the same Sr isotope composition at the same time and if the Rb/Sr ratio of the system remains undisturbed. If these conditions are met, growth in  $^{87}\text{Sr}$  will be strictly proportional to the Rb/Sr ratio of the rock or mineral. In this case the present day  $^{87}\text{Sr}/^{86}\text{Sr}$  ratio of a group of samples will define a line whose slope is proportional to the age of the samples and whose y-intercept (Rb/Sr=0) gives the initial  $^{87}\text{Sr}/^{86}\text{Sr}$  ratio of the samples.

Rb, Sr, and  $^{87}\text{Sr}/^{86}\text{Sr}$  analyses of 15 rocks from the Kilbuck terrane do not clearly define a line, or isochron.



Table 2. Additional trace element data for selected samples—Continued

Rock type	Amphibolite						Metapelite
Sample no.	88JB 187d	88JB 175g	88JB 196a	89JB 042	89JB 047	89JB 048a	88JB 188a
La ppm	16.4	7.25	20.5	9.2	7.2	8.2	28.5
Ce	40.3	19.8	49	23.0	19.0	20.0	66.5
Nd	25.7	16.9	30.5	18.0	14.0	14.0	13.6
Sm	5.6	5.3	8.2	6.3	4.7	5.1	3.7
Eu	1.66	1.69	2.24	1.960	1.580	1.660	1.15
Gd	4.79	5.96	8.94	nd	nd	nd	5.76
Tb	.701	1.08	1.55	1.24	.95	1.1	.977
Ho	.866	1.56	2.28	nd	nd	nd	1.38
Tm	.352	.654	.981	nd	nd	nd	.61
Yb	2.16	4.12	6.06	3.79	3.00	4.46	3.8
Lu	.313	.59	.914	.54	.43	.63	.558
Ni	108	65.5	32.9	70	100	99	51.3
Zn	141	118	166	135	120	145	95.2
Cr	71.1	74.1	9.96	75.8	137	79.5	74.1
U	.479	.267	1.13	.39	<3	.32	1.86
Th	1.06	.679	4.38	.78	.54	.67	10.6
Ta	1.41	1.77	2.17	.68	.53	.58	1.96
Hf	2.49	3.35	5.53	4.35	3.36	3.6	4.78
Co	90.9	108	91.3	51.5	50.4	52.8	61.9
Sc	29.8	47.5	35.2	40.4	40.5	46.5	20.5
Sb	.0795	.212	.156	<.09	<2	<1	.121

This nonlinear trend indicates either that the suites were not isotopically uniform when they formed or that the Rb-Sr systematics were disturbed by metamorphism. Data for the granite gneiss suite scatter about a 1800-Ma reference isochron (fig. 12A); data for the tonalite gneiss suite scatter about a 2070-Ma reference isochron (fig. 12B). Data for the amphibolites do not define a line, and only one sample of pelitic schist was analyzed (table 5). Assuming an age of 2.1 Ga, the tonalite gneiss suite samples had initial  $^{87}\text{Sr}/^{86}\text{Sr}$  ratios of 0.7013–0.7031. Some of the granite gneisses (88JB181e, 88JB200a, 88JB203a) give unreasonably low initial  $^{87}\text{Sr}/^{86}\text{Sr}$  ratios (less than 0.7000) when an age of 2.1 Ga is used to calculate their initial ratio (table 5), indicating that they are probably younger than the tonalite gneiss suite or that their Rb/Sr ratios were modified during metamorphism. Lack of coherency in the Sr isotopic data for the amphibolites underscores their variability and incompatibility. Sr isotope data for sample 88JB187d, which had major and trace element affinities with the tonalite gneiss suite, show a Sr isotopic composition (0.7074 at 2.1 Ga) that precludes an affinity unless the Rb, Sr, or  $^{87}\text{Sr}/^{86}\text{Sr}$  ratio has been altered. The

single Sr isotope analysis of the metapelite sample is difficult to interpret. This sample has a high Rb/Sr ratio that gives unreasonably low initial  $^{87}\text{Sr}/^{86}\text{Sr}$  ratios for ages greater than 850 Ma (table 5) indicating that the rock is either much younger than the tonalite gneiss suite or contains highly altered Rb and Sr.

## DISCUSSION

The tonalite gneiss suite forms a chemically and isotopically coherent suite that appears to represent a variably deformed and metamorphosed composite intrusion. The pyroxene diorite gneiss represents the less deformed part of this intrusion because igneous textures are commonly preserved in this rock type. The tonalite gneisses represent the more strongly metamorphosed and recrystallized parts of the intrusion. Although Nd model ages for the tonalite gneiss suite are approximately the same as its U-Pb zircon ages, it is unlikely that tonalite or trondhjemitic magmas formed by direct partial melting of depleted mantle. Tonalite and trondhjemitic magmas gen-

erally form by partial melting of basaltic sources or by fractionation of basaltic magmas rather than by partial melting of ultramafic mantle (Barker, 1979, p. 8). Data for the tonalite gneiss suite display on spidergrams the characteristic enrichments and depletions of arc magmas. Thus, the tonalite and trondhjemite magmas most likely formed either by fractionation of arc basalts at approximately 2 Ga or by rapid remelting of basaltic arc rocks shortly after formation at 2 Ga.

The relations of the amphibolites and the granite gneisses to the tonalite gneiss suite is less certain. Field relations suggested that at least some of the granite gneisses intruded rocks of the tonalite gneiss suite. At least one sample of granite gneiss (88ML022b) yields a U-Pb age that is similar to that of the tonalite gneiss suite, but it has a Late Archean Nd model age. This older Nd model age indicates that its protolith either formed from Archean crust or interacted with Archean crust or sediments derived from Archean crust. In addition to the geochemistry, this provides further evidence that the 2-Ga rocks of the Kilbuck terrane did not form in an intraoceanic island arc far removed from the continental margin. Although only one sample gave an Archean Nd model age, it is likely that the entire arc was either located in a continental margin consisting in part of Archean

rocks or was close enough to a continental margin for some of the magmas to interact with sediments derived from such a margin. This interpretation implies that the sample with an Archean model age represents a relatively small proportion of magma that was sufficiently contaminated by the country rock to alter its Nd isotopic composition. Miller and others (1991) also reported a single Archean model age of 2.5 Ga on a sample of granite gneiss from the Idono complex (fig. 1), confirming that a latest Archean or earliest Proterozoic component is also present there. Other granite gneisses may also be the same

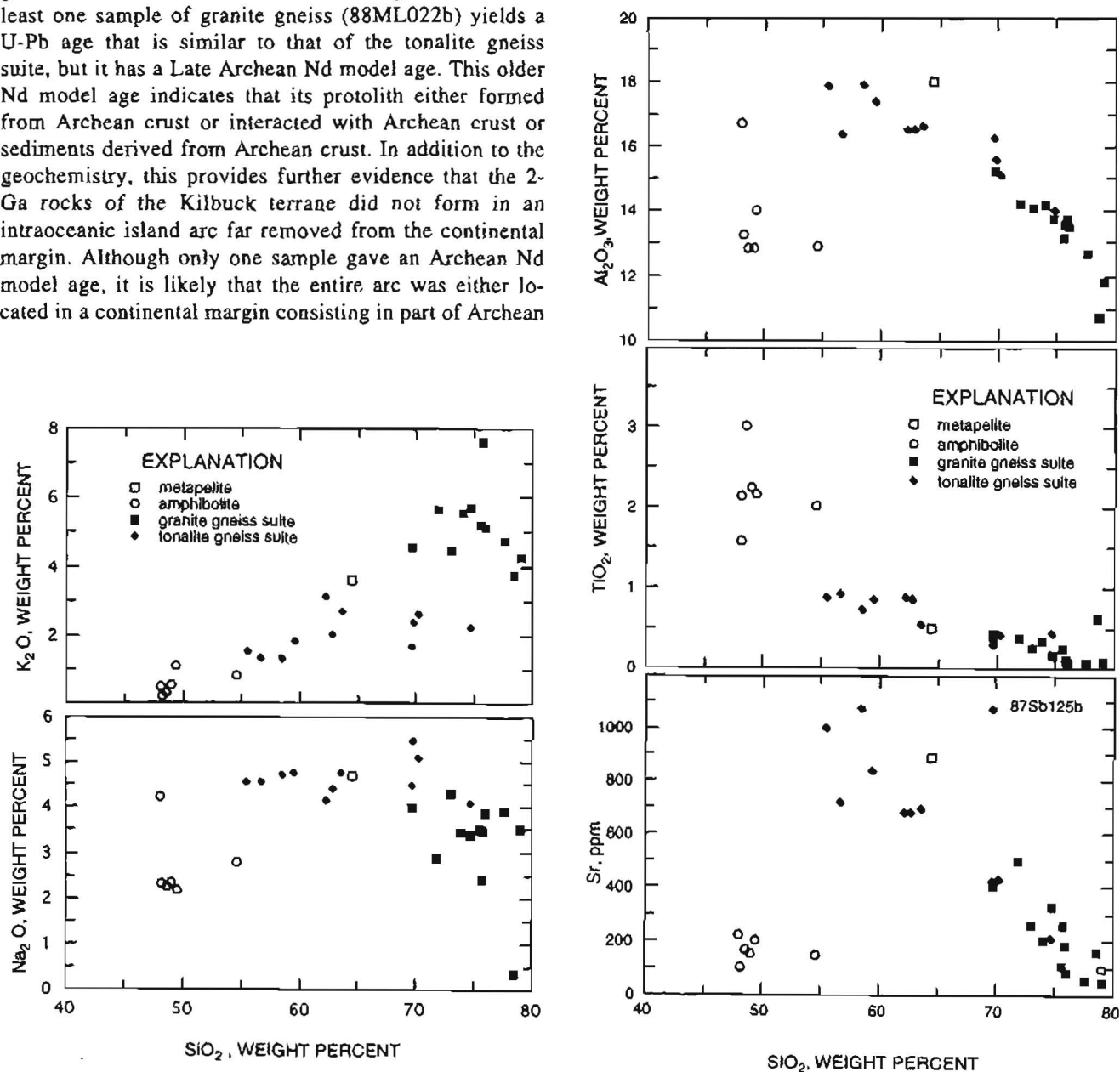
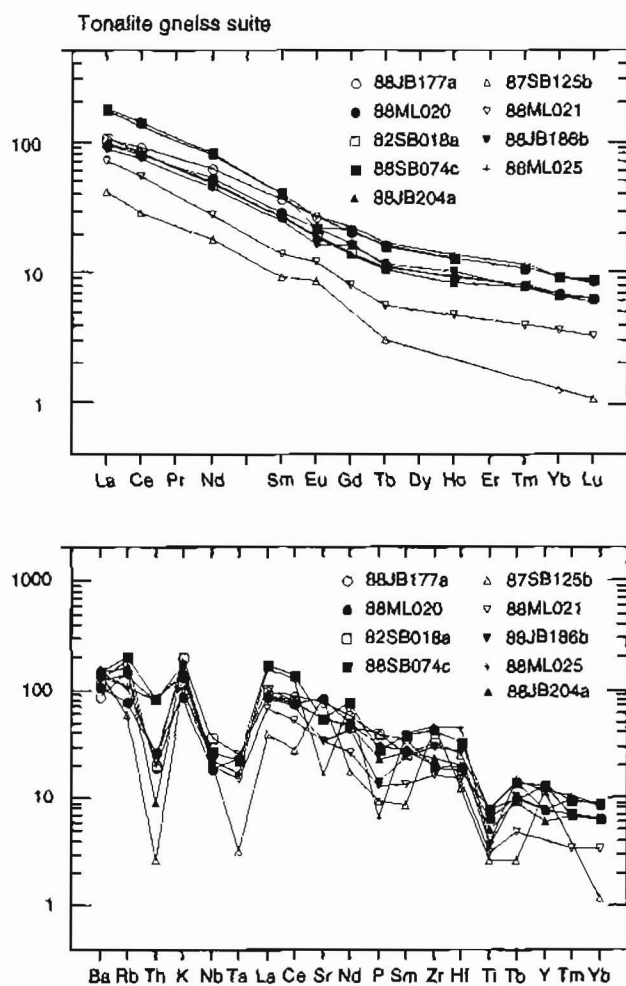


Figure 4. Plots of  $\text{K}_2\text{O}$ ,  $\text{Na}_2\text{O}$ ,  $\text{Al}_2\text{O}_3$ ,  $\text{TiO}_2$ , and Sr versus  $\text{SiO}_2$  for data from the tonalite gneiss suite, granite gneiss suite, amphibolite, and metapelite rocks in the Kilbuck terrane. ppm, parts per million.

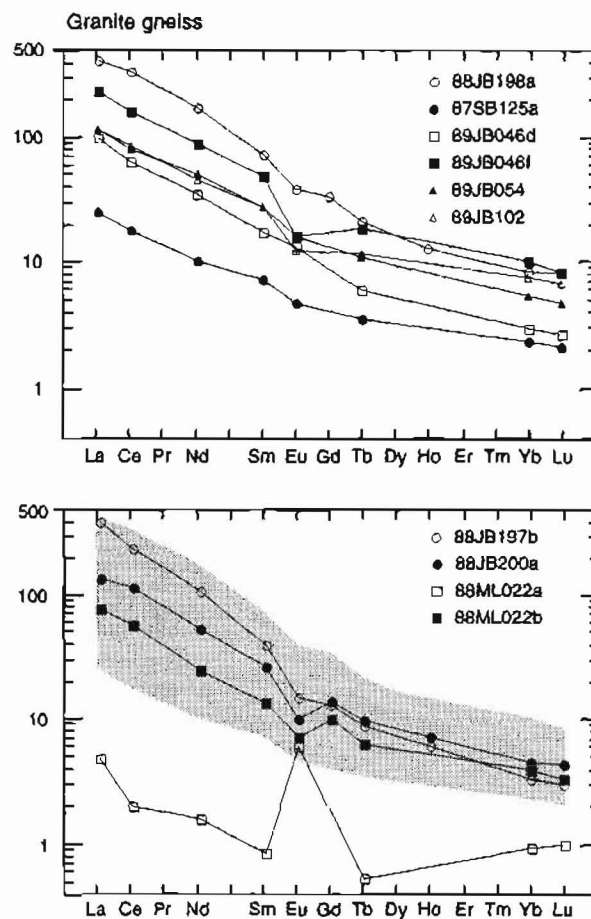
age as the tonalite gneiss suite; two granite gneisses (88JB200a and 88JB197b) in the Kilbuck terrane give Nd model ages similar to those for the tonalite gneiss suite, but these samples did not yield zircons for U-Pb dating. Initial  $^{87}\text{Sr}/^{86}\text{Sr}$  ratios for some of the granite gneisses (88JB181e, 88JB200a, 88JB203a) are unrealistically low (less than 0.7000) if these ratios are calculated using an age of 2100 Ma. This discrepancy indicates either that these gneisses are younger than 2100 Ma or that their Rb/Sr ratios have been modified since formation. We calculated initial Sr isotope ratios for these three granites using a hypothetical age of 1800 Ma (table 5) because data for the granites scatter about a 1800-Ma reference isochron. Although the data have too much scatter to define an age, the Sr isotopic compositions do not plot randomly

on figure 12, suggesting that there is some relation between samples. Perhaps the granite gneisses had initial Sr isotope ratios that were nearly homogeneous or had Rb/Sr ratios that were only slightly disturbed. Although all three granitic gneiss samples give reasonable initial Sr ratios using an age of 1800 Ma, their real age is unknown and could be much younger or much older if their Rb and Sr contents have been disturbed. Major and trace element data do not fall along smooth curves when combined with data from the tonalite gneiss suite, indicating that not all of the granite gneisses can be related to the tonalite gneiss suite or to each other by igneous processes such as crystal fractionation. If some of the granites are younger than the dominant tonalite gneiss suite, they could have been derived by melting of the tonalites at midcrustal pressure (Skjerlie and Johnston, 1993). Such granites would have the same Nd model ages as the tonalites but younger absolute ages in keeping with the poorly constrained Rb-Sr data.

Most of the amphibolites appear chemically and isotopically distinct from the tonalite gneiss suite or the gran-



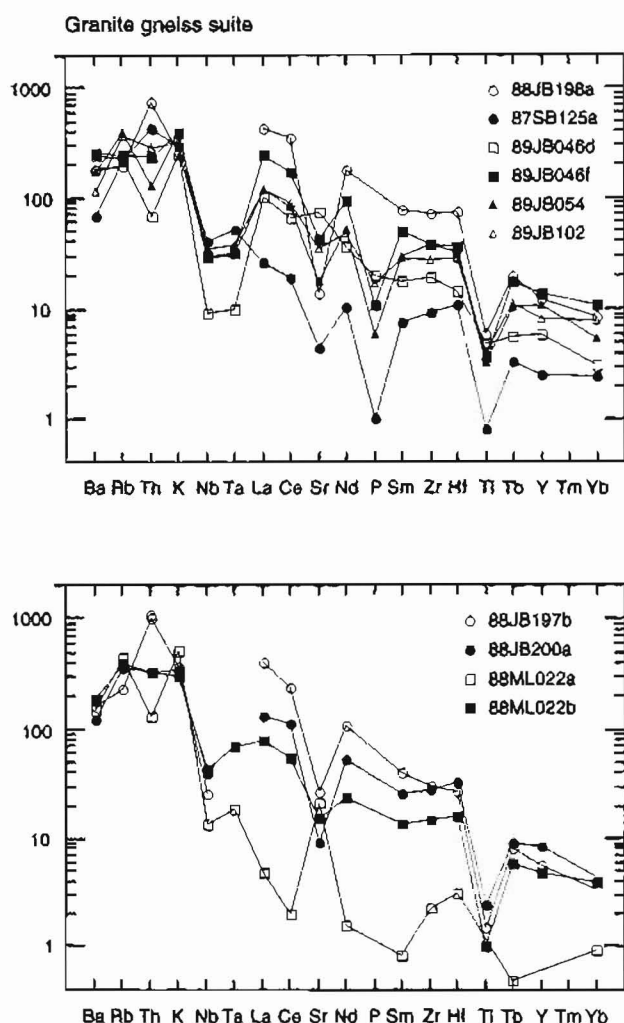
**Figure 5.** REE and spidergram plots for rocks from the tonalite gneiss suite. Values plotted on the spidergram are normalized to chondritic abundances except for K, P, and Ti; values are given in Thompson (1982). Ta contents in samples with the prefix 88JB are not shown because they are elevated relative to Nb owing to contamination from a tungsten-carbide shatterbox. Diagrams drawn using the program of Wheatley and Rock (1988).



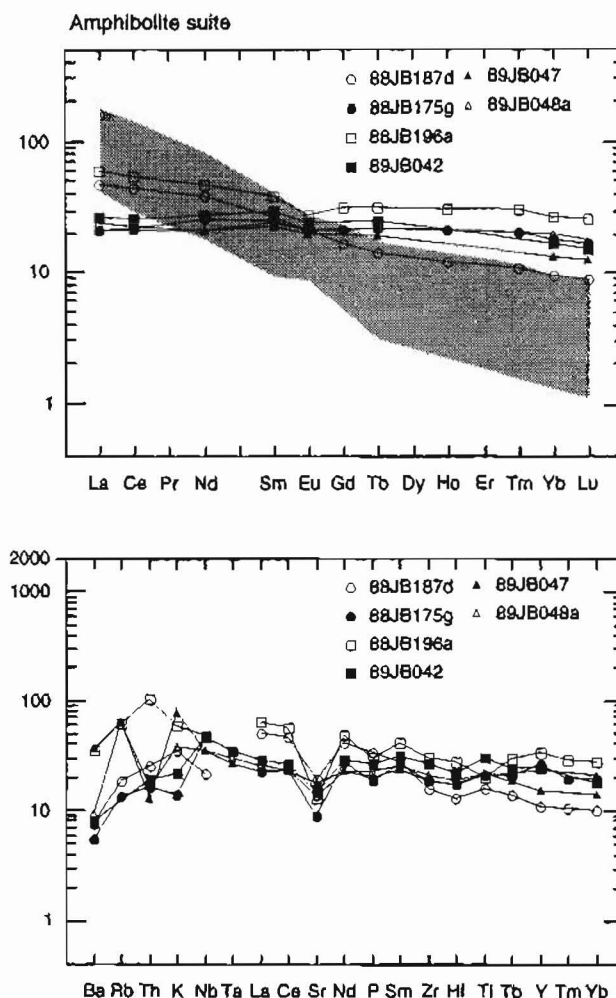
**Figure 6.** REE plots for rocks from the granite gneiss suite. Shaded area on the lower diagram shows the field for granites in the upper diagram. Diagrams drawn using the program of Wheatley and Rock (1988).

ite gneiss suite and form at least three groups that are chemically distinct from each other. Only sample 88JB187d, which was taken from a mafic layer in a tonalite gneiss, appears to be related to the tonalite gneiss suite. It has a Nd model age of 2.06 Ga and a REE pattern with similar HREE contents but lower LREE contents than nearby rocks in the tonalite gneiss suite (fig. 8). Sample 88JB196a is only slightly less siliceous than the most mafic tonalite gneiss but has considerably less  $Al_2O_3$  and Sr and more  $TiO_2$  and total Fe than sample 88JB187d. The other amphibolite samples are iron-rich tholeiites. The tholeiitic samples and sample 88JB196a

have flat or near-flat REE patterns and therefore give unreliable Nd model ages (table 4). The age of these amphibolites is unknown. In the field, the amphibolites appear to intrude rocks of the tonalite gneiss suite, and we presume that most of the amphibolites are younger than the tonalite gneiss suite. However, the various types of



**Figure 7.** Spidergram plots for data from the granite gneiss suite. Most of the rocks have negative Nb and Ta anomalies relative to the alkali elements (Ba, Rb, Th, and K) and the LREE (La, Ce). Ta contents in samples with the prefix 88JB are not shown because they are elevated relative to Nb owing to contamination from a tungsten-carbide shatterbox. The tonalite and granite gneiss suites show higher alkali and LREE contents relative to Nb and Ta on spidergrams; this is the characteristic pattern of subduction-related magmas.



**Figure 8.** REE and spidergram plots of amphibolites from the Kilbuck terrane. Shaded area shows field for tonalite gneiss from figure 5 for comparison. All of the amphibolites, except 88JB187d, have flat REE patterns and higher HREE contents than those of the dominant tonalite gneiss suite. In addition, these amphibolites do not have negative Nb and Ta anomalies. For these reasons, the amphibolites appear to be chemically and isotopically unrelated to the dominant tonalite gneiss suite with the possible exception of one sample, 88JB187d, which is LREE enriched and has a small Nb anomaly. This sample may be a more mafic part of the tonalite gneiss suite. Ta contents in samples with the prefix 88JB are not shown because they are elevated relative to Nb owing to contamination from a tungsten-carbide shatterbox. Uncontaminated Ta contents are usually about the same as Nb contents on normalized spidergrams. REE and spidergram diagrams were made using the program of Wheatley and Rock (1988).

amphibolite may be dikes or sills that were intruded at different times.

Recent map, gravity, and magnetic data indicate that the Kilbuck terrane is a shallow, isolated sliver of old continental-margin arc crust that does not extend beneath the adjacent Paleozoic to Mesozoic oceanic terranes and does not form the basement in this region (Box and others, 1991). Our preliminary Sr and Nd isotope data on latest Cretaceous and Tertiary plutonic and volcanic rocks confirm this interpretation because none of the young rocks show evidence for interaction with Precambrian crust

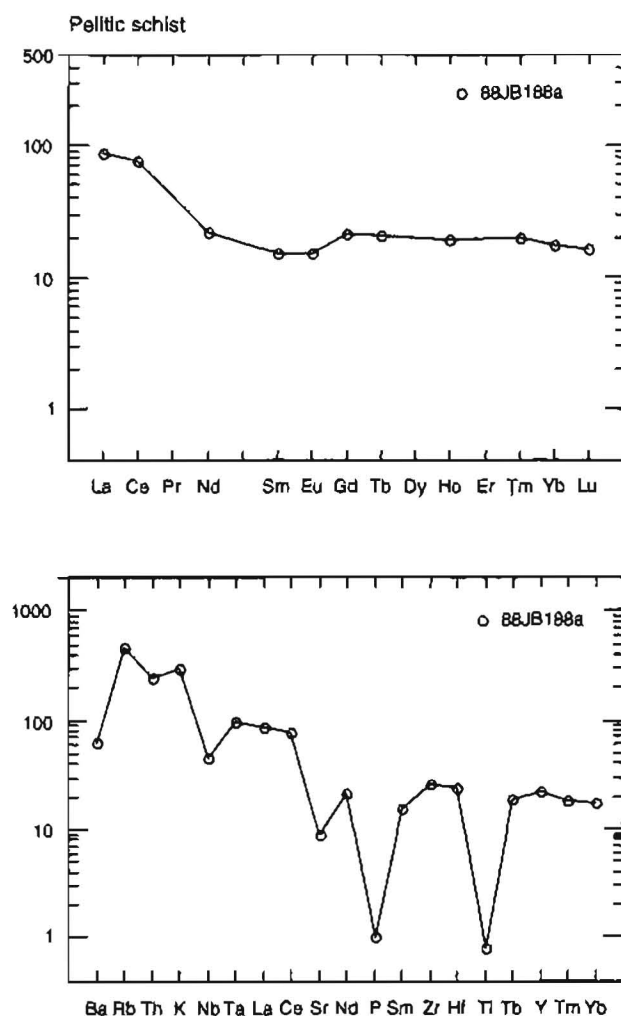
having very low  $\epsilon_{Nd}$  like the Kilbuck terrane (figs. 11, 13).

The similarity in U-Pb zircon ages, Nd model ages, rock types, and metamorphic grade suggest that the Kilbuck terrane is correlative with the Idono complex (Miller and others, 1991), about 250 km to the northeast (fig. 1). The two terranes were probably offset from each other along strike-slip faults, but the original location of either the Kilbuck terrane or the Idono complex is unknown. There are no known rocks that have both U-Pb zircon and Nd model ages of about 2 Ga in the North American Cordillera (R.R. Parrish, oral commun., 1990). In the Canadian Cordillera, rocks that have 2-Ga zircon ages have older Nd model ages, and those that have 2-Ga Nd model ages have younger U-Pb zircon ages (Parrish, 1990, 1991). Possible Precambrian terranes are known in the Russian Far East, but none have been dated by U-Pb methods. Some workers have suggested that the Kilbuck terrane may be displaced from Asia and may be correlative with the Omolon terrane in northeastern Russia (W.J. Nokleberg, oral commun., 1994), but the Omolon terrane has a much wider variety of rock types and ages compared with the Kilbuck terrane (Nokleberg and others, 1994).

## CONCLUSIONS

The isotopic data clearly indicate that most of the Kilbuck terrane (diorite, tonalite, and trondhjemite gneiss suite) formed as either new crust or rapidly recycled crust at about 2 Ga. Most of the Kilbuck terrane has a major and trace element composition that is compatible with an origin in an environment like that of modern arcs. The relations between the dominant tonalite gneiss suite and the amphibolites and granite gneiss suite is uncertain. At least one of the granite gneisses formed at 2 Ga, but it interacted with Archean crust. This result suggests that the arc formed on, or near, an Archean continental margin, although only one sample was sufficiently contaminated by the Archean crust to give an Archean Nd model age. One amphibolite has a Nd model age of 2 Ga and is probably related to the tonalite gneiss suite. Other granite gneisses and amphibolites appear chemically unrelated to the tonalite gneiss suite and are probably younger. The age of metamorphism is not well established, but it may be about 1770 Ma as indicated by the U-Pb sphene age and Rb-Sr data. Alternatively, some of the granite gneisses may have been intruded at about 1770 Ma during metamorphism.

**Acknowledgments.**—Steve Box, Greg Grimsich, and Mike Mullen took part in the field studies upon which this work is based. We were helped in our interpretations of the data by an the earlier unpublished manuscript on the Kilbuck terrane by Don L. Turner, John N. Aleinikoff, and C.E. Hedge.



**Figure 9.** REE and spidergram plots for a sample of pelitic schist from the Kilbuck terrane. This rock type is fairly rare in the Kilbuck terrane. The sample has relatively low REE contents and is LREE enriched. The sample was unfortunately powdered in a tungsten-carbide shatterbox, and its elevated Ta content is probably the result of contamination. Uncontaminated Ta contents are usually about the same as Nb contents on normalized spidergrams. Nb is lower than normalized alkali and LREE contents, indicating that the rock probably has a negative Nb-Ta anomaly.



Table 3. U-Pb data for the Kilbuck terrane

Sample <sup>1</sup>		U, ppm <sup>2</sup>	Pb, ppm <sup>2</sup>	Atomic ratios <sup>3</sup>		Ages, Ma <sup>4</sup>				Measured	
				Pb <sup>206</sup> / U <sup>238</sup>	Pb <sup>207</sup> / U <sup>235</sup>	Pb <sup>207</sup> / Pb <sup>206</sup>	Pb <sup>206</sup> / U <sup>238</sup>	Pb <sup>207</sup> / U <sup>235</sup>	Pb <sup>207</sup> / Pb <sup>206</sup>	Pb <sup>206</sup> / Pb <sup>204</sup>	Pb <sup>208</sup> / Pb <sup>206</sup>
<b>87SB125b</b>	<b>zircon</b>										
NM+102	343	127	0.34209	5.9657	0.12648	1897	1971	2050	10870	0.1276	
NM-63	240	93	.35886	6.2913	.12715	1977	2017	2059	12660	.1322	
NM63-102	278	105	.35089	6.1470	.12706	1939	1997	2058	16230	.1215	
<b>88JB177a</b>	<b>zircon</b>										
NM+163	202	80	.35740	6.2641	.12712	1970	2013	2059	14970	.1647	
M+163	176	70	.35631	6.2501	.12722	1965	2011	2060	13370	.1639	
M 63-102	176	71	.35657	6.2554	.12724	1966	2012	2060	4968	.1812	
<b>88JB204a</b>	<b>zircon</b>										
NM 102-163	132	50	.33160	5.8090	.12705	1846	1948	2058	5525	.1799	
NM-63	155	60	.33687	5.8990	.12700	1872	1961	2057	7692	.1937	
M +163	126	48	.33120	5.8157	.12735	1844	1949	2062	1613	.1999	
M 63-102	143	58	.33485	5.8621	.12697	1862	1956	2057	725	.2270	
<b>88ML022b</b>	<b>zircon</b>										
NM R7	386	122	.28387	4.8445	.12377	1611	1793	2011	1715	.1470	
NM R8	726	214	.26590	4.4977	.12268	1520	1731	1996	2645	.1552	
NM R9	1589	330	.19283	3.1690	.11919	1137	1450	1944	2139	.1193	
<b>DT-75-86</b>	<b>zircon</b>										
+150	375	117	.28367	4.9360	.12620	1610	1808	2046	5224	.1432	
-150+200	403	129	.29226	5.0879	.12626	1653	1834	2046	13674	.1432	
-325	414	132	.29001	5.0474	.12623	1642	1827	2046	33205	.1523	
<b>DT-75-86</b>	<b>sphene</b>										
+150	8.4	16.7	.31205	4.6671	0.10847	1751	1761	1773	28.322	1.660	

<sup>1</sup> NM (nonmagnetic) and M (magnetic) splits at 1.7 A on a Franz Isodynamic separator. Sizes are in micrometers. Sample 88ML022b is a bulk-size fraction split into increasingly more nonmagnetic fractions.

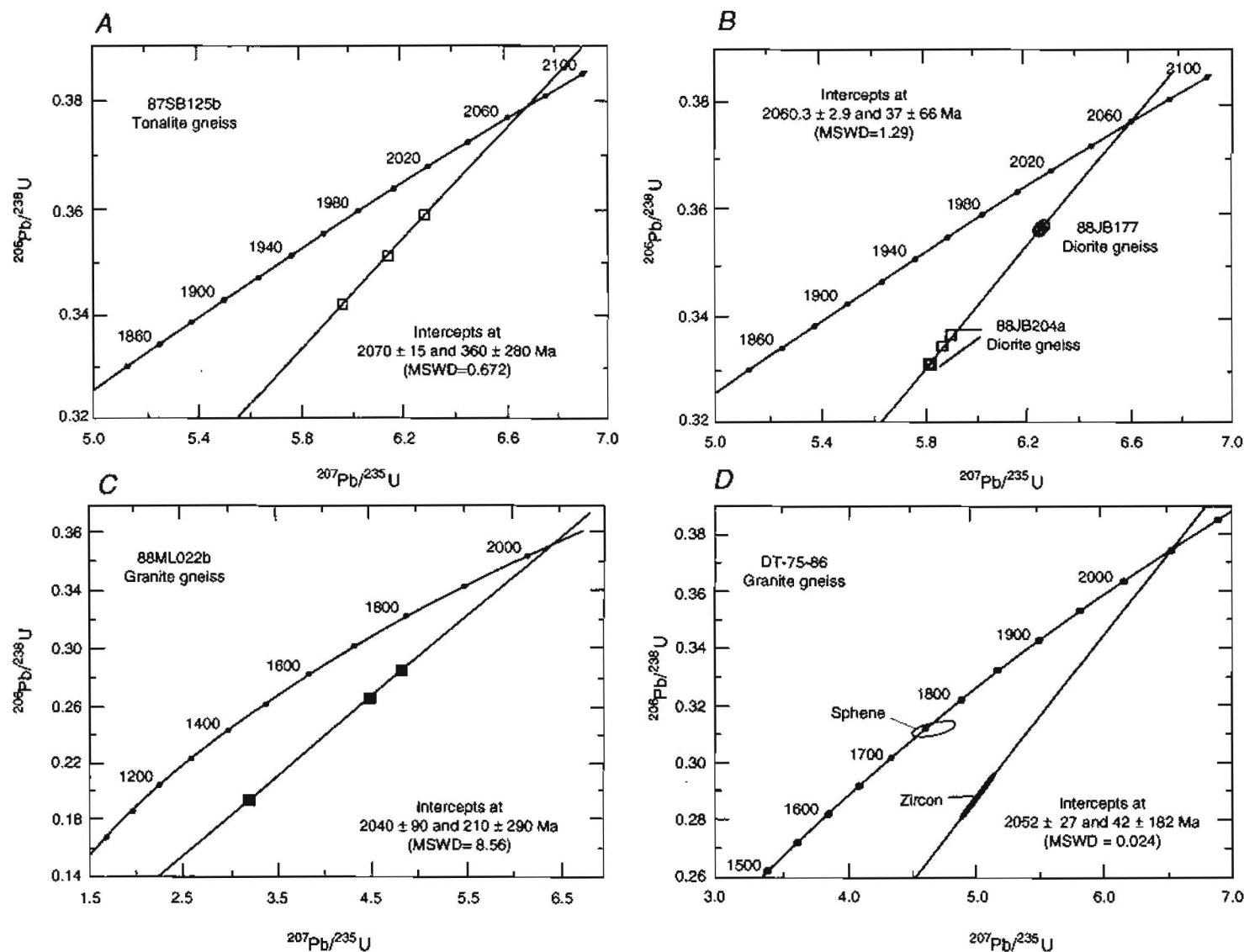
<sup>2</sup> U and Pb concentrations for total element determined on an aliquot of dissolved sample using a mixed <sup>235</sup>U-<sup>208</sup>Pb spike.

<sup>3</sup> Atomic ratios corrected for analytical blank (0.3 ng Pb and 0.01 ng U) and common Pb using measured <sup>206</sup>Pb/<sup>204</sup>Pb and Pb isotopic composition from Stacey and Kramers (1975) for an age of 2100 Ma. Measured Pb isotopic ratios corrected for 0.10 percent per mass unit fractionation. All isotopic ratios measured in static mode on a multicollector Finnigan-Mat mass spectrometer in the Pb lab at USGS, Menlo Park, Calif. except for sample DT-75-86 measured on a single collector NBS 12-in. mass spectrometer at the USGS lab in Denver, Colo.

<sup>4</sup> Ages calculated using the decay constants and <sup>238</sup>U/<sup>235</sup>U recommended by Steiger and Jäger (1977).

## REFERENCES CITED

- Arndt, N. T., and Goldstein, S.L., 1987, Use and abuse of crust-formation ages: *Geology*, v. 15, p. 893-895.
- Baedecker, P.A., ed., 1987, *Methods for geochemical analysis*: U.S. Geological Survey Bulletin 1770, 132 p.
- Barker, Fred, 1979, *Trondhjemite, dacites, and related rocks*: New York, Elsevier Scientific Publications, 659 p.
- Bowring, S.A., and Podosek, F.A., 1989, Nd isotopic evidence from Wopmay Orogen for 2.0-2.4 Ga crust in western North America: *Earth and Planetary Science Letters*, v. 94, p. 217-230.
- Box, S.E., Moll-Stalcup, E.J., Wooden, J.L., and Bradshaw, J.Y., 1991, Kilbuck terrane: oldest known rocks in Alaska: *Geology*, v. 18, p. 1219-1222.
- DePaolo, D.J., 1981, Neodymium isotopes in the Colorado Front Range and crust-mantle evolution in the Proterozoic: *Nature*, v. 291, p. 193-196.
- Hanson, G.N., Catanzaro, E.J., and Anderson, D.H., 1971, U-Pb ages from sphene in a contact metamorphic zone: *Earth and Planetary Science Letters*, v. 12, p. 231-237.
- Hawkesworth, C.J., Gallagher, K., Hergt, J.M., and McDermott, F., 1993, Mantle and slab contributions in arc magmas: *Annual Review of Earth and Planetary Sciences*, v. 21, p. 175-204.
- Hoare, J.M., and Coonrad, W.L., 1961, *Geologic map of the Goodnews quadrangle, Alaska*: U.S. Geological Survey Miscellaneous Geologic Investigations Map I-339, scale 1:250,000.
- , 1979, The Kanektok metamorphic complex, a rootless



**Figure 10.** U-Pb concordia plots for zircon samples from the tonalite gneiss suite and the granite gneiss suite. *A*, A trondhjemitic gneiss yields an independent age of 2070±15 Ma. *B*, Two tonalitic gneisses have insufficient spread in their Pb-U ratios to yield an age, but together they give an age of 2060.3±3 Ma. *C*, Granite gneiss gives an age of 2040±90 Ma, but this age is more discordant than the other ages. *D*, An additional age run in another lab (sample DT-75-86) gives an age of 2052±27 Ma. A sphene from the same sample give an age of 1770 Ma. The zircon and sphene ages shown in part *D* were cited by Turner and others (1983); data are given in table 3.

Table 4. Nd isotope data and model ages for the Kilbuck terrane

Sample no.	Sm, <sup>1</sup> ppm	Nd, <sup>1</sup> ppm	<sup>147</sup> Sm/ <sup>144</sup> Nd	<sup>143</sup> Nd/ <sup>144</sup> Nd <sub>m</sub> (Measured)	Mass spectrometer precision	f Sm/Nd	T CHUR	E <sub>Nd(0)</sub>	E <sub>Nd(t)</sub>
Tonalitic gneiss									
88JB177a	7.6	40.4	0.1133	0.51162	0.000008	-0.4237	1854	-19.82	1.73
88ML020	6.0	33.7	.1078	.51157	.000008	-0.4518	1831	-20.88	2.1
88JB204a	5.7	32.5	.1054	.51154	.000005	-0.4639	1830	-21.42	2.18
88JB186b	5.3	29.4	.1090	.51156	.000006	-0.4456	1871	-21.04	1.63
87SB125b	1.9	11.7	.0997	.51149	.000010	-0.4926	1792	-22.32	2.74
Granitic gneiss									
88JB181e	5.0	29.1	.1041	.51151	.000006	-0.4706	1858	-22.07	1.87
88JB197b	8.5	71.9	.0713	.51098	.000009	-0.6371	2011	-32.35	0.06
88JB200a	5.6	35.9	.0938	.511356	.000009	-0.523	1895	-25.01	1.6
88ML022b	2.9	16.1	.1094	.51119	.000006	-0.4435	2522	-28.29	-5.73
Amphibolites									
88JB187d	5.6	25.7	.1321	.511857	.000009	-15.24	1842	-15.24	1.44
88JB175g	5.3	16.9	.1910	.51292	.000007	-0.0283	-7884	5.46	6.9
88JB196a	8.2	30.5	.1621	.512563	.000010	-0.1754	334	-1.47	7.45

<sup>1</sup> Sm and Nd analyses by isotope dilution mass spectrometry. Precision is less than 0.5 percent.

- belt of Precambrian rocks in southwestern Alaska, in Johnson, K.M., and Williams, J.R., eds., *The United States Geological Survey in Alaska: Accomplishments during 1978: U.S. Geological Survey Circular 804-B*, p. 72-74.
- Krogh, T. E., 1973, A low-contamination method for hydrothermal decomposition of zircon and extraction of U and Pb for isotopic age determination: *Geochimica et Cosmochimica Acta*, v. 37, p. 485-494.
- Liew, T.C. and McCulloch, M.T., 1985, Genesis of granitoid batholiths of peninsular Malaysia and implications for models of crustal evolution: evidence from a Nd-Sm isotopic and U-Pb zircon study: *Geochimica et Cosmochimica Acta*, v. 49, p. 587-600.
- Miller, M.L., Bradshaw, J.Y., Kimbrough, D.L., Stern, T.W., and Bundtzen, T.K., 1991, Isotopic evidence for early Proterozoic age of the Idono Complex, west-central Alaska: *Journal of Geology*, v. 99, p. 209-223.
- Nokleberg, W.J., Moll-Stalcup, E.J., Miller, T.P., Jr., Brew, D.A., Grantz, Arthur, Reed, J.C., Jr., Plafker, George, Moore, T.E., Silva, S.R., and Patton, W.W., Jr., 1994, Tectonostratigraphic terrane and overlap assemblage map of Alaska: U.S. Geological Survey Open-File Report 94-194, 54 p., 1 sheet, scale 1:2,500,000.
- Norton, D.R., and Papp, C.S., 1990, Determination of moisture and total water in silicate rocks, in Arbogast, B.F., ed., *Quality assurance manual for the Branch of Geochemistry: U.S. Geological Survey Open-File Report 90-668*, p. 73-82.
- Papp, C.S.E., Aruscavage, P., and Brandt, E., 1990, Determination of ferrous oxide in geologic materials by potentiometric titration, in Arbogast, B.F., ed., *Quality assurance manual for the Branch of Geochemistry: U.S. Geological Survey Open-File Report 90-668*, p. 139-145.
- Parrish, R.R., 1990, Review of the Precambrian basement of the cordillera [abs.]: Geological Association of Canada Annual Meeting Program with Abstracts, v. 15, p. A101.
- , 1991, Precambrian basement rocks of the Canadian cordillera, in Gabrielse, H., and Yorath, C.J., eds., *Geology of the Cordilleran orogen in Canada: Geological Survey of Canada, Geology of Canada*, no. 4, p. 87-96.
- Plank, Terry, and Langmuir, C.H., 1993, Tracing trace elements from sediment input to volcanic output at subduction zones: *Nature*, v. 362, p. 739-743.
- Schnetzler, C.C., and Philpotts, J.A., 1970, Partition coefficients of rare-earth elements between igneous matrix material and rock-forming mineral phenocrysts-II: *Geochimica et Cosmochimica Acta*, v. 34, p. 331-340.
- Skjerlie, K.P., and Johnston, A.D., 1993, Fluid-absent melting behavior of an F-rich tonalite gneiss at mid-crustal pressures: implications for the generation of anorogenic granites: *Journal of Petrology*, v. 34, p. 785-815.
- Stacey, J.S., and Kramers, J.D., 1975, Approximation of terrestrial lead evolution by a two-stage model: *Earth and Planetary Science Letters*, v. 26, p. 207-221.
- Steiger, R.H., and Jäger, E., 1977, Subcommittee on geochronology: convention on the use of decay constants in geo-

and cosmochemistry: *Earth and Planetary Science Letters*, v. 36, p. 359–362.

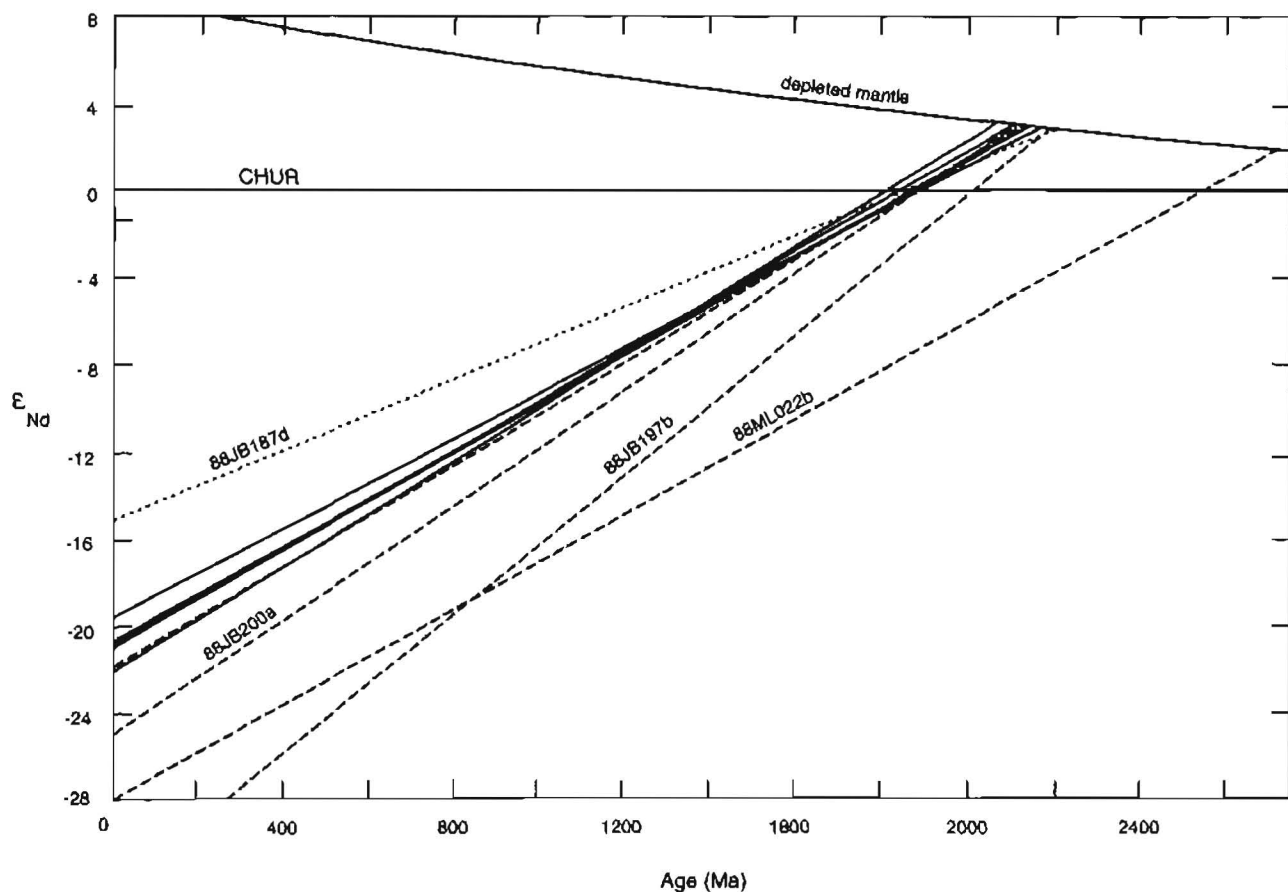
Taggart, J.E., Jr., Bartel, A., and Siems, D.F., 1990, High precision major element analyses of rocks and minerals by wavelength dispersive X-ray fluorescence spectroscopy, in Arbogast, B.F., ed., *Quality assurance manual for the Branch of Geochemistry*; U.S. Geological Survey Open-File Report 90-668, p. 166–172.

Thompson, R.N., 1982, Magmatism of the British Tertiary volcanic province; *Scottish Journal of Geology*, v. 18, p. 49–107.

Turner, D.L., Forbes, R.B., Aleinikoff, J.N., Hedge, C.E., and McDougall, I., 1983, Geochronology of the Kilbuck terrane in southwestern Alaska [abs.]; *Geological Society of America Abstracts with Programs*, v. 15, p. 407.

Wheatley, M.R., and Rock, N.M.S., 1988, Spider: a Macintosh program to generate normalized multi-element "spidergrams"; *American Mineralogist*, v. 73, p. 919–921.

Reviewers: Robert Ayuso and Steve Box.



**Figure 11.** Plot showing Nd model ages for rocks from the Kilbuck terrane. Solid lines are rocks from the tonalite gneiss suite, dashed lines are rocks from the granite gneiss suite, and dotted lines are for an amphibolite. The tonalite gneiss suite samples, two samples from the granite gneiss suite, and the one sample of amphibolite have depleted mantle model ages (2.05–2.2 Ga) similar to their U-Pb zircon ages. These rocks probably represent newly formed crust generated from the mantle at about 2 Ga. One granitic gneiss sample (88ML022b) has a much older Nd model age (depleted mantle model age of about 2.7 Ga), although it gave a zircon U-Pb age of 2.04 Ga, similar to the other samples. The old model age indicates that the rock formed at least partly from preexisting Archean crust. The most likely mechanisms would either be partially melted Archean crust or contamination of a more mafic parent magma by Archean crust. The depleted mantle curve is from DePaolo (1981). Abbreviation: CHUR, chondritic uniform reservoir.

## APPENDIX 1. PETROGRAPHIC DESCRIPTIONS OF ANALYZED SAMPLES

### Tonalite gneiss suite:

Sample 88JB177a: Pyroxene diorite gneiss. Distinctive coarse-grained, weakly foliated and lineated rock with a partly recrystallized relict igneous texture. Composed predominantly of plagioclase, clinopyroxene, hornblende, biotite, and minor garnet. Contains trace opaque oxides, quartz, and apatite. Pyroxene locally replaced by hornblende and biotite; biotite locally intergrown with garnet. Reaction between biotite and plagioclase has locally produced fine-grained garnet.

Sample 88JB181d: Streaky hornblende-biotite-plagioclase dioritic gneiss.

Sample 88ML020: Hornblende-biotite gneiss. Strongly deformed showing undulous and recrystallized quartz. Feldspars show some remnant albite twinning. Contains minor epidote, sphene and chlorite.

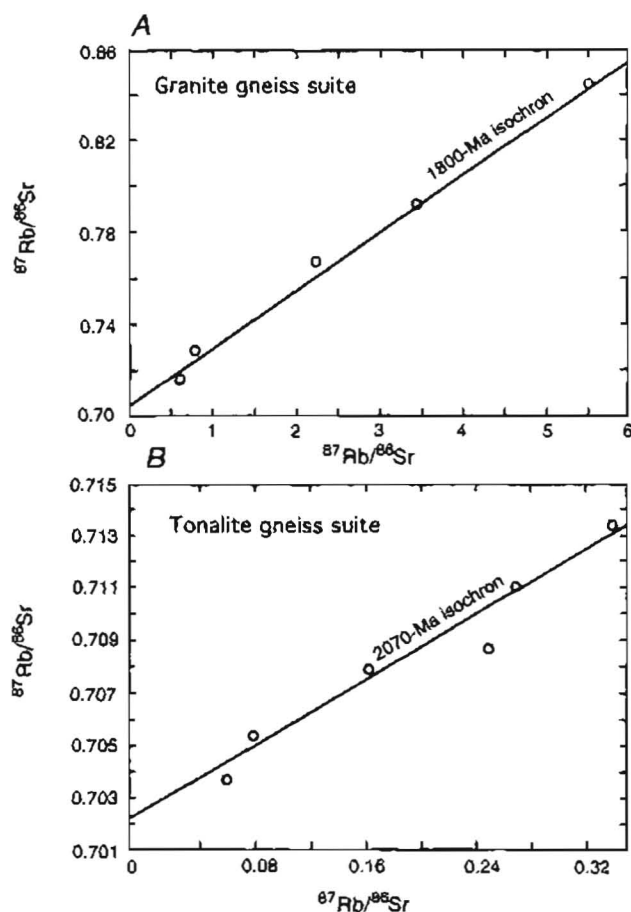


Figure 12. Sr isotope data for rocks of the Kilbuck terrane. A, Plot for the granite gneiss suite, shown with an 1800-Ma isochron. B, Plot for the tonalite gneiss suite, shown with a 2070-Ma reference isochron. Both data sets have too much scatter to yield reliable isochron ages, either because the rocks did not have a uniform isotopic composition at formation or because their Rb/Sr ratios were disturbed during metamorphism.

Sample 88JB178b: Dark gray, medium- to fine-grained hornblende-biotite diorite gneiss.

Sample 82SB018a: Biotite-hornblende-quartz-potassium feldspar-plagioclase granodiorite gneiss. Displays weak foliation defined by thin layers enriched in hornblende and biotite.

Sample 88SB074c: Tonalitic gneiss. Displays ductily deformed elongate quartz.

Sample 88JB204a: Hornblende-biotite dioritic gneiss. Streaky, well lineated. Contains minor K-feldspar.

Sample 87SB125b: Biotite trondhjemite gneiss. Contains quartz having undulatory extinction and plagioclase with remnant albite twinning. Contains trace interstitial K-feldspar, zircon, apatite, chlorite, and zoisite.

Sample 88ML021: Biotite trondhjemite gneiss. Composed of 5 percent biotite, 45 percent plagioclase, 35 percent quartz, and 10-15 percent K-feldspar. Contains minor epidote.

Sample 88JB186b: Biotite-plagioclase granodiorite gneiss. Light colored, well foliated, scaly.

Sample 88ML025: Trondhjemite gneiss. Composed of twinned plagioclase, quartz, biotite, muscovite, epidote, calcite, and magnetite. Granoblastic or weakly aligned quartz and feldspar. Contains trace potassium feldspar.

### Granite gneiss suite:

88JB181e: Pink leucogranitic vein. Composed dominantly of quartz, plagioclase, potassium feldspar, biotite, epidote, and muscovite. Contains trace sphene and zircon.

88JB197b: Lineated and foliated pink medium-grained muscovite-biotite granite gneiss. Composed dominantly of quartz,

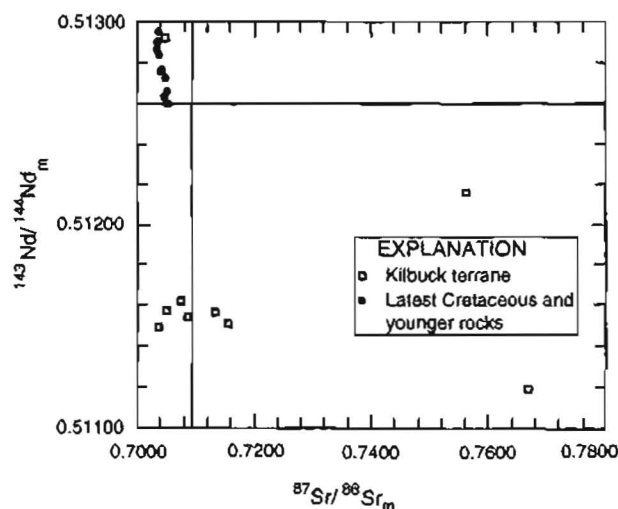


Figure 13. Measured (m)  $^{87}\text{Sr}/^{86}\text{Sr}$  and  $^{143}\text{Nd}/^{144}\text{Nd}$  ratios for rocks from the Kilbuck terrane and for latest Cretaceous and younger magmatic rocks from the surrounding region. The young magmatic rocks do not appear to be contaminated by crust having the isotopic composition of the Kilbuck terrane because the Kilbuck rocks have much lower  $^{143}\text{Nd}/^{144}\text{Nd}$  ratios. None of the younger rocks have  $^{143}\text{Nd}/^{144}\text{Nd}$  values that exceed those produced from oceanic mantle. These data support the model that the Kilbuck terrane is an isolated crustal sliver and not a terrane that underlies an extensive area in southwestern Alaska.



Table 5. Sr isotope data for the Kilbuck terrane

Sample no.	Unit	Rb, <sup>1</sup> ppm	Sr, <sup>1</sup> ppm	<sup>87</sup> Rb/ <sup>86</sup> Sr	<sup>87</sup> Sr/ <sup>86</sup> Sr <sup>2</sup> (Measured)	Mass spectrometer precision <sup>3</sup>	Age, Ma <sup>4</sup>	Initial <sup>87</sup> Sr/ <sup>86</sup> Sr
88JB187d	amphibolite	6.29	222.32	0.0818	.70981	0.000011	2060	0.70738
88JB175g	amphibolite	4.58	104.35	.1269	.70483	.000012	2060	.70106
88JB196a	amphibolite	20.93	151.1	.4009	.71345	.000010	2060	.70155
88JB177a	tonalitic gneiss	56.36	1000.24	.1630	.70761	.000013	2060	.70277
88ML020	tonalitic gneiss	29.35	1073.33	.0791	.70514	.000012	2060	.70279
88JB204a	tonalitic gneiss	59.83	695.85	.2487	.70864	.000012	2060	.70126
88ML021	tonalitic gneiss	39.74	425.61	.2702	.71081	.000012	2060	.70279
88JB186b	tonalitic gneiss	51.9	429.65	.3493	.71344	.000012	2060	.70307
87SB125b	tonalitic gneiss	22.03	1074.98	.0593	.70363	.000012	2060	.70187
88JB181e	granitic gneiss	54.19	263.31	.5952	.71578	.000011	1800	.70037
88JB197b	granitic gneiss	88.36	328.36	.7786	.72855	.000012	2060	.70544
88JB200a	granitic gneiss	135.99	114.66	3.4300	.79150	.000011	1800	.70270
88ML022b	granitic gneiss	144.07	187.18	2.2259	.76691	.000011	2060	.70084
88JB203a	granitic gneiss	164.93	86.62	5.5066	.84452	.000015	1800	.70196
88JB188a	metapelite	162.99	102.64	4.5924	.75613	0.000016	850	.70036

<sup>1</sup>Rb and Sr analyses by isotope dilution mass spectrometry. Precision is less than 0.5 percent.

<sup>2</sup>Sr isotopic ratios normalized to <sup>87</sup>Sr/<sup>86</sup>Sr=0.11940. NBS SRM987 gave a value of 0.710240 on runs during the year (1989).

<sup>3</sup>Precision of mass spectrometry on an individual sample reported as 2 sigma of the mean.

<sup>4</sup>Ages used for calculation of initial ratios are not necessarily the age of the rocks and were chosen as follows: 2060, average of all U-Pb zircon ages; 1800, age of reference isochron for granite used in cases where initial Sr ratio is too low using 2060; 850, age at which initial Sr ratio exceeds 0.7000. See text for more explanation.

plagioclase, potassium feldspar, muscovite, biotite, and epidote. Contains minor calcite, sphene, and apatite.

88JB200a: Pink, medium-grained biotite granite gneiss. Composed dominantly of quartz, plagioclase, potassium feldspar, and biotite. Well-developed lineation defined by biotite. Contains trace muscovite, sphene, opaque oxides, zircon, garnet, chlorite, apatite and allanite.

88ML022a: Pink leucogranitic vein in granitic gneiss (88ML22b). Consists almost entirely of quartz (50 percent), plagioclase, and K-feldspar. Rare coarse-grained biotite is recrystallized to fine-grained biotite along the grain boundaries. Sparse muscovite also present.

88ML022b: Pinkish granitic gneiss. Composed chiefly of muscovite, quartz, K-feldspar, and biotite. Contains some skeletal garnet and trace epidote. Quartz is strained and elongate parallel to the foliation defined by the micaceous layers.

88JB203a: Equigranular, pinkish-yellow leucogranitic gneiss. Composed dominantly of quartz, plagioclase, and potassium feldspar. Contains sparse biotite and trace muscovite.

88JB185a: Medium-grained leucogranite pink granite gneiss. Composed dominantly of quartz, plagioclase, and potassium feldspar; and trace muscovite, biotite, garnet, sphene and zircon.

88JB198a: Muscovite-rich granite gneiss. Leucocratic, light colored, and well foliated. Composed dominantly of quartz, plagioclase, muscovite, epidote/clinozoisite, sphene, and zircon. Contains trace garnet and apatite.

87SB125a: Muscovite granitic gneiss. Contains strained quartz, plagioclase having remnant albite twinning, and K-feldspar having microcline twinning. Minor biotite, zoisite, chlorite,

apatite, and zircon also present.

88JB046d: Biotite granodiorite-granite gneiss.

89JB046f: Coarse-grained biotite granite gneiss with pink potassium feldspar.

89JB054: Lineated pink granite gneiss with muscovite and minor biotite.

89JB102: Very coarse grained augen gneiss that has pink augen about 1 cm across.

#### **Amphibolite:**

88JB187d: Well-foliated and lineated coarse-grained hornblende-garnet-plagioclase amphibolite from a mafic layer within the dioritic suite. Contains streaky, lineated clots of garnet and quartz. Much coarser grained and feldspar rich than the other amphibolites.

88JB175g: Fine-grained hornblende-garnet-clinopyroxene-quartz amphibolite collected from distinct podlike body. Very dense rock.

88JB196a: Medium-grained hornblende-garnet-quartz-plagioclase amphibolite from layer within complex sequence of diorite gneiss, granitic gneiss, and pyroxene gneiss. Coarser grained and more felsic than 88JB175g.

89JB042: Garnet amphibolite. Contains hornblende and sphene.

89JB047: Garnet amphibolite. Lineated hornblende-rich rock containing minor garnet, plagioclase, epidote, and sphene.

89JB048a: Garnet clinopyroxene amphibolite. Lineated rock with high-pressure mineral assemblage.

#### **Metapelite:**

88JB188a: Garnet, muscovite, quartz, tourmaline, rutile, and trace plagioclase. Contains snowball garnets.

# U-Pb Zircon and Titanite Ages for Augen Gneiss from the Divide Mountain Area, Eastern Yukon-Tanana Upland, Alaska, and Evidence for the Composite Nature of the Fiftymile Batholith

By Cynthia Dusel-Bacon and John N. Aleinikoff

## ABSTRACT

Zircons from two compositional variants of augen gneiss from the Divide Mountain area in the northeastern Tanacross quadrangle of east-central Alaska yield nearly concordant U-Pb ages of  $353 \pm 4$  Ma and  $356 \pm 2$  Ma. Both samples were obtained from the western part of a 900-km<sup>2</sup> augen gneiss body named the Fiftymile batholith in Yukon Territory. This batholith is part of a southeast-trending, 400-km-long belt of megacrystic granitoids, metamorphosed and deformed to augen gneiss, that spans the Alaska-Yukon Territory international boundary. One sample is garnet-bearing hornblende-biotite augen gneiss, a very unusual composition in the belt, and the other is biotite-muscovite augen gneiss that is typical of most augen gneiss bodies in the belt. In Alaska, the augen gneiss bodies are a diagnostic element of the Lake George subterrane of the Yukon-Tanana terrane.

U-Pb systematics and the presence of visible xenocrystic cores within many zircon grains confirm the presence of a significant inherited Precambrian component; this is the case with all of the Alaskan samples of orthogneiss and many, but not all, of those in Yukon Territory. U-Pb zircon analyses made by other workers of a sample of biotite-muscovite augen gneiss from the eastern part of the Fiftymile Batholith indicate a U-Pb upper intercept age of  $364 \pm 4$  Ma, interpreted as an emplacement age, and only a limited inherited xenocrystic zircon component. This slightly older age from the eastern part of the batholith suggests that intrusion of the Fiftymile Batholith may have begun as early as 368 Ma (maximum age of uncertainty range determined for the sample from the eastern part of the batholith) and continued to as late as 349 Ma (minimum age of uncertainty range determined for the younger of the samples from the Divide Mountain area). This potentially long interval for crystallization, together with the difference in the degree of inheritance between samples from the western and eastern parts of the batholith and the range in composition illustrated by

the two samples of our study, suggest that the batholith was probably intruded in multiple stages, from slightly differing sources, and hence may be composite. <sup>206</sup>Pb/<sup>238</sup>U data on titanite from one of our gneiss samples indicate that it cooled through about 600°C at 135 Ma. We interpret this cooling to have occurred during the final stages of Mesozoic metamorphism of the batholith, specifically during a widespread mid-Cretaceous episode of ductile deformation and southeast-directed extension. This extension has been proposed to have resulted in the exhumation of the Yukon-Tanana terrane from beneath allochthonous terranes that were emplaced in latest Early to early Middle Jurassic time.

## INTRODUCTION

Batholith-sized bodies of augen gneiss compose a 400-km-long, southeast-trending belt that spans the Alaska-Yukon Territory international boundary (Dusel-Bacon and Aleinikoff, 1985; Mortensen and Jilson, 1985). These bodies are a diagnostic element of the Lake George subterrane of the Yukon-Tanana terrane in east-central Alaska (Dusel-Bacon and Hansen, 1992). They also form part of an even more extensive mid-Paleozoic magmatic belt that extends for 5,000 km along the length of the North American Cordillera (Rubin and others, 1990). Crystallization ages of plutons from the extensive Cordilleran belt range from Late Devonian to Early Mississippian, and isotopic signatures and Proterozoic U-Pb upper intercept (inheritance) ages imply that basement was composed of both continental crust and transitional or oceanic crust overlain by continent-derived sedimentary rocks (Rubin and others, 1990).

The purpose of our U-Pb study was to determine the crystallization ages and assess the amount and average age of inheritance of the granitoid protoliths of two compositionally distinct samples of augen gneiss (one hornblende-biotite-garnet bearing and the other biotite-

muscovite bearing) from different localities in the Divide Mountain area of the northeastern Tanacross  $1^{\circ} \times 3^{\circ}$  quadrangle. We also hoped to determine a U-Pb age on titanite that would provide a high-temperature ( $\sim 600^{\circ}\text{C}$ ) metamorphic cooling age for the rocks of the Lake George subterrane in the Divide Mountain area. These augen gneiss samples are part of a  $900\text{-km}^2$  augen gneiss body that has been referred to as the Fiftymile batholith in Yukon Territory (Tempelman-Kluit and Wanless, 1980).

Zircons from one of the samples from this study (14C) were previously dated in an earlier U-Pb study that we conducted, which focused primarily on dating a body of augen gneiss in the Big Delta quadrangle about 170 km to the northwest of our study area (Aleinikoff and others, 1986). This previous attempt to determine the crystallization age of the granitoid protoliths (discussed in a subsequent section) was hampered by large amounts of inherited radiogenic lead that resulted in highly discordant ages and by our reliance on extrapolation to lower intercept ages (Aleinikoff and others, 1986). In order to arrive at more accurate crystallization ages for the two augen samples in the Divide Mountain area, we used an improved zircon selection and preparation procedure in which we analyzed only hand-picked zircon fractions that were devoid of visible xenocrystic cores and abraded all fractions in order to remove possible overgrowths or damaged areas.

Using these more accurate crystallization ages, we could then compare the crystallization ages and pattern of inheritance for our two samples with each other, with other U-Pb ages from gneiss mapped as part of the Fiftymile Batholith in Yukon Territory, and with other nearby bodies. Our new data thus help characterize the mid-Paleozoic magmatic event in east-central Alaska and adjacent parts of Yukon Territory.

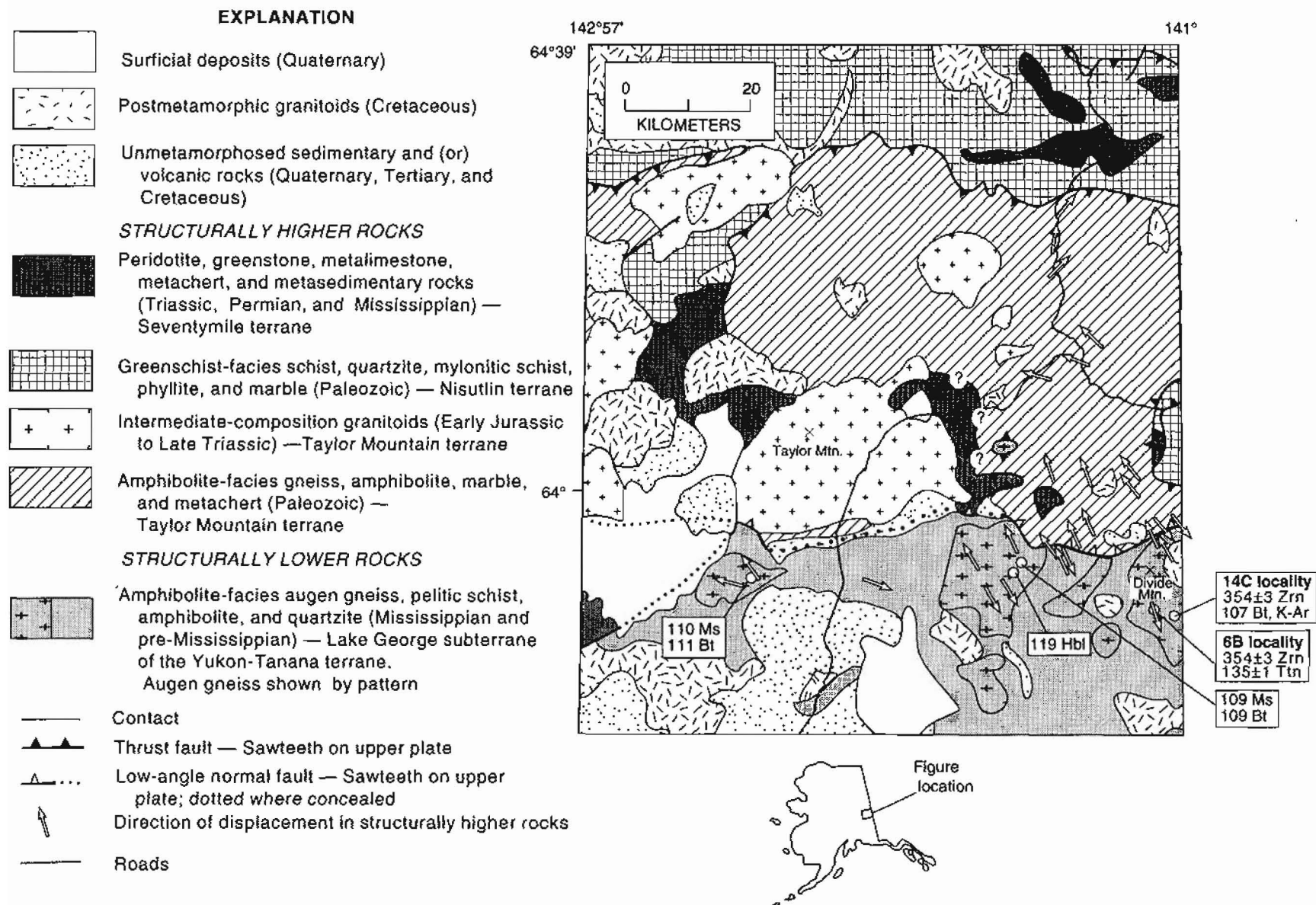
## REGIONAL GEOLOGIC SETTING

The augen gneisses in the Divide Mountain area form part of the Lake George subterrane of the Yukon-Tanana terrane. This subterrane comprises amphibolite-facies quartz-biotite schist and gneiss, augen gneiss, pelitic schist, garnet amphibolite, and quartzite, and it has been interpreted to represent a continental-margin assemblage intruded by a middle Paleozoic arc (Dusel-Bacon and Aleinikoff, 1985; Nokleberg and Aleinikoff, 1985). In the eastern Yukon-Tanana upland (fig. 1), the Lake George subterrane is structurally overlain by the Taylor Mountain terrane, an assemblage of (1) garnet amphibolite, biotite $\pm$ hornblende gneiss, marble, quartzite, metachert, and pelitic schist; (2) small masses of hornblende, metadiabase, metagabbro, pyroxenite, and serpentinitized peridotite; and (3) crosscutting granitoids of intermediate composition, including the Late Triassic to Early Jurassic

Taylor Mountain batholith (Foster, 1976; Dusel-Bacon and Hansen, 1992). Lithologic associations and isotopic data from the granitoids suggest an oceanic-arc or marginal-basin origin for the Taylor Mountain terrane (Dusel-Bacon and Hansen, 1992). Metamorphic cooling ages (K-Ar,  $^{40}\text{Ar}/^{39}\text{Ar}$ , U-Pb titanite) from the Lake George subterrane are almost entirely Early Cretaceous, whereas those from the Taylor Mountain terrane are latest Triassic to earliest Middle Jurassic (Hansen, 1990; Hansen and others, 1991; Pavlis and others, 1993). Postmetamorphic Cretaceous granitoids and unmetamorphosed Cretaceous and Tertiary sedimentary and volcanic rocks crop out in both terranes (fig. 1).

The structurally highest rocks that crop out in the eastern Yukon-Tanana upland (fig. 1) are part of a belt of fault-bounded slices of serpentinitized alpine-type peridotite, weakly metamorphosed mafic volcanic rocks, and Mississippian to Late Triassic sedimentary rocks. These rocks are assigned to the Seventymile terrane, and some of them in the Eagle quadrangle have been described as parts of a dismembered ophiolite (Foster and others, 1994). Commonly associated with the Seventymile terrane, and structurally underlying it, is a sequence of greenschist-facies, quartz-rich clastic metasedimentary rocks, mafic and intermediate metavolcanic rocks, and marble. These rocks have been variously assigned to the Nisutlin terrane (Hansen and others, 1991; see also fig. 1) or the Butte subterrane of the Yukon-Tanana terrane (Pavlis and others, 1993).

Geothermobarometry indicates that moderate- to high-pressure (7–12 kbar) amphibolite-facies conditions accompanied metamorphism of both the Taylor Mountain terrane and the structurally underlying Lake George subterrane (Dusel-Bacon and Hansen, 1992; Dusel-Bacon and others, 1995). Structural and thermochronologic data, together with the geothermobarometry, are consistent with a model in which metamorphism of the Taylor Mountain terrane and the Lake George subterrane took place during different phases of a late Paleozoic through early Mesozoic shortening episode that resulted from closure of an ocean basin (now represented by klippen of the Seventymile terrane) and collision of an outboard-arc and marginal-basin assemblage (Taylor Mountain terrane) with the ancient continental margin of western North America (Yukon-Tanana terrane) (Hansen, 1990; Hansen and others, 1991; Dusel-Bacon and Hansen, 1992). Metamorphism of the Taylor Mountain terrane began, perhaps as early as late Paleozoic time, within a southwest-dipping (present-day coordinates) subduction system that developed off the continental margin (Hansen, 1990). Continued metamorphism of the tectonites at the structural base of the obducted Taylor Mountain terrane and initial metamorphism of the underlying Yukon-Tanana terrane, including the augen gneiss bodies of this study, took place in Early to Middle Jurassic time as a result of the accretion of the



**Figure 1.** Geologic map of the northeastern Tanacross and southeastern Eagle quadrangles (modified from Dusel-Bacon and others, 1995) showing locations of dated samples; U-Pb zircon ages for emplacement of augen gneiss protoliths; titanite, hornblende, and mica metamorphic cooling ages (Ma) for rocks of the Yukon-Tanana terrane; and direction of tectonic transport of upper plate rocks (Dusel-Bacon and others, 1995; V.L. Hansen, Southern Methodist University, written commun., 1994). Mineral abbreviations: Bt, biotite; Hbl, hornblende; Ms, muscovite; Ttn, titanite; Zrn, zircon. With the exception of the Bt K-Ar age, all Bt, Ms, and Hbl ages are  $^{40}\text{Ar}/^{39}\text{Ar}$  incremental heating ages.  $^{40}\text{Ar}/^{39}\text{Ar}$  metamorphic cooling ages for Ms and Bt from Hansen and others (1991) and for Hbl from T.M. Harrison (University of California, Los Angeles, written commun., 1986, in Dusel-Bacon and others, 1995). Bt K-Ar metamorphic age from Nora Shew (U.S. Geological Survey, written commun., 1985, in Dusel-Bacon and others, 1995).  $^{206}\text{Pb}/^{238}\text{U}$  Ttn metamorphic cooling age and U-Pb Zrn crystallization ages are from this study.



outboard arc and basin and imbrication of the continental margin. The northwest-directed shear shared by the structurally lower (southern) part of the Taylor Mountain terrane and the northern Lake George subterrane (fig. 1) reflect this collisional event (Dusel-Bacon and others, 1995; V.L. Hansen, written commun., 1994). The Early Cretaceous metamorphic cooling ages that characterize the rocks of the Yukon-Tanana terrane have been proposed to date the exhumation of this previously buried lower plate during a widespread extensional event that probably was related to the development of a northeast-dipping (present-day coordinates) subduction system outboard of the continental margin (for example, Hansen and others, 1991; Dusel-Bacon and Hansen, 1992; Pavlis and others, 1993). A top-to-the-southeast fabric, documented in structural studies from several widely separated areas in the Yukon-Tanana upland (including the augen gneiss bodies shown in fig. 1), is interpreted to have developed during this extensional event (Dusel-Bacon and Hansen, 1992; Pavlis and others, 1993; Dusel-Bacon and others, 1995; V.L. Hansen, Southern Methodist Univ., written commun., 1994).

## LOCAL GEOLOGIC SETTING AND PETROGRAPHY OF DATED SAMPLES

We obtained two large (~60 kg) samples from two exposures of augen gneiss that crop out in the Divide Mountain area of the northeastern Tanacross  $1^{\circ} \times 3^{\circ}$  quadrangle during field studies conducted in 1981 and 1990. The samples differ in mineralogy and texture but occur within the same 900-km<sup>2</sup> augen gneiss body that has been referred to as the Fiftymile batholith in Yukon Territory (Tempelman-Kluit and Wanless, 1980). Both augen gneiss samples (90ADb6B, herein abbreviated 6B, and 81ADb14C, herein abbreviated 14C) were collected from large outcrops along the flat top of a southeast-trending ridge (Fig. 1). Sample 14C was collected at a site (lat  $63^{\circ}45'10''$  N., long  $141^{\circ}01'30''$  W.) located about 1 km west of the Alaska-Yukon Territory international boundary, and sample 6B at a site (lat  $63^{\circ}46'34''$  N., long  $141^{\circ}06'26''$  W.) about 5 km to the northwest of sample 14C.

The Divide Mountain area is dominantly composed of granitic orthogneiss, primarily biotite±muscovite gneiss and augen gneiss, with lesser amounts of quartz-feldspar-biotite-hornblende gneiss and augen gneiss. Locally, orthogneisses contain trace amounts of pinhead-sized garnets. The orthogneisses form shallow to moderately ( $10^{\circ}$ – $30^{\circ}$ ) (generally) north-dipping, tabular bodies that crop out along flat ridgetops. Quartz-biotite-muscovite±garnet schist, less resistant than the orthogneiss, underlies intervening saddles, where it is exposed as platy rubble and, locally, as outcrop. The gneisses are generally both foli-

ated and lineated, but locally either fabric element may be weakly developed. Folding, seen at outcrop scale at a few exposures of augen gneiss, is probably also present at larger scales. Mineral lineation trends northwest. The only kinematic data available in the Divide Mountain area indicate S.  $20^{\circ}$  E.-vergent shear (V.L. Hansen, written commun., 1994; Dusel-Bacon and others, 1995) and were determined at the outcrop from which augen gneiss sample 6B was collected.

Sample 6B was collected from a large outcrop of variably foliated, garnet-bearing hornblende-biotite augen gneiss. The augen are generally 1–2 cm in the longest dimension and range from the characteristic eye shape to strongly flattened. Sample 6B is strongly lineated but poorly foliated, in part owing to a dense packing of the K-feldspar augen. In thin section, the rock is blastomylonitic and consists of K-feldspar augen in a gneissic matrix of (in order of decreasing abundance) plagioclase, quartz, biotite, and hornblende, with accessory garnet, titanite, apatite, zircon, and a few grains of zoisite and allanite. K-feldspar occurs primarily as augen that are locally bordered by patches of myrmekite or plagioclase, but a minor amount of finer grained, 1-mm-long, subidioblastic grains of K-feldspar also are present in the matrix. Quartz shows only moderately developed undulose extinction and polygonization into subgrain domains; grain boundaries are elongate parallel to the foliation and range from straight to only moderately sutured. Quartz is mostly fine grained (0.5–1.5 mm) but locally forms larger (2.5 mm) grains aggregated into augenlike domains. Plagioclase (0.5–1.5 mm) is polysynthetically twinned and of probable oligoclase composition, based on a preliminary determination of extinction angles. Biotite forms 1–2 mm-long grains that exhibit dark-reddish-brown to tan pleochroism and define continuous and closely spaced folia. Hornblende is much less abundant than biotite and forms medium-green elongate grains that are generally 1–2 mm in length but reach a maximum of 4 mm. Garnet, although minor in abundance, is ubiquitous in thin section and forms 0.5-mm-diameter grains that are either atoll shaped, subidioblastic, or form a concentration of granules that imply a former crystal outline. Titanite, like garnet, is minor but ubiquitous and occurs as concentrations of minute (~0.25 mm long) rhombohedra adjacent to biotite or hornblende. Zircon is primarily included within biotite, where it is surrounded by dark pleochroic haloes.

Sample 14C was collected from a 15-m-high vertical face of a torlike outcrop of homogeneous augen gneiss. The augen reach a maximum of about 8 cm and average about 3–4 cm in longest dimension. The largest K-feldspar augen have preserved fairly rectangular outlines, whereas smaller augen have the characteristic eyeshape befitting the flaser texture of the gneiss. This preferential preservation of the euhedral crystal shape of the larger



megacrysts (greater than approximately 3 cm in longest dimension) is characteristic of the augen gneiss bodies of the Yukon-Tanana terrane (Dusel-Bacon and Aleinikoff, 1985). In thin section, sample 14C consists of K-feldspar augen in a gneissic matrix of (in order of decreasing abundance) plagioclase, quartz, biotite, and muscovite, with accessory apatite, zircon, and Fe-Ti oxides. This sample differs from sample 6B not only mineralogically (in that it contains no hornblende or garnet and instead contains white mica as a minor phase), but also texturally. It has larger K-feldspar augen and quartz that is more mylonitic and less recrystallized. Quartz forms ribbonlike bands made up of elongate subgrains (~1.5 mm in length) with irregular, toothlike margins. Biotite has dark-reddish- or greenish-brown to tan pleochroism and forms 1–2 mm-long, thin subidioblastic books. Muscovite forms 1-mm-long books that are present adjacent to biotite or are included within K-feldspar augen. Plagioclase of probable oligoclase composition forms small (0.25–0.5 mm) grains. Fe-Ti oxides form small clots of irregularly shaped grains that are commonly associated with biotite. Minor kaolinitization of K-feldspar and rare chloritization of biotite indicate a moderate degree of low-temperature alteration.

## GEOCHRONOLOGY

Because previous experience showed that most of the zircons from augen gneiss in the Yukon-Tanana terrane contain significant components of inherited Proterozoic zircons (Aleinikoff and others, 1981, 1986), only grains that appeared to be wholly magmatic without visible xenocrystic cores were chosen for analysis (that is, elongate, prismatic, euhedral, clear, colorless crystals). Zircons from sample 6B were handpicked from the (–100+150) mesh fraction, whereas the coarsest available zircons from sample 14C were obtained from the (–150+200) mesh fraction. All fractions consisted of fewer than 20 grains (seven of eight fractions weighed less than 50 µg; table 1). All analyzed grains, both zircon and titanite, were abraded (Aleinikoff and others, 1990; modified from Krogh, 1982).

Zircons were dissolved in concentrated HF and HNO<sub>3</sub> in PFA Teflon microcapsules within a Parr bomb in an oven at about 230°C for about 3 days (method modified from Parrish, 1987). Titanite was dissolved in concentrated HF and HNO<sub>3</sub> in a screw top PFA Teflon container on a hot plate at about 150°C for 3 days. The samples were spiked with a mixed <sup>205</sup>Pb-<sup>233</sup>U-<sup>236</sup>U tracer. After standard chemical extraction of Pb and U (method modified from Krogh, 1973), Pb was loaded on a single rhenium filament with 0.2 N H<sub>3</sub>PO<sub>4</sub> and silica gel, whereas U was loaded on a single rhenium filament with 0.5 N HNO<sub>3</sub> and aquadag (very fine, suspended graphite). Iso-

topic ratios were measured on a VG 54E single collector mass spectrometer with Daly multiplier, and data were reduced and plotted using the programs of Ludwig (1991a,b, 1992).

Despite our efforts to select pristine magmatic grains without xenocrystic cores, only three of the eight fractions of zircon from the two samples are apparently free of inheritance (fig. 2), indicated by nearly concordant <sup>206</sup>Pb/<sup>238</sup>U, <sup>207</sup>Pb/<sup>235</sup>U, and <sup>207</sup>Pb/<sup>206</sup>Pb ages (table 1). <sup>207</sup>Pb/<sup>206</sup>Pb ages range from 349 to 1077 Ma. A regression forced through 0±50 Ma establishes an age for sample 6B of 353±4 Ma; a concordant fraction from sample 14C has U-Pb ages of 356±2 Ma [earliest Mississippian, according to the DNAG time scale of Palmer (1983)]. We interpret these ages as the times of emplacement of the augen gneiss protoliths. Isotopic data from the five fractions that contain inheritance do not form a linear array, in contrast to previously published results by Aleinikoff and others (1981, 1986).

A fraction of titanite from sample 6B has a <sup>206</sup>Pb/<sup>238</sup>U age of 135 Ma. Because this sample has very high common Pb contents (as shown by the very low <sup>206</sup>Pb/<sup>204</sup>Pb ratio of 29.381; table 1), only the <sup>206</sup>Pb/<sup>238</sup>U age is reliable.

## DISCUSSION

### CRYSTALLIZATION AGE OF THE AUGEN GNEISS PROTOLITHS IN ALASKA

Previous attempts at dating a biotite±muscovite-bearing augen gneiss body in the Big Delta 1°×3° quadrangle, about 170 km to the northwest of our study area, resulted in ages of 344±3 Ma (Aleinikoff and others, 1981) and 341±3 Ma (Aleinikoff and others, 1986). Both dates were calculated by extrapolating to a lower intercept through five discordant fractions with <sup>207</sup>Pb/<sup>206</sup>Pb ages ranging from 523 to 1420 and 1362 Ma, respectively. Several other fractions in each study plotted below discordia, presumably owing to variable amounts of modern Pb loss. We concluded that all fractions contained significant inherited components and interpreted the lower intercept as the age of emplacement based on the assumptions that all fractions used in the regressions (1) contained inheritance of a single age (interpreted to be the upper intercept age of 2.16 or 2.28 Ga), and (2) had not lost radiogenic Pb since the time of emplacement. Two zircon fractions from sample 14C were analyzed by Aleinikoff and others (1986); results are shown in table 1. Although the analyses from these two fractions were not used in the calculation of the discordia of Aleinikoff and others (1986), the analyses plotted on the discordia that gave a 341±3-Ma intercept.

**Table 1.** U-Pb isotopic data from zircon and titanite from augen gneiss, Tanacross quadrangle, Alaska[Constants:  $^{235}\lambda = 9.8485 \text{ E-10/yr}$ ;  $^{238}\lambda = 1.55125 \text{ E-10/yr}$ ;  $^{238}\text{U}/^{235}\text{U} = 137.88$  (Steiger and Jäger, 1977)]

Fraction <sup>1</sup>	Weight (mg)	Concentrations (ppm)		measured	Pb composition <sup>2</sup>				Ratios (percent error) <sup>3</sup>			Ages (Ma) <sup>4</sup>		
		U	Pb		$\frac{^{206}\text{Pb}}{^{204}\text{Pb}}$	$\frac{^{206}\text{Pb}}{^{204}\text{Pb}}$	$\frac{^{206}\text{Pb}}{^{207}\text{Pb}}$	$\frac{^{206}\text{Pb}}{^{206}\text{Pb}}$	$\frac{^{206}\text{Pb}}{^{238}\text{U}}$	$\frac{^{207}\text{Pb}}{^{235}\text{U}}$	$\frac{^{207}\text{Pb}}{^{206}\text{Pb}}$	$\frac{^{206}\text{Pb}}{^{238}\text{U}}$	$\frac{^{207}\text{Pb}}{^{235}\text{U}}$	$\frac{^{207}\text{Pb}}{^{206}\text{Pb}}$
81ADb14C														
(-150+200)EC1	0.046	607.0	36.11	5201.0	9957.9	16.683	15.466	0.0614(.22)	0.4951(.30)	0.0585(.20)	384	408	548	
(-150+200)EC2	.094	593.3	34.36	6330.0	9113.8	17.547	11.600	.0588(.31)	.4490(.34)	.0554(.14)	368	377	428	
(-150+200)EC3	.020	297.1	17.52	1388.0	3720.8	17.365	6.8771	.0567(.49)	.4184(.55)	.0537(.25)	355	356	357	
(-150+200)EC4	.016	969.5	53.90	1359.6	1782.5	15.900	14.766	.0566(.20)	.4267(.22)	.0547(.08)	355	361	400	
(+150)NM <sup>5</sup>	8.09	722.3	46.58	1501.2	1772.6	13.716	7.8170	.0618	.5516	.0648	386	446	766	
(-150+200)NM <sup>5</sup>	9.43	862.0	51.54	1729.1	1997.1	15.476	7.1075	.0571	.4514	.0573	358	378	504	
90ADb6B														
(-100+150)EC1	0.028	686.8	43.96	4759.7	13197	15.806	6.3577	0.0609(.23)	0.5217(.24)	0.0622(.07)	381	426	680	
(-100+150)EC2	.032	387.2	27.04	2753.0	5793.1	12.859	6.7518	.0660(.30)	.6854(.31)	.0753(.10)	412	530	1077	
(-100+150)EC3	.018	505.6	29.40	1236.3	1974.6	16.391	6.7537	.0554(.44)	.4091(.49)	.0536(.20)	347	348	354	
(-100+150)EC4	.014	551.6	35.75	498.40	596.16	12.817	4.5867	.0563(.42)	.4149(.57)	.0535(.36)	353	352	349	
titanite	.110	44.78	6.480	29.381	29.276	1.8124	.7464	.0212(.55)	.1452(3.2)	.0496(3.0)	135	138	176	

<sup>1</sup> All grains were abraded. Abbreviations: E (euhedral), C (clear), NM (nonmagnetic).<sup>2</sup> Blank (ranged from 10-20 pg  $\pm$  50 percent) and fractionation (0.14  $\pm$  .03 percent) corrected. Assumed blank composition is 204:206:207:208 = 1:18.8:15.65:38.65.<sup>3</sup> 2 $\sigma$  uncertainties.<sup>4</sup> Common lead corrections from Stacey and Kramers (1975) for 360-Ma (zircon) and 135-Ma (titanite) model Pb.<sup>5</sup> Previously published in Aleinikoff and others (1986).

Lack of U-Pb data for the Big Delta augen gneiss body (Aleinikoff and others, 1986) that are comparable to results for the Divide Mountain gneisses of this study (that is, nearly concordant U-Pb ages from abraded zircons devoid of visible xenocrystic cores) precludes a definitive comparison of the crystallization ages of the two batholiths. The  $353 \pm 4$ -Ma and  $356 \pm 2$ -Ma emplacement ages we determined for the two augen gneisses in the Divide Mountain area are a more accurate estimation of the ages of emplacement of their protoliths than is the  $341 \pm 3$ -Ma age determined previously for the protolith of the Big Delta augen gneiss body (Aleinikoff and others, 1986). The Divide Mountain ages, based on concordant and nearly concordant fractions, are about 180 m.y. younger than the youngest  $^{207}\text{Pb}/^{206}\text{Pb}$  age obtained in the previous studies. The lower intercept ages in Aleinikoff and others (1981, 1986) may be younger than our new data because the Big Delta augen gneiss body is truly 10 to 15 m.y. younger than the protoliths of the Divide Mountain augen gneisses. Alternatively, the lower intercept ages may be younger because some of the zircons in the previously analyzed fractions (composed of several milligrams each) may have experienced a minor amount of modern Pb loss, thereby lowering the discordia to a slightly younger lower intercept. Note that two previously analyzed fractions from sample 14C plot below a reference chord we have constructed (fig. 2) between the 355-Ma concordant age for sample 14C determined in this study and the 2160-Ma upper intercept age determined in the study of the Big Delta augen gneiss body. The scatter in our new data both above and below the reference chord indicates that the assumption of a single inheritance age is incorrect, and that our assumed inheritance age prob-

ably represents an approximate average age of inheritance. The interpretation of the upper intercept age as an average age of inheritance was proposed by Mortensen (1990b), who found that single detrital zircons from a quartzite in the Cleary sequence of the western Yukon-Tanana terrane had  $^{207}\text{Pb}/^{206}\text{Pb}$  ages ranging from 1.2 to 3.4 Ga.

### AGE COMPARISON OF THE DIVIDE MOUNTAIN AUGEN GNEISS PROTOLITHS WITH NEARBY BODIES IN YUKON TERRITORY

Similar latest Devonian to earliest Mississippian crystallization ages have been determined by U-Pb analyses of abraded zircon fractions from orthogneiss bodies in Yukon Territory east of our study area. Some of these metaplutonic bodies consist of biotite-bearing augen gneisses, whereas others are augen-free biotite-hornblende granodioritic gneisses. Unlike the bodies in Alaska, some of those in Yukon Territory show little to no inheritance of Precambrian zircons.

A  $364 \pm 4$ -Ma upper intercept age, interpreted as the crystallization age, was determined for a sample of gneissic K-feldspar augen-bearing biotite quartz monzonite from the eastern part of the Fiftymile batholith (fig. 3) (Mortensen, 1986; Mortensen and Sullivan, 1991). Rocks of that composition make up the bulk of the Fiftymile batholith (Tempelman-Kluit and Wanless, 1980), the body that adjoins the orthogneiss of the Divide Mountain area. Unlike both samples from the Divide Mountain area, the sample from the Fiftymile batholith contains only limited evidence for an inherited xenocrystic zircon component from either grain appearance (cores) or from isotopic systematics (Mortensen, 1986).

A virtually identical lower intercept age of  $364 \pm 2$  Ma, based on a three-point discordia and interpreted as the crystallization age (Mortensen, 1990a), was determined for a sample of peraluminous augen gneiss from a body farther east. This body, referred to as the Mt. Burnham orthogneiss (fig. 3), is in a geologic setting comparable to the augen gneiss bodies of the Lake George subterrane in that its contacts appear to be conformable with compositional layering in schist, micaceous quartzite, and amphibolite. It is also compositionally similar to the typical augen gneiss in the Lake George subterrane and consists of subhedral to strongly flattened K-feldspar augen up to 8 cm in length surrounded by medium to coarsely crystalline biotite, muscovite, quartz, and feldspar, and, locally, minor amounts of garnet and tourmaline. Zircons from the dated sample of the Mt. Burnham orthogneiss include a significant inherited component, with  $^{207}\text{Pb}/^{206}\text{Pb}$  ages between 441 and 844 Ma (Mortensen, 1990a), similar to U-Pb systematics in zircons from the two samples from our study.

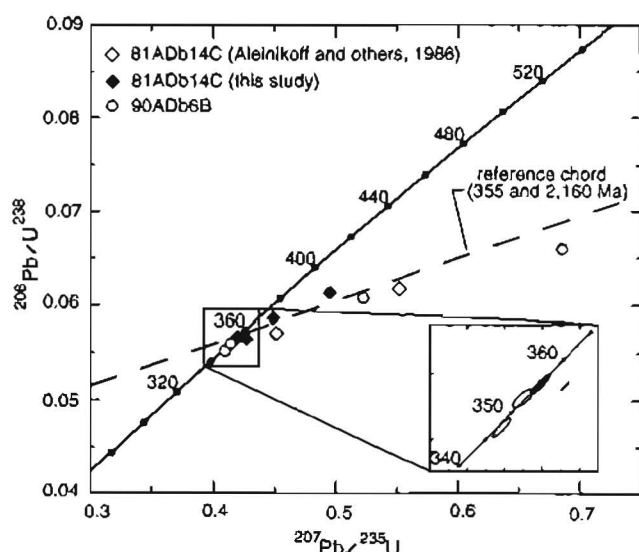


Figure 2. Concordia plot of data from augen gneisses in the Divide Mountain area. Upper intercept of reference chord in this diagram is from Aleinikoff and others (1986).

Samples from three augen-free, biotite-hornblende granodiorite gneiss bodies yielded slightly younger crystallization ages than the Mt. Burnham gneiss. The first sample, collected approximately 170 km southeast of Divide Mountain (fig. 3), is from the Selwyn Gneiss. The Selwyn Gneiss is compositionally homogeneous but extremely variable in its degree of deformation and recrystallization; it occurs as a gently dipping sheet about 2 km thick that is preserved in a syncline above siliceous mylonite (Tempelman-Kluit and Wanless, 1980). The sample from this body gave an upper intercept age of  $352 \pm 4$  Ma (Mortensen and Sullivan, 1991) and showed no evidence for an inherited zircon component (Mortensen, 1986).

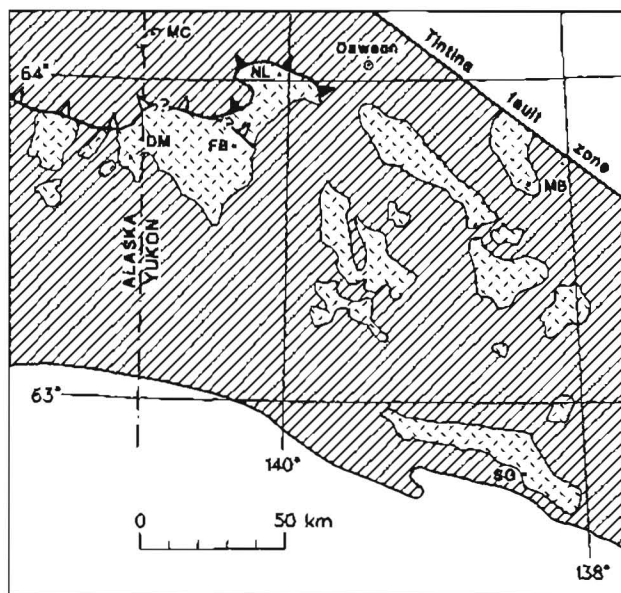
The second sample of augen-free, biotite-hornblende granodiorite (NL on fig. 3), collected about 60 km north-east of Divide Mountain, is from a body that has been interpreted to be the northeastern lobe of the Fiftymile batholith (Tempelman-Kluit and Wanless, 1980; Morten-

sen and Sullivan, 1991). However, this northeastern "lobe" appears to be separated from the K-feldspar-bearing augen gneiss to the south, which forms the dominant part of the batholith, by a shallow northeast-dipping shear zone that is tentatively interpreted as a low-angle normal fault (J.K. Mortensen, written commun., 1993). Along its northern and western margins, the northeastern body structurally underlies carbonaceous quartzite and schist with interlayered marble and locally abundant mafic metavolcanic rocks (Mortensen, 1988) (a lithologic association referred to as the Nasina assemblage by Wheeler and McFeely (1987) that we include in the Nisutlin terrane shown on fig. 1). Nowhere along its contact is the granodiorite gneiss shown to intrude the adjacent units, because where not in fault contact with the adjacent metamorphic rocks (along its eastern margin), it is overlain by unmetamorphosed Upper Cretaceous volcanic rocks (Tempelman-Kluit, 1974) (fig. 3). Two zircon fractions from the hornblende granodiorite of the proposed northeastern lobe yielded nearly concordant ages of  $347 \pm 1$  Ma. Only one fraction showed minor inheritance [ $^{207}\text{Pb}/^{206}\text{Pb}$  age of 421 Ma (Mortensen and Sullivan, 1991; J.K. Mortensen, written commun., 1993)].

A similar age of  $348 \pm 1$  Ma was determined for a sample from the third augen-free, biotite-hornblende granodiorite gneiss body: the Moose Creek orthogneiss (Mortensen and Sullivan, 1991), a small body north of our study area (fig. 3) that crops out within an area of Nasina assemblage rocks (J.K. Mortensen, written commun., 1993). Zircons from this sample indicated a moderate degree of inheritance [ $^{207}\text{Pb}/^{206}\text{Pb}$  ages up to 600 Ma (J.K. Mortensen, written commun., 1993)].

### POSSIBLE COMPOSITE NATURE OF THE FIFTYMILE BATHOLITH

The continuity of augen gneiss in the area of Divide Mountain (Foster, 1970) with augen gneiss of the adjacent Fiftymile batholith in Yukon Territory (Tempelman-Kluit and Wanless, 1980; Mortensen, 1986) suggests that a continuous batholith spans the international boundary. The  $353 \pm 4$ -Ma and  $356 \pm 2$ -Ma U-Pb ages determined for the two Divide Mountain augen gneisses viewed together with the  $364 \pm 4$ -Ma age determined for the augen gneiss from the eastern part of the Fiftymile batholith suggests that intrusion of the Fiftymile batholith may have begun as early as 368 Ma (maximum age of uncertainty range determined for the sample from the eastern part of the batholith) and continued to as late as 349 Ma (minimum age of uncertainty range determined for the younger of the samples from the Divide Mountain area). We propose that the apparent range in crystallization ages, degree of inheritance, and composition for different parts of the batholith indicate a possible composite origin for the



**Figure 3.** Distribution of granitic and granodioritic orthogneiss bodies (stippled) within the undivided bedrock of eastern Alaska and western Yukon Territory (hachured) (modified from Mortensen, 1986; Dusel-Bacon and others, 1993, and J.K. Mortensen, unpublished mapping, 1993). The undivided bedrock contains rocks included in the Nisutlin, Teslin-Taylor Mountain, and Yukon-Tanana terranes as defined by Hansen and others (1991) and revised by Dusel-Bacon and Hansen (1992). Dots show location of dated samples discussed in text: DM, Divide Mountain area; FB, Fiftymile batholith; NL, presumed northeastern lobe of Fiftymile batholith; MC, Moose Creek orthogneiss; MB, Mt. Burnham orthogneiss; SG, Selwyn Gneiss. Low-angle normal fault shown by open-toothed fault, and thrust fault shown by closed-tooth fault (sawteeth on upper plate); other faults between the metamorphic packages (terrane or subterrane) not shown.



Fiftymile batholith, an idea previously proposed by Mortensen (1986) on the basis of preliminary geochemical and U-Pb zircon differences between the eastern and western parts of the batholith. Our evidence for this interpretation is based on the fact that (1) two compositionally distinct augen gneiss samples of our study yield overlapping to slightly different crystallization ages (differing by a maximum of 9 m.y.), and (2) sample 14C and the sample from the eastern part of the Fiftymile batholith are compositionally similar but give different crystallization ages and show very different degrees of inheritance. Differences in magmatic residence time within the crust and degree of assimilation of crustal material of different batches of magma could account for the differences in the composition and xenocrystic zircon component. Our interpretation of a prolonged Late Devonian to Early Mississippian magmatic event is consistent with the wide range of middle Paleozoic crystallization ages that have been determined along the length of a 5,000-km-long magmatic belt that intruded the continental margin of ancestral North America (Rubin and others, 1990).

Uncertainty regarding the original geologic setting of the largely fault-bounded,  $347 \pm 1$ -Ma granodiorite gneiss body that is proposed to be the northeastern lobe of the Fiftymile batholith precludes speculation about its relation to the rest of the batholith. It is possible that the granodiorite gneiss body and the Fiftymile batholith may have originated in separate parts of the middle Paleozoic magmatic belt.

The range in crystallization ages, degree of inheritance, and composition within a body we propose may have been a site of continued magmatism during a 2- to 19-m.y. period (based on the maximum and minimum age differences allowed by the age ranges for the oldest and youngest samples) bears on an observation made by (Mortensen, 1992) regarding the distribution of the two suites of Late Devonian to Early Mississippian plutons. These two suites are (1) hornblende-bearing metaluminous plutons with only minor inheritance, and (2) peraluminous plutons (augen gneiss) with abundant inheritance. Mortensen (1992) proposed that the bulk of the metaluminous plutons and presumably cogenetic metavolcanic rocks crop out mainly south and west of, or occur in structurally higher thrust sheets than, the peraluminous suite of plutons. Mortensen (1992) concluded that this relation implied that the metaluminous belt developed outboard of the coeval peraluminous belt, and, by analogy with other magmatic belts, that the Late Devonian to Early Mississippian arc was produced by north- or northeast-dipping subduction. In applying this hypothesis to the gneisses shown in figure 3, no simple spatial relation of the metaplutonic bodies to the presumed outer (southern) margin of the Cordilleran magmatic belt in terms of their composition and degree of inheritance appears to be present. However, the hornblende-bearing plutons with

moderate, little, or no zircon inheritance (Moose Creek orthogneiss, presumed northeastern lobe of Fiftymile batholith, and Selwyn Gneiss, respectively) all either intrude or structurally overlie rocks included by Hansen and others (1991) and Dusel-Bacon and Hansen (1992) in the upper plate Nisutlin terrane (comparable to that shown in fig. 1). According to the model of Hansen (1990) and Dusel-Bacon and Hansen (1992), these rocks originated outboard of their current position and were juxtaposed on top of the peraluminous augen gneiss bodies during crustal shortening. The variation in composition and U-Pb systematics that exists within the composite Fiftymile batholith indicates that additional complexities may exist on the scale of a single batholith, and it argues for more detailed characterizations of the gneissic bodies.

## INTERPRETATION AND SIGNIFICANCE OF THE EARLY CRETACEOUS TITANITE AGE

Previous structural and metamorphic studies of the augen gneiss and associated metasedimentary and metaigneous tectonites in the northeastern Tanacross quadrangle (Hansen and others, 1991; Dusel-Bacon and Hansen, 1992; Dusel-Bacon and others, 1995) have shown that northwest-vergent shear is generally recorded in the northern part of the area and southeast-vergent shear in the southern part (fig. 1). Where the two shear senses are present in the same rocks (primarily near the northern margin of the Lake George subterrane), fabrics that record northwest-vergent shear are more penetrative and preceded fabrics that record southeast-vergent shear. The northwest-vergent fabrics were interpreted in these previous studies to have formed during latest Early to early Middle Jurassic emplacement of the structurally higher, allochthonous oceanic and marginal-basin rocks of the Taylor Mountain and Seventymile terranes onto the ancient continental margin of North America (interpreted to include the Lake George subterrane of the Yukon-Tanana terrane). High-pressure (7–12 kbar) dynamothermal metamorphism of the structurally higher Taylor Mountain terrane probably began during the late Paleozoic in a west-dipping subduction system and continued until the Early to Middle Jurassic, at which time the outboard terrane was obducted onto the underlying continental margin. High-pressure (also 7–12 kbar) metamorphism of the Lake George subterrane is interpreted to have occurred as a result of crustal thickening caused by obduction of the outboard terranes and imbrication of the continental margin (Dusel-Bacon and Hansen, 1992; Dusel-Bacon and others, 1995).

The southeast-vergent deformation recorded in tectonites within our study area, and for over 300 km across the Yukon-Tanana terrane to the northwest of our study area, has been interpreted to have accompanied



southeast-directed extension and exhumation of the Yukon-Tanana terrane (Hansen and others, 1991; Dusel-Bacon and Hansen, 1992; Pavlis and others, 1993). Early Cretaceous metamorphic cooling ages establish a chronology for this proposed event. The 135-Ma  $^{206}\text{Pb}/^{238}\text{U}$  age on titanite from sample 6B (from an outcrop in which southeast-vergent deformation is present) indicates the time at which augen gneiss at this locality cooled through about 600°C (closure temperatures referred to in this discussion generalized from Heaman and Parrish, 1991). We suggest that this age records cooling from ductile deformation because geothermometric data indicate that rocks at a nearby locality on this ridge attained a peak metamorphic temperature of 640 to 700°C (Dusel-Bacon and others, 1995). This cooling age is virtually identical to the 135-Ma U-Pb titanite age determined for compositionally similar augen gneiss from a body 275 km to the northwest (Aleinikoff and others, 1981). K-Ar and  $^{40}\text{Ar}/^{39}\text{Ar}$  ages on hornblende, muscovite, and biotite (see summary in Pavlis and others, 1993) are also consistent over a widespread area of the Yukon-Tanana terrane. The cooling history determined for the rocks of the Lake George subterrane in the northeastern Tanacross quadrangle—namely, cooling to 500°C (hornblende  $^{40}\text{Ar}/^{39}\text{Ar}$  closure temperature) at 119 Ma followed by cooling to ~350–250°C (muscovite and biotite  $^{40}\text{Ar}/^{39}\text{Ar}$  closure temperatures) at 109 Ma (fig. 1)—mirrors the cooling history determined for other tectonites across the Yukon-Tanana terrane.

## CONCLUSIONS

Zircon fractions from two compositionally distinct samples of augen gneiss from the Divide Mountain area, located near the Alaska-Yukon Territory international boundary, yield nearly concordant ages that we interpret as 353±4-Ma and 356±2-Ma crystallization ages for the protoliths of the gneisses. A significant component of inherited xenocrystic zircon is indicated for both samples by  $^{207}\text{Pb}/^{206}\text{Pb}$  ages that range from 349 to 1077 Ma for the younger sample and 357 to 766 Ma for the older sample. Sample 14C is a biotite-muscovite augen gneiss in which K-feldspar augen reach up to 8 cm in longest dimension; this mineralogy and the large size of the megacrystic augen are typical of most of the augen gneiss bodies in the Lake George subterrane of the Yukon-Tanana terrane, of which the Divide Mountain samples form a part. Sample 6B is a garnet-bearing hornblende-biotite augen gneiss in which augen are generally only 1–2 cm in longest dimension; this mineralogy is unusual for the augen gneiss bodies of the Lake George subterrane.

Both gneisses are located in the western part of the Fiftymile batholith. U-Pb zircon analyses made by Mortensen (1986) and Mortensen and Sullivan (1991) of

a sample of biotite-muscovite augen gneiss from the eastern part of the Fiftymile batholith indicate a U-Pb upper intercept age, interpreted as an emplacement age, of 364±4 Ma. There is only limited evidence for an inherited xenocrystic zircon component in their sample. The range in crystallization ages, degree of inheritance, and composition within the Fiftymile batholith suggests that the batholith is composite. A  $^{206}\text{Pb}/^{238}\text{U}$  age of 135 Ma on titanite from one of the dated samples establishes the time of cooling through about 600°C. We believe the cooling occurred during a widespread mid-Cretaceous episode of ductile deformation and southeast-directed extension. This extension has been proposed to have resulted in the exhumation of the Yukon-Tanana terrane from beneath allochthonous terranes that were emplaced in latest Early to early Middle Jurassic time (Hansen and others, 1991; Dusel-Bacon and Hansen, 1992; Pavlis and others, 1993).

**Acknowledgments.**— We thank C.R. Bacon and H.L. Foster for assistance during 1981 fieldwork and S.L. Douglass and V.L. Hansen for assistance during 1990 fieldwork. Our interpretation of the U-Pb dates and deformational history of the augen gneiss bodies has benefited greatly from discussions and sharing of data with V.L. Hansen, H.L. Foster, and J.K. Mortensen. We thank M. Walter for chemical procedures and A. Walker for mineral separations.

## REFERENCES CITED

- Aleinikoff, J.N., Dusel-Bacon, Cynthia, and Foster, H.L., 1986, Geochronology of augen gneiss and related rocks, Yukon-Tanana terrane, east-central Alaska: *Geological Society of America Bulletin*, v. 97, p. 626–637.
- Aleinikoff, J.N., Dusel-Bacon, Cynthia, Foster, H.L., and Futa, Kiyoto, 1981, Proterozoic zircon from augen gneiss, Yukon-Tanana Upland, east-central Alaska: *Geology*, v. 9, p. 469–473.
- Aleinikoff, J.N., Winegarden, D.L., and Walter, M., 1990, U-Pb ages of rims of zircon: a new analytical method using the air-abrasion technique: *Chemical Geology (Isotope Geoscience Section)*, v. 80, p. 351–363.
- Dusel-Bacon, Cynthia, and Aleinikoff, J.N., 1985, Petrology and tectonic significance of augen gneiss from a belt of Mississippian granitoids in the Yukon-Tanana terrane, east-central Alaska: *Geological Society of America Bulletin*, v. 96, no. 4, p. 411–425.
- Dusel-Bacon, Cynthia, Csejtey, Béla, Jr., Foster, H.L., Doyle, E.O., Nokleberg, W.J., and Plafker, George, 1993, Distribution, facies, ages, and proposed tectonic associations of regionally metamorphosed rocks in east- and south-central Alaska: *U.S. Geological Survey Professional Paper 1497-C*, 73 p., 2 pls., scale 1:1,000,000.
- Dusel-Bacon, Cynthia, and Hansen, V.L., 1992, High-pressure amphibolite-facies metamorphism and deformation within the Yukon-Tanana and Taylor Mountain terranes, eastern Alaska, in Bradley, D.C., and Dusel-Bacon, Cynthia, eds., *Geologic studies in Alaska by the U.S. Geological Survey:*

- U.S. Geological Survey Bulletin 2041, p. 140–159.
- Dusel-Bacon, Cynthia, Hansen, V.L., and Scala, J.A., 1995, High-pressure amphibolite facies dynamic metamorphism and the Mesozoic tectonic evolution of an ancient continental margin, east-central Alaska: *Journal of Metamorphic Geology*, v. 13, p. 9–24.
- Foster, H.L., 1970, Reconnaissance geologic map of the Tanacross quadrangle, Alaska: U.S. Geological Survey Miscellaneous Geologic Investigations Map I-593, scale 1:250,000.
- , 1976, Geologic map of the Eagle quadrangle, Alaska: U.S. Geological Survey Miscellaneous Geologic Investigations Map I-922, scale 1:250,000.
- Foster, H.L., Keith, T.E.C., and Menzie, W.D., 1994, Geology of the Yukon-Tanana area of east-central Alaska, in Plafker, George, and Berg, H.C., eds., *The geology of Alaska: Boulder, Colo., Geological Society of America, The Geology of North America*, v. G-1, p. 205–240.
- Hansen, V.L., 1990, Yukon-Tanana terrane: a partial acquittal: *Geology*, v. 18, p. 365–369.
- Hansen, V.L., Heizler, M.T., and Harrison, T.M., 1991, Mesozoic thermal evolution of the Yukon-Tanana composite terrane: new evidence from  $^{40}\text{Ar}/^{39}\text{Ar}$  data: *Tectonics*, v. 10, p. 51–76.
- Heaman, Larry, and Parrish, Randy, 1991, U-Pb geochronology of accessory minerals, in Heaman, L., and Ludden, J.N., eds., *Applications of radiogenic isotope systems to problems in geology: Mineralogical Association of Canada, Short course handbook*, v. 19, p. 59–102.
- Krogh, T.E., 1973, A low-contamination method for hydrothermal decomposition of zircon and extraction of U and Pb for isotopic age determination: *Geochimica et Cosmochimica Acta*, v. 37, p. 485–494.
- , 1982, Improved accuracy of U-Pb zircon ages by the creation of more concordant systems using an air abrasion technique: *Geochimica et Cosmochimica Acta*, v. 46, p. 637–649.
- Ludwig, K.R., 1991a, PBDAT — A computer program for processing Pb-U-Th isotope data, version 1.20: U.S. Geological Survey Open-File Report 88-542, Revision of March 19, 1991, 34 p.
- , 1991b, ISOPLOT — A plotting and regression program for radiogenic-isotope data: U.S. Geological Survey Open-File Report 91-445, 41 p.
- , 1992, ANALYST — A computer program for control of a thermal-ionization, single collector mass-spectrometer, version 2.20: U.S. Geological Survey Open-File Report 92-543, 93 p.
- Mortensen, J.K., 1986, U-Pb ages for granitic orthogneiss from western Yukon Territory: Selwyn Gneiss and Fiftymile Batholith revisited, in *Current Research, Part B: Geological Survey of Canada, Paper 86-1B*, p. 141–146.
- , 1988, Geology of southwestern Dawson map area, Yukon Territory (NTS 116 B, C): Geological Survey of Canada Open File 1927.
- , 1990a, Geology and U-Pb geochronology of the Klondike District, west-central Yukon Territory: *Canadian Journal of Earth Sciences*, v. 27, p. 903–914.
- , 1990b, Significance of U-Pb ages for inherited and detrital zircons from Yukon-Tanana terrane, Yukon and Alaska [abs.]: Geological Association of Canada—Mineralogical Association of Canada Program with Abstracts, v. 15, p. A91.
- , 1992, Pre-mid-Mesozoic tectonic evolution of the Yukon-Tanana terrane, Yukon and Alaska: *Tectonics*, v. 11, p. 836–853.
- Mortensen, J.K., and Jilson, G.A., 1985, Evolution of the Yukon-Tanana terrane: evidence from southeastern Yukon Territory: *Geology*, v. 13, p. 806–810.
- Mortensen, J.K., and Sullivan, R.W., 1991, U-Pb zircon ages, Nd isotopic compositions and tectonic significance of middle and late Paleozoic magmatism in the Yukon-Tanana terrane, western Yukon Territory, Canada [abs.]: Geological Society of America Abstracts with Programs, v. 23, no. 5, p. A434.
- Nokleberg, W.J., and Aleinikoff, J.N., 1985, Summary of stratigraphy, structure, and metamorphism of Devonian igneous-arc terranes, northeastern Mount Hayes quadrangle, eastern Alaska Range, in Bartsch-Winkler, Susan, ed., *The United States Geological Survey in Alaska: Accomplishments during 1984: U.S. Geological Survey Circular 967*, p. 66–71.
- Palmer, A.R., 1983, The Decade of North American geology 1983 geologic time scale: *Geology*, v. 11, no. 9, p. 503–504.
- Parrish, R.R., 1987, An improved microcapsule for zircon dissolution in U-Pb geochronology: *Chemical Geology*, v. 66, p. 99–102.
- Pavlis, T.L., Sisson, V.B., Foster, H.L., Nokleberg, W.J., and Plafker, George, 1993, Mid-Cretaceous extensional tectonics of the Yukon-Tanana terrane, Trans-Alaskan Crustal Transect (TACT), east-central Alaska: *Tectonics*, v. 12, p. 103–122.
- Rubin, C.M., Miller, M.M., and Smith, G.M., 1990, Tectonic development of Cordilleran mid-Paleozoic volcano-plutonic complexes: evidence for convergent margin tectonism, in Harwood, D.S., and Miller, M.M., eds., *Paleozoic and early Mesozoic paleogeographic relations: Sierra Nevada, Klamath Mountains, and related terranes: Boulder, Colo., Geological Society of America Special Paper 255*, p. 1–16.
- Stacey, J.S., and Kramers, J.D., 1975, Approximation of terrestrial lead isotope evolution by a two stage model: *Earth and Planetary Science Letters*, v. 26, p. 207–221.
- Steiger, R.H., and Jäger, E., 1977, Subcommittee on geochronology: convention on the use of decay constants in geo- and cosmochronology: *Earth and Planetary Science Letters*, v. 36, p. 359–362.
- Tempelman-Kluit, D.J., 1974, Reconnaissance geology of Aishihik Lake, Snag, and part of Stewart River map-areas, west-central Yukon: Geological Survey of Canada, Paper 79-14, 27 p.
- Tempelman-Kluit, Dirk, and Wanless, R.K., 1980, Zircon ages for the Pelly Gneiss and Klotassin granodiorite in western Yukon: *Canadian Journal of Earth Sciences*, v. 17, p. 297–306.
- Wheeler, J.O., and McFeeley, P., 1987, Tectonic assemblage map of the Canadian Cordillera and adjacent parts of the United States of America: Geological Survey of Canada Open File 1565, scale 1:2,000,000.



# Late Cretaceous Age of the Middle Fork Caldera, Eagle Quadrangle, East-Central Alaska

By Charles R. Bacon and Marvin A. Lanphere

## ABSTRACT

Welded tuff associated with the  $10 \times 18$  km Middle Fork caldera in the southwest quarter of the Eagle  $1^\circ \times 3^\circ$  quadrangle is dated at  $69.10 \pm 0.19$  Ma. The reported age is the weighted mean of five  $^{40}\text{Ar}/^{39}\text{Ar}$  laser-fusion analyses of individual biotite phenocrysts. This result indicates that this area has experienced comparatively little uplift and erosion since the Late Cretaceous. Silicic volcanic fields and collapse calderas probably also existed above presently exposed Cretaceous and early Tertiary plutons in more extensively unroofed, high-angle fault-bounded areas to the northwest and southeast in the Yukon-Tanana region.

## INTRODUCTION

Four elliptical masses of unmetamorphosed volcanic rocks in the Tanacross and in the Eagle  $1^\circ \times 3^\circ$  quadrangles (Foster, 1970, 1976) were identified as caldera-fill deposits by Bacon and others (1990). The three Tanacross occurrences are rhyolites, erupted about 93 Ma (two are dated), that have geochemical affinities with modern continental margin volcanic arcs. Identification of the Middle Fork caldera in the Eagle quadrangle by Bacon and others (1990) was based on interpretation of then-existing collections and field notes of H. L. Foster and co-workers. Following publication of the Eagle and Tanacross  $1^\circ \times 3^\circ$  quadrangle geologic maps, private companies explored the areas now recognized as caldera fill for Cu, Mo, and Au deposits.

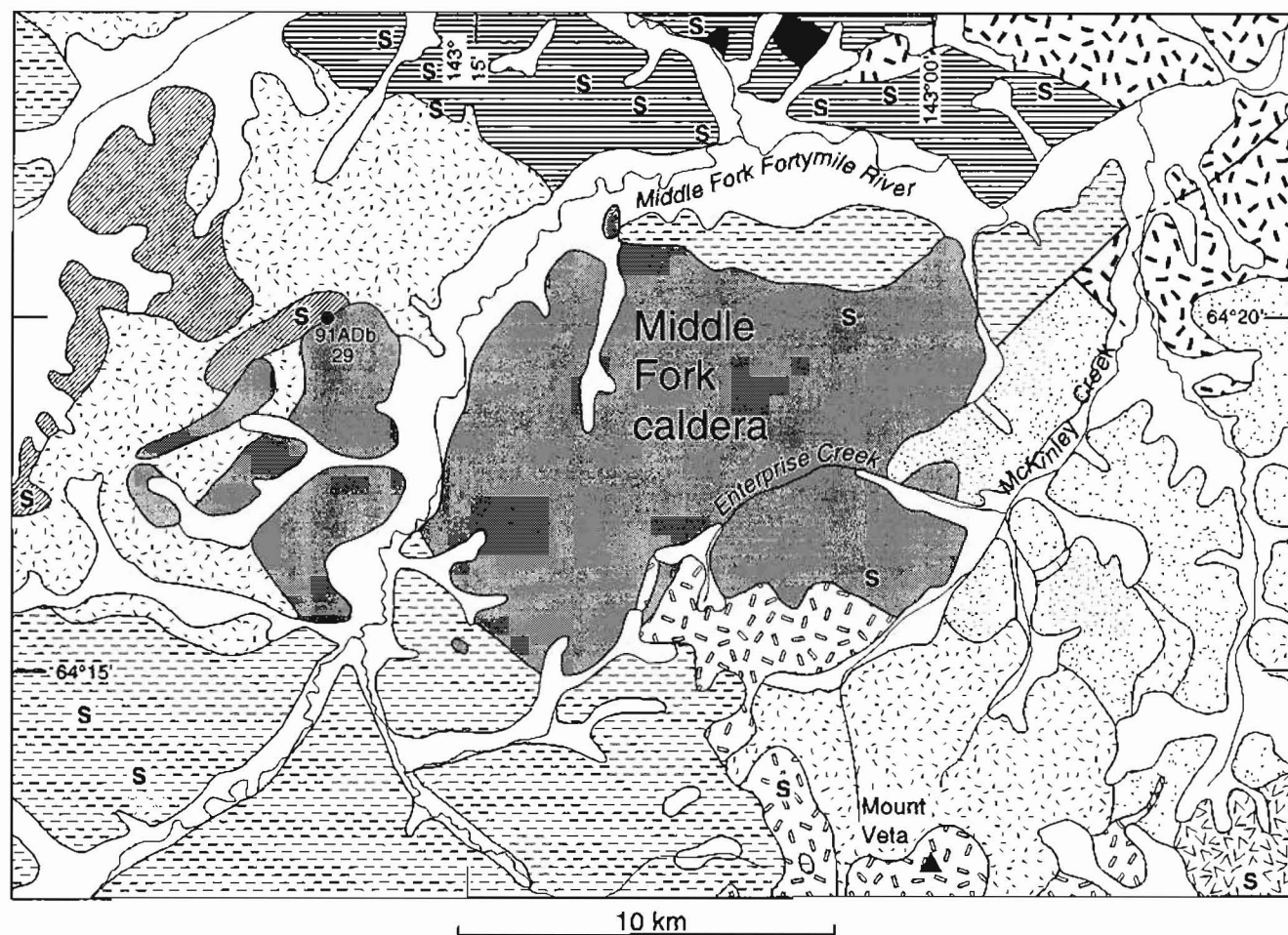
This note presents the results of  $^{40}\text{Ar}/^{39}\text{Ar}$  laser-fusion dating of five biotite phenocrysts from a large sample of fresh rhyolitic welded tuff obtained in 1991 from the Middle Fork caldera. Although suitable for dating, the welded tuff sample was not chemically analyzed because it contains abundant lithic fragments and lacks mechanically separable fiamme (collapsed pumice lumps). This geochronologic information is of significance to the history of igneous activity in the region and the degree of uplift and erosion since the caldera formed.

## THE MIDDLE FORK CALDERA

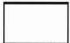
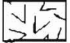


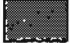

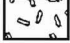
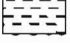


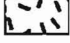


The Middle Fork caldera is marked by a  $10 \times 18$  km occurrence of felsic volcanic and shallow intrusive rocks in the southwest quarter of the Eagle quadrangle mapped by Foster (1976) (fig. 1; see also fig. 1 of Bacon and others, 1990). Although well exposed in comparison to the Tanacross calderas, the geology of the Middle Fork caldera-fill deposit is incompletely known because the occurrence is remote and most traverses were made along ridges during reconnaissance mapping of the Eagle quadrangle by H. L. Foster and coworkers (unpub. data, 1970). The volcanic and hypabyssal rocks are interpreted as intracaldera tuff and postcaldera intrusions on the basis of reexamination of specimens collected by Foster and coworkers. The exposed thickness of intracaldera tuff is over 700 m where it is cut by the Middle Fork of the Fortymile River near the western margin of the caldera and over 850 m south of Enterprise Creek near the southeastern limit of the deposit where it abuts the Jurassic syenite of Mount Veta. The base of the caldera fill apparently is not exposed. The original caldera depression, now destroyed by erosion, may have been larger in diameter than the caldera-fill deposit (compare Lipman, 1976). Boundaries of the caldera are not indicated in figure 1 because it is uncertain in many places whether mapped limits of felsic rocks reflect margins of the caldera structure or contacts between intracaldera tuff and megabreccia blocks within the tuff (compare Lipman, 1976).

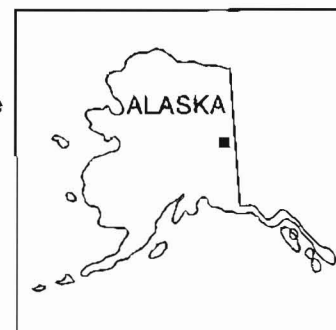
## THE DATED SAMPLE

The sample described in this paper was collected during a brief visit to the western limit of rock exposures thought to be related to the Middle Fork caldera while participating in helicopter-supported field work for another project in 1991. The base of a remnant of proximal outflow tuff, or possibly the upper contact of a megabreccia block, is exposed near the 4,500-ft elevation in the hills west of the Middle Fork of the Fortymile River, about 5 km southwest of the locality where our sample



## EXPLANATION

	Surficial deposits (Quaternary)		Greenstone (Paleozoic?)
	Granitic rocks, undivided (Tertiary and Mesozoic)		Hornfels (Paleozoic?)
	Felsic volcanic and shallow intrusive rocks (Late Cretaceous)		Quartz-mica schist and greenschist (Paleozoic?)
	Syenite of Mount Veta (Jurassic)		Biotite schist, quartzite, and marble (Paleozoic?)
	Pyroxenite and hornblendite (Jurassic)		Biotite gneiss and amphibolite (Paleozoic?)
	Hornblende granodiorite (Mesozoic)		Sample locality
			Sulfide occurrence



**Figure 1.** Geologic map of the Middle Fork caldera and vicinity (modified from Foster, 1976), showing locality of sample 91ADb29.



was collected (fig. 1). The elevation of the sample locality is 4,100 ft and is on the projected continuation of the base of the tuff. We believe that the dated sample thus is correlative with, or part of, the intracaldera tuff of the Middle Fork caldera.

The dated sample contains about 50 percent crystals in a devitrified matrix in which relict glass shards are visible in thin section. The phenocryst content of the magma may have been closer to 20 percent according to the approximate modal abundance in a collapsed pumice clast. The most abundant phenocrysts in the tuff are plagioclase, quartz, and biotite. Plagioclase forms discrete euhedral or broken crystals up to 3 mm in size which are replaced to varying degrees by sericite and carbonate. Quartz mainly occurs as discrete embayed crystals up to 2 mm in size. Polycrystalline quartz and quartz in biotite granite fragments also tend to have embayed margins, which implies that some free quartz crystals may be xenocrysts. Some quartz crystals smaller than about 0.5 mm are sharply euhedral, however, and must be phenocrysts. Brown biotite is present as hexagonal books up to 2 mm across and as much as 1 mm thick. The biotite commonly is intergrown with quartz  $\pm$  plagioclase  $\pm$  opaque oxide and contains apatite and rare zircon inclusions. Partially chloritized, subhedral biotite crystals are much less abundant and probably are xenocrysts. Common opaque oxide crystals believed to be phenocrysts are up to 0.5 mm in diameter, as are comparatively rare, euhedral brown amphibole crystals. Oxide and amphibole crystals contain apatite inclusions, and the amphibole also carries opaque oxides. Basement rock fragments are present, including muscovite schist and altered biotite granite. Petrographic examination thus indicates that the erupted magma contained a phenocryst assemblage of quartz + plagioclase + biotite + Fe-Ti oxide(s) + minor amphibole, with inclusions of apatite  $\pm$  zircon.

Euhedral biotite phenocrysts approximately 1 mm in diameter and free of adhering matrix were selected for  $^{40}\text{Ar}/^{39}\text{Ar}$  laser-fusion analysis. By analyzing individual, well-formed crystals belonging to the phenocryst population, it was possible to avoid contamination by xenocrysts.

### $^{40}\text{Ar}/^{39}\text{Ar}$ RESULTS

Five laser-fusion  $^{40}\text{Ar}/^{39}\text{Ar}$  analyses of individual biotite phenocrysts are presented in table 1. Analyses were made on the GLM ("Great Little Machine") continuous laser system (Dalrymple, 1989). The irradiation parameter,  $J$ , for the reaction  $^{39}\text{K}(n,p)^{39}\text{Ar}$  is determined by irradiating a monitor mineral of known age along with the samples whose age is to be determined (Dalrymple and Lanphere, 1971). The K/Ca ratios in table 1 are low for biotite as a result of plagioclase and apatite inclusions

in the analyzed biotite crystals; these inclusions do not affect the validity of the age determinations. Calculated ages range from  $68.58 \pm 0.41$  to  $69.55 \pm 0.42$  (1 $\sigma$ ) Ma. We believe that the weighted mean age of  $69.10 \pm 0.19$  is an accurate determination of the time of emplacement of the welded tuff and collapse of the Middle Fork caldera. The 69-Ma age of the Middle Fork caldera is consistent with aeromagnetic data cited by Bacon and others (1990) as evidence for a post-83-Ma age for this feature.

### REGIONAL SIGNIFICANCE OF THE LATE CRETACEOUS AGE

The 69-Ma age of the Middle Fork caldera is considerably younger than the ~93-Ma ages of the two dated calderas to the south in the Tanacross quadrangle that were reported by Bacon and others (1990). However, both ages lie within periods of widespread igneous activity indicated by maps and histograms of radiometric ages (Wilson and others, 1985, 1994). The mid-Cretaceous rocks occur within a magmatic belt that extends from the Canadian Cordillera through Alaska to the Russian Far East (Armstrong, 1988; Plafker and Berg, 1994). The Middle Fork caldera probably belongs to the Late Cretaceous to Paleogene Kluane arc, evidenced now mainly by volcanoclastic sedimentary rocks of the Southern Margin composite terrane (Plafker and Berg, 1994). Volcanic rocks of ~70-Ma age also are preserved in southwestern Yukon Territory (Grond and others, 1984).

Vertical stability of this part of the Yukon-Tanana region since the Late Cretaceous is evidenced by preservation of thick caldera-fill deposits and remnants of outflow tuff that do not appear to have experienced significant regional tilting. Although little remains of the outflow sheets, the tops of the caldera-fill deposits must be very close to the Late Cretaceous ground surface. The situation is similar for the ~95-Ma South Fork Volcanics in Yukon Territory (Wood and Armstrong, 1982; Gordey, 1988). Stability of the Tanacross quadrangle and Eagle quadrangle caldera localities is in striking contrast to the region south of the Denali fault, where dramatic uplift has occurred in the Alaska Range. Nevertheless, modest Quaternary uplift and northward tilting near the Middle Fork caldera are evident from entrenchment of the Middle Fork of the Fortymile River, as well as from entrenchment of and extensive high-level terraces elsewhere along the Fortymile and Seventymile Rivers (Foster and others, 1994).

The eastern Yukon-Tanana region (Foster, 1992) is segmented into several blocks, bounded by southwest-northeast-trending fault zones (Wilson and others, 1985) that have been differentially uplifted (Foster and others, 1994; Newberry and others, 1995). This province of monotonous, low to moderate topographic relief, therefore,

**Table 1.**  $^{40}\text{Ar}/^{39}\text{Ar}$  analytical data for sample 91ADb29 biotite.

[Sample 91ADb29 from Eagle B-5 15' quadrangle (lat 64°19'53", long 143°19'54"). Ratios corrected for  $^{37}\text{Ar}$  decay (half-life=35.1 days) and  $^{39}\text{Ar}$  decay (half-life=269 years). K/Ca ratios computed from  $\text{K/Ca}=0.52 \times [^{39}\text{Ar}_{\text{K}}/^{37}\text{Ar}_{\text{Ca}}]$  for the TRIGA reactor. Subscripts: rad, radiogenic; K, potassium derived; Ca, calcium derived. Decay constants:  $\lambda_{\text{K}}=0.581 \times 10^{-10}/\text{yr}$ ,  $\lambda_{\text{Ca}}=4.962 \times 10^{-10}/\text{yr}$ . Errors assigned are estimates of the standard deviation of analytical precision and do not include the error in the irradiation parameter,  $J$ , which is 0.5 percent.  $J = 0.010325$ . Weighted mean age is weighted by the inverse of variances of the individual determinations;  $\sigma_{\text{best}}$  is the weighted standard deviation where the weighting is also done by the inverse of the variances]

No. of grains	$^{40}\text{Ar}/^{39}\text{Ar}$	$^{37}\text{Ar}/^{39}\text{Ar}$	$^{36}\text{Ar}/^{39}\text{Ar}$	$^{40}\text{Ar}_{\text{rad}}$ ( $10^{-13}\text{mol}$ )	$^{40}\text{Ar}_{\text{rad}}$ (percent)	$^{39}\text{Ar}_{\text{Ca}}$ (percent)	$^{36}\text{Ar}_{\text{Ca}}$ (percent)	K/Ca	Age (Ma)
1	3.9892	0.09671	0.000627	9.404	95.4	0.01	4.15	5.07	69.55 $\pm$ 0.42
1	3.9830	0.09918	0.000712	15.00	94.8	0.01	3.74	4.94	68.99 $\pm$ 0.41
1	3.9965	0.06541	0.000827	11.26	93.9	0.01	2.13	7.49	68.58 $\pm$ 0.41
1	4.2035	0.06270	0.001464	14.27	89.7	0.01	1.15	7.81	68.91 $\pm$ 0.41
1	3.9514	0.04602	0.000501	11.50	96.2	0.01	2.47	10.65	69.47 $\pm$ 0.42
<b>weighted mean and <math>\sigma_{\text{best}} = 69.10 \pm 0.19</math></b>									

exposes bedrock characteristic of contrasting depths in the different blocks. Caldera-fill deposits are only preserved in the relatively downdropped blocks, where Cretaceous and older plutonic rocks and large areas of metamorphic rocks also are exposed. The block to the northwest of the Mount Harper lineament, the fault zone proposed by Wilson and others (1985, fig. 1) to lie immediately northwest of the Middle Fork caldera, has a much greater proportion of exposed Cretaceous plutonic rocks and apparently lacks caldera-fill deposits belonging to volcanic fields associated with the Cretaceous plutons. This block appears to have been unroofed to a greater extent than the blocks to the southeast in Alaska, which contain the 69-Ma Middle Fork and mid-Cretaceous calderas of Bacon and others (1990), so that any major accumulations of Cretaceous and early Tertiary volcanic rocks have been eroded away. Late Cretaceous and early Tertiary plutons (70 to 50 Ma) are present in the western part of the block northwest of the Mount Harper lineament and more abundantly in the next block to the west, northwest of the Shaw Creek fault (Wilson and others, 1985; Foster, 1992; Foster and others, 1994). Silicic volcanic fields, and probably collapse calderas, may have existed above the present level of exposure of Cretaceous and early Tertiary plutons in the more uplifted blocks.

## REFERENCES CITED

- Armstrong, R.L., 1988, Mesozoic and early Cenozoic magmatic evolution of the Canadian Cordillera, in Clark, S.P., Jr., Burchfiel, B.C., and Suppe, J., Processes in continental lithospheric deformation: Geological Society of America Special Paper 218, p. 55-91.
- Bacon, C.R., Foster, H.L., and Smith, J.G., 1990, Rhyolitic calderas of the Yukon-Tanana terrane, east central Alaska: volcanic remnants of a mid-Cretaceous magmatic arc: *Journal of Geophysical Research*, v. 95, p. 21,451-21,461.
- Dalrymple, G.B., 1989, The GLM continuous laser system for  $^{40}\text{Ar}/^{39}\text{Ar}$  dating: description and performance characteristics, in Shanks, W.C. III, and Criss, R.E., eds., *New frontiers in stable isotopic research: laser probes, ion probes, and small-sample analysis*: U.S. Geological Survey Bulletin 1890, p. 89-96.
- Dalrymple, G.B., and Lanphere, M.A., 1971,  $^{40}\text{Ar}/^{39}\text{Ar}$  technique of K-Ar dating: a comparison with the conventional technique: *Earth and Planetary Science Letters*, v. 12, p. 300-308.
- Foster, H.L., 1970, Reconnaissance geologic map of the Tanacross quadrangle, Alaska: U.S. Geological Survey Miscellaneous Geologic Investigations Map 1-593, scale 1:250,000.
- , 1976, Geologic map of the Eagle quadrangle, Alaska: U.S. Geological Survey Miscellaneous Geologic Investigations Map 1-922, scale 1:250,000.
- , 1992, Geologic map of the eastern Yukon-Tanana region, Alaska: U.S. Geological Survey Open-File Report 92-313, scale 1:500,000.
- Foster, H.L., Keith, T.E.C., and Menzie, W.D., 1994, Geology of the Yukon-Tanana area of east-central Alaska, in Plafker, George, and Berg, H.C., eds., *The geology of Alaska: Boulder, Colo., Geological Society of America, The Geology of North America*, v. G-1, p. 205-240.
- Gordey, S.P., 1988, The South Fork Volcanics: mid-Cretaceous caldera fill tuffs in east-central Yukon: *Papers of the Geological Survey of Canada*, 88-1E, p. 13-18.
- Grond, H.C., Churchill, S.J., Armstrong, R.L., Harakal, J. E., and Nixon, G.T., 1984, Late Cretaceous age of the Hutshi, Mount Nansen, and Carmacks groups, southwestern Yukon Territory and northwestern British Columbia: *Canadian*

- Journal of Earth Sciences, v. 21, p. 554-558.
- Lipman, P.W., 1976, Caldera-collapse breccias in the western San Juan Mountains, Colorado: Geological Society of American Bulletin, v. 87, p. 1397-1410.
- Newberry, R.J., Solie, D.N., Burns, L.E., Wiltse, M.A., Hammond, W.R., and Swainbank, R., 1995, Geophysical and geological evidence for pervasive, northeast-trending, left-lateral faults in eastern interior Alaska [abs.]: Geological Society of America Abstracts with Programs, v. 27, no. 5, p. 68.
- Plafker, George, and Berg, H.C., 1994, Overview of the geology and tectonic evolution of Alaska, in Plafker, George, and Berg, H.C., eds., The Geology of Alaska: Boulder, Colorado, Geological Society of America, The Geology of North America, v. G-1, p. 989-1021, pls. 3, 7, and 12.
- Wilson, F.H., Shew, Nora, and DuBois, G.D., 1994, Map and table showing isotopic age data in Alaska, in Plafker, George, and Berg, H.C., eds., The geology of Alaska: Boulder, Colo., Geological Society of America, The Geology of North America, v. G-1, pl. 8.
- Wilson, F.H., Smith, J.G., and Shew, Nora, 1985, Review of radiometric data from the Yukon Crystalline Terrane, Alaska and Yukon Territory: Canadian Journal of Earth Sciences, v. 22, p. 525-537.
- Wood, D.H., and Armstrong, R.L., 1982, Geology, chemistry, and geochronometry of the Cretaceous South Fork Volcanics, Yukon Territory: Papers of the Geological Survey of Canada, 82-1A, p. 309-316.

Reviewers: J.G. Smith and P.W. Lipman



# Correlation of Rock Sequences Across the Denali Fault in South-Central Alaska

By Béla Csejtey, Jr., Chester T. Wrucke, Arthur B. Ford, Michael W. Mullen,  
J. Thomas Dutro, Jr., Anita G. Harris, and Phil F. Brease

## ABSTRACT

Recent geologic investigations in the Mt. McKinley region of south-central Alaska strongly suggest that a thick sequence of Paleozoic marine sedimentary rocks north of the Denali fault correlates with similar Paleozoic rocks south of the fault. The presence of these Paleozoic and other correlative rock sequences and geologic features on both sides of the fault indicates that in south-central Alaska the Denali fault is not a terrane-bounding fault, and that the total Cenozoic right-lateral offset along the fault is minimal.

## INTRODUCTION

The Cenozoic Denali fault is one of the longest and topographically best expressed structural features of southern Alaska, with a sharply northward-convex surface trace over 1,200 km long across the entire width of the state (Beikman, 1980). Despite its prominence, displacement directions and magnitudes along the fault are inadequately known and are the subject of ongoing controversy. Several researchers have postulated that along its entire length, the Denali fault is a terrane-bounding fault and primarily a Cenozoic strike-slip feature with several hundred kilometers of right-lateral displacement (for instance, Nokleberg and others, 1985; Plafker and others, 1989). In contrast, Csejtey and others (1982, 1992) argued that along the sharp bend of its surface trace in south-central Alaska, the western segment of the Denali fault has changed into a dominantly dip-slip feature with at most only a few tens of kilometers of Cenozoic dextral offset. Csejtey and others (1982) further postulated that in eastern Alaska, east of the sharp bend, the Denali fault is dominantly a strike-slip fault, but only with a moderate amount of Cenozoic right-lateral offset. Csejtey and others (1982) suggested that in eastern Alaska, the Denali fault developed along an old Cretaceous transform fault, which explains why in that region the fault separates diverse and unrelated rock sequences of pre-Cenozoic age. West of the

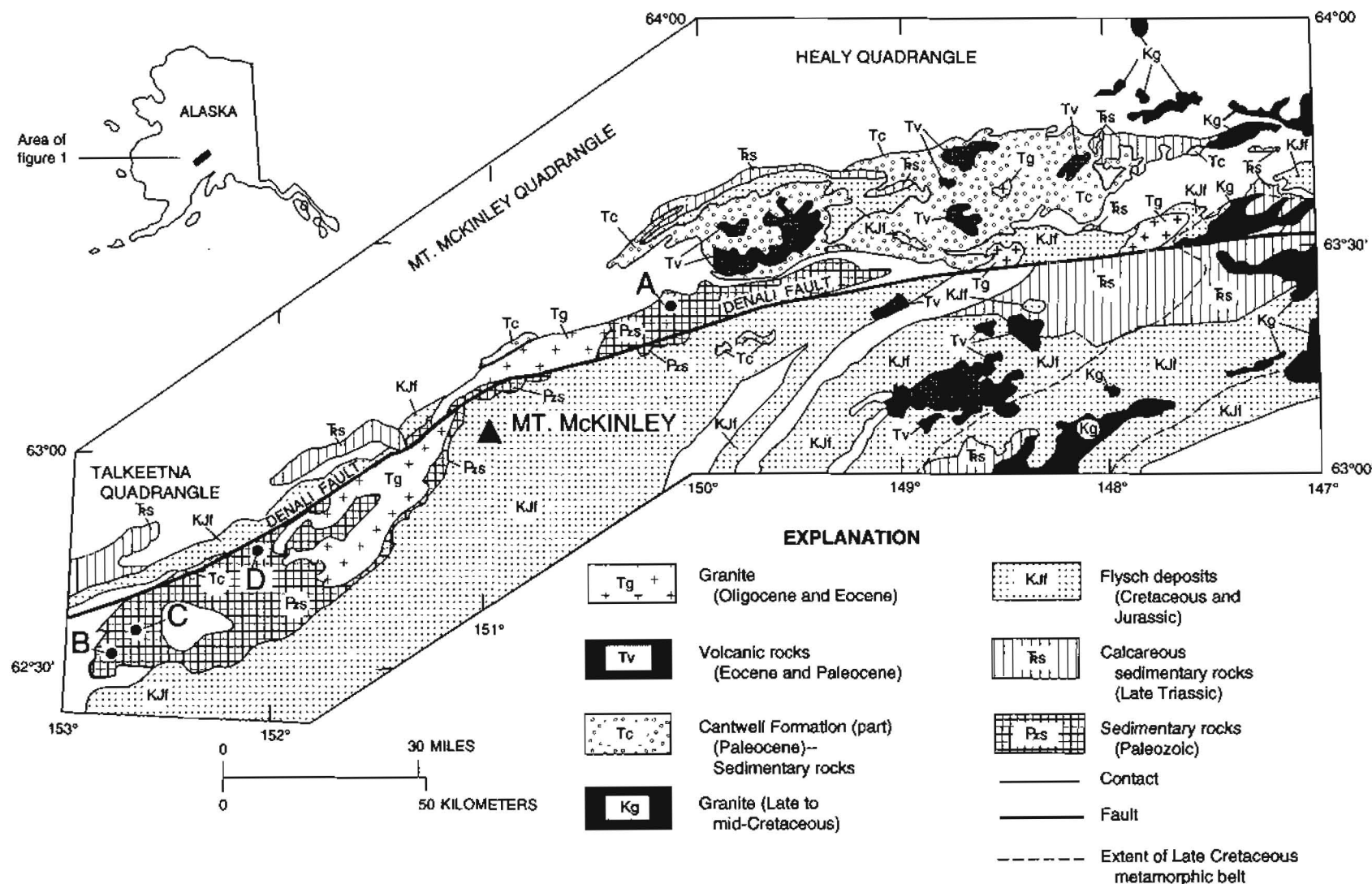
sharp bend, the Denali fault does not appear to follow any preexisting sutures, and because of its apparently minimal lateral movement in Cenozoic time, the western segment of the Denali fault does not appear to be a terrane-bounding fault. If so, the Denali fault probably played only a limited role in the Cenozoic tectonic evolution of Alaska.

The primary aim of this paper is to report briefly on newly obtained fossil data and to propose a correlation for a previously mapped but poorly dated, intensely deformed, thick Paleozoic marine sedimentary sequence. This sequence, composed dominantly of flysch deposits, crops out north of the Denali fault in the Mt. McKinley region of south-central Alaska (unit DOs of Csejtey and others, 1992; fig. 1). We propose here that these Paleozoic rocks north of the Denali fault are correlative with at least parts of a depositionally and structurally complex sequence of Paleozoic, dominantly marine flyschoid sedimentary rocks that lie south of the Denali fault near Mt. McKinley (units P<sub>2</sub> and D<sub>1</sub> of Reed and Nelson, 1980; figs. 1, 2). The proposed correlation of these rocks is important because it limits the displacement magnitudes of the Denali fault system of Alaska. This correlation is consistent with other stratigraphic sequences and igneous and metamorphic rocks that already have been interpreted to correlate across the Denali fault in south-central Alaska (Csejtey and others, 1992), including granitic rocks that have been used to indicate dextral displacement of only a few tens of kilometers along the fault in the Mt. McKinley area (Reed and Lanphere, 1974; Lanphere, 1978).

## PALEOZOIC ROCKS NORTH OF THE DENALI FAULT

Paleozoic sedimentary rocks on the north side of the Denali fault are present in an elongate fault-bounded block about 128 km long and, on average, approximately 8 km wide. The block extends from the western Healy quadrangle into the southern Mt. McKinley quadrangle (fig. 1). Rocks of the block comprise an upward-shallowing



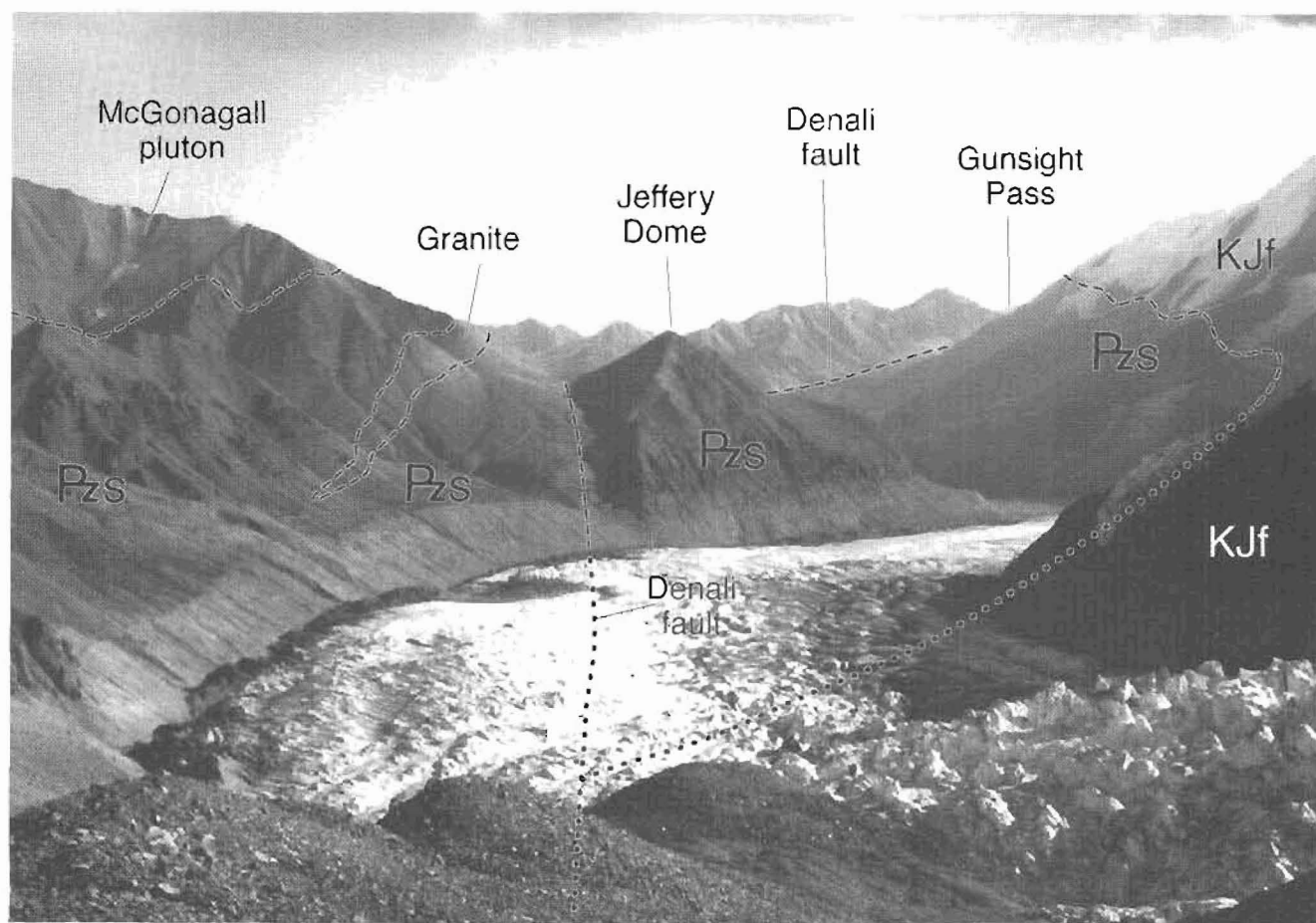


**Figure 1.** Generalized map showing the areal distribution of two Paleozoic sequences (Ps) and other rock units, interpreted to be correlative, on both sides of the Denali fault in the Mt. McKinley region of south-central Alaska. The map also shows the areal extent of a Late Cretaceous metamorphic belt. Distribution of rocks from Reed and Nelson (1980), Csejty and others (1992), and B. Csejty, Jr., unpub. data (1994). Within outcrop areas of correlative rocks, surficial deposits and noncorrelative plutonic and volcanic rocks are not shown. Dots and capital letters indicate locations of paleontologically examined samples, discussed in text, from the two Paleozoic sequences: A, 94ACy-6a, 6b, and 6c; B, 74AR-43; C, 74AR-135; and D, 74AR-129.

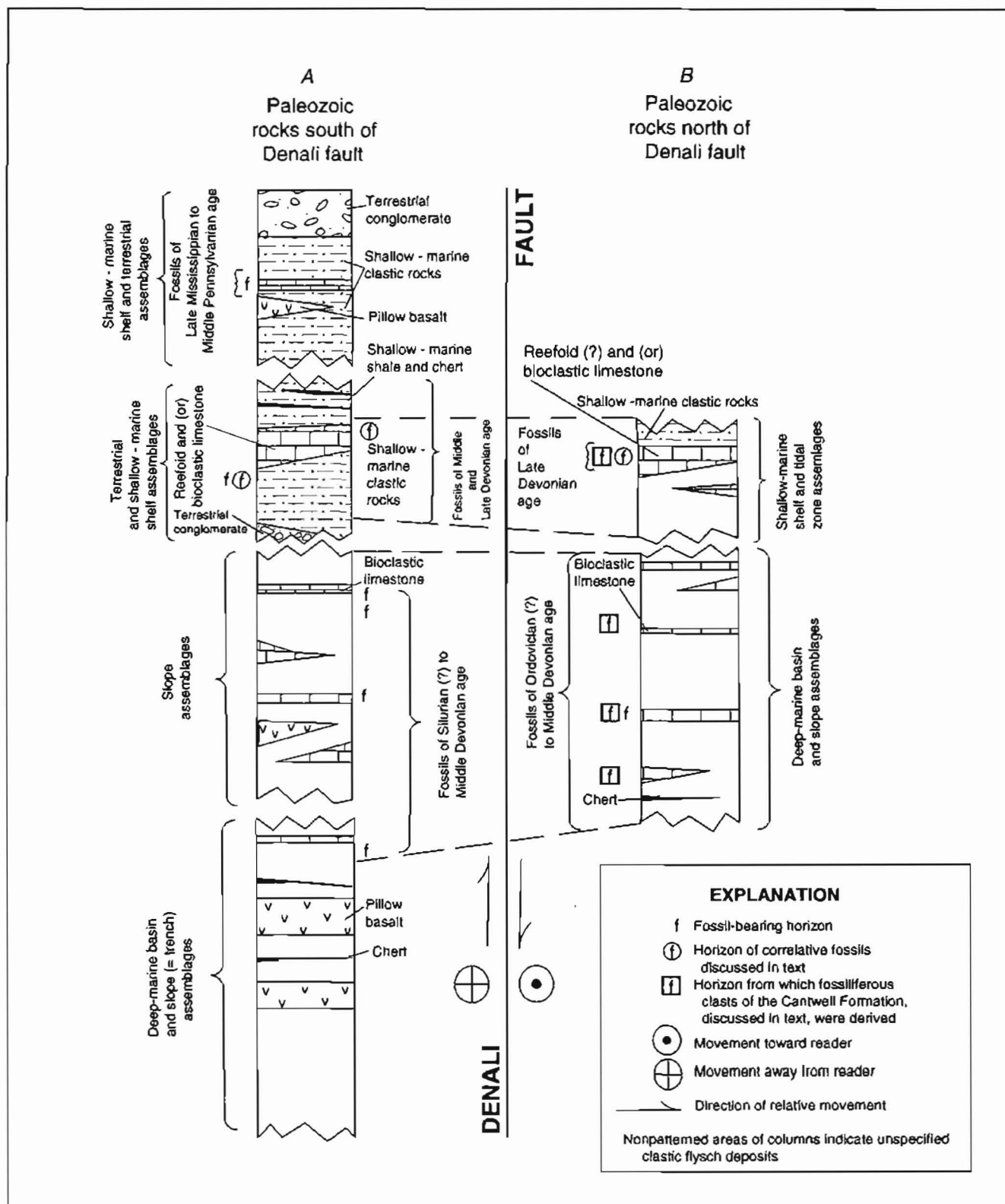
marine sequence composed of dominantly slope and basinal turbidites and hemipelagic deposits overlain by subordinate amounts of shelf-type deposits. The sequence is complexly faulted and folded such that its thickness cannot be reliably established, although it is estimated to be greater than 1,000 m. The metamorphic grade of the sequence is mostly subgreenschist facies and only locally reaches the lower greenschist facies of Turner (1968). A reconstructed stratigraphic column of the sequence is shown in Section B of figure 3.

The Paleozoic rocks north of the Denali fault have been described as unit DOs by Csejtey and others (1992) and as units DOs and DIs by Mullen and Csejtey (1986). These rocks consist of "medium- to dark-gray, thinly bedded to laminated, commonly graded, medium- to fine-grained sandstone; dark-gray to black argillite and siltstone; intercalated layers, a few tens of meters thick,

of dark-gray, generally fine-grained and thinly bedded to laminated, locally medium-bedded limestone and dark-gray argillite and minor chert; and, near the top of the sequence, an approximately 40- to 70-m-thick interval of medium- to light-gray, massive, finely to medium-crystalline, partly dolomitic limestone" (Csejtey and others, 1992). The sandstones contain abundant quartz and chert grains and fewer grains of mica, feldspar, and minor pyroxene, suggesting a dominantly continental, partly volcanic source. Most of the sandstones and the thinly to medium-bedded limestones and argillite interlayers appear to be turbidites, based on the presence of Bouma sequences. The turbidites were deposited in a continental-slope and deep-marine basin environment. The massive limestone at the top of the sequence crops out along strike for over 45 km, but in most places it is sheared and recrystallized, and primary sedimentary features and pos-



**Figure 2.** Photograph showing Paleozoic sedimentary rocks (Pzs), interpreted to be correlative, on both sides of the Denali fault in the upper Peters Glacier area of Denali National Park, south-central Alaska. View is toward the northeast along the surface trace of the Denali fault. Northward-facing slope on the right is part of the Wickersham Wall of Mt. McKinley. The Paleozoic rocks north of the fault have been intruded by the McGonagall pluton of Reed and Lanphere (1974). The Paleozoic rocks south of the Denali fault are in fault contact with Jurassic and Cretaceous flysch (unit KJf of Csejtey and others, 1992). Note the sharp bend in the surface trace of the vertical to subvertical Denali fault



**Figure 3.** Reconstructed stratigraphic columns for the two Paleozoic sedimentary sequences on opposite sides of the Denali fault in the Mt. McKinley region of south-central Alaska. *A*, Column for the Paleozoic sequence south of the Denali fault. *B*, Column for the Paleozoic sequence north of the Denali fault. Dashed tie lines delineate correlative segments of the two columns.

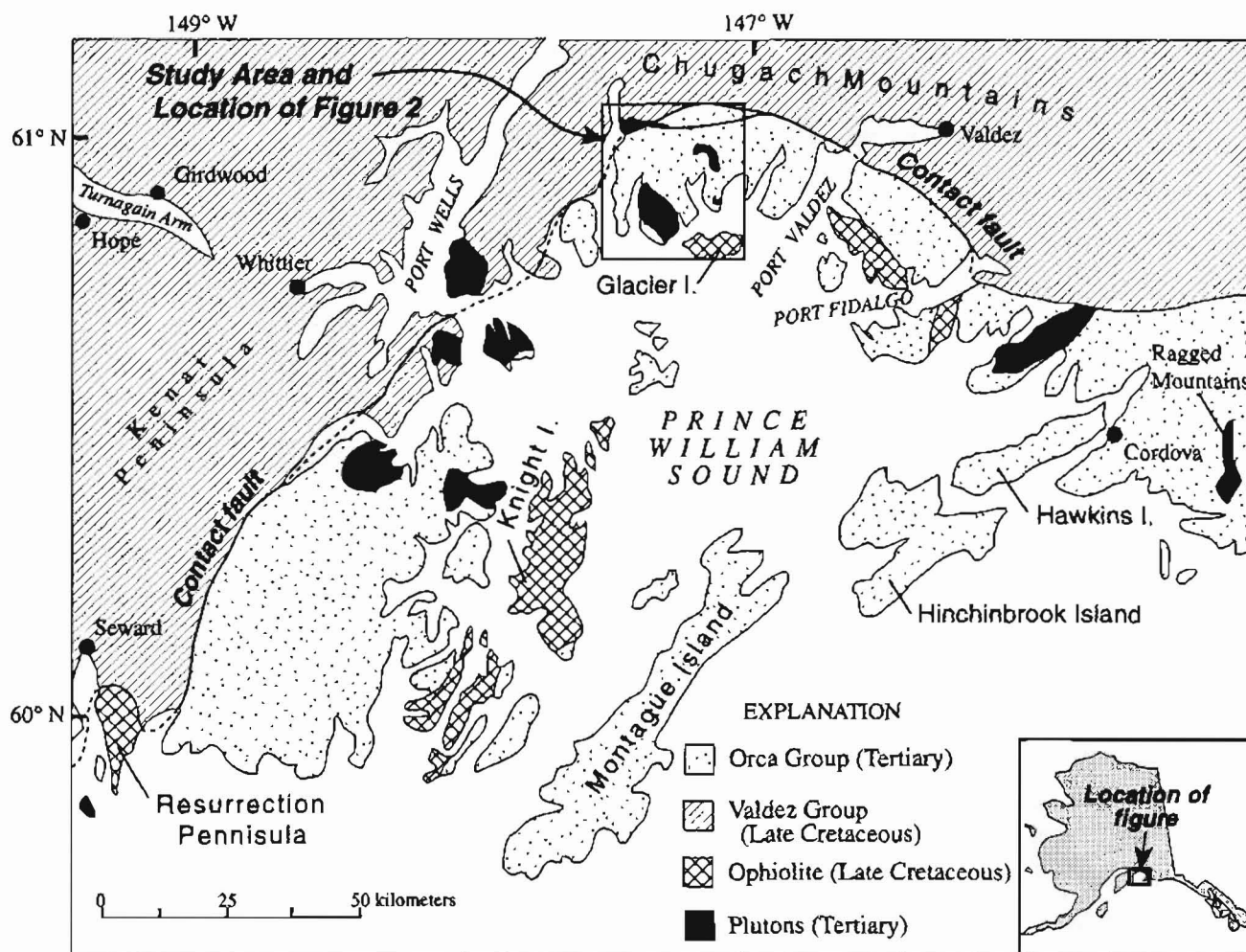
Groups form part of a Late Cretaceous to early Tertiary accretionary prism that was related to subduction of the Kula-Farallon plate (Bol and others, 1992; Farmer and others, 1993).

Both units have been folded, faulted, metamorphosed, and intruded by Tertiary plutons (Nelson and others, 1985; Goldfarb and others, 1986). Metamorphic grade in the study area ranges from laumontite to hornblende-hornfels facies. Upper greenschist and hornblende-hornfels facies mineral assemblages are developed adjacent to intrusions (S.W. Nelson and others, unpub. mapping, 1994).

The Valdez and Orca Groups are generally separated by the Contact fault system (Winkler and Plafker, 1981; Jones and others, 1981; fig. 2). Recent work shows that that no major compositional, lithologic, or metamorphic differences exist between the Valdez and Orca Groups and suggests that they constitute parts of a single terrane, the Chugach-Prince William composite terrane (Dumoulin, 1988; Bol and Gibbons, 1992).

The Valdez Group, exposed in the northwestern part of the study area (figs. 1, 2), consists of turbiditic sandstone, siltstone, and shale. The Orca Group is present throughout the rest of the study area and, like the Valdez Group, consists predominantly of turbidites and other sediment gravity-flow deposits that are composed of sandstone and lesser conglomerate and shale. The Orca Group sedimentary rocks are interbedded with, and intruded by, mafic volcanic rocks. The Orca Group also includes an ophiolitic section that consists of ultramafic rocks, gabbro, sheeted dikes, and pillow basalt (Nelson and others, 1985; Crowe and others, 1992; Nelson and Nelson, 1993).

Two fault-bounded packages of volcanoclastic rocks and limestone (TKvv) may be, at least in part, older than the Campanian and Maastrichtian Valdez Group (Nelson and others, 1994). These rocks occur within the outcrop area of the Orca Group (fig. 2; Nelson and others, 1994; S.W. Nelson and others, unpub. mapping, 1994) and consist of volcanic mudstone, pillow breccia, purple and green



**Figure 1.** Location of the study area in the Chugach National Forest, northern Prince William Sound, and general geology of the region (modified from Nelson and others, 1994).

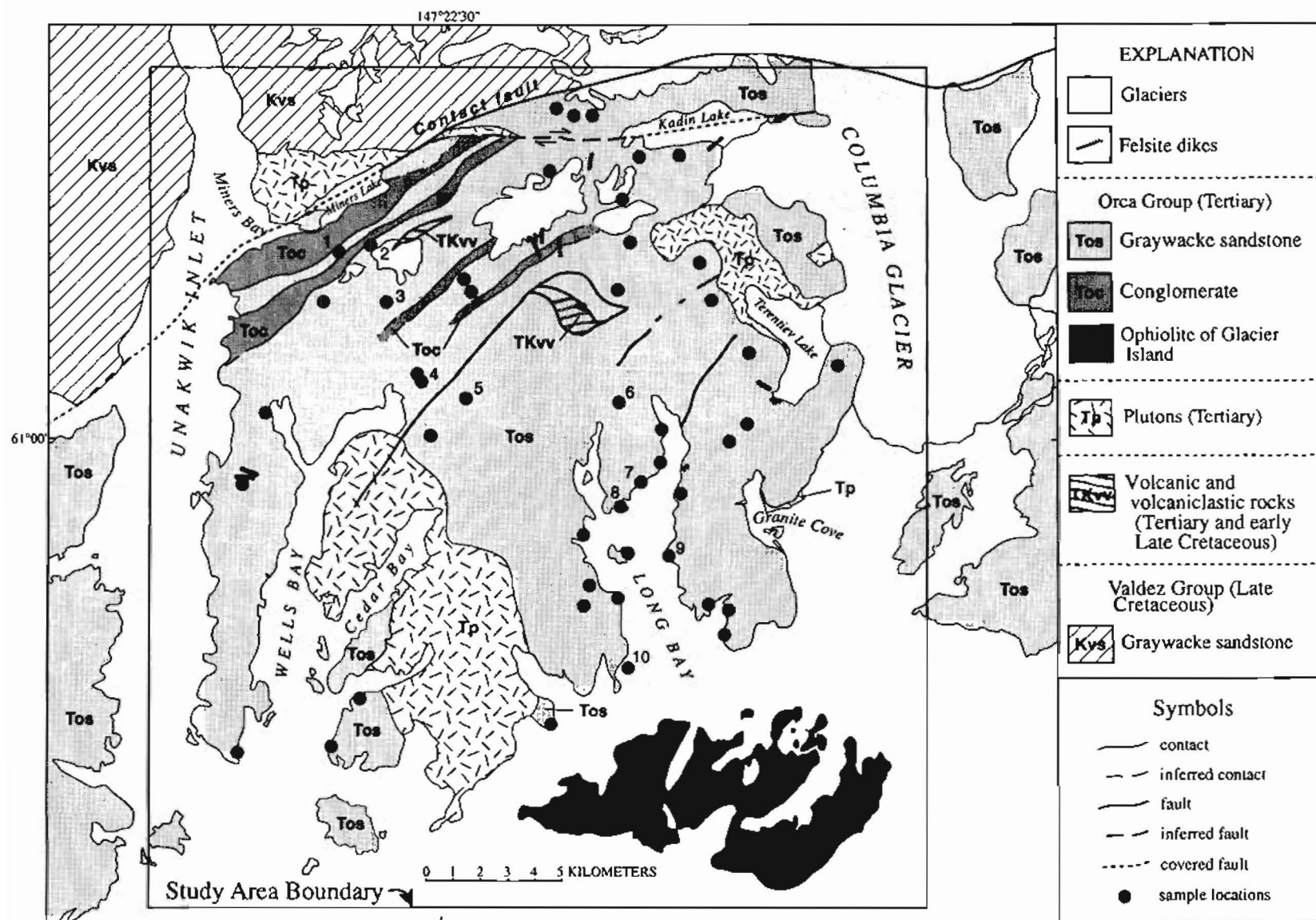


Figure 2. Sample locations and geology of the study area, northern Chugach National Forest. Sample transect numbers refer to table 4 (modified from Nelson and others, 1994).



calcareous shale, and thin beds of gray, green, and purple limestone (Nelson and others, 1994). Limestone from one package yields microfossils of Coniacian to early Santonian age, whereas apparently identical beds in the second package contain Tertiary (middle Eocene) microfossils (R. Rosen, TGS-Calibre Geophysical Company, written commun., 1992; W. Sliter, USGS, written commun., 1994).

In the study area, S.W. Nelson and others (unpub. mapping, 1994) have divided the Orca Group into several lithofacies based on the classification of Mutti and Ricci-Lucchi (1978). Samples in the present study are largely from the B and C turbidite facies sandstones (table 1). Only a few samples are from turbidite facies A, facies BD, facies D, and facies F sandstones. Facies A consists of predominantly coarse-grained sandstones and conglomerates in thick to massive beds. Facies B consists of medium- to fine- and coarse-grained sandstones in thick, lenticular beds. Facies C consists of medium- to fine-grained, rhythmically bedded sandstones and shales that contain typical turbidite sedimentary structures such as graded beds, whereas facies D consists mainly of shale with sandstone interbeds. Facies BD, as used by Nelson and others (1994) and in table 1, contains both B facies and D facies sandstones. Facies F is composed of various sediment types deformed by mass movement.

## SEDIMENTARY PETROLOGY

### METHODS

One hundred and seventeen sandstone samples of the Orca Group in the study area were examined for alteration, grain size, percentage matrix, and cement. Of this number, 47 samples (fig. 2) met petrographic criteria for point counting. These criteria include medium grain size (to ensure standardization of point-counting procedures and to facilitate comparison with data from previous studies), and the presence of less than 25 percent combined matrix and cement (Dickinson and Suczek, 1979). Rocks were stained for potassium feldspar, and in each thin section at least 300 detrital framework grains were counted (table 1). Identification of grain types and point-count procedures were based on criteria developed by Dickinson (1970) and Dickinson and Rich (1972). Classification and symbols used for grain types are given in table 2. Phenocrysts greater than 0.0625 mm present within rock fragments were counted as individual mineral grains instead of as lithic fragments, following methods established by Dickinson (1970).

Detrital framework modes were calculated for quartz, feldspar, and lithic fragments (table 3). Lithic fragments were subdivided into volcanic, metamorphic, and sedi-

mentary types. Recognized volcanic types include vitric, felsitic, microlitic, and lathwork grains, representing a continuum of composition types from siliceous to intermediate to more mafic volcanic rocks.

### ALTERATION

Valid detrital modes can be determined for sandstones only where diagenetic or metamorphic changes of the original mineralogy and texture have not obscured the initial grain population (Dickinson and Rich, 1972). Although many sandstones in the study area show alteration of volcanic lithic and plagioclase grains, original grain lithology is still recognizable. Metamorphic alteration of labile volcanic lithic grains in the studied samples typically involves formation of secondary chlorite, white mica, and some epidote. In many samples, plagioclase is partially or (less commonly) completely albitized. It is probable that some K-feldspar has also been albitized, as was described in graywacke samples from the Franciscan Complex (Cowan, 1974; Dickinson and others, 1982). Other plagioclase grains are replaced by epidote, white mica, and (or) calcite.

The samples studied show prehnite-pumpellyite and lower-middle greenschist metamorphic assemblages. Although some samples show minor lineation or semischistosity, the lithologies of grains were still recognizable in the counted samples. Veins in the Orca Group are filled with prehnite, epidote, feldspar, quartz+calcite, and prehnite+epidote+quartz. Calcite is sometimes present as incomplete or patchy cement and as replacement for plagioclase, lithic grains, and sparse pyroxene.

### RESULTS

Most sandstones of the Orca Group in the study area are moderately to well-sorted arkose to lithic arkose (Folk, 1968) or feldspathic graywackes (Pettijohn, 1957). Modal analyses of sandstones are plotted on the triangular diagrams of Dickinson (1985; fig. 3). On the Q-F-L and Qm-F-Lt plots (figs. 3A, B), the data lie predominantly in the field of magmatic arc provenances. Data are clustered in the dissected arc realm toward the Q-F join, which indicates that the Orca Group sandstones have a more feldspathic and less lithic character.

Detailed age relationships within the faulted accretionary prism of the Orca Group are not well known, but it is assumed that overall the sequence becomes younger to the southeast or outboard area (Dumoulin, 1987). Samples from the inboard part of the study area were compared with samples from the outboard part of the area to determine if any time-related compositional trends exist. Latitude, longitude, and Q-F-L data for samples

Table 1. Point-count data for Orca Group sandstones

[Turbidite facies type listed for each sample. Category abbreviations: Qm, monocrystalline quartz; undul, undulatory; strain, strained; Qp, polycrystalline quartz; eq, equigranular; ineq, inequigranular; fol, foliated; cht, chert; pl, plagioclase; Ksp, K-feldspar; alt, feldspar too altered to be recognized as plagioclase or K-feldspar (not used in normalization); Lv, volcanic lithic grains; vit, vitric; flsit, felsitic; ml, microlitic; lw, lathwork; Ls, sedimentary lithic grains; slst, siltstone; mds, mudstone; Lm, metamorphic lithic grains; slt, slate; sch, schist; hrofl, hornfels; Lms, metasedimentary lithic grains; Lmv, metavolcanic lithic grains; bt, biotite; ms, muscovite; am, amphibole; px, pyroxene; op, opaques; ep, epidote; cm, cement; mx, matrix; alt, alteration such as chlorite, white mica, prehnite, pumpellyite, and laumontite (included with cement and matrix as nonframework grains)]

Sample no.	Facies type	Qm		Qp				Feldspar			Lv				Ls		Lm			Lms	Lmv	bt	ms	am	px	op	cp	other	cm	mx	alt
		undul	strain	eq	ineq	fol	cht	pl	Ksp	alt	vit	flsit	ml	lw	slst	mdst	slt	sch	hroft												
82ADU142A	B	76	7	12	14	5	1	166	47	0	23	20	10	9	1	0	0	0	0	0	0	5	0	0	0	3	3	0	23	37	4
92ANS3A	B	72	4	2	3	1	0	127	43	0	7	22	8	4	0	0	0	0	0	0	4	5	0	0	0	0	0	16	30	11	
92ANS6B	B	68	11	9	12	9	0	85	27	1	16	27	3	5	0	0	0	8	1	0	0	4	0	0	1	1	0	5	28	21	
92ANS7A	B	70	2	2	1	14	0	142	12	0	13	20	3	4	0	0	1	2	0	0	1	2	0	0	5	1	8	18	28	5	
92ANS12A	B	71	12	3	6	3	3	117	15	2	7	26	6	7	0	0	1	2	0	0	3	1	0	0	0	2	13	29	52	13	
92ANS27A	B	72	9	0	8	5	1	125	15	1	5	26	5	6	1	0	2	8	0	0	4	2	0	0	0	2	2	42	67	36	
92ANS33A	BD	85	9	6	8	7	2	140	21	1	1	8	1	0	0	0	0	3	0	0	2	0	1	0	1	0	2	35	36	12	
92ANS46A	B	61	0	3	3	0	1	145	23	0	4	22	21	12	0	0	1	3	0	0	0	0	0	0	0	5	0	30	45	42	
92ANS48A	A	52	0	4	1	26	0	68	7	0	8	47	6	7	8	0	9	24	0	2	30	0	0	0	0	3	0	40	40	17	
92ANS58A	BD	84	10	5	12	20	2	110	8	0	1	27	3	4	0	0	1	5	0	0	7	0	0	0	0	0	3	16	20	28	
92ANS68A	B	35	5	3	7	15	2	123	8	1	8	63	9	7	0	0	1	7	0	0	2	3	0	0	0	1	0	36	37	9	
92ANS69A	B	53	7	4	5	4	0	162	17	0	1	25	4	7	0	0	1	1	0	0	5	1	1	0	1	0	3	11	33	37	
92ANS70A	BD	67	10	2	2	6	3	119	13	0	3	43	2	1	0	0	4	16	0	0	8	0	3	0	0	1	3	29	62	19	
92ANS74A	C	75	12	0	6	8	2	159	3	0	1	17	1	3	0	0	0	10	0	0	1	0	0	0	3	0	5	28	50	11	
92ANS75A	B	63	11	5	6	14	0	108	8	0	10	29	18	14	0	0	0	23	0	0	3	1	0	0	1	2	2	11	32	11	
92ANS81A	C	46	7	1	1	1	0	147	34	0	25	21	4	9	0	0	0	0	0	0	0	0	0	0	0	4	0	34	55	6	
92ANS82A	C	61	7	0	0	5	1	134	30	0	6	19	3	5	1	0	6	14	0	0	2	1	0	0	0	3	2	10	36	5	
92ANS86C	B	54	5	1	1	6	1	159	21	0	10	16	5	3	5	0	0	5	0	0	5	0	1	0	0	0	2	0	9	67	4
92ANS200A	B	78	0	2	7	5	0	112	25	2	5	40	7	4	0	0	0	3	0	0	2	5	0	0	0	2	3	21	48	14	
92ANS201A	B	59	16	3	7	4	2	121	28	0	3	31	6	3	0	0	1	7	0	1	0	1	0	0	1	5	6	11	34	16	
92ANS202A	A	77	13	9	6	5	2	135	6	0	8	11	4	2	2	2	0	0	0	0	2	0	2	0	0	4	0	47	56	36	
92ANS204A	B	83	5	4	4	1	0	127	32	0	1	14	10	5	0	0	1	5	0	0	0	5	1	0	0	1	1	25	30	10	
92AM206A	B	133	2	9	12	2	1	71	18	5	5	18	10	6	1	0	1	9	0	1	0	2	2	0	0	1	1	18	35	4	
92AM209A	C	84	0	3	2	0	0	138	31	0	3	23	3	8	0	0	0	1	0	0	1	1	0	0	3	0	5	9	34	7	
92AM210A	B	65	3	5	4	2	1	129	19	0	4	36	12	4	1	0	1	8	0	1	1	1	0	0	1	2	4	4	24	7	
92AM212A	B	82	4	5	12	6	0	149	1	0	5	17	6	3	1	0	2	3	0	0	1	2	0	0	0	1	2	21	28	5	
92AM214B	F	72	3	6	6	2	2	134	21	0	4	21	7	4	0	0	3	10	0	0	2	3	0	0	0	0	3	14	60	1	
92AM215A	F	84	12	2	5	1	0	136	22	1	5	10	3	2	0	0	1	7	0	0	0	0	0	1	3	2	6	21	82	13	
92AM218A	C	72	5	2	10	9	0	137	19	0	8	11	6	3	0	0	1	12	0	0	0	1	0	0	1	2	4	19	27	5	
92AM219A	B	65	6	1	3	13	0	141	24	0	1	9	4	4	0	0	4	14	0	0	3	5	0	0	0	4	7	0	33	40	5
92AM220B	F	52	0	1	1	10	0	146	30	0	7	34	3	2	2	0	0	7	0	0	2	2	0	0	2	0	5	21	58	11	
92AM230A	C	61	13	2	8	10	0	151	13	1	5	18	3	5	0	0	0	2	0	0	2	0	1	0	4	0	1	17	30	8	
92AM231A	C	55	4	6	4	2	0	163	32	0	6	16	5	1	1	0	0	0	0	0	2	0	0	0	1	2	5	10	55	6	
92AM232A	B	73	6	3	8	1	0	105	33	0	9	32	9	2	2	0	3	3	0	0	5	0	0	0	0	4	1	6	9	12	
92AM237B	BD	52	8	3	6	7	1	127	23	3	8	27	1	2	2	0	7	18	1	0	2	0	0	1	2	2	6	36	54	29	
92AM239A	C	55	4	7	9	0	0	131	33	0	11	26	14	3	1	0	0	0	0	0	7	0	0	0	0	0	8	10	25	15	
92AM241A	B	52	4	0	0	3	0	133	15	0	9	45	24	3	6	0	1	0	0	0	2	0	1	0	0	2	0	29	41	18	
92AM241B	A	73	4	8	7	1	0	124	35	0	10	37	0	1	0	0	0	0	0	0	0	0	0	0	0	2	0	12	36	4	
92AM242A	C	74	5	5	5	4	0	131	21	1	9	14	6	2	0	0	7	8	0	3	0	2	2	0	0	1	3	23	21	1	
92AM246A	C	67	6	10	14	9	1	146	8	0	13	7	2	2	0	0	3	11	0	0	0	2	0	0	0	0	1	10	29	5	
92AM248A	BD	61	5	2	3	5	0	139	114	25	14	20	7	3	0	0	8	13	0	0	3	3	0	2	4	0	5	2	41	6	
92AM249A	C	80	4	5	1	8	1	150	135	15	5	6	0	7	0	0	0	0	0	0	10	0	6	1	9	0	5	5	37	8	
92AM250A	C	63	12	5	6	4	0	156	20	0	21	16	1	14	0	0	0	1	0	0	0	0	0	0	0	2	0	6	46	9	
92AM252A	C	73	5	0	1	6	0	124	30	0	4	20	6	6	0	0	4	7	0	0	1	1	0	0	2	1	6	23	56	3	
92AM253A	C	68	2	1	0	13	0	107	24	0	15	25	21	9	1	0	2	1	0	0	2	1	0	0	2	0	6	11	51	12	
92AM256A	C	51	7	1	3	3	0	176	6	0	6	16	3	15	0	0	0	5	0	0	0	0	0	1	1	0	4	31	20	9	
92AM257A	B	77	3	3	1	3	0	124	25	0	13	18	9	9	0	0	0	1	0	0	0	3	0	0	5	2	8	14	75	1	

**Table 2.** Classification and symbols of grain types

[Classification after Dickinson and others (1982) and Dickinson (1985). Point-count data were normalized to 100 percent and categories summed to produce grain populations used in evaluating provenance trends on triangular diagrams]

Symbols	Grain types	Summations
Q	Total quartzose grains	
Qm	Monocrystalline quartz	$Q = Qm + Qp$
Qp	Polycrystalline quartz (or chert)	
F	Total feldspar grains	
P	Plagioclase grains	$F = P + K$
K	K-feldspar grains	
L	Total unstable lithic fragments	$L = Lv + Ls$
Lv	Volcanic/metavolcanic fragments	
	v m l	$Lv = v + m + l$
	vitric + felsitic volcanic fragments	
	microlitic volcanic fragments	
	lathwork volcanic fragments	
Ls	Sedimentary/metasedimentary lithic fragments	
Lt	Total aphanitic lithic fragments (both unstable and quartz)	$Lt = L + Qp$

**Table 3.** Mean framework modes of primary and secondary parameters of sandstone samples of the Orca Group in the study area, Chugach National Forest

[Secondary grain parameters are ratios of the primary grain populations, which help extract trends and provenance type by identifying significant population variables]

Framework modes	Mean values or ratios
Q-F-L	30-51-19
Qm-F-Lt	25-51-24
Qp-Lv-Ls	23-52-25
Qm-P-K	33-58-9
v-m-l	73-14-13
Qp/Q	0.17
P/F	0.86
V/L	0.76

along a northwest to southeast transect through the study area are given in table 4. From inboard to outboard, samples show generally increasing quartz and decreasing lithic values. All sample points that fall in the transitional arc area of the Q-F-L and Qm-F-Lt diagrams (figs. 3A, B) represent inboard (presumably older) rocks. This result suggests that older parts of the Orca Group formed dur-

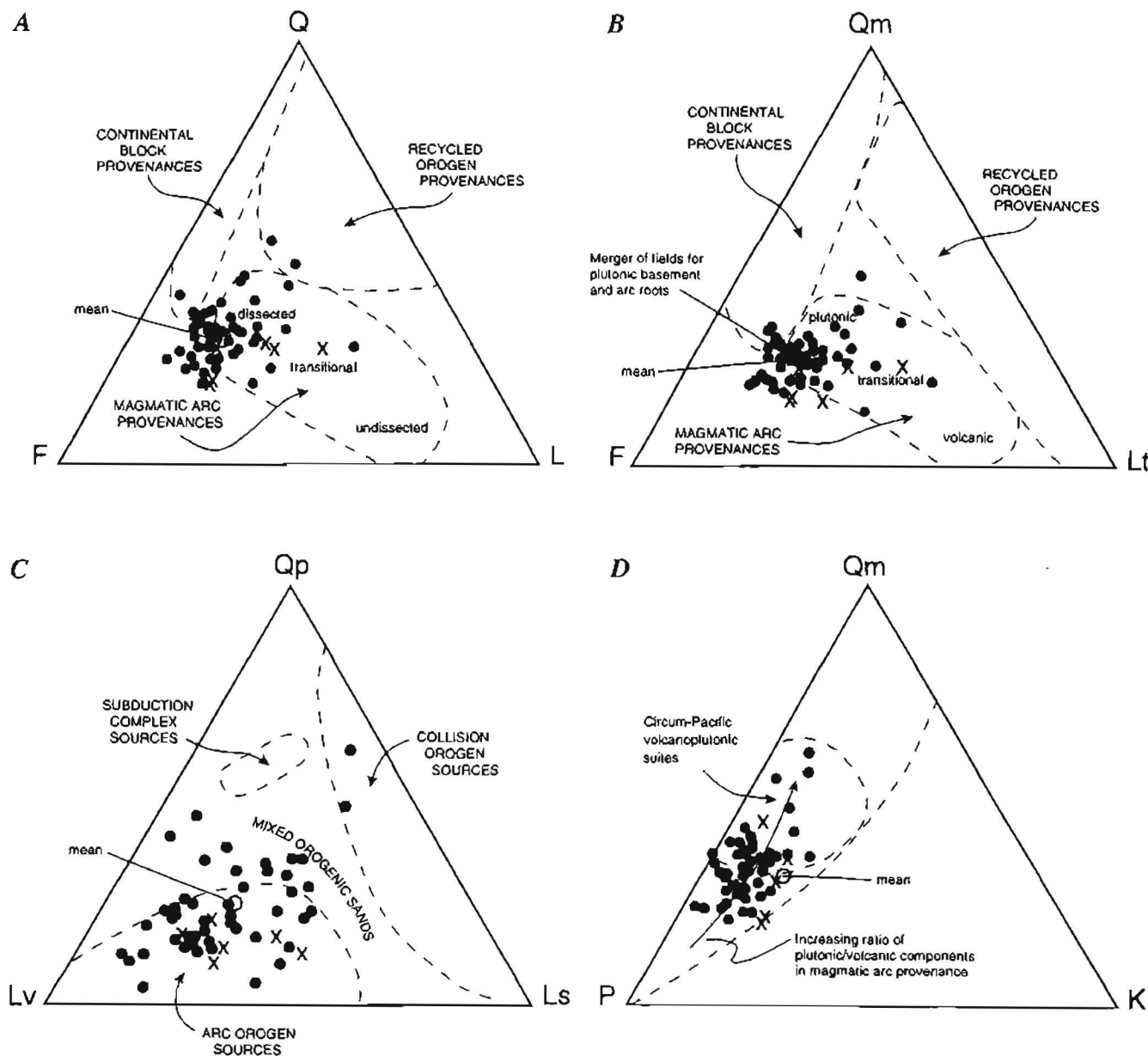
ing progressive unroofing of the arc, whereas younger parts were derived from a more fully dissected arc. Several points occur in the merger of fields on the Qm-F-Lt plot (fig. 3B), indicating deep dissection of the magmatic arc into plutonic basement and batholithic roots. Some scatter of data suggests minor contribution from continental block sources, possibly local uplifted basement provenances, and recycled orogen provenances. Overall, there is a trend of decreasing total lithic fragments and increasing quartz from inboard to outboard locations.

On the Qp-Lv-Ls (fig. 3C) diagram, data from the Orca Group fall primarily in the arc orogen source region, with some scatter into the mixed orogenic sands field. A few points fall into the collision orogen source field. The mean for Qp-Lv-Ls is 23-52-25, which emphasizes that high proportions of volcanic lithic fragments are present. Sedimentary grains are chiefly siltstone with some shale fragments and do not exceed 3.5 percent of total framework grains. An increase in chert grains (included with Qp) accounts for an overall increase in Qp, relative to Lv and Ls (fig. 3C). Volcanic lithic grains ranged from 3 to 29 percent of total framework grains, and the V/L ratio was 0.76 (table 3). Total Lv of the samples has a mean v-m-l of 73-14-13. Volcanic lithic grains have mostly felsitic or vitric textures (73 percent of total Lv), suggesting a source rich in silicic volcanic rocks.

A few percent coarse holocrystalline rock fragments, representing probable plutonic and hypabyssal debris, were noted in nine of the samples. These grains are not evident in tables 1 and 3, however, because they were counted not as lithic fragments but as individual mineral grains

owing to their coarse size (clast size greater than 0.0625 mm in diameter). Several grains of microcline, myrmekite, and perthite were also noted in the samples. Mafic minerals, including pyroxene, amphibole, biotite, muscovite,

and opaques make up as much as 7 percent of total framework grains. Abundant amounts of pyroxene and amphibole support a volcanic origin, whereas the presence of biotite and muscovite point to a plutonic source.



#### EXPLANATION

- Samples from Orca Group, Chugach National Forest study area,  $n = 47$
- Mean of Orca Group, this study
- × Samples from Orca Group (Dumoulin, 1987),  $n = 7$
- - - Provenance fields (Dickinson, 1985)

Figure 3. Triangular plots showing framework modes of sandstones of the Orca Group from the study area, Chugach National Forest, compared with analyses of the Orca Group from the same area from Dumoulin's (1987) study.

**Table 4.** Location of samples and Q-F-L values along a northwest-southeast transect showing inboard to outboard variations

[Transect numbers refer to fig. 2]

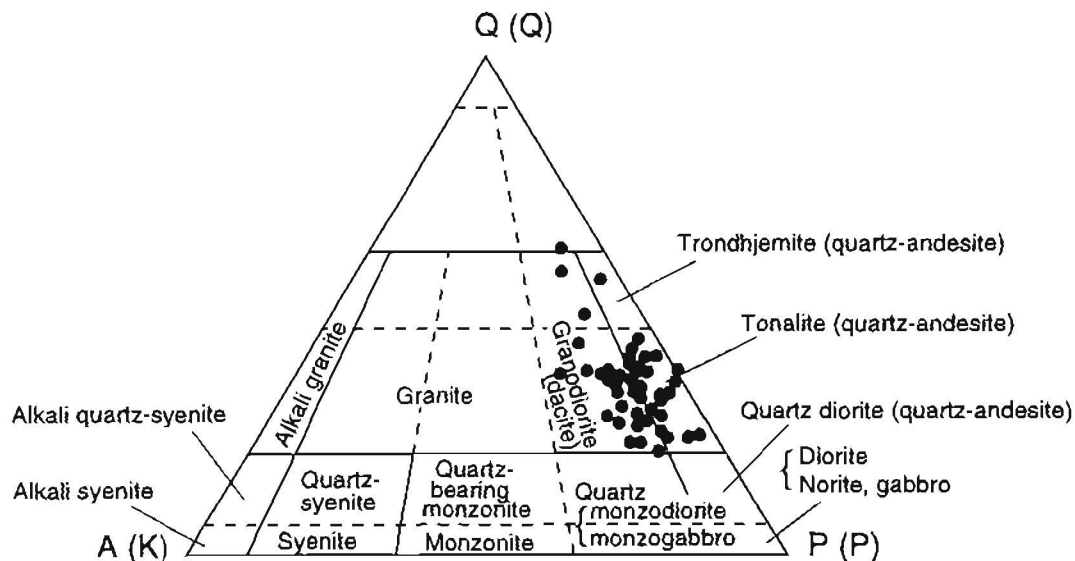
Transect no.	Sample no.	Latitude (degrees)	Longitude (degrees)	Q	F	L
1	92ANS48A	61.0606	147.4487	27.8	25.1	47.2
2	92ANS68A	61.0604	147.4213	22.6	44.6	32.8
3	92ANS75A	61.0469	147.4065	31.7	37.2	31.1
4	92AM241A	61.0267	147.3898	18.9	49.8	30.3
5	92ANS27A	61.0183	147.3498	32.3	47.6	19.7
6	92ANS86C	61.0316	147.2562	22.9	60.6	16.5
7	92AM219A	60.9868	147.2353	30.1	69.9	13.4
8	92AM215A	60.9679	147.2798	35.4	54.1	10.5
9	92ANS202A	60.9431	147.1947	38.0	47.8	14.2
10	92AM212A	60.9258	147.2469	36.6	50.3	13.1

Metamorphic rock fragments, including schist, slate, and rare hornfels fragments, range up to 12.8 percent of total framework grains. These grains probably represent erosion of the wall rocks around batholiths.

The monocrystalline quartz component is shown in the Qm-P-K (fig. 3D) plot. The mean of the data for Qm-P-K is 33-58-9. Rocks in the Chugach National Forest study area have high framework modes of plagioclase (generally greater than 50 percent) and relatively low K-feldspar (usually less than 20 percent). Influence from a plutonic source is indicated by a few points (with out-

board locations) positioned closer to the Qm pole. The average P/F ratio for all samples is 0.86 (table 3).

Abundant plagioclase probably indicates the presence of lavas rich in plagioclase and of intrusive source rocks that contain more plagioclase than K-feldspar in the source area. Qm-P-K data, plotted as a reverse image on a Streckeisen (1967) Q-A-P diagram (fig. 4), indicate that source rocks of the Orca Group consisted predominantly of dacite, quartz-andesite, granodiorite, and tonalite compositions, with a few samples plotting in the trondhjemite field.



**Figure 4.** Streckeisen's (1967) classification of plutonic rocks in the triangle Q-A-P with Q-P-K data from Orca Group sandstones reversely plotted (Q-K-P). K-feldspar is plotted to the left on the alkali side, and plagioclase is plotted on the right side. (Volcanic rock names are also given for classification fields where data occur.)



Samples were plotted according to turbidite facies types to see if compositional variations exist between facies units (table 1). There are no turbidite facies controls of Orca Group sandstone composition. Petrographic data from all facies types plot randomly on triangular diagrams.

## PROVENANCE

All four triangular diagrams collectively point to a dissected magmatic arc provenance of mixed volcanic and plutonic detritus. Overall, a trend of unroofing from a transitional arc to a more dissected arc is suggested by the Q-F-L and Qm-F-Lt plots. Dumoulin (1987, 1988) analyzed seven samples from the area of the present study. Data from these samples are plotted on figure 3 and generally compare well with the data from the present study. A large number of samples in the present study ( $n=47$ ) cluster in a relatively small area of the figure and indicate the primary character of the source area. The remaining scattered data are interpreted as secondary aspects of provenance. Q-P-K data in this study suggest that the primary source rocks included dacite and quartz-andesite volcanic rocks and intrusive tonalite, granodiorite, and minor trondhjemite (fig. 4). The plot of Qm-F-Lt data (fig. 3B) shows many samples plotting in the plutonic basement and arc roots region, emphasizing erosion deep into the arc. Secondary aspects of provenance include chert and metamorphic rocks that may be associated with even older basement of the arc.

Results of previous point-count studies indicated that the most likely source for the Orca Group was a progressively eroded magmatic arc (Winkler, 1976; Dumoulin, 1987, 1988). Earlier geologic and petrologic studies suggested two possible source areas (Dumoulin, 1987, 1988; Plafker and others, 1989; Farmer and others, 1993): the adjacent Wrangellia and Peninsular terranes to the north, and the Coast Mountains of southeastern Alaska and British Columbia (the Coast Mountains Complex) to the southeast. Petrographic data presented here cannot definitively indicate which of these two source areas is more likely, but by combining the detailed analysis of a small study area with regional sedimentologic and paleomagnetic studies, more constraints can be applied to the delineation of the source area for the Orca Group.

Sedimentological data suggest that much of the sediment in the Orca Group came from the direction of southeastern Alaska and British Columbia, with transport northwestward along the continental margin (Winkler, 1976; Plafker and others, 1989). The nearest paleocurrent data available from the Orca Group are those that Winkler (1976) obtained 12-50 km to the southeast of the Chugach National Forest study area. Winkler's (1976) analyses indicate that the transport direction was dominantly from

the northeast near Port Fidalgo and west-northwestward on Hinchinbrook and Hawkins Islands.

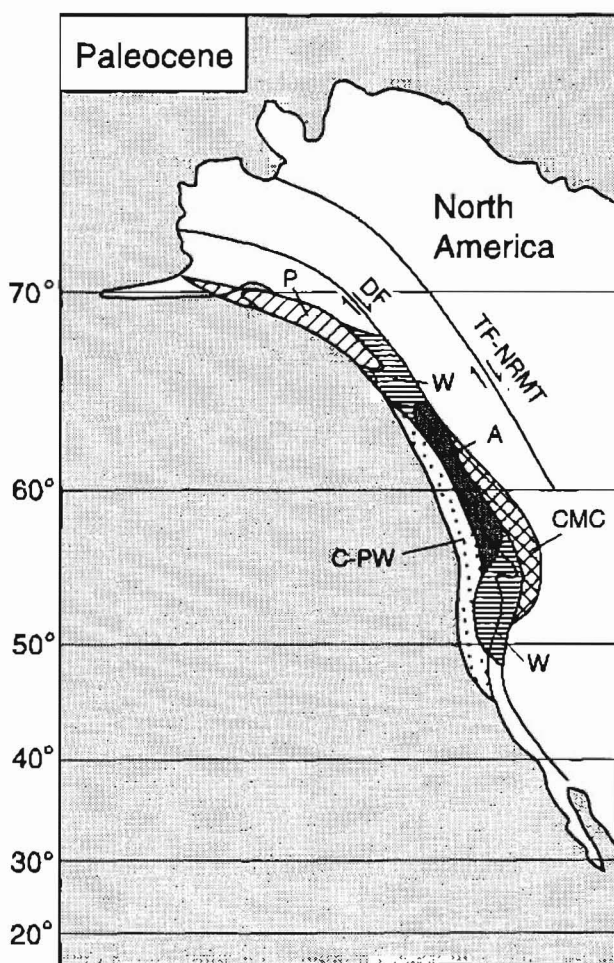
Paleomagnetic and tectonic analyses of rocks in the Prince William Sound area (Nokleberg and others, 1989; Pavlis and Crouse, 1989; Plafker and others, 1989; Bol, 1993; Bol and others, 1992) have documented structural events related to subduction-related accretion or terrane accretion along the Border Ranges and Contact fault systems (Nokleberg and others, 1989; Plafker and others, 1989). These data indicate that the Mesozoic and Tertiary accretionary complex of the Chugach-Prince William composite terrane originated 13-25° of latitude to the south of its present position (Plumley and others, 1983; Bol and others, 1992) and was emplaced by right-lateral movement along the Border Ranges and Contact fault systems (Nokleberg and others, 1989; Pavlis and Crouse, 1989; Bol, 1993). The tectonic setting for the southern Alaskan and Canadian Cordillera during the Paleocene is shown in figure 5 (from Bol and others, 1992).

Both the Wrangellia and Peninsular terranes and the Coast Mountains Complex are possible sources based on point-count data, but isotopic data from Farmer and others (1993) strongly indicate a Coast Mountains provenance as the preferred source. Nd, Sr, and Pb isotopic compositions of both the Valdez and Orca Groups overlap values for the intrusive igneous rocks exposed in the northern part of the Coast Mountains Complex in western British Columbia and equivalent rocks in southern Alaska (Farmer and others, 1993). This complex consists of a deeply eroded plutonic belt of Late Cretaceous and early Tertiary age built on terranes lying inboard of the Wrangellia terrane (Farmer and others, 1993; fig. 5).

Rocks occurring in the Coast Mountains Complex have compositions that are compatible with petrographic data from the Orca Group. The Coast Mountains Complex is one of the main tectonic elements of the northern Cordillera and extends for over 1,700 km in southern Alaska and western British Columbia (Samson and others, 1991). Several workers have described different parts of the complex and have found a compositional range from diorite to granite, but by far the most common rock types are quartz diorite, tonalite, and granodiorite (Crawford and others, 1987; Arth and others, 1988; Brew, 1988; Samson and others, 1991). Felsic and subordinate andesitic volcanic rocks that are older than 110 Ma make up about 60 percent of the lithologies that were present before intrusion of the plutons (Crawford and others, 1987). Thus, the composition of both the Coast Mountains Complex and its country rocks matches that suggested by this study for the source rocks of the Orca Group sandstones (fig. 4).

The isotopic study by Farmer and others (1993) suggested that trondhjemitic clasts in the Orca Group were derived from a Precambrian source in the Nisling/Yukon-Tanana terrane. Petrographic data presented here support

a minor trondhjemitic source and erosion deep into basement (figs. 3, 4). In addition, secondary sources of mixed orogenic sands (fig. 3C) are indicated by point-count data. These sands may have been derived from local uplifted blocks, such as the fault-bounded volcanic and volcanoclastic rocks (TKvv) within the study area (fig. 2); such blocks could have shed chert and limestone, as well as volcanic and volcanoclastic debris, as the accretionary prism evolved. Alternatively, other uplifted block provenances located farther away to the southeast (perhaps also in British Columbia and southeast Alaska) could have been a source of mixed orogenic sands.



**Figure 5.** Tectonic setting for the southern Alaskan and Canadian Cordillera during the Paleocene (after Bol and others, 1992). The Chugach-Prince William terrane lies 13° of latitude south of its present position and adjacent to the Peninsula-Wrangellia-Alexander terrane. Map abbreviations: A, Alexander terrane; C-PW, Chugach-Prince William terrane; CMC, Coast Mountains Complex; DF, Denali fault; P, Peninsular terrane; TF-NRMT, Tintina fault-Northern Rocky Mountain trench; W, Wrangellia terrane.

## CONCLUSIONS

Detrital modes of sandstones of the Orca Group suggest that the Orca Group was derived from a transitional to deeply dissected magmatic arc source, exposing plutonic basement and arc roots. Volcanic and associated plutonic rocks, together with subordinate metamorphic and sedimentary rocks, were the primary source rocks. Regional geologic relations imply that the provenance was located to the southeast in the Coast Mountains Complex of British Columbia and southeast Alaska. The Wrangellia and Peninsular terranes to the north and east are possible alternative sources but are inconsistent with published isotopic data.

High ratios of P/F and V/L in Orca Group sandstones suggest sources rich in plagioclase and volcanic lithic fragments, with relatively short transport distances into the trench area. Secondary sources include mixed orogenic sands derived from local uplifted blocks such as those in the study area. Such blocks could have provided sedimentary lithic grains and volcanoclastic debris to the trench and trench-slope basins as the accretionary prism evolved.

## REFERENCES CITED

- Arth, J.G., Barker, Fred, and Stern, T.W., 1988, Coast batholith and Taku plutons near Ketchikan, Alaska: petrography, geochronology, geochemistry, and isotopic character: *American Journal of Science*, v. 288-A, p. 461-489.
- Bol, A.J., 1993, Overprint magnetizations in support of northward displacement of the Chugach-Prince William terrane, Alaska: *Journal of Geophysical Research*, v. 98, p. 22,389-22,400.
- Bol, A.J., Coe, R.S., Grommé, C.S., and Hillhouse, J.W., 1992, Paleomagnetism of the Resurrection Peninsula, Alaska: implications for the tectonics of southern Alaska and the Kula-Farallon ridge: *Journal of Geophysical Research*, v. 97, p. 17,213-17,232.
- Bol, A.J., and Gibbons, Helen, 1992, Tectonic implications of out-of-sequence faults in an accretionary prism, Prince William Sound, Alaska: *Tectonics*, v. 11, p. 1288-1300.
- Brew, D.A., 1988, Latest Mesozoic and Cenozoic igneous rocks of southeastern Alaska—a synopsis: U.S. Geological Survey Open-File Report 88-405, 29 p.
- Brew, D.A., Ford, A.B., Himmelberg, G.R., and Drinkwater, J.L., in press, The Coast Mountains Complex of southeastern Alaska and adjacent regions, in Koozmín, E.D., ed., *Stratigraphic notes—1994*: U.S. Geological Survey Bulletin.
- Cowan, D.S., 1974, Deformation and metamorphism of the Franciscan subduction complex northwest of Pacheco Pass, California: *Geological Society of America Bulletin*, v. 85, p. 1623-1634.
- Crawford, M.L., Hollister, L.S., and Woodsworth, G.J., 1987, Crustal deformation and regional metamorphism across a terrane boundary, Coast Plutonic Complex, British Columbia: *Tectonics*, v. 6, p. 343-361.

- Crowe, D.E., Nelson, S.W., Brown, P.E., Shanks, W.C. III, and Valley, J.W., 1992, Geology and geochemistry of volcanogenic massive sulfide deposits and related igneous rocks, Prince William Sound, south-central Alaska: *Economic Geology*, v. 87, p. 1722-1746.
- Dickinson, W.R., 1970, Interpreting detrital modes of graywacke and arkose: *Journal of Sedimentary Petrology*, v. 40, p. 695-707.
- , 1985, Interpreting provenance relations from detrital modes of sandstones, in Zuffa, G.G., ed., *Provenance of arenites*: Boston, D. Reidel, p. 333-362.
- Dickinson, W.R., Ingersoll, R.V., Cowan, D.S., Helmhold, K.P., and Suczek, C.A., 1982, Provenance of Franciscan graywackes in coastal California: *Geological Society of America Bulletin*, v. 93, p. 95-107.
- Dickinson, W.R., and Rich, E.I., 1972, Petrologic intervals and petrofacies in the Great Valley Sequence, Sacramento, California: *Geological Society of America Bulletin*, v. 83, p. 3007-3024.
- Dickinson, W.R., and Suczek, C.A., 1979, Plate tectonics and sandstone compositions: *American Association of Petroleum Geologists Bulletin*, v. 63, p. 2164-2182.
- Dumoulin, J.A., 1987, Sandstone composition of the Valdez and Orca Groups, Prince William Sound, Alaska: *U.S. Geological Survey Bulletin* 1774, 37 p.
- , 1988, Sandstone petrographic evidence and the Chugach-Prince William terrane boundary in southern Alaska: *Geology*, v. 16, p. 456-460.
- Farmer, G.L., Ayuso, Robert, and Plafker, George, 1993, A Coast Mountains provenance for the Valdez and Orca Groups, southern Alaska, based on Nd, Sr, and Pb isotopic evidence: *Earth and Planetary Science Letters*, v. 116, p. 9-21.
- Folk, R.L., 1968, *Petrology of sedimentary rocks*: Austin, Tex., Hemphill's Bookstore, 170 p.
- Goldfarb, R.J., Leach, D.L., Miller, M.L., and Pickthorn, W.J., 1986, Geology, metamorphic setting, and genetic constraints of epigenetic lode-gold mineralization within the Cretaceous Valdez Group, south-central Alaska, in Keppie, J.D., Boyle, R.W., and Haynes, S.J., eds., *Turbidite-hosted gold deposits*: *Geological Association of Canada Special Paper* 32, p. 87-105.
- Jones, D.L., Silberling, N.J., Berg, H.C., and Plafker, George, 1981, Map showing tectonostratigraphic terranes of Alaska, columnar sections, and summary description of terranes: *U.S. Geological Survey Open-File Report* 81-792, scale 1:2,500,000, 2 sheets, 20 p. text.
- McGlasson, J.A., 1976, *Geology of central Knight Island, Prince William Sound region, Alaska*: Golden, Colo., Colorado School of Mines, M.S. thesis, 136 p.
- Murri, Emiliano, and Ricci-Lucchi, Franco, 1978, Turbidites of the northern Apennines: introduction to facies analysis: *American Geophysical Institute, Reprint Series* 3, p. 127-166.
- Nelson, S.W., Dumoulin, J.A., and Miller, M.L., 1985, Geologic map of the Chugach National Forest, Alaska: *U.S. Geological Survey Miscellaneous Field Studies Map* MF-1645-B, 16 p., scale 1:250,000.
- Nelson, S.W., Miller, M.L., Goldfarb, R.J., Snee, L.W., Sherman, G.E., Roe, C.H., and Balen, M.D., 1994, Mineral resource assessment of the Chugach National Forest Special Study Area in northern Prince William Sound, Alaska: *U.S. Geological Survey Open-File Report* 94-272, 21 p.
- Nelson, S.W., and Nelson, M.S., 1993, Geochemistry of ophiolitic rocks from Knight Island, Prince William Sound, Alaska, in Dusel-Bacon, Cynthia and Till, A.B., *Geologic Studies in Alaska by the U.S. Geological Survey, 1992*: *U.S. Geological Survey Bulletin* 2068, p. 130-142.
- Nokleberg, W.J., Plafker, George, Lull, J.S., Wallace, W.K., and Winkler, G.R., 1989, Structural analysis of the southern Peninsular, southern Wrangellia, and northern Chugach terranes along the Trans-Alaska Crustal Transect, northern Chugach Mountains, Alaska: *Journal of Geophysical Research*, v. 94, p. 4297-4320.
- Pavlis, T. L., and Crouse, G.W., 1989, Late Mesozoic strike slip movement on the Border Ranges fault system in the eastern Chugach Mountains, southern Alaska: *Journal of Geophysical Research*, v. 94, p. 4321-4332.
- Pettijohn, F.J., 1957, *Sedimentary rocks* (2d ed.): New York, Harper and Bros., 628 p.
- Plafker, George, Jones, D.L., and Pessagno, E.A., Jr., 1977, A Cretaceous accretionary flysch and melange terrane along the Gulf of Alaska margin, in Blean, K.M., ed., *The United States Geological Survey in Alaska: Accomplishments during 1976*: *U.S. Geological Survey Circular* 751-B, p. 41-43.
- Plafker, George, Keller, Gerta, Nelson, S.W., Dumoulin, J.A., and Miller, M.L., 1985, Summary of data on the age of the Orca Group, Alaska: *U.S. Geological Survey Open-File Report* 85-429, 24 p.
- Plafker, George, Nokleberg, W.J., and Lull, J.S., 1989, Bedrock geology and tectonic evolution of the Wrangellia, Peninsular, and Chugach terranes along the Trans-Alaska Crustal Transect in the Chugach Mountains and southern Copper River basin: *Journal of Geophysical Research*, v. 94, p. 4255-4295.
- Plumley, P.W., Coe, R.S., and Byrne, Tim, 1983, Paleomagnetism of the Paleocene Ghost Rocks Formation, Prince William terrane, Alaska: *Tectonics*, v. 2, p. 295-314.
- Samson, S.D., Patchett, P.J., McClellan, W.C., and Gehrels, G.E., 1991, Nd and Sr isotopic constraints on the petrogenesis of the west side of the northern Coast Mountains batholith, Alaskan and Canadian Cordillera: *Canadian Journal of Earth Sciences*, v. 28, p. 939-946.
- Schrader, F.C., 1900, A reconnaissance of a part of Prince William Sound and the Copper River district, Alaska, in 1898: *U.S. Geological Survey 20th Anniversary Report*, p. 341-423.
- Sureckisen, Albert, 1967, Classification and nomenclature of igneous rocks (final report of an inquiry): *Neues Jahrbuch für Mineralogie Abhandlungen*, v. 107, p. 144-240.
- Winkler, G.R., 1976, Deep-sea fan deposition of the lower Tertiary Orca Group, eastern Prince William Sound, Alaska, in Miller, T.P., ed., *Recent and ancient sedimentary environments in Alaska*: Anchorage, Alaska Geological Society, Symposium Proceedings, p. R1-R20.
- Winkler, G.R., and Plafker, George, 1981, Geologic map and cross-sections of the Cordova and Middleton Island quadrangles, southern Alaska: *U.S. Geological Survey Open-File Report* 81-1164, 26 p., scale 1:250,000.



# The Pliosaurid *Megalneusaurus*: A Newly Recognized Occurrence in the Upper Jurassic Naknek Formation of the Alaska Peninsula

By Robert E. Weems and Robert B. Blodgett

## ABSTRACT

A fragmentary humerus of the pliosaurid *Megalneusaurus*, from the Upper Jurassic Naknek Formation of the Alaska Peninsula, represents the only plesiosaurian known from Alaska and only the second Jurassic pliosauroid occurrence reported from the modern Arctic region. Elsewhere, *Megalneusaurus* is known only from Wyoming. The restricted geographic occurrence of *Megalneusaurus*, in the absence of any well-known European genera of Jurassic plesiosaurians or ichthyosaurs in marine strata from northwestern North America, suggests that there may have been biogeographic provincialism among Late Jurassic marine reptiles.

## INTRODUCTION

In June of 1922, W.R. Smith of the U.S. Geological Survey (USGS) received from Jack Mason two large fossil bone fragments collected along the Kejulic River in the Alaska Peninsula (fig. 1). The specimens, proximal and distal ends of a large humerus, came from siltstone in the Upper Jurassic Naknek Formation. The fragments were accessioned with the United States National Museum (USNM, now the Smithsonian Institution's National Museum of Natural History) under the number 372857, and they were assigned a specimen number of USNM 418489. Two cards accompany these specimens. The first is a USGS locality information card stating that the specimens are from locality F 38, which is "sh [shale] in uppermost Naknek" located "On Kejulic River. N.E. of Becharof Lake. Found by Jack Mason." The second is a USNM card with much of the same information.

The only published reference to the plesiosaurian material here described is in a list of fossils from the Naknek Formation (Martin, 1926, p. 215), where a plesiosaurian is noted from locality F 38. This reference is obscure, and later workers (such as Tarlo, 1960; Persson, 1963) apparently were unaware of the existence of an

Alaskan Jurassic plesiosaurian. The present paper places this geographically important material more obviously within the formal literature.

## GEOGRAPHIC LOCATION AND STRATIGRAPHIC HORIZON

Martin (1926, p. 212) stated that the pliosaurid fossil was found "near mouth of Kejulic River" by "W.R. Smith, 1922." This taxonomic assignment was based on an unpublished report, dated October 30, 1922, provided to W. R. Smith by J.W. Gidley of the U.S. National Museum. Gidley reported that the specimens were found "near mouth of Kejulic River" in "shales" from the "Upper Jurassic, Upper Naknek." The collector was listed as W.R. Smith and the field locality as F 38. Gidley concluded that: "The pieces of this lot belong to a large species of plesiosaur, probably of the *Baptanodon* group [i.e., of Middle Jurassic Cordilleran affinity]. The large piece seems to be the distal end of a humerus. The genus and species cannot be determined on this material."

W.R. Smith and A.A. Baker were involved during the summer of 1922 in USGS geologic and topographic mapping of the Alaska Peninsula. Smith (Field Notebook II, 1922, p. 8) made the following field notes regarding the discovery of these bone fragments. "June 21. Fog. Walked to head of Ugashik Creek. Mason Bros. gave me some fossils from Garcolik River bank. One a piece of dinosaur bone." Presumably the "dinosaur bone" was one of the pliosaurid bone fragments because no other bone fragments were accessioned with the USNM. The Garcolic (also spelled Garkolik) River is an earlier alternate name for the Kejulic River of current usage (see Capps, 1923, p. 88, 103).

A. A. Baker (Field Notebook 22ABII, 1922, p. 10, entry for 24 June) provided a bit more information about this discovery: "Jack Mason reports an anticline in the Kejulics. As he described it to me the Kejulic River runs through the structure which follows the same structural



trend as the Cold Bay country or possibly a little more southerly. The rock is a hard, bluish gray shale with thin ss [sandstone] beds which Mason says is uppermost Naknek. He found a gastropod and some bones in this formation."

Two USGS field parties, one including Smith and the other including Baker, had their camps situated close to Pearl Creek dome, southeast of Mount Peulik, at the time the Mason brothers donated their fossil specimens. However, it is unclear what relationship other than proximity the Mason brothers might have had with the USGS parties working in the area at that time. It seems plausible that the brothers were involved with oil exploration and drilling being conducted in this region on the Pearl Creek dome. Certainly they had been involved previously in mineral exploration, for Smith (1925, p. 207) recorded that "in 1915 placer gold was discovered by Fred and Jack Mason in a small stream about 2 miles in length rising in the snow fields of Mount Kubugakli and entering the strait at the point of the cape just west of the southwest boundary of the Katmai National Monument."

Neither the pliosaurid nor gastropod collection locality is shown on the geologic map of the Kejulik River valley that was published with the results of work for that year (Smith and Baker, 1924, pl. IX), nor is either locality described in that work. However, Smith, on October 24, 1922, submitted a request for examination of invertebrate fossils to T.W. Stanton of the USGS that included the fossil gastropod (*Amberleya*) mentioned by Baker. Smith provided field data for this specimen under field locality F 37 (cited in Martin, 1926, p. 212, 214 as USGS Mesozoic locality 11363), which he described as "Naknek. Shale on bank of Kejulic River, N.E. of Becharof Lake. With vertebrates found by Jack Mason." This statement might imply that locality F 37 was the same as locality F 38. Yet Martin (1926, p. 214) gives slightly different site descriptions for F 37 (=11363) and F 38, suggesting that the collection sites were different. Thus, although it is certain that the pliosaurid bone fragments were found somewhere along the banks of the Kejulik River (fig. 1), most likely near its mouth, we can neither locate precisely where they were found nor say for sure if they were found together with the specimen of *Amberleya*.

Although the original USGS locality information card states that these fossils came from the "uppermost Naknek," recent mapping suggests that the uppermost Naknek does not occur along the Kejulik River. Instead, the Kejulik River valley is largely floored by rocks of the Snug Harbor Siltstone Member, which lies near the middle of the Naknek Formation (Detterman and others, in press; Wilson and others, in press). This member of the Naknek has been dated as late Oxfordian to Kimmeridgian in age (Detterman and others, in press).

## TAXONOMY

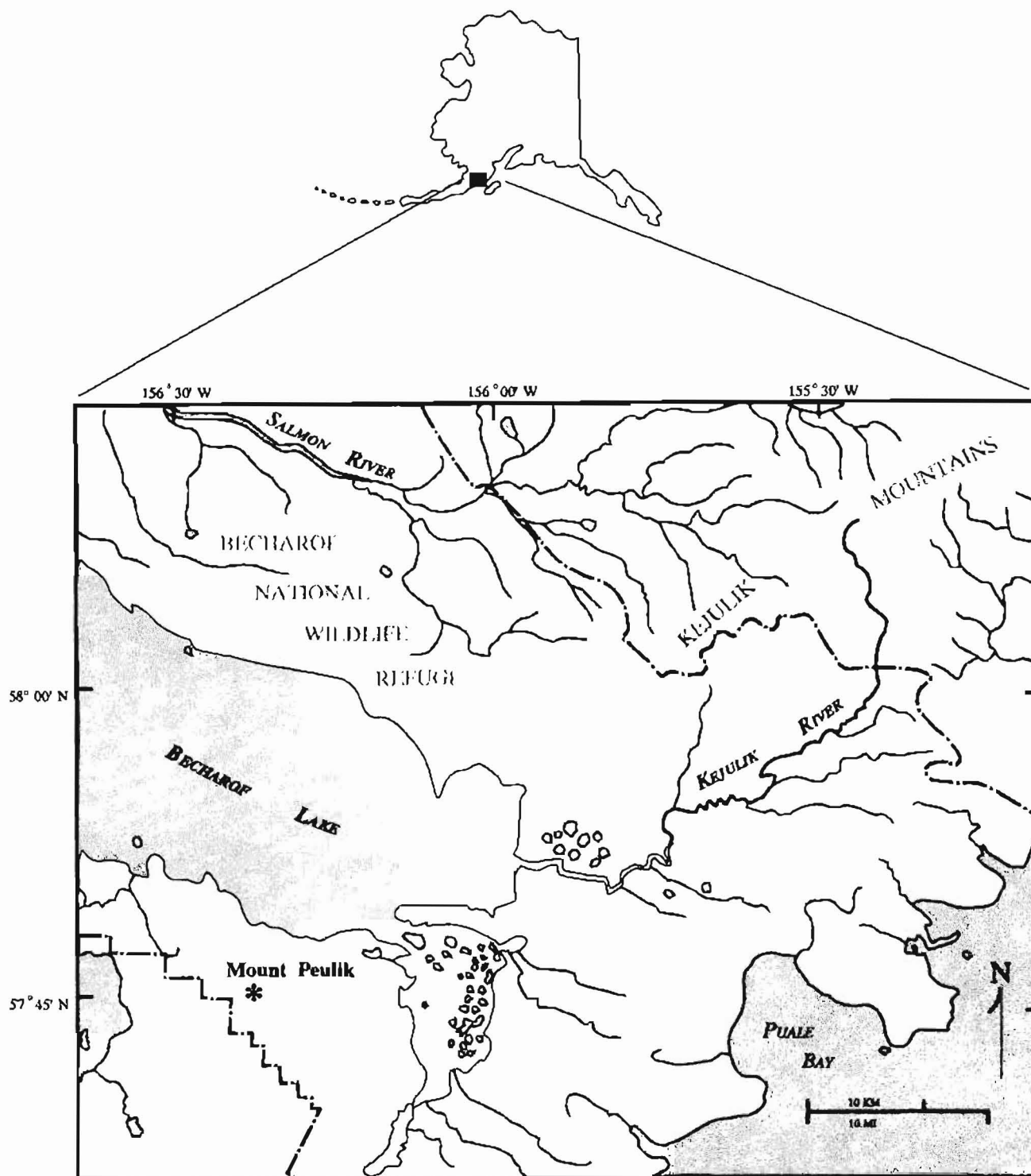
The two fragments (fig. 2) are proximal and distal ends of a plesiosaurian humerus. The two fragments do not make contact with each other, so it cannot be rigorously demonstrated that they pertain to the same animal. However, the pieces are not overlapping, are from the same size animal, have color and texture that are identical, and come from the same locality. Therefore, it is very likely that these two pieces represent opposite ends of the same bone (fig. 3). The proximal fragment has a robust and rounded head, a pronounced lateral tubercle centered medially in dorsal view, and a stout but rounded shaft. The distal end is only modestly expanded when compared to other plesiosaurians. These characteristics are diagnostic for the superfamily Pliosauroidae (Tarlo, 1960, p. 181), which includes plesiosaurians with large heads, short necks, and barrel-shaped bodies (fig. 4). Traditionally, the superfamily Pliosauroidae includes all other plesiosaurians, which are forms with long necks and much smaller heads. However, Bakker (1993) has argued convincingly that the Pliosauroidae is polyphyletic and thus in need of taxonomic revision.

The Pliosauroidae are grouped either within the single family Pliosauridae (Tarlo, 1960; Carroll, 1988) or as three families (Persson, 1963). In the latter classification, some forms are placed in the family Pliosauridae, but others are placed in the families Rhomaleosauridae and Polycotylidae. Among the Rhomaleosauridae, the humeri of the Late Jurassic taxa *Simolestes* and *Leptocleidus* have distal ends that are more expanded than in the Alaskan specimen and proximal heads that are much less robust and less expanded (Tarlo, 1960, pl. 27; Andrews, 1922, pl. 15). The Polycotylidae are known only from the Cretaceous (Persson, 1963). Thus, the specimens at hand belong in the family Pliosauridae by either taxonomic system.

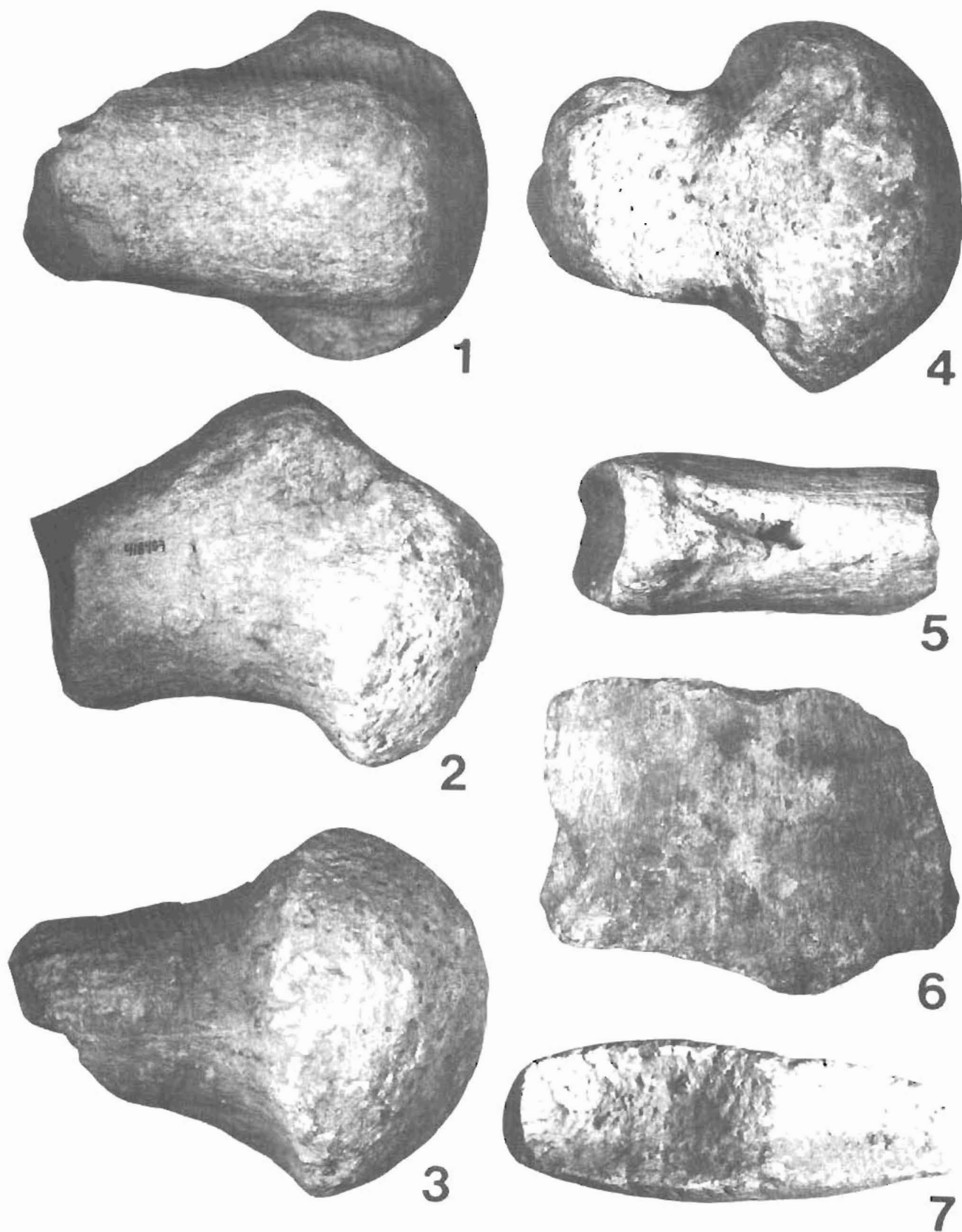
Among genera universally placed in the Pliosauridae, only the Late Jurassic North American genus *Megalneusaurus* provides a close match to the Alaskan material, both in its general appearance and in the details of the cross-sectional shape of the head and the tubercle. Even so, there are three discernible differences: (1) The crest of the tubercle on the Alaskan specimen is not quite as high in profile as it is in the type of *Megalneusaurus*. (2) Although the distal end of the Alaskan humerus shows a degree of lateral expansion similar to that seen in *Megalneusaurus* in dorsal view, in lateral view its relative thickness seems to be slightly less. (3) The type humerus of *Megalneusaurus rex* is nearly twice as large as that of the Alaskan specimen. While the observed differences might represent a species level of distinction between the type humerus of *Megalneusaurus* and the specimen from the Naknek Formation, they more probably represent allometric variation due to age or individual variation. As isolated plesiosaurian humeri are

considered diagnostic at the generic level of taxonomy but not at the species level (Tarlo, 1960, p. 149), it is pointless to assign taxonomic significance to the observed minor differences on the basis of one specimen.

Humeri of other genera of described pliosaurids are much less similar in appearance to the Alaskan material. The genus *Pliosaurus* has a tubercle that is nearly equal in size to the head of the humerus (Tarlo, 1959a), while



**Figure 1.** Map showing location of the Kejulik River on the Alaska Peninsula. A fragmentary pliosaurid humerus (*Megalneusaurus* sp.) was recovered from the banks of this river in strata of the Upper Jurassic Naknek Formation. Dashed lines mark the boundaries of the Becharof National Wildlife Refuge.



**Figure 2.** *Megalneusaurus* sp. (USNM 418489) from the Naknek Formation. 1-4, Dorsal, lateral, ventral, and proximal views of proximal end of humerus. 5-7, Lateral, dorsal, and distal views of distal end of humerus. All views  $\times 0.5$ .

*Liopleurodon* and *Peloneustes* both have heads much less expanded and less rounded than the head of the Alaskan specimen (Linder, 1913, pl. 35, fig. 7 per Tarlo, 1960, p. 167; Andrews, 1913, p. 57). The Alaskan specimen compares rather favorably to *Stretosaurus* in its general proportions (Tarlo, 1959b), but the shape of the proximal head, the lateral tubercle, and the distal end do not match in detail. The humerus is unknown for *Strongylokrotaphus* from Russia (Novozhilov, 1948, 1964), and for *Sinopliosaurus*, *Bishanopliosaurus*, and *Yuzhoupliosaurus* from China (Young, 1944; Hou and others, 1975; Zhang, 1985; Dong, 1980), so direct comparisons cannot be made with any of those genera. If any of these taxa eventually prove to be synonymous with *Megalneusaurus*, the American name has priority.

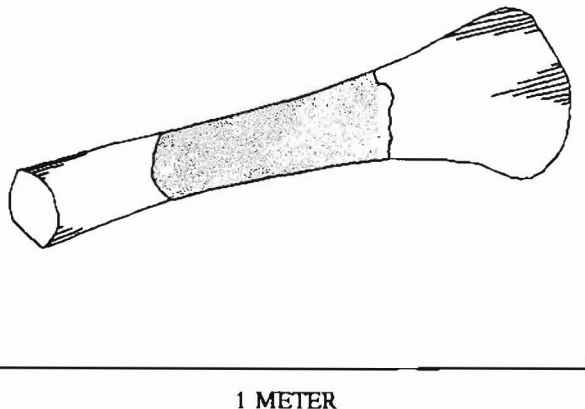


Figure 3. Estimation of the relative proportions of missing (stippled) and preserved bone for the Alaskan humerus specimen of *Megalneusaurus* sp. Missing portion shown here is estimated by comparison with the humerus of *Megalneusaurus rex* shown here in lateral view (Knight, 1898) (scale is for *M. rex*).

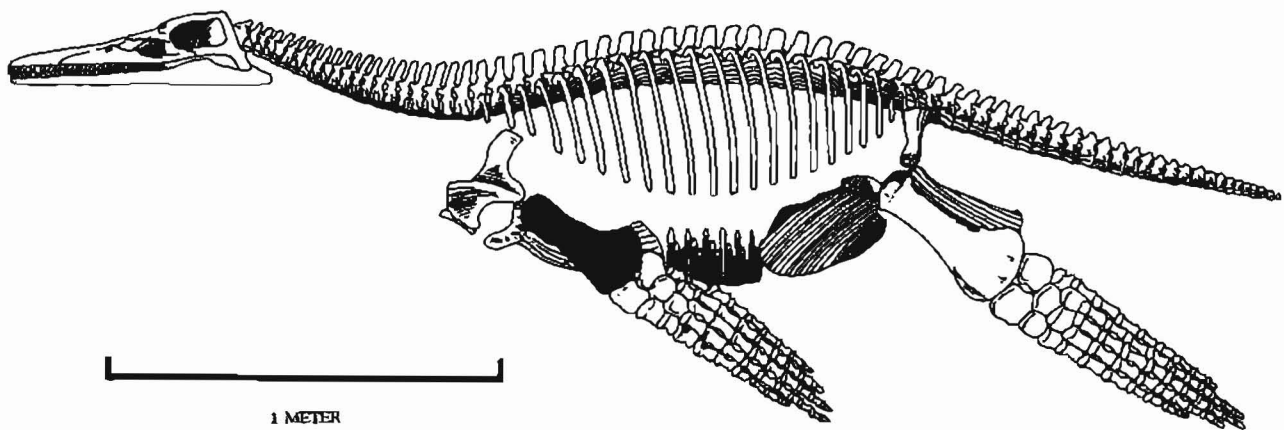


Figure 4. Restored skeleton of one of the better known small pliosaurids, *Peloneustes philarchus* (Seeley), as envisioned by Andrews (1913). The humerus is shown in black. The relatively longer humerus of *Megalneusaurus* (see fig. 3), as compared with *Peloneustes*, suggests that *Megalneusaurus* had a more powerful swimming stroke than *Peloneustes*.

## STRATIGRAPHIC RANGE OF *MEGALNEUSAURUS*

Persson (1963, p. 37) stated that *Megalneusaurus rex* came from the "Como Stage" = Morrison Formation (Kimmeridgian-L. Portlandian). Natrona County (Wyoming). Although the locality is correctly listed, the stratigraphic horizon is wrong. This error occurred because Knight (1898), in the same article that he described *Megalneusaurus*, also proposed that the beds containing this fossil be formally named the "Como group." However, W.B. Scott (1897) already had proposed the name "Como beds" for what today is called the Morrison Formation. Apparently, Knight was initially unaware of this; later, he changed his terminology and adopted Scott's term "Como beds" (as the "Como stage") for beds equivalent to the Morrison and renamed the *Megalneusaurus*-bearing beds as the "Shirley stage." The "Shirley" beds today are the upper part of the Sundance Formation (Imlay, 1952). Unfortunately, Knight never explicitly renounced his original usage of "Como group" for the upper part of the Sundance Formation (Knight, 1900; Wilmarth, 1957, p. 499). Because Knight (1900) later listed *Megalneusaurus* as a "Shirley" fossil, it is certain that he collected it from the upper part of the Sundance Formation of late Oxfordian age. However, Persson understandably but incorrectly assumed that that "Como stage" and "Como group" were synonymous concepts. In so doing, he unwittingly moved the provenance of *Megalneusaurus* out of the upper Oxfordian part of the Sundance Formation and into the Kimmeridgian part of the Morrison Formation.

The base of the Naknek Formation in the Kejulik River area is, like the upper part of the Sundance Formation, Oxfordian in age. But the Snug Harbor Siltstone

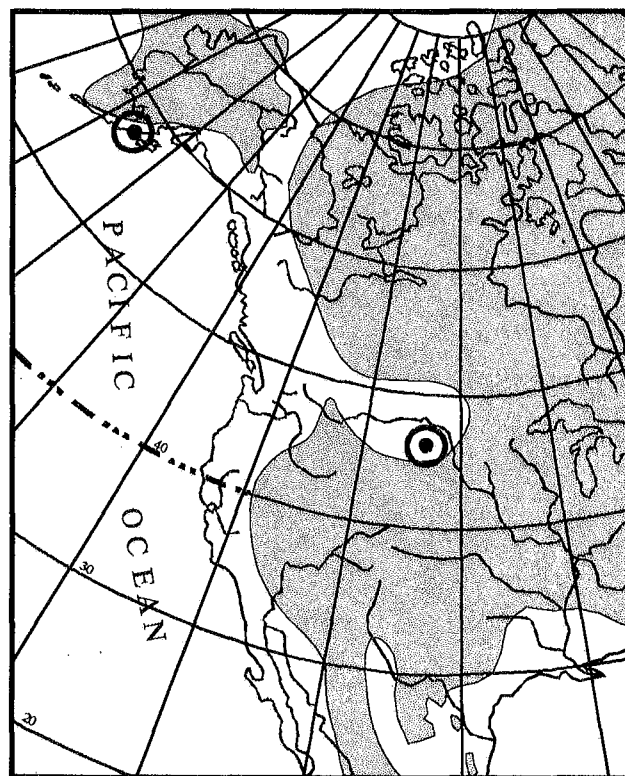
Member of the Naknek, which floors the Kejulik River valley, also ranges upward into the Kimmeridgian stage (Detterman and others, in press). Thus the Alaskan specimen of *Megalneusaurus* could be either the same age as the Wyoming occurrences of *Megalneusaurus rex* or slightly younger. As the Late Jurassic has been considered to be a time of relative ecological and taxonomic stability among marine reptiles (Bakker, 1993), an Oxfordian to Kimmeridgian range for *Megalneusaurus* would not be surprising.

## BIOGEOGRAPHIC AND PALEOECOLOGIC IMPLICATIONS

The occurrence of *Megalneusaurus* in Alaska has interesting implications for the biogeography of marine reptiles in the Late Jurassic. None of the plesiosaurian species described from the Upper Jurassic of northwestern North America are synonymous with European species, and assignments previously made to European genera are all questioned (Persson, 1963). Similarly, ichthyosaurs (another major group of Jurassic marine reptiles) are represented in the Upper Jurassic of western North America by species of the endemic genus *Baptanodon* (Gilmore, 1905, 1906) and two poorly known endemic species originally assigned (probably incorrectly) to *Ichthyosaurus* (Camp, 1942; Camp and Koch, 1966). Upper Jurassic ichthyosaur genera known from Europe (*Ophthalmosaurus*, *Grendelius*, and ?*Nannopterygius*) have not been reported from western North America (Carroll, 1988). This apparent provincialism among the western North American marine reptiles may be significant in view of the fact that invertebrate fossils from northwestern North America (for example, *Buchia* and *Amoeboceras*) are part of a distinct Late Jurassic biogeographic Boreal realm that differs markedly from the circumequatorial Tethyan realm invertebrate faunas found farther south (Khudoley, 1979, p. 60; Detterman, 1988, p. 8–9, 24; Hillebrandt and others, 1992, p. 351). The occurrence of *Megalneusaurus* widely across this province, both in Wyoming and Alaska but not elsewhere (fig. 5), hints that the marine reptiles within the Late Jurassic Boreal Realm may have been endemic to this province. A later Mesozoic biogeographic provincialism in the Pacific Coast region has been documented for plesiosaurians and mosasaurs in the Late Cretaceous (Russell, 1993), so it will be most interesting to see if future finds continue to suggest an earlier provincialism among Late Jurassic marine reptiles of the northern Pacific region.

There has been much controversy concerning the location of the Peninsular terrane and associated southern Alaskan terranes during the Mesozoic. On the basis of paleomagnetic data (for example, Packer and Stone, 1974;

Stone and Packer, 1979; Stone and others, 1982), it has been suggested that these terranes lay far south of their present position during the Jurassic, perhaps even south of the equator. However, both the low diversity of the Naknek molluscan fauna and its strong similarity to molluscan faunas of similar age in Siberia, Franz Joseph Land, Arctic Canada, and Greenland offer compelling evidence that by Late Jurassic time the Peninsular terrane was located at or near its present position in a cool to cold boreal setting (Taylor and others, 1984; Detterman, 1988; Hillebrandt and others, 1992). Similarly, the scarcity of Upper Jurassic calcareous sediments in the Naknek Formation suggests that the Peninsular terrane was located in cool to cold water (Imlay, 1965, p. 1033). In contrast to the Naknek beds, the Oxfordian upper part of the Sundance Formation of Wyoming, which contains the other occurrence of *Megalneusaurus*, appears to have been deposited in somewhat warmer waters. The upper part of the



**Figure 5.** Late Jurassic paleogeography of western North America (modified from Imlay, 1984), showing the relative locations of the type area occurrence of *Megalneusaurus* in the Sundance Formation of Wyoming and the presently reported occurrence in the Naknek Formation of Alaska. Stippled area represents estimated extent of land during this time period. In this figure, Alaska is assumed to have reached nearly its present geologic configuration by the Late Jurassic. The transition between the circumequatorial Tethyan realm and the Boreal realm lies at about 40°N. latitude.



Sundance Formation has common bedded limestones, a much more diverse invertebrate fauna, and an abundant and taxonomically diverse population of the bivalve genus *Gryphaea*. The latter genus is totally unknown from Naknek fossil collections.

The presence of a large reptile such as *Megalneusaurus* on the Alaska Peninsula does not necessarily contradict the above cited faunal and sedimentological evidence. Although this is the first plesiosaurian known from Alaska, a Late Jurassic pliosaurid (*Peloneustes* cf. *philarchus*) also has been reported in the circumpolar region from Franz Joseph Land northeast of Norway (Persson, 1963, p. 35). According to recent paleogeographic reconstructions (Smith and others, 1993), both of these pliosaurid occurrences were higher than 60° paleolatitude in the Late Jurassic. It might be argued that pliosaurid reptile remains at very high paleolatitudes indicate that the Late Jurassic polar region was much warmer than today. However, it must be remembered that the only living fully marine reptile of remotely comparable bulk (the leatherback sea turtle *Dermochelys*) ranges north to Labrador, Iceland, and Alaska during the summer months (Ernst and Barbour, 1989). In cold water, leatherbacks can maintain body temperatures up to 18°C higher than that of surrounding water (Frair and others, 1972). It is quite possible that pliosaurids were comparable to *Dermochelys* in their wide-ranging habits and in their ability to survive in cool or cold waters. Massare (1987) has concluded that pliosaurids probably were opportunistic predators like modern killer whales. Based on one case of preserved stomach contents, some pliosauroids definitely preyed upon cephalopods. Their tooth morphology, however, suggests that they also could have caught and consumed fish, sea turtles, and (or) small ichthyosaurs as well. Thus, *Megalneusaurus* may have been a wide-ranging, opportunistic marine predator that visited the waters of the Alaska Peninsula only seasonally.

**Acknowledgments.**—We are grateful to Frederic H. Wilson for providing us a copy of the unpublished faunal report of J.W. Gidley on these fossils, and also to Jill L. Schneider, who arranged for a loan of the field notebooks of W.R. Smith and A.A. Baker. Thomas R. Holtz, Jr., and Frederic H. Wilson reviewed the manuscript and made helpful suggestions and revisions.

## REFERENCES CITED

- Andrews, C.W., 1913, A descriptive catalogue of the marine reptiles of the Oxford Clay, v. 2: London, British Museum of Natural History, 206 p.
- 1922, Description of a new plesiosaur from the Weald Clay of Berwick (Sussex): Quarterly Journal of the Geological Society of London, v. 78, p. 285–298.
- Bakker, R.T., 1993, Plesiosaur extinction cycles—events that mark the beginning, middle and end of the Cretaceous, in Caldwell, W.G.E., and Kauffman, E.G., eds., Evolution of the Western Interior Basin: Geological Association of Canada Special Paper 39, p. 641–664.
- Camp, C.L., 1942, Ichthyosaur rostra from central California: Journal of Paleontology, v. 16, no. 3, p. 362–371.
- Camp, C.L., and Koch, J.G., 1966, Late Jurassic ichthyosaur from coastal Oregon: Journal of Paleontology, v. 40, no. 1, p. 204–205.
- Capps, S.R., 1923, The Cold Bay district, in Brooks, A.H., and others, eds., Mineral resources of Alaska, report on progress of investigations in 1921: U.S. Geological Survey Bulletin 739-C, p. C77–C116.
- Carroll, R.L., 1988, Vertebrate paleontology and evolution: New York, W.H. Freeman and Company, 698 p.
- Detterman, R.L., 1988, Mesozoic biogeography of southern Alaska with implications for the paleogeography: U.S. Geological Survey Open-File Report 88–662, 27 p.
- Detterman, R.L., Case, J.E., Miller, J.W., Wilson, F.H., and Yount, M.E., in press, Stratigraphic framework of the Alaska Peninsula: U.S. Geological Survey Bulletin 1969-A.
- Dong, Z.M., 1980, A new plesiosauria from the Lias of Sichuan basin: Vertebata Palasiatica, v. 18, p. 191–197.
- Ernst, C.H., and Barbour, R.W., 1989, Turtles of the world: Washington, D.C., Smithsonian Institution Press, 313 p.
- Frair, W., Ackman, R.G., and Mrosovsky, N., 1972, Body temperature of *Dermochelys coriacea*: warm turtle from cold water: Science v. 177, p. 791–793.
- Gilmore, C.W., 1905, Osteology of *Baptanodon* (Marsh): Memoirs of the Carnegie Museum, v. 2, no. 2, p. 77–129.
- 1906, Notes on osteology of *Baptanodon* with a description of a new species: Memoirs of the Carnegie Museum, v. 2, no. 9, p. 325–337.
- Hillebrandt, A. von, Westermann, G.E.G., Callomon, J.H., and Detterman, R.L., 1992, Ammonites of the circum-Pacific region, in Westermann, G.E.G., ed., The Jurassic of the circum-Pacific: International Geological Correlation Programme Project 171: New York, Cambridge University Press, p. 342–359.
- Hou, L.H., Yeh, H.K., and Zhao, X.J., 1975, Fossil reptiles from Fusui Kwangshi: Vertebata Palasiatica, v. 13, p. 24–33.
- Imlay, R.W., 1952, Correlation of the Jurassic formations of North America, exclusive of Canada: Bulletin of the Geological Society of America, v. 63, p. 953–992.
- 1965, Jurassic marine faunal differentiation in North America: Journal of Paleontology, v. 39, no. 5, p. 1023–1038.
- 1984, Jurassic ammonite successions in North America and biogeographic implications, in Westermann, G.E.G., ed., Jurassic-Cretaceous biochronology and paleogeography of North America: Geological Association of Canada Special Paper 27, p. 1–12.
- Khudoley, K.M., 1979, Kimeridzhskii vek, in Khudoley, K.M. and Rzhonsnitskaya, M.A., eds., Paleobiogeograficheskii altas tikhookeanskogo podvishnogo poyasa i tikhogo okeana: Moskva, "Aerogeologiya," p. 59–60.
- Knight, W.C., 1898, Some new Jurassic vertebrates from Wyoming: American Journal of Science, ser. 4, v. 5, p. 378–381.

- 1900, Jurassic rocks of southeastern Wyoming: Bulletin of the Geological Society of America, v. 11, p. 377–388.
- Linder, H., 1913, Beiträge zur Kenntnis der Plesiosaurier-Gattungen *Peloneustes* und *Pliosaurus*. Nebst Anhang: Ueber die beiden ersten Halswirbel der Plesiosaurier: Geologische und Paläontologische Abhandlungen, Neue Folge, v. 11, no. 5, p. 339–409.
- Martin, G.C., 1926, The Mesozoic stratigraphy of Alaska: U.S. Geological Survey Bulletin 776, 493 p.
- Massare, J.A., 1987, Tooth morphology and prey preference of Mesozoic marine reptiles: Journal of Vertebrate Paleontology, v. 7, p. 121–137.
- Novozhilov, N.I., 1948, Dva novykh pliozavra iz nizhnego volzhskogo yarusa povolzhya: Doklady Akademii Nauk SSSR, v. 60, p. 115–118.
- 1964, Nadsemeistvo Pliosauroida, in Rozhdestvenskii, A.K., and Tatarinov, L.I., eds., Zemnovodnye, presmykayushchiesya i ptitsy, v. 12, Osnovy Paleontologii: Moskva, "Nauka," p. 327–332.
- Packer, D.R., and Stone, D.B., 1974, Paleomagnetism of Jurassic rocks from southern Alaska and the tectonic implications: Canadian Journal of Earth Sciences, v. 11, p. 976–997.
- Persson, P.O., 1963, A revision of the classification of the Plesiosauria with a synopsis of the stratigraphical and geographical distribution of the group: Lunds Universitets Årsskrift, Ny Följd, Avd. 2, v. 59, no. 1, p. 1–59.
- Russell, D.A., 1993, Vertebrates in the Cretaceous Western Interior Sea, in Caldwell, W.G.E., and Kauffman, E.G., eds., Evolution of the Western Interior Basin: Geological Association of Canada Special Paper 39, p. 665–680.
- Scott, W.B., 1897, Introduction to geology: New York, The Macmillan Company, 573 p.
- Smith, A.G., Smith, D.G., and Funnell, B.M., 1993, Atlas of Mesozoic and Cenozoic coastlines: New York, Cambridge University Press, 99 p.
- Smith, W.R., 1925, The Cold Bay-Katmai district: U.S. Geological Survey Bulletin 773, p. 183–207.
- Smith, W.R., and Baker, A.A., 1924, The Cold Bay-Chignik district: U.S. Geological Survey Bulletin 755, p. 151–218.
- Stone, D.B., and Packer, D.R., 1979, Paleomagnetic data from the Alaska Peninsula: Geological Society of America Bulletin, v. 90, p. 545–560.
- Stone, D.B., Panuska, B.C., and Packer, D.R., 1982, Paleolatitudes versus time for southern Alaska: Journal of Geophysical Research, v. 87, p. 3697–3707.
- Tarlo, L.B., 1959a, *Pliosaurus brachyspondylus* (Owen) from the Kimmeridge Clay: Palaeontology, v. 1, p. 283–291.
- 1959b, *Stretosaurus* gen. nov., a giant pliosaur from the Kimmeridge Clay: Palaeontology, v. 2, p. 39–55.
- 1960, A review of Upper Jurassic pliosaurs: Bulletin of the British Museum of Natural History, Geology Series, v. 4, no. 5, p. 147–189.
- Taylor, D.G., Callomon, J.H., Hall, R., Smith, P.L., Tipper, H.W., and Westermann, G.E.G., 1984, Jurassic ammonite biogeography of western North America: the tectonic implications, in Westermann, G.E.G., ed., Jurassic-Cretaceous biochronology and paleogeography of North America: Geological Association of Canada Special Paper 27, p. 121–141.
- Wilmarth, M.G., 1957, Lexicon of geologic names of the United States (including Alaska): U.S. Geological Survey Bulletin 896, pt. 1, p. 1–1244.
- Wilson, F.H., Detterman, R.L., and DuBois, G.D., in press, Geologic framework of the Alaska Peninsula, southwest Alaska, and the Alaska Peninsula terrane: U.S. Geological Survey Bulletin 1969–B.
- Young, C.C., 1944, On the reptilian remains from Weiyuan, Szechuan, China: Bulletin of the Geological Society of China, v. 24, nos. 3–4, p. 187–210.
- Zhang, Y.H., 1985, A new plesiosaur from the Lias of Sichuan Basin: Vertebrata Palasiatica, v. 23, p. 235.

Reviewers: Thomas R. Holtz, Jr., and Frederic H. Wilson

# Geochemistry of the Andesitic Admiralty Island Volcanics, An Oligocene Rift-Related Basalt to Rhyolite Volcanic Suite of Southeastern Alaska

By Arthur B. Ford, Curtis A. Palmer, and David A. Brew

## ABSTRACT

The Admiralty Island Volcanics of Oligocene age on southernmost Admiralty Island is an approximately 1,000-km<sup>2</sup> by 3,000-m-thick field of low-MgO, medium- and low-K, dominantly andesitic rocks. Compositions are mostly low-SiO<sub>2</sub> andesite and range from basalt and high-SiO<sub>2</sub> andesite to less abundant dacite and rhyolite of high-K, high-SiO<sub>2</sub> type. Volatile-free SiO<sub>2</sub> content of flow rocks ranges from 47 to 77 weight percent, with a SiO<sub>2</sub> gap at 62–68 weight percent. Numerous comagmatic dikes cut the flow rocks and probably represent fissure feeders for the flows. Most flow and dike rocks contain normative hypersthene and are free of normative olivine. Major-element compositions are generally typical for orogenic, arc-related volcanic suites, but critical incompatible trace elements (Nb, Ta, Hf, Th) show characteristics of a within-plate extensional setting of volcanism that was not related to subduction of a slab of oceanic lithosphere.

The volcanism on Admiralty Island occurred about 10 m.y. after termination of Kula plate convergence at 43 Ma and during right-lateral transform motion of an ancestral Queen Charlotte–Fairweather Fault between the Pacific and North American plates. The transform setting of this volcanic activity contrasts with that of the subduction setting of arc volcanism of the 26- to 0.2-Ma Wrangell volcanic field of southern Alaska and Canada, early phases of which have been correlated with the Admiralty Island Volcanics. The volcanic field of Admiralty Island is part of the 35- to 5-Ma Tkopec–Portland Peninsula magmatic belt that approximately parallels the continental margin. The setting inferred for the Admiralty Island Volcanics suggests that this belt is a major, transform-related Cenozoic extensional feature of southeastern Alaska. Extension may be related to weakening of the lithosphere by upwelling of mafic asthenosphere in an area of transform activity.

## INTRODUCTION

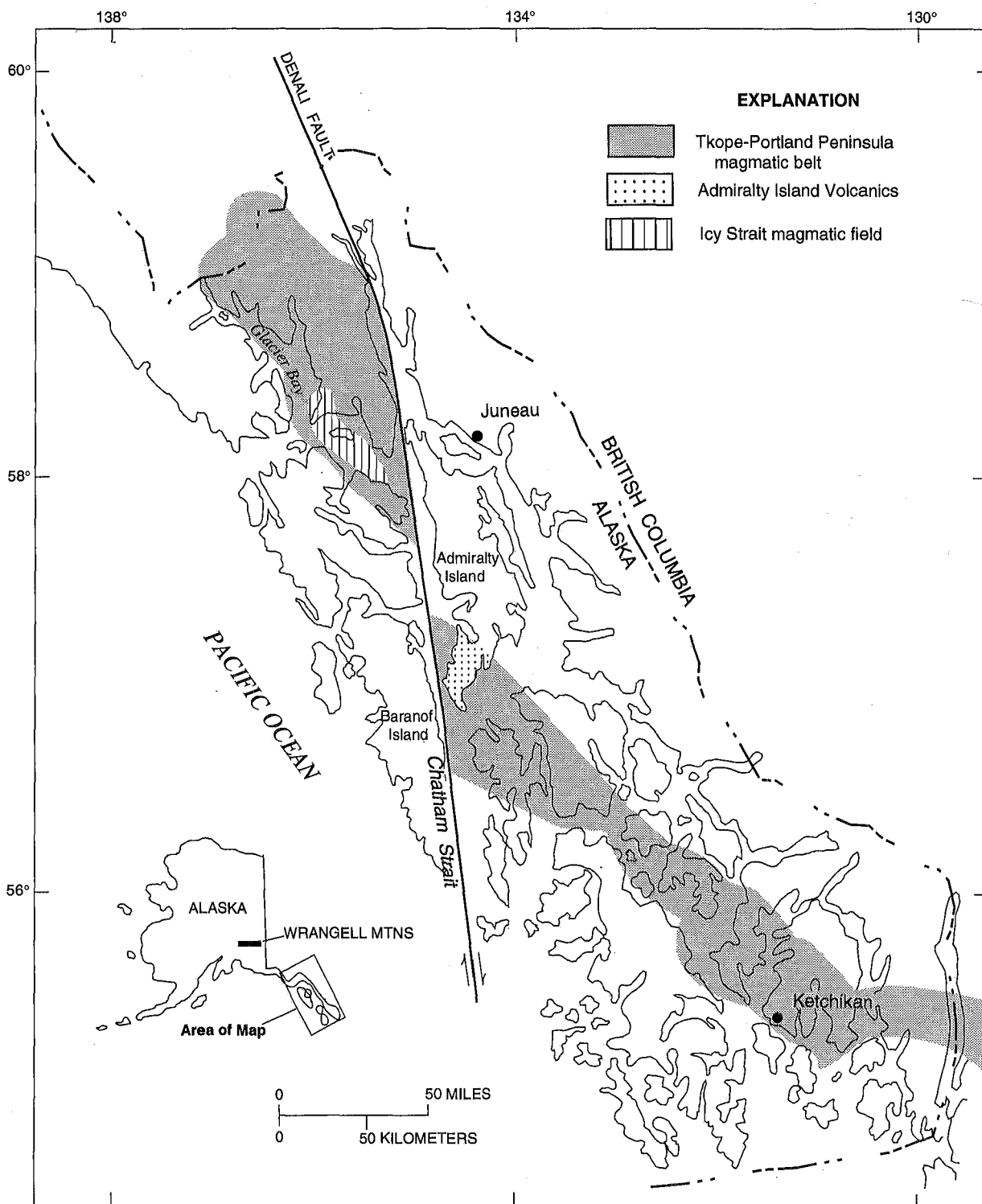
The Admiralty Island Volcanics (Loney, 1964) forms a volcanic field of about 1,000-km<sup>2</sup> area and 3,000-m thickness on southernmost Admiralty Island (fig. 1). The suite of rocks is largely andesitic, but varies from basalt to rhyolite. Numerous dikes intrude the volcanic sequence. The formation was assigned a late Eocene and Oligocene age by Loney (1964) and has yielded a K-Ar age of 27 Ma (Oligocene). The Admiralty Island Volcanics and the smaller 25- to 16-Ma Icy Strait magmatic field of Brew (1994) near Glacier Bay (fig. 1) are members of the 35- to 5-Ma Tkopec–Portland Peninsula magmatic belt of Brew (1994) that extends along most of southeastern Alaska. The northern part of the belt is displaced from central and southern parts by about 150 km of Cenozoic right-lateral separation along the Chatham Strait fault (fig. 1), a segment of the Denali fault (St. Amand, 1957). The fault also has a large component of vertical movement, in which the Baranof Island side is uplifted several kilometers relative to the Admiralty Island side (Loney and others, 1967). Whereas Tertiary rocks of Baranof Island are deeply eroded, those of southern Admiralty Island remain close to the elevations of their formation near or slightly above sea level (Loney and others, 1967).

The volcanism of the Admiralty Island Volcanics and the Icy Strait magmatic field has been suggested to be related to early phases of the extensive 26- to 0.2-Ma age Wrangell volcanic field in southern Alaska and Canada (Richter and others, 1990). The Wrangell volcanic field is characterized by medium-K, calc-alkalic lavas typical of continental volcanic arcs located along convergent plate margins (Richter and others, 1990). Wrangell lavas in southern Alaska, like the Admiralty Island Volcanics, are predominantly andesitic and range from basalt to rhyolite (Richter and others, 1990, 1993). The Wrangell lavas extend southeastward into Canada, where they are similar in character to rocks of the type locality in the Wrangell

Mountains but formed in an arc-transform transition zone (Skulski and others, 1991, 1992).

The field of the Admiralty Island Volcanics lies near the continental margin in a zone of complex Cenozoic interactions between the eastern Pacific and North Ameri-

can plates (Bradley and others, 1993; Plafker and others, 1994). Paleomagnetic data show that volcanism of the field occurred after the accretion of the Wrangellia and other allochthonous terranes of the area (Panuska and Decker, 1985). The Canadian continental margin to the



**Figure 1.** Index map of southeastern Alaska, showing the location of the Admiralty Island Volcanics, the Icy Strait magmatic field, and the Tkope-Portland Peninsula magmatic belt of Brew (1994). Modified from Brew (1994).

south records an abrupt transition from rapid plate convergence and subduction to highly oblique transcurrent motion between North America and the Pacific plate in the middle Eocene (Hamilton and Dostal, 1993). The transition may have been related to a reorientation of Pacific plate motion after cessation of Kula ridge spreading at 43 Ma (Lonsdale, 1988). By about 37 Ma (Irving and Wynne, 1991), relative movements between southeastern Alaska and the Pacific plate were transcurrent along the offshore Transition fault system of Plafker and others (1994), a transform fault ancestral to the later Cenozoic Queen Charlotte–Fairweather fault system. The Admiralty Island Volcanics records a volcanic episode related to plate activity about 10 m.y. after the transition from subduction to transcurrent motion along this part of the North American continent. To the north, eruptive centers of alkalic basalt, trachyte, and rhyolite of the Wrangell field in Canada formed at 18–10 Ma during transition between subduction- and transform-margin-related settings (Skulski and others, 1991, 1992). In southern Alaska, oblique convergence and subduction between the Pacific plate and southern Alaska persisted throughout the 26- to 0.2-Ma arc volcanism of the Wrangell volcanic field (Richter and others, 1990).

Volcanic rocks with the wide compositional range of the Admiralty Island Volcanics are found in settings as varied as subduction-related continental margin arcs (Condie and Hayslip, 1975; Cole, 1981; Gill, 1981; Thorpe and others, 1982), back-arc basins (Rudnick, 1983; Gamble and others, 1995), intraoceanic subduction systems (Gill and Stork, 1979), and intracontinental extensional rift zones (Chapin and Zidek, 1989; Nicholson, 1992; Giese and Bühn, 1993). Interpretation of the tectonic setting of volcanism can be complicated by the presence of rocks of both convergent- and extensional-related tectonic regimes within a single volcanic field (Ewart, 1982; Sawlan, 1991; Wharton and others, 1995). The tectonic setting of magmatism has been shown in many studies to influence the geochemistry of volcanic rocks, particularly in trace elements (Pearce and Cann, 1973; Wood, 1980; Pearce, 1982, 1983). The present study investigates the geochemical signatures of the Admiralty Island Volcanics, with emphasis on trace elements, in an attempt to determine the tectonic setting of this volcanism of Oligocene age. The setting of the Admiralty Island volcanism is used to interpret the origin of the Tko-pe-Portland Peninsula magmatic belt, which is a major tectonomagmatic feature that parallels the coast of southeastern Alaska (fig. 1).

## PREVIOUS AND PRESENT STUDIES

The volcanic rocks of southwestern Admiralty Island investigated in this study were first mapped in Wright's (1906) reconnaissance investigations of southeastern Alaska. The field of volcanic rocks was mapped in more

detail by Loney (1964) and Lathram and others (1965). Rocks correlated with the Admiralty Island Volcanics occur on nearby islands to the south of Admiralty Island (Buddington and Chapin, 1929; Muffler, 1967; Brew and others, 1984, 1985; Brew, 1994). Previously published chemical data for the Admiralty Island Volcanics are limited to major-element analyses of six flows of basalt, basaltic andesite, andesite, and "altered lavas," and one dike (Loney, 1964). A plot of rare-earth elements of one sample, for which the locality, lithology, and major-element content were not reported, was shown by Brew (1994).

Thirty-five samples of flows and samples of eight dikes from the field of the Admiralty Island Volcanics were analyzed for this study. The rocks were broken into small pieces on the outcrop in order to exclude as much weathered material, veinlets, and amygdules as possible. Nonetheless, unusually small amygdules and veinlets, which could not be excluded from some samples even with later hand picking, may be reflected in unusually high contents of volatiles ( $H_2O$ ,  $CO_2$ ) and anomalous mobile-element variations. Samples were obtained from elevations ranging from sea level to the highest topographic exposures of the field (Bear Pass Mountain, elevation 3,853 ft; fig. 2), so that as much of the stratigraphy of the volcanic field as possible was collected. However, the abundance of steep faults with unknown displacement (Loney, 1964; Lathram and others, 1965) precludes measurement of detailed stratigraphic sections across the entire sequence of flows. Accordingly, the compositional variation of the flows with stratigraphic position in the volcanic sequence has not been determined.

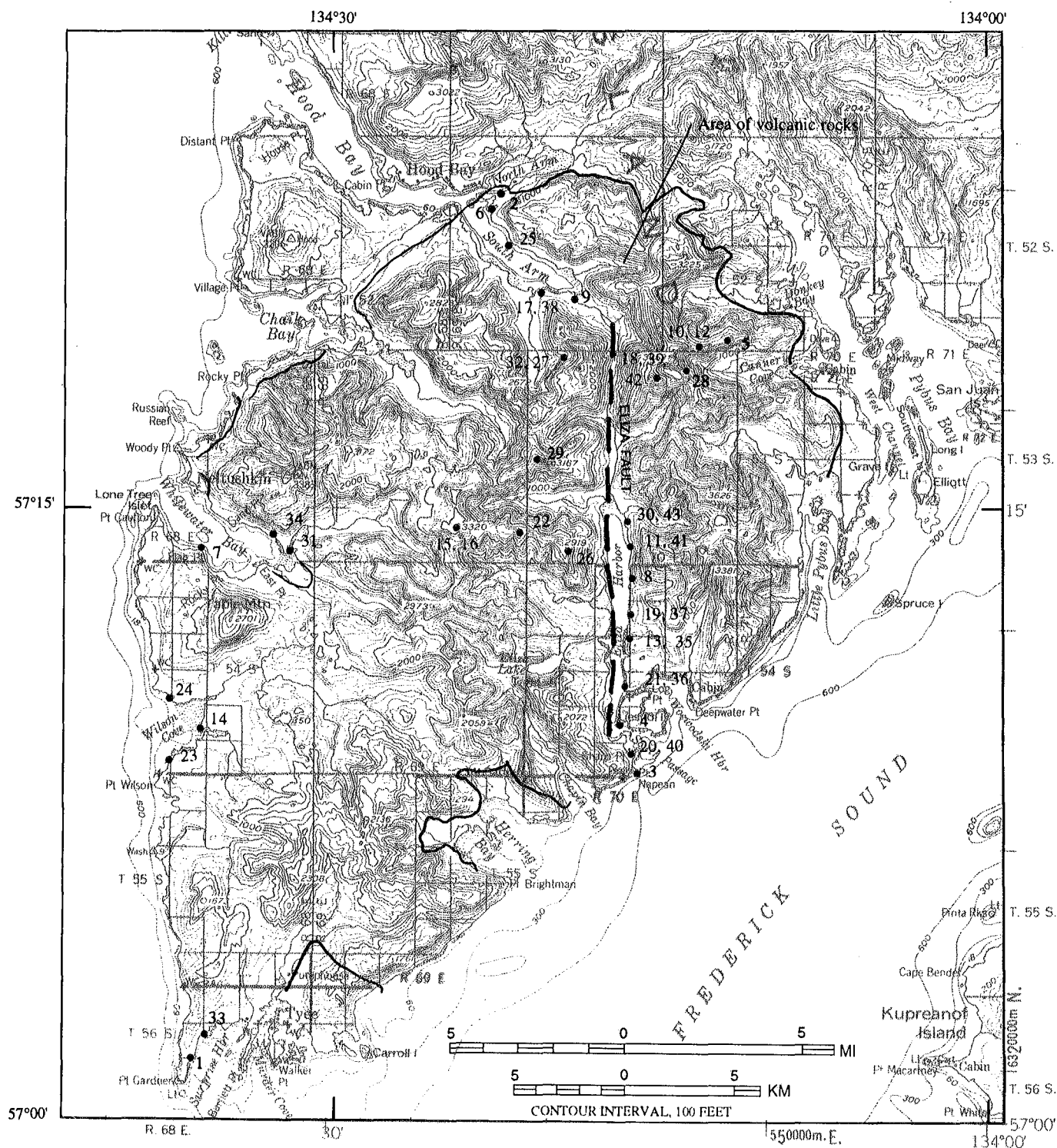
## DESCRIPTION OF THE ADMIRALTY ISLAND VOLCANICS

The Admiralty Island Volcanics consists predominantly of andesitic flows that are interlayered with flows of basalt and minor dacite and rhyolite and minor pyroclastic rock. Approximately 23 percent of the rocks of this study are basalt, 43 percent are low- $SiO_2$  andesite, 23 percent are high- $SiO_2$  andesite, and 11 percent are dacite and rhyolite, as described below. Loney (1964) described the volcanic field as a "...thick sequence of gently dipping andesitic and basaltic flows and minor rhyolitic breccia and tuff." The volcanic field is probably of terrestrial origin, as suggested by relations with partly coeval terrestrial clastic rocks (Kootznahoo Formation; Lathram and others, 1965) and an absence of pillow lavas. The volcanic rocks are best exposed along shorelines. The total exposed thickness of the field is about 3,050 m, but because the top is erosional the original thickness is unknown (Lathram and others, 1965). The thickness of



the volcanic pile is highly variable, owing in part to well-developed topographic relief under the sequence of flows (Buddington and Chapin, 1929). The overall form of the volcanic field appears to be that of a north-trending, block-faulted synclinal structure, the axial trace of which ap-

proximately coincides with the trace of the Eliza fault (Loney, 1964). In places, the origin of dark, dense, and structureless rocks is indistinguishable by field characteristics alone. Samples collected from Wilson Cove and Whitewater Bay, for example, were interpreted in the field



**Figure 2.** Distribution of the Admiralty Island Volcanics, southern Admiralty Island, showing sample localities (see table 1). Area of volcanic rocks slightly modified from Lathram and others (1965). Base map from U.S. Geological Survey, Sitka quadrangle 1951.

to be hornfelsed metasedimentary rocks, but were later found in thin-section study to be volcanic (localities 23, 34; fig. 2, table 1).

Dikes are present throughout the volcanic field and seem to be especially concentrated as swarms in central areas near Eliza Harbor and Bear Pass Mountain (localities 39, 42; fig. 2). Loney (1964) reported that the dikes are petrographically and compositionally similar to the flows. The dikes range in thickness from 0.6 cm to 6.1 m, and their average attitude (N. 32° E. strike, 75° S. dip) is about normal to axial planes of second-generation folds in pre-Tertiary rocks of the area and approximately parallel with high-angle faults (Loney, 1964). The abundance of dikes within a zone about 2 km wide surrounding the volcanic field and their scarcity beyond that distance suggest that volcanism did not extend far beyond the present area of the field (Loney, 1964). The "numerous vents and craters" that Wright (1906) believed were the source of the lavas were not found in our field work.

The volcanic rocks of this study have varied mineralogy, texture, and structure, and show a wide range in alteration (table 1; Loney, 1964). Fragmental rocks, including breccia and tuff, are present locally but were not collected for this study. Amygdaloidal structure is found in flows of basalt and andesite sampled from near sea level (localities 6, 20, 25; fig. 2, table 1) and higher elevations (localities 28, 29; fig. 2, table 1). Xenoliths have not been found in any of the flows. Most rocks are porphyritic and contain phenocrysts principally of plagioclase. In our samples, clinopyroxene (cpx) is common only as a groundmass phase, but Loney (1964) reported clinopyroxene to be a common phenocryst phase, although much lower in abundance than plagioclase. Hornblende is not present as a phenocryst phase in the samples, but green amphibole of apparent secondary origin is locally present in the groundmass. Alteration products from primary minerals include highly variable amounts of clay, chlorite, mica, amphibole, and carbonate minerals, and many rocks contain small amounts of interstitial devitrified material.

The volumetrically minor and poorly exposed dacitic and rhyolitic rocks of the Admiralty Island Volcanics are intercalated with basaltic and andesitic flows at localities from sea level (Eliza Harbor, localities 13, 35; Surprise Harbor, localities 1, 33; fig. 2) to high elevations (west of Bear Pass Mountain, localities 27, 32; fig. 2). In the absence of observed intrusive relations the silicic rocks of the field are interpreted to be extrusive rather than hypabyssal intrusive in origin. However, an origin of some of the silicic bodies by hypabyssal intrusion is possible, as is the case with the silicic intrusive bodies mapped in other basalt to rhyolite suites (Wrangell volcanic field; Chapin and Zidek, 1989; Nicholson, 1992; Richter and others, 1993). The silicic rocks of the Admiralty Island Volcanics commonly show convoluted flow banding. In

the absence of shards and pumice fragments typical of silicic volcanic rocks of ash-flow origin (Chapin and Zidek, 1989), the silicic extrusive rocks of the Admiralty Island Volcanics are interpreted to represent lava flows.

## AGE

The age of the Admiralty Island Volcanics is not well constrained because paleontologic and isotopic age data are available from few localities and only for rocks of low stratigraphic position. Wright (1906) ascribed a post-Eocene age to the Admiralty Island Volcanics. Loney (1964) considered the formation to be late Eocene to Oligocene, based on the relations between flows of a lower part of the volcanic field at Little Pybus Bay with underlying Eocene(?) conglomerate of the terrestrial Kootznahoo Formation, a unit of Paleocene through Miocene age (Lathram and others, 1965). An Oligocene age of volcanic rocks of a lower part of the sequence is indicated by plant fossils in sedimentary rocks interbedded with the volcanic rocks (J.A. Wolfe, quoted in Lathram and others, 1965). A volcanic rock from near the head of Chaik Bay (locality in Wilson and others, 1994; data from George Plafker, written comm., 1986, quoted in Brew, 1994) yielded a whole-rock K-Ar age of 27 Ma (Oligocene; time scale of Harland and others, 1990). The stratigraphic position of the sample was unreported. The locality, near sea level, is somewhere within the lower part of the volcanic sequence. Ages of intermediate and upper flows of the field have not been determined. Loney (1964) suggested that the oldest volcanic rocks of the field may be Eocene because conglomerate of the Kootznahoo Formation contains volcanic clasts. Although a wider age range is possible, an age of Oligocene is here ascribed to the Admiralty Island Volcanics because the only direct evidence available indicates such an age for the volcanic field.

## NOMENCLATURE

The volcanic-rock nomenclature used in this report follows that of Gill (1981). The commonly used classification by CIPW minerals (Irvine and Baragar, 1971) is unsatisfactory owing to the generally poor correspondence between CIPW and modal mineralogy (Le Bas and others, 1986). Moreover, amounts of the normative minerals quartz (Q), orthoclase (or), and olivine (ol) that are critical for classification are dependent on iron-oxidation ratio ( $\text{Fe}_2\text{O}_3/\text{FeO}$ ; Middlemost, 1989), a ratio that probably has been modified by alteration in rocks of this study. In Gill's (1981) classification, rock names are based primarily on  $\text{SiO}_2$  content recalculated to a volatile-free amount

Table 1. Sample locations and petrographic features of the Admiralty Island Volcanics

[Rock groups: BA, basalt; AN-L, low-SiO<sub>2</sub> andesite; AN-H, high-SiO<sub>2</sub> andesite; SIL, dacite and rhyolite; DK, dike. Widths given for dikes. Thin-section textures and structures: Am, amygdaloidal; Pp, porphyritic; Gl, glomeroporphyritic; Fl, flow structure; Ho, holocrystalline; Is, intersertal; Ig, intergranular; Mp, microporphyritic; Op, ophiitic; Dv, devitrification features. Minerals: PL, plagioclase (abundant, all samples except dacite and rhyolite); QZ, quartz; CPX, clinopyroxene; AM, amphibole; OX, opaque oxides (minor, all samples); CA, carbonate; EP, epidote; CL, clays, chlorite, secondary mica. \*, phenocrysts; #, groundmass; +, abundant; tr, minor. Textures underlined.]

Field No.	Plot symbol	Rock group	Latitude	Longitude	Location	Petrographic features and notes
91AF085A	21	AN-L	57°10'43"	134°16'52"	Eliza Harbor	Fresh. <u>Mp, Fl, Dv(?)</u> . PL, *, #; OX, #.
91AF085B	36	DK	57°10'43"	134°16'52"	Eliza Harbor	Dike, 1.4 m. Altered (CA, CL, tr). <u>Ho, Ig</u> . PL, OX, CPX.
91AF086A	35	SIL	57°11'40"	134°16'59"	Eliza Harbor	Altered. <u>Dv, Fl, QZ</u> . CL. Banded.
91AF086B	13	AN-L	57°11'40"	134°16'59"	Eliza Harbor	Altered, minor (CL, CA, tr.). PL; CPX, tr.; QZ, tr.
91AF087A	19	AN-L	57°12'20"	134°16'47"	Eliza Harbor	Altered, minor (CA, CL). <u>Dv, Ig</u> . PL; CPX, tr; OX.
91AF087B	37	DK	57°12'20"	134°16'47"	Eliza Harbor	Dike, 2 m. Altered, minor (CA, CL, tr.) <u>Pp</u> . PL+, *, #.
91AF088A	8	BA	57°13'17"	134°16'47"	Eliza Harbor	Altered (CL, EP, tr). <u>Dv(?)</u> . PL; CPX, tr.; OX.
91AF089A	11	AN-L	57°14'03"	134°16'45"	Eliza Harbor	Altered (CL, CA, tr). <u>Dv, Pp, Is</u> . PL; CPX, tr; OX
91AF089B	41	DK	57°14'03"	134°16'45"	Eliza Harbor	Dike, 2 m. Altered (CA, CL, AM, prehnite). <u>Ho, Pp</u> . PL, *, #; CPX, *, #.
91AF090B	30	AN-H	57°14'39"	134°17'01"	Eliza Harbor	Altered (CL, EP). <u>Dv (?)</u> . PL.
91AF090C	43	DK	57°14'39"	134°17'01"	Eliza Harbor	Dike, > 30 cm. Altered (CL, EP, AM) <u>Pp, Dv</u> . PL, *, #. AM, #, tr., OX.
91AF091A	4	BA	57°09'48"	134°17'19"	South of Eliza Harbor	Fresh. <u>Pp, Fl</u> . PL, *, #; CPX, #; OX, CA, tr.
91AF092A	20	AN-L	57°09'07"	134°16'29"	South of Eliza Harbor	Altered (CA, CL). <u>Pp, Fl, Am</u> . PL, *, #; OX.
91AF092B	40	DK	57°09'07"	134°16'29"	South of Eliza Harbor	Dike, 3 m. Altered (CA, CL). <u>Mp, Dv, Am, varioles</u> . PL, OX.
91AF093A	3	BA	57°08'34"	134°16'35"	South of Eliza Harbor	Fresh. <u>Ho, Pp, Fl</u> . PL, *, #; CPX, #; OX.
91AF095A	1	BA	57°01'30"	134°36'25"	Surprise Harbor	Fresh. <u>Pp, Op, Fl</u> . PL, *, #; CPX, *, #; OX; CL, tr.
91AF096A	33	SIL	57°02'04"	134°35'48"	Surprise Harbor	Altered(?). <u>Pp, Dv</u> .
91AF097A	14	AN-L	57°09'31"	134°36'08"	Wilson Cove, head	Fresh. <u>Pp, Ho, Fl</u> . PL, *, #; CPX, #tr; OX, #tr.
91AF098A	24	AN-H	57°10'34"	134°37'30"	Wilson Cove, N. side	Fresh. <u>Mp, Ho, Fl</u> (strong). PL*.
91AF099A	34	SIL	57°14'22"	134°32'10"	Whitewater Bay, head	Altered. <u>Dv, Pp</u> . Flow(?) banded.
91AF100A	31	AN-H	57°13'35"	134°32'20"	Whitewater Bay, head	Altered. <u>Pp, Dv(?)</u> . PL, *.
91AF101A	7	BA	57°14'02"	134°36'08"	Whitewater Bay, S. side	(No thin section)
91AF102A	2	BA	57°22'44"	134°22'40"	Hood Bay, North Arm	Fresh. <u>Pp, Op</u> . PL, *, #; CPX, #; OX, #.
91AF103A	6	BA	57°22'17"	134°23'09"	Hood Bay, South Arm	Fresh. <u>Pp, Am</u> . PL, *, #.
91AF104A	25	AN-H	57°21'29"	134°21'59"	Hood Bay, South Arm	Altered(?). <u>Ho, Mp, Fl, Am</u> . PL, *, #.
91AF105A	17	AN-L	57°20'22"	134°20'34"	Hood Bay, South Arm	Fresh. <u>Ho, Fl</u> . PL, #.
91AF105C	38	DK	57°20'22"	134°20'34"	Hood Bay, South Arm	Dike, 2 m. Fresh. <u>Ho</u> . PL, #.
91AF106A	9	AN-L	57°21'19"	134°19'19"	Hood Bay, South Arm	Fresh. <u>Ig, Fl</u> . PL, #.
91DB034A	23	AN-L	57°08'44"	134°37'32"	South of Wilson Cove	Fresh. <u>Ho, Fl</u> . PL, #; CPX, #.
92AF023A	10	AN-L	57°03'58"	134°13'17"	East of Bear Pass Mtn	Altered (?). <u>Pp, Ho, Gl</u> . PL, *, #; CPX, #.
92AF023B	12	AN-L	57°03'58"	134°13'17"	East of Bear Pass Mtn	Altered (?). <u>Pp, Ho, Gl</u> . PL, *, #; CPX, #.
92AF024A	5	BA	57°04'13"	134°12'09"	East of Bear Pass Mtn	Altered (?). <u>Ho, Mp, Fl</u> . PL, *, #.
92AF025A	28	AN-H	57°03'18"	134°14'08"	South of Bear Pass Mtn	Altered. <u>Pp, Dv, Am, Is</u> . PL, *, CA, tr. Glass (?) present.
92AF026A	18	AN-L	57°03'10"	134°15'12"	Southwest, Bear Pass Mtn	Altered. <u>Dv, Fl</u> . PL, #, tr, CA, EP.
92AF026B	39	DK	57°03'10"	134°15'12"	Southwest, Bear Pass Mtn	Dike, 2 m. Altered. <u>Pp</u> . PL, *, #; CA, +, #.
92AF026C	42	DK	57°03'10"	134°15'12"	Southwest, Bear Pass Mtn	Dike, 3 m. Altered. <u>Pp, Fl, Dv(?)</u> . Quartz (?), *.
92AF027A	32	SIL	57°03'31"	134°18'42"	West of Bear Pass Mtn	Fresh (?). <u>Pp, Dv, Fl</u> . PL, *, #; CPX, *. Glass (?) present.
92AF027B	27	AN-H	57°03'31"	134°18'42"	West of Bear Pass Mtn	Fresh (?). <u>Pp, Dv, Fl</u> . PL, *, #. Glass (?) present
92AF028A	29	AN-H	57°16'26"	134°20'57"	3167' pk, SE, Chaik Bay	Altered. <u>Pp, Am</u> . PL, *, #; CA, +. CA in veinlets and vesicles.
92AF029A	26	AN-H	57°14'13"	134°19'55"	2919' pk, W., Eliza Harbor	Fresh. <u>Mp, Fl, Is</u> . PL, *, #.
92AF030A	22	AN-L	57°14'29"	134°21'55"	West of Eliza Harbor	Altered. <u>Pp, Gl</u> . PL, *, #; CPX, *, #; CA.
92AF031A	16	AN-L	57°14'28"	134°14'25"	3320' pk, W., Eliza Harbor	Fresh. <u>Mp, Fl</u> . PL, *, #; CPX, #; OX, #.
92AF031B	15	AN-L	57°14'28"	134°14'25"	3320' pk, W., Eliza Harbor	Fresh. <u>Mp, Fl</u> . PL, *, #; CPX, #; OX, #.

(basalt, <53 percent; andesite, 53-63 percent; dacite, 63-70 percent; rhyolite, >70 percent). Andesites, typically containing normative hypersthene (hy), are further subdivided into low-silica (or basaltic) andesite ( $\text{SiO}_2$ , 53-57 percent) and high-silica andesite ( $\text{SiO}_2$ , 57-63 percent), following Gill (1981). Normative plagioclase composition at  $\text{An}_{50}$  (Thompson, 1972) distinguishes basalt from andesite in most rocks of this study.

The alterations indicated by secondary minerals in many rocks (table 1) resulted in variable increases in volatile constituents ( $\text{H}_2\text{O}$ ,  $\text{CO}_2$ ) that affect the relative amounts of major elements analyzed. Therefore, CIPW norms, ratios, and major-element plots in this report are based on amounts of major elements normalized to volatile-free amounts for comparison of rock compositions within this volcanic field and with rocks of other areas, and for rock classification. CIPW norms were calculated using the PETCAL program of Binger and others (1976), as modified by R.D. Koch (written commun., 1992), and using  $\text{FeO}/\text{Fe}_2\text{O}_3$  ratios of original analyses (Le Bas and others, 1986).

## MAJOR-ELEMENT CHEMISTRY

The  $\text{SiO}_2$  content (volatile-free basis) of flow rocks ranges widely from about 47 to 77 weight percent (table 2). Most flow and dike rocks of the volcanic field are Q normative and most contain hy, with minor ol in a few basalts. The flow rocks show a  $\text{SiO}_2$  gap at 62-68 weight percent (fig. 3), separating andesitic from dacitic compositions, which is about the same as that of the Icy Strait magmatic field (61-68 weight percent; Brew, 1994). Other volcanic suites commonly show a lower  $\text{SiO}_2$  gap separating basalt from andesite (Thompson, 1972). The average major-element composition of the silicic flow rocks (table 2D) is intermediate between average rhyolite and rhyodacite of Le Maitre (1976). The dike rocks have a narrower  $\text{SiO}_2$  range than flow rocks (48-65 weight percent; table 2E), with  $\text{SiO}_2$  contents that lie within the  $\text{SiO}_2$  gap of flow rocks (fig. 3).

The flow and dike rocks of the Admiralty Island field are dominantly andesitic in composition, as indicated in the total alkali and silica (TAS) diagram of figure 4. The rocks have medium- to low-K characteristics (fig. 5), except for rocks of silicic flows that have high-K characteristics (average  $\text{K}_2\text{O}/\text{Na}_2\text{O}$ , 1.2; table 2D, fig. 5). The weak bimodality in frequency distribution of  $\text{SiO}_2$  content in the Admiralty Island Volcanics differs from distributions in typical volcanic bimodal suites (Condie and Hayslip, 1975; Giese and Bühn, 1993) in the abundance of andesitic compositions (figs. 3, 4). The metaluminous character of the basalt and andesite flow and dike rocks is shown by  $\text{A}/\text{CNK}$  [ $\text{Al}_2\text{O}_3/(\text{CaO} + \text{Na}_2\text{O} + \text{K}_2\text{O})$ ] values less than 1.0 (tables 2A-C, E). Rocks of silicic flows, how-

ever, have higher, strongly peraluminous  $\text{A}/\text{CNK}$  values (1.08-1.32; table 2D).  $\text{A}/\text{CNK}$  values generally vary inversely with  $\text{CaO}$  content and increase with  $\text{SiO}_2$  content (averages: basalt, 0.73; low- $\text{SiO}_2$  andesite, 0.79; high- $\text{SiO}_2$  andesite, 0.87; dacite and rhyolite, 1.20; tables 2A-D). Higher normative-corundum contents also show the more aluminous character of silicic flow rocks compared with intermediate and mafic flow rocks of the field (table 2A-D). A moderate- to low-MgO character of the rocks is shown by MgO contents (mostly < 6 weight percent; table 2) and by low values of Mg numbers [ $100 \times \text{Mg}^{2+}/(\text{Mg}^{2+} + \text{Fe}^{2+})$ , in molecular amounts], which vary inversely with  $\text{SiO}_2$  content (averages, basalt: 56; low- $\text{SiO}_2$  andesite, 54; high- $\text{SiO}_2$  andesite, 52; silicic rocks, 37; tables 2A-D).

Major-element contents of the Admiralty Island Volcanics show different relations in different diagrams. For example, flow and dike rocks are subalkalic (fig. 4), but the rocks form slightly calcic suites according to their alkali-lime "Peacock" index (62; fig. 6). The flow and dike rocks show mixed calc-alkalic and tholeiitic compositions in a diagram of total alkali ( $\text{Na}_2\text{O} + \text{K}_2\text{O}$ ), total iron calculated as  $\text{FeO}$  ( $\text{FeO}^* = \text{FeO} + 0.9 \times \text{Fe}_2\text{O}_3$ ), and MgO relations (AFM; fig. 7). All rocks, however, show tholeiitic characteristics when classified by the variation between  $\text{SiO}_2$  and  $\text{FeO}^*/\text{MgO}$  (fig. 8).  $\text{SiO}_2$  and  $\text{TiO}_2$  contents of the dike and flow rocks are similar and show inverse covariation (fig. 9).

## TRACE-ELEMENT CHEMISTRY

Trace-element contents of the volcanic rocks of Admiralty Island (table 3) show many variations related to  $\text{SiO}_2$  content. Increases with  $\text{SiO}_2$  content, for example, are shown by Zr abundance in flow rocks, which averages 150 ppm in basalt, 200 ppm in low- $\text{SiO}_2$  andesite, 199 ppm in high- $\text{SiO}_2$  andesite, and 378 ppm in silicic rocks. Th content increases with  $\text{SiO}_2$  content to a maximum abundance in silicic rocks (11.4 ppm; table 3D), and U content also increases with  $\text{SiO}_2$  content (table 3). Total abundance of rare-earth elements (REE) generally increases with  $\text{SiO}_2$  content, from an average 70.7 ppm in basalt, 93.8 ppm in low- $\text{SiO}_2$  andesite, and 98.1 ppm in high- $\text{SiO}_2$  andesite, to 172 ppm in silicic rocks ( $\Sigma\text{REE}$ ; table 3). The ratio between chondrite-normalized light-rare-earth elements (LREE) to heavy-rare-earth elements (HREE) also generally increases with  $\text{SiO}_2$  content, as discussed below. Vanadium content (averages: basalt, 233 ppm; low- $\text{SiO}_2$  andesite, 168 ppm; high- $\text{SiO}_2$  andesite, 135 ppm; silicic rocks, 31 ppm; table 3) and  $\text{K}/\text{Rb}$  value (averages: basalt, 494 ppm; low- $\text{SiO}_2$  andesite, 409 ppm; high- $\text{SiO}_2$  andesite, 347 ppm; silicic rocks, 342 ppm; table 3), in contrast, vary inversely with  $\text{SiO}_2$  content.

The flow and dike rocks of the Admiralty Island Volcanics are characterized by low to moderate REE con-

**Table 2.** Major-element chemical composition (weight percent) of flow and dike rocks of the Admiralty Island Volcanics in order of increasing SiO<sub>2</sub> content recalculated in volatile-free amount, and CIPW norms based on volatile-free oxide amount

[Major-element analyses, in weight percent, by methods described in Baedeker (1987) and Taggart and others (1987, 1990). Samples prepared by methods in Taylor (1990). FeO, H<sub>2</sub>O, and CO<sub>2</sub> by methods in Jackson and others (1987). LOI, Loss on ignition at 925°C. Analysis in U.S. Geological Survey Laboratories. Analysts: J.S. Mee, D.F. Siems, except FeO, H<sub>2</sub>O and CO<sub>2</sub> by T.L. Fries, S.T. Pribble. Indexes A/CNK and Mg number defined in text]

A. Basalt flows									
Field No.	91AF095A	91AF102A	91AF093A	91AF091A	92AF024A	91AF103A	91AF101A	91AF088A	average
Symbol	1	2	3	4	5	6	7	8	BA
SiO <sub>2</sub> -----	46.3	45.3	47.4	48.2	49.3	47.2	50.3	48.5	47.8
Al <sub>2</sub> O <sub>3</sub> -----	16.1	16.8	16.0	18.0	15.7	17.5	16.9	16.4	16.7
Fe <sub>2</sub> O <sub>3</sub> -----	2.94	2.41	3.60	4.10	3.99	2.73	2.37	2.72	3.11
FeO -----	8.96	8.09	9.27	6.30	7.12	5.68	7.41	5.71	7.32
MgO -----	7.63	7.14	4.53	5.29	5.71	2.39	5.01	5.44	5.39
CaO -----	9.40	8.81	9.91	10.30	9.78	10.3	9.25	8.03	9.47
Na <sub>2</sub> O -----	2.84	2.61	2.90	3.07	3.12	3.13	3.47	3.81	3.12
K <sub>2</sub> O -----	.34	.51	.58	.38	.61	.46	.46	.37	.46
H <sub>2</sub> O+ -----	2.04	3.84	.96	1.06	.60	1.73	.65	3.35	1.78
H <sub>2</sub> O- -----	1.01	1.07	.71	.72	.88	.29	.22	.63	.69
TiO <sub>2</sub> -----	1.99	1.53	2.13	1.58	2.18	1.68	1.48	1.15	1.72
P <sub>2</sub> O <sub>5</sub> -----	.24	.21	.33	.25	.59	.33	.43	.23	.33
MnO -----	.21	.18	.20	.16	.20	.14	.18	.13	.18
CO <sub>2</sub> -----	.28	1.31	1.53	.38	.03	6.10	1.50	3.66	1.85
Total	100.3	99.8	100.0	99.8	99.8	99.7	99.6	100.1	99.9
LOI -----	2.15	5.21	2.05	1.36	.97	7.13	1.58	6.56	3.38
Analyses recalculated in volatile-free amount									
SiO <sub>2</sub> -----	47.8	48.4	48.9	49.4	50.2	51.6	51.7	52.4	50.1
Al <sub>2</sub> O <sub>3</sub> -----	16.6	18.0	16.5	18.4	16.0	19.1	17.4	17.7	17.5
Fe <sub>2</sub> O <sub>3</sub> -----	3.03	2.58	3.72	4.20	4.06	2.98	2.44	2.94	3.24
FeO -----	9.24	8.64	9.57	6.45	7.24	6.21	7.62	6.17	7.64
MgO -----	7.87	7.63	4.68	5.42	5.81	2.61	5.15	5.88	5.83
CaO -----	9.70	9.41	10.23	10.55	9.95	11.25	9.51	8.68	9.91
Na <sub>2</sub> O -----	2.93	2.79	2.99	3.15	3.17	3.42	3.57	4.12	3.27
K <sub>2</sub> O -----	.35	.55	.60	.39	.62	.50	.47	.40	.49
TiO <sub>2</sub> -----	2.05	1.64	2.20	1.62	2.22	1.84	1.52	1.24	1.79
P <sub>2</sub> O <sub>5</sub> -----	.25	.22	.34	.26	.60	.36	.44	.25	.34
MnO -----	.22	.19	.21	.16	.20	.15	.19	.14	.18
Total	100.0	100.0	100.0	100.0	100.0	100.0	100.0	100.0	100.0
Indexes									
A/CNK -----	0.73	0.81	0.68	0.74	0.67	0.72	0.73	0.77	0.73
Mg number ---	60.3	61.1	46.6	59.9	58.8	42.9	54.7	62.9	55.9
Normative minerals									
Q -----	0.00	0.00	0.20	0.26	1.87	3.86	.96	0.00	0.89
or -----	2.07	3.22	3.54	2.30	3.67	2.97	2.80	2.36	2.87
ab -----	24.79	23.60	25.34	26.61	26.86	28.93	30.19	34.86	27.65
an -----	31.13	34.85	29.87	35.04	27.50	35.33	30.00	28.71	31.55
di -----	12.49	8.45	15.43	12.61	14.49	14.98	11.72	10.31	12.56
hy -----	9.07	12.46	15.27	13.42	14.13	5.28	16.88	16.00	12.81
ol -----	11.58	10.06	.00	.00	.00	.00	.00	.56	2.78
mt -----	4.40	3.73	5.39	6.09	5.89	4.32	3.53	4.26	4.70
il -----	3.90	3.11	4.18	3.07	4.21	3.49	2.89	2.36	3.40
ap -----	.57	.52	.79	.59	1.39	.84	1.02	.58	.79
Total	100.00	100.00	100.00	100.00	100.00	100.00	100.00	100.00	100.00
Normative plagioclase An percent	55.67	59.63	54.10	56.84	50.59	54.98	49.84	45.17	53.4



**Table 2.** Major-element chemical composition (weight percent) of flow and dike rocks of the Admiralty Island Volcanics in order of increasing SiO<sub>2</sub> content recalculated in volatile-free amount, and CIPW norms based on volatile-free oxide amount—Continued

B. Low-SiO <sub>2</sub> andesite flows																
Field No.	91AF106A	92AF023A	91AF089A	92AF023B	91AF086B	91AF097A	92AF031B	92AF031A	91AF105A	92AF026A	91AF087A	91AF092A	91AF085A	92AF030A	91DB034A	average
Symbol	9	10	11	12	13	14	15	16	17	18	19	20	21	22	23	AN-L
SiO <sub>2</sub> -----		51.1	51.4	52.5	47.6	53.0	54.3	54.4	53.8	54.5	50.6	52.5	53.3	55.4	55.4	52.7
Al <sub>2</sub> O <sub>3</sub> -----	17.4	17.8	18.9	17.8	14.6	15.7	17.1	17.2	17.5	16.8	14.9	14.3	14.9	17.5	15.3	16.5
Fe <sub>2</sub> O <sub>3</sub> -----	3.50	3.28	1.35	3.86	2.20	3.74	3.71	3.77	3.89	1.38	2.32	5.31	2.18	3.76	4.28	3.24
FeO -----	4.67	5.26	5.29	4.91	6.17	6.44	4.40	4.07	3.86	6.64	6.08	6.74	7.94	3.45	5.96	5.46
MgO -----	4.96	3.15	4.95	3.06	3.33	4.31	4.68	4.49	4.42	4.27	3.22	1.47	2.51	4.68	2.47	3.73
CaO -----	9.33	9.43	8.38	8.92	6.07	6.30	8.54	8.41	7.23	8.13	7.21	6.14	6.18	7.90	5.68	7.59
Na <sub>2</sub> O -----	3.68	3.26	3.50	3.54	3.33	4.04	3.49	3.60	4.12	3.66	3.24	3.68	4.08	3.47	4.57	3.68
K <sub>2</sub> O -----	.32	.55	.70	.65	2.19	1.20	.93	.98	.87	1.02	.73	1.34	1.08	.80	1.40	.98
H <sub>2</sub> O+ -----	.96	1.87	2.73	1.64	1.36	1.11	.62	.72	.85	1.49	3.39	.76	.48	1.14	.43	1.30
H <sub>2</sub> O -----	1.61	.48	.27	.39	.65	1.55	.83	.53	2.36	.10	.77	.67	.31	1.28	.87	.84
TiO <sub>2</sub> -----	1.19	1.27	.93	1.27	1.45	1.52	1.30	1.22	1.10	1.36	1.68	1.70	1.76	1.00	1.60	1.36
P <sub>2</sub> O <sub>5</sub> -----	.30	.32	.20	.33	.29	.28	.31	.30	.28	.32	.39	.54	.59	.26	.64	.36
MnO -----	.14	.14	.12	.14	.12	.13	.13	.13	.17	.15	.15	.22	.20	.11	.20	.15
CO <sub>2</sub> -----	.11	2.13	.89	1.10	10.9	.01	.03	.05	.05	<.02	5.06	4.36	4.29	.06	.02	2.08
Total -----	99.6	100.0	99.6	100.1	100.3	99.3	100.4	99.9	100.5	99.8	99.7	99.7	99.8	100.8	98.8	99.9
LOI -----	1.95	3.83	3.06	2.70	11.7	1.50	1.05	0.81	1.75	0.80	8.0	4.58	4.08	1.96	0.39	3.21
Analyses recalculated in volatile-free amount																
SiO <sub>2</sub> -----	53.1	53.5	53.7	54.1	54.5	54.8	54.9	55.2	55.3	55.5	55.9	55.9	56.3	56.3	56.8	55.1
Al <sub>2</sub> O <sub>3</sub> -----	18.0	18.6	19.7	18.4	16.7	16.2	17.3	17.5	18.0	17.1	16.5	15.2	15.7	17.8	15.7	17.2
Fe <sub>2</sub> O <sub>3</sub> -----	3.61	3.43	1.41	3.98	2.52	3.87	3.75	3.83	4.00	1.41	2.56	5.65	2.30	3.82	4.39	3.37
FeO -----	4.82	5.50	5.53	5.06	7.06	6.66	4.45	4.13	3.97	6.76	6.72	7.18	8.38	3.51	6.11	5.72
MgO -----	5.12	3.30	5.17	3.16	3.81	4.46	4.73	4.56	4.55	4.35	3.56	1.57	2.65	4.76	2.53	3.89
CaO -----	9.63	9.87	8.76	9.20	6.95	6.52	8.64	8.53	7.44	8.28	7.97	6.54	6.52	8.03	5.83	7.91
Na <sub>2</sub> O -----	3.80	3.41	3.66	3.65	3.81	4.18	3.53	3.65	4.24	3.73	3.58	3.92	4.31	3.53	4.69	3.85
K <sub>2</sub> O -----	.33	.58	.73	.67	2.51	1.24	.94	.99	.90	1.04	.81	1.43	1.14	.81	1.44	1.04
TiO <sub>2</sub> -----	1.23	1.33	.97	1.31	1.66	1.57	1.32	1.24	1.13	1.38	1.86	1.81	1.89	1.02	1.64	1.42
P <sub>2</sub> O <sub>5</sub> -----	.31	.34	.21	.34	.33	.29	.31	.30	.29	.33	.43	.58	.62	.26	.66	.37
MnO -----	.14	.15	.13	.14	.14	.13	.13	.13	.18	.15	.17	.23	.21	.11	.21	.16
Total -----	100.0	100.0	100.0	100.0	100.0	100.0	100.0	100.0	100.0	100.0	100.0	100.0	100.0	100.0	100.0	100.0
Indexes																
A/CNK -----	0.74	0.77	0.87	0.78	0.77	0.81	0.77	0.77	0.84	0.77	0.77	0.77	0.78	0.84	0.79	0.79
Mg # -----	65.4	51.6	62.5	52.6	49.0	54.4	65.5	66.3	67.1	53.4	48.6	28.0	36.1	70.7	42.5	54.3
Normative minerals																
Q -----	3.62	6.68	1.75	7.54	1.68	4.77	7.32	7.34	5.88	4.93	9.65	12.14	7.50	10.0	8.78	6.64
or -----	1.95	3.40	4.32	3.96	14.81	7.34	5.56	5.88	5.29	6.14	4.77	8.43	6.74	4.81	8.49	6.13
ab -----	32.14	28.87	30.94	30.89	32.26	35.36	29.86	30.90	35.85	31.53	30.29	33.15	36.45	29.86	39.66	32.53
an -----	30.98	33.81	35.30	31.72	21.09	21.89	28.56	28.28	27.44	26.87	26.46	19.74	20.22	30.32	17.54	26.68
di -----	11.83	10.57	5.50	9.48	9.24	6.96	9.76	9.59	6.01	9.93	8.42	7.50	6.80	6.18	5.82	8.24
hy -----	11.20	8.40	17.81	7.38	13.34	14.40	10.28	9.41	10.91	15.19	12.17	6.08	13.99	10.75	8.71	11.33
mt -----	5.24	4.98	2.05	5.77	3.65	5.61	5.44	5.55	5.80	2.04	3.72	8.20	3.34	5.54	6.37	4.89
il -----	2.33	2.52	1.85	2.49	3.15	2.99	2.50	2.35	2.15	2.63	3.53	3.44	3.53	1.93	3.12	2.70
ap -----	.72	.78	.48	.79	.77	.67	.73	.71	.67	.75	1.00	1.33	1.44	.61	1.52	.86
Total -----	100.00	100.00	100.00	100.00	100.00	100.00	100.00	100.00	100.00	100.00	100.00	100.00	100.00	100.00	100.00	100.00
Normative plagioclase An percent	49.1	53.9	53.3	50.7	39.5	38.2	48.9	47.8	43.4	46.0	46.6	37.3	35.7	50.4	30.7	44.8

**Table 2.** Major-element chemical composition (weight percent) of flow and dike rocks of the Admiralty Island Volcanics in order of increasing SiO<sub>2</sub> content recalculated in volatile-free amount, and CIPW norms based on volatile-free oxide amount —Continued

C. High-SiO <sub>2</sub> andesite flows									
Field No.	91AF098A	91AF104A	92AF029A	92AF027B	92AF025A	92AF028A	91AF090B	91AF100A	average
Symbol	24	25	26	27	28	29	30	31	AN-HI
SiO <sub>2</sub> -----	55.9	53.0	57.2	56.8	52.9	55.8	58.1	56.6	55.8
Al <sub>2</sub> O <sub>3</sub> -----	15.8	15.5	16.2	16.6	15.5	17.1	16.3	14.8	16.0
Fe <sub>2</sub> O <sub>3</sub> -----	3.98	2.42	3.34	3.12	1.42	4.63	1.49	2.26	2.83
FeO-----	5.51	4.47	5.14	4.34	6.08	2.19	5.02	6.94	4.96
MgO-----	2.80	2.50	3.04	3.82	3.06	3.93	4.25	1.27	3.08
CaO-----	6.08	9.12	6.31	6.91	6.59	5.38	6.65	4.99	6.50
Na <sub>2</sub> O-----	4.33	2.90	4.19	3.59	2.80	3.37	3.34	3.46	3.50
K <sub>2</sub> O-----	1.39	.45	1.15	1.12	.31	1.28	.73	.41	.86
H <sub>2</sub> O+-----	.41	2.41	.71	.86	4.43	3.15	1.76	3.05	2.10
H <sub>2</sub> O-----	.84	.83	.58	.61	1.01	1.40	.29	.52	.76
TiO <sub>2</sub> -----	1.54	1.10	1.53	1.11	1.28	.90	1.00	1.38	1.23
P <sub>2</sub> O <sub>5</sub> -----	.48	.28	.34	.25	.39	.20	.26	.62	.35
MnO-----	.17	.12	.16	.12	.13	.09	.13	.09	.13
CO <sub>2</sub> -----	<.01	4.32	.48	1.00	4.53	1.65	.02	2.98	2.14
Total	99.2	99.4	100.4	100.2	100.4	101.1	99.3	99.4	99.9
LOI-----	0.45	6.42	1.07	1.88	8.93	5.24	1.53	5.30	3.85
Analyses recalculated in volatile-free amount									
SiO <sub>2</sub> -----	57.1	57.7	58.0	58.1	58.5	58.8	59.7	61.0	58.6
Al <sub>2</sub> O <sub>3</sub> -----	16.1	16.9	16.4	17.0	17.1	18.0	16.8	15.9	16.8
Fe <sub>2</sub> O <sub>3</sub> -----	4.06	2.63	3.39	3.19	1.57	4.88	1.53	2.44	2.96
FeO-----	5.62	4.87	5.21	4.44	6.72	2.31	5.16	7.48	5.23
MgO-----	2.86	2.72	3.08	3.91	3.38	4.14	4.37	1.37	3.23
CaO-----	6.21	9.93	6.40	7.07	7.29	5.67	6.84	5.38	6.85
Na <sub>2</sub> O-----	4.42	3.16	4.25	3.67	3.10	3.55	3.43	3.73	3.66
K <sub>2</sub> O-----	1.42	.49	1.17	1.15	.34	1.35	.75	.44	.89
TiO <sub>2</sub> -----	1.57	1.20	1.55	1.14	1.42	.95	1.03	1.49	1.29
P <sub>2</sub> O <sub>5</sub> -----	.49	.31	.35	.26	.43	.21	.27	.67	.37
MnO-----	.17	.13	.16	.12	.14	.10	.13	.10	.13
Total	100.0	100.0	100.0	100.0	100.0	100.0	100.0	100.0	100.00
Indexes									
A/CNK----	0.80	0.71	0.83	0.84	0.92	1.02	0.89	0.97	0.87
Mg #----	47.5	49.9	51.3	61.1	47.3	76.2	60.1	24.6	52.3
Normative minerals									
Q-----	9.25	14.34	10.99	11.84	15.96	15.26	14.28	21.63	14.19
C-----	.00	.00	.00	.00	.00	.91	.00	1.16	.26
or-----	8.38	2.90	6.89	6.77	2.03	7.97	4.44	2.61	5.25
ab-----	37.39	26.71	35.96	31.07	26.19	30.06	29.05	31.54	31.00
an-----	19.97	30.42	22.31	26.46	31.85	26.76	28.09	22.31	26.02
di-----	6.22	13.80	5.85	5.58	1.23	.00	3.32	.00	4.50
hy-----	8.78	5.04	9.35	10.91	16.79	10.32	16.02	12.85	11.26
mt-----	5.89	3.82	4.91	4.63	2.28	5.00	2.22	3.53	4.04
hm-----	.00	.00	.00	.00	.00	1.43	.00	.00	.18
il-----	2.99	2.27	2.95	2.16	2.69	1.80	1.95	2.82	2.45
ap-----	1.13	.71	.80	.59	1.00	.49	.62	1.55	.86
Total	100.00	100.00	100.00	100.00	100.00	100.00	100.00	100.00	100.00
Plagioclase normative An percent	34.8	53.3	38.3	46.0	54.9	47.1	49.2	41.4	45.6

**Table 2.** Major-element chemical composition (weight percent) of flow and dike rocks of the Admiralty Island Volcanics in order of increasing SiO<sub>2</sub> content recalculated in volatile-free amount, and CIPW norms based on volatile-free oxide amount —Continued

D. Silicic flows					
Field No.	92AF027A	91AF096A	91AF099A	91AF086A	average
Symbol	32	33	34	35	SIL
SiO <sub>2</sub> -----	67.1	68.6	71.0	75.8	70.6
Al <sub>2</sub> O <sub>3</sub> -----	15.8	14.0	12.9	12.4	13.8
Fe <sub>2</sub> O <sub>3</sub> -----	4.80	.88	.88	1.39	1.99
FeO -----	.18	2.30	2.16	.42	1.27
MgO -----	.13	.58	.23	.20	.29
CaO -----	1.61	1.16	1.62	.06	1.11
Na <sub>2</sub> O -----	4.93	1.94	3.43	2.72	3.26
K <sub>2</sub> O -----	2.54	4.91	3.07	4.70	3.81
H <sub>2</sub> O+ -----	1.24	2.10	1.44	.81	1.40
H <sub>2</sub> O- -----	.44	1.64	.60	.36	.76
TiO <sub>2</sub> -----	.78	.20	.27	.17	.36
P <sub>2</sub> O <sub>5</sub> -----	.26	.03	.03	.03	.09
MnO -----	.05	.05	.07	.01	.04
CO <sub>2</sub> -----	.04	1.34	1.43	<.01	.94
Total	99.9	99.7	99.1	99.1	99.5
LOI -----	1.50	3.72	2.90	1.16	2.32
Analyses recalculated in volatile-free amount					
SiO <sub>2</sub> -----	68.34	72.48	74.2	77.43	73.1
Al <sub>2</sub> O <sub>3</sub> -----	16.09	14.79	13.5	12.67	14.3
Fe <sub>2</sub> O <sub>3</sub> -----	4.89	.93	.92	1.42	2.04
FeO -----	.18	2.43	2.26	.43	1.33
MgO -----	.13	.61	.24	.20	.30
CaO -----	1.64	1.23	1.69	.06	1.16
Na <sub>2</sub> O -----	5.02	2.05	3.59	2.78	3.36
K <sub>2</sub> O -----	2.59	5.19	3.21	4.80	3.95
TiO <sub>2</sub> -----	.79	.21	.28	.17	.36
P <sub>2</sub> O <sub>5</sub> -----	.27	.03	.03	.03	.09
MnO -----	.05	.05	.07	.01	.05
Total	100.00	100.00	100.00	100.00	100.00
Indexes					
A/CNK -----	1.15	1.32	1.08	1.21	1.20
Mg # -----	56.3	31.0	15.9	45.8	37.3
Normative minerals					
Q -----	26.27	35.68	35.79	42.54	35.07
C -----	2.68	3.65	1.11	2.86	2.58
or -----	15.29	30.65	18.96	28.37	23.32
ab -----	42.49	17.34	30.34	23.51	28.42
an -----	6.41	5.87	8.20	.10	5.15
hy -----	.33	4.97	3.66	.51	2.37
mt -----	.00	1.35	1.33	.91	.90
hm -----	4.89	.00	.00	.79	1.42
ru -----	.53	.00	.00	.00	.13
il -----	.00	.40	.54	.33	.44
ap -----	.61	.07	.07	.07	.21
Total	100.00	100.00	100.00	100.00	100.00
Normative plagioclase An percent	13.1	25.3	21.3	0.4	15.0

tent ( $\Sigma$ REE for flow rocks, given above; average for dike rocks, 113 ppm; table 3E). Basalt and andesite flow and dike rocks of the field have chondrite-normalized HREE values that are much lower than those of silicic rocks (basalt and andesite, - 8 to 20 times chondrite; silicic rocks, - 20 to 40 times chondrite; fig. 10). The flow and dike rocks of the field show moderate enrichment in LREE in chondrite-normalized REE variation (fig. 10). The degree of fractionation in a REE pattern can also be expressed by the ratio between chondrite-normalized contents of a LREE (La or Ce) to a HREE (Yb or Y) (Rollinson, 1993). The volcanic rocks of the Admiralty Island field have moderate chondrite-normalized Ce/Yb [(Ce/Yb)<sub>N</sub>] values that generally increase with SiO<sub>2</sub> content (averages: basalt, 2.45; low-SiO<sub>2</sub> andesite, 3.31; silicic rocks, 3.32; high-SiO<sub>2</sub> andesite, 3.65; table 3).

The origin of the small, positive, chondrite-normalized Gd anomaly shown by many rocks of the Admiralty Island Volcanics (fig. 10) and the much larger positive Gd anomaly in rocks of the Icy Strait magmatic field (Brew, 1994) is uncertain. Gd anomalies of this type are not reported for other andesitic suites (for example, Gill, 1981; Sawlan, 1991). Analysis of Gd by instrumental neutron-activation analysis (INAA), such as used in the present study, is difficult (de Baar and others, 1985). de Baar and others (1985) considered the positive Gd anomalies by INAA analysis to be significant in their study. The common, small, negative Eu anomalies [(Eu/Eu\*)<sub>N</sub> < 1; table 3; fig. 10] in the basalt and andesite flow and dike rocks might be attributed to inaccuracy in analysis of neighboring Gd, and so their significance is uncertain. The silicic rocks of the field, however, have much more pronounced, negative Eu anomalies that are not dependent on uncertainty of Gd analysis (fig. 10).

A variety of geochemical signatures using immobile trace elements have been found to fingerprint magmas that formed in different tectonic settings (for example, Wood, 1980; Pearce, 1982; Rollinson, 1993). The covariation between the immobile elements Ti, Zr, and Y used by Pearce and Cann (1973) to discriminate between a variety of tectonic settings of basaltic volcanism, however, does not indicate well the tectonic setting of the basaltic rocks of the Admiralty Island Volcanics (fig. 11). TiO<sub>2</sub> and Zr covariations in basalts of the Admiralty Island Volcanics plot within the field of ocean-floor basalt in the diagram of figure 12 and show characteristics of within-plate rather than volcanic-arc magmatism according to diagrams of Pearce (1982). The basalt and andesite flow rocks have closely similar MORB-normalized, multi-element variation patterns (fig. 13). Silicic rocks show greater enrichment in incompatible elements and strong depletions in Sr, P, Ti, and Cr compared with the more mafic rocks (fig. 13).

The relatively immobile high-field-strength elements (HFSE) afford the best indicators of tectonic setting in



altered volcanic rocks according to many authors (for example, Wood, 1980; Pearce, 1983; Arculus, 1987). Wood's (1980) diagram using the HFSE Th, Hf, and Ta can be applied to basaltic, intermediate, and silicic rocks and is particularly good for discriminating subduction-related volcanic-arc rocks from rocks of other origins (Rollinson, 1993). All rocks of the field of the Admiralty Island Volcanics, including the dikes, plot within Wood's Th-Hf-Ta field for within-plate volcanic rocks and lie in a field distinctly apart from volcanic rocks of either a subduction-related or a MORB origin (fig. 14). The covariation between MgO and TiO<sub>2</sub> contents additionally

suggests a nonsubduction setting for the silicic rocks of the field (fig. 15).

## DISCUSSION

Plate reconstructions (Plafker and others, 1994) show that northern southeastern Alaska had a transform tectonic setting by the time of formation of the Admiralty Island Volcanics in the Oligocene. The mostly andesitic volcanic rocks show geochemical characteristics of rocks formed in an extensional tectonic setting. Studies of other

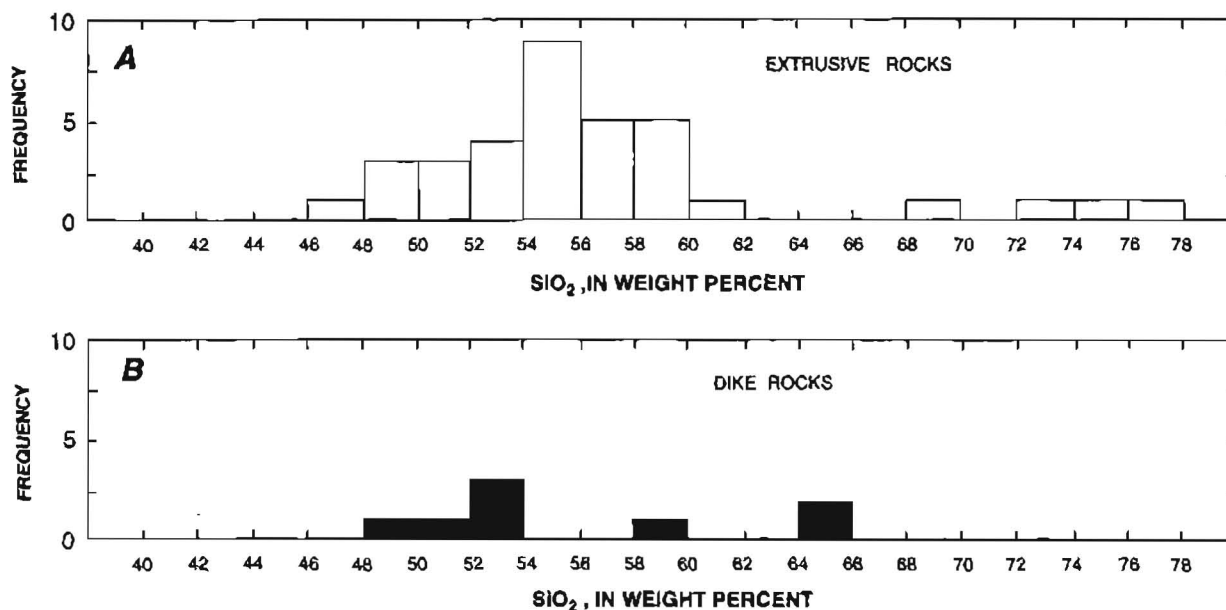


Figure 3. Histogram showing distribution of SiO<sub>2</sub> in flows (A) and dikes (B) of the Admiralty Island Volcanics.

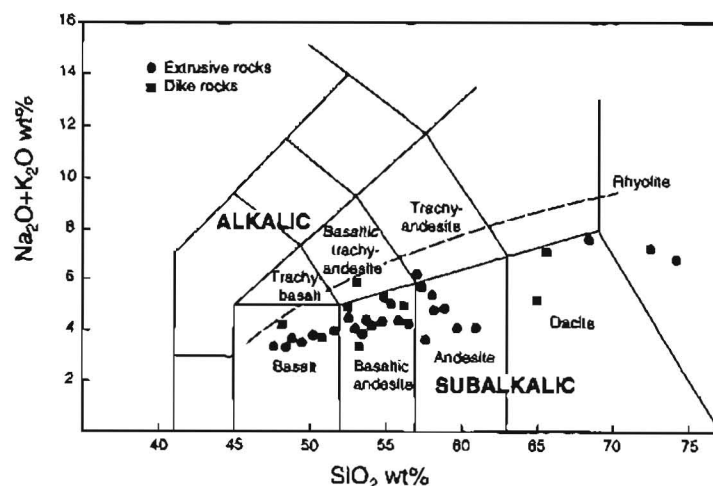


Figure 4. Nomenclature of flow and dike rocks of the Admiralty Island Volcanics based on the classification of Le Bas and others (1986). Heavy dashed line shows division between alkalic and subalkalic rocks of Irvine and Baragar (1971).



extensional zones of transform margins have shown that magmatic activity, which is typically of intermediate composition, was generated from heterogeneous mantle under varied tectonic settings (Pe-Piper and others, 1994). The identification of magmas formed in such a transform-margin setting by geochemical methods, however, is difficult (Pe-Piper and others, 1994). The Admiralty Island rocks show some features of orogenic-arc rocks but others of nonsubduction-related, within-plate extensional magmatism. The rocks of the field lack the alkalic characteristics of rocks typically found in within-plate, intracontinental-rift zones (Hess, 1989; Harangi, 1994),

and the abundance of andesitic rocks in the field contrasts with the limited abundance of such rocks of intermediate composition found in transform-related, bimodal basalt-rhyolite volcanic suites of other areas (Lipman and others, 1978).

The volcanism on Admiralty Island followed a long history of magmatic-arc activity in northern southeastern Alaska that was related to Pacific plate slab subduction (62-48 Ma; Plafker and others, 1994). After subduction, the development of a transform plate boundary by Oligocene time led to the formation of a "slab-free" region along this part of southeastern Alaska, analogous to the

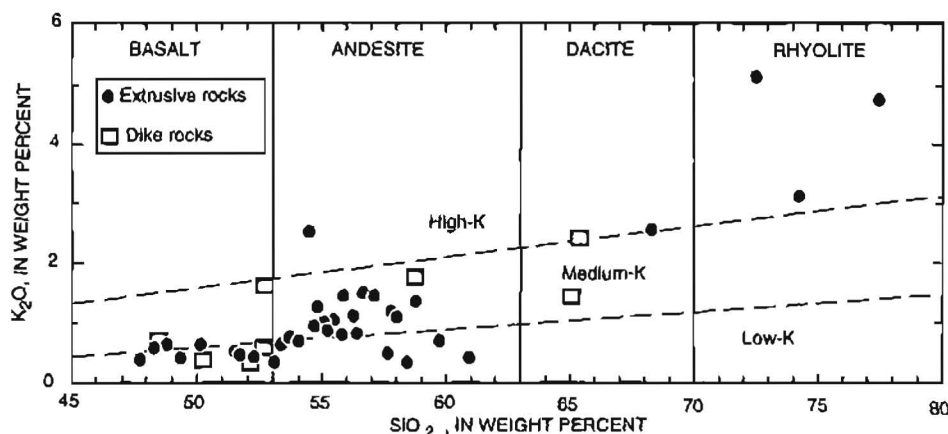


Figure 5.  $K_2O$  versus  $SiO_2$  variation in flow and dike rocks of the Admiralty Island Volcanics, based on diagram of Gill (1981).

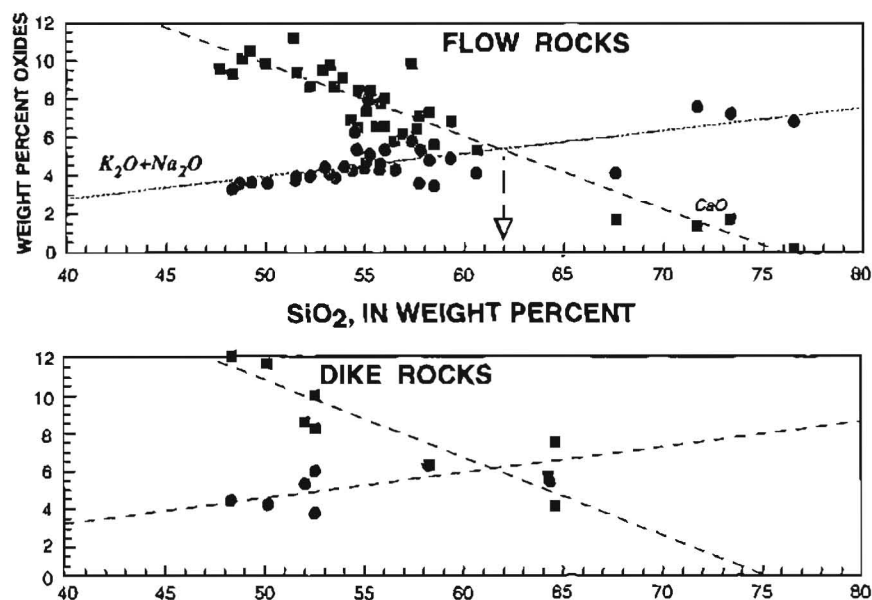
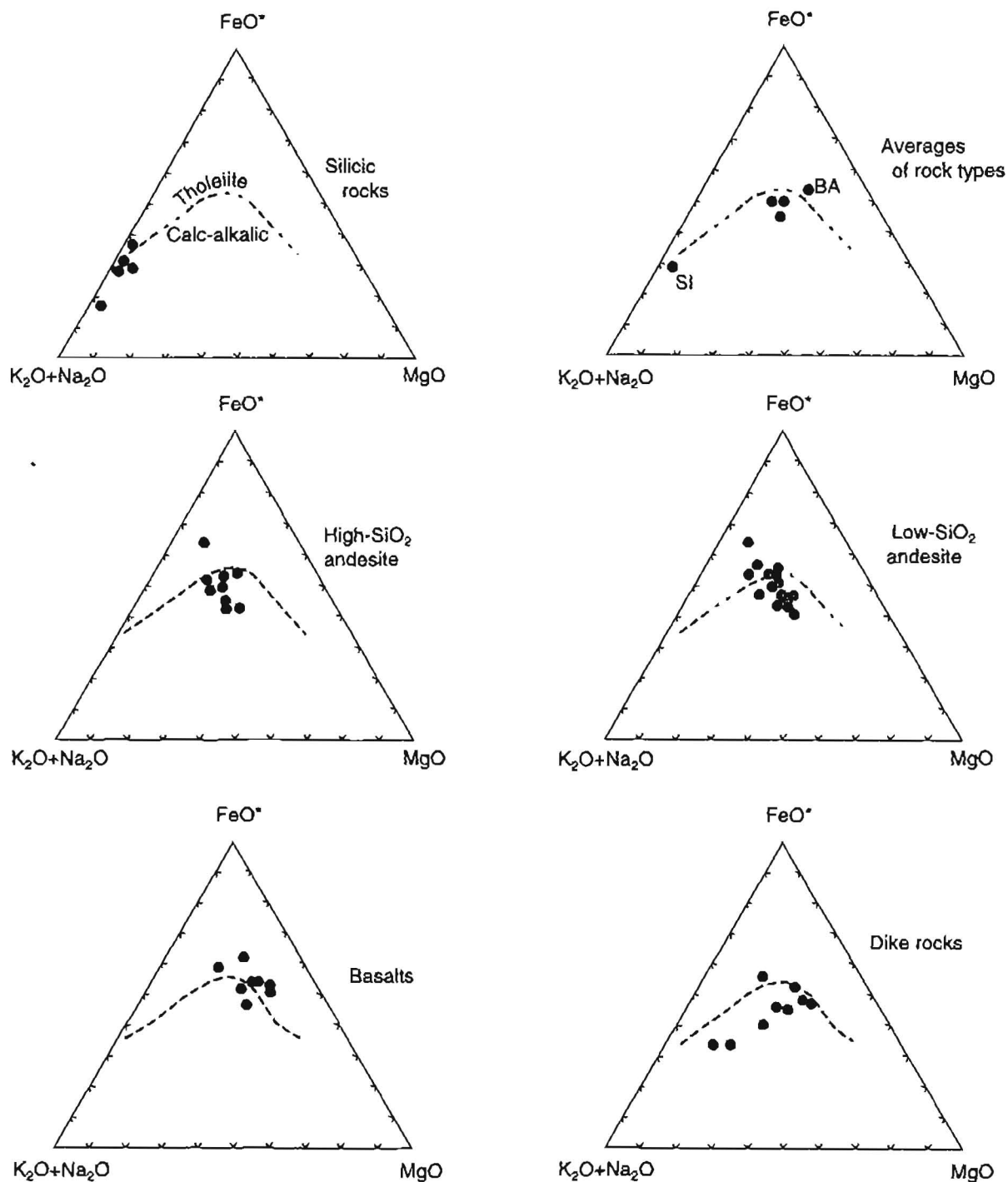


Figure 6. Variation of  $CaO$  and  $Na_2O+K_2O$  with  $SiO_2$  in flow and dike rocks of the Admiralty Island Volcanics. Lines show best fit of data points by least-squares regression. "Peacock" (alkali-lime) index from intersection (Peacock, 1931), marked by arrow.

situation behind the San Andreas transform fault of California following termination of subduction activity (Dickinson and Snyder, 1979). The Admiralty Island volcanism occurred about 300 km east of the transform fault marking the boundary between the Pacific and North American plates.

The flows and dikes of the Admiralty Island volcanic field represent derivative melts, as shown by Mg numbers that are much lower than those of primary melts of mantle origin ( $>67$ ; Gill, 1981) and by Ni contents of the most mafic rocks (20-86 ppm, table 3A) that are much below values in rocks of primary mantle origin (300-400



**Figure 7** Ternary (AFM) diagrams, showing variation of (A)  $\text{Na}_2\text{O} + \text{K}_2\text{O}$ , (F)  $\text{FeO}^*$  ( $\text{FeO} + 0.9 \times \text{Fe}_2\text{O}_3$ ), and (M)  $\text{MgO}$  for the Admiralty Island Volcanics. Tholeiitic and calc-alkalic fields from Irvine and Baragar (1971).

ppm; Harangi, 1994). The lack of isotopic data limits conjecture on the nature of the source. Many compositional variations of the rocks can be attributed to fractionation. An absence of hornblende phenocrysts in flow rocks is possibly explained by removal of hornblende from the melt, as is suggested by the inverse variation between A/CNK value and CaO content (Liggett, 1990) in the rocks of this volcanic field. The origin of the pronounced negative Eu anomaly of the silicic rocks (fig. 10) can be

explained by fractionation of plagioclase (Rollinson, 1993).

The petrologic nature and tectonic setting of the Admiralty Island Volcanics inferred from geochemical characteristics show differences according to different major and minor elements. Major-element compositions of the rocks, for example, are generally typical for orogenic, arc-related volcanic suites, but the suite lacks the high-K, shoshonitic basalt and andesite compositions that characterize some subduction-related orogenic andesitic suites (Ewart, 1982). The rocks of the field have tholeiitic composition rather than the alkalic characteristics of subduction-related volcanic rocks of Baja California (Sawlan, 1991). The tholeiitic nature of the Admiralty Island Volcanics does not exclude a subduction-related origin, however, because rocks of tholeiitic composition are found in arc and back-arc rift settings (Sawlan, 1991; Tamura, 1994; Wharton and others, 1995).

The trace-element characteristics show the principal differences between the Admiralty Island Volcanics and volcanic-arc (orogenic) rocks formed by subduction processes. Although Th contents of the Admiralty Island Volcanics are generally within the range found in orogenic andesite (1-5 ppm; Gill, 1981), Zr abundances are much higher than typical for such rocks (50-150 ppm; Gill, 1981). Average K/Rb values of rocks of the Admiralty Island field are similar to those of calc-alkalic suites and much lower than those of island-arc tholeiitic suites (respectively, 400-500, 1000; Jakes and Gill, 1970). The average  $\text{TiO}_2$  content of the basalt flows (1.8 weight percent, table 2A) is generally higher than typical for arc-related volcanic rocks (<1.3 weight percent; Gill, 1981) and about the same as for rift-related tholeiite of the Gulf of California (1.1-2.6 weight percent; Sawlan, 1991). The Admiralty Island volcanic rocks have more fractionated chondrite-normalized REE patterns and much higher HREE contents (10-20 times chondrite values) than is typical for island-arc tholeiite (Jakes and Gill, 1970) and for MORB. Chondrite-normalized REE patterns for all rocks of the field are closely similar to those of a (Proterozoic) bimodal, calc-alkalic, continental-margin volcanic arc reported by Condie and Shadel (1984).

The Admiralty Island rocks generally show the enrichments in incompatible elements (fig. 13) that characterize volcanic rocks of a within-plate setting and that differ from the typical depletion of these elements in subduction-related volcanic rocks (Pearce, 1983). Rocks of the Admiralty Island field lack the Ta and Nb depletions, relative to Th and Ce (fig. 13), that typify subduction-related rocks of volcanic arcs (Pearce, 1983; Sawlan, 1991; Wharton and others, 1995) and back-arc basins (Gamble and others, 1995). Multielement variation diagrams of the Admiralty Island rocks (fig. 13) are also more like those of nonsubduction-related rift-zone volcanic rocks than subduction-related rocks of the Gulf of California (Sawlan,

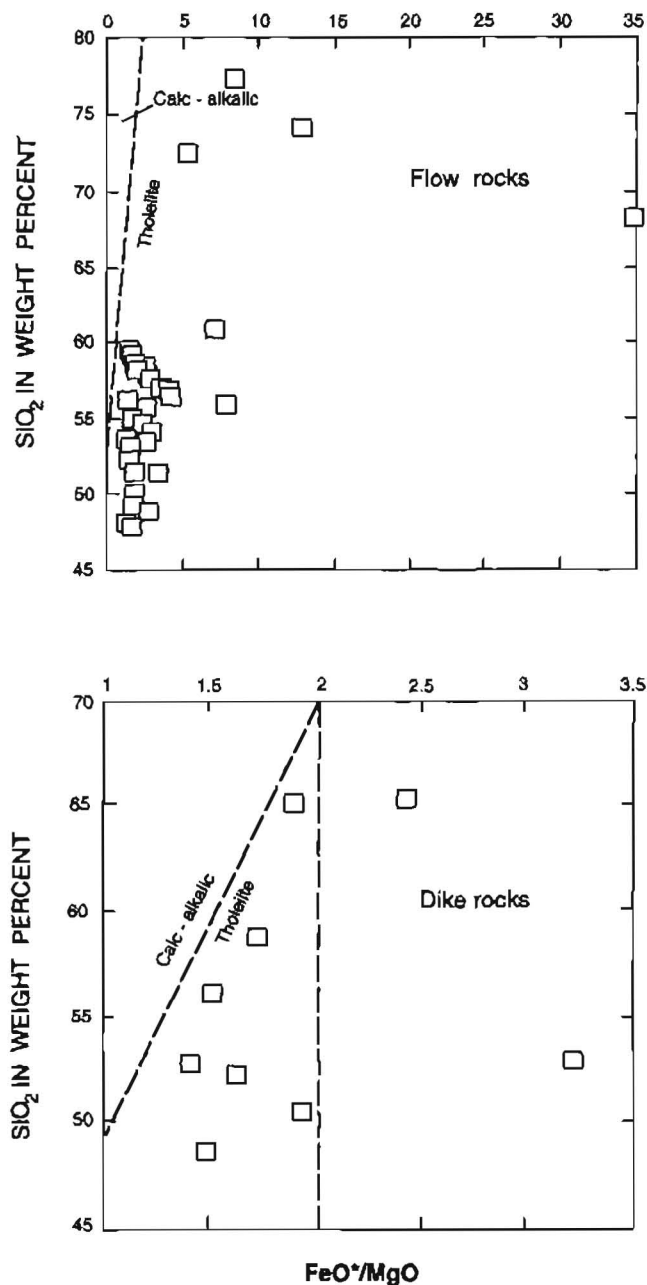


Figure 8. Variation between  $\text{SiO}_2$  and  $\text{FeO}^*/\text{MgO}$  in rocks of the Admiralty Island Volcanics, showing dividing line of calc-alkalic and tholeiitic compositions of Miyashiro (1974).

1991). The tectonic setting of the Admiralty Island volcanism is therefore interpreted to be that of within-plate extension (fig. 14). The rifting in this area did not progress to the stage of development of new oceanic crust as in the Gulf of California (Sawlan, 1991; Sawlan and Smith, 1984).

### RELATION TO TKOPE-PORTLAND PENINSULA MAGMATIC BELT

The Admiralty Island Volcanics is the largest volcanic field of the Tko-pe-Portland Peninsula magmatic belt, which extends along almost all of southeastern Alaska. This report on the Admiralty Island Volcanics provides the first critical trace-element data for rocks of this belt. The approximate parallelism of the belt with the continental margin and its proximity to the margin (fig. 1) are suggestive of a back-arc rift setting, but the geochemical characteristics of the rocks and the cessation of subduction before the volcanism indicate that back-arc processes were not involved in the magma generation. The Tko-pe-Portland Peninsula magmatic belt differs from typical intracontinental-rift belts in that it apparently lacks alkalic rocks typical of such belts (Hess, 1989; Harangi, 1994). The origin of the magmatic belt does not appear to be related to the Chatham Strait segment of the Denali fault system, which crosses the belt at a low angle and in which right-lateral transcurrent movement began by about 62 Ma according to Plafker and others (1994) and continued until after the time of the Admiralty Island volcanism (fig. 1). The spacial relation of the fault to the Admiralty Island volcanic field, however, suggests that fault activity may have played a role in the development of a conduit system for eruption of the volcanic rocks.

The origin of the Admiralty Island Volcanics and the Tko-pe-Portland Peninsula magmatic belt may be related to processes of extension and crustal thinning developed in an area thermally weakened by asthenosphere upwelling and crustal underplating by intrusion of mafic magmas (Liu and Furlong, 1994; Keen and others, 1994), as proposed for the origin of magmas in the "slab-window" of the San Andreas transform fault (Dickinson and Snyder, 1979). The linear zone of coast-parallel extension and volcanism of the belt may have resulted from lithospheric instability following the Eocene and older subduction activity. The long duration of magmatism in the Tko-pe-Portland magmatic Peninsula belt (35-5 Ma; Brew, 1994) is similar to that of other transform-related regions (Dickinson and Snyder, 1979). To the north, the late Cenozoic parts of the Wrangell volcanic field in Canada record a transition from a subduction margin to a transform margin (Skulski and others, 1991), while the Wrangell field in Alaska continued to record arc volcanism associated with subduction of the north-moving Pacific plate (Richter and others, 1990).

### SUMMARY AND CONCLUSIONS

The Admiralty Island Volcanics consists of a 3,000-m-thick field of low-MgO, medium- and low-K, mostly andesitic flows and dikes that covers an area of about 1,000 km<sup>2</sup> on southernmost Admiralty Island. The volcanic field is composed dominantly of low-SiO<sub>2</sub> andesite flows that are interlayered with flows of high-SiO<sub>2</sub> andesite, basalt, and much less abundant dacite and rhyolite. Volatile-free SiO<sub>2</sub> content of flow rocks ranges from 47 to 77 weight percent and shows a SiO<sub>2</sub> gap at 62-68

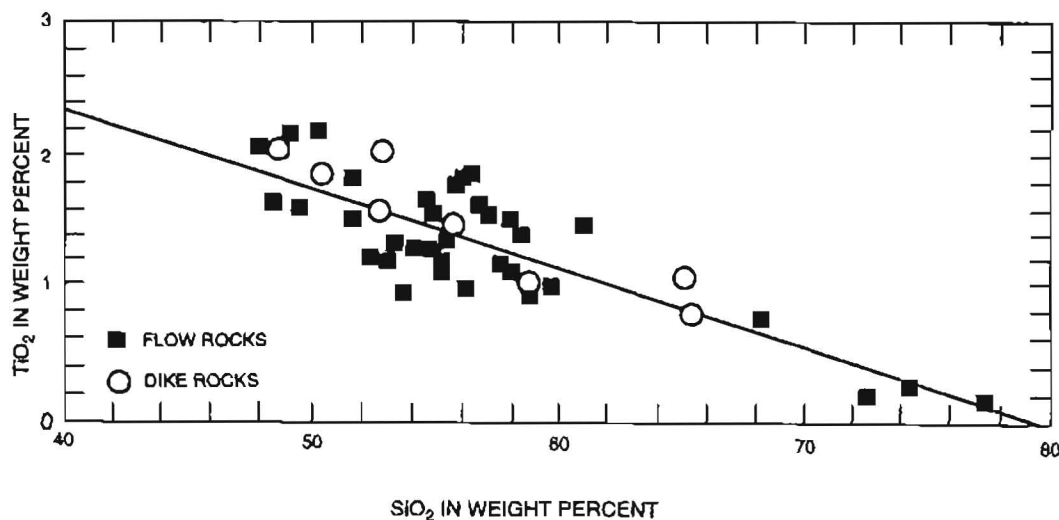


Figure 9. Variation between TiO<sub>2</sub> and SiO<sub>2</sub> in rocks of the Admiralty Island Volcanics. Line shows best fit of data points by least-squares regression.

**Table 3.** Average trace-element content (parts per million) and ratios for flow and dike rocks of the Admiralty Island Volcanics

[Samples analyzed in laboratories of the U.S. Geological Survey by methods described in Baedecker (1987); X-ray fluorescence (XRF) methods described in Johnson and King (1987) and King and Lindsay (1990); V, by method in Golightly and others (1987); instrumental neutron-activation analysis (INAA) methods in Baedecker and McKown (1987); nd, not determined. Analysis: energy-dispersive XRF methods (#), Judith Kent, B.W. King; INAA (Δ), C.A. Palmer; direct-current arc emission spectrographic analysis (@), P.J. Lamothe]

A. Basalt flows									
Field No.	91AF095A	91AF102A	91AF093A	91AF091A	92AF024A	91AF103A	91AF101A	91AF088A	average
Plot symbol	1	2	3	4	5	6	7	8	BA
K-group elements									
Ba <sup>#</sup> -----	64	770	240	168	270	345	250	150	282
Cs <sup>Δ</sup> -----	.23	.45	.27	<.16	<.17	.27	.74	.19	.38
Rb <sup>Δ</sup> -----	16	4.8	15	4.5	10	7.3	11	<6	10
Sr <sup>#</sup> -----	250	385	275	315	450	360	395	300	341
REE group elements									
La <sup>Δ</sup> -----	7.96	7.13	12.5	8.46	16.8	16.1	15.2	11.1	11.9
Ce <sup>Δ</sup> -----	20	17	28.6	19	37	34.1	33.7	24	27
Nd <sup>Δ</sup> -----	14	10	18	14	24	18	19	13	16
Sm <sup>Δ</sup> -----	4.46	3.73	5.34	3.58	6.14	5.09	5.24	3.79	4.67
Eu <sup>Δ</sup> -----	1.6	1.3	1.7	1.3	2.1	1.6	1.7	1.3	1.6
Gd <sup>Δ</sup> -----	6.3	4.4	7.0	4.6	8.0	6.8	6.7	4.5	6.0
Tb <sup>Δ</sup> -----	.86	.71	.993	.68	.98	.87	.861	.67	.83
Tm <sup>Δ</sup> -----	nd	nd	nd	nd	nd	nd	nd	nd	nd
Yb <sup>Δ</sup> -----	2.8	2.6	3.2	2.3	2.9	3.1	3.06	2.3	2.8
Lu <sup>Δ</sup> -----	.414	.403	.458	.330	.428	.435	.428	.340	.405
Sum REE-----	58.0	46.9	77.3	53.9	97.9	85.7	85.5	60.7	70.7
Y <sup>#</sup> -----	40	32	38	33	34	27	34	20	32
Th group									
Th <sup>Δ</sup> -----	0.70	0.52	1.56	0.71	1.40	2.52	1.40	1.40	1.28
U <sup>Δ</sup> -----	.24	<.20	.56	2.00	.43	.87	.68	.52	.76
Ti group									
Zr <sup>#</sup> -----	140	122	176	120	168	174	168	134	150
Hf <sup>Δ</sup> -----	3.24	2.61	3.85	2.60	3.50	3.72	3.50	2.93	3.24
Nb <sup>#</sup> -----	16	13	17	14	20	16	18	<10	16
Ta <sup>Δ</sup> -----	.63	.45	.838	.55	.95	.88	.77	.52	.70
Compatible group									
Co <sup>Δ</sup> -----	46.9	44.9	39.9	37.4	34.0	25.0	29.5	31.1	36.1
Cr <sup>Δ</sup> -----	87.2	77.8	60.1	117	92	34.6	96	132	87
Ni <sup>#</sup> -----	51	86	44	32	43	20	29	35	43
Sc <sup>Δ</sup> -----	32.5	31.9	30.7	31.2	33.0	25.2	28.9	25.8	29.9
V <sup>@</sup> -----	240	220	270	260	264	230	190	190	233
Chalcophile group									
Cu <sup>#</sup> -----	31	31	39	42	22	27	23	19	29
Zn <sup>Δ</sup> -----	87	72	95	67	84	85	.86	68	80
Ratios									
K/Rb	176	882	321	701	506	523	347.2	nd	494
Rb/Sr	.06	.01	.05	.01	.02	.02	.03	nd	.03
(Eu/Eu*) <sub>N</sub>	.93	.98	.84	.98	.92	.84	.89	.97	.92
(Ce/Yb) <sub>N</sub>	1.82	1.66	2.27	2.10	3.24	2.80	2.80	2.65	2.45



Table 3. Average trace-element content (parts per million) and ratios for flow and dike rocks of the Admiralty Island Volcanics—Continued

B. Low-SiO <sub>2</sub> andesite flows																
Field No. Plot symbol	91AF106A 9	92AF023A 10	91AF089A 11	92AF023B 12	91AF086B 13	91AF097A 14	92AF031B 15	92AF031A 16	92AF105A 17	92AF026A 18	91AF087A 19	91AF092A 20	91AF085A 21	92AF030A 22	91DB034A 23	average AN-L
K-group elements																
Ba <sup>#</sup>	196	255	300	295	250	580	370	375	310	405	850	750	465	285	560	416
Ca <sup>Δ</sup>	<.14	.20	.54	<.24	.3	.41	.21	.30	.16	.38	.81	.34	.23	.36	.51	.57
Rb <sup>Δ</sup>	<11	9.4	14	11	81	26	16	20	18	22	13	27	20	18	32	23
Sr <sup>#</sup>	395	390	435	385	194	290	480	460	345	415	330	290	365	385	305	364
REE group elements																
La <sup>Δ</sup>	17.5	16.4	12.1	16.9	14.7	19.8	18.2	17.9	18.1	18.5	19.0	23.4	23.2	17.3	28.6	18.8
Ce <sup>Δ</sup>	35.6	33.4	25.0	34.6	31.0	42.0	35.0	35.0	35.6	36.0	39.2	50.0	48.0	33.0	58.7	38.1
Nd <sup>Δ</sup>	18	18	12	18	16	23	17	18	17	18	19	29	25	17	31	20
Sm <sup>Δ</sup>	4.73	4.61	3.16	4.78	4.34	6.90	4.42	4.40	4.42	4.43	4.99	8.55	7.19	4.18	8.82	5.33
Eu <sup>Δ</sup>	1.41	1.60	1.10	1.70	1.40	1.90	1.40	1.40	1.32	1.40	1.50	2.44	2.09	1.30	2.46	1.63
Gd <sup>Δ</sup>	5.9	5.5	4.5	6.0	5.4	7.8	5.5	4.9	5.1	5.4	6.0	10	7.7	5.9	10	6.4
Tb <sup>Δ</sup>	.777	.750	.530	.790	.700	1.21	.680	.670	.714	.710	.760	1.48	1.18	.680	1.40	.87
Tm <sup>Δ</sup>	nd	nd	nd	nd	nd	nd	nd	nd	nd	nd	nd	nd	nd	nd	nd	-
Yb <sup>Δ</sup>	2.71	2.56	1.90	2.63	2.40	4.50	2.24	2.20	2.39	2.20	2.30	5.27	3.90	2.20	4.60	2.93
Lu <sup>Δ</sup>	.387	.387	.250	.402	.345	.659	.300	.300	.360	.330	.337	.749	.541	.340	.659	.420
Sum REE <sup>Δ</sup>	86.63	82.82	60.29	85.40	75.94	107.11	84.44	84.47	84.64	86.64	92.75	130.14	118.66	81.56	145.58	93.80
Y <sup>#</sup>	25	25	23	30	30	54	25	26	27	30	30	51	49	26	52	34
Th group																
Th <sup>Δ</sup>	2.19	1.99	1.90	2.10	2.20	3.17	2.50	2.60	2.71	2.80	3.00	3.33	3.30	2.50	4.10	2.69
U <sup>Δ</sup>	.77	.72	.62	.82	.83	1.6	.99	.99	.99	1.10	.98	1.50	1.10	.91	1.50	1.03
Compatible group																
Zr <sup>#</sup>	184	174	126	182	154	405	150	154	198	160	184	265	245	152	265	200
Hf <sup>Δ</sup>	3.91	3.60	2.60	3.68	3.30	7.75	3.33	3.40	3.99	3.44	3.90	5.97	5.13	3.40	5.72	4.21
Nb <sup>#</sup>	17	16	<10	16	14	20	13	14	18	14	20	21	27	14	24	18
Ta <sup>Δ</sup>	.88	.82	.612	.86	.78	.91	.816	.809	.878	.746	.95	1.20	1.24	.79	1.30	.91
Co <sup>Δ</sup>	30.4	25.5	27.6	25.8	22.8	31.0	27.2	27.0	26.4	22.0	23.9	18.3	16.2	29.0	14.1	24.5
Cr <sup>Δ</sup>	101	26.0	108	26.0	28.1	24.6	75.1	74.6	50.6	65.3	5.90	3.10	2.60	140	<4	52.2
Ni <sup>#</sup>	57	15	60	11	10	36	24	26	46	15	11	<10	<10	63	<10	31
Sc <sup>Δ</sup>	22.8	27.1	19.3	27.5	23.9	21.6	23.8	23.8	18.7	24.7	21.8	24.6	25.0	20.0	22.1	23.1
V <sup>@</sup>	180	179	140	164	205	180	196	172	150	188	240	150	150	132	95	168
Chalcophile group																
Cu <sup>#</sup>	45	45	39	43	25	26	42	36	28	15	27	22	<10	47	17	33
Zn <sup>Δ</sup>	78	80	59	80	74	111	74	74	75	71	81	138	100	66	110	85
Ratios																
K/Rb	nd	486	415	491	224	383	483	407	401	385	466	412	448	369	363	409
Rb/Sr	nd	.02	.03	.03	.42	.09	.03	.04	.05	.05	.04	.09	.05	.05	.10	.08
(Eu/Eu*) <sub>N</sub>	.82	.97	.90	.98	.89	.79	.87	.92	.85	.88	.84	.81	.86	.80	.80	.87
(Ce/Yb) <sub>N</sub>	3.34	3.32	3.35	3.35	3.29	2.37	3.97	4.05	3.79	4.16	4.33	2.41	3.13	3.82	3.25	3.31

**Table 3.** Average trace-element content (parts per million) and ratios for flow and dike rocks of the Admiralty Island Volcanics—Continued

C. High-SiO <sub>2</sub> andesite flows									
Field No.	91AF098A	91AF104A	92AF029A	92AF027B	92AF025A	92AF028A	91AF090B	91AF100A	average
Plot symbol	24	25	26	27	28	29	30	31	AN-H
K-group elements									
Ba <sup>#</sup> -----	510	350	415	445	365	390	300	310	386
Cs <sup>Δ</sup> -----	.44	<.16	.33	.39	.34	.87	.55	.33	.46
Rb <sup>Δ</sup> -----	33	11	23	25	8.6	29	21	<9	22
Sr <sup>#</sup> -----	310	315	355	355	410	250	395	245	329
REE-group elements									
La <sup>Δ</sup> -----	25.4	17.4	20.8	17.8	19.3	17.6	16.9	27.7	20.4
Ce <sup>Δ</sup> -----	52.4	35.1	41.0	34.6	38.1	27.6	33.4	59.5	40.2
Nd <sup>Δ</sup> -----	27	17	21	17	20	16	15	35	21
Sm <sup>Δ</sup> -----	7.30	4.11	5.29	4.26	4.60	3.93	3.55	9.12	5.27
Eu <sup>Δ</sup> -----	2.0	1.3	1.6	1.3	1.6	1.1	1.1	2.7	1.6
Gd <sup>Δ</sup> -----	8.0	5.3	6.4	4.8	5.6	4.5	4.2	9.4	6.0
Tb <sup>Δ</sup> -----	1.20	.66	.85	.72	.71	.60	.564	1.48	.85
Tm <sup>Δ</sup> -----	nd	nd	nd	nd	nd	nd	nd	nd	nd
Yb <sup>Δ</sup> -----	4.0	2.2	2.9	2.4	2.1	1.8	1.8	5.3	2.8
Lu <sup>Δ</sup> -----	.57	.310	.434	.352	.290	.271	.250	.75	.40
Sum REE-----	127.30	83.07	99.84	82.89	92.01	73.13	76.55	150.20	98.12
Y <sup>#</sup> -----	43	25	39	26	25	28	25	57	34
Th group									
Th <sup>Δ</sup> -----	4.15	3.29	3.50	3.52	2.90	2.70	3.72	3.28	3.38
U <sup>Δ</sup> -----	1.4	1.1	1.5	1.3	1.7	.9	1.3	1.3	1.3
Ti group									
Zr <sup>#</sup> -----	245	164	215	172	158	146	168	320	199
Hf <sup>Δ</sup> -----	5.32	3.59	4.50	3.81	3.57	3.13	3.50	6.71	4.27
Nb <sup>#</sup> -----	22	14	19	18	12	15	18	26	18
Ta <sup>Δ</sup> -----	1.16	.84	1.00	.844	.829	.654	.82	1.50	.96
Compatible group									
Co <sup>Δ</sup> -----	17.1	19.6	21.0	24.2	21.5	20.5	24.7	17.1	20.7
Cr <sup>Δ</sup> -----	10	13	6	61	13	121	101	2.2	41
Ni <sup>#</sup> -----	<10	<10	5	26	5	46	62	<10	29
Sc <sup>Δ</sup> -----	21.6	19.7	21.6	21.4	18.3	19.2	16.8	24.7	20.4
V <sup>@</sup> -----	150	150	197	145	150	124	130	37	135
Chalcophile group									
Cu <sup>#</sup> -----	19	18	22	30	16	35	12	15	21
Zn <sup>Δ</sup> -----	102	73	77	78	90	72	69	168	91
Ratios									
K/Rb	350	340	415	372	299	366	289	nd	347
Rb/Sr	.11	.03	.06	.07	.02	.12	.05	nd	.07
(Eu/Eu*) <sub>N</sub>	.80	.86	.84	.89	.97	.80	.91	.89	.87
(Ce/Yb) <sub>N</sub>	3.33	4.06	3.60	3.67	4.61	3.90	4.72	2.86	3.65

weight percent between rocks of andesitic and dacitic composition, which is similar to the gap recorded in other rocks of the Tkope-Portland Peninsula magmatic belt. The flows were probably fed from fissure eruptions that are represented by numerous dikes that cut the volcanic se-

quence. Although the rocks show enrichments in incompatible elements that are characteristic of a within-plate extensional setting and lack the Ta and Nb depletions that typify subduction-related rocks, the major-element geochemistry is similar to that of subduction-related oro-

**Table 3.** Average trace-element content (parts per million) and ratios for flow and dike rocks of the Admiralty Island Volcanics—Continued

D. Silicic flows					
Field No.-- Plot symbol-	92AF027A 32	91AF096A 33	91AF099A 34	91AF086A 35	average SIL
K-group elements					
Ba <sup>#</sup> -----	970	740	1500	880	1023
Cs <sup>Δ</sup> -----	1.0	1.5	1.3	.94	1.2
Rb <sup>Δ</sup> -----	51	158	64.8	129	101
Sr <sup>#</sup> -----	180	25	84	53	86
REE-group elements					
La <sup>Δ</sup> -----	51.1	36.6	37.6	38.2	40.9
Ce <sup>Δ</sup> -----	89.0	68.0	73.7	58.0	72.2
Nd <sup>Δ</sup> -----	47.1	29.0	34.0	28.0	34.5
Sm <sup>Δ</sup> -----	11.70	7.05	3.58	6.53	7.22
Eu <sup>Δ</sup> -----	2.50	1.14	1.25	.391	1.32
Gd <sup>Δ</sup> -----	13.0	7.6	9.6	7.3	9.4
Tb <sup>Δ</sup> -----	1.80	1.20	1.52	1.09	1.40
Tm <sup>Δ</sup> -----	nd	nd	nd	nd	nd
Yb <sup>Δ</sup> -----	6.10	4.90	6.30	4.74	5.51
Lu <sup>Δ</sup> -----	.879	.690	.894	.618	.770
Sum REE-	222.3	155.5	167.6	144.3	172.4
Y <sup>#</sup> -----	73	53	68	52	62
Th group					
Th <sup>Δ</sup> -----	6.60	13.10	9.37	16.50	11.39
U <sup>Δ</sup> -----	3.00	5.19	3.86	5.87	4.48
Ti group					
Zr <sup>#</sup> -----	450	385	455	220	378
Hf <sup>Δ</sup> -----	9.30	9.10	9.83	6.34	8.64
Nb <sup>#</sup> -----	35	21	19	17	23
Ta <sup>Δ</sup> -----	2.00	1.56	1.30	1.07	1.48
Compatible group					
Co <sup>Δ</sup> -----	4.10	.62	.46	.77	1.49
Cr <sup>Δ</sup> -----	2.0	<1.7	2.1	1.6	1.9
Ni <sup>#</sup> -----	5	<10	<10	<10	5
Sc <sup>Δ</sup> -----	12.0	5.44	10.7	2.18	7.6
V <sup>@</sup> -----	31	<10	<10	<10	31
Chalcophile group					
Cu <sup>#</sup> -----	11	<10	12	<10	12
Zn <sup>Δ</sup> -----	100	84.6	98.4	65.1	87.0
Ratios					
K/Rb	413.4	258.0	393.3	302.5	341.8
Rb/Sr	.28	6.32	.77	2.43	2.45
(Eu/Eu*) <sub>N</sub>	.62	.48	.62	.17	.47
(Ce/Yb) <sub>N</sub>	3.71	3.53	2.98	3.11	3.32

genic andesite and basalt. The subalkaline character of the rocks differs from the typically alkalic character of intracontinental-rift volcanic rocks.

The volcanism on Admiralty Island occurred about 10 m.y. after termination of Kula plate convergence and during right-lateral transform motion of an ancestral Queen Charlotte-Fairweather fault between the Pacific and North American plates. The Admiralty Island Volcanics is part of the Tkoep-Portland Peninsula magmatic belt that extends along most of southeastern Alaska. Although the major-element composition of the Admiralty Island field and spatial distribution of the Tkoep-Portland Peninsula magmatic belt are broadly suggestive of subduction-related volcanism, the trace-element composition and the age of the belt are inconsistent with such an origin. The position, timing, and trace-element composition instead suggest that the Admiralty Island Volcanics is the result of magmatic processes in a setting continentward of a transform fault. The Admiralty Island Volcanics differs from other transform-related volcanic fields in that rocks of andesitic composition are abundant. We suggest that the magmatism of the belt may be related to asthenospheric upwelling in a slab-window region following change from subduction to transform tectonism. Although coeval with early phases of arc volcanism of the Wrangell volcanic field, the Oligocene volcanism of the Admiralty Island field marks the cessation of subduction magmatism in southeastern Alaska and the onset of transform motion that continues in the area today.

**Acknowledgments.**—We thank Richard D. Koch, Glen R. Himmelberg, and Byron J. Richards for aid in field work.

## REFERENCES CITED

- Arculus, R.J., 1987, The significance of source versus process in the tectonic controls of magma genesis: *Journal of Volcanology and Geothermal Research*, v. 32, p. 1–12.
- Baedecker, P.A., ed., 1987, *Methods for geochemical analysis: U.S. Geological Survey Bulletin 1770*, p. A-1–K-5.
- Baedecker, P.A., and McKown, D.M., 1987, Instrumental neutron activation analysis of geochemical samples, in Baedecker, P.A., ed., *Methods for geochemical analysis: U.S. Geological Survey Bulletin 1770*, p. H-1–H-14.
- Bingler, E.C., Trexler, D.T., Kemp, W.R., and Banham, H.F., Jr., 1976, PETCAL: A basic language computer program for petrologic calculations: *Nevada Bureau of Mines and Geology Report 28*, 27 p.
- Bradley, D.C., Haeussler, P.J., and Kusky, T.M., 1993, Timing of early Tertiary ridge subduction in southern Alaska, in Dusei-Bacon, Cynthia, and Till, A.B., eds., *Geologic studies in Alaska by the U.S. Geological Survey, 1992: U.S. Geological Survey Bulletin 2068*, p. 163–177.
- Brew, D.A., 1994, Latest Mesozoic and Cenozoic magmatism in southeastern Alaska, in Plafker, George, and Berg, H.C., eds., *The Geology of Alaska: Boulder, Colorado, Geological Society of America, The Geology of North America*, v. G-1, p. 621–656.

**Table 3.** Average trace-element content (parts per million) and ratios for flow and dike rocks of the Admiralty Island Volcanics—Continued

E. Dikes									
Field No.	91AF085B	91AF087B	91AF105C	92AF026B	91AF092B	91AF089B	92AF026C	91AF090C	average
Plot symbol	36	37	38	39	40	41	42	43	DK
K-group elements									
Ba <sup>#</sup> -----	435	600	205	290	610	510	405	750	476
Cs <sup>Δ</sup> -----	.17	.56	<.09	1.60	.67	1.10	.64	.82	.79
Rb <sup>Δ</sup> -----	5.5	5.4	<4	11	31	35	37	57	26
Sr <sup>#</sup> -----	850	760	390	610	340	530	310	285	509
REE-group									
La <sup>Δ</sup> -----	20.5	21.5	19.6	24.2	16.1	24.2	39.5	30.1	24.5
Ce <sup>Δ</sup> -----	47.0	46.8	38.4	50.0	36.0	45.5	70.0	57.8	48.9
Nd <sup>Δ</sup> -----	27	23	19	25	20	19	29	24	23
Sm <sup>Δ</sup> -----	6.33	5.76	4.73	5.74	5.61	4.55	6.14	5.62	5.56
Eu <sup>Δ</sup> -----	1.90	1.70	1.35	1.70	1.71	1.32	1.20	1.29	1.52
Gd <sup>Δ</sup> -----	5.9	6.3	5.6	6.4	7.1	5.1	6.7	5.4	6.1
Tb <sup>Δ</sup> -----	.800	.722	.760	.730	.957	.630	.780	.830	.780
Tm <sup>Δ</sup> -----	nd	nd	nd	nd	nd	nd	nd	nd	nd
Yb <sup>Δ</sup> -----	1.90	1.80	2.62	2.00	3.23	2.00	2.65	3.10	2.41
Lu <sup>Δ</sup> -----	.270	.270	.399	.320	.483	.290	.370	.440	.355
Sum REE-----	111.3	107.6	92.1	115.8	90.7	102.3	156.0	128.1	113.0
Y <sup>#</sup> -----	24	21	20	23	39	23	34	32	27
Th group									
Th <sup>Δ</sup> -----	1.20	1.60	2.89	2.00	2.30	3.80	6.50	7.79	3.51
U <sup>Δ</sup> -----	.51	.55	1.10	.80	1.10	1.40	2.50	3.00	1.37
Ti group									
Zr <sup>#</sup> -----	168	162	198	196	186	205	265	320	213
Hf <sup>Δ</sup> -----	3.15	3.30	4.25	4.00	4.12	4.07	5.50	7.00	4.42
Nb <sup>#</sup> -----	20	15	14	20	15	19	20	17	18
Ta <sup>Δ</sup> -----	.93	.97	.96	1.24	.849	1.10	1.40	1.40	1.11
Compatible group									
Co <sup>Δ</sup> -----	32.4	29.1	27.2	29.5	24.2	20.4	13.3	10.9	23.4
Cr <sup>Δ</sup> -----	170	88.8	51.4	140	12.0	87.8	3.0	28.6	72.7
Ni <sup>#</sup> -----	65	34	43	75	<10	41	5	17	40
Sc <sup>Δ</sup> -----	27.5	22.5	19.3	17.9	31.1	13.9	11.5	10.8	19.3
V <sup>@</sup> -----	250	210	160	128	250	110	79	59	156
Chalcophile group									
Cu <sup>#</sup> -----	34	31	40	33	<10	24	14	23	28
Zn <sup>Δ</sup> -----	73.3	80.3	81.1	86	86	76.9	9.3	75	71
Ratios									
K/Rb	891	446	362	375	415	328	361	454	196
Rb/Sr	.01	.01	nd	.02	.09	.07	.12	.20	.07
(Eu/Eu*) <sub>N</sub>	.94	.86	.80	.86	.83	.84	.57	.71	.80
(Ce/Yb) <sub>N</sub>	6.29	6.61	5.79	4.74	2.83	3.73	6.36	6.72	5.16

Brew, D.A., Karl, S.M., and Tobey, E.F., 1985, Re-interpretation of the age of the Kuiu-Etolin belt volcanic rocks, Kupreanof Island, southeastern Alaska, in, Bartsch-Winkler, Susan, and Reed, K.M., eds., *The United States Geological Survey in Alaska: Accomplishments during 1983*; U.S.

Geological Survey Circular 945, p. 86–88.  
 Brew, D.A., Ovenshine, A.T., Karl, S.M., and Hunt, S.J., 1984, Preliminary reconnaissance geologic map of the Petersburg and parts of the Port Alexander and Sumdum 1:250,000 quadrangles, southeastern Alaska: U.S. Geologi-

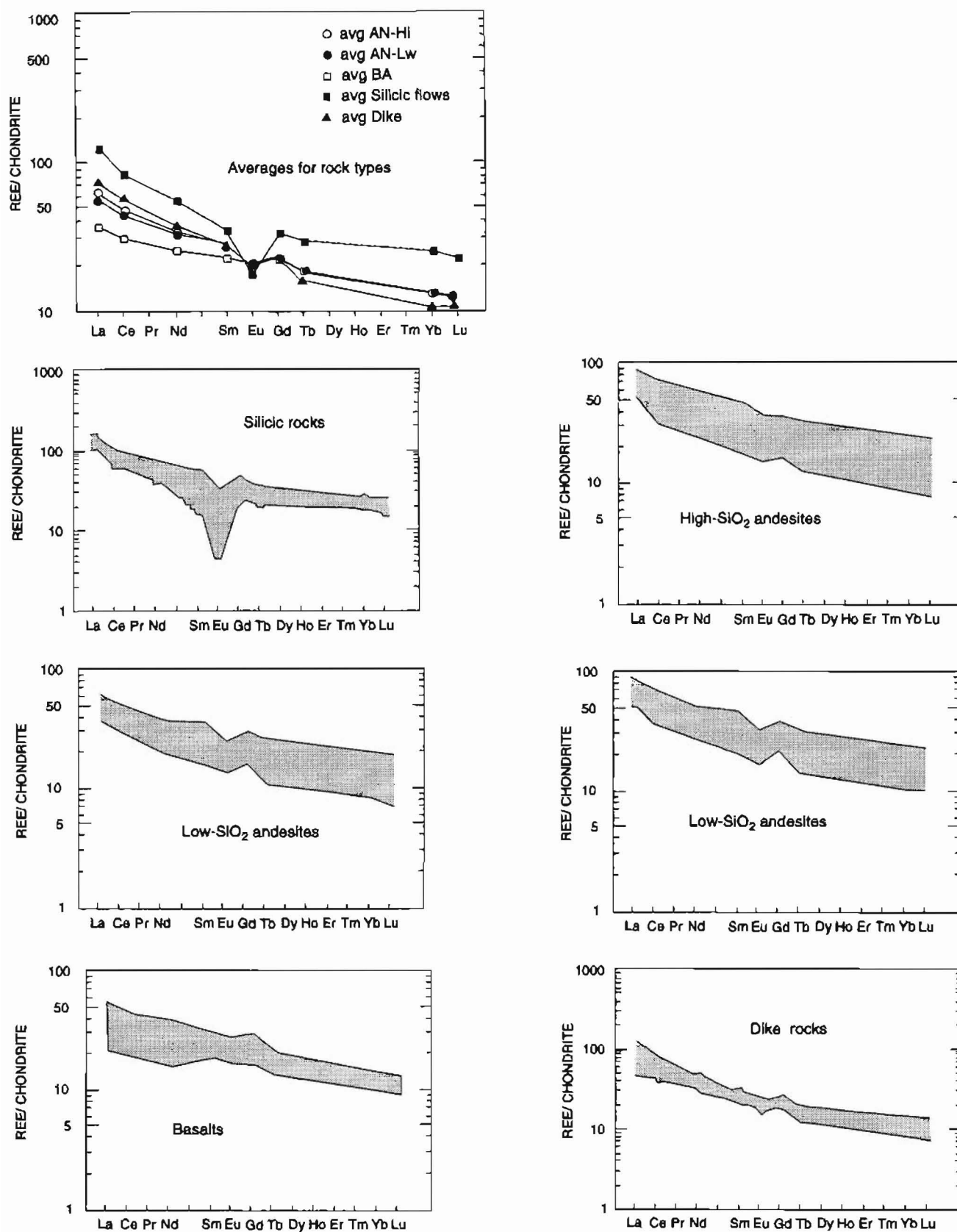


Figure 10. Rare-earth element abundances (log scale) in rocks of the Admiralty Island Volcanics normalized to chondritic meteorite values by method of Wheatley and Rock (1988).



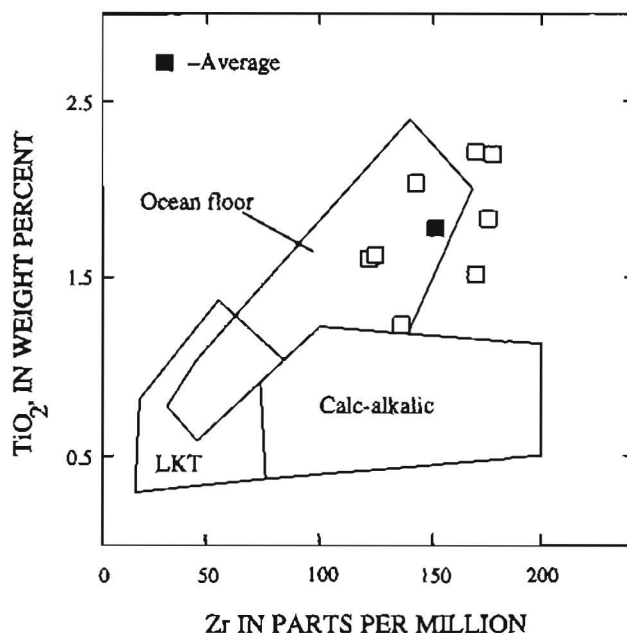


Figure 11. Variation between Zr, Y ( $\times 3$ ), and Ti ( $/100$ ) in basaltic flow rocks of the Admiralty Island Volcanics, showing Pearce and Cann's (1973) fields of low-K tholeiite (LKT), ocean-floor basalt (OFB), calc-alkalic basalt (CAB), and within-plate basalt (WPB).

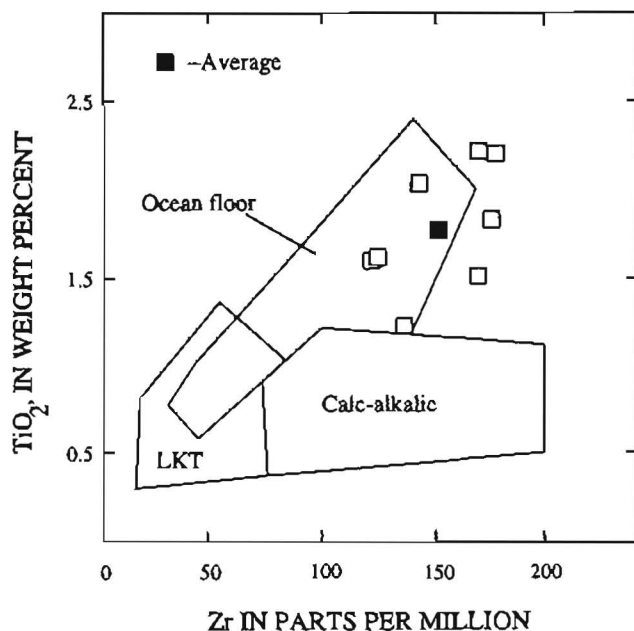


Figure 12. Variation between  $\text{TiO}_2$  and Zr contents of basaltic flow rocks of the Admiralty Island Volcanics, showing Pearce and Cann's (1973) fields of low-K tholeiite (LKT), ocean-floor, and calc-alkalic rocks.

cal Survey Open-File Report 84-405, 1 sheet, scale 1:250,000.

- Buddington, A.F., and Chapin, Theodore, 1929, *Geology and mineral deposits of southeastern Alaska*: U.S. Geological Survey Bulletin 800, 398 p.
- Chapin, C.E., and Zidek, Jiri, 1989, eds., *Field excursions to volcanic terranes in the western United States, Volume I: Southern Rocky Mountain region*: New Mexico Bureau of Mines and Mineral Resources, Memoir 46, 486 p.
- Cole, J.W., 1981, Genesis of lavas of the Taupo Volcanic Zone, North Island, New Zealand: *Journal of Volcanology and Geothermal Research*, v. 10, p. 317-337.
- Condie, K.C., and Hayslip, D.L., 1975, Young bimodal volcanism at Medicine Lake volcanic center, northern California: *Geochimica et Cosmochimica Acta*, v. 39, p. 1165-1178.
- Condie, K.C., and Shadel, C.A., 1984, An early Proterozoic volcanic arc succession in southeastern Wyoming: *Canadian Journal of Earth Sciences*, v. 21, p. 415-427.
- de Baar, H.J.W., Brewer, P.G., and Bacon, M.P., 1985, Anomalies in rare earth distributions in seawater: Gd and Tb: *Geochimica et Cosmochimica Acta*, v. 49, p. 1961-1969.
- Dickinson, W.R., and Snyder, W.S., 1979, Geometry of subducted slabs related to San Andreas transform: *Journal of Geology*, v. 87, p. 609-627.
- Ewart, A., 1982, *The mineralogy and petrology of Tertiary-Recent orogenic volcanic rocks: with special reference to the andesitic-basaltic compositional range*, in: Thorpe, R.S., ed., *Andesites*: New York, John Wiley & Sons, p. 25-87.

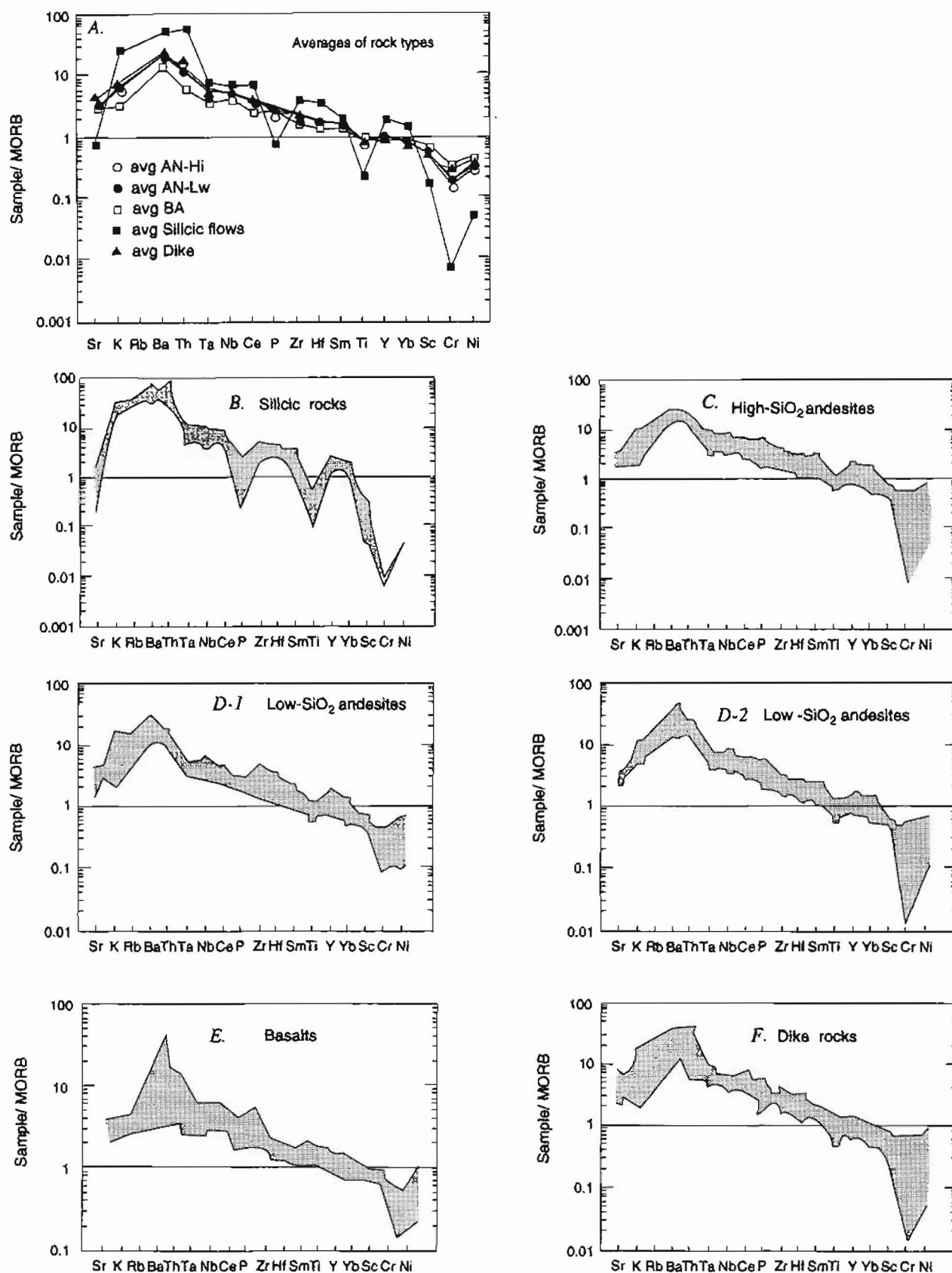


Figure 13. MORB-normalized element abundances (log scale) in rocks of the Admiralty Island Volcanics, by method of Wheatley and Rock (1988). MORB values of Pearce (1983).

- Gamble, J.A., Wright, I.C., Woodhead, J.D., and McCulloch, M.T., 1995, Arc and back-arc geochemistry in the southern Kermadec arc-Ngatoro Basin and offshore Taupo Volcanic Zone, SW Pacific, in Smellie, J.L., ed., *Volcanism associated with extension at consuming plate margins*: London, Geological Society Special Publication 81, p. 193-212.
- Giese, U., and Bühn, B., 1993, Early Paleozoic rifting and bimodal volcanism in the Ossa-Morena Zone of south-west Spain: *Geologische Rundschau*, v. 83, p. 143-160.
- Gill, J.B., 1981, *Orogenic andesites and plate tectonics*: New York, Springer-Verlag, 390 p.
- Gill, J.B., and Stork, A.L., 1979, Miocene low-K dacites and trondhjemites of Fiji, in Barker, Fred, ed., *Trondhjemites, dacites, and related rocks*: New York, Elsevier, p. 629-649.
- Golightly, D.W., Dorrzapf, A.F., Jr., Mays, R.E., Fries, T.L., and Conklin, N.M., 1987, Analysis of geologic materials by direct-current arc emission spectrography and spectrometry, 1987, in Baedeker, P.A., ed., *Methods for geochemical analysis*: U.S. Geological Survey Bulletin 1770, p. A1-A13.
- Hamilton, T.S., and Dostal, J., 1993, *Geology, geochemistry and petrogenesis of Middle Tertiary volcanic rocks of the Queen Charlotte Islands, British Columbia (Canada)*: *Journal of Volcanology and Geothermal Research*, v. 59, p. 77-99.
- Harangi, S., 1994, Geochemistry and petrogenesis of the Early Cretaceous continental rift-type volcanic rocks of the Mecsek Mountains, South Hungary: *Lithos*, v. 33, p. 303-321.
- Harland, W.B., Armstrong, R.L., Cox, A.V., Craig, L.E., Smith, A.G., Smith, D.G., 1990, *A geologic time scale 1989*: Cambridge, Cambridge University Press, 263 p.
- Hess, P.C., 1989, *Origins of igneous rocks*: Cambridge, Harvard University Press, 336 p.
- Irvine, T.N., and Baragar, W.R.A., 1971, A guide to the chemical classification of the common volcanic rocks: *Canadian Journal of Earth Sciences*, v. 8, p. 523-548.
- Irving, E., and Wynne, P.J., 1991, Paleomagnetism: Review and tectonic implications, in Gabrielse, H., and Yarath, C.J., eds., *Geology of the Cordilleran orogen in Canada*: Boulder, Colorado, Geological Society of America, *The Geology of North America*, v. G-2, p. 63-86.
- Jackson, L.L., Brown, F.W., and Neil, S.T., 1987, Major and minor elements requiring individual determination, classi-

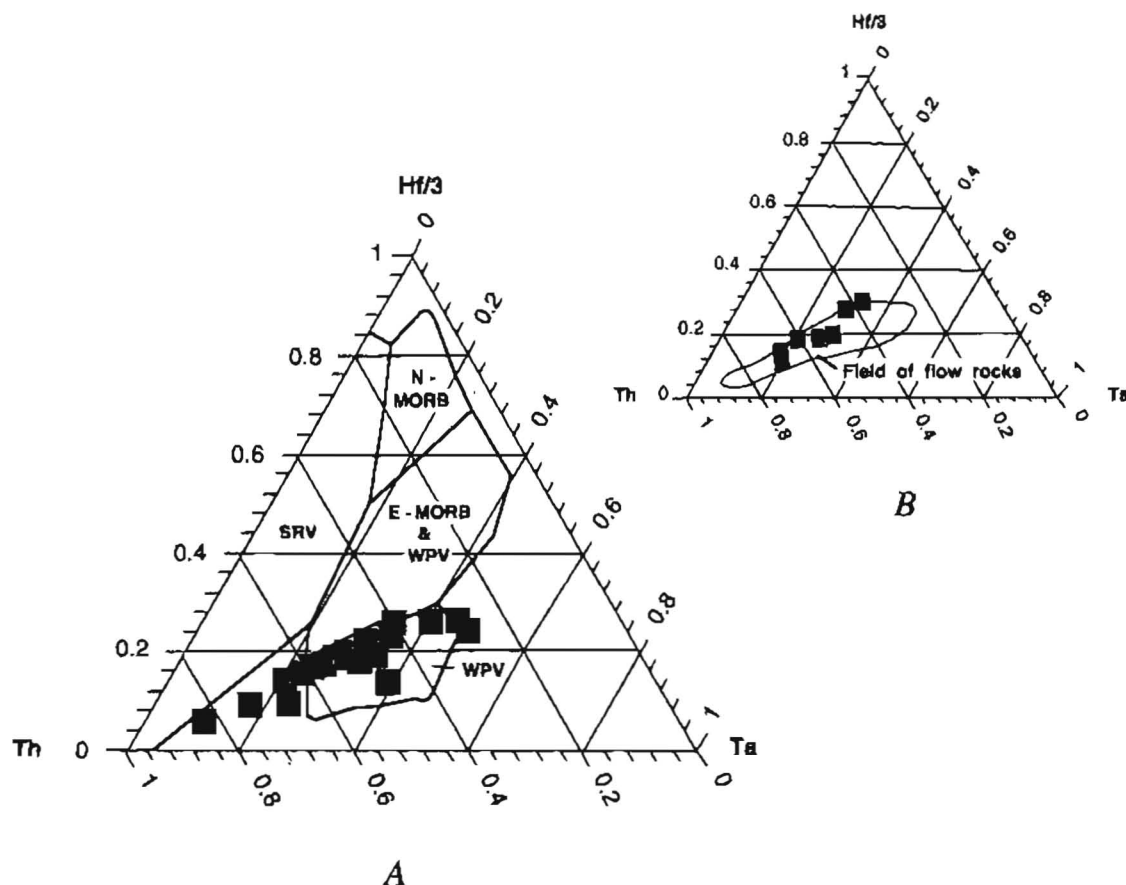


Figure 14. Variations between Th, Hf, and Ta in rocks of the Admiralty Island Volcanics, showing fields of volcanic settings of Wood (1980). Abbreviations: SRV, subduction-related volcanic rocks; WPV, within-plate volcanic rocks; N- and E-MORB, normal and enriched mid-ocean-ridge basalt. A, Flow rocks; B, Dike rocks, showing field of flow rocks.

- cal whole rock analysis, and rapid rock analysis, in Baedeker, P.A., ed., *Methods for geochemical analysis*: U.S. Geological Survey Bulletin 1770, p. G1–G23.
- Jakes, P., and Gill, J.B., 1970, Rare earth elements and the island arc tholeiitic series: *Earth and Planetary Science Letters*, v. 9, p. 17–28.
- Johnson, R.G., and King, B.-S., L., 1987, Energy-dispersive X-ray fluorescence spectrometry, in Baedeker, P.A., ed., *Methods for geochemical analysis*: U.S. Geological Survey Bulletin 1770, p. F1–F5.
- Keen, C.E., Courtney, R.C., Dehler, S.A., and Williamson, M.C., 1994, Decompression melting at rifted margins: comparison of model predictions with the distribution of igneous rocks on the eastern Canadian margin: *Earth and Planetary Science Letters*, v. 121, p. 403–416.
- King, Bi-Shia, and Lindsay, J.R., 1990, Determination of 12 selected trace elements in geological materials by energy-dispersive X-ray fluorescence spectroscopy, in Arbogast, B.F., ed., *Quality assurance manual for the Branch of Geochemistry*, U.S. Geological Survey: U.S. Geological Survey Open-File Report 90-668, p. 161–165.
- Lathram, E.H., Pomeroy, J.S., Berg, H.C., and Loney, R.A., 1965, Reconnaissance geology of Admiralty Island, Alaska: U.S. Geological Survey Bulletin 1181-R, 48 p.
- Le Bas, M.J., Le Maitre, R.W., Streckeisen, A., and Zanettin, B., 1986, A chemical classification of volcanic rocks based on the total alkali-silica diagram: *Journal of Petrology*, v. 27, p. 745–750.
- Le Maitre, R.W., 1976, The chemical variability of some common igneous rocks: *Journal of Petrology*, v. 17, p. 589–637.
- Liggett, D.L., 1990, Geochemistry of the garnet-bearing Tharps

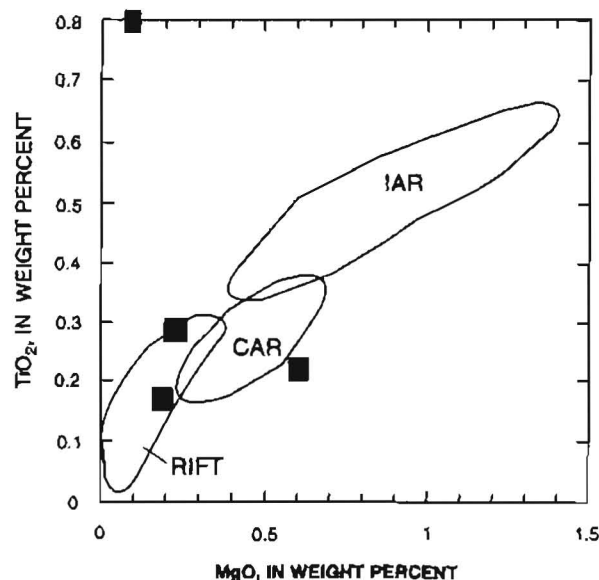


Figure 15.  $\text{TiO}_2$  and  $\text{MgO}$  variation in silicic rocks of the Admiralty Island Volcanics, showing tectonic setting in fields of Condie and Shadel (1984). Abbreviations: IAR, island-arc rhyolites; CAR, calc-alkalic rhyolites; RIFT, continental-rift rhyolites.

- Peak granodiorite and its relation to other members of the Lake Kaweah intrusive suite, southwestern Sierra Nevada, California, in Anderson, J.L., ed., *The nature and origin of Cordilleran magmatism*: Boulder, Colorado, Geological Society of America Memoir 174, p. 225–236.
- Lipman, P.W., Doe, B.R., Hedge, C.E., and Steven, T.A., 1978, Petrologic evolution of the San Juan volcanic field, southwestern Colorado: Pb and Sr isotope evidence: *Geological Society of America Bulletin*, v. 89, p. 59–82.
- Liu, Mian, and Furlong, K.P., 1994, Intrusion and underplating of mafic magmas: thermal-rheological effects and implications for Tertiary tectonomagmatism in the North American Cordillera: *Tectonophysics*, v. 237, p. 175–187.
- Loney, R.A., 1964, Stratigraphy and petrography of the Pybus-Gambier area, Admiralty Island, Alaska: U.S. Geological Survey Bulletin 1178, 103 p.
- Loney, R.A., Brew, D.A., and Lanphere, M.A., 1967, Post-Paleozoic radiometric ages and their relevance to fault movements, northern southeastern Alaska: *Geological Society of America Bulletin*, v. 78, p. 511–526.
- Lonsdale, Peter, 1988, Paleogene history of the Kula plate: Offshore evidence and onshore implications: *Geological Society of America Bulletin*, v. 100, n. 5, p. 733–754.
- Middlemost, E.A.K., 1989, Iron oxidation ratios, norms and the classification of volcanic rocks: *Chemical Geology*, v. 77, p. 19–26.
- Miyashiro, Akiho, 1974, Volcanic rock series in island arcs and active continental margins: *American Journal of Science*, v. 274, p. 321–355.
- Muffer, L.J.P., 1967, Stratigraphy of the Keku Islets and neighboring parts of Kuiu and Kupreanof islands, southeastern Alaska: U.S. Geological Survey Bulletin 1241-C, 52 p.
- Nicholson, S.W., 1992, Geochemistry, petrography, and volcanology of rhyolites of the Portage Lake Volcanics, Keweenaw Peninsula, Michigan: U.S. Geological Survey Bulletin 1970B, 57 p.
- Panaska, B.C., and Decker, John, 1985, Reconnaissance paleomagnetic study of the Eocene Admiralty Island Volcanics, southeast Alaska: Evidence for pre-late Eocene accretion: *Geological Society of America, Abstracts with Programs*, v. 17, n. 7, p. 684.
- Pe-Piper, Georgia, Jansa, L.F., and Palacz, Zen, 1994, Geochemistry and regional significance of the Early Cretaceous bimodal basalt-felsic associations on Grand Banks, eastern Canada: *Geological Society of America Bulletin*, v. 106, p. 1319–1331.
- Peacock, M.A., 1931, Classification of igneous rock series: *Journal of Geology*, v. 39, p. 54–67.
- Pearce, J.A., 1982, Trace element characteristics of lavas from destructive plate boundaries, in Thorpe, R.S., ed., *Andesites*: New York, John Wiley & Sons, p. 525–548.
- , 1983, Role of the sub-continental lithosphere in magma genesis at active continental margins, in Hawkesworth, C.J., and Norry, M.J., eds., *Continental basalts and mantle xenoliths*: Nantwich, Shiva, p. 230–249.
- Pearce, J.A., and Cann, J.R., 1973, Tectonic setting of basic volcanic rocks determined using trace element analyses: *Earth and Planetary Science Letters*, v. 19, p. 290–300.
- Plafker, George, Moore, J.C., and Winkler, G.R., 1994, Geology of the southern Alaska margin, in Plafker, George,

- and Berg, H.C., eds., *The Geology of Alaska*: Boulder, Colorado, Geological Society of America, *The Geology of North America*, v. G-1, p. 389-449.
- Richter, D.H., Smith, J.G., Lanphere, M.A., Dalrymple, G.B., Reed, B.L., and Shew, Nora, 1990, Age and progression of volcanism, Wrangell volcanic field, Alaska: *Bulletin of Volcanology*, v. 53, p. 29-44.
- Richter, D.H., Smith, J.G., Schmoll, H.R., and Smith, R.L., 1993, Geologic map of the Nabesna B-6 quadrangle, south-central Alaska: U.S. Geological Survey Map GQ-1688, scale 1:63,360.
- Rollinson, H.R., 1993, *Using geochemical data: Evaluation, presentation, interpretation*: New York, John Wiley & Sons, 352 p.
- Rudnick, R.L., 1983, Geochemistry and tectonic affinities of a Proterozoic bimodal igneous suite, west Texas: *Geology*, v. 11, n. 6, p. 352-355.
- Sawlan, M.G., 1991, Magmatic evolution of the Gulf of California rift, in Dauphin, J.P., and Simoneit, B.R.T., eds., *The Gulf and Peninsular provinces of the Californias*: American Association of Petroleum Geologists, Memoir 47, p. 301-369.
- Sawlan, M.G., and Smith, J.G., 1984, Petrologic characteristics, age and tectonic setting of Neogene volcanic rocks in northern Baja California Sur, Mexico, in Frizzell, V.A., Jr., ed., *Geology of the Baja California peninsula*: Society of Economic Paleontologists and Mineralogists, v. 39, p. 237-251.
- Skulski, Thomas, Francis, Don, and Ludden, John, 1991, Arc-transform magmatism in the Wrangell volcanic belt: *Geology*, v. 19, p. 11-14.
- , 1992, Volcanism in an arc-transform transition zone: the stratigraphy of the St. Clare Creek volcanic field, Wrangell volcanic belt, Yukon, Canada: *Canadian Journal of Earth Science*, v. 29, p. 446-461.
- St. Amand, Pierre, 1957, Geological and geophysical synthesis of the tectonics of portions of British Columbia, the Yukon Territory, and Alaska: *Geological Society of America Bulletin*, v. 68, p. 1343-1370.
- Taggart, J.E., Jr., Bartel, Ardith, and Siems, D.F., 1990, in Arbogast, B.F., ed., *Quality assurance manual for the Branch of Geochemistry*, U.S. Geological Survey: U.S. Geological Survey Open-File Report 90-668, p. 166-172.
- Taggart, J.E., Jr., Lindsay, J.R., Scott, B.A., Vivit, D.V., Bartel, A.J., and Stewart, K.C., 1987, in Baedeker, P.A., ed., *Methods for geochemical analysis*: U.S. Geological Survey Bulletin 1770, p. E1-E19.
- Tamura, Y., 1994, Genesis of island arc magmas by mantle-derived bimodal magmatism: evidence from the Shirahama Group, Japan: *Journal of Petrology*, v. 35, p. 619-645.
- Taylor, C.D., 1990, Physical preparation of rock samples, in Arbogast, B.F., ed., *Quality assurance manual for the Branch of Geochemistry*, U.S. Geological Survey: U.S. Geological Survey Open-File Report 90-668, p. 21-25.
- Thompson, R.N., 1972, Evidence for a chemical discontinuity near the basalt-andesite transition in many anorogenic volcanic suites: *Nature*, v. 236, p. 106-110.
- Thorpe, R.S., Francis, P.W., Hammill, M., and Baker, M.C.W., 1982, *The Andes*, in Thorpe, R. S., ed., *Andesites*: New York, John Wiley & Sons, p. 187-205.
- Wharton, M.R., Hathaway, B., and Colley, H., 1995, Volcanism associated with extension in an Oligocene-Miocene arc, southwestern Viti Levu, Fiji, in Smellie, J.L., ed., *Volcanism associated with extension at consuming plate margins*: London, Geological Society Special Publication 81, p. 95-114.
- Wheatley, Michael, and Rock, N.M.S., 1988, SPIDER: A Macintosh program to generate normalized multi-element "spidergrams": *American Mineralogist*, v. 73, p. 919-921.
- Wilson, F.H., Shew, Nora, and DuBois, G.D., 1994, Map and table showing isotopic age data in Alaska, in Plafker, George, and Berg, H.C., eds., *The Geology of Alaska*: Boulder, Colorado, Geological Society of America, v. G-1, plate 8. Scale: 1:2,500,000.
- Wood, D.A., 1980, The application of a Th-Hf-Ta diagram to problems of tectonomagmatic classification and to establishing the nature of crustal contamination of basaltic lavas of the British Tertiary volcanic province: *Earth and Planetary Science Letters*, v. 50, p. 11-30.
- Wright, C.W., 1906, A reconnaissance of Admiralty Island, Alaska, in Spencer, A.C., *The Juneau gold belt, Alaska*: U.S. Geological Survey Bulletin 287, p. 138-154.

Reviewers: Robert A. Loney and James P. Calzia

# Reports about Alaska in Non-USGS Publications Released in 1994 that Include USGS Authors

Compiled by Ellen R. Reiser

{Some reports dated 1993 did not become available for indexing until 1994; they are included in this listing. USGS authors are marked with asterisks(\*)}

## ABBREVIATIONS

Eos	Eos (American Geophysical Union Transactions), v. 75, no. 44, suppl., 1994 fall meeting, 795 p.
G-1	Plafker, George, and Berg, H.C., eds., 1994, The geology of Alaska: Boulder, Colo., Geological Society of America, The Geology of North America, v. G-1, 1055 p., 14 pls.
GSA	Geological Society of America Abstracts with Programs, v. 26, no. 7, 533 p., and Index, 20 p.
ICAM	International Conference on Arctic Margins, 1994, Magadan, Russia, Abstracts.
MMS	Thurston, D.K., and Fujita, Kazuya, eds., International Conference on Arctic Margins, 1992, Anchorage, Alaska, Proceedings: Minerals Management Service OCS Study MMS 94-0040, 408 p.

- \*Ager, T.A., Matthews, J.V., Jr., and \*Yeend, Warren, 1994, Pliocene terrace gravels of the ancestral Yukon River near Circle, Alaska: palynology, paleobotany, paleoenvironmental reconstruction and regional correlation: Quaternary International, v. 22/23, p. 185-206.
- Anderson, M.P., Robinson, M.R., Jiang, T.M., Sonafrank, G.H.C., and \*Ward, P.L., 1994, Alaska seismic network database management and analysis software at the University of Alaska Geophysical Institute [abs.]: Seismological Research Letters, v. 65, no. 1, p. 51.
- \*Arth, J.G., 1994, Isotopic composition of the igneous rocks of Alaska, in G-1, p. 781-795, pls. 1-3.
- \*Barker, Fred, \*Aleinikoff, J.N., \*Box, S.E., Evans, B.W., Gehrels, G.E., Hill, M.D., Irving, A.J., \*Kelley, J.S., Leeman, W.P., \*Lull, J.S., \*Nokleberg, W.J., \*Pallister, J.S., Patrick, B.E., \*Plafker, George, and Rubin, C.M., 1994, Some accreted volcanic rocks of Alaska and their elemental abundances, in G-1, p. 555-587, pls. 2, 6, and 13.
- Barnett, D.E., Bowman, J.R., Pavlis, T.L., Rubenstone, J.R., \*Snee, L.W., and Onstott, T.C., 1994, Metamorphism and near-trench plutonism during initial accretion of the Cretaceous Alaskan forearc: Journal of Geophysical Research, v. 99, no. B12, p. 24,007-24,024.
- \*Bartsch-Winkler, Susan, and \*Schmoll, H.R., 1994, What can reconnaissance studies of intertidal stratigraphy reveal about relative sea-level changes at convergent plate margins? — examples from Upper Cook Inlet, Alaska, and Isla Chiloe, Chile [abs.]: GSA, p. 138.
- Baxter, M.E., and \*Blodgett, R.B., 1994, A new species of *Droharhynchia* (Brachiopoda) from the lower Middle Devonian (Eifelian) of west-central Alaska: Journal of Paleontology, v. 68, no. 6, p. 1235-1240.
- \*Beaudoin, B.C., \*Fuis, G.S., \*Lutter, W.J., \*Mooney, W.D., and \*Moore, T.E., 1994, Crustal velocity structure of the northern Yukon-Tanana upland, central Alaska: results from TACT refraction/wide-angle reflection data: Geological Society of America Bulletin, v. 106, no. 8, p. 981-1001.
- \*Belkin, H.E., 1993, Fluid inclusion systematics of epithermal mercury-antimony mineralization, southwestern Alaska, USA [abs.]: Archiwum Mineralogiczne, v. 49, no. 1, p. 25-26. [12th biennial Symposium for European Current Research on Fluid Inclusions, Warsaw-Krakow, Poland, 1993.]
- Benson, C.S., \*Friedman, I., and \*Gleason, J., 1994, Anthropogenic water in the ice fog of Fairbanks, Alaska and sea level rise [abs.]: Eos, p. 244-245.
- \*Benz, H.M., \*Chouet, B.A., \*Dawson, P.B., \*Lahr, J.C., \*Page, R.A., and Hole, J.A., 1994, Three-dimensional P and S-wave velocity structure of Redoubt Volcano, Alaska [abs.]: Seismological Research Letters, v. 65, no. 1, p. 55.
- \*Blodgett, R.B., and Johnson, J.G., 1994, First recognition of the genus *Verneuillia* Hall and Clarke (Brachiopoda, Spiriferida) from North America (west-central) Alaska: Journal of Paleontology, v. 68, no. 6, p. 1240-1242.
- Bogue, S.W., \*Grommé, C.S., and \*Hillhouse, J.W., 1994, Paleomagnetism, magnetic anisotropy and Cretaceous paleolatitude of the Duke Island (Alaska) ultramafic complex [abs.]: GSA, p. 460.
- \*Brew, D.A., 1994, Latest Mesozoic and Cenozoic magmatism



- in southeastern Alaska, in G-1, p. 621-656.
- 1994, Metallogenic factors and metallogenic belts of southeastern Alaska [abs.]: GSA, v. 26, no. 7, p. 27-28.
- \*Brew, D.A., Himmelberg, G.R., \*Ford, A.B., and \*Loney, R.A., 1994, Metamorphic belts, plutonic-metamorphic complexes, major structures, and tectonic causes, North American Cordillera, southeastern Alaska [abs.]: Geological Society of America Abstracts with Programs, v. 26, no. 2, p. 41.
- Brigham-Grette, J., Hopkins, D.M., \*Carter, L.D., Kaufman, D.S., and \*Marincovich, L., 1994, Character and climate of the last interglacial (oxygen isotope substage 5E) in the Bering Strait and Arctic Alaska as determined from nearshore marine deposits [abs.]: GSA, p. 514.
- \*Brocher, T.M., \*Fuis, G.S., \*Fisher, M.A., \*Plafker, George, \*Moses, M.J., Taber, J.J., and Christensen, N.I., 1994, Mapping the megathrust beneath the northern Gulf of Alaska using wide-angle seismic data: Journal of Geophysical Research, v. 99, no. B6, p. 11,663-11,685.
- \*Brouwers, E.M., 1994, Late Pliocene paleoecologic reconstructions based on ostracode assemblages from the Sagavanirktok and Gubik Formations, Alaskan North Slope: Arctic, v. 47, no. 1, p. 16-33.
- \*Brouwers, E.M., and De Deckker, Patrick, 1994, Maastrichtian/Danian(?) ostracode assemblages from northern Alaska: paleoenvironments and paleobiogeographic relations, in MMS, p. 89-93.
- \*Bufe, C.G., \*Nishenko, S.P., and \*Varnes, D.J., 1994, Seismicity trends and potential for large earthquakes in the Alaska-Aleutian region: Pure and Applied Geophysics (Pageoph), v. 142, no. 1, p. 83-99.
- Burkett, P.J., Bennett, R.H., \*Olsen, H.W., and \*Schmoll, H.R., 1994, TEM microfabric of Alaska's Bootlegger Cove Formation, in MMS, p. 357-362.
- \*Carlson, P.R., Cowan, E.A., Cai, Jinkui, and Powell, R.D., 1994, Turbidite systems of Glacier Bay compared to Gulf of Alaska systems [abs.]: GSA, v. 26, no. 7, p. 364.
- \*Carter, L.D., and \*Whelan, J.F., 1994, The last interglacial along the Arctic coast of Alaska [abs.]: GSA, v. 26, no. 7, p. 236.
- \*Casadevall, T.J., 1994, The 1989-1990 eruption of Redoubt Volcano, Alaska: impacts on aircraft operations: Journal of Volcanology and Geothermal Research, v. 62, no. 1/4, p. 301-316.
- \*Casadevall, T.J., \*Doukas, M.P., \*Neal, C.A., \*McGimsey, R.G., and \*Gardner, C.A., 1994, Emission rates of sulfur dioxide and carbon dioxide from Redoubt Volcano, Alaska during the 1989-1990 eruptions: Journal of Volcanology and Geothermal Research, v. 62, no. 1/4, p. 519-530.
- \*Chouet, B.A., \*Page, R.A., \*Stephens, C.D., \*Lahr, J.C., and \*Power, J.A., 1994, Precursory swarms of long-period events at Redoubt Volcano (1989-1990), Alaska: their origin and use as a forecasting tool: Journal of Volcanology and Geothermal Research, v. 62, no. 1/4, p. 95-135.
- Christiansen, P.P., and \*Snee, L.W., 1994, Structure, metamorphism, and geochronology of the Cosmos Hills and Ruby Ridge, Brooks Range schist belt, Alaska: Tectonics, v. 13, no. 1, p. 193-213.
- \*Clow, G.D., 1994, Climate monitoring and reconstruction in the Alaskan Arctic utilizing a "solid-earth" climate observatory [abs.], in Bridges of the science between North America and the Russian Far East, Arctic Science Conference, 45th, Anchorage, Alaska and Vladivostok, Russia, 1994: Vladivostok, Russia, Dalnauka, v. 1, p. 171-172.
- \*Clow, G.D., and \*Saltus, R.W., 1994, USGS program for reconstruction of climate variations in the Alaskan Arctic from borehole temperature measurements—current progress and plans [abs.]: Eos, p. 85.
- \*Cole, F., \*Howell, D.G., and \*Bird, K., 1994, Geometry and timing of deformation in the north-central Brooks Range, Alaska [abs.]: Eos, p. 646-647.
- \*Cole, Frances, \*Bird, K.J., and \*Howell, D.G., 1994, Tectonic subsidence and uplift in the North Slope foreland basin, Alaska—responses to Canada Basin rifting and Brooks Range orogenesis [abs.]: GSA, p. 149.
- \*Collett, T.S., 1994, Secondary gas migration within the Prudhoe Bay-Kuparuk River area of northern Alaska [abs.]: AAPG [American Association of Petroleum Geologists] Annual Convention, Official Program, v. 3, p. 125.
- Cowan, E.A., Powell, R.D., \*Carlson, P.R., and Nall, C.A., 1994, Marine record of the October 8, 1986 Hubbard Glacier jokulhlaup [abs.]: GSA, p. 176-177.
- \*Cronin, T.M., \*Holtz, T.R., and Whatley, R.C., 1994, Quaternary paleoceanography of the deep Arctic Ocean based on quantitative analysis of Ostracoda: Marine Geology, v. 119, no. 3/4, p. 305-332.
- Decker, John, Bergman, S.C., Blodgett, R.B., \*Box, S.E., Bundtzen, T.K., Clough, J.G., \*Coonrad, W.L., Gilbert, W.G., \*Miller, M.L., \*Murphy, J.M., Robinson, M.S., and Wallace, W.K., 1994, Geology of southwestern Alaska, in G-1, p. 285-310, pl. 3.
- \*Dorava, J.M., 1994, Water generation and lahar formation from melting snow and ice during future eruptions of Crater Peak, Spurr Volcano, Alaska [abs.]: GSA, p. 113.
- \*Dorova, J.M., and \*Meyer, D.F., 1994, Hydrologic hazards in the lower Drift River basin associated with the 1989-1990 eruptions of Redoubt Volcano, Alaska: Journal of Volcanology and Geothermal Research, v. 62, no. 1/4, p. 387-407.
- \*Dover, J.H., 1994, Geology of part of east-central Alaska, in G-1, p. 153-204, pl. 3.
- \*Dumoulin, J.A., and \*Harris, A.G., 1994, Correlation of pre-Carboniferous carbonate successions of northern Alaska, in MMS, p. 65-69.
- \*Dumoulin, J.A., \*Harris, A.G., and \*Schmidt, J.M., 1994, Deep-water facies of the Lisburne Group, west-central Brooks Range, Alaska, in MMS, p. 77-82.
- \*Dusel-Bacon, Cynthia, 1994, Metamorphic history of Alaska, in G-1, p. 495-533, pls. 4A and 4B.
- Dzurisin, D., Iwatsubo, E.Y., Kleinman, J.W., Murray, T.L., \*Power, J.A., and \*Paskievitch, J.F., 1994, Deformation monitoring at Augustine Volcano, AK [abs.]: Eos, p. 62.
- Elias, S.A., Short, S.K., \*Phillips, R.L., and \*Nelson, C.H., 1994, New evidence on the timing of inundation of the Bering Land Bridge, based on radiocarbon ages of macrofossils [abs.]: Eos (American Geophysical Union Transactions), v. 75, no. 3, suppl., p. 198.
- Farmer, G.L., \*Ayuso, R., and \*Plafker, George, 1994, Derivation of late Cretaceous-early Tertiary flysch in southern Alaska from erosion of the northern Coast Mountains [abs.]: GSA, p. 149.

- \*Ferrians, O.J., Jr., 1994, Permafrost in Alaska, in G-1, p. 845-854.
- \*Foster, H.L., \*Keith, T.E.C., and Menzie, W.D., 1994, Geology of the Yukon-Tanana area of east-central Alaska, in G-1, p. 205-240, pl. 11.
- \*Fouch, T.D., \*Carter, L.D., \*Kunk, M.J., Smith, C.A.S., and White, J.M., 1994, Miocene and Pliocene lacustrine and fluvial sequences, Upper Ramparts and Canyon Village, Porcupine River, east-central Alaska: Quaternary International, v. 22/23, p. 11-29.
- \*Fuis, G.S., Levander, A.R., \*Lutter, W.J., Wissinger, E.S., \*Moore, T.E., and Oldow, J.S., 1994, Seismic images of the Brooks Range, Arctic Alaska, reveal crustal-scale duplexing [abs.]: Seismological Research Letters, v. 65, no. 1, p. 17.
- \*Fuis, G.S., \*Lutter, W.J., \*Moore, T.E., Levander, A.R., and Wissinger, E.S., 1994, Interpretation of the deep structure of the Brooks Range, Arctic Alaska [abs.]: Eos, p. 646.
- Galloway, B.K., Klemperer, S.L., \*Childs, J.R., and Bering-Chukchi Working Group, 1994, New seismic reflection profiles of the continental crust and Moho, Bering and Chukchi Seas transect, Alaska [abs.]: Eos, p. 642.
- \*Gann, J.T., O'Connell, W.M., Greene, H.G., Wakefield, W., and \*Bruns, T.R., 1994, Characterization of rockfish habitats of the offshore Mt. Edgecumbe lava field and Fairweather Ground, southeast Alaska, using side scan sonar [abs.]: Eos, p. 319.
- \*Gardner, C.A., \*Neal, C.A., \*Waitt, R.B., and Janda, R.J., 1994, Proximal pyroclastic deposits from the 1989-1990 eruption of Redoubt Volcano, Alaska—stratigraphy, distribution, and physical characteristics: Journal of Volcanology and Geothermal Research, v. 62, no. 1/4, p. 213-250.
- Gehrels, G.E., Dickinson, W.R., Ross, G.M., \*Stewart, J.H., and \*Howell, D.G., 1994, Provenance of detrital zircons in strata of the Cordilleran miogeocline and selected outboard terranes [abs.]: GSA, p. 384.
- \*Geist, E.L., and \*Scholl, D.W., 1994, Large-scale deformation related to the collision of the Aleutian Arc with Kamchatka: Tectonics, v. 13, no. 3, p. 538-560.
- \*Gerlach, T.M., Westrich, H.R., \*Casadevall, T.J., and Finnegan, D.L., 1994, Vapor saturation and accumulation in magmas of the 1989-1990 eruption of Redoubt Volcano, Alaska: Journal of Volcanology and Geothermal Research, v. 62, no. 1/4, p. 317-337.
- \*Grantz, Arthur, \*May, S.D., and \*Hart, P.E., 1994, Geology of the Arctic continental margin of Alaska, in G-1, p. 17-48.
- \*Gray, J.R., \*Hart, R.J., and \*Molnia, B.F., 1994, 1994 changes in physical and sedimentary characteristics of proglacial Vitus Lake resulting from the surge of Bering Glacier, Alaska [abs.]: Eos, p. 63.
- \*Haeussler, P.J., Davis, J.S., Roeske, S.M., and \*Karl, S.M., 1994, Late Mesozoic and Cenozoic faulting at the leading edge of North America, Chichagof and Baranof Islands, southeastern Alaska [abs.]: GSA, p. 317.
- \*Hamilton, T.D., 1994, Interglacial and interstadial deposits from the western Noatak River basin, northwest Alaska [abs.]: GSA, p. 236.
- \*Hamilton, T.D., 1994, Late Cenozoic glaciation of Alaska, in G-1, p. 813-844.
- \*Harris, A.G., Krumhardt, A.P., and Watts, K.F., 1994, Conodont-based correlation of the Lisburne Group (Carboniferous), northeast Brooks Range, Alaska [abs.]: ICAM, p. 48-49.
- \*Hillhouse, J.W., and Coe, R.S., 1994, Paleomagnetic data from Alaska, in G-1, p. 797-812.
- Himmelberg, G.R., \*Brew, D.A., and \*Ford, A.B., 1994, Inverted Barrovian metamorphic sequence, western metamorphic belt, Coast Mountains plutonic-metamorphic complex, North American Cordillera, southeastern Alaska [abs.]: Geological Society of America Abstracts with Programs, v. 26, no. 2, p. 59.
- \*Hinkley, T.K., 1994, Composition and sources of atmospheric dusts in snow at 3200 meters in the St. Elias Range, southeastern Alaska, USA: Geochimica et Cosmochimica Acta, v. 58, no. 15, p. 3245-3254.
- \*Hoblitt, R.P., 1994, An experiment to detect and locate lightning associated with eruptions of Redoubt Volcano: Journal of Volcanology and Geothermal Research, v. 62, no. 1/4, p. 499-517.
- \*Howell, D.G., 1994, Northern Cordillera tectonics and the where and why of petroleum [abs.]: GSA, p. 21.
- \*Ishman, S.E., 1994, Benthic foraminifer distribution in the Canada Basin, Arctic Ocean: application to quantitative paleoenvironmental estimates [abs.]: Paleobios, v. 16, no. 2, suppl., p. 37. [Forams '94, International Symposium on Foraminifera, Berkeley, University of California, Abstracts with Programs]
- Jolly, A.D., \*Lahr, J.C., \*Power, J.A., \*Stihler, S.D., \*Ward, P.L., and McNutt, S.R., 1994, Velocity models for locations of shallow seismicity along the northeastern portion of the Aleutian volcanic arc [abs.]: Eos, p. 423-424.
- Jolly, A.D., \*Page, R.A., and \*Power, J.A., 1994, Seismicity and stress in the vicinity of Mount Spurr volcano, south central Alaska: Journal of Geophysical Research, v. 99, no. B8, p. 15,305-15,318.
- Kable, M.W., Murray, R.W., \*Howell, D.G., and Pflaum, R.C., 1994, Characterizing sources of Antler-aged Cordilleran chert-pebble conglomerates: an example from the National River FM., east-central Alaska [abs.]: GSA, p. 384.
- \*Kelley, J.S., \*Wrucke, C.T., and Lane, L.S., 1994, Pre-Mississippian rocks in the Clarence and Malcolm Rivers area, Alaska, and the Yukon Territory, in MMS, p. 59-64.
- \*Kimmel, R.M., 1994, Photogrammetric measurement of geometric changes of Bering Glacier during the 1993-94 surge [abs.]: Eos, p. 62.
- \*Krohn, M.D., \*Hogan, Maura, Harman, R.D., and Harrington, W.H., 1994, Documenting persistence of volcanic ash clouds from pilot reports (PIREPS): Sept. 17, 1992, eruption of Mt. Spurr, Alaska [abs.]: Eos (American Geophysical Union Transactions), v. 75, no. 16 suppl., p. 77.
- Krumhardt, A.P., \*Harris, A.G., and Watts, K.F., 1994, Conodont biofacies of the Wahoo Limestone (Carboniferous), northeast Brooks Range, Alaska [abs.]: Geological Society of America Abstracts with Programs, v. 26, no. 5, p. 24.
- 1994, Conodont biostratigraphy and biofacies of the Wahoo Limestone (Carboniferous), eastern Sadlerochit Mountains, Brooks Range, Alaska, in MMS, p. 83-88.
- \*Kunk, M.J., \*Rieck, Hugh, \*Fouch, T.D., and \*Carter, L.D.,

- 1994,  $^{40}\text{Ar}/^{39}\text{Ar}$  age constraints on Neogene sedimentary beds, Upper Ramparts, Half-way Pillar and Canyon Village sites, Porcupine River, east-central Alaska: *Quaternary International*, v. 22/23, p. 31-42.
- \*Kvenvolden, K.A., \*Lorenson, T.D., \*Barnes, P.W., Popp, B.N., Sansone, F.J., Rust, T.M., Lilley, M.D., and Olson, E.J., 1994, Possible source of methane in seasonal ice of the Alaskan Beaufort Sea [abs.]: *Eos*, p. 77.
- \*Lahr, J.C., \*Chouet, B.A., \*Stephens, C.D., \*Power, J.A., and \*Page, R.A., 1994, Earthquake classification, location, and error analysis in a volcanic environment: implications for the magmatic system of the 1989-1990 eruptions at Redoubt Volcano, Alaska: *Journal of Volcanology and Geothermal Research*, v. 62, no. 1/4, p. 137-151.
- \*Lahr, J.C., \*Stephens, C.D., and \*Page, R.A., 1994, Possible early signs of re-organization of the Pacific-North American plate boundary in the Gulf of Alaska [abs.]: *GSA*, p. 139.
- Larson, K.M., and \*Lisowski, Michael, 1994, Strain accumulation in the Shumagin Islands: results of initial GPS measurements: *Geophysical Research Letters*, v. 21, no. 6, p. 489-492.
- Lea, P.D., Buppert, G.D., and \*Waythomas, C.F., 1994, Last-glacial eolian deposits in central and southwestern Alaska [abs.]: *GSA*, p. 512.
- Levander, A., \*Fuis, G.S., Wissinger, E.S., \*Lutter, W.J., Oldow, J.S., and \*Moore, T.E., 1994, Seismic images of the Brooks Range fold and thrust belt, Arctic Alaska, from an integrated seismic reflection/refraction experiment: *Tectonophysics*, v. 232, no. 1/4, p. 12-30.
- Lu, Zhong, Wyss, Max, Tytgat, Guy, McNutt, Steve, and \*Stihler, Scott, 1994, Aftershocks of the 13 May 1993 Shumagin Alaska earthquake: *Geophysical Research Letters*, v. 21, no. 6, p. 497-500.
- \*Magoon, L.B., III, 1994, Petroleum resources in Alaska, in G-1, p. 905-936, pls. 3 and 7.
- \*Marincovich, Louie, Jr., 1994, Earliest Tertiary paleogeography of the Arctic Ocean, in *MMS*, p. 45-48.
- 1994, Late Pliocene marine paleoclimate during the Bigbendian transgression, Alaska [abs.]: *ICAM*, p. 72.
- \*Marlow, M.S., \*Cooper, A.K., and \*Fisher, M.A., 1994, Geology of the eastern Bering Sea continental shelf, in G-1, p. 271-284, pl. 3.
- McGeary, Susan, Diebold, J.B., Bangs, N.L., and Bond, Gerard, 1994, Preliminary results of the Pacific to Bering shelf seismic experiment [abs.]: *Eos*, p. 643.
- \*McGimsey, R.G., \*Waythomas, C.F., and \*Neal, C.A., 1994, High stand and catastrophic draining of intracaldera Surprise Lake, Aniakchak Crater, Alaska [abs.]: *GSA*, p. 138.
- Meier, Mark, Lundstrom, Scott, Stone, Dan, Kamb, Barclay, Engelhardt, Hermann, Humphrey, Neil, Dunlap, W.W., Fahnestock, Mark, \*Krimmel, R.M., and \*Walters, Roy, 1994, Mechanical and hydrologic basis for the rapid motion of a large tidewater glacier—1. Observations: *Journal of Geophysical Research*, v. 99, no. B8, p. 15,219-15,229.
- Merrand, Y., Hallet, B., \*Molnia, B.F., \*Gray, J., and \*Hart, R., 1994, Bering Glacier: toward a sediment budget [abs.]: *Eos*, p. 63-64.
- Miller, L.D., \*Goldfarb, R.J., Gehrels, G.E., and \*Snee, L.W., 1994, Genetic links among fluid cycling, vein formation, regional deformation, and plutonism in the Juneau gold belt, southeastern Alaska: *Geology*, v. 22, no. 3, p. 203-206.
- \*Miller, T.P., 1994, Dome growth and destruction during the 1989-1990 eruption of Redoubt Volcano: *Journal of Volcanology and Geothermal Research*, v. 62, no. 1/4, p. 197-212.
- 1994, Geothermal resources in Alaska, in G-1, p. 979-987, pl. 12.
- 1994, Pre-Cenozoic plutonic rocks in mainland Alaska, in G-1, p. 535-554, pls. 4, 6, and 13.
- \*Miller, T.P., and \*Chouet, B.A., 1994, The 1989-1990 eruptions of Redoubt volcano: an introduction: *Journal of Volcanology and Geothermal Research*, v. 62, no. 1/4, p. 1-10.
- \*Miller, T.P., and \*Chouet, B.A., eds., 1994, The 1989-1990 eruptions of Redoubt Volcano, Alaska: *Journal of Volcanology and Geothermal Research*, v. 62, no. 1/4, special issue, 530 p.
- \*Miller, T.P., and Kirianov, V.Yu., 1994, Timing of large Holocene volcanic events in the western Aleutian arc, Alaska [abs.]: *Eos*, p. 731.
- \*Miller, T.P., and \*Richter, D.H., 1994, Quaternary volcanism in the Alaska Peninsula and Wrangell Mountains, Alaska, in G-1, p. 759-779.
- \*Moll-Stalcup, E.J., 1994, Latest Cretaceous and Cenozoic magmatism in mainland Alaska, in G-1, p. 589-619, pls. 5 and 12.
- 1994, The origin of the Bering Sea basalt province, western Alaska [abs.]: *ICAM*, p. 76.
- \*Moll-Stalcup, E.J., and \*Till, A.B., 1994, The origin of effusive cone-building lavas from Redoubt Volcano, easternmost Aleutian Arc, Alaska [abs.]: *Eos (American Geophysical Union Transactions)*, v. 75, no. 16 suppl., p. 358.
- \*Molnia, Bruce [B.F.], 1994, Modern surge of glacier comes to an end: *Eos (American Geophysical Union Transactions)*, v. 75, no. 47, p. 549. ["The latest surge of Bering Glacier may be over."]
- \*Molnia, B.F., \*Post, Austin, \*Trabant, D.C., and \*Krimmel, R.M., 1994, The 1993-94 surge of Bering Glacier, Alaska: an overview [abs.]: *Eos*, p. 62.
- \*Moore, T.E., \*Fuis, G.S., O'Sullivan, P.B., and Murphy, J.M., 1994, Evidence of Laramide age deformation in the Brooks Range, Alaska [abs.]: *GSA*, p. 383.
- \*Moore, T.E., \*Grantz, Arthur, and Roeske, S.M., 1994, Continent-ocean transition in Alaska: the tectonic assembly of eastern Denali, in Speed, R.C., ed., *Phanerozoic evolution of North American continent-ocean transitions*: Boulder, Colo., Geological Society of America, Summary volume to accompany the Decade of North American Geology continent-ocean transect series, p. 399-441.
- \*Moore, T.E., Wallace, W.K., \*Bird, K.J., \*Karl, S.M., Mull, C.G., and Dillon, J.T., 1994, Geology of northern Alaska, in G-1, p. 49-140, pl. 6, 13.
- \*Moore, T.E., Wallace, W.K., and \*Fuis, G.S., 1994, Shingled tectonic wedges in the central Brooks Range orogen [abs.]: *Eos*, p. 646.
- Morrissey, M.M., and \*Chouet, B.A., 1994, Choked-flow model

- for triggering and intermittency of long-period events at Redoubt Volcano 1989-90 [abs.]: *Seismological Research Letters*, v. 65, no. 1, p. 56.
- 1994, Masses of magmatic volatiles estimated by different methods for the 1989 eruptive onset of Redoubt Volcano, Alaska [abs.]: *GSA*, p. 452.
- \*Mullen, M.W., 1994, Miocene benthic foraminiferal assemblages from central Arctic Ocean cores and possible implications for Arctic paleoenvironments [abs.]: *Paleobios*, v. 16, no. 2, suppl., p. 49. [Forams '94, International Symposium on Foraminifera, Berkeley, University of California, Abstracts with Programs]
- \*Nelson, C.H., \*Phillips, R.L., \*McRea, James, Jr., \*Barber, J.H., Jr., \*McLaughlin, M.W., and \*Chin, J.L., 1994, Gray whale and Pacific walrus benthic feeding grounds and sea floor interaction in the Chukchi Sea: U.S. Minerals Management Service, OCS Study, MMS 93-0042, variously pagged. [Technical report for Minerals Management Service / IA No. 14157.]
- Nelson, R.E., and \*Carter, L.D., 1994, Pliocene marine palynology documents first appearance of lowland tundra in northern Alaska [abs.]: *GSA*, p. 142.
- \*Nokleberg, W.J., \*Brew, D.A., \*Grybeck, Donald, \*Yeend, Warren, Bundtzen, T.K., Robinson, M.S., Smith, T.E., Berg, H.C., Andersen, G.L., Chipp, E.R., Gaard, D.R., Burton, P.J., Dunbar, John, Scherckenbach, D.A., Foley, J.Y., Thurow, Gregory, Warner, J.D., Freeman, C.J., \*Gamble, B.M., \*Nelson, S.W., \*Schmidt, J.M., Hawley, C.C., Hitzman, M.W., Jones, B.K., Lange, I.M., Maars, C.D., Puchner, C.C., Steefel, C.I., \*Menzie, W.D., Metz, P.A., Modene, J.S., Plahuta, J.T., Young, L.E., Nauman, C.R., Newkirk, S.R., Newberry, R.J., Rogers, R.K., Rubin, C.M., Swainbank, R.C., Smith, P.R., and Stephens, J.E., 1994, Metallogeny and major mineral deposits of Alaska. in G-1, p. 855-903, pls. 3 and 11.
- \*Nokleberg, W.J., Bundtzen, T.K., and \*Plafker, George, 1994, Tectonic controls for metallogenesis of mainland Alaska [abs.]: *GSA*, p. 28.
- \*Nokleberg, W.J., Bundtzen, T.K., Shpikerman, V.I., Eremin, R.A., and Goryachev, N.I., 1994, Metallogenic model for the Russian Northeast and mainland Alaska [abs.]: *ICAM*, p. 81.
- \*Nokleberg, W.J., \*Plafker, G., \*Scholl, D.W., \*Vallier, T.L., Monger, J.W.H., Norton, I.O., Parfenov, L.M., Byalobzhesky, S.G., Khanchuk, A.I., Fujita, K., and Stone, D.B., 1994, Correlations of major terranes and overlap assemblages around [sic] Circum-North Pacific [abs.]: *ICAM*, p. 81-82.
- \*Nokleberg, W.J., \*Plafker, George, and \*Wilson, F.H., 1994, Geology of south-central Alaska, in G-1, p. 311-366, pls. 4, 7, 11, and 12.
- Nolan, M.A., Moryka, R.J., Echelmeyer, K., and \*Trabant, D., 1994, Ice thickness measurements of Taku Glacier, Alaska, and their implications [abs.]: *Eos*, p. 222.
- Nürnberg, D., Wollenburg, I., Dethleff, D., Eicken, H., Kassens, H., Letzig, T., \*Reimnitz, E., and Thiede, J., 1994, Sediments in Arctic sea ice: implications for entrainment, transport and release: *Marine Geology*, v. 119, no. 3/4, p. 185-214.
- Nye, C.J., Swanson, S.E., Avery, V.F., and \*Miller, T.P., 1994, Geochemistry of the 1989-1990 eruption of Redoubt Volcano: Part I. Whole-rock major- and trace-element chemistry: *Journal of Volcanology and Geothermal Research*, v. 62, no. 1/4, p. 429-452.
- Ort, M.H., Wohletz, K.H., and \*Neal, C.A., 1994, Complex interactions of ground water and basaltic magma during the eruption of the Ukinrek maars, Alaska [abs.]: *GSA*, p. 378.
- O'Sullivan, P.B., Murphy, J.M., Blythe, A.E., and \*Moore, T.E., 1994, Fission track evidence indicates that the present-day Brooks Range, Alaska, is a Cenozoic, not Early Cretaceous physiographic feature [abs.]: *Eos*, p. 646.
- \*Page, R.A., \*Lahr, J.C., \*Chouet, B.A., \*Power, J.A., and \*Stephens, C.D., 1994, Statistical forecasting of repetitive dome failures during the waning eruption of Redoubt Volcano, Alaska, February-April 1990: *Journal of Volcanology and Geothermal Research*, v. 62, no. 1/4, p. 183-196.
- Patrick, B., \*Till, A.B., and Dinklage, W.S., 1994, An inverted metamorphic field gradient in the central Brooks Range, Alaska and implications for exhumation of high-pressure/low-temperature metamorphic rocks: *Lithos*, v. 33, no. 1/3, p. 67-83. [Walker Lake]
- \*Patton, W.W., Jr., \*Box, S.E., and \*Grybeck, D.J., 1994, Ophiolites and other mafic-ultramafic complexes in Alaska, in G-1, p. 671-686.
- \*Patton, W.W., Jr., \*Box, S.E., \*Moll-Stalcup, E.J., and \*Miller, T.P., 1994, Geology of west-central Alaska, in G-1, p. 241-269.
- \*Pierson, T.C., and \*Janda, R.J., 1994, Volcanic mixed avalanches: a distinct eruption-triggered mass-flow process at snow-clad volcanoes: *Geological Society of America Bulletin*, v. 106, no. 10, p. 1351-1358. [Redoubt Volcano is one of the examples used.]
- \*Plafker, George, and Berg, H.C., 1994, Introduction, in G-1, p. 1-16, pl. 1-13.
- 1994, Overview of the geology and tectonic evolution of Alaska, in G-1, p. 989-1021, pls. 3, 7, and 12.
- \*Plafker, George, Moore, J.C., and \*Winkler, G.R., 1994, Geology of the southern Alaska margin, in G-1, p. 389-449, pl. 12.
- Popov, L.Y., \*Blodgett, R.B., and Anderson, A.V., 1994, First occurrence of the genus *Bicarinata* (Brachiopoda, Inarticulata) from the Middle Devonian in North America (Alaska): *Journal of Paleontology*, v. 68, no. 6, p. 1214-1218.
- \*Power, J.A., and Jolly, A.D., 1994, Seismicity at 10- to 45-km depth associated with the 1992 eruptions of Crater Peak vent, Mount Spurr, Alaska [abs.]: *Eos*, p. 715.
- \*Power, J.A., \*Lahr, J.C., \*Page, R.A., \*Chouet, B.A., Stephens, C.D., \*Harlow, D.H., Murray, T.L., and Davies, J.N., 1994, Seismic evolution of the 1989-1990 eruption sequence of Redoubt Volcano, Alaska: *Journal of Volcanology and Geothermal Research*, v. 62, no. 1/4, p. 69-94.
- \*Quinterno, P.J., \*McDougall, Kristin, \*Mullen, M.W., and \*Reimnitz, Erk, 1994, Foraminifers in sea ice from the Alaskan Beaufort Sea - indicators of cross-shelf transport [abs.]: *Paleobios*, v. 16, no. 2, suppl., p. 54. [Forams '94, International Symposium on Foraminifera, Berkeley, University of California, Abstracts with Programs]
- \*Reimnitz, Erk, Dethleff, Dirk, and Nürnberg, Dirk, 1994, Con-



- trasts in Arctic shelf sea-ice regimes and some implications: Beaufort Sea versus Laptev Sea: *Marine Geology*, v. 119, no. 3/4, p. 215-225.
- 1994, The danger of extrapolating from Beaufort Sea knowledge to other shallow Arctic shelf settings [abs.]: *Eos (American Geophysical Union Transactions)*, v. 75, no. 3, suppl., p. 73.
- \*Richter, D.H., \*Moll-Stalcup, E.J., \*Miller, T.P., \*Lanphere, M.A., \*Dalrymple, G.B., and \*Smith, R.L., 1994, Eruptive history and petrology of Mount Drum volcano, Wrangell Mountains, Alaska: *Bulletin of Volcanology*, v. 56, no. 1, p. 29-46.
- \*Riehle, J.R., 1994, Heterogeneity, correlatives, and proposed stratigraphic nomenclature of Hayes tephra set H, Alaska: *Quaternary Research*, v. 41, no. 3, p. 285-288.
- \*Riehle, J.R., \*Budahn, J.R., \*Lanphere, M.A., and \*Brew, D.A., 1994, Rare earth element contents and multiple mantle sources of the transform-related Mount Edgecumbe basalts, southeastern Alaska: *Canadian Journal of Earth Sciences*, v. 31, no. 5, p. 852-864.
- \*Riehle, J.R., and \*Meyer, C.E., 1994, Reconnaissance Holocene tephrochronology of the eastern Aleutian Arc, AK. [abs.]: *GSA*, p. 138.
- \*Riehle, J.R., Rose, W.I., Schneider, D.J., \*Casadevall, T.J., and Langford, J.S., 1994, Unmanned aerial sampling of a volcanic ash cloud: *Eos (American Geophysical Union Transactions)*, v. 75, no. 12, p. 137, 138. [Mt. Spurr volcano]
- 1994, Unmanned aerial sampling of a volcanic ash cloud. When Alaska's Mount Spurr erupted, emitted particles of a thick cloud in the air that threatened the safety of airplane passengers traveling through the cloud's path: *Earth in Space (For teachers and students of science)*, v. 6, no. 8, p. 10-11.
- Rohr, D.M., and \*Blodgett, R.B., 1994, *Palliseria* (middle Ordovician gastropoda) from east-central Alaska and its stratigraphic and biogeographic significance: *Journal of Paleontology*, v. 68, no. 3, p. 674-675.
- \*Scholl, D.W., \*Stevenson, A.J., Mueller, Steve, \*Geist, Eric, \*Vallier, T.L., and Engebretson, D.C., 1994, Regional-scale strain partitioning leading to escape tectonism and formation of offshore arc-trench systems, Alaska-Aleutian-Bering Sea region [abs.]: *GSA*, p. 110.
- \*Scott, W.E., and \*McGimsey, R.G., 1994, Character, mass, distribution, and origin of tephra-fall deposits of the 1989-1990 eruption of Redoubt Volcano, south-central Alaska: *Journal of Volcanology and Geothermal Research*, v. 62, no. 1/4, p. 251-272.
- Shelton, K.L., Underwood, M.B., and \*Howell, D.G., 1994, Regional stable isotope variations of calcite veins from Lisburne corridor, frontal Brooks Range, north-central Alaska: indicators of thermal maturity and hydrocarbon migration [abs.]: *Eos*, p. 647.
- \*Starratt, S.W., 1994, Benthonic foraminifers from Pervenets Canyon, Bering Sea: sedimentological and oceanographic controls [abs.]: *Paleobios*, v. 16, no. 2, suppl., p. 60. [Forams '94, International Symposium on Foraminifera, Berkeley, University of California, Abstracts with Programs]
- \*Stephens, C.D., and \*Chouet, B.A., 1994, Evolution of the precursory long-period event swarm of the December 14, 1989 eruption of Redoubt Volcano, Alaska [abs.]: *Seismological Research Letters*, v. 65, no. 1, p. 55.
- \*Stephens, C.D., \*Chouet, B.A., \*Page, R.A., \*Lahr, J.C., and \*Power, J.A., 1994, Seismological aspects of the 1989-1990 eruptions at Redoubt Volcano, Alaska: the SSAM perspective: *Journal of Volcanology and Geothermal Research*, v. 62, no. 1/4, p. 153-182.
- \*Stevenson, A.J., and \*Bruns, T.R., 1994, Sediment transport and fan deposition in the southern Gulf of Alaska: effects of transform motion recorded by deep-sea sedimentation [abs.]: *GSA*, p. 194.
- Swanson, S.E., Nye, C.J., \*Miller, T.P., and Avery, V.F., 1994, Geochemistry of the 1989-1990 eruption of Redoubt Volcano: Part II. Evidence from mineral and glass chemistry: *Journal of Volcanology and Geothermal Research*, v. 62, no. 1/4, p. 453-468.
- \*Taylor, C.D., \*Goldfarb, R.J., \*Snee, L.W., \*Gent, C.A., \*Karl, S.M., and \*Haeussler, P.J., 1994, New age data for gold deposits and granites, Chichagof mining district, SE Alaska: evidence for a common origin [abs.]: *GSA*, p. 140.
- \*Till, A.B., and \*Dumoulin, J.A., 1994, Geology of Seward Peninsula and Saint Lawrence Island, in G-1, p. 141-152.
- \*Till, A.B., \*Yount, M.E., and Bevier, M.L., 1994, The geologic history of Redoubt Volcano, Alaska: *Journal of Volcanology and Geothermal Research*, v. 62, no. 1/4, p. 11-30.
- \*Trabant, D.C., 1994, Measured propagation of a kinematic wave through a small piedmont lobe near Redoubt Volcano, Alaska [abs.]: *Eos*, p. 224.
- \*Trabant, D.C., and \*Molnia, B.F., 1994, Ice speed, ice thickness, and proglacial-lake stage and turbidity trends at the surging Bering Glacier, Alaska [abs.]: *Eos*, p. 63.
- \*Trabant, D.C., \*Waitt, R.B., and \*Major, J.J., 1994, Disruption of Drift glacier and origin of floods during the 1989-1990 eruptions of Redoubt Volcano, Alaska: *Journal of Volcanology and Geothermal Research*, v. 62, no. 1/4, p. 369-385.
- \*Vallier, T.L., \*Scholl, D.W., \*Fisher, M.A., \*Bruns, T.R., \*Wilson, F.H., \*von Huene, Roland, and \*Stevenson, A.J., 1994, Geologic framework of the Aleutian arc, Alaska, in G-1, p. 367-388.
- von Huene, R., Flueh, E., and the Kodiak Seis/Vent research group, GEOMAR, \*Fisher, Mike, and Jones, Kevin, 1994, Shipboard results from the Kodiak Seis cruise, Gulf of Alaska [abs.]: *Eos*, p. 597.
- \*Wahrhaftig, Clyde, \*Bartsch-Winkler, Susan, and \*Stricker, G.D., 1994, Coal in Alaska, in G-1, p. 937-978, pls. 1, 2, and 7.
- \*Waitt, R.B., \*Gardner, C.A., \*Pierson, T.C., \*Major, J.J., and \*Neal, C.A., 1994, Unusual ice diamicts emplaced during the December 15, 1989 eruption of Redoubt Volcano, Alaska: *Journal of Volcanology and Geothermal Research*, v. 62, no. 1/4, p. 409-428.
- \*Waitt, R.B., \*Mastin, L.G., and \*Miller, T.P., 1994, Velocities and spin of hydromagmatic ballistics from Mt. Spurr (Alaska) 1992 [abs.]: *IAVCEI, International Volcanological Congress, 1994, Ankara, Turkey, Abstracts: Ankara, Turkey, Middle East Technical University, Department of Geological Engineering, Special Publications no. 2, n.p.*
- Wallace, W.K., \*Moore, T.E., and \*Plafker, George, 1994, A multi-story duplex of thrust-truncated detachment folds,

- north-central Brooks Range, Alaska [abs.]: GSA, p. 527-528.
- 1994, Variations in structure from the Endicott Mountains allochthon to the parautochthon, north-central Brooks Range, Alaska [abs.]: Eos, p. 646.
- Watts, K.F., and \*Harris, A.G., 1994, Sequence stratigraphy and paleogeography—Carboniferous Lisburne Group of NE Alaska [abs.]: ICAM, p. 125-126.
- \*Waythomas, C.F., 1994, Hydrologic processes at Alaska volcanoes [abs.]: GSA, p. 377.
- 1994, New evidence for Holocene volcanic activity on northern Adak Island, Alaska [abs.]: GSA, p. 137-138.
- \*Waythomas, C.F., \*Miller, T.P., and Kirianov, V.Yu., 1994, Post-glacial evolution of northern Adak Island, Alaska [abs.]: American Quaternary Association, Biennial meeting, 13th, University of Minnesota, Minneapolis, Minn., Program and Abstracts, p. 179.
- White, J.M., and \*Ager, T.A., 1994, Palynology, paleoclimatology and correlation of middle Miocene beds from Porcupine River (locality 90-1), Alaska: Quaternary International, v. 22/23, p. 43-77.
- Wiles, G.C., Post, Austin, Muller, E.H., and \*Molnia, B.F., 1994, Tree-ring crossdating as a stratigraphic tool: examples from Bering Glacier, Alaska [abs.]: GSA, p. 309.
- \*Wilson, F.H., 1994, Overview of Quaternary glacial volcanic, and tectonic interactions of the Alaska Peninsula [abs.]: GSA, p. 137.
- Wissinger, E.S., Levander, A., \*Fuis, G.S., and \*Lutter, W.J., 1994, Crustal wedging in the Brooks Range, Alaska [abs.]: Eos, p. 646.
- Wissinger, E.S., Levander, Alan, Oldow, J.S., \*Fuis, G.S., and \*Lutter, W.J., 1994, Seismic images of the Brooks Range fold and thrust belt, arctic Alaska [abs.]: GSA, p. 146.
- \*Wolfe, J.A., 1994, An analysis of Neogene climates in Beringia: Palaeogeography, Palaeoclimatology, Palaeoecology, v. 108, no. 3/4, p. 207-216.

## CORRECTION

The following incorrect reference:

\*Casadevall, T., \*Chouet, B., \*Davies, J., \*Dorava, M., \*Doukas, M., \*Ellersieck, I., \*Gardner, C., \*Hoblitt, R., \*Jolly, A., \*Keith, T., \*Lahr, J., \*Matox, T., \*May, B., \*McGimsey, G., \*Meyer, D., \*Miller, T., \*Neal, C., \*Page, R., \*Paskievitch, J., \*Power, J., \*Stephens, C., \*Trabant, T., \*Waitt, R., Beget, J., Dean, K., Eichelberger, J., Harbin, M., Kienle, J., McNutt, S., Swanson, S., Tytgat, G., March, G., Motyka, R., and Nye, C., principal investigators, 1993, Mt. Spurr's 1992 eruptions: Eos (American Geophysical Union Transactions), v. 74, no. 19, p. 217, 221, and 222.

appeared in

Till, A.B., and Moore, T.E., eds., 1994, Geologic studies in Alaska by the U.S. Geological Survey, 1993: U.S. Geological Survey Bulletin 2107, p. 212.

the CORRECT REFERENCE follows:

Alaska Volcano Observatory, 1993, Mt. Spurr's 1992 eruptions: Eos (American Geophysical Union Transactions), v. 74, no. 19, p. 217, 221, and 222.





# U.S. Geological Survey Reports on Alaska Released in 1994\*

Compiled by Ellen R. Reiser

\*[One report dated 1992 and several reports dated 1993 did not become available for indexing until 1994: they are included in this listing.]

## ABBREVIATIONS

- B2047 Casadevall, T.J., ed., 1994, Volcanic ash and aviation safety: Proceedings of the First International Symposium on Volcanic Ash and Aviation Safety: U.S. Geological Survey Bulletin 2047, 450 p.
- B2107 Till, A.B., and Moore, T.E., eds., 1994, Geologic studies in Alaska by the U.S. Geological Survey, 1993: U.S. Geological Survey Bulletin 2107, 217 p.
- OF94-176 Jacobson, M.L., compiler, 1994, National Earthquake Hazards Reduction Program, summaries of technical reports, v. XXXV: U.S. Geological Survey Open-File Report 94-176, v. 1, 906 p., v. 2, 906 p.
- SUBCON Interdisciplinary Conference on the Subduction Process, Catalina Island, Calif., 1994, conveners: Dave Scholl, Gray Bebout, and Steve Kirby, sponsors: U.S. Geological Survey, JOL/USSAC, and NSF, 311 p., 19 leaves. [This is an unpublished version of the conference proceedings. The Menlo Park, Calif. U.S. Geological Survey Library has a copy. A final version is expected to be issued in late 1995 or early 1996.]

- Ager, T.A., 1994, Terrestrial palynological and paleobotanical records of Pliocene age from Alaska and Yukon Territory [abs.]: U.S. Geological Survey Open-File Report 94-23, p. 2-3.
- Aho, John, 1994, Potential effects of a major earthquake on structures in the Anchorage area: U.S. Geological Survey Open-File Report 94-218, p. 55-60.
- Alpha, T.R., and Ford, A.B., 1994, Oblique maps of southeastern Alaska, showing major mineral localities: U. S. Geological Survey Miscellaneous Field Studies Map MF-2271, 2 sheets.
- Babcock, L.E., Blodgett, R.B., and St. John, James, 1994, New Late(?) Proterozoic-age formations in the vicinity of Lone Mountain, McGrath quadrangle, west-central Alaska: B2107, p. 143-155.
- Bayhurst, G.K., Wohletz, K.H., and Mason, A.S., 1994, A method for characterizing volcanic ash from the December 15, 1989 eruption of Redoubt Volcano, Alaska: B2047, p. 13-17.
- Beavan, John, 1994, Crustal deformation measurements in the Shumagin seismic gap, Alaska: OF94-176, v. 1, p. 195-205.
- Belkin, H.E., and Sparck, H.M., 1994, Heavy-metal contents of sediment from the Kuskokwim River, Bethel, Alaska — a baseline study [abs.]: U.S. Geological Survey Circular 1103-A, p. 7-8.
- Boyd, T.M., [1993], Analysis of the 1957 Andreanof Islands earthquake: U.S. Geological Survey contract report, 14-08-0001-G1766, 11 p.
- Brabets, T.P., 1994, Scour assessment at bridges from Flag Point to Million Dollar Bridge, Copper River Highway, Alaska: U.S. Geological Survey Water-Resources Investigations Report 94-4073, 57 p.
- Bradley, Dwight, Haeussler, Peter, Kusky, Tim, and Goldfarb, Rich, 1994, Near-trench magmatism, deformation, and gold mineralization during Paleogene ridge subduction in Alaska: SUBCON, p. 219-221.
- Brantley, S.R., 1994, Volcanoes of the United States: U.S. Geological Survey, 44 p. [Alaskan volcanoes: p. 24-33, and 43 and one photo each on front- and back-covers. Public interest pamphlet.]
- Brew, D.A., and Ford, A.B., 1994, The Coast Mountains plutonic-metamorphic complex and related rocks between Haines, Alaska, and Fraser, British Columbia—tectonic and geologic sketches and Klondike Highway road log: U.S. Geological Survey Open-File Report 94-268, 25 p.
- Brew, D.A., Ford, A.B., Koch, R.D., Diggles, M.F., Drinkwater, J.L., Loney, R.A., and Smith, J.G., 1994, GPS versus template—simple field and office experiments concerning GPS-determined positions and template-scaled map locations: B2107, p. 199-205.
- Brouwers, E.M., 1993 [released 1994], Systematic paleontology of Quaternary ostracode assemblages from the Gulf of Alaska, Part 2: Families *Trachyleberididae*, *Hemicytheri-*

- dae, Loxoconchidae, Paracytherideidae*: U.S. Geological Survey Professional Paper 1531, 47 p., 16 pls.
- 1994, Systematic paleontology of Quaternary Ostracode assemblages from the Gulf of Alaska, Part 3—Family *Cytheruridae*: U.S. Geological Survey Professional Paper 1510, 45 p., 24 pls.
- Brunett, J.O., Solin, G.L., Carr, M.R., Glass, R.L., Nelson, G.L., and Buchmiller, R.C., 1992, Water-quality and soil assessment at 28 exploratory wellsites in the National Petroleum Reserve in Alaska, 1989-90: U.S. Geological Survey Open-File Report 91-458, 118 p., 68 pls., 13 diskettes, 5 1/4 in., 1.2 MB.
- Carver, G.A., 1993, Comparison of paleoseismic geology of subduction zone earthquakes in Alaska and Cascadia: U.S. Geological Survey Open-File Report 93-542, p. 23.
- Cathrall, J.B., 1994, Geochemical survey of the Craig Study Area—Craig and Dixon Entrance quadrangles and the western edges of the Ketchikan and Prince Rupert quadrangles, southeast Alaska: U.S. Geological Survey Bulletin 2082, 52 p., 1 sheet, scale 1:250,000.
- Church, S.E., Riehle, J.R., and Goldfarb, R.J., 1994, Interpretation of exploration geochemical data for the Mount Katmai quadrangle and adjacent parts of the Afognak and Naknek quadrangles, Alaska: U.S. Geological Survey Bulletin 2020, 67 p., 3 sheets, scale 1:250,000.
- Cieutat, B.A., Goldfarb, R.J., Borden, J.C., McHugh, John, and Taylor, C.D., 1994, Environmental geochemistry of mesothermal gold deposits, Kenai Fjords National Park, south-central Alaska: B2107, p. 21-25.
- Cole, Frances, Bird, Kenneth, and Howell, David, 1994, Preliminary results of a tectonic subsidence analysis of the central North Slope, Alaska: B2107, p. 115-132.
- Combellick, Rodney, 1994, Geologic evidence of earthquake frequency in southcentral Alaska: U.S. Geological Survey Open-File Report 94-218, p. 19-29.
- Combellick, Rodney, Head, Roger, and Updike, Randall, 1994, Earthquake Alaska—are we prepared?: U.S. Geological Survey Open-File Report 94-128, 192 p. [Proceedings of a conference on the status of knowledge and preparedness for earthquake hazards in Alaska, November 19-20, 1992, Anchorage, Alaska]
- Csejtey, Béla, Jr., Breace, P.F., Ford, A.B., and Nelson, W.H., 1994, Possible occurrence of lower to middle Paleozoic rocks south of the Denali fault, Denali National Park, Alaska, and implications for Denali fault displacement: B2107, p. 157-160.
- Davies, John, 1994, Earthquake sources in Alaska: U.S. Geological Survey Open-File Report 94-218, p. 9-18.
- Dmowska, Renata, and Rice, J.R., 1994, Integrated approach to earthquake hazard assessment of a subduction segment: a case study of the Shumagin Islands region, Alaska (grant 1434-93-G-2325): OF94-176, v. 1, p. 296-300.
- Dolton, G.L., Bird, K.J., Varnes, K.L., and Gautier, D.L., 1993, Onshore oil and gas resource assessment areas - Alaska: U.S. Geological Survey Open-File Report 93-331, 1 sheet, scale 1:5,000,000.
- Dorava, J.M., 1994, Environmental overview and hydrogeologic conditions at Aniak, Alaska: U.S. Geological Survey Open-File Report 94-85, variously paged.
- 1994, Overview of environmental and hydrogeologic conditions at McGrath, Alaska: U.S. Geological Survey Open-File Report 94-119, variously paged.
- Dorava, J.M., Ayres, R.P., and Sisco, W.C., 1994, Overview of environmental and hydrogeologic conditions at Moses Point, Alaska: U.S. Geological Survey Open-File Report 94-310, 11 p.
- Dorava, J.M., and Sokup, J.M., 1994, Overview of environmental and hydrogeologic conditions at the Merle K. "Mudhole" Smith airport near Cordova, Alaska: U.S. Geological Survey Open-File Report 94-328, variously paged.
- Doukas, M.P., McGimsey, R.G., and Dorava, J.M., 1994, Videotaped studies of ten years of volcanic eruptions in Alaska [abs.]: U.S. Geological Survey Open-File Report 94-134, p. 17.
- Drinkwater, J.L., Brew, D.A., and Ford, A.B., 1994, Chemical characteristics of major plutonic belts of the Coast plutonic-metamorphic complex near Juneau, southeastern Alaska: B2107, p. 161-172.
- Drinkwater, J.L., and Calzia, J.P., 1994, Geochemical reconnaissance of alkalic plutons on Prince of Wales Island, southeastern Alaska: B2107, p. 173-184.
- Dutro, J.T., Jr., Blodgett, R.B., and Mull, C.G., 1994, *Cyrtospirifer* from Upper Devonian rocks of the Endicott Group, west-central Brooks Range, Alaska: B2107, p. 133-141.
- Elder, W.P., and Miller, J.W., 1994, Mesozoic macrofossil locality information for the Mount Katmai and part of the Afognak quadrangles, Alaska: U.S. Geological Survey Open-File Report 93-713, 83 p., 1 sheet, scale 1:250,000.
- Eppinger, R.G., Motooka, J.M., and Sutley, S.J., 1994, High arsenic content in sediments from the Koyukuk National Wildlife Refuge, west-central Alaska: B2107, p. 15-20.
- Fisher, D.M., Brantley, S.L., Everett, Mark, and Wambold, Brett, 1994, Anatomy of a regionally extensive fracture network in the Kodiak accretionary prism: U.S. Geological Survey Open-File Report 94-228, p. 107-137. [Proceedings of Workshop LXIII: The mechanical involvement of fluids in faulting: National Earthquake Hazards Reduction Program]
- Flores, R.M., Stricker, G.D., and Roberts, S.B., 1994, Miocene coal-bearing strata of the Tyonek Formation: braided-stream deposits in the Chuit Creek-Chuitna River drainage basin, southern Alaska: B2107, p. 95-114.
- Frederiksen, N.O., Edwards, L.E., Fouch, T.D., Carter, L.D., and Collett, T.S., 1994, Palynomorph biostratigraphy of Eocene samples from the Sagavanirktok Formation at Franklin Bluffs, North Slope of Alaska: U.S. Geological Survey Open-File Report 94-653, 32 p.
- Galloway, J.P., and Carter, L.D., 1994, Paleowind directions for late Holocene dunes on the western Arctic Coastal Plain, northern Alaska: B2107, p. 27-30.
- Gautier, D.L., and Varnes, K.L., compilers, 1993, Plays for assessment in Region I, Alaska, as of October 4, 1993, 1995 National assessment of oil and gas: U.S. Geological Survey Open-File Report 93-596-A, 7 p.
- Gehrels, G.E., Dickinson, W.R., Ross, G.M., Stewart, J.H., and Howell, D.G., 1994, Detrital zircon geochronology of Cambrian to Triassic strata of the Cordilleran miogeocline, western North America [abs.], in Lanphere, M.A., Dalrymple, G.B., and Turrin, B.D., eds., Abstracts of the Eighth Inter-

- national Conference on Geochronology, Cosmochronology, and Isotope Geology: U.S. Geological Survey Circular 1107, p. 109.
- Gilpin, Lou, Ward, Steve, Anderson, Robert, Moore, J.C., and Carver, Gary, 1994, Holocene interseismic deformation and stratigraphic modeling of the earthquake cycle, Kodiak Islands, Alaska, Award no. 1434-93-G-2316: OF94-176, v. 1, p. 339-344.
- Goldfarb, R.J., Gent, C.A., Gray, J.E., and Nelson, S.W., 1994, Isotopic constraints on the genesis of base-metal-bearing mineral occurrences near Columbia Glacier, northern Prince William Sound, Alaska: B2107, p. 73-82.
- Gray, John, Theodorakos, Peter, Budahn, Jim, and O'Leary, Richard, 1994, Mercury in the environment and its implications, Kuskokwim River region, southwestern Alaska: B2107, p. 3-13.
- Haeussler, Peter, [1994], The next big earthquake in southern Alaska may come sooner than you think. Are you prepared?: U.S. Geological Survey, 24 p.
- , 1994, Possible active fault traces on or near the Castle Mountain fault between Houston and the Hatcher Pass road: B2107, p. 49-58.
- Heiken, Grant, 1994, Volcanic ash: what it is and how it forms: B2047, p. 39-45. [Augustine Volcano]
- Himmelberg, G.R., Brew, D.A., and Ford, A.B., 1994, Evaluation and application of garnet amphibolite thermobarometry, western metamorphic belt near Juneau, Alaska: B2107, p. 185-198.
- , 1994, Petrologic characterization of pelitic schists in the western metamorphic belt, Coast plutonic-metamorphic complex, near Juneau, southeastern Alaska: U.S. Geological Survey Bulletin 2074, 18 p.
- Jones, S.H., and Fahl, C.B., 1994, Magnitude and frequency of floods in Alaska and conterminous basins of Canada: U.S. Geological Survey Water-Resources Investigations Report WR93-4179, 122 p., 2 sheets, scale 1:250,000.
- Kelley, K.D., Bailey, E.A., Cieutat, B.A., and Borden, J.C., 1994, Gold in heavy-mineral-concentrate samples from the Howard Pass quadrangle, Brooks Range, Alaska: B2107, p. 83-89.
- King, H.D., Risoli, D.A., and Cooley, E.F., 1994, Analytical results and sample locality maps of samples of the ash of dwarf arctic birch, black spruce, white spruce, and tamarack from the Medfra quadrangle, west-central Alaska: U.S. Geological Survey Open-File Report 94-277-A, 102 p., 3 sheets, scale 1:250,000 (paper version); 94-277-B (diskette version).
- Kvenvolden, K.A., Lorenson, T.D., and Barber, Valerie, 1994, Methane in the Fox permafrost tunnel near Fairbanks, Alaska: B2107, p. 31-37.
- Lachenbruch, A.H., 1994, Permafrost, the active layer, and changing climate: U.S. Geological Survey Open-File Report 94-694, 43 p. [Transcript with minor editorial changes of a plenary address to the Sixth International Conference on Permafrost, Beijing, July 6, 1993.]
- Lahr, J.C., Stephens, C.D., Page, R.A., and Fogleman, K.A., 1994, Characteristics of the Aleutian Wadati-Benioff zone seismicity beneath southern Alaska: SUBCON, p. 301-303.
- Madden-McGuire, D.J., and Winkler, G.R., 1994, Mineral resource potential maps of the Anchorage 1° x 3° quadrangle, southern Alaska: U.S. Geological Survey Miscellaneous Investigations Series Map I-2393, scale 1:250,000.
- McCarthy, K.A., 1994, Overview of environmental and hydrogeologic conditions at Barrow, Alaska: U.S. Geological Survey Open-File Report 94-322, 17 p.
- McCormick, Michael, and Barnes, P.W., 1994, Studies of sediment transported by Beaufort gyre pack ice, Arctic Ocean, 1993: concentrations, textural and carbon data: U.S. Geological Survey Open-File Report 94-25, 30 p.
- McCoy, D., Layer, P.W., Newberry, R.J., Bakke, A., Masterman, S., and Goldfarb, R., 1994, Timing and source of lode gold in the Fairbanks district, interior Alaska [abs.], in Lanphere, M.A., Dalrymple, G.B., and Turrin, B.D., eds., Abstracts of the Eighth International Conference on Geochronology, Cosmochronology, and Isotope Geology: U.S. Geological Survey Circular 1107, p. 210.
- McDougall, Kristin, 1994, Late Cenozoic benthic foraminifers of the HLA borehole series, Beaufort Sea shelf, Alaska: U.S. Geological Survey Bulletin 2055, 100 p., 4 pls.
- McGimsey, Game, 1993, Volcanic activity in Alaska: September 1991-September 1992: Earthquakes and Volcanoes, v. 24, no. 2, p. 60-73.
- McGimsey, R.G., and Dorava, J.M., 1994, Video of the August 18, 1992, eruption of Crater Peak vent on Spurr volcano, Alaska: U.S. Geological Survey Open-File Report 94-614-A, videotape, Open-File Report 94-614-B, 14 p. [The videotape contains raw footage taken during observation flight.]
- McGimsey, R.G., Waythomas, C.F., and Neal, C.A., 1994, High stand and catastrophic draining of intracaldera Surprise Lake, Aniakchak volcano, Alaska: B2107, p. 59-71.
- McNutt, S.R., 1994, Eruptions of Pavlof Volcano, Alaska, and their possible modulation by ocean load and tectonic stresses: implications for the Shumagin seismic gap: SUBCON, p. 286-288.
- Miller, M.L., and Bundtzen, T.K., 1994, Generalized geologic map of the Iditarod quadrangle, Alaska, showing potassium-argon, major-oxide, trace element, fossil, paleocurrent, and archaeological sample localities: U.S. Geological Survey Miscellaneous Field Studies Map MF-2219-A, 48 p., 1 sheet, scale 1:250,000.
- Molnia, Bruce, 1994, International workshop on Arctic contamination: U.S. Geological Survey yearbook, fiscal year 1993, p. 72-73.
- Morin, R.L., 1994, Principal facts for gravity data in the Bethel and Russian Mission 1°x3° quadrangles, Alaska: U.S. Geological Survey Open-File Report 94-14-A, 6 p., 94-14-B, gravity data on diskette.
- Mortera-Gutiérrez, C.A., Carlson, R.L., and Scholt, D.W., 1994, Accommodation of stresses along the western Aleutian Trench: inferences from outer slope fault patterns: SUBCON, p. 55-58.
- Murray, T.L., Bauer, C.I., and Paskievich, J.F., 1994, Using a personal computer to obtain predicted plume trajectories during the 1989-90 eruption of Redoubt Volcano, Alaska: B2047, p. 253-256.
- Myers, J.D., 1994, The tale of three Aleutian volcanic centers: the influence of time and space on magmatic processes in subduction zones: SUBCON, p. 283-285.

- Neal, C.A., McGimsey, R.G., Doukas, M.P., and Ellersieck, Inyo, 1994 [release date], Photographs of the 1992 eruptions of Crater Peak, Spurr Volcano, Alaska: U.S. Geological Survey Open-File Report 93-707, 9 p., 20 color slides.
- Nelson, S.W., 1994, Importance of landslides in the geomorphic development of the upper Caribou Creek area, Talkeetna Mountains, Alaska: B2107, p. 43-47.
- Nelson, S.W., Miller, M.L., Goldfarb, R.J., Snee, L.W., Sherman, G.E., Roe, C.H., and Balen, M.D., 1994, Mineral resource assessment of the Chugach National Forest Special Study Area in northern Prince William Sound, Alaska: U.S. Geological Survey Open-File Report 94-272, 21 p.
- Nokleberg, W.J., Moll-Stalcup, E.J., Miller, T.F., Brew, D.A., Grantz, Arthur, Reed, J.C., Jr., Plafker, George, Moore, T.E., Silva, S.R., and Patton, W.W., Jr., 1994, Tectonostratigraphic terrane and overlap assemblage map of Alaska: U.S. Geological Survey Open-File Report 94-194, 54 p., 1 sheet, scale 1:2,500,000.
- Page, [Robert], R.A., 1994, Comparison of knowledge of earthquake potential in the San Francisco Bay and Anchorage regions: U.S. Geological Survey Open-File Report 94-218, p. 31-42.
- Page, R.A., Brocher, T.M., Stephens, C.D., Lahr, J.C., Fogleman, K.A., and Fisher, M.A., 1994, Piggyback subduction at the eastern end of the Aleutian trench and the giant asperity that ruptured in the Great 1964 earthquake: SUBCON, p. 152-154.
- Plafker, George, 1994, A look back at the Great 1964 Alaska and 1960 Chile subduction zone earthquakes: SUBCON, p. 310-311.
- Poore, R.Z., Ishman, S.E., Phillips, R.L., and McNeil, D.H., 1994, Quaternary stratigraphy and paleoceanography of the Canada basin, western Arctic Ocean: U.S. Geological Survey Bulletin 2080, 32 p. [Northwind Ridge]
- Prose, Doug, 1994, Alaska: U.S. Geological Survey Open-File Report 94-179-D, VHS videotape. [Raw footage of scenery, some aerial views of Anchorage. Of most interest to people making videos, according to the author.]
- Richter, D.H., Duffield, W.A., Sawyer, D.A., Ratté, J.C., and Schmoll, H.R., 1994, Geologic map of the Gulkana A-1 quadrangle, south-central Alaska: U.S. Geological Survey Geologic Quadrangle Map GQ-1728, scale 1:63,360.
- Rickman, R.L., 1993, Alaska, stream water quality: U.S. Geological Survey Water Supply Paper 2400, p. 163-170.
- Riehle, J.R., Church, S.E., Detterman, R.L., and Miller, J.W., 1994, Mineral-resource assessment in Alaska—background information to accompany maps and reports about the geology and undiscovered-mineral-resource potential of the Mount Katmai quadrangle and adjacent parts of the Naknek and Afognak quadrangles, Alaska Peninsula: U.S. Geological Survey Circular 1106, 13 p.
- Riehle, J.R., Detterman, R.L., Yount, M.E., and Miller, J.W., 1994, Geologic map of the Mount Katmai quadrangle and adjacent parts of the Naknek and Afognak quadrangles, Alaska: U.S. Geological Survey Miscellaneous Investigations Series Map I-2204, 1 sheet, scale 1:250,000.
- Rowe, Charlotte, 1994, Historic seismicity in Alaska: U.S. Geological Survey Open-File Report 94-218, p. 3-8.
- Ryan, H.F., 1994, Geologic setting of great Aleutian subduction-zone earthquakes: SUBCON, p. 155-157.
- Satake, Kenji and Boyd, T.M., [1993], The 1957 Andreanof Islands earthquake; constraints and implications on seismic hazard analysis and structural style of the Aleutian Arc; final report: U.S. Geological Survey contract report, award no. 1434-92-G-2187, 11 p.
- Satake, Kenji, and Ruff, L.J., 1994, Earthquake source process and tsunami generation in Aleutian-Alaska-Cascadia: OF94-176, v. 1, p. 112-114.
- Schlatter, T.W., and Benjamin, S.G., 1994, A mesoscale data assimilation system adapted for trajectory calculations over Alaska: B2047, p. 269-275.
- Schneider, D.J., and Rose, W.I., 1994, Observations of the 1989-90 Redoubt Volcano eruption clouds using AVHRR satellite imagery: B2047, p. 405-418.
- Schneider, J.L., ed., 1994, 1994 annual report on Alaska's mineral resources: U.S. Geological Survey Circular 1113, 69 p.
- Scholl, D.W., 1994, Initiation of new trench-arc-backarc systems of crustal growth in response to regional plate-boundary events that promote trench advance or retreat: examples from the Lau Tonga and Aleutian-Bering Sea regions: SUBCON, p. 115-119.
- Singer, Bradley, Rogers, Nick, Thirlwall, Matthew, and Leeman, William, 1994, Does fracture zone subduction increase sediment flux and mantle melting in the Aleutian arc?: evidence from trace element concentrations in Aleutian basalt: SUBCON, p. 289-291.
- Sokolowski, T.J., and Whitmore, P.M., 1994, Regional tsunami potential: U.S. Geological Survey Open-File Report 94-218, p. 43-54.
- Stephens, C.D., Page, R.A., Lahr, J.C., Fogleman, K.A., Brocher, T.M., Fisher, M.A., and Geist, E.L., 1993, Seismicity, stress orientation and configuration of the Aleutian megathrust in the vicinity of the Great 1964 Alaska Earthquake: U.S. Geological Survey Open-File Report 93-542, p. 94-104.
- Tanaka, H.L., 1994, Development of a prediction scheme for volcanic ash fall from Redoubt Volcano, Alaska: B2047, p. 283-291.
- Till, A.B., and Moore, T.E., 1994, Introduction: B2107, p. 1-2.
- Udike, Randall, 1994, A hypothetical earthquake on the Castle Mountain fault: U.S. Geological Survey Open-File Report 94-218, p. 61-67.
- Waythomas, C.P., 1994, Overview of environmental and hydrogeologic conditions at King Salmon, Alaska: U.S. Geological Survey Open-File Report 94-323, 16 p.
- Weber, F.R., Blodgett, R.B., Harris, A.G., and Dutro, J.T., Jr., 1994, Paleontology of the Livengood quadrangle, Alaska: U.S. Geological Survey Open-File Report 94-215, 24 p., 1 sheet, scale 1:250,000.
- White, E.R., 1994, Reports about Alaska in non-USGS publications released in 1993 that include USGS authors: B2107, p. 211-217.
- , 1994, U.S. Geological Survey reports on Alaska released in 1993: B2107, p. 207-210.
- Wilson, F.H., Shew, Nora, DuBois, G.D., and Bie, S.W., 1994, Sample locality map and analytical data for potassium-argon ages in the Port Moller, Stepovak Bay, and Simeonof Island quadrangles, Alaska Peninsula: U.S. Geological Survey Miscellaneous Field Studies Map MF-2155-E, 18



- p., 1 sheet, scale 1:250,000.
- Yeend, Warren, 1994, Calculated gold resource in Circle and Fortymile placers: B2107, p. 91-93.
- Yehle, L.A., and Rosenkrans, Danny, 1994, The 1993 Nelson Mountain landslide, Chitina Valley, southern Alaska, an aerial view: B2107, p. 39-41.
- Yehle, L.A., and Schmoll, H.R., 1994, Surficial geologic map of the Tyonek B-4 quadrangle, south-central Alaska: U.S. Geological Survey Miscellaneous Field Studies Map MF-2258, scale 1:31,680.

